December 2020

Electron-rich Alkynes and Azodicarboxylates Chemistry Towards Vicinal Diamine Motif Containing Small Molecules and N-Heterocycles

Chandima Jeewantha Narangoda
Clemson University, cjnarangoda.usjp@gmail.com

ELECTRON-RICH ALKYNES AND AZODICARBOXYLATES CHEMISTRY TOWARDS VICINAL DIAMINE MOTIF CONTAINING SMALL MOLECULES AND *N*-HETEROCYCLES

A Dissertation
Presented to
the Graduate School of
Clemson University

In Partial Fulfillment
of the Requirements for the Degree
Doctor of Philosophy
Chemistry

---

by
Chandima Jeewantha Narangoda
December 2020

Accepted by:
Dr. Daniel C. Whitehead, Committee Chair
Dr. William T. Pennington
Dr. Rhett Smith
Dr. Modi Wetzler

ABSTRACT

Heterocyclic molecules that contain nitrogens and consist of four, five and six-membered rings such as azetidinones (eg: β-lactams), pyrroles, indoles, azoles, triazoles, oxadiazines, and oxadiazinones, etc. are ubiquitous in the use of pharmaceutical fields. This also reflected in the recently FDA approved unique small-molecule pharmaceuticals, where about 90% of those molecules contain a nitrogen heterocycle. Particularly, the vicinal diamino motif has been appeared in leading drug directing candidates such as penicillin, cephalosporins, and oseltamivir (Tamiflu) over the past years.

Historically, there has been minimal interest in synthesizing a broad scope of vicinal diamino motif-containing small molecules and heterocyclic compounds for the purpose of using them in the medicinal fields. Therefore, synthesizing the vicinal diamino motif in a few synthetic steps with a broad substrate scope has remained challenging. In this work, we assess the potential to access the vicinal diamino skeleton through the reactivity of various azodicarboxylates (as the main nitrogen source) with various electron-rich alkynes. With further investigations, this chemistry leads us to develop novel methods to generate several classes of vicinal diamino motif-containing products, such as diazacyclobutenes (four-membered heterocyclic compound) and 2-iminothioimidates (acyclic vicinal diimino compounds), and highly substituted tetrahydroindoles (fused bicyclic compound consist of a five-membered *N*-heterocycle) in good yields with a broad substrate scope.

Additionally, with the divergent reactivity of this chemistry under the catalytic environment; a novel compound consist of a 6-membered 1,3,4-oxadiazin-2-one heterocyclic skeleton was produced. This dissertation further discloses the substrate dependent reactivity, divergent reactivity, mechanistic investigations and variable temperature dynamic NMR studies of these novel compounds.

In overall, this electron-rich alkynes and azodicarboxylates chemistry described in this document has been validated a novel protocol to rapidly access diverse vicinal diamino motif containing acyclic and cyclic compounds which have potential utility in organic synthesis and medicinal chemistry.

Last part of this dissertation describes the development of a protocol for the in-house synthesis of the cellulose nanocrystals, optimization and scale up synthesis of the poly(etheleneimne) functionalized cellulose nanocrystals to investigate the possibility of reducing the cost of the synthesis while maintaining the environmental remediation properties of these functionalized materials at the same efficiency.

DEDICATION

I dedicate this work to the memory of my dearest mother, Leela Goonasekara.

ACKNOWLEDGMENTS

I would like to give my sincere gratitude to my supervisor Dr. Whitehead for his continuous guidance in this research project, great flexibility he gave to develop this chemistry and for providing me all the necessities to make this project successful. I would like to give my appreciation and thank to Dr. Colin McMillen for his commitment and swift actions on solving crystal structures on this project which helped to keep the momentum of this work. I offer my special thanks Dr. Pennington, Dr. Smith and Dr. Wetzler for serving as my committee members.

I wish to thank current and past members of Whitehead research group including Dr. McKenzie Campbell, Dr. Heeren Gordhan, Dr. Timothy Lex, Dr. Maria Swasy, Anthony Santilli, Beau Brummel, Soham Panda, Kerrick Rees, and Brock Miller. Also my special thanks go to Dr. Timothy Lex for his support for the substrate scope studies in diazacyclobutenes and 2-iminothioimidates, Brock Miller for his support on collaborative broad catalytic development studies, Mohamed F. Attia for the support on cytotoxicity studies, Dr. Kristi Whitehead on antimicrobial studies, Dr. James Morris, Jillian Milanes, Neil Monaghan for antiparasitic studies.

Dr. James Jackson and Tayeb Kakeshpour from the Department of Chemistry, Michigan State University deserves a special mention for their computational support throughout this work. I would also like to thank the support given by Dr. Sheryl L. Wiskur and Brandon K. Redden in the Department of Chemistry and Biochemistry,

University of South Carolina for their support on react-IR studies. My big appreciation also goes to the undergraduate students who worked with me in this project including Madelyn Moore, Emma Frank, Samantha Carter, John Weller, Alex Pierce, Alec Suttle.

I acknowledged the National Science Foundation (grant number CHE-1725919) for allowing us to perform the most recent NMR experiments on a 500 MHz Bruker Avance NEO NMR instrument. My sincere gratitude goes to Dr. Alex Kitaygorodskiy for his training given for special NMR tasks, guidance throughout these experiments.

I am very grateful to my parents Leela Goonasekara, Sarath Narangoda and to all my teachers in education since preschool for laying out the foundation for my education. Also I thank my brother Anushka Narangoda and his family, father in law Ananda Kolambage and the sister in law Harshani for constantly sending me their love all the way from Sri Lanka.

Most of all I thank my wonderful wife Muditha Kolambage for the immense love and support she gave through this entire Ph.D journey.

LIST OF ABBREVIATIONS

Å	Angstrom
ATR	Attenuated Total Reflection
°C	Degrees centigrade
CNC	Cellulose nanocrystals
CNC-*f*-PEI	Poly(etheleneimne) functionalized cellulose nanocrystals
COSY	Correlation spectroscopy
d	doublet
DCM	Dichloromethane
DEAD	Diethyl azodicarboxylate
DIAD	Diisopropyl azodicarboxylate
DFT	Density-functional Theory
DMF	N,N'-Dimethyl formamide
DMSO	Dimethyl sulfoxide
DTBAD	Di-*tert*-butyl azodicarboxylate
equiv	Equivalence
EtOAc	Ethyl acetate
FTIR	Fourier Transform Infrared spectroscopy
g	Gram
GC	Gas Chromatography
h	hour
HMQC	Heteronuclear Multiple-Quantum Correlation
HPLC	High pressure liquid chromatography
HRMS	High resolution mass spectrum or spectrometry
m	multiplet
MeOH	Methanol
mg	Milligram
mmol	Milli moles
mol	Moles
M.pt.	Melting point
MS	Mass spectrometry
MW	Molecular Weight
NMR	Nuclear Magnetic Resonance
NOE(SY)	Nuclear overhauser effect (spectroscopy)
PEI	Polyethylenimine
q	Quartet
RT	Room temperature
t	triplet
TCEAD	Bis(2,2,2-trichloroethyl) azodicarboxylate
Tf	Triflate
THF	Tetrahydrofuran
TLC	Thin layer chromatography
VOCs	Volatile Organic Compounds

TABLE OF CONTENTS

Page

Table of Content (continued)

Page

Table of Content (continued)

Page

Table of Content (continued)

Page

Table of Content (continued)

Page

Table of Content (continued)

Page

Table of Content (continued)

Page

LIST OF TABLES

List of Tables (continued)

Table Page

List of Tables (continued)

Table Page

LIST OF SCHEMES

List of Schemes (continued)

Scheme Page

List of schemes (Continued)

Scheme Page

LIST OF FIGURES

List of figures (Continued)

Figure Page

List of figures (Continued)
Figure Page

List of figures (Continued)
Figure Page

List of figures (Continued)

Figure Page

List of figures (Continued)
Figure Page

CHAPTER ONE

INTRODUCTION

1.1 Importance of the *N*-heterocycles and vicinal diamines

1.1.1 Biological importance of the N-heterocyclic compounds

Nitrogen containing heterocyclic compounds have been widely used as pharmaceutical drug candidates.[1–4] The frequency of the use of nitrogen containing heterocyclic compounds is evident in the United States FDA drug approvals. Statistical surveys published in 2014 and 2018 revealed that about 60% of the U.S. FDA approved unique small molecule drugs contained a nitrogen heterocycle.[2,3] This high frequency of *N*-heterocycles was also reflected in the list of approved 2019 U.S FDA drugs, where 90% of the small molecule candidates contained *N*-heterocycles.[5] Further analysis of the 2014 survey showed that five and six-membered N-heterocycles are highly prevalent among those pharmaceuticals.[1] These studies show the ubiquity of the *N*-heterocycles and the biological importance of them as pharmaceuticals. Another significant factor pertaining to the *N*-heterocycles is the presence of the nitrogen atom in their structure as a high impact element, which could give rise to substantial improvements of the pharmacological properties of the drug candidate.[6] Previous biomedical research studies have shown that nitrogen can be utilized successfully to optimize the pharmacological parameters by replacing a CH group of the drug molecule with nitrogen atom. It has been found that substitution of a select CH group in a drug candidate with nitrogen can enhance and optimize the pharmacological properties and increase the drug potency.

Some of the noticeable properties arise from the nitrogen atom are increasing the binding affinity to the target receptor,[7,8] increasing the hydrogen bonding donor-acceptor capability,[9] facilitates intra- and inter-molecular interactions. In addition some specific features such as providing a conformational preference to the structure and changing the electrostatic potential map of the molecule with substituting nitrogen in place of a carbon atom in aromatic molecules could play key roles in governing these pharmacological properties.[6]

In order to highlight the biological importance of the *N*-heterocycles; **Figure 1.1** lays out some of selected examples of *N*-heterocycles that have been used as synthetic pharmaceuticals in the pharmaceutical industry. Compound **I-1** contains a four-membered *N*-heterocycle and can be categorized as a leading drug family of antibiotics known as penicillins.[10] Econazole (**I-2**) contains a five-membered *N*-heterocycle which is also a well-known antifungal drug used to treat skin infections.[11–13] Another broadly medicinally used family of five-membered *N*-heterocyclic scaffold is the triazole which is highlighted in the example of compound **I-3** for its antifungal activity.[14] The final example of **Figure 1.1** shows a six-membered *N*-heterocyclic compound **I-4**, which has a 1,3,4-oxadiazine-5-one scaffold. It has been found that some of these derivatives demonstrated significant antibacterial and appreciable antifungal properties.[15,16]

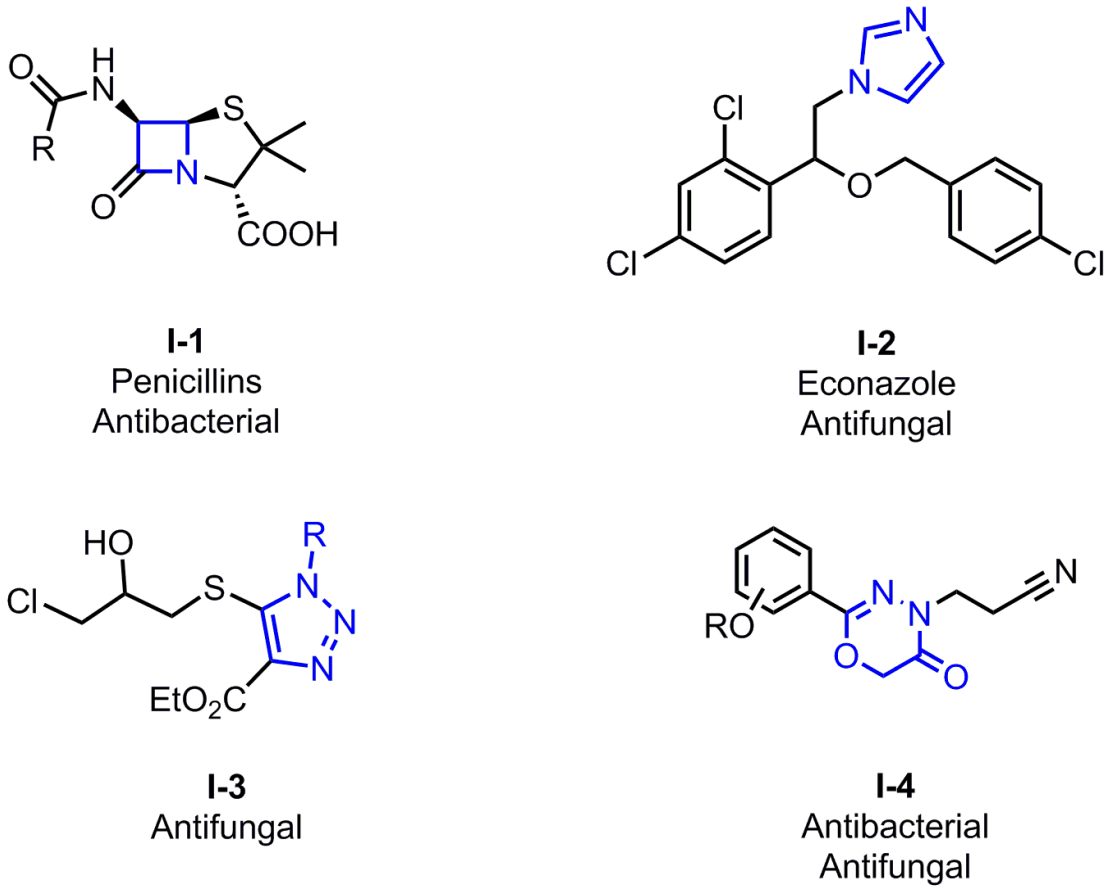

Figure 1.1 Selected examples of biologically important 4-, 5-, 6-membered *N*-heterocycles.

Moreover, six-membered 1,3,4-oxadiazinone structural motif is one of the versatile building block that has been widely seen in compounds used in pharmaceutical, agrochemical and pesticide industry.[17]

Since *N*-heterocycles enjoy a wide variety of applications in pharmaceutical, agrochemical, pesticide, and material industry, the synthesis of *N*-heterocycles by convenient routes via atom-economical pathways, with a lack of significant waste generation are popular research areas nowadays. Also, there are many synthetic methodologies that utilize transition metal catalyzed routes for *N*-heterocycle synthesis.[18–21] Nonetheless, due to the fact that trace impurities of some metals could be toxic to bacteria and fungi, carrying out synthetic operations which rely on transition metal ions could potentially contaminate the final bio-active product with trace metal impurities, leading to falsely potent lead compounds. So, developing transition metal free synthetic methodologies to access *N*-heterocycles in fewer synthetic steps with readily available starting materials is a worthy area of study.[22]

1.1.2 Biological importance of the 1,2-diamino compounds

Another biologically and synthetically important structural motif is the 1,2-diamine or the vicinal diamino structural motif. There has been significant methodology development towards 1,2-diamination reactions of alkenes over the past due to the appearance of the 1,2-diamine scaffold in a large number of biologically important natural products and in ligands for asymmetric catalysis.[10]

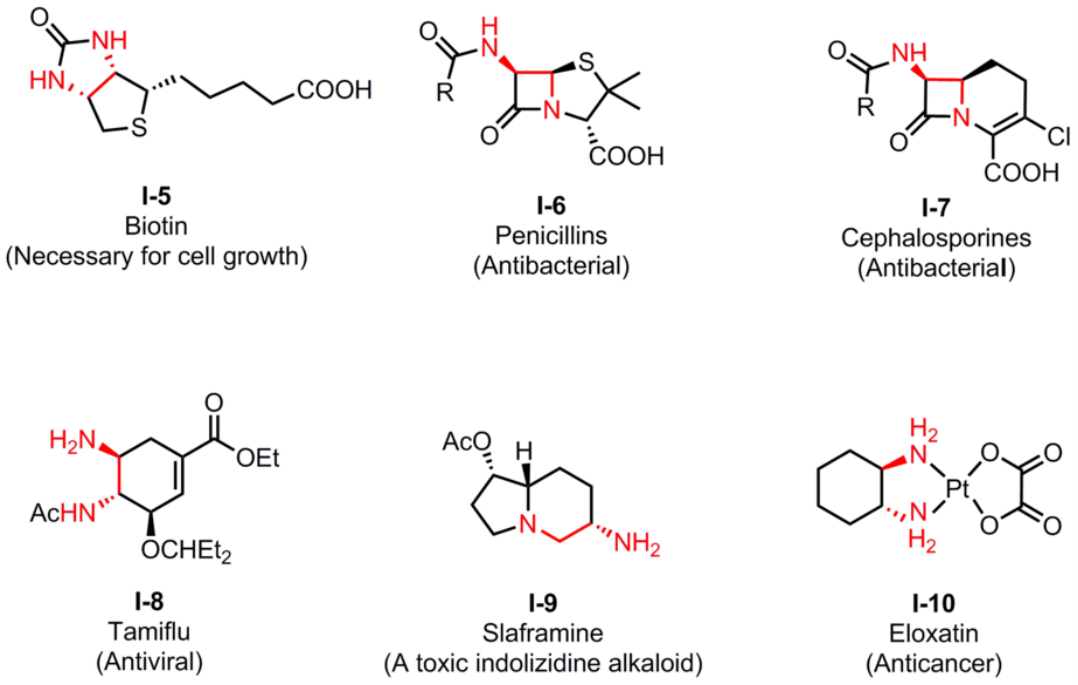

Figure 1.2 Selected examples of biologically important 1,2-diamine structural motif containing compounds.

Figure 1.2 shows some selected examples of naturally occurring compounds and synthetic pharmaceuticals that contain the vicinal diamino motif exhibiting broad spectrum of biological activity.[10,23,24]

Compound **I-5** (Figure 1.2) is known as biotin (or vitamin H or vitamin B7) which is a water-soluble vitamin which is necessary for cell growth and the metabolism of fats and amino acids. Biotin shows its vicinal diamine moiety in the imidazolidinone ring. Penicillins (**I-6)** and Cephalosporines (**I-7)** are well-known, naturally occurring, potent antibiotics with a 1,2-diamine motif within the azetidine ring. Tamiflu (**I-8**) and Slaframine (**I-9**) both contains the 1,2-diamine motif and are antiviral and cytotoxic indolizidine alkaloid respectively.

As a result of the success of diamino platinum compounds in the field of antitumor chemotherapy in mid 1960s, synthetic chemists turned towards synthesizing different 1,2-diamino platinum compounds to evaluate and identify compounds having greater potency and less toxicity. The compound illustrated in **I-10** (Eloxatin) is one of the examples of a 1,2-diaminoplatinum compound that was tested in the 1960s for its anticancer activity that now has been used as a clinical therapeutic agent.[23,25]

1.2 Vicinal diamination or 1,2-diamination

1.2.1 Previous studies of the vicinal diamination of alkenes

The versatile applications of the 1,2-diamine (vicinal diamino) motif have placed the development of synthetic methodologies for accessing a broad substrate scope of vicinal diamines in high demand. Despite their utility in medicine and organic synthesis, robust and general means for their preparation are sparse. The previous progress toward the vicinal diamination of alkenes is discussed in this section.

Many established approaches for the synthesis of *vic*-diamines suffer from lengthy processes, tedious operations, and sometimes poor yield. As an historical example, initially formed diols from an alkene must then undergo alcohol activation, azide replacement and reduction to generate the vicinal diamine motif (Scheme 1.1, eq. 1).[23,24,26]

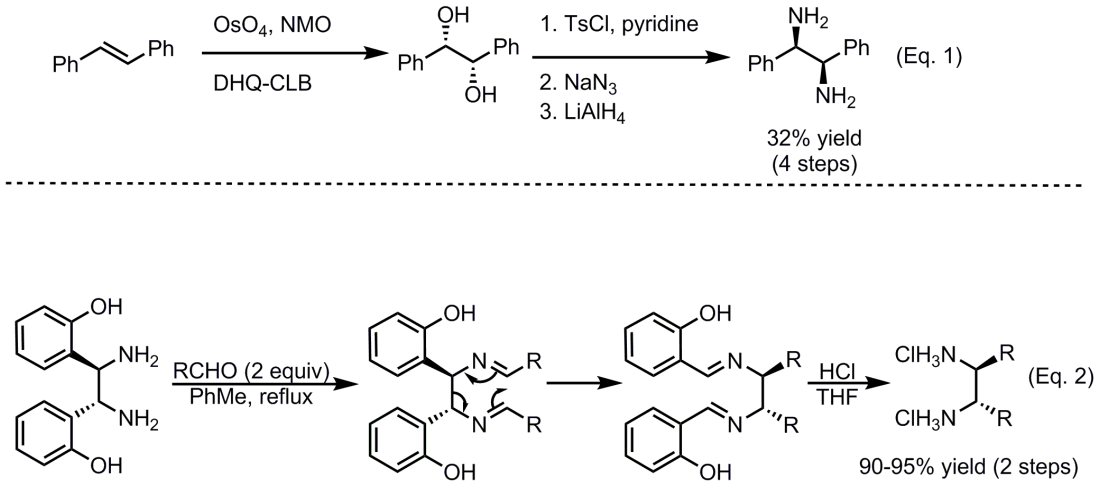

Scheme 1.1 Equation 1: A typical multi-step linear sequence for the enantioselective preparation of *vic*-diamines from alkenes. Equation 2: The diaza-Cope strategy for the preparation of chiral *vic*-diamines.

Analogous methods have been adapted which involves the stepwise operation of a single functional group in β-amino alcohols, β-halogenoalkylamines, aldehydes and amino acid derived ketimines.[23,24] Some other strategies of *vic*-diamine synthesis have originated from substrates other than generic alkenes which rely on nucleophilic addition into nitro alkene, ring opening from aziridinium ion intermediates, or the reductive coupling of imines, amides and oximes.[23,24] Further, Chin and Kim developed a somewhat general methodology using the diaza-Cope rearrangement (DCR) strategy (Scheme 1.1, eq. 2) however this strategy also has its own limitations due to the requirement of a specialized chiral diamine source as the initial substrate.[27]

All of these strategies have limitations such as further synthetic operations to obtain the desired products, use of expensive starting materials, multiple steps, and the use of toxic substances such as azides. Further, none of these methods displays a generalized method for the preparation of a broad scope of vicinal diamines from commonly available starting materials.

From a theoretical standpoint, the direct addition of two nitrogen atoms across a carbon-carbon double bond is perhaps the most straightforward means for the preparation of vicinal diamines.[28] However, this approach is not as well developed as related processes such as dihydroxylations,[29] aminohydroxlyations,[30] and epoxidations.[31–33]

Initial attempts towards direct vicinal diamination of alkenes have focused on a variety of different metal catalyzed processes. In previous studies, researchers have done a remarkable amount of work on metal-catalyzed intramolecular 1,2-diamination reactions which enabled access to vicinal diamines. Several protocols utilizing palladium catalysis, copper catalysis and some higher oxidation state metals have become available, which served to significantly broaden the ability to access these 1,2-diamino compounds.[34–36] As mentioned earlier, due to the potential for trace metal contamination, these metal catalyzed approaches may be less desirable for biomedical research areas. Thus, exploring new metal-free approaches toward vicinal diamination is important.

Several groups have done vicinal diamination reactions of alkenes utilizing metal-free approaches, mostly aided by halogenation event or hypervalent iodine catalysis. Scheme 1.2 shows a brief outline of these efforts and highlights a few examples. In 2012, Muñiz and coworkers were used an alkene with a tethered sulfonamide group (*e.g.* **I-11**) to carry out an intramolecular diamination event while avoiding the use of transition metals. This reaction was promoted by the *in situ* oxidation of KBr, leading to bicyclic diamine products such as **I-12** in high yield (Scheme 1.2, Eq. 1).[37,38] Later this protocol was modified by Wirth and co-workers by employing a chiral hypervalent iodine catalyst, **I-13**, to perform a highly stereoselective diamination (*i.e.*, (*R*)-**I-14** in 92% *ee*, Eq. 2) in good yield.[39] These methods allowed rapid access to the vicinal diamino motif containing cyclic sulfamide derivatives, which are medicinally useful due to their proven biological

activities such as the inhibition of serine proteases,[40] antidepressant activity,[41] antibacterial activity,[42] and antiviral activity.[43,44]

Furthermore, the Muñiz group applied this hypervalent iodine chemistry for alkenes[35,37,45,46] and conjugated dienes[47] to facilitate intra- and intermolecular diaminations (examples are not shown).

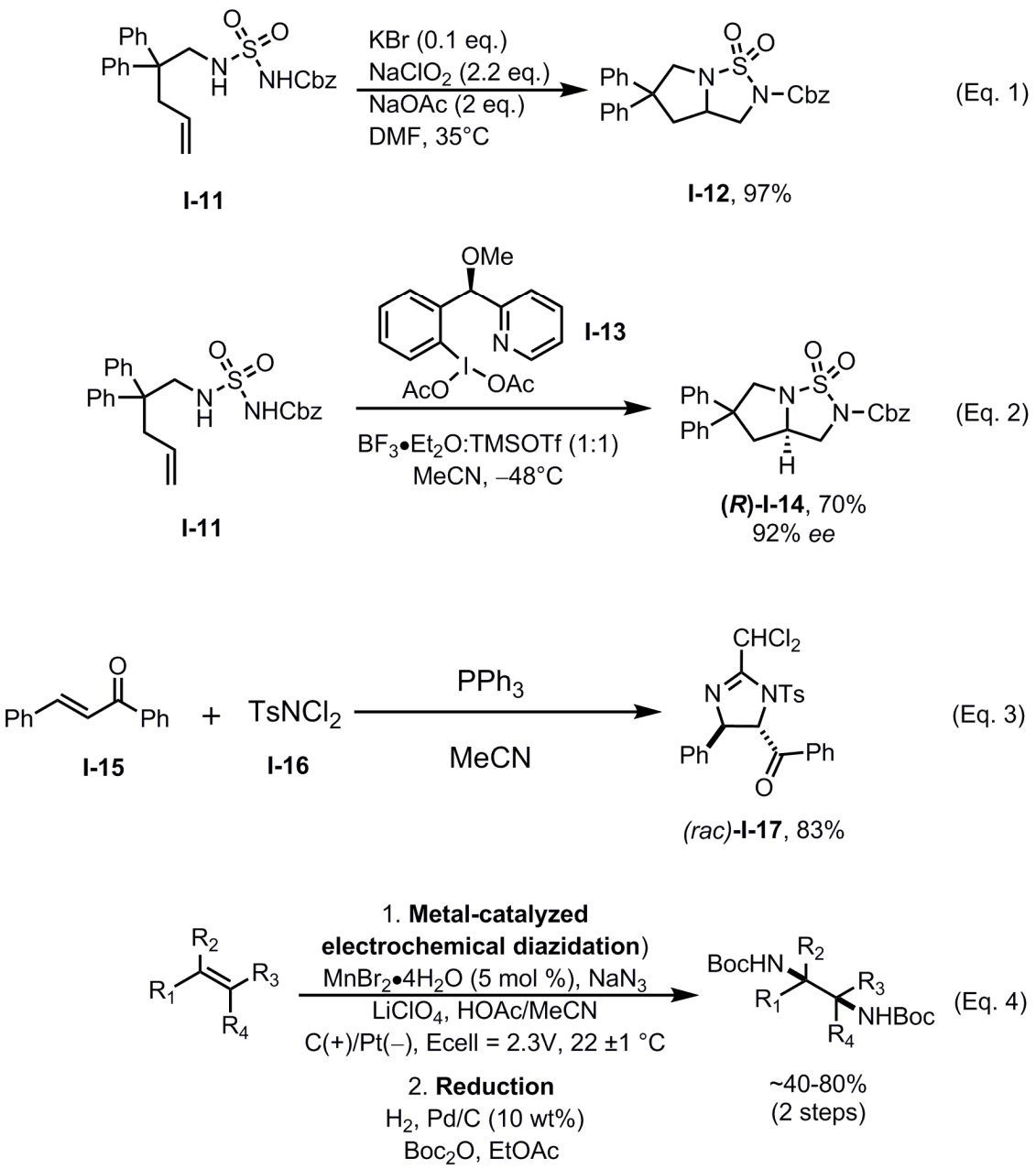

Scheme 1.2 Selected examples of metal-free and recent electrocatalytic vicinal diaminations of alkenes.

Moreover, similar synthetic strategies were also reported by several other research groups for the intramolecular diamination of olefins, which were facilitated by *N*-iodosuccinimide and tethered amine nucleophiles such as amidine, urea and thiourea. Significant contributions were made by the groups of Zhang,[48,49] Widenhoefer,[50] and Hennecke.[51] Equally, other research groups, including those of Chiba,[52] Blakey,[53] and Chang[54] reported related intramolecular diamination reactions with hypervalent iodine reagents.

In most of these methods, the nitrogen sources for the diamination were already housed within the substrate to promote the intramolecular deamination, which was further mediated by a halonium promoter or oxidative diamination step. Due to this limitation of using specialized substrates in these methods, they necessarily require the synthesis of specialized starting materials by means of several steps. However, Pan and co-workers demonstrated a Ritter-like cyclization of chalcones (**I-15**) assisted by an external nitrogen source such as $TsNCl_2$ (**I-16**), with the use of triphenylphosphine, and acetonitrile, thus generating racemic 2-imidazolines in high yield (*i.e.*, (*rac*)-**I-17**, in Eq. 3).[55]

In recent literature, the vicinal diamination of alkenes was achieved by the Lin group using electrocatalytic diazidation by means of a metal-mediated azidyl radical transfer reaction. This approach enabled dual carbon-nitrogen bond formation followed by subsequent reduction to the corresponding vicinal diamines (Scheme 1.2, Eq. 4).[36] This electrocatalytic methodology served as a good generalized method with broad

functional group compatibility, while the handling of toxic azide reagents seems to be the only drawback. Very recently, the selenide-catalyzed 1,2-diamination of alkenes has been developed utilizing sulfonamide nucleophiles.[56] However, this process requires a specialized catalyst and also suffers from a somewhat limited functional group tolerance. As described so far, the 1,2-diamination of alkenes is a well-developed and actively ongoing research area.

In comparison with alkene diamination, the synthesis of the vicinal diamine motif contained within *N*-heterocycles is another broadly developed research domain due to the biological importance of these motifs, as described earlier. There are many other classes of 5- and 6-membered heterocyclic compounds containing the *vic*-diamine motif, while also containing oxygen, sulfur, carbonyl, sulfoxide, and sulfone groups within the heterocyclic ring. Due to our interest in the main vicinal diamino scaffold, the examples and the literature studies of these compounds have not been extensively discussed here. Nevertheless, a few selected examples of recent studies, related developments, and apparent downsides of the methodologies are highlighted and discussed in the following paragraphs in order to highlight some aspects of this area of study.

Vast number of 5-membered heterocycles containing the vicinal diamine motif such as imidazoles and imidazolines have been synthesized and evaluated for their biological activities over the past.[57–64] This area is well-documented in the literature. The

preparation of these scaffolds have been enriched with number of different synthetic protocols since 1950s.[58,59]

Six-membered *vic*-diamine motifs containing heterocycles such as piperizines, quinoxalines, tetrahydroquinoxalines are also important structural elements in medicinal chemistry.[65–73] In recent studies, the vicinal diamination of arenes have been carried out under mild conditions with the *in situ* generation of benzynes (**II-19)** from trimethylsilylaryl triflates (**II-18**) followed by reaction with sulfamides (*e.g.***II-20**) to produce the benzothiadiazole-2,2-dioxide motif (*e.g.***II-21**) consisting of a 1,2-diamino motif (Scheme 1.3, Eq. 1).[74,75] Lately, *o*-phenylendiamine have been used as precursors to produce quinoxalines and tetrahydroquinoxalines via metal-catalyzed and metal-free strategies. With the inspiration of the pioneering work of nickel-catalyzed borrowing hydrogen and dehydrogenative coupling protocols,[76–78], the Kundu[79] and Tang[80] groups have utilized vicinal diols for the synthesis of quinoxalines and tetrahydroquinoxalines. One example for this type of transformation appears in Scheme 1.3, Eq. 2, where a vicinal diol (*e.g.***II-23**) reacts with *o*-phenylendiamine (*e.g.***II-22**) to form quinoxaline (*e.g.***II-24**) in the presence of a Ni(II) catalyst.[79] Even though these strategies are compatible with a broad scope, some required well-define catalysts, specialized ligands, additives, high temperatures, and longer reaction times.[79,80]

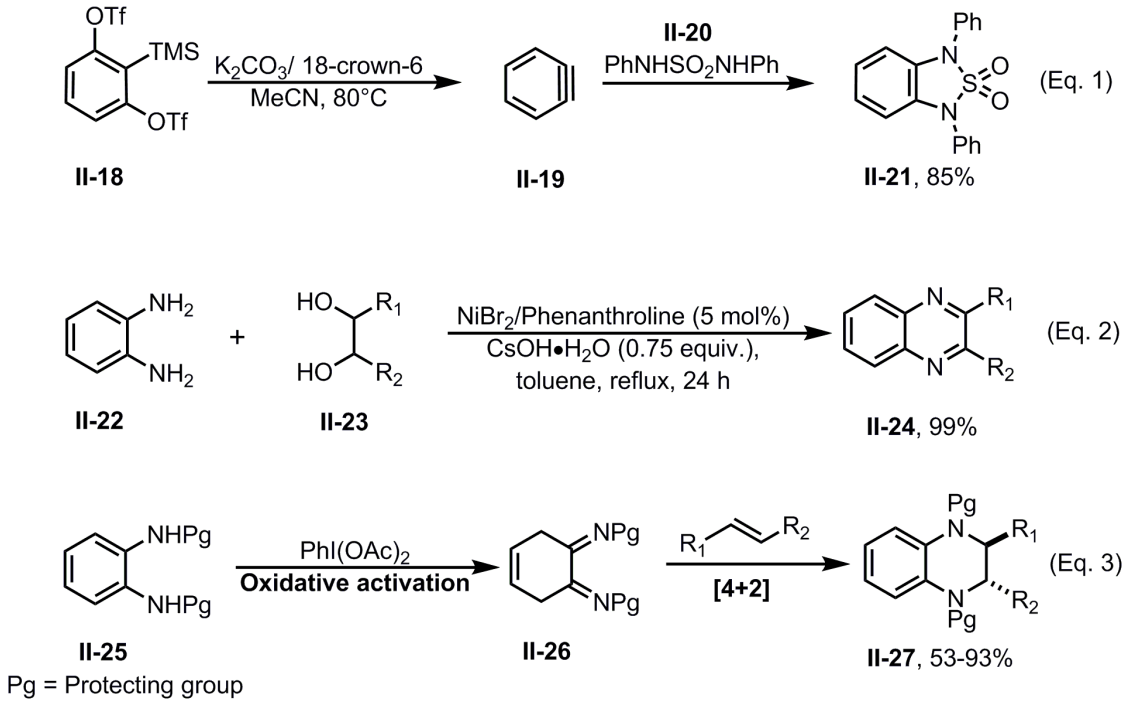

Scheme 1.3 Selected examples for the synthesis of 5- and 6-membered *vic*-diamine motif containing *N*-heterocycles.

In very recent studies, Wang *et al*. used a metal-free oxidative [4+2] cycloaddition approach to produce an assembly of tetrahydroquinoxalines (Scheme 1.3, Eq.3).[70] In this example, first *o*-phenylenediamines (**II-25**) were chemoselectively oxidized into quinine diimide intermediates (**II-26**) and subsequently reacted with various alkenes to perform the [4+2] cycloaddition in order to obtain the corresponding tetrahydroquinoxalines (**II-27**) (Scheme 1.3, Eq.3). However, this protocol was also limited by the necessary use of electron-withdrawing *o*-phenylendiamine to obtain higher yields.

Despite these synthetic methodologies, facile and efficient protocols to rapidly access the vicinal diamine motif and quickly increase structural diversity as well as enantioselective methods are still highly beneficial to this research area. Particularly, when compared to the synthetic strategies of five- and six-membered *vic*-diamine motif containing *N*-heterocycles, methods accessing four-membered *N*-heterocycles harboring the *vic*-diamine motif are relatively rare.

1.2.2 Four-membered N-heterocycles consist of 1,2-diamino motif

This section will review the previously reported synthetic methodologies for the synthesis of four-membered *N*-heterocycles containing of 1,2-diamino motif. Four-membered heterocycles that contain the 1,2-diamino motif can be categorized into three main classes. They are called as 1,2-diazetidines, 1,2-diazetines, and 1,2-diazetes. These compounds consist of two adjacent nitrogen atoms and two adjacent carbon atoms in a four-membered ring. They have been named according to Hantzch-Widman IUPAC nomenclature system depending on their degree of unsaturation. Efforts to synthesize these types of compounds go back over the past 100 years.

The 1,2-Diazetidines have no additional degrees of unsaturation beyond their cyclic structure (see **Figure 1.3**). The 1,2-diazetines have one pi bond and depending on the position of the pi bond, they are named differently (see **Figure 1.3**).[81] If the double bond or the pi bond is at the first position of the four-membered ring (*i.e.,* numbering from the first nitrogen atom through the second), the compound is called as Δ^1-1,2-diazetine. Similarly, if the double bond is at the second and the third position of the four-membered ring, it is called a Δ^2-1,2-diazetine and Δ^3-1,2-diazetine, respectively. Furthermore, the Δ^3-1,2-diazetine motif can be obtained by replacing the saturated carbons of the cyclobutene motif with two nitrogen atoms. Thus, Δ^3-1,2-diazetines are also known as diazacyclobutenes where “diaza” refers to the two nitrogen atoms in the scaffold.

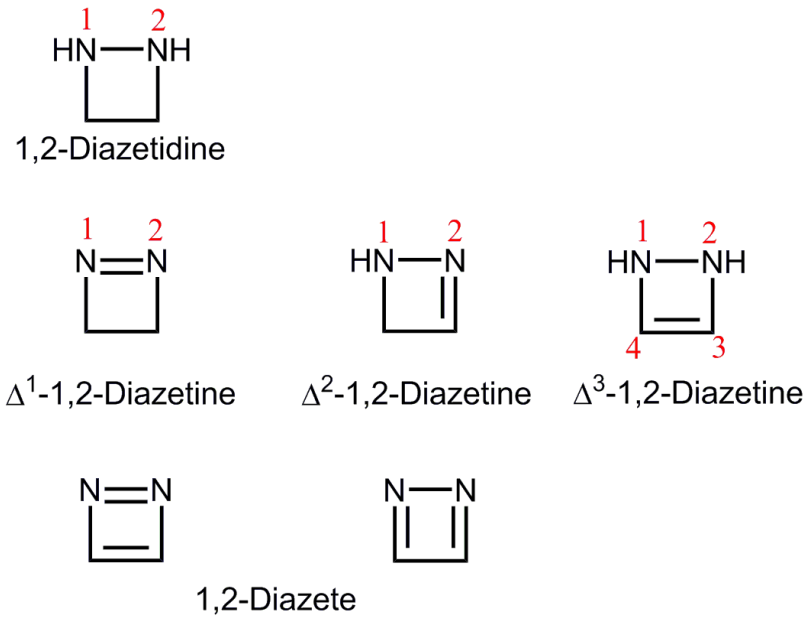

Figure 1.3 1,2-Diazetidines, diazetines and diazetes.

The first example of a 1,2-diazetidine was synthesized by Herman Staudinger from diphenylketene and *trans*-azobenzene using a [2+2] ketene cycloaddition.[82–85] There are many derivatives of 1,2-diazetidines known to date, and their synthesis, properties, and chemistry are well known.[81]

Some of the selected synthetic strategies for 1,2-diazetidines are summarized in Scheme 1.4. One of the common strategies that to synthesize 1,2-diazetidines is the formal [2+2] cycloaddition of cyclic or acyclic azodicarboxylates (*e.g.* **II-28**) with substrates bearing an olefin functionality such as tetrafluroethylene,[86] indene,[87] vinyl ethers,[88] tetracyclopropylethylene,[89] and allenamide[90] (Scheme 1.4, Eq. 1). However this approach is limited by the high substrate dependency of these reactions and moderate yields. Alternatively, Diels-Alder reactions of cyclobutadiene (*e.g.* **II-29**) with various azo compounds[91,92], and 4π–photocyclization of a 1,2-dihydropyridazine (*e.g.* **II-30**)[93,94] have been reported to obtain bicycle 1,2-diazetidines (Scheme 1.4, Eq. 2). However, some of the drawbacks associated with these methods such as impracticality on larger scale, the requirement for a cyclobutadiene precursor (*e.g.* the corresponding iron tricarbonyl complex) which are not commercially available, poor atom economy, and expensive preparation of precursors narrowed the broad applicability of these methods.

Further, Hall and Brigard showed that 1,2-dialkyl-1,2-diazetidines can be prepared from a direct reaction of 1,2-dibromoethane (**II-31**) and 1,2-dialkylhydrazines (**II-32**) in hot xylene in the presence of a base such as sodium carbonate (Scheme 1.4, Eq.

3).[95] Later Miao*et al.* reported a one-pot synthesis of substituted 1,2-diazetidines from readily available aldehydes. They first transformed the aldehyde (**II-33**) into a corresponding dialkyl 1-(1-hydroxy-3-phenylpropan-2-yl)-hydrazine-1,2-dicarboxylate such as **II-34** by reacting with a protected azodicarboxylate (**II-28**) in the presence of catalytic proline. Next, the hydroxyl group of **II-34** was activated to a better leaving group such as a mesylate, which could then be displaced with a nitrogen nucleophile within the **II-34** via intramolecular cyclization to form the substituted 1,2-diazetidines (**II-35)** (Scheme 1.4, Eq. 4).[96]

In addition, the Shipman group developed a protocol to access a wide range of 1,2-diazetidines such as **II-37** by applying a Cu(I)-catalyzed 4-exo ring closure from a previously synthesized cyclization precursor such as **II-36** (Scheme 1.4, Eq. 5).[97] Later, this method was further modified to obtain enantioenriched C-3 substituted 1,2-diazetidines and 1,2-diamines.[98,99] Regardless of the efficiency, these methods also have their own downsides such as multistep synthesis, use of additives, and the formation of less substituted 1,2-diazetidine derivatives. Overall, despite the fact that the synthesis of 1,2-diazetidines are rather well developed, still there are more opportunities for synthetic chemists to expand and develop new synthetic protocols to access a broader scope of these compounds with lack of drawbacks which mentioned above.

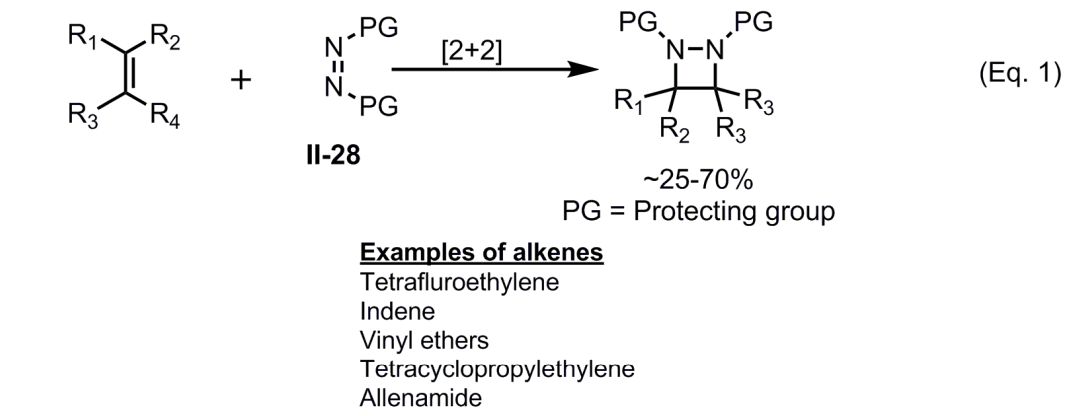

(Eq. 1)

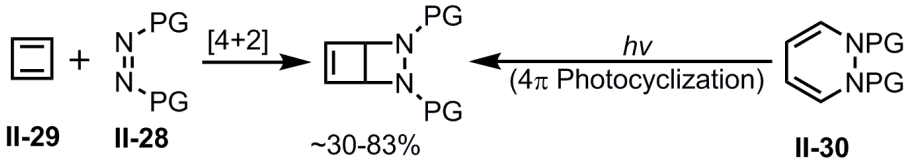

(Eq. 2)

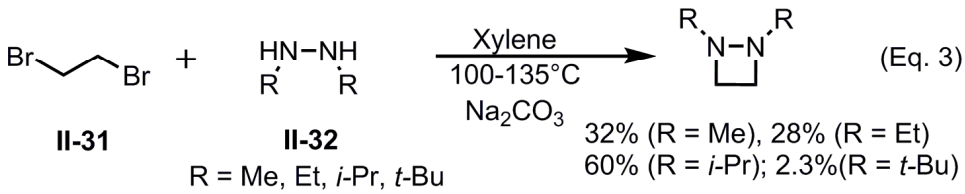

(Eq. 3)

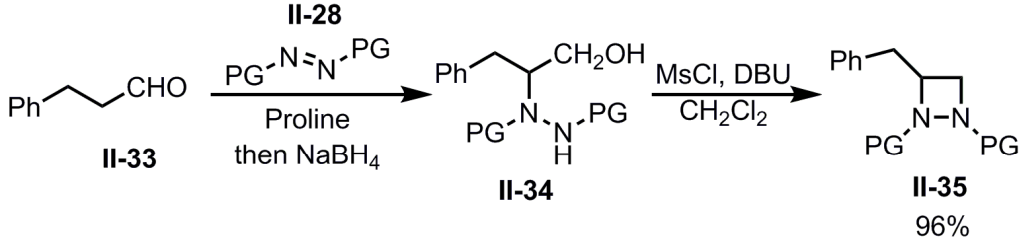

(Eq. 4)

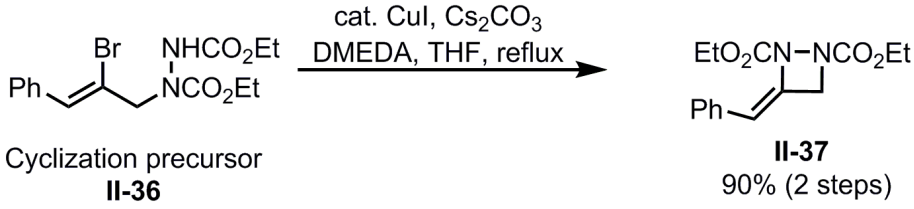

(Eq. 5)

Scheme 1.4 Selected examples for the synthesis of 1,2-diazetidines.

The first diazetine derivative (**II-39**) was synthesized in 1962 by Emeleus and Hurst from the fluorination of cyanogens (**II-38**) (Scheme 1.5, Eq. 1).[100,101] A few attempts were made to synthesize Δ^1-1,2-diazetine-1,2-dioxides (**II-41**) by oxidizing the corresponding 1,2-*bis*-hydroxylamines (**II-40**) or 1,2-diamine with an oxidant such as bromine, dimethyldioxirane (DMDO), or sodium hypobromite (Scheme 1.5, eq. 2).[102–106] This oxidation method provided very low to moderate yields when the hydroxylamino group or amino groups of the substrates are at tertiary carbon atoms and phenyl substituted secondary carbon atoms. In contrast, the substrates bearing tertiary carbon atoms with less sterically hindered shorter alkyl groups such as methyl and secondary carbon atoms in cyclic analogs provided very high yields. Δ^1-1,2-diazetine-1,2-dioxides were found to be highly effective low-energy triplet quenchers due to their ability to absorb short wavelengths of light, and the absence of both singlet quenching and triplet reactivity.[102,106]

Furthermore, these Δ^1-1,2-diazetine-1,2-dioxides were investigated as vasodilators due to their ability to liberate two molecules of NO upon moderate heating.[106–108] These studies show that Δ^1-1,2-diazetine-1,2-dioxides can be identified as a new class of effective vasorelaxant agents which will be a good substituent for some of the currently used vasorelaxants, such as nitroglycerin, due to the side effects associated with nitroglycerin.[107]

Alternatively, Breton and co-workers applied a Diels-Alder approach to afford the corresponding Δ^1-1,2-diazetine in high synthetic yields.[109,110] This method utilizes a less substituted Δ^3-1,2-diazetine analog such as **II-43** as a dienophile to react with a diene **II-42** to afford a Diels-Alder cycloadduct **II-44**, followed by hydrolysis and oxidation of **II-44** to furnish the final Δ^1-1,2-diazetine derivative **II-45** (Scheme 1.5, eq. 3). However, this method was also limited by the poor yield of the Δ^3-1,2-diazetine analog which is used as the dienophile.

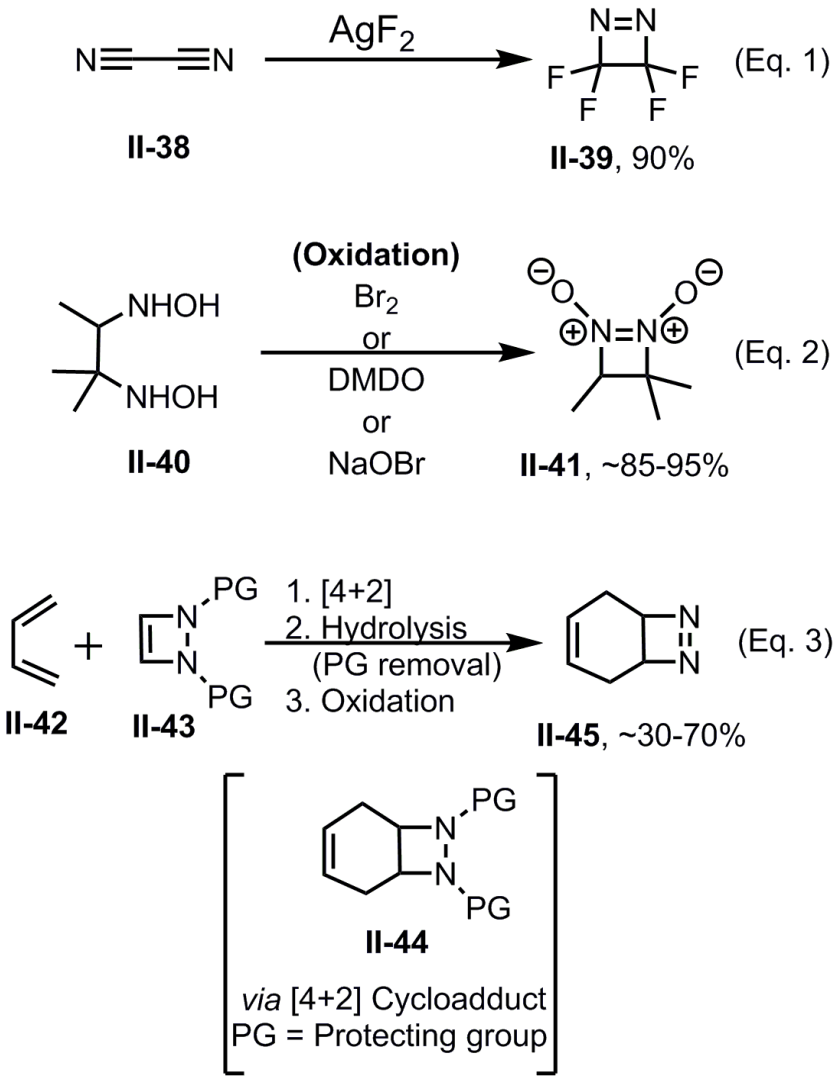

Scheme 1.5 Selected examples for the synthesis of Δ^1-1,2-diazetines.

Examples of the Δ^2-1,2-diazetine structural architecture also appeared in the literature since the 1980s. Sharp and co-workers showed that bicyclic Δ^2-1,2-diazetines (**II-47**) can be formed through the rapid photoisomerization of the corresponding 1,2-diazepine (**II-46**) in quantitative yields (Scheme 1.6, Eq.1).[111–114] In 1984, the Taylor group accidentally found that pivaloylation of 1,2-diazetidine-3-ones bearing a bulky group at N1 (**II-48**) can produce the corresponding Δ^2-1,2-diazetine(**II-49**) in moderate to good yields (Scheme 1.6, Eq. 2).[115] Beckert and co-workers developed an efficient procedure to access the Δ^2-1,2-diazetine motif (**II-52**) by reacting an amidrazone such as **II-50** with thebis(imidoyl) chlorides of oxalic acid such as **II-51**while eliminating benzonitrile (Scheme 1.6, Eq. 3).[116,117] They further illustrated that this synthesis can also be performed by the cycloacylation reaction of monoalkylhydrazines (**II-53**) instead of using amidrazones.[117] However, in some cases these Δ^2-1,2-diazetines were found to be light sensitive and degrade to fluorubine byproducts which exhibit fluorescence.[117] Beckert and co-workers further modified this protocol to produce pyridazines and biologically relevant 1,3,4-oxadizines by ring expansion reactions.[118,119]

Some other transformations were also developed for the synthesis of Δ^2-1,2-diazetines by using the reaction between nitrilimines and isocyanides, nitrosation of aziridines and irradiation of pyridazines. Nevertheless, these strategies are highly substrate dependent and the products generated in these transformations are heat sensitive, tending to form byproducts through cycloreversion, ring expansion, and fragmentation.[116]

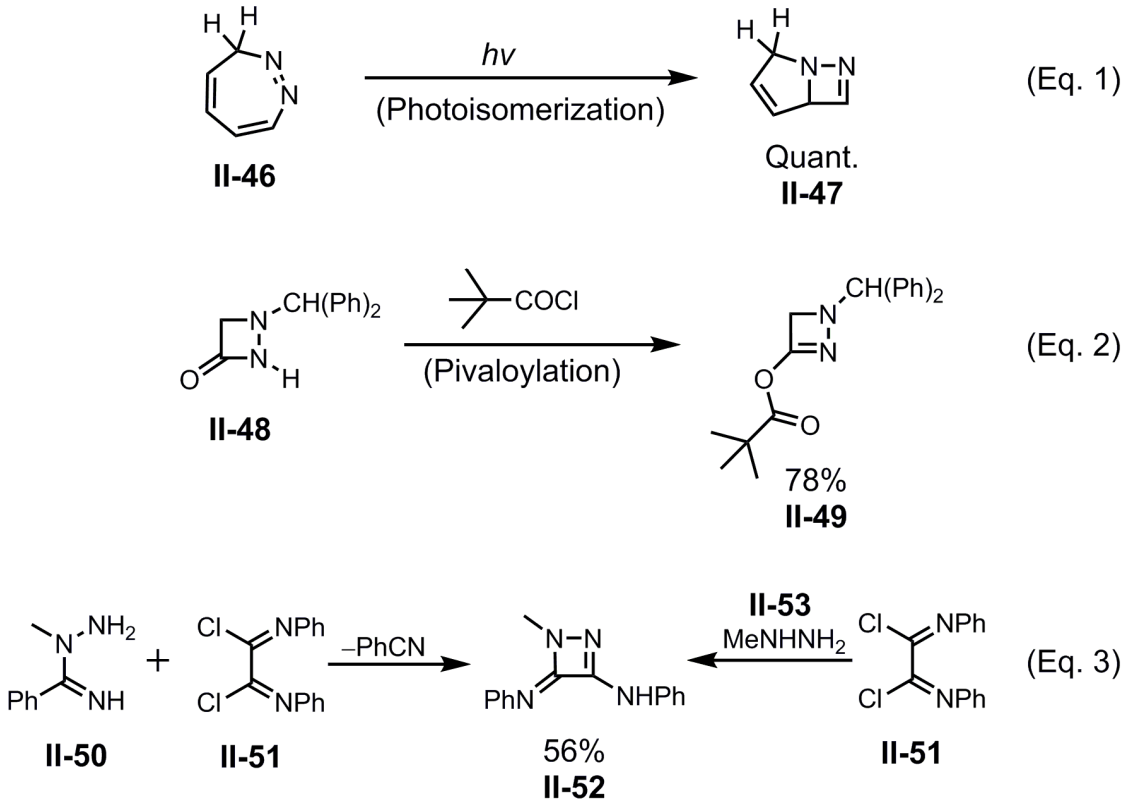

Scheme 1.6 Selected examples for the synthesis of Δ^2-1,2-diazetines.

When compared with the Δ^1-1,2-diazetines and Δ^2-1,2-diazetines less attention has been paid to the diazacyclobutenes (Δ^3-1,2-diazetines) and just a few synthetic protocols are available for the synthesis of diazacyclobutenes so far.[92,101,109,120–123]

Diazacyclobutenes are also fairly strained four membered rings consisting of a carbon-carbon double bond and two adjacent nitrogen atoms. These heterocycles have gained some attention in the literature owing to the electronic framework resident in the diazetine moiety that formally follows the Hückel (4n+2) rule of aromaticity.[81,92,123,124] There has been some debate in the literature about the possible aromaticity of diazacyclobutenes, but a thorough investigation has been difficult due to relatively limited access to these molecules.[92,123,124] Those diazacyclobutenes that are isolable and stable have proven to be synthetically useful as dienophiles in Diels-Alder cycloadditions and precursors to Δ^1-1,2-diazetine derivatives which was illustrated previously (Scheme 1.5, Eq. 3).[109]

The first diazacyclobutene (Δ^3-1,2-diazetine) derivative (**II-56**) was reported by Effenberger and Maier in 1966.[120] They reacted ketene-*N*,*N*-acetals (**II-54**) and azosulfone (**II-55**) to afford the corresponding diazacyclobutene derivative (Scheme 1.7, Eq. 1). Nevertheless, their characterization did not include spectroscopic information and did not prove the regiospecificity and the stability of the products. Even though it has been more than 50 years since this initial report on the synthesis of diazacyclobutenes, less than a dozen examples of the scaffold have been reported so far in the literature due

to a general lack of synthetic routes to access the diazacyclobutene moiety in high yield.[92,109,120,121]

Warrener and Nunn reported dimethyl Δ^3-1,2-diazetine-1,2-dicarboxylate **II-57** in 1972, which was synthesized in very poor yield (5% in 3 steps). It was found to be thermally unstable at room temperature and cycloreversed to make a stable diimine derivative **II-58** (Scheme 1.7, Eq. 2).[92,122] In 1984, Greene synthesized diazacyclobutene **II-60** in 21-26% yield by reacting 4-phenyl-1,2,4-triazole-3,5-dione (PTAD) with a hindered acetylene **II-59** in dichloromethane for 4-5 days. They observed that the reaction proceeded to make 1:1 and 1:2 (Acetylene: PTAD) adducts (Scheme 1.7, eq. 3).[121]

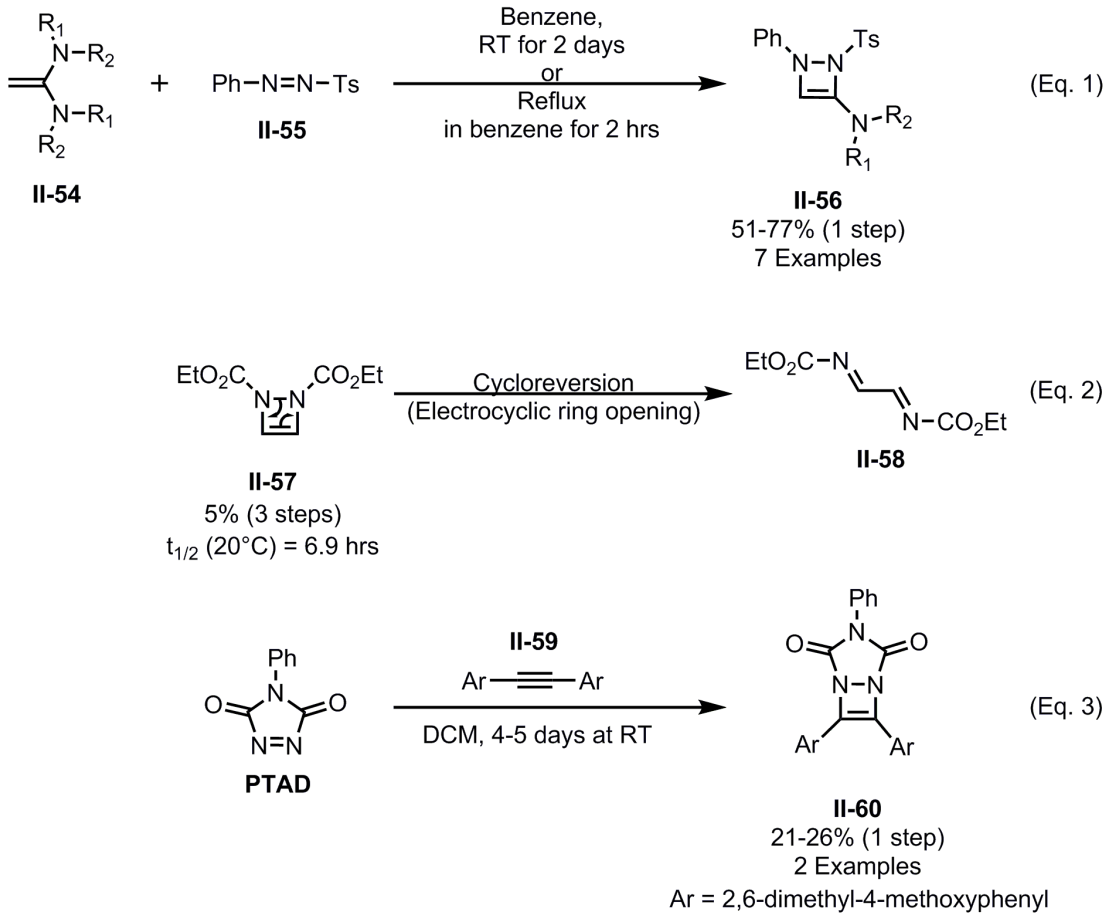

Scheme 1.7 Synthesis of diazacyclobutenes (Δ^3-1,2-diazetines).

Breton and coworkers developed a method to produce the diazacyclobutene moiety in 3 steps by reacting vinyl sulfide (**II-62**) and *N*-methyltriazolinedione (**II-61,** MTAD) to yield a [2+2] adduct (**II-63**) followed by an oxidation with *m*-CPBA and solution-phase pyrolysis to yield the desired diazacyclobutene derivative (**II-65**) (Scheme 1.8).[109] The overall yield of the sequence was about 8-10% which was attributed to the formation of a polymeric byproduct that competes with the desired cycloaddition reaction.[88]

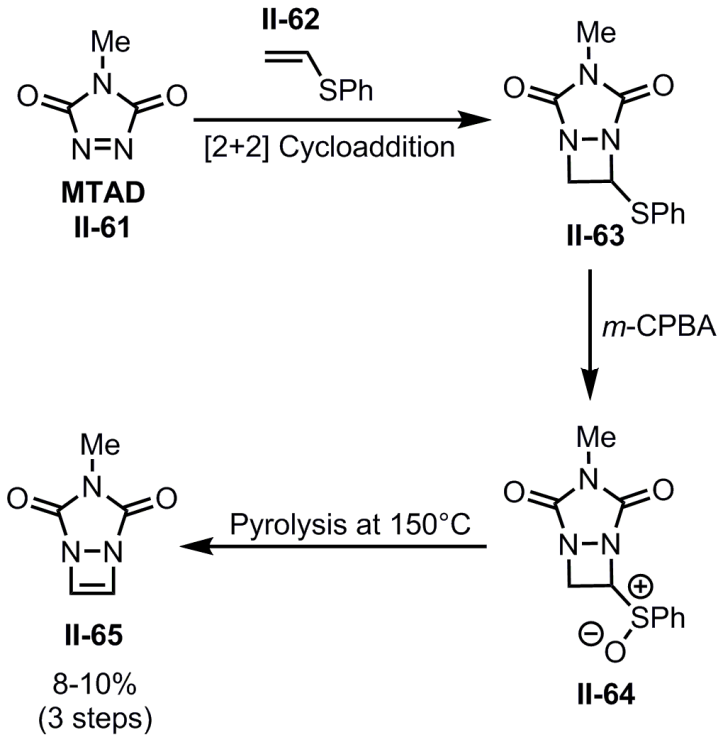

Scheme 1.8 Diazacyclobutene synthesis with vinyl sulfide and N-methyltriazolinedione (MTAD)

Tandon and Chhor were able to prepare 1,2-diazete (**II-67**) in moderate yields (56%) by refluxing 1,4-dichloro-1,4-disubstituted-2,3-diaza-1,3-butadiene (**II-66)** with Beryllium (Be) in dry THF.[125] The 1,2-diazetes are the cyclobutadiene analogues of these heterocycles and so far only one study has been carried out to access diazete heterocycles.[125]

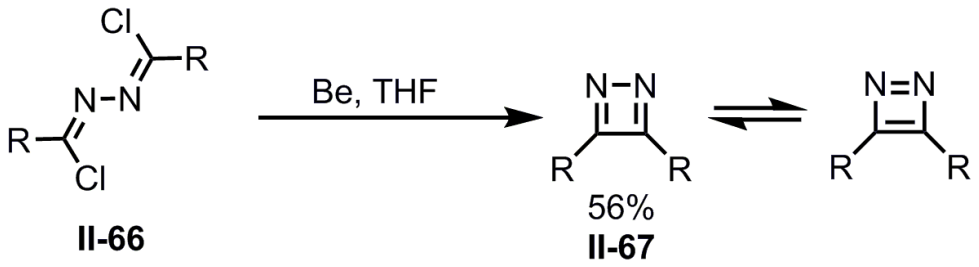

II-66 **II-67**

Scheme 1.9 Synthesis of 1,2-diazetes.

In addition to the above examples, enzyme mediated vicinal diamino motif synthesis has been also appeared in recent literature.[126,127] One of the remarkable example for this is; biocatalytic asymmetric C(sp^3)-H amination that has been developed by Arnold group (examples are not shown).[127] Despite the fact that this enzymatic methodology was able to provide diverse array of synthetically valuable chiral diamines in excellent enantioselectivity, the requirement of the nitrogen source which housed within the substrate (similar to the Scheme 1.2, Eq. 1) and the synthesis of the specialized precursors such as sulfomyl azide substrates in multiple steps are the major drawbacks in this transformation.

Due to the versatile use of 1,2-diamines and 1,2-diamino motif containing heterocycles in synthetic organic chemistry and medicinal chemistry, we wished to investigate more efficient protocols to access these types of compounds. Research studies for the synthesis of the 1,2-diamino-motif-containing 4, 5, and 6-membered *N*-heterocycles can still benefit from new, efficient synthetic strategies with higher reagent economy, higher atom economy, straight forward approaches, less substrate specificity, metal-free synthesis, and less additives.

Further, the studies on the chemical properties, biological activities and reactivities of some of the *vic*-diamino motif containing *N*-heterocycles – for instance diazacyclobutenes – are stymied by a lack of simple methods for their preparation. Some of these *N*-heterocycles are useful as precursors for further chemical transformations to

obtain biologically important compounds. These reasons have validated the need for the development of facile synthetic methods to prepare these compounds.

In the second chapter of this dissertation, we describe the design of an efficient formal [2+2] cycloaddition protocol to access the *vic*-diamino motif in the form of four-membered *N*-heterocycles known as Δ^3-1,2-diazetines or diazacyclobutenes from electron-rich alkynes and azodicarboxylates. Chapter 2 discusses the development of this chemistry and the optimization of the protocol, the initial substrate scope, investigation of their potential aromaticity, additional improvements of the substrate scope and biological activity of these diazacyclobutenes. Some of the content in this second chapter were adapted with permission from (Narangoda, C. J.; Lex, T. R.; Moore, M. A.; McMillen, C. D.; Kitaygorodskiy, A.; Jackson, J. E.; Whitehead, D. C. Accessing the Rare Diazacyclobutene Motif. *Org. Lett.* **2018**, *20* (24), 8009–8013. https://doi.org/10.1021/acs.orglett.8b03590), Copyright (2018) American Chemical Society.

Chapter 3 describes the further exploration of this chemistry in terms of substrate dependent reactivities such as comparing the reactivity of acyclic vs cyclic azodicarboxylates, ene reaction competition with the initially developed formal [2+2] cycloaddition protocol, and anomalous behavior in the presence of catalysts. This chapter introduces novel protocols for the synthesis of 5-membered *N*-heterocycles known as tetrahydroindoles and a 6-membered *N*-heterocycle known as 1,3,4-oxadiazin-2-ones by

utilizing the electron-rich alkyne and azodicarboxylate chemistry. Some of the content in this third chapter were adapted with permission from (Narangoda, C. J.; Kakeshpour, T.; Lex, T. R.; Redden, B. K.; Moore, M. A.; Frank, E. M.; McMillen, C. D.; Wiskur, S. L.; Kitaygorodskiy, A.; Jackson, J. E.; Whitehead, D. C. Cycloaddition/Electrocyclic Ring Opening Sequence between Alkynyl Sulfides and Azodicarboxylates To Provide N,N-Dicarbamoyl 2-Iminothioimidates. *J. Org. Chem.* **2019**, *84* (15), 9734–9743. https://doi.org/10.1021/acs.joc.9b01515), Copyright (2019) American Chemical Society.

Chapter Four describes the use of polyethyleneimine (PEI) functionalized cellulose nanocrystals (CNC) in the use of environmental remediation. This chapter discusses the synthesis of CNC, optimization of the functionalization reaction of CNC with PEI, environmental remediation studies of PEI functionalized CNC and further modifications of the functionalization protocol with halogenation reactions for the synthesis of antimicrobial agents.

1.3 References

(1) Vitaku, E.; Smith, D. T.; Njardarson, J. T. Analysis of the Structural Diversity, Substitution Patterns, and Frequency of Nitrogen Heterocycles among U.S. FDA Approved Pharmaceuticals. *J. Med. Chem.* **2014**, *57* (24), 10257–10274. https://doi.org/10.1021/jm501100b.

(2) G. de la Torre, B.; Albericio, F. The Pharmaceutical Industry in 2018. An Analysis of FDA Drug Approvals from the Perspective of Molecules. *Molecules* **2019**, *24* (4), 809. https://doi.org/10.3390/molecules24040809.

(3) de la Torre, B. G.; Albericio, F. The Pharmaceutical Industry in 2019. An Analysis of FDA Drug Approvals from the Perspective of Molecules. *Molecules* **2020**, *25* (3), 745. https://doi.org/10.3390/molecules25030745.

(4) Das, P.; Delost, M. D.; Qureshi, M. H.; Smith, D. T.; Njardarson, J. T. A Survey of the Structures of US FDA Approved Combination Drugs. *J. Med. Chem.* **2019**, *62* (9), 4265–4311. https://doi.org/10.1021/acs.jmedchem.8b01610.

(5) Research, C. for D. E. and. Novel Drug Approvals for 2019. *FDA* **2020**.

(6) Pennington, L. D.; Moustakas, D. T. The Necessary Nitrogen Atom: A Versatile High-Impact Design Element for Multiparameter Optimization. *J. Med. Chem.* **2017**, *60* (9), 3552–3579. https://doi.org/10.1021/acs.jmedchem.6b01807.

(7) Verheij, M. H. P.; Thompson, A. J.; van Muijlwijk-Koezen, J. E.; Lummis, S. C. R.; Leurs, R.; de Esch, I. J. P. Design, Synthesis, and Structure–Activity Relationships of Highly Potent 5-HT3 Receptor Ligands. *J. Med. Chem.* **2012**, *55* (20), 8603–8614. https://doi.org/10.1021/jm300801u.

(8) Borrmann, T.; Abdelrahman, A.; Volpini, R.; Lambertucci, C.; Alksnis, E.; Gorzalka, S.; Knospe, M.; Schiedel, A. C.; Cristalli, G.; Müller, C. E. Structure−Activity Relationships of Adenine and Deazaadenine Derivatives as Ligands for Adenine Receptors, a New Purinergic Receptor Family. *J. Med. Chem.* **2009**, *52* (19), 5974–5989. https://doi.org/10.1021/jm9006356.

(9) Henry, J. R.; Kaufman, M. D.; Peng, S.-B.; Ahn, Y. M.; Caldwell, T. M.; Vogeti, L.; Telikepalli, H.; Lu, W.-P.; Hood, M. M.; Rutkoski, T. J.; Smith, B. D.; Vogeti, S.; Miller, D.; Wise, S. C.; Chun, L.; Zhang, X.; Zhang, Y.; Kays, L.; Hipskind, P. A.; Wrobleski, A. D.; Lobb, K. L.; Clay, J. M.; Cohen, J. D.; Walgren, J. L.; McCann, D.; Patel, P.; Clawson, D. K.; Guo, S.; Manglicmot, D.; Groshong, C.; Logan, C.; Starling, J. J.; Flynn, D. L. Discovery of 1-(3,3-Dimethylbutyl)-3-(2-Fluoro-4-Methyl-5-(7-Methyl-2-(Methylamino)Pyrido[2,3- *d*]Pyrimidin-6-Yl)Phenyl)Urea (LY3009120) as a Pan-RAF Inhibitor with Minimal Paradoxical Activation and Activity against *BRAF* or *RAS* Mutant Tumor Cells. *J. Med. Chem.* **2015**, *58* (10), 4165–4179. https://doi.org/10.1021/acs.jmedchem.5b00067.

(10) Cardona, F.; Goti, A. Metal-Catalysed 1,2-Diamination Reactions. *Nature Chem* **2009**, *1* (4), 269–275. https://doi.org/10.1038/nchem.256.

(11) Albertini, B.; Passerini, N.; Di Sabatino, M.; Vitali, B.; Brigidi, P.; Rodriguez, L. Polymer–Lipid Based Mucoadhesive Microspheres Prepared by Spray-Congealing for the Vaginal Delivery of Econazole Nitrate. *European Journal of Pharmaceutical Sciences* **2009**, *36* (4–5), 591–601. https://doi.org/10.1016/j.ejps.2008.12.009.

(12) Godefroi, E. F.; Heeres, J.; Van Cutsem, J.; Janssen, P. A. J. Preparation and Antimycotic Properties of Derivatives of 1-Phenethylimidazole. *J. Med. Chem.* **1969**, *12* (5), 784–791. https://doi.org/10.1021/jm00305a014.

(13) Carrieo-mufioz, A. J.; Torres-rodriguez, J. M. *In-Vitro Antifungal Activity of Sertaconazole, Econazole, and Bifonazole against Candida Spp.*

(14) Ding, S.; Jia, G.; Sun, J. Iridium-Catalyzed Intermolecular Azide–Alkyne Cycloaddition of Internal Thioalkynes under Mild Conditions. *Angewandte Chemie International Edition* **2014**, *53* (7), 1877–1880. https://doi.org/10.1002/anie.201309855.

(15) Seki, J.; Shimada, N.; Takahashi, K.; Takita, T.; Takeuchi, T.; Hoshino, H. Inhibition of Infectivity of Human Immunodeficiency Virus by a Novel Nucleoside, Oxetanocin, and Related Compounds. *Antimicrob Agents Chemother* **1989**, *33* (5), 773–775.

(16) Khan, K. M.; Rahat, S.; Choudhary, M. I.; Atta-ur-Rahman; Ghani, U.; Perveen, S.; Khatoon, S.; Dar, A.; Malik, A. Synthesis and Biological Screening of 2-Substituted 5,6-Dihydro-5-Oxo- 4H-1,3,4-Oxadiazine-4-Propanenitriles and of Their Intermediates. *Helvetica Chimica Acta* **2002**, *85* (2), 559–570. https://doi.org/10.1002/1522-2675(200202)85:2<559::AID-HLCA559>3.0.CO;2-A.

(17) Ke, S.; Cao, X.; Liang, Y.; Wang, K.; Yang, Z. Synthesis and Biological Properties of Dihydro-Oxadiazine-Based Heterocyclic Derivatives http://www.ingentaconnect.com/content/ben/mrmc/2011/00000011/00000008/art00002 (accessed Mar 20, 2020). https://doi.org/info:doi/10.2174/138955711796268769.

(18) Han, J.; Xu, B.; Hammond, G. B. Highly Efficient Cu(I)-Catalyzed Synthesis of *N* -Heterocycles through a Cyclization-Triggered Addition of Alkynes. *J. Am. Chem. Soc.* **2010**, *132* (3), 916–917. https://doi.org/10.1021/ja908883n.

(19) Dong, H.; Shen, M.; Redford, J. E.; Stokes, B. J.; Pumphrey, A. L.; Driver, T. G. Transition Metal-Catalyzed Synthesis of Pyrroles from Dienyl Azides. *Org. Lett.* **2007**, *9* (25), 5191–5194. https://doi.org/10.1021/ol702262f.

(20) Zeni, G.; Larock, R. C. Synthesis of Heterocycles via Palladium-Catalyzed Oxidative Addition. *Chem. Rev.* **2006**, *106* (11), 4644–4680. https://doi.org/10.1021/cr0683966.

(21) Kaur, N. Palladium Catalysts: Synthesis of Five-Membered *N* -Heterocycles Fused with Other Heterocycles. *Catalysis Reviews* **2015**, *57* (1), 1–78. https://doi.org/10.1080/01614940.2014.976118.

(22) Mao, J.; Wang, Z.; Xu, X.; Liu, G.; Jiang, R.; Guan, H.; Zheng, Z.; Walsh, P. J. Synthesis of Indoles through Domino Reactions of 2-Fluorotoluenes and Nitriles. *Angewandte Chemie International Edition* **2019**, *58* (32), 11033–11038. https://doi.org/10.1002/anie.201904658.

(23) Lucet, D.; Gall, T. L.; Mioskowski, C. The Chemistry of Vicinal Diamines. *Angewandte Chemie International Edition* **1998**, *37* (19), 2580–2627. https://doi.org/10.1002/(SICI)1521-3773(19981016)37:19<2580::AID-ANIE2580>3.0.CO;2-L.

(24) Kotti, S. R. S. S.; Timmons, C.; Li, G. Vicinal Diamino Functionalities as Privileged Structural Elements in Biologically Active Compounds and Exploitation of Their Synthetic Chemistry. *Chemical Biology & Drug Design* **2006**, *67* (2), 101–114. https://doi.org/10.1111/j.1747-0285.2006.00347.x.

(25) Rosenberg, B.; Vancamp, L.; Trosko, J. E.; Mansour, V. H. Platinum Compounds: A New Class of Potent Antitumour Agents. *Nature* **1969**, *222* (5191), 385–386. https://doi.org/10.1038/222385a0.

(26) PINI, D.; IULIANO, A.; ROSINI, C.; SALVADORI, P. An Efficient and Practical Route to Enantiomerically Pure ( )-(1R,2R)- and (-)-(1S,2S)-1,2-Diphenylethane-1,2-Diamines. *Synthesis (Stuttg.)* **1990**, No. 11, 1023–1024.

(27) Kim, H.; So, S. M.; Chin, J.; Kim, B. M. Preparation of Chiral Diamines by the Diaza-Cope Rearrangement (DCR). *ALDRICHIMICA ACTA* **2008**, *41* (3), 77–88.

(28) de Jong, S.; Nosal, D. G.; Wardrop, D. J. Methods for Direct Alkene Diamination, New & Old. *Tetrahedron* **2012**, *68* (22), 4067–4105. https://doi.org/10.1016/j.tet.2012.03.036.

(29) Kolb, H. C.; VanNieuwenhze, M. S.; Sharpless, K. B. Catalytic Asymmetric Dihydroxylation. *Chem. Rev.* **1994**, *94* (8), 2483–2547. https://doi.org/10.1021/cr00032a009.

(30) O'Brien, P. Sharpless Asymmetric Aminohydroxylation: Scope, Limitations, and Use in Synthesis. *Angewandte Chemie International Edition* **1999**, *38* (3), 326–329. https://doi.org/10.1002/(SICI)1521-3773(19990201)38:3<326::AID-ANIE326>3.0.CO;2-T.

(31) Katsuki, T. Chiral Metallosalen Complexes: Structures and Catalyst Tuning for Asymmetric Epoxidation and Cyclopropanation. *Advanced Synthesis & Catalysis* **2002**, *344* (2), 131–147. https://doi.org/10.1002/1615-4169(200202)344:2<131::AID-ADSC131>3.0.CO;2-T.

(32) Wong, O. A.; Shi, Y. Organocatalytic Oxidation. Asymmetric Epoxidation of Olefins Catalyzed by Chiral Ketones and Iminium Salts. *Chem. Rev.* **2008**, *108* (9), 3958–3987. https://doi.org/10.1021/cr068367v.

(33) Pfenninger, A. Asymmetric Epoxidation of Allylic Alcohols: The Sharpless Epoxidation. *Synthesis* **1986**, *1986* (02), 89–116. https://doi.org/10.1055/s-1986-31489.

(34) Muñiz, K.; Martínez, C. Development of Intramolecular Vicinal Diamination of Alkenes: From Palladium to Bromine Catalysis. *J. Org. Chem.* **2013**, *78* (6), 2168–2174. https://doi.org/10.1021/jo302472w.

(35) Muñiz, K.; Hövelmann, C. H.; Campos-Gómez, E.; Barluenga, J.; González, J. M.; Streuff, J.; Nieger, M. Intramolecular Diamination of Alkenes with Palladium(II)/Copper(II) Bromide and IPy2BF4: The Role of Halogenated Intermediates. *Chemistry – An Asian Journal* **2008**, *3* (4), 776–788. https://doi.org/10.1002/asia.200700373.

(36) Fu, N.; Sauer, G. S.; Saha, A.; Loo, A.; Lin, S. Metal-Catalyzed Electrochemical Diazidation of Alkenes. *Science* **2017**, *357* (6351), 575–579. https://doi.org/10.1126/science.aan6206.

(37) Muñiz, K. Metal-Free Catalytic Vicinal Diamination of Alkenes. *Pure Appl. Chem.* **2013**, *85* (4), 755–761. https://doi.org/10.1351/PAC-CON-12-10-23.

(38) Chávez, P.; Kirsch, J.; Hövelmann, C. H.; Streuff, J.; Martínez-Belmonte, M.; Escudero-Adán, E. C.; Martin, E.; Muñiz, K. Metal-Free Diamination of Alkenes Employing Bromide Catalysis. *Chem. Sci.* **2012**, *3* (7), 2375–2382. https://doi.org/10.1039/C2SC20242E.

(39) Mizar, P.; Laverny, A.; El-Sherbini, M.; Farid, U.; Brown, M.; Malmedy, F.; Wirth, T. Enantioselective Diamination with Novel Chiral Hypervalent Iodine Catalysts. *Chemistry – A European Journal* **2014**, *20* (32), 9910–9913. https://doi.org/10.1002/chem.201403891.

(40) Yang, Q.; Li, Y.; Dou, D.; Gan, X.; Mohan, S.; Groutas, C. S.; Stevenson, L. E.; Lai, Z.; Alliston, K. R.; Zhong, J.; Williams, T. D.; Groutas, W. C. Inhibition of Serine Proteases by a New Class of Cyclosulfamide-Based Carbamylating Agents. *Archives of Biochemistry and Biophysics* **2008**, *475* (2), 115–120. https://doi.org/10.1016/j.abb.2008.04.020.

(41) Giannotti, D.; Viti, G.; Sbraci, P.; Pestellini, V.; Volterra, G.; Borsini, F.; Lecci, A.; Meli, A.; Dapporto, P.; Paoli, P. New Dibenzothiadiazepine Derivatives with Antidepressant Activities. *J. Med. Chem.* **1991**, *34* (4), 1356–1362. https://doi.org/10.1021/jm00108a018.

(42) Fouzia, B.; Sihem, H.; Hadjer, C.; Malika, B.; Becheker, I.; Nour-Eddine, A. Efficient Synthesis and Antibacterial Activity of Novel Cyclic Sulfamides. *Rasayan Journal of Chemistry* **2013**, *6*, 175.

(43) Giannotti, D.; Viti, G.; Nannicini, R.; Pestellini, V.; Bellarosa, D. Synthesis and Anti HIV-1 Activity of New Thiadiazepindioxides. *Bioorganic & Medicinal Chemistry Letters* **1995**, *5* (14), 1461–1466. https://doi.org/10.1016/0960-894X(95)00257-T.

(44) Dou, D.; Mandadapu, S. R.; Alliston, K. R.; Kim, Y.; Chang, K.-O.; Groutas, W. C. Cyclosulfamide-Based Derivatives as Inhibitors of Noroviruses. *European Journal of Medicinal Chemistry* **2012**, *47*, 59–64. https://doi.org/10.1016/j.ejmech.2011.10.019.

(45) Souto, J. A.; González, Y.; Iglesias, A.; Zian, D.; Lishchynskyi, A.; Muñiz, K. Iodine(III)-Promoted Intermolecular Diamination of Alkenes. *Chemistry – An Asian Journal* **2012**, *7* (5), 1103–1111. https://doi.org/10.1002/asia.201101025.

(46) Röben, C.; Souto, J. A.; Escudero-Adán, E. C.; Muñiz, K. Oxidative Diamination Promoted by Dinuclear Iodine(III) Reagents. *Org. Lett.* **2013**, *15* (5), 1008–1011. https://doi.org/10.1021/ol3034884.

(47) Lishchynskyi, A.; Muñiz, K. An Approach to the Regioselective Diamination of Conjugated Di- and Trienes. *Chemistry – A European Journal* **2012**, *18* (8), 2212–2216. https://doi.org/10.1002/chem.201103435.
(48) Zhang, J.; Zhang, G.; Wu, W.; Zhang, X.; Shi, M. Metal-Free Aminoamidiniumation Employing N-Iodosuccinimide: Facile Syntheses of Bicyclic Imidazolidiniums and Cyclic Vicinal Diamines. *Chem. Commun.* **2014**, *50* (95), 15052–15054. https://doi.org/10.1039/C4CC07082H.
(49) Zhang, J.; Zhang, X.; Wu, W.; Zhang, G.; Xu, S.; Shi, M. Intramolecular Aminochalcogenation and Diamination of Alkenes Employing N-Iodosuccinimide. *Tetrahedron Letters* **2015**, *56* (12), 1505–1509. https://doi.org/10.1016/j.tetlet.2015.01.154.
(50) Li, H.; Widenhoefer, R. A. Intramolecular Diamination and Alkoxyamination of Alkenes with N-Sulfonyl Ureas With N-Iodosuccinimide. *Tetrahedron* **2010**, *66* (26), 4827–4831. https://doi.org/10.1016/j.tet.2010.03.082.
(51) Müller, C. H.; Fröhlich, R.; Daniliuc, C. G.; Hennecke, U. Efficient Synthesis of Chiral 2,2′-Bipyrrolidines by an Anti-Selective Alkene Diamination. *Org. Lett.* **2012**, *14* (23), 5944–5947. https://doi.org/10.1021/ol302855z.
(52) Chen, H.; Kaga, A.; Chiba, S. Diastereoselective Aminooxygenation and Diamination of Alkenes with Amidines by Hypervalent Iodine(III) Reagents. *Org. Lett.* **2014**, *16* (23), 6136–6139. https://doi.org/10.1021/ol503000c.
(53) Kong, A.; Blakey, S. B. Intramolecular Olefin Diamination for the Stereoselective Synthesis of 3-Aminopiperidines. *Synthesis* **2012**, *44* (8), 1190–1198. https://doi.org/10.1055/s-0031-1290591.
(54) Kim, H. J.; Cho, S. H.; Chang, S. Intramolecular Oxidative Diamination and Aminohydroxylation of Olefins under Metal-Free Conditions. *Org. Lett.* **2012**, *14* (6), 1424–1427. https://doi.org/10.1021/ol300166q.
(55) Wu, H.; Ji, X.; Sun, H.; An, G.; Han, J.; Li, G.; Pan, Y. Organocatalyzed Regio- and Stereoselective Diamination of Functionalized Alkenes. *Tetrahedron* **2010**, *66* (25), 4555–4559. https://doi.org/10.1016/j.tet.2010.04.054.
(56) Tabor, J. R.; Obenschain, D. C.; Michael, F. E. Selenophosphoramide-Catalyzed Diamination and Oxyamination of Alkenes. *Chem. Sci.* **2020**, *11* (6), 1677–1682. https://doi.org/10.1039/C9SC05335B.
(57) Jat, Dr. R.; Vihar, G. REVIEW OF IMIDAZOLE HETEROCYCLIC RING CONTAINING COMPOUNDS WITH THEIR BIOLOGICAL ACTIVITY. October 10, 2010.
(58) Fox, S. W. Chemistry of the Biologically Important Imidazoles. *Chem. Rev.* **1943**, *32* (1), 47–71. https://doi.org/10.1021/cr60101a002.
(59) Ferm, R. J.; Riebsomer, J. L. The Chemistry of the 2-Imidazolines and Imidazolidines. *Chem. Rev.* **1954**, *54* (4), 593–613. https://doi.org/10.1021/cr60170a002.
(60) Krasavin, M. Biologically Active Compounds Based on the Privileged 2-Imidazoline Scaffold: The World beyond Adrenergic/Imidazoline Receptor Modulators. *European Journal of Medicinal Chemistry* **2015**, *97*, 525–537. https://doi.org/10.1016/j.ejmech.2014.11.028.

(61) Katritzky, A. R.; Suzuki, K.; He, H.-Y. Convenient Syntheses of Unsymmetrical Imidazolidines. *J. Org. Chem.* **2002**, *67* (9), 3109–3114. https://doi.org/10.1021/jo010868n.
(62) Liu, H.; Du, D.-M. Recent Advances in the Synthesis of 2-Imidazolines and Their Applications in Homogeneous Catalysis. *Advanced Synthesis & Catalysis* **2009**, *351* (4), 489–519. https://doi.org/10.1002/adsc.200800797.
(63) Sharma, A. K. A Convenient Approach for the Synthesis of Imidazole Derivatives Using Microwaves. *Der Pharmacia Lettere* **2012**.
(64) Bon, R. S.; van Vliet, B.; Sprenkels, N. E.; Schmitz, R. F.; de Kanter, F. J. J.; Stevens, C. V.; Swart, M.; Bickelhaupt, F. M.; Groen, M. B.; Orru, R. V. A. Multicomponent Synthesis of 2-Imidazolines. *J. Org. Chem.* **2005**, *70* (9), 3542–3553. https://doi.org/10.1021/jo050132g.
(65) Gettys, K. E.; Ye, Z.; Dai, M. Recent Advances in Piperazine Synthesis. *Synthesis* **2017**, *49* (12), 2589–2604. https://doi.org/10.1055/s-0036-1589491.
(66) Mamedov, V. A.; Zhukova, N. A. Chapter 1 - Progress in Quinoxaline Synthesis (Part 2). In *Progress in Heterocyclic Chemistry*; Gribble, G. W., Joule, J. A., Eds.; Elsevier, 2013; Vol. 25, pp 1–45. https://doi.org/10.1016/B978-0-08-099406-2.00001-7.
(67) Antoniotti, S.; Duñach, E. Direct and Catalytic Synthesis of Quinoxaline Derivatives from Epoxides and Ene-1,2-Diamines. *Tetrahedron Letters* **2002**, *43* (22), 3971–3973. https://doi.org/10.1016/S0040-4039(02)00715-3.
(68) Bachhav, H. M.; Bhagat, S. B.; Telvekar, V. N. Efficient Protocol for the Synthesis of Quinoxaline, Benzoxazole and Benzimidazole Derivatives Using Glycerol as Green Solvent. *Tetrahedron Letters* **2011**, *52* (43), 5697–5701. https://doi.org/10.1016/j.tetlet.2011.08.105.
(69) Pereira, J. A.; Pessoa, A. M.; Cordeiro, M. N. D. S.; Fernandes, R.; Prudêncio, C.; Noronha, J. P.; Vieira, M. Quinoxaline, Its Derivatives and Applications: A State of the Art Review. *European Journal of Medicinal Chemistry* **2015**, *97*, 664–672. https://doi.org/10.1016/j.ejmech.2014.06.058.
(70) Wang, D.; Yu, H.; Sun, S.; Zhong, F. Intermolecular Vicinal Diaminative Assembly of Tetrahydroquinoxalines via Metal-Free Oxidative [4 + 2] Cycloaddition Strategy. *Org. Lett.* **2020**, *22* (6), 2425–2430. https://doi.org/10.1021/acs.orglett.0c00624.
(71) Law, R. P.; Atkinson, S. J.; Bamborough, P.; Chung, C.; Demont, E. H.; Gordon, L. J.; Lindon, M.; Prinjha, R. K.; Watson, A. J. B.; Hirst, D. J. Discovery of Tetrahydroquinoxalines as Bromodomain and Extra-Terminal Domain (BET) Inhibitors with Selectivity for the Second Bromodomain. *J. Med. Chem.* **2018**, *61* (10), 4317–4334. https://doi.org/10.1021/acs.jmedchem.7b01666.
(72) Millan, D. S.; Kayser-Bricker, K. J.; Martin, M. W.; Talbot, A. C.; Schiller, S. E. R.; Herbertz, T.; Williams, G. L.; Luke, G. P.; Hubbs, S.; Alvarez Morales, M. A.; Cardillo, D.; Troccolo, P.; Mendes, R. L.; McKinnon, C. Design and Optimization of Benzopiperazines as Potent Inhibitors of BET Bromodomains. *ACS Med. Chem. Lett.* **2017**, *8* (8), 847–852. https://doi.org/10.1021/acsmedchemlett.7b00191.

(73) Jacobsen, E. J.; Stelzer, L. S.; Belonga, K. L.; Carter, D. B.; Im, W. B.; Sethy, V. H.; Tang, A. H.; VonVoigtlander, P. F.; Petke, J. D. 3-Phenyl-Substituted Imidazo[1,5-a]Quinoxalin-4-Ones and Imidazo[1,5-a]Quinoxaline Ureas That Have High Affinity at the GABAA/Benzodiazepine Receptor Complex. *J. Med. Chem.* **1996**, *39* (19), 3820–3836. https://doi.org/10.1021/jm960070+.

(74) Li, L.; Qiu, D.; Shi, J.; Li, Y. Vicinal Diamination of Arenes with Domino Aryne Precursors. *Org. Lett.* **2016**, *18* (15), 3726–3729. https://doi.org/10.1021/acs.orglett.6b01747.

(75) He, J.; Qiu, D.; Li, Y. Strategies toward Aryne Multifunctionalization via 1,2-Benzdiyne and Benzyne. *Acc. Chem. Res.* **2020**, *53* (2), 508–519. https://doi.org/10.1021/acs.accounts.9b00608.

(76) Singh, K.; Kabadwal, L. M.; Bera, S.; Alanthadka, A.; Banerjee, D. Nickel-Catalyzed Synthesis of N-Substituted Pyrroles Using Diols with Aryl- and Alkylamines. *J. Org. Chem.* **2018**, *83* (24), 15406–15414. https://doi.org/10.1021/acs.joc.8b02666.

(77) Chakraborty, G.; Sikari, R.; Das, S.; Mondal, R.; Sinha, S.; Banerjee, S.; Paul, N. D. Dehydrogenative Synthesis of Quinolines, 2-Aminoquinolines, and Quinazolines Using Singlet Diradical Ni(II)-Catalysts. *J. Org. Chem.* **2019**, *84* (5), 2626–2641. https://doi.org/10.1021/acs.joc.8b03070.

(78) Singh, K.; Vellakkaran, M.; Banerjee, D. A Nitrogen-Ligated Nickel-Catalyst Enables Selective Intermolecular Cyclisation of β- and γ-Amino Alcohols with Ketones: Access to Five and Six-Membered N-Heterocycles. *Green Chemistry* **2018**, *20* (10), 2250–2256. https://doi.org/10.1039/C8GC00318A.

(79) Shee, S.; Panja, D.; Kundu, S. Nickel-Catalyzed Direct Synthesis of Quinoxalines from 2-Nitroanilines and Vicinal Diols: Identifying Nature of the Active Catalyst. *J. Org. Chem.* **2020**, *85* (4), 2775–2784. https://doi.org/10.1021/acs.joc.9b03104.

(80) Yang, P.; Zhang, C.; Gao, W.-C.; Ma, Y.; Wang, X.; Zhang, L.; Yue, J.; Tang, B. Nickel-Catalyzed Borrowing Hydrogen Annulations: Access to Diversified N-Heterocycles. *Chem. Commun.* **2019**, *55* (54), 7844–7847. https://doi.org/10.1039/C9CC03975A.

(81) Richter, R.; Ulrich, H. Four-Membered Rings Containing Two Nitrogenc Heteroatoms. In *Chemistry of Heterocyclic Compounds*; John Wiley & Sons, Ltd, 2008; pp 443–545. https://doi.org/10.1002/9780470187197.ch3.

(82) Staudinger, H. *Die ketene*; F. Enke, 1912.

(83) Hall, J. H.; Krishnan, G. The 2 + 2 Cycloaddition of 4-Substituted-1,2,4-Triazoline-3,5-Diones to Diphenylketene. *J. Org. Chem.* **1984**, *49* (13), 2498–2500. https://doi.org/10.1021/jo00187a040.

(84) Gheorghiu, M. D.; Parvulescu, L.; Popescu, A.; Cimpoia, R. A. The Reaction of Ketene with Carbon-Carbon .Sigma. Bonds. The Case of Moore's Ketene. *J. Org. Chem.* **1990**, *55* (12), 3713–3714. https://doi.org/10.1021/jo00299a005.

(85) Hyatt, J. A.; Raynolds, P. W. Ketene Cycloadditions. In *Organic Reactions*; American Cancer Society, 2004; pp 159–646. https://doi.org/10.1002/0471264180.or045.02.

(86) Kauer, J. C.; Schneider, A. K. Methoxydifluoromethyl Isocyanate by Thermal Cleavage of a Diazetidine. *J. Am. Chem. Soc.* **1960**, *82* (4), 852–853. https://doi.org/10.1021/ja01489a022.
(87) Huebner, C. F.; Strachan, P. L.; Donoghue, E. M.; Cahoon, N.; Dorfman, L.; Margerison, R. B.; Wenkert, E. Diels-Alder Reactions of Indene. *J. Org. Chem.* **1967**, *32* (4), 1126–1130. https://doi.org/10.1021/jo01279a060.
(88) Hall, J. H.; Jones, M. L. Reactions of Azodiones with Electron-Rich Alkenes. 1,2,4-Triazoline-3,5-Diones and Vinyl Ethers. *J. Org. Chem.* **1983**, *48* (6), 822–826. https://doi.org/10.1021/jo00154a014.
(89) Kim, D. K.; O'Shea, K. E. The Reaction of N-Methyl-1,2,4-Triazoline-3,5-Dione with Tetracyclopropylethylene. Formation of an Unusual Meso-Ionic Product and Its Rearrangement to the Diazetidine. *J. Am. Chem. Soc.* **2004**, *126* (3), 700–701. https://doi.org/10.1021/ja038359l.
(90) Okitsu, T.; Kobayashi, K.; Kan, R.; Yoshida, Y.; Matsui, Y.; Wada, A. 3-Methylene-4-Amido-1,2-Diazetidine as a Formal 1,4-Dipole Precursor: Lewis Acid-Catalyzed Nucleophilic Addition with Silylated Nucleophiles. *Org. Lett.* **2017**, *19* (17), 4592–4595. https://doi.org/10.1021/acs.orglett.7b02194.
(91) Masamune, S.; Nakamura, N.; Sapadaro, J. 1,2-Bis(.Beta.-Tosylethoxycarbonyl)Diazene. Application to the 2,3-Diazabicyclo[2.2.0]Hexene System. *J. Am. Chem. Soc.* **1975**, *97* (4), 918–919. https://doi.org/10.1021/ja00837a053.
(92) Warrener, R. N.; Nunn, E. E.; Paddon-Row, M. N. The Synthesis and Properties of Dimethyl 1,2-Diazetine-1,2-Dicarboxylate, a Potentially Aromatic Molecule. *Aust. J. Chem.* **1979**, *32* (12), 2659–2674. https://doi.org/10.1071/ch9792659.
(93) Whitman, D. W.; Carpenter, B. K. Experimental Evidence for Nonsquare Cyclobutadiene as a Chemically Significant Intermediate in Solution. *J. Am. Chem. Soc.* **1980**, *102* (12), 4272–4274. https://doi.org/10.1021/ja00532a055.
(94) Britten, T. K.; Kemmitt, P. D.; Halcovitch, N. R.; Coote, S. C. 4-π-Photocyclization of 1,2-Dihydropyridazines: An Approach to Bicyclic 1,2-Diazetidines with Rich Synthetic Potential. *Org. Lett.* **2019**, *21* (22), 9232–9235. https://doi.org/10.1021/acs.orglett.9b03613.
(95) Hall, J. H.; Bigard, W. S. 1,2-Diazetidine Conformation. Double Nitrogen Inversion. *J. Org. Chem.* **1978**, *43* (14), 2785–2788. https://doi.org/10.1021/jo00408a009.
(96) Miao, W.; Xu, W.; Zhang, Z.; Ma, R.; Chen, S.-H.; Li, G. A Novel and Efficient Method for the Synthesis of 1,2-Diazetidines. *Tetrahedron Letters* **2006**, *47* (38), 6835–6837. https://doi.org/10.1016/j.tetlet.2006.07.075.
(97) Brown, M. J.; Clarkson, G. J.; Inglis, G. G.; Shipman, M. Synthesis and Functionalization of 3-Alkylidene-1,2-Diazetidines Using Transition Metal Catalysis. *Org. Lett.* **2011**, *13* (7), 1686–1689. https://doi.org/10.1021/ol200193n.
(98) Rajkumar, S.; Clarkson, G. J.; Shipman, M. Regio- and Stereocontrolled Synthesis of 3-Substituted 1,2-Diazetidines by Asymmetric Allylic Amination of Vinyl Epoxide. *Org. Lett.* **2017**, *19* (8), 2058–2061. https://doi.org/10.1021/acs.orglett.7b00653.

(99) P. Iacobini, G.; W. Porter, D.; Shipman, M. Chemo- and Enantioselective Rh-Catalysed Hydrogenation of 3-Methylene-1,2-Diazetidines: Application to Vicinal Diamine Synthesis. *Chemical Communications* **2012**, *48* (79), 9852–9854. https://doi.org/10.1039/C2CC35445D.
(100) Hart, A. C. Silver(II) Fluoride. In *Encyclopedia of Reagents for Organic Synthesis*; American Cancer Society, 2007. https://doi.org/10.1002/047084289X.rn00740.
(101) Emeléus, H. J.; Hurst, G. L. 70. Fluorination of Cyanogen and Cyanogen Chloride with Metal Fluorides. *J. Chem. Soc.* **1964**, *0* (0), 396–399. https://doi.org/10.1039/JR9640000396.
(102) Ullman, E. F.; Singh, P. 3,3,4,4-Tetramethyl-1,2-Diazetine 1,2-Dioxide, a Useful Low-Energy Triplet Quencher. *J. Am. Chem. Soc.* **1972**, *94* (14), 5077–5078. https://doi.org/10.1021/ja00769a048.
(103) Mazhukin, D. G.; Volodarskii, L. B.; Tikhonova, L. A.; Tikhonov, A. Ya. Synthesis of 3,4-Dihydro-1,2-Diazete 1,2-Dioxides Based on 1,2-Bishydroxylamines and 1,2-Nitroso Oxime. *Mendeleev Communications* **1992**, *2* (1), 29–30. https://doi.org/10.1070/MC1992v002n01ABEH000111.
(104) Gagnon, J. L.; Zajac, W. W. Oxidative Cleavage of Cis-1,2-Diamino-1,2-Dimethyl-Cyclobutane to 2,5-Hexanedione. *Tetrahedron Letters* **1995**, *36* (11), 1803–1804. https://doi.org/10.1016/0040-4039(95)00147-5.
(105) Breton, G. W.; Nickerson, J. E.; Greene, A. M.; Oliver, L. H. Thermal Decomposition of Meso- and d,l-3,4-Diethyl-3,4-Dimethyldiazetine N,N‘-Dioxide. *Org. Lett.* **2007**, *9* (16), 3005–3008. https://doi.org/10.1021/ol0710414.
(106) Breton, G. W.; Oliver, L. H.; Nickerson, J. E. Synthesis of a Stereochemically Defined 1,2-Diazetine N,N‘-Dioxide and a Study of Its Thermal Decomposition. *J. Org. Chem.* **2007**, *72* (4), 1412–1416. https://doi.org/10.1021/jo062357c.
(107) Shvarts, G.; Grigor’ev, N.; Severina, I.; Ryaposova, I.; Lapitskaia, A.; Volodarskii, L.; Tikhonov, A.; Kurbnikova, I.; Mazhukin, D.; Granik, V. Derivatives of 1,2-Diazetine-1,2-Dioxide: A New Class of Nitric Oxide Generators Exhibiting Vasodilator Activity. *Pharmaceutical Chemistry Journal* **1994**, *28*, 261–266. https://doi.org/10.1007/BF02219799.
(108) Kirilyuk, I. A.; Utepbergenov, D. I.; Mazhukin, D. G.; Fechner, K.; Mertsch, K.; Khramtsov, V. V.; Blasig, I. E.; Haseloff, R. F. Thiol-Induced Nitric Oxide Release from 3-Halogeno-3,4-Dihydrodiazete 1,2-Dioxides. *J. Med. Chem.* **1998**, *41* (7), 1027–1033. https://doi.org/10.1021/jm960737s.
(109) Breton, G. W.; Shugart, J. H.; Hughey, C. A.; Perala, S. M.; Hicks, A. D. Synthesis of Δ1-1,2-Diazetines via a Diels−Alder Cycloaddition Approach. *Org. Lett.* **2001**, *3* (20), 3185–3187. https://doi.org/10.1021/ol0164942.
(110) Erden, I. Unusual Cycloadditions of 4-Phenyl-1,2,4-Triazolin-3,5-Dione to Endo- and Exo-Tricyclo[3.2.1.02,4]Oct-6-Enes. *Chem. Lett.* **1981**, *10* (2), 263–266. https://doi.org/10.1246/cl.1981.263.

(111) Munro, D. P.; Sharp, J. T. The Synthesis of 1H- and 5H-Thieno[1,2]Diazepines by the Electrocyclisation of α-(2-Alkenylthienyl)Diazoalkanes, and Some Observations on Their Photochemical Reactivity and Ring Inversion. *J. Chem. Soc., Perkin Trans. 1* **1980**, No. 0, 1718–1723. https://doi.org/10.1039/P19800001718.
(112) Robertson, I. R.; Sharp, J. T. The Photochemical Reactions of α,β,γ,δ -Unsaturated Diazo Compounds at Low Temperature. *Tetrahedron* **1984**, *40* (16), 3113–3116. https://doi.org/10.1016/S0040-4020(01)82435-2.
(113) Anderson, C. D.; Sharp, J. T. Photochemical Isomerisation of 3H-1,2-Diazepines to 4,6a-Dihydro[1,2]Diazeto[1,4-a]Pyrroles. *J. Chem. Soc., Perkin Trans. 1* **1980**, No. 0, 1230–1232. https://doi.org/10.1039/P19800001230.
(114) O'leary, Margaret. A.; Wege, D. Approaches to Pseudoindene: Products Derived from the Carbenes Benzocyclobuten-1-Ylcarbene, 2-Methylbenzocyclobutenylidene and o-Styrylcarbene. *Tetrahedron* **1981**, *37* (4), 801–811. https://doi.org/10.1016/S0040-4020(01)97701-4.
(115) Taylor, E. C.; Davies, H. M. L.; Lavell, W. T.; Jones, N. D. N- vs. O-Acylation of 4,5-Dihydro-1,3-Oxadiazin-6-Ones by Ring Enlargement. *J. Org. Chem.* **1984**, *49* (12), 2204–2208. https://doi.org/10.1021/jo00186a026.
(116) Moderhack, D. Dihydro-1,2-Diazetes – the Preparative Chemistry since 1980. *Chem Heterocycl Comp* **2019**, *55* (1), 3–24. https://doi.org/10.1007/s10593-019-02412-w.
(117) Fleischhauer, J.; Beckert, R.; Jüttke, Y.; Hornig, D.; Günther, W.; Birckner, E.; Grummt, U.-W.; Görls, H. From Byproducts to Efficient Fluorophores: A Route to the Synthesis of Fluorubines. *Chemistry – A European Journal* **2009**, *15* (46), 12799–12806. https://doi.org/10.1002/chem.200901961.
(118) Fleischhauer, J.; Beckert, R.; Günther, W.; Görls, H. Ring Strain and Weak Bonds: Δ2-1,2-Diazetines as Building Blocks for Pyridazines. *Synthesis* **2006**, *2006* (17), 2885–2890. https://doi.org/10.1055/s-2006-942524.
(119) Fleischhauer, J.; Beckert, R.; Weston, J.; Schmidt, M.; Flammersheim, H.-J.; Görls, H. Δ2-1,2-Diazetines: Regioselective Acylation Reactions and Rearrangement into 4H-1,3,4-Oxadiazines. *Synthesis* **2006**, *2006* (03), 514–518. https://doi.org/10.1055/s-2006-926272.
(120) Effenberger, F.; Maier, R. Cycloaddition of Azosulfones and Sulfonylimines. *Angew. Chem. Int. Ed. Engl.* **1966**, *5* (4), 416–417. https://doi.org/10.1002/anie.196604162.
(121) Cheng, C. C.; Greene, F. D.; Blount, J. F. Reaction of Triazolinediones with Acetylenes. Electrophilic Addition. *J. Org. Chem.* **1984**, *49* (16), 2917–2922. https://doi.org/10.1021/jo00190a015.
(122) Nunn, E. E.; Warrener, R. N. Dimethyl Δ3-1,2-Diazetine-1,2-Dicarboxylate: A New Four-Membered 6π-Ring System. *J. Chem. Soc., Chem. Commun.* **1972**, No. 14, 818–819. https://doi.org/10.1039/C39720000818.
(123) Breton, G. W.; Martin, K. L. Are 1,2-Dihydrodiazetes Aromatic? An Experimental and Computational Investigation. *J. Org. Chem.* **2002**, *67* (19), 6699–6704. https://doi.org/10.1021/jo026082m.

(124) Vol'pin, M. E. NON-BENZENOID AROMATIC COMPOUNDS AND THE CONCEPT OF AROMATICITY. *Russ. Chem. Rev.* **1960**, *29* (3), 129. https://doi.org/10.1070/RC1960v029n03ABEH001224.
(125) Tandon, V. K.; Chhor, R. B. Metal Mediated Dechlorination - A New Route to Nitriles http://www.ingentaconnect.com/contentone/ben/loc/2004/00000001/00000001/art00010 (accessed Mar 26, 2020). https://doi.org/info:doi/10.2174/1570178043488680.
(126) Jia, Z.-J.; Gao, S.; Arnold, F. H. Enzymatic Primary Amination of Benzylic and Allylic C(Sp3)–H Bonds. *J. Am. Chem. Soc.* **2020**, *142* (23), 10279–10283. https://doi.org/10.1021/jacs.0c03428.
(127) Yang, Y.; Cho, I.; Qi, X.; Liu, P.; Arnold, F. H. An Enzymatic Platform for the Asymmetric Amination of Primary, Secondary and Tertiary C(Sp3)–H Bonds. *Nat. Chem.* **2019**, *11* (11), 987–993. https://doi.org/10.1038/s41557-019-0343-5.

CHAPTER TWO

DEVELOPMENT OF THE ELECTRON-RICH ALKYNE AND AZODICARBOXYLATE CHEMISTRY

2.1 Motivating Goal: To design a straightforward methodology for the access of vicinal diamine motif

Despite the significant advances described in Chapter I, a general methodology that provides rapid access to the vicinal diamine motif in a variety of substitution patterns from readily available starting materials is still relatively elusive, and the field could benefit from new strategies to solve this difficult problem. This synthetic demand to access the vicinal diamine motif triggered our desire to develop a straightforward approach to synthesize these compounds. An efficient strategy to access vicinal diamines from unsaturated carbon-carbon multiple bonds is not well developed compared to similar processes such as dihydroxylations,[1] aminohydroxlyations,[2] and epoxidations.[3,4] Theoretically, the direct addition of two nitrogen atoms across a carbon-carbon multiple bonds is conceptually the most simple way to prepare a vicinal diamino functionality. Such an approach would be more economically efficient in terms of reagents and yields.[5]

We started to investigate the direct addition of two nitrogen atoms across carbon-carbon multiple bonds using electron rich alkenes and alkynes, while taking azodicarboxylates as the nitrogen source. Azodicarboxylates have been used in wide range of applications in different research disciplines.[6–9] Due to the large number of applications in synthetic organic chemistry, azodicarboxylates are readily available

starting materials with a variety of derivatives that are commercially available. Scheme 2.1 briefly highlights the wide range of reactions of azodicarboxylates. Azodicarboxylates participates in many different synthetic organic reactions such as Mitsunobu reactions,[10] terminal alkyne addition reactions,[11] aza-Baylis–Hillman reactions,[12–14] rearrangements,[15] and heterocycle syntheses (Scheme 2.1).[15–17] Azodicarboxylates are also known to perform amination reactions with aryl boronic compounds,[18] β-ketoesters,[19] enamines,[7] enol ethers,[20,21] vinyl acetates[22] and oxindoles[23] (Scheme 2.1).

Furthermore, cyclic azodicarboxylates, for instance the triazolinediones (TADs), are very reactive species that participate in diverse range of reactions such as [2+2] cycloadditions,[24–26] Alder-ene reactions,[27] aza-Diels-Alder reactions,[28–31] amination reactions[32] and photochemical reactions[33] (Scheme 2.2). Despite their wide range of applications of these compounds, a common protocol to obtain a broad range of *vic*-diamines through the reaction of azodicarboxylates with alkenes has not been developed.[34–36]

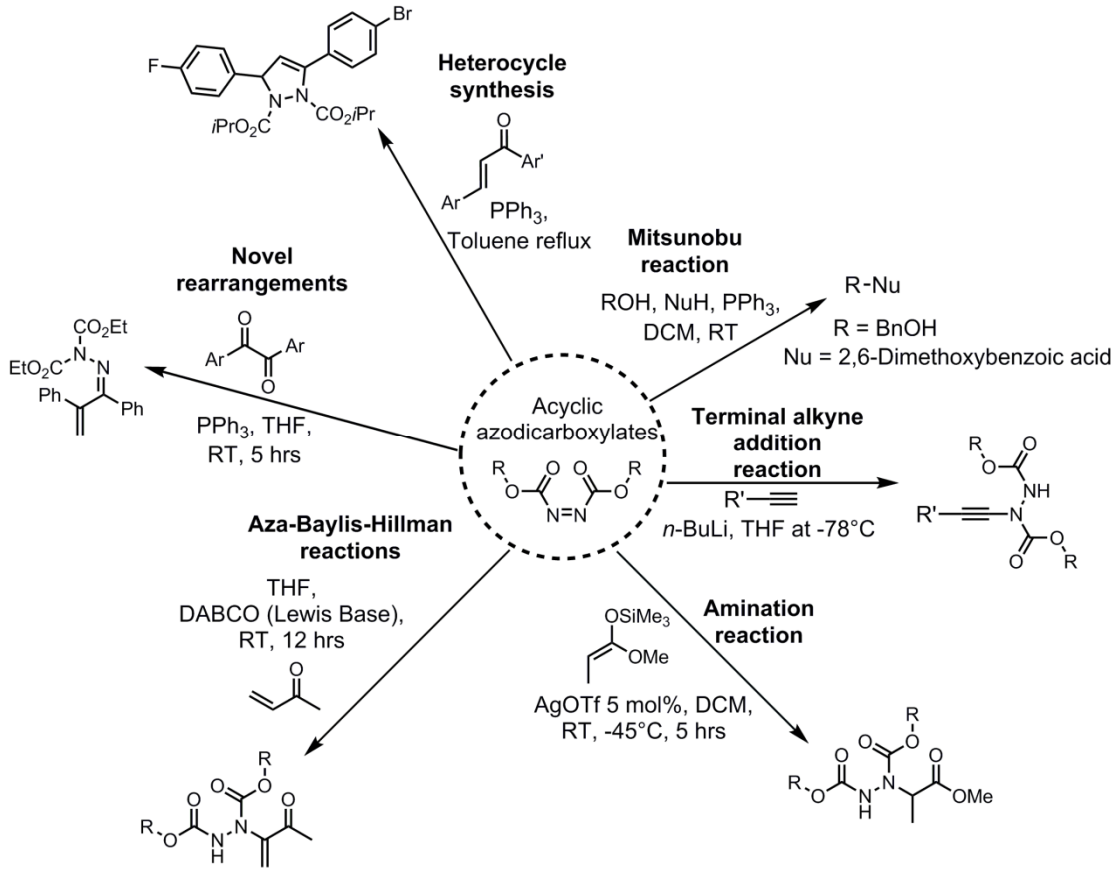

Scheme 2.1. Brief outline of the reactions of acyclic azodicarboxylates.

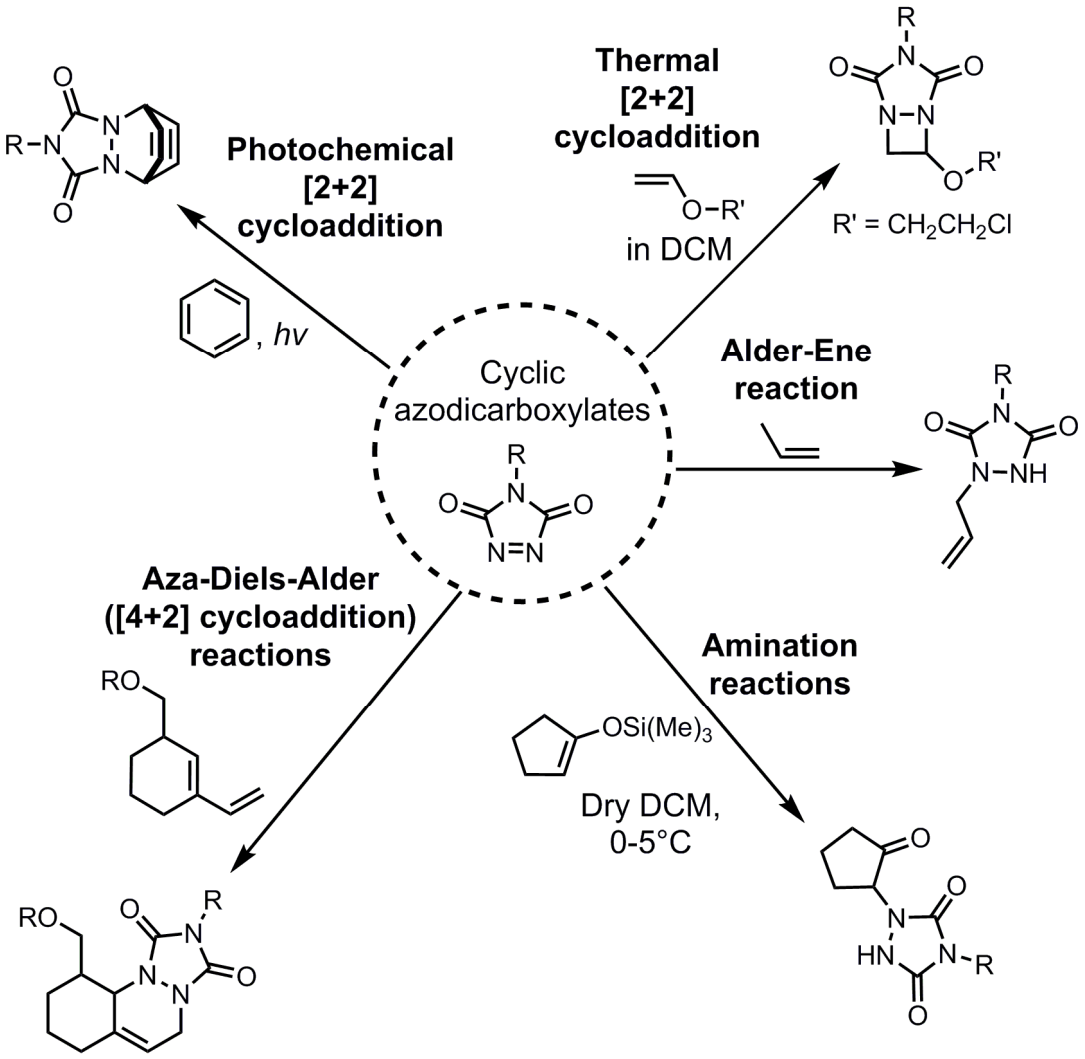

Scheme 2.2. Brief outline of the reactions of cyclic azodicarboxylates.

Another interesting feature of azodicarboxylates is the presence of the carbamate functionality on the molecule. Organic carbamates have been broadly used as structural elements of many approved therapeutic agents.[37,38] These functionalities show amide-ester hybrid features. In most cases, carbamates demonstrate very good chemical and proteolytic stabilities, which are some of the key factors for therapeutic agents. Medicinal chemists utilize this functionality as a substitution for a peptide bond in their therapeutic drugs due to their excellent chemical stability, metabolic stability, and cell permeability. Furthermore, having carbamate groups in the final product allows for late stage modifications to the structure which can ultimately help to modulate inter- and intramolecular interactions with target enzymes or receptors. Moreover, carbamate groups help to modulate the pharmacological properties of compounds such as absorption, distribution, metabolism, and excretion in order to enhance the desired therapeutic effect.[37,38]

We decided to choose azodicarboxylates as our nitrogen source due to the above properties of the carbamate group, two adjacent nitrogen atoms, and their electron deficiency. On the other hand, alkenes are commodity petrochemicals and alkynes are also readily available starting materials. Both alkenes and alkynes are available in a broad range of substitution patterns. Thus, we hypothesized that alkenes and alkynes will be the most suitable two carbon candidates for the construction of the vicinal diamine motif.

We began our initial goal to test the reactivity of a series of azodicarboxylates with electron rich alkene and alkyne substrates in order to access the corresponding vicinal diamine motif in the form of four-membered 1,2-diazetidine and diazacyclobutene (Δ^3-1,2-diazetine) *N*-heterocycles. Even though we tested the reactivity of many analogs of the alkenes and alkynes with azodicarboxylates, the key trials that lead to the discovery and development of this chemistry have been outlined in this section. In our early attempts, we converted the azodicarboxylate into an electron-rich betaine intermediate to react with an alkene bearing an electron withdrawing group (EWG) [Scheme 2.3 Eq. 1].[10] Furthermore, different substrates were screened to test the possibility in this aspect such as epoxides and copper acetalides under different conditions. However, all of these attempts were unsuccessful, and even trace amounts of the expected product were not observed.

Secondly, we attempted the same reactions with electron rich alkenes which bears an electron donating group (EDG) [Scheme 2.3 Eq. 2].[20,21,24,32] Since azodicarboxylates are known to be good electrophiles,[6,7] we thought that the inherent electrophillic nature of the azodicarboxylates would possibly provide a reasonable amount of reactivity.

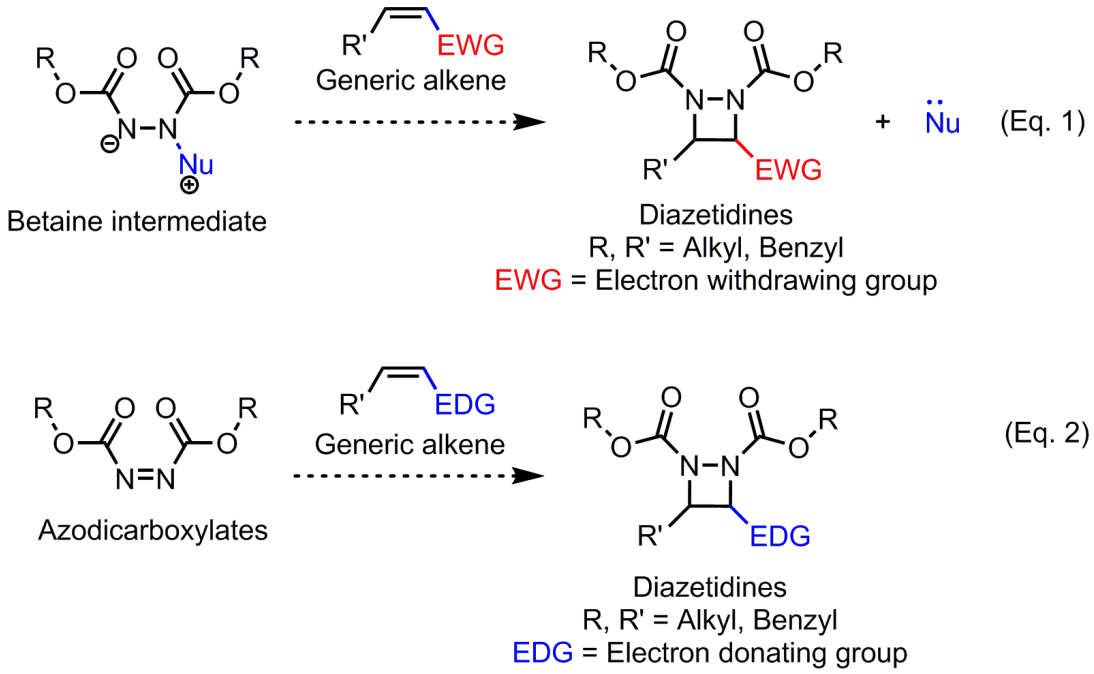

Scheme 2.3. Original plan to synthesize four-membered 1,2-diazetidines.

As we expected, we saw a reaction between azodicarboxylates **II-1** and the electron-rich silyl enol ether **II-2** (Scheme 2.4). However, the transformation returned hydrazine diesters like **II-4** which failed to undergo subsequent cyclization to provide the desired diazetidines.[20,21,24,32] We abandoned this route due to the possible increase in the number of synthetic steps to access the desired diazetidines.

Nevertheless, when we carefully considered the possible mechanism of the formation of the *N*-substituted hydrazine diester, we suspected that two pitfalls prevented the desired cyclization to form the desired 1,2-diazetidine derivative (Scheme 2.4).[24] First, the formation of a stable carbonyl group with the simultaneous loss of the silyl group may prevent further reaction. The second potential drawback is due to the effect of the resonance-stabilized negative charge that is formed after the initial attack on the azodicarboxylate depicted in intermediate **II-3**, rendering this intermediate less nucleophilic, and thus less prone to cyclization (Scheme 2.4).[20,21,32]

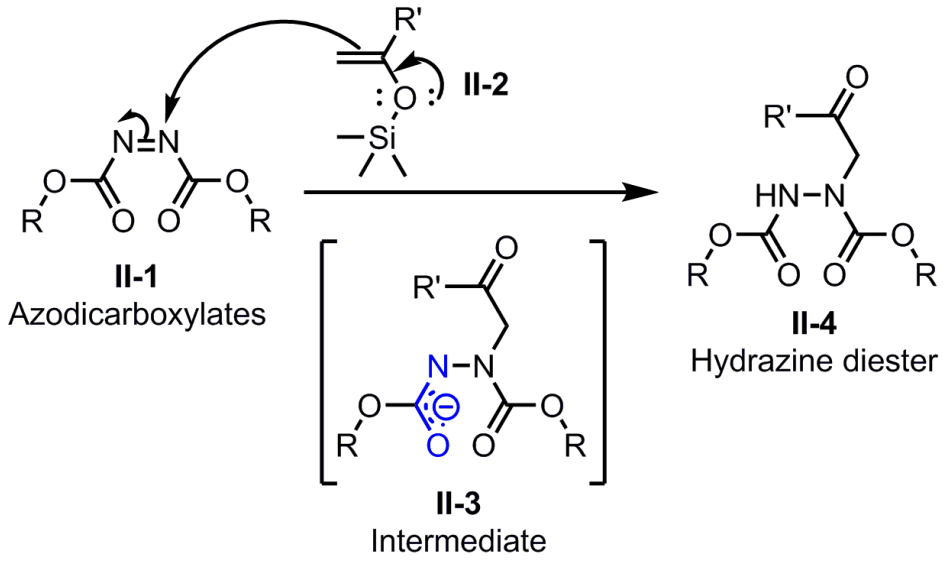

Scheme 2.4. Possible mechanism of *N*-Substituted hydrazine diester formation.

2.2 Synthesis of four-membered 1,2-diamino motif containing *N*-heterocycle: diazacyclobutenes (Δ^3-1,2-diazetines)

In order to understand the lack of previous synthetic studies toward diazacyclobutenes and for the convenience of the reader; a very brief outline of the historical examples of the diazacyclobutenes are illustrated in Scheme 2.5 and a short discussion is also provided. Nevertheless, these literature studies have also been discussed in detail in Chapter I. The first diazacyclobutene derivative **II-5** was reported by Effenberger and Maier in 1966.[39] Even though it has been over 50 years since this initial report on the synthesis of diazacyclobutenes, less than a dozen diazacyclobutene derivatives have been reported in the literature due to a lack of feasible synthetic routes to access the motif in high yield.[5,40–42]

Warrener and Nunn reported dimethyl Δ^3-1,2-diazetine-1,2-dicarboxylate or diazacyclobutene **II-6** in 1972, although the molecule was thermally unstable and rapidly underwent electrocyclic ring opening at room temperature to form the stable diimine carbamate derivative **II-7** (Scheme 2.5).[43] In 1984, Greene synthesized diazacyclobutene **II-8** in a 21–26 % yield by reacting PTAD with a hindered diarylacetylene in dichloromethane for 5 days.[44] In 2001, Breton and coworkers developed a method to produce the diazacyclobutene moiety in 3 operations to afford the desired diazacyclobutene **II-9** in an 8–10% overall yield (Scheme 2.5).[45] The aforementioned synthetic methods allowed access to the diazacyclobutene moiety; however their strategies suffer from low yields and narrow substrate scopes.

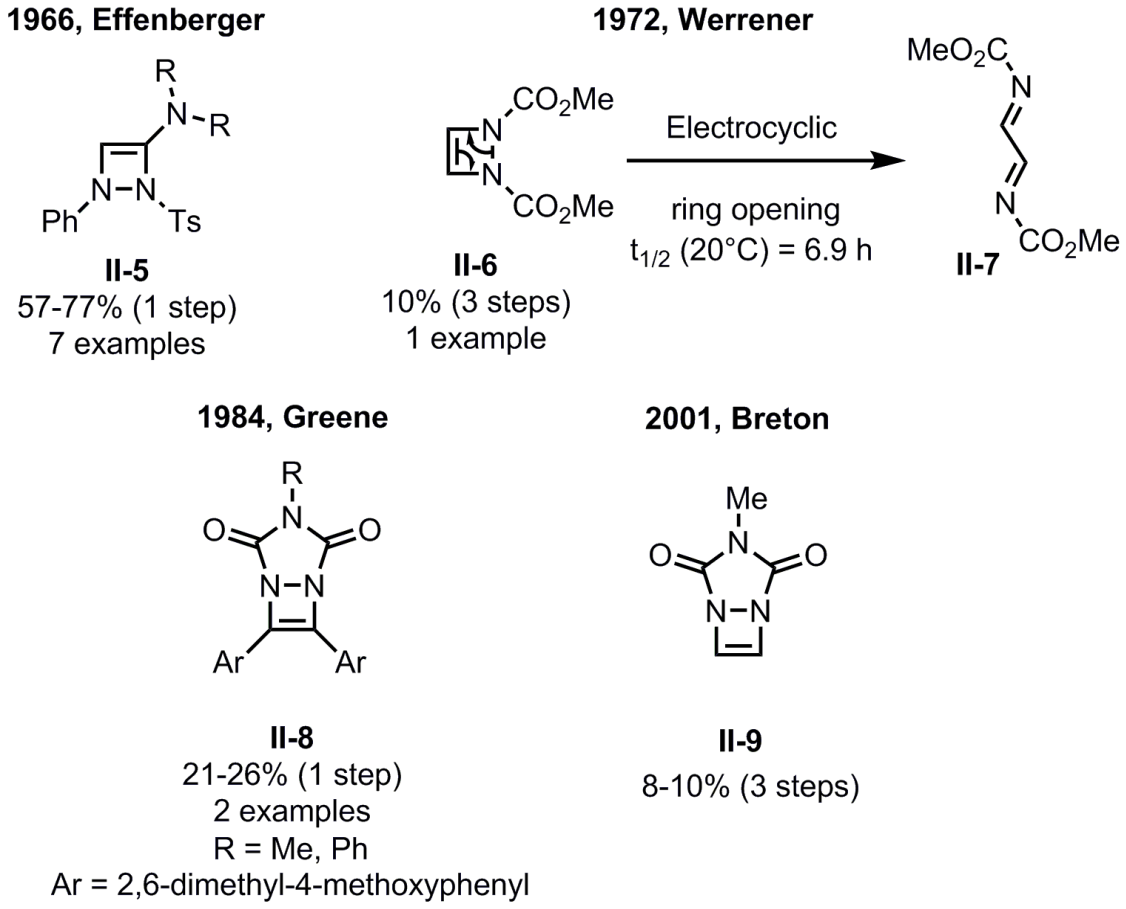

Scheme 2.5. Historical examples of diazacyclobutene synthesis.

Our initial failures to make four membered heterocyclic compounds with electron rich and deficient alkenes (Scheme 2.2) brought our focus on the potential use of electron rich alkynes instead of alkenes. Our initial idea was that if we used an electron rich alkyne **II-10** which has an electron donating group attached to the alkyne functionality, it could possibly push electrons towards the pi system and attack one of the electrophillic nitrogen on the azodicarboxylates **II-11**, thus making a zwitterionic species **II-12** which contains ketene functionality (Scheme 2.6). Due to the high reactivity of the ketene functionality, the zwitterionic species **II-12** could possibly undergo a rapid ring closure to produce the expected diazacyclobutene moiety **II-13**.[46–48]

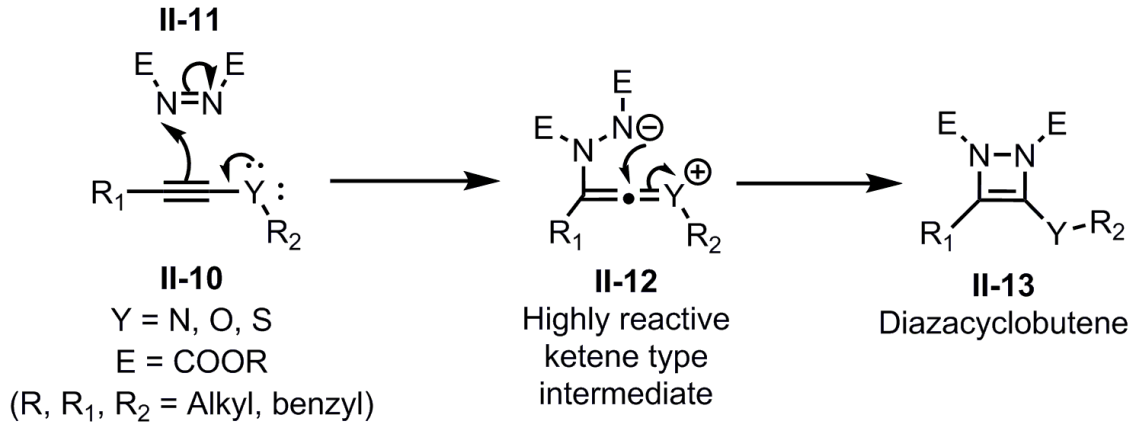

Scheme 2.6. Proposed mechanism for the synthesis of diazacyclobutenes.

In order to test this hypothesis outlined in Scheme 2.6, we synthesized several sulfur analogues of electron rich alkynes (alkylacetylene sulfides) which are displayed in Table 2.1 and 2.2. We used two methods to synthesize different alkyne substrates that modulated R_1 and R_2.[49–51]

The first procedure shown in Table 2.1 was performed mainly to make alkylacetylene sulfides with different R_2 groups by starting with a terminal alkyne and then deprotonating it with *n*-butyl lithium at –78°C to form the acetylide ion followed by addition of elemental sulfur to make the thiolate ion and finally carrying out a nucleophilic substitution with a corresponding alkyl halide.

Similarly in the second procedure, a corresponding dialkyl disulfide was added after the acetylide ion formation to synthesize bearing alkylacetylene sulfides bearing different R_1 and R_2 groups (See Table 2.2).

Table 2.1. Synthesis of alkylacetylene sulfides.

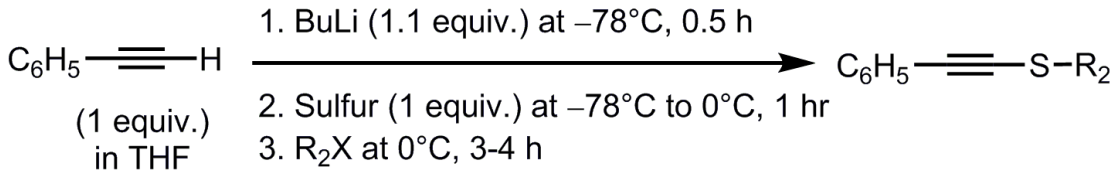

Entry	R_2	Yield%[a]
1	Me	90
2	Et	82
3	*n*-Pr	83
4	*n*-Bu	76
5	*n*-C_5H_{11}	69
6	*n*-C_8H_{17}	75
7	Bn	85

[a]Isolated yields after column chromatography.

Table 2.2. Synthesis of alkylacetylene sulfides.

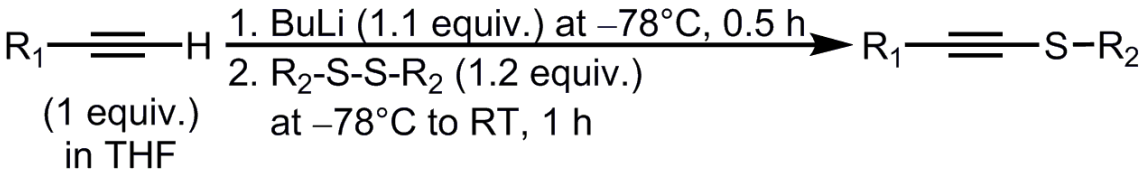

Entry	R_1	Chalcogen atom (S or Se)	R_2	Yield%[a]
1	C_6H_5	S	C_6H_5	92
2	4-Me-C_6H_4	S	Me	78
3	4-Me-C_6H_4	S	Et	90
4	4-MeO-C_6H_4	S	Me	98
5	4-Cl-C_6H_4	S	Me	65
6	4-CF_3-C_6H_4	S	Me	43
7	*n*-Bu	S	Me	28
8	*n*-Bu	S	*n*-Bu	67
9	Cyclopropyl	S	Me	38
10	C_6H_5	Se	Me	86
11	C_6H_5	Se	C_6H_5	94

[a]Isolated yields after column chromatography

Then we tested our hypothesis outlined in Scheme 2.6 by reacting methylphenylacetylene sulfide with 4-phenyl-1,2,4-triazoline-3,5,dione (PTAD) (Table 2.3). Intriguingly, we saw the formation of the expected diazacyclobutene derivative. The success of this initial reaction encouraged us to explore the optimization of the transformation and to probe the substrate scope of this reaction with a range of alkylacetylene sulfides.

We first examined the reaction yields under reflux conditions for 24 hours using a series of common solvents while keeping the equivalence of PTAD (**II-14**) and thio-acetylene **II-15a** as 1:1.3 (Table 2.3, entries 1-5). Among the common solvents examined, acetonitrile was found to afford the highest yield (89%, entry 5) of the diazacyclobutene product **II-16a**. Chloroform and dichloromethane gave yields of 82% and 78%, respectively, whereas tetrahydrofuran and toluene provided lower yields of 68% and 67% (entries 1-4). The reaction conditions were further tuned by conducting a time study, varying the reactant equivalence, and reducing the total volume of solvent by half (Table 2.3, entry 6-11). Refluxing in acetonitrile for 6 h and 12 h did not significantly influence the yield (entries 6-7). Furthermore, decreasing the equivalence of the thio-acetylene lowered the yields about 20% (entries 8-10). Finally, when the reaction volume was reduced to half, the yield was further lower (entry 11). These studies indicate that optimal yields are obtained when the reactants are refluxed in acetonitrile for 24 hours while using a 1:1.3 ratio of PTAD to alkylacetylene sulfide.

Table 2.3. Optimization of the reaction conditions.

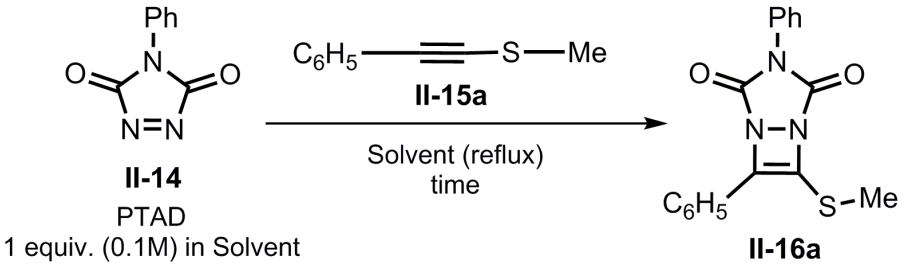

Entry	Solvent	Equivalence of the Alkynyl Sulfide(**II-15a**)	Reaction time	Yield[a](%)
1	Chloroform	1.3	24 h	82
2	Dichloromethane	1.3	24 h	78
3	THF	1.3	24 h	68
4	Toluene	1.3	24 h	67
5	**Acetonitrile**	**1.3**	**24 h**	**89**
6	Acetonitrile	1.3	6 h	80
7	Acetonitrile	1.3	12 h	83
8	Acetonitrile	1	24 h	71
9	Acetonitrile	1.1	24 h	69
10	Acetonitrile	1.2	24 h	72
11[b]	Acetonitrile	1.3	24 h	75

[a]Isolated Yields. [b]5mL of total volume used.

With the optimized conditions in hand, we successfully synthesized several derivatives of diazacyclobutenes in good yield (Scheme 2.7). Alkylphenylacetylene sulfides (**II-15a to II-15d)** with *S*-substituted methyl, ethyl, *n*-propyl, *n*-butyl were successfully converted into their corresponding diazacyclobutene derivatives **II-16a to II-16d** in 77–89% yields (Scheme 2.7). Diazacyclobutenes bearing longer *S*-alkyl chains (**II-16e to II-16f**) with *n*-pentyl or *n*-octyl were generated in 78% and 81% yields, respectively. The *S*-benzyl diazacyclobutene derivative **II-16g** was also produced in a moderate 62% yield. The *S*-phenyl analog **II-16h** was afforded in 85% yield. A gram scale (6 mmol) reaction to produce the same analog proceeded in 81% yield (1.87 g).

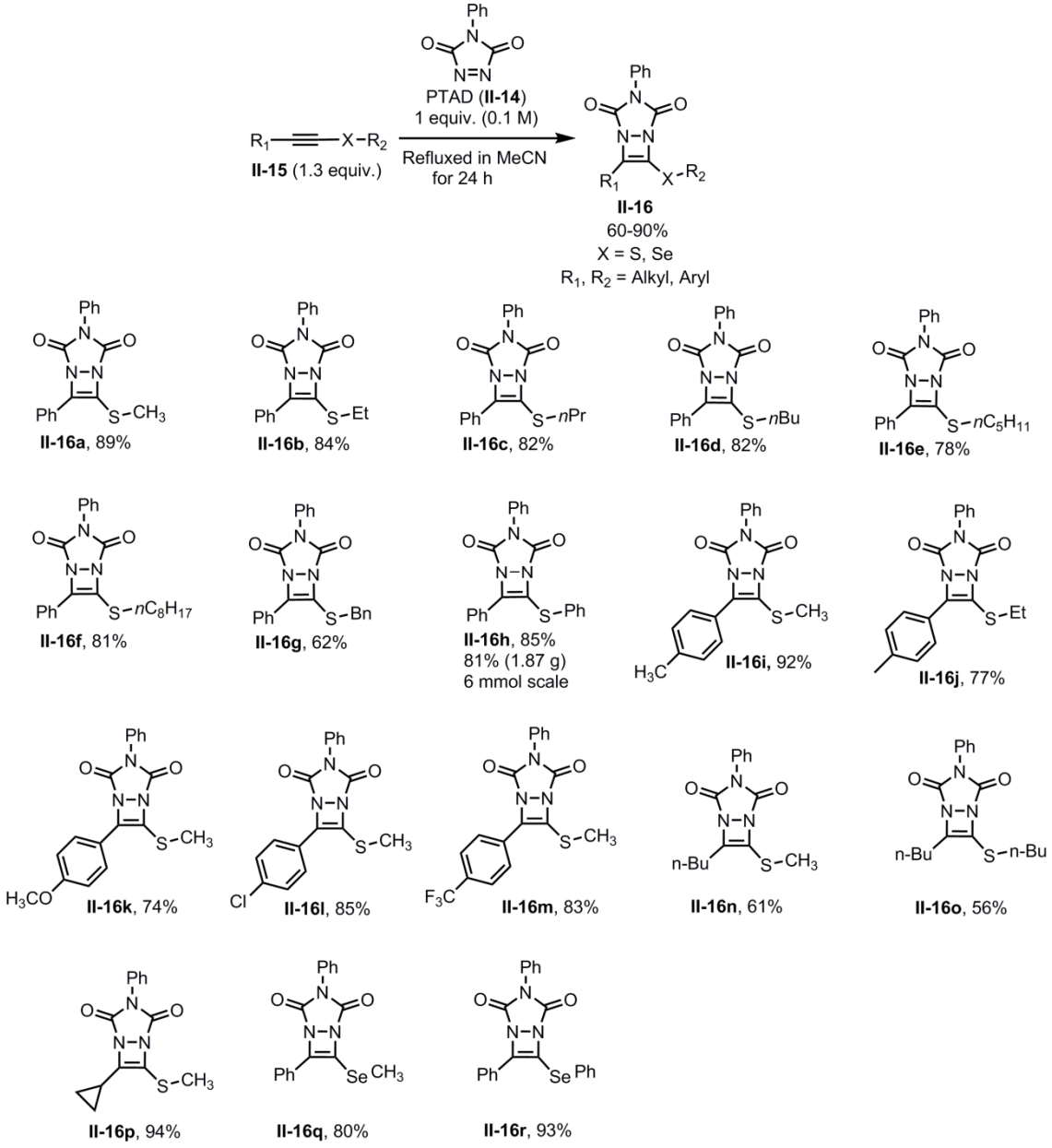

Scheme 2.7. Substrate scope of diazacyclobutene derivatives from the cycloaddition of PTAD and alkyl acetylene sulfides

We then examined the reactivity of alkylphenylacetylene sulfides with *para*-substituted electron donating and withdrawing substituents on the phenyl group. Two analogs (R_2 = Me, Et) of the alkynylsulfides bearing *p*-methylphenyl as R_1 group were converted to their corresponding diazacyclobutene in 92% and 77% yield, respectively (Scheme 2.7, **II-16i** and **II-16j**). Alkylphenylacetylenes with electron donating groups such as *p*-methoxy and electron withdrawing substituents such as *p*-chloro and *p*-trifluoromethyl (**II-16k-m**) generated the corresponding diazacyclobutene derivatives in good yields ranging from 74–85%. We also synthesized a couple of derivatives (R_2 = Me, *n*-Bu) that had R_1 substituted with an alkyl group such as *n*-butyl. These examples were made in moderate yields, 56% and 61%, respectively (Scheme 2.7, **II-16n** and **II-16o**).

In addition, we were able to synthesize a diazacyclobutene analog **II-16p** which bore a cyclopropyl group at the R_1 position in 94% yield. Furthermore we explored this chemistry with selenium analogs by changing the chalcogen atom on the electron-rich alkyne. These attempts yielded the corresponding diazacyclobutenes **II-16q** and **II-16r** (where R_2 = Me, Ph) in 80% and 93% yield, respectively.

2.3 Potential Aromaticity of diazacyclobutenes (Δ^3-1,2-diazetines)

Due to the fact that the diazacyclobutene (Δ^3-1,2-diazetine) electronic framework consists of 6π electrons in a four-membered ring, the Hūckel rule[52,53] of aromaticity predicts that the motif may have aromatic character (Figure 2.1).There have been some computational studies reported previously to assess the potential aromatic character of diazacyclobutenes.[43,54–59] Nonetheless, these computational studies could not be validated experimentally due to the lack of simple synthetic methods to access the motif.

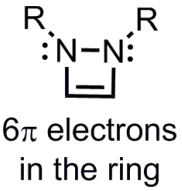

.

Figure 2.1. Central diazacycobutene ring

When diazacyclobutenes were first reported in 1966, no experiments probing their potential aromaticity were performed. Nevertheless, six years prior to this study, a similar structural moiety with sulfur as heteroatoms instead of nitrogens was reported.[60] This molecule was known as bis-(trifluoromethyl)-l,2-dithietene (**II-17,** Scheme 2.8) and theoretically this molecule also follows the Hückel rule. Surprisingly, this molecule **II-17** exhibited a rather high boiling point (95–96˚C), and existed as a liquid presumably due to its aromatic stability.[60]

In 1972, Warrener synthesized dimethyl Δ^3-1,2-diazetine-1,2-dicarboxylate **II-18** (Scheme 2.8) and found that even at ambient temperatures the compound isomerizes to the corresponding ring opened analog **II-19 [**$t_{1/2}$ (20˚C) = 6.9 h], suggesting that **II-18** does not benefit from aromatic stability. In 1979, Warrener and co-workers reported the first broader discussion about the potential aromaticity of the diazacyclobutene motif and suggested that the compounds were non-aromatic – or perhaps even antiaromatic – due to the destabilizing interactions arising from the lone pair repulsion between the two nitrogen atoms and the repulsion between the lone pairs of the nitrogen atoms and the C=C double bond.[58]

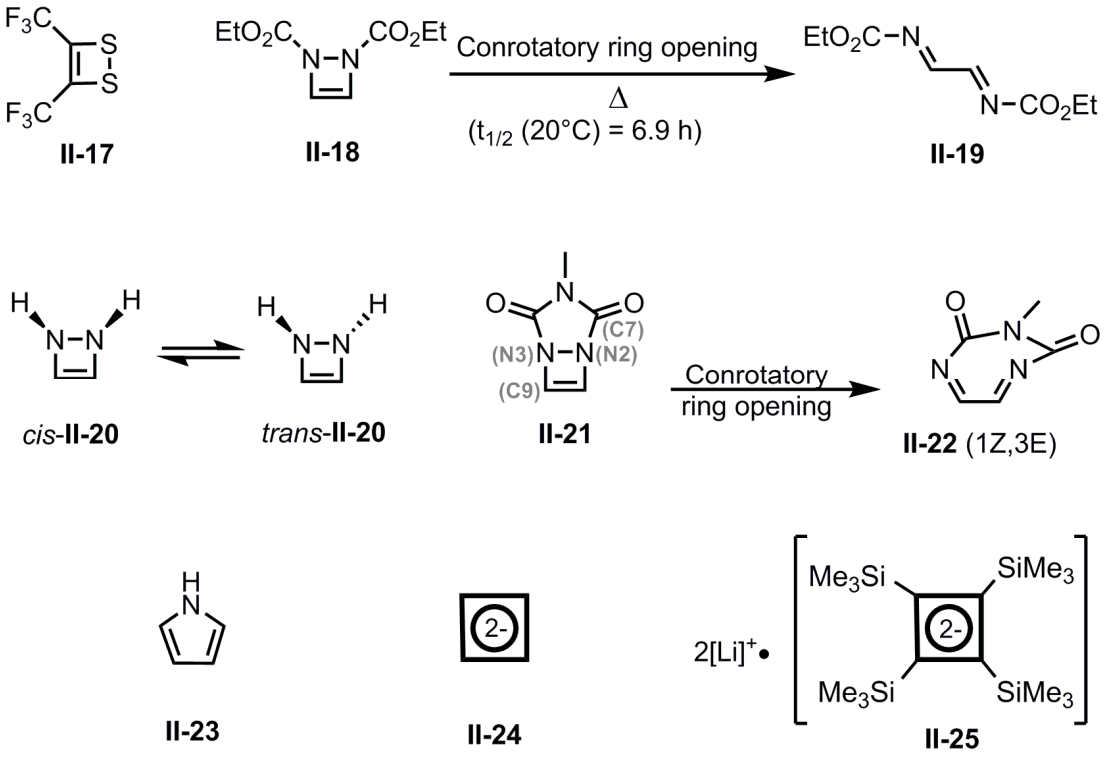

Scheme 2.8. Various examples used to examine the potential aromaticity.

Warrener and co-workers further reported that diazacyclobutene **II-20** can undergo rapid *cis-trans* isomerization through NH outer plane deformations (Scheme 2.8). They further stated that these NH deformations reduce the N-N and C-N overlap and thereby compensate the hitherto mentioned destabilizing interactions of the molecule.[58] Successive computational studies on the conrotatory ring opening of the diazacyclobutenes, molecular orbital analysis done by Budzelaar *et al.*[54] Mó*et al.*[55] and Bachrach *et al.*[56] were also in good agreement with Warrener's initial conclusions of the non-aromaticity of the diazacyclobutenes.

In 2002, Breton and his co-workers probed the aromaticity of diazacyclobutene **II-21** (Scheme 2.8) with the help of an X-ray crystal structure study, further reaction studies, and computational investigations.[59] They first noticed the non-aromatic character of diazacyclobutene **II-21** based on the pyramidal nature of the two nitrogen atoms in the four-membered ring that were readily extracted from the crystal structure. The pyramidal nature of the two nitrogen atoms were observed from the C7-N2-N3-C9 torsion angle of 120.4° (Scheme 2.8, **II-21**) which directly suggest that the diazacyclobutene is not aromatic. If the four-membered ring is aromatic, it would be a planar molecule and the torsion angle should be 180˚. Furthermore, the non-aromatic character based on the pyramidal nature of the nitrogen atoms in this diazacyclobutene system **II-21** can be compared with pyrrole **II-23** (Scheme 2.8) (*i.e.,* as a prototype heteroaromatic five-membered aromatic ring system), which has a trigonal planar nitrogen atom. However, there were cases where the extent of the pyramidality of the phosphorous heteroatom

atom in some phospholes is not directly correlated with their aromaticity.[61,62] So, they further investigated the non-delocalized character of the bonds in the four-membered ring of **II-21** (Scheme 2.8). They found that the bond length values of C=C, C-N and N-N do not show any intermediate values. Rather, they are similar to the corresponding standard bond lengths for single and double bonds, which ultimately suggest that the diazacyclobutene ring has no significant ring current.[59] It is also important to note that diazacyclobutene **II-21** survived higher temperature conditions (*i.e.,* 150˚C for several hours) during the solution phase pyrolysis step of its synthesis (described also in Chapter I, Scheme 1.8).[45] This enhanced thermal stability is not a manifestation of the aromatic stability of bicyclic diazacyclobutene **II-21** since it should also present in the more labile monocyclic diazacyclobutene **II-18**. Rather, this is probably due to the restriction caused by the fused urozole ring of **II-21**. The conrotatory ring opening process would yield a strained ring-opened product: a (1*Z*,3*E*)-cycloheptadienyl heterocyclic ring (**II-22,** Scheme 2.8).[59] This improved thermal stability was also seen in the bicyclic diazacyclobutenes that we synthesized. Figure 2.2 shows the thermogravimetric analysis (TGA) of diazacyclobutene **II-16b**.

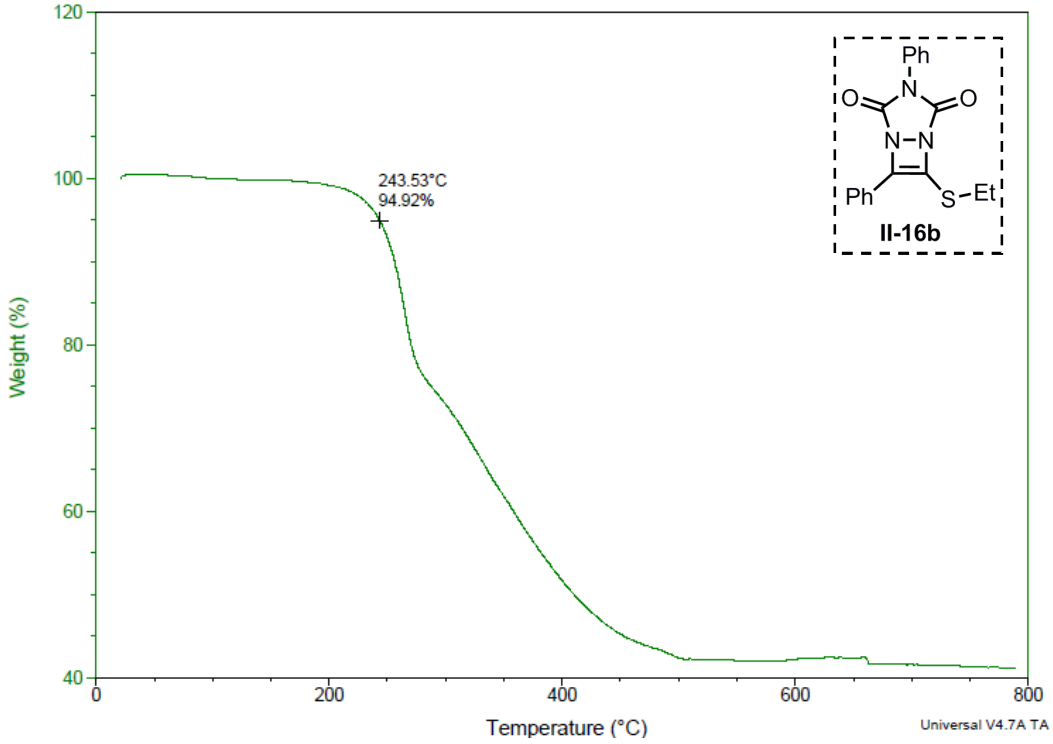

Figure 2.2. Thermogravimetric analysis (TGA) of diazacyclobutene**II-16b**

This TGA curve (Figure 2.2) shows that compound **II-16b** is stable up to *ca.* 240˚C. Due to the enhanced stability of **II-21**, Breton and co-workers performed alkene-like reactions with the compound such as hydrogenation, bromination, and Diels-Alder cycloaddition to further experimentally prove the non-aromatic behavior of the diazacyclobutene **II-21**.[59]

Although the debate on the potential aromaticity of the diazacyclobutene is fairly settled at this point, further attempts to make different derivatives of diazacyclobutenes and to evaluate their potential aromaticity has been hindered due to a lack of simple synthetic protocols to generate the compounds.[39,43–45]A similar debate about the aromaticity of cyclobutadienyl dianion **II-24** (Scheme 2.8) (*i.e.*, a compound that is isoelectronic with the diazacyclobutene core ring) also persisted over the past.[63–65] Eventually, it was shown that electronic effects, substituent effects, and steric effects can stabilize the π-electron system of the cyclobutadienyl dianion **II-24**.[66] For example Sekiguchi *et al.* reported that the dilithium salt of tetrakis(trimethylsilyl)cyclobutadiene dianion **II-25** (Scheme 2.8) was planar and almost square according to X-ray crystallographic data.[66] The observed C-C bond lengths for that compound were in between the typical C-C (1.54Å) and C=C (1.34Å) bond lengths. These results suggested that the dilithium salt of tetrakis(trimethylsilyl)cyclobutadiene dianion **II-25** may be aromatic.[66]

Since we were able to produce an array of diazacyclobutene derivatives with our simple two-step synthetic protocol and inspired by the aromaticity investigation studies of cyclobutadienyl dianion derivatives,[63–66] we generated crystals from our suites of diazacyclobutene derivatives to get an initial idea about their potential aromaticity based on the X-ray crystallographic data.[59,62] We thought that this might provide us the initial understanding of how electronic effects, substituent effects, and steric effects influence the electronic nature and potential aromaticity of our suite of diazacyclobutene derivatives.[66]

The crystal structures of our diazacyclobutene derivatives are shown in Figure 2.3 and Figure 2.4. In order to investigate the possibility of aromaticity in our diazacyclobutenes, several important bond lengths are reported in Table 2.4. Similar to Breton's experimental results, the observed C9-C10,C9-N3, C10-N2 and N2-N3 bond lengths are approximately similar to the standard single bond lengths (*i.e.*, C-C of cyclobutene = 1.34 Å; C-N of CH_3NH_2 = 1.47 Å; N-N of N_2H_4 = 1.45 Å). As explained earlier, if the diazacyclobutene possessed ring current due to potential aromaticity, it would result in a lengthening of the C9-C10 bond lengths and simultaneous shortening of C9-N3, C10-N2 and N2-N3 bond lengths compared to the corresponding standard bond lengths of the reference compounds. The XRD data suggests that there is no such alteration of the bond lengths, consistent with a non-aromatic compound.

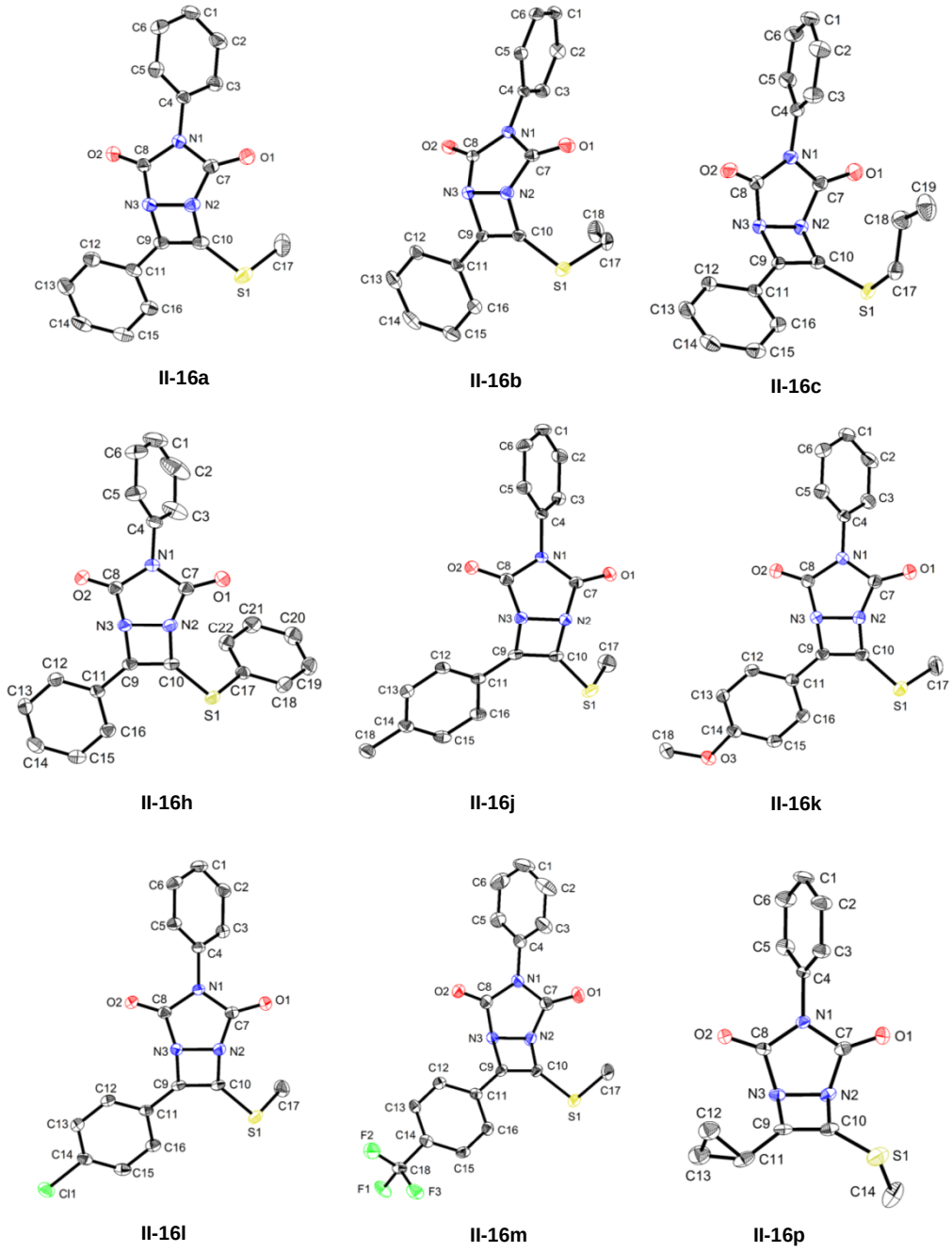

Figure 2.3. Structures of the sulfur-based diazacyclobutenes determined by single crystal X-ray diffraction, shown as 50% probability ellipsoids.

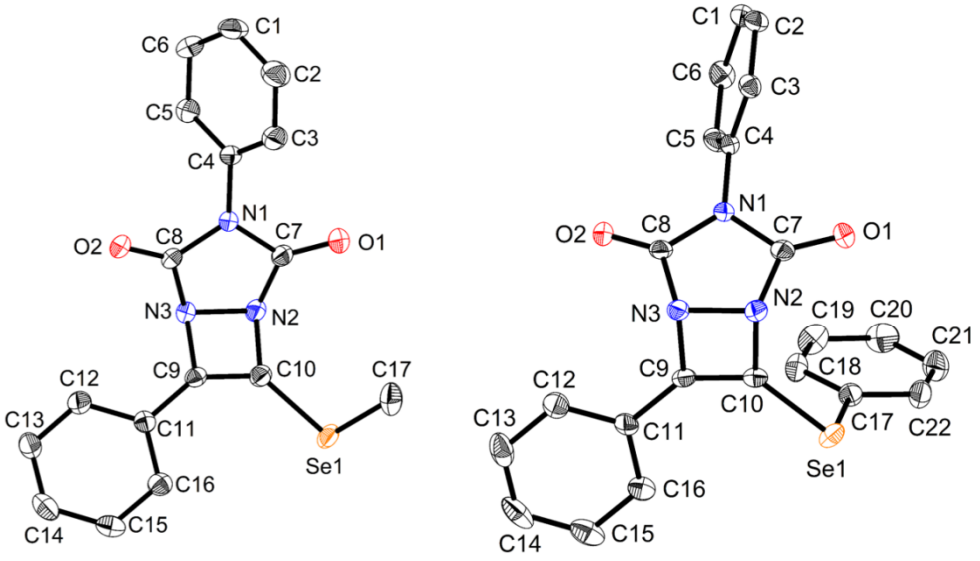

Figure 2.4. Structures of the selenium-based diazacyclobutenes determined by single crystal X-ray diffraction, shown as 50% probability ellipsoids.

Table 2.4. Bond lengths of diazacyclobutene crystal structures. Note that the asymmetric units of the compounds of **II-16j**, **II-16l**, **II-16m**, and **II-16p** have two unique molecules, and the corresponding bond lengths and angles of both unique molecules are listed below. Compounds **II-16q** and **II-16r** are the Se-based molecules.

Entry	R_1	R_2	Bond lengths (Å)			
			C9-C10	**C9-N3**	**C10-N2**	**N3-N2**
II-16a	C_6H_5	CH_3	1.346(3)	1.463(2)	1.475(2)	1.467(2)
II-16b	C_6H_5	CH_2CH_3	1.3505(17)	1.4700(15)	1.4799(16)	1.4712(14)
II-16c	C_6H_5	$CH_2CH_2CH_3$	1.3514(19)	1.4691(16)	1.4713(16)	1.4746(15)
II-16h	C_6H_5	C_6H_5	1.351(2)	1.468(2)	1.479(2)	1.471(2)
II-16j	4-CH_3-C_6H_4	CH_3	1.350(3) 1.352(3)	1.464(2) 1.466(2)	1.482(2) 1.480(2)	1.468(2) 1.471(2)
II-16k	4-MeO-C_6H_4	CH_3	1.352(2)	1.462(2)	1.487(2)	1.4635(17)
II-16l	4-Cl-C_6H_4	CH_3	1.350(2) 1.350(2)	1.464(2) 1.463(2)	1.479(2) 1.480(2)	1.4658(19) 1.4698(19)
II-16m	4-CF_3-C_6H_4	CH_3	1.337(12) 1.348(13)	1.474(11) 1.468(11)	1.477(11) 1.468(11)	1.460(10) 1.472(11)
II-16p	C_3H_5	CH_3	1.341(5) 1.329(5)	1.474(4) 1.475(4)	1.480(4) 1.469(4)	1.475(4) 1.471(4)
II-16q	C_6H_5	CH_3	1.348(4)	1.459(3)	1.475(3)	1.462(3)
II-16r	C_6H_5	C_6H_5	1.349(3)	1.470(2)	1.470(2)	1.475(2)

In addition, we also evaluated the degree of planarity of the diazacyclobutene ring by analyzing the C9-N3-N2-C10 torsion angle (Table 2.5). This revealed that the central four-membered ring is nearly planar. For instance the C9-N3-N2-C10 torsion angle is lower than 2.74(9)˚ for all of the diazacyclobutenes we studied.

However, as described in Breton's study,[59] the pyramidal versus planar nature of the nitrogen atoms in the diazacyclobutene ring could be taken as an additional measurement to further confirm the aromatic or non-aromatic character of the compounds. Since the N2-N3 bond of all the diazacyclobutene crystal structures (Figure 2.2 and Figure 2.3) is shared between the four-membered diazacyclobutene ring and the top five-membered urozole ring, the angle between the four-five ring planes is a direct indication of whether the nitrogen atoms are planar or pyramidal. The 4/5 ring planar angles (Table 2.6) for our derivatives were ranging from 50˚ to 60˚. If the compounds were aromatic one would expect that the angle would be closer to 180˚. Angles between 50–60˚clearly indicate that in all of the cases, the N2 and N3 atoms are pyramidal in nature.[59,62] Therefore, both the bond lengths and 4/5 planar angles suggest that our suite of diazacyclobutenes are not aromatic, but instead resemble strained four-membered rings with a localized double bond. These studies are also in good agreement with the previously reported studies.[43,54–59,61,62] However, further studies on more changes to the diazacyclobutene scaffold with different electronic and steric substituents to examine the influence to the aromaticity are underway.

Table 2.5. Evaluating the planarity of the diazacyclobutene ring by C9-N3-N2-C10 torsion angle. Note that compounds **II-16j**, **II-16l**, **II-16m**, and **II-16p** and have two unique molecules in their asymmetric units, and the corresponding torsion angles of both unique molecules are listed. Compounds **II-16q** and **II-16r** are the Se-based molecules.

Entry	**R_1**	**R_2**	**Diazacyclobutene Torsion Angle (°) C9-N3-N2-C10**	**RMS deviation (Å) from C9-N3-N2-C10 plane**
II-16a	C_6H_5	CH_3	1.08(12)	0.0072
II-16b	C_6H_5	CH_2CH_3	2.24(8)	0.0150
II-16c	C_6H_5	$CH_2CH_2CH_3$	2.74(9)	0.0183
II-16h	C_6H_5	C_6H_5	1.46(12)	0.0098
II-16j	4-CH_3-C_6H_4	CH_3	1.13(13) 2.01(14)	0.0076 0.0124
II-16k	4-MeO-C_6H_4	CH_3	1.03(11)	0.0068
II-16l	4-Cl-C_6H_4	CH_3	1.27(12) 1.83(13)	0.0085 0.0111
II-16m	4-CF_3-C_6H_4	CH_3	1.0(6) 1.1(7)	0.0068 0.0068
II-16p	C_3H_5	CH_3	0.0(2) 1.0(2)	0.0001 0.0059
II-16q	C_6H_5	CH_3	0.74(19)	0.0049
II-16r	C_6H_5	C_6H_5	1.66(13)	0.0111

Table 2.6. Four-fiveplanar angles of diazacyclobutene crystal structures. Note that the compounds **II-16q** and **II-16r** are the Se-based molecules.

Entry	R_1	R_2	Angle between 4/5 planes (°)
			N2-N3-C9-C10 N1-C7-C8-N2-N3
II-16a	C_6H_5	CH_3	53.90(8)
II-16b	C_6H_5	CH_2CH_3	58.28(6)
II-16c	C_6H_5	$CH_2CH_2CH_3$	57.91(6)
II-16h	C_6H_5	C_6H_5	54.79(8)
II-16j	4-CH_3-C_6H_4	CH_3	54.53(8) 55.87(8)
II-16k	4-MeO-C_6H_4	CH_3	52.38(6)
II-16l	4-Cl-C_6H_4	CH_3	54.09(7) 55.74(7)
II-16m	4-CF_3-C_6H_4	CH_3	52.8(4) 54.4(4)
II-16p	C_3H_5	CH_3	56.21(11) 56.45(13)
II-16q	C_6H_5	CH_3	53.18(11)
II-16r	C_6H_5	C_6H_5	58.58(9)

2.4 Dynamic studies of diazacyclobutenes (Δ^3-1,2-diazetines)

Generally diazacyclobutenes can be crystallized without much difficulty aside from those bearing long alkyl chains on the chalcogen. One of the common features we noticed in these crystal structures is the puckered geometry about the four- and five-member ring junction. For example the puckered nature of the diazacyclobutene **II-16cb** is evident in the X-ray crystal structure (Figure 2.5). The side view of **II-16cb** in Figure 2.5 clearly shows the angle between the planes of the four-membered diazacyclobutene ring and the five-membered urozole ring (4/5 ring planes) is 118°. This angle is also similar to the angle of C8-N3-C9 in **II-16bc** (Figure 2.5). This puckered nature was evident in all the diazacyclobutenes we synthesized.

Unlike previous diazacyclobutenes, due to this puckered nature and the 3, 4-disubstitution of the diazacyclobutene ring (*i.e.,* C9 and C10 substitutions based on the crystal structure numbering, *see* Figure 2.3 and 2.4), these molecules can exist as enantiomers. Surprisingly, when we carefully analyzed the crystal structures of these diazacyclobutenes, we saw the evidence of the enantiomers in the crystal structure.

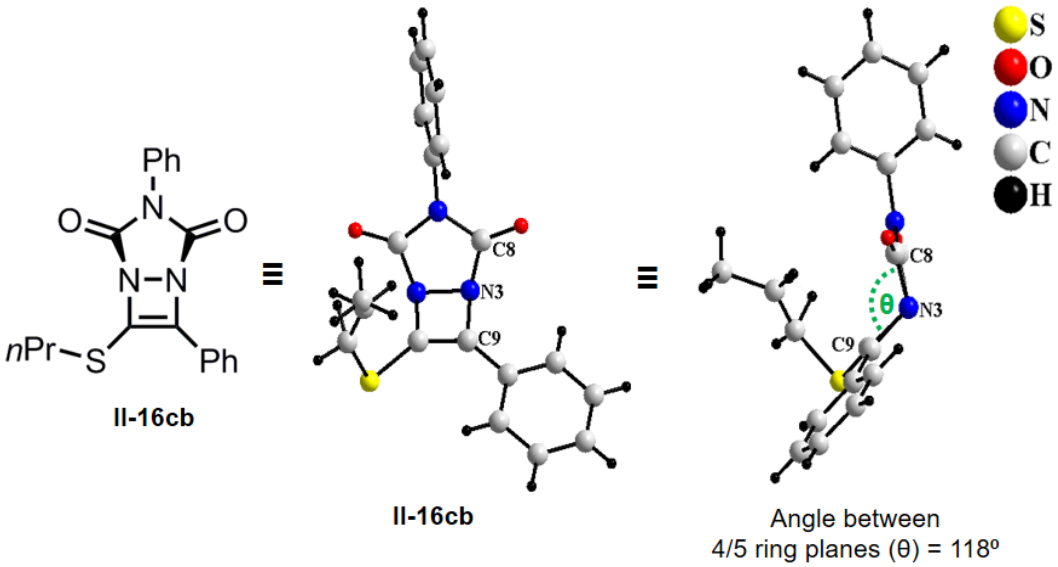

Figure 2.5. Puckered nature of the diazacyclobutene **II-16cb** evident in the X-ray crystal structure.

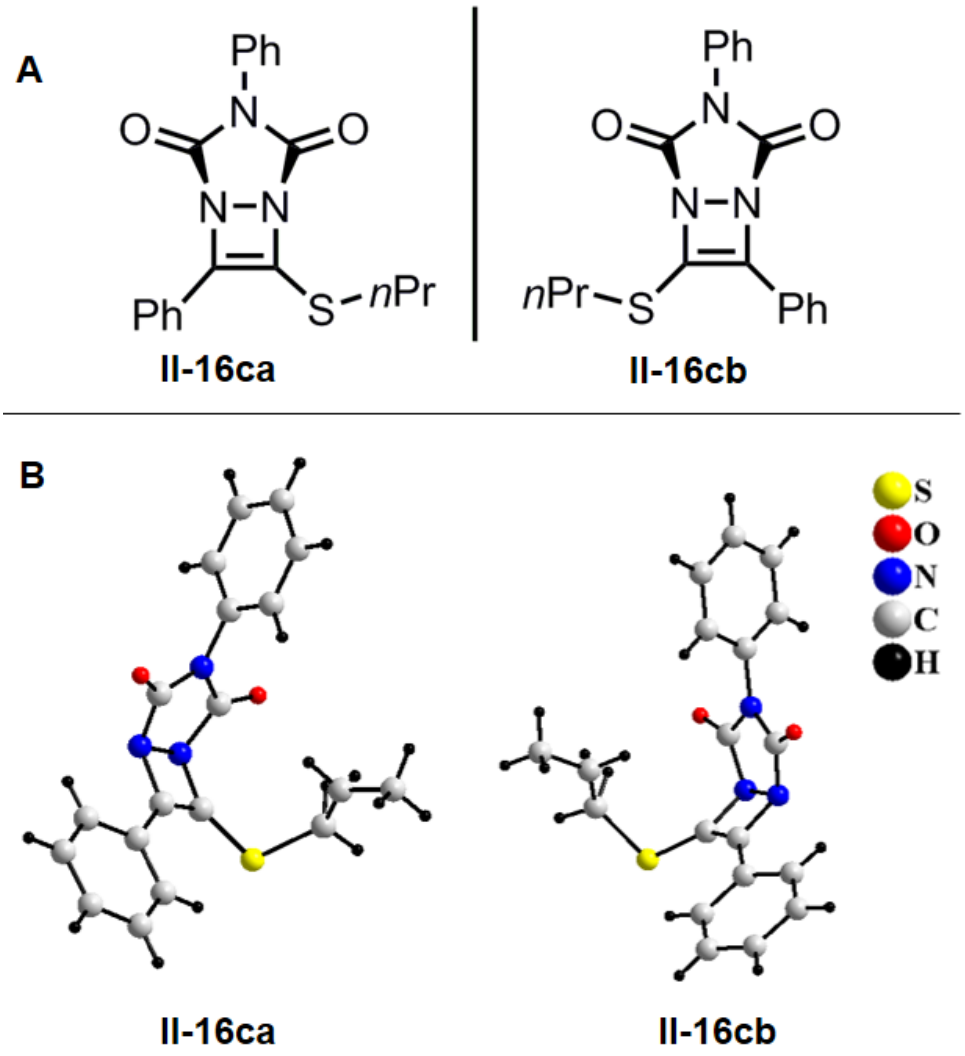

Figure 2.6. A. Chemical structures for the enantiomers of **II-16c** (**II-16ca** and **II-16cb**).

B. Enantiomers of **II-16c** evident in X-ray crystal structure.

Figure 2.6 illustrates the enantiomers evident in the X-ray crystal structure of diazacyclobutene **II-16c**. Isomer **II-16ca** and **II-16cb** are nonsuperimposable mirror images due to the puckered geometry and the 3,4-disubstitution. This characteristic behavior of diazacyclobutenes attracted us. We then tried to isolate these enantiomers in solution based studies by hoping that the successful isolation of these types of molecules could further expand this research area.

Isolation of the enantiomers using high performance liquid chromatography (HPLC) was unsuccessful. Then we turned to variable temperature NMR studies to carefully investigate the behavior of the diazacyclobutene enantiomers in solution. We took **II-16g** as the model compound to investigate this behavior. At room temperature, **II-16g** shows a clean singlet at 4.21 ppm (300 MHz ^{1}H NMR spectra in Figure 2.7) corresponding to the signal for the benzylic methylene protons. However, when **II-16g** is slowly cooled to –25˚C, the singlet at first broadens and then transforms to a coalescence point followed by resolution into a clean AB quartet or doublet of doublet (4.22 ppm, 4.15 ppm, J = 12.8 Hz, see stacked spectra in Figure 2.7).

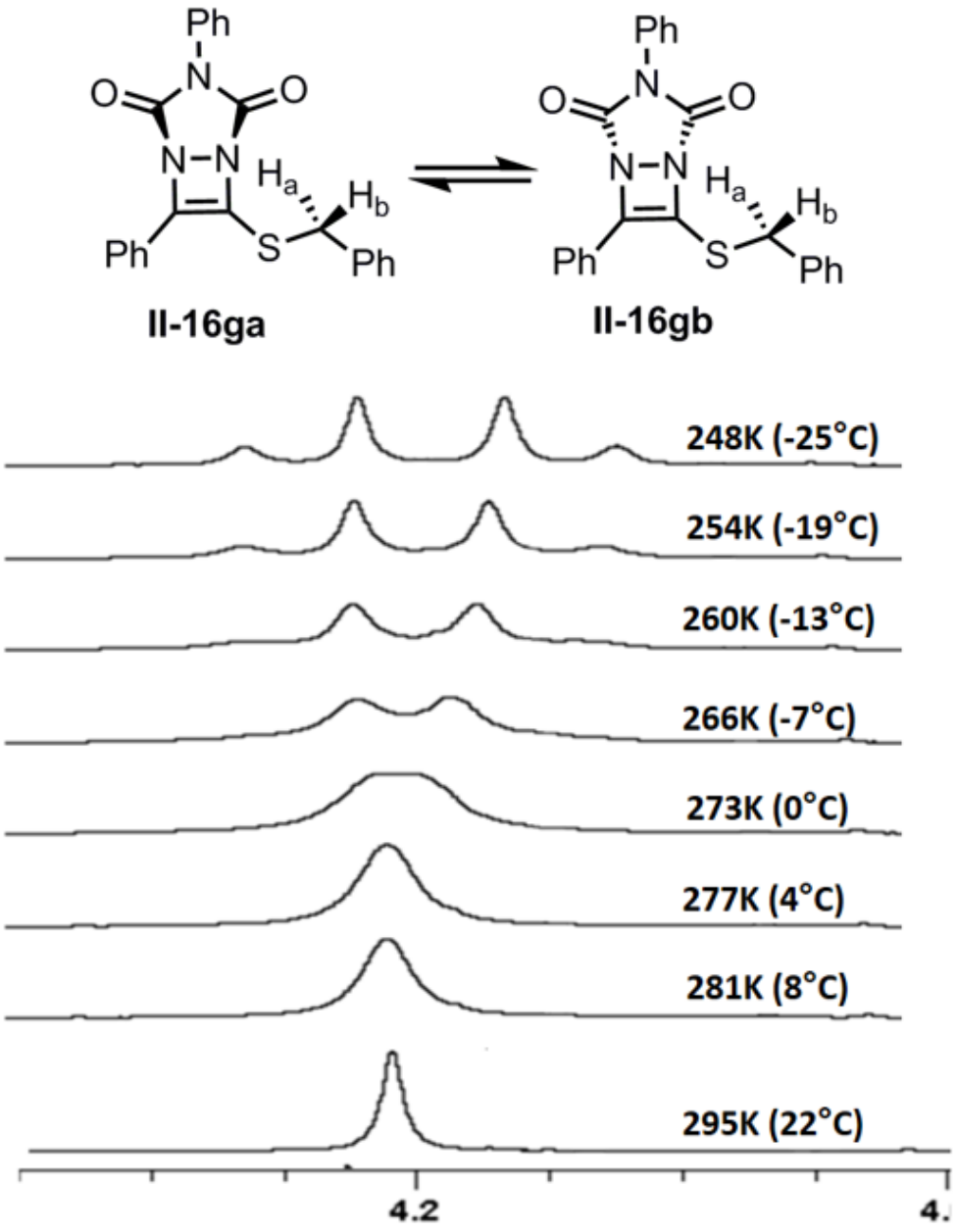

Figure 2.7. Temperature-dependent 300 MHz ^{1}H NMR experimental spectra of compound **II-16g** in $CDCl_3$.

This phenomenon is caused due to the diastereotopicity of the benzylic methylene protons at lower temperatures. At low temperatures (–25 ˚C), the barrier to nitrogen inversion is longer than the NMR time scale, thus rendering the two benzylic protons diastereomeric. Due to this phenomenon, H_a and H_b split each other into doublets in the NMR time scale and resolve into an AB quartet or doublet of doublet.

We then went forward and analyzed the double nitrogen inversion barrier for this isomerization process with the help of dynamic NMR (DNMR) line shape analysis.[67–69] Thus, we were able to simulate a theoretical spectrum for each experimental ^{1}H NMR spectrum of **II-16g** at the specific temperatures denoted above (Figure 2.7). This analysis was performed using Bruker Topspin version 3.5 software. First, the coupling constants (*J*, Hz) and the chemical shifts (δ, ppm) were extracted from the completely resolved doublet of doublet at the lowest temperature (–25˚C spectrum in Figure 2.7). Next, these *J* values and δ values were entered to the Bruker software and subsequently the exchange rate constant (K_{ex}) was varied until the best match of the theoretical spectrum was obtained for the corresponding experimental spectrum.

After this DNMR analysis, exchange rate constant (K_{ex}) values for each spectrum at each temperature [T (k)] were extracted and an Eyring plot (Figure 2.8) was generated by taking [1000/T] for the x-axis and [(Ln K_{ex} / T)] for the y-axis. Using the Eyring plot, the enthalpy barrier ($\Delta H^{\ddagger}$) for the double nitrogen inversion of **II-16g** and the entropy ($\Delta S^{\ddagger}$) for this process were calculated as 14.4 ± 0.7 kcal/mol and 3.2 ± 2.7 cal/mol·K,

respectively. Finally, the activation energy barrier for the inversion, ($\Delta G^{\ddagger}$) was determined to be 13.4 ± 0.7 kcal/mol at 298 K (25 ˚C).

The same analysis was performed for the S-ethyl methylene protons in **II-16b** and S-benzyl methylene protons of **II-16s** (R_1 = *p*-$CF_3C_6H_4$-), and the corresponding $\Delta G^{\ddagger}$ values at 298 K (25 ˚C) of all the compounds that were analyzed in this manner appear in Table 2.7.

These data show that the *para*-substituted electron withdrawing CF_3 group does not significantly influence the inversion barrier (Table 2.7). Additional studies on investigating the electronic and steric influence to the N-inversion barrier are currently in progress. The main idea here is to investigate the electronic influence, steric influence and the effect of additives such as Lewis acids/Brønsted acids on the barrier to double nitrogen inversion. Since these types of molecules have potential use in enantioselective organic reactions, this type of study will further our understanding on the possibility of "locking" one enantiomer of the diazacyclobutene over the other.

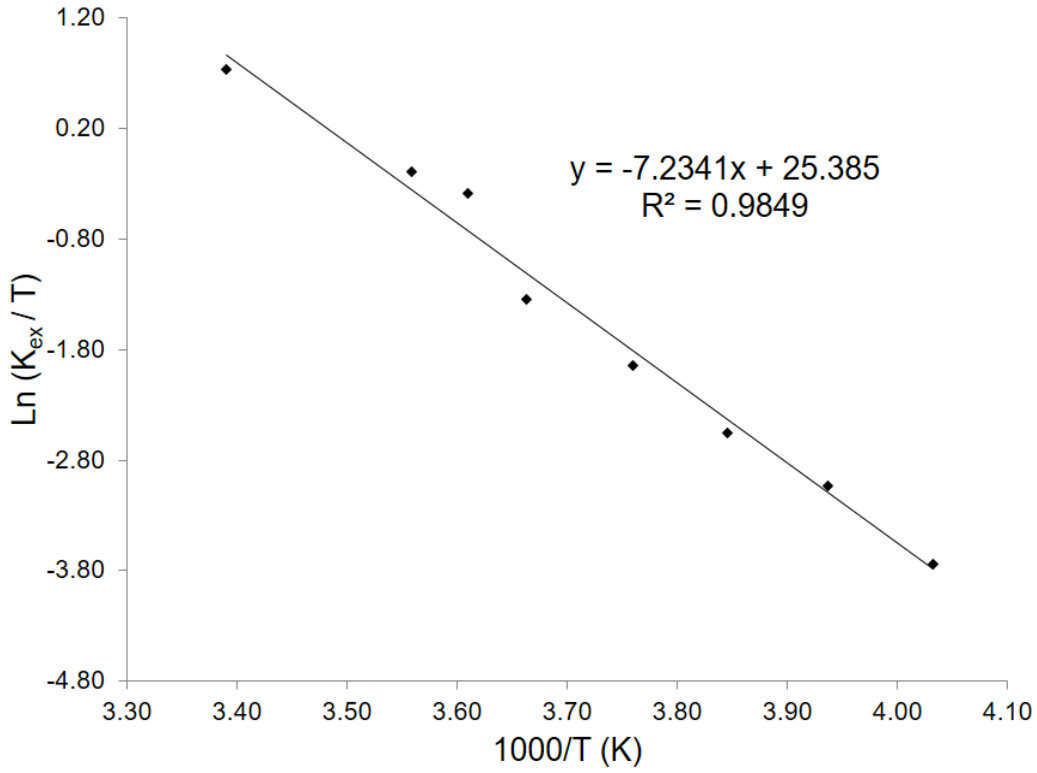

Figure 2.8. Eyring plot originated from simulated spectra for **II-16g** in $CDCl_3$.

Table 2.7. The activation energy barrier for the double nitrogen inversion ($\Delta G^{\ddagger}$) at 298 K (25 ˚C) for the compounds **II-16g, II-16b** and **II-16s**.

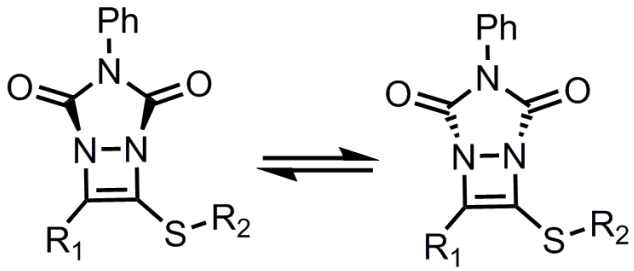

Compound No	R_1	R_2	$\Delta G^{\ddagger}$ (kcal/mol) at 298 K (25 °C)
II-16g	C_6H_5-	Bn	13.4 ± 0.7
II-16b	C_6H_5-	Et	13.6±0.5
II-16s	*p*-$CF_3C_6H_4$-	Bn	13.8±0.3

Based on the experimental results for **II-16g**, the exchange rate constant K_{ex} at 248K (–25˚C) =*ca.* 6 S^{-1} (*i.e.*, 6 inversions per second) and K_{ex} at 295K (22˚C) = *ca.* 600 S^{-1} (*ca.*600 inversions per second). This clearly indicates that enantiomers of the diazacyclobutene **II-16g** (**II-16ga** and **II-16gb**) are undergoing a rapid isomerization via double nitrogen inversion at room temperature.[35] It is apparent that during the double nitrogen inversion, the diazacyclobutene must isomerize via the intermediacy of a nearly planar transition state. Theoretically, this near planar transition state has the most overlap between the lone pairs of the two nitrogen atoms and the C=C double bond, which is the expected characteristic feature for a putative aromatic diazacyclobutene ring. Therefore, this rapid double nitrogen inversion of the diazacyclobutenes indirectly confirms that the planar diazacyclobutene intermediate is unstable relative to their puckered ground state geometry which is in good agreement with previous studies.

As mentioned earlier we also wished to further analyze the possibility of locking the diazacyclobutene enantiomers and to utilize them for further organic reactions. However, immediately we recognized that these types of variable temperature studies and calculations of the $\Delta G^{\ddagger}$ values and K_{ex} are tedious task for these types of screening studies. So we needed a quick read out method to understand whether we can lock or isolate the diazacyclobutene enantiomers while tuning the above mentioned factors. We realized that the simplest way to do this is to look for are solved ^{1}H NMR splitting correspond to the diastereotopic protons (as seen in Figure 2.7,–25˚C spectrum) or look for ^{1}H NMR peaks which has a higher line broadening (LB) correspond to the

diastereotopic protons (as seen in Figure 2.7, 0˚C spectrum at the coalescence point). This quick read out will save a lot of time in terms of searching for a method to lock these enantiomers. We studied the effect of several Lewis acids and Brønsted acids to see the possibility of locking **II-16g** diazacyclobutene enantiomers in solution via protonating the nitrogens of the diazacyclobutene ring. However, so far such attempts were unsuccessful. Further studies on these locking attempts will require further modifications of the diazacyclobutene molecule and such attempts are currently under progress.

Meanwhile, a more sterically bulky, dimeric diazacyclobutene compound was accessed using a bis-alkyne (**II-26**) and PTAD (**II-14**) by applying our previously optimized conditions (Scheme 2.9). Bis-alkyne (**II-26)** was first synthesized using the protocol described by Hoye's group by means of the deprotonation of the terminal alkyne followed by performing a nucleophilic substitution with an alkyl dihalide (Scheme 2.9, Eq. 1)[70]

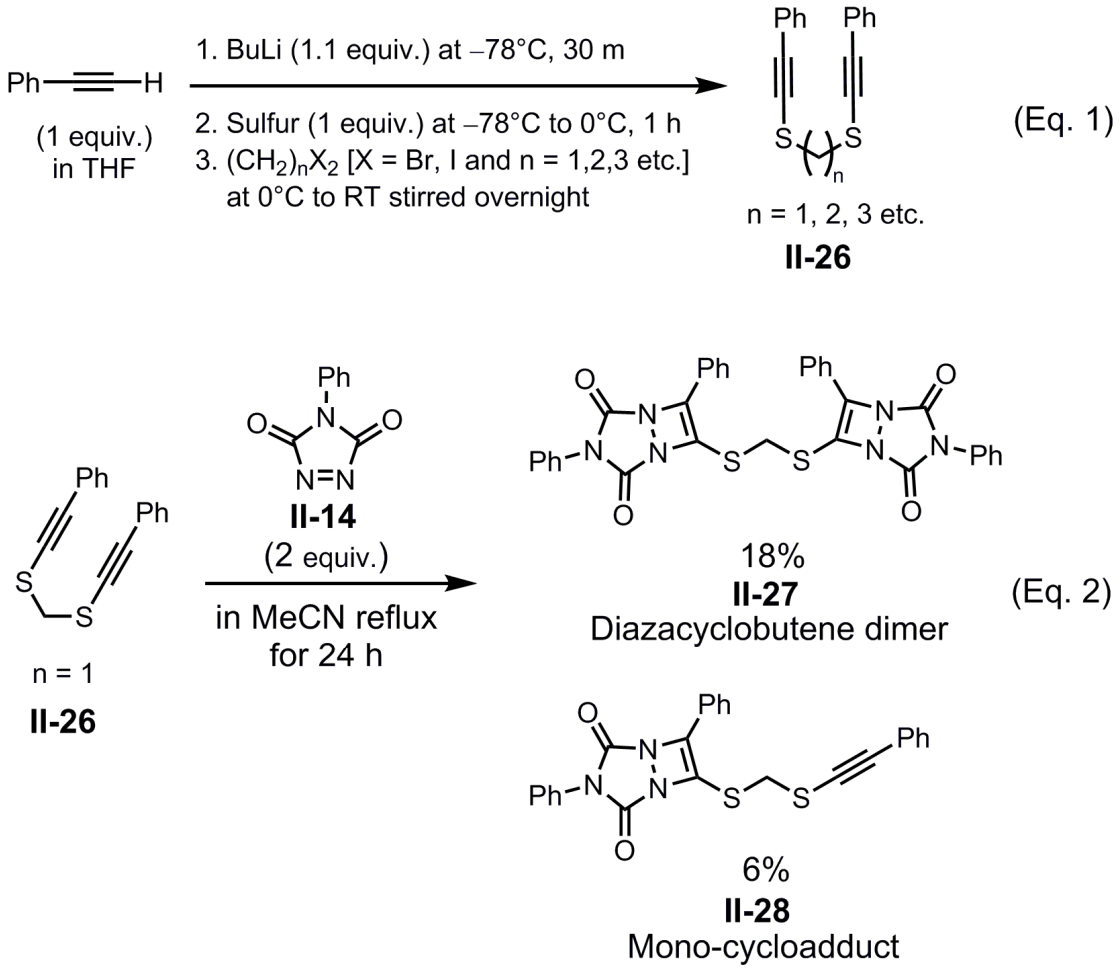

Scheme 2.9. Synthetic scheme for diazacyclobutene dimer.

Then the bis-alkyne (**II-26**) was reacted with 2 equivalents of PTAD (**II-14**) by refluxing in acetonitrile for 24 h in order to obtain a maximum yield of the diazacyclobutene dimer **II-27**. However, even with our previously optimized thermal conditions, we obtained 18% of the diazacyclobutene dimer **II-27** and also the mono-adduct **II-28** in 6% yield (Scheme 2.9, Eq. 2).

This diazacyclobutene dimer (**II-27,** n=1) is bridged by the sulfur-methylene-sulfur linkage. Interestingly, we saw that the line broadening (LB) value for the singlet corresponding to that bridged methylene protons of **II-27** was 24 Hz at room temperature ^{1}H NMR spectrum. Typical line broadening for unexchanged protons or rapidly isomerizing diastereotopic protons are about 1-2 Hz in ^{1}H NMR. Therefore, this high LB value was surprising. We then performed a variable temperature NMR study to reveal more insights of this molecule. This bridged methylene protons of **II-27** which appeared as a broad singlet at room temperature, was transformed to a clean doublet of doublet and a clean singlet upon gradual cooling to a very low temperature (<–30°C) (*see* Figure 2.9).

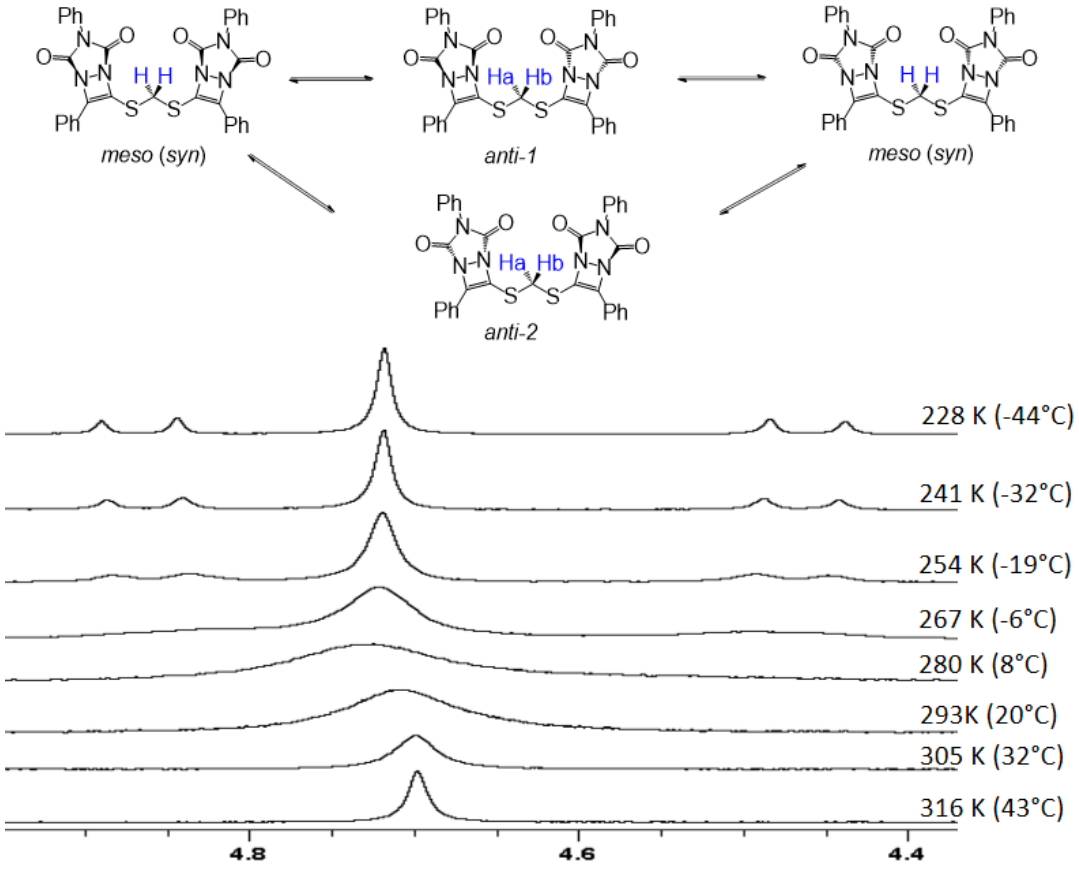

Figure 2.9. "Two hands waving dynamic effect" of the diazacyclobutene dimer (**II-27)** evident in variable temperature NMR in $CDCl_3$ (300 MHz ^1H NMR spectra).

We found that this singlet corresponds to a *meso (syn)* conformational isomer of **II-27**, whereas the doublet of doublets corresponds to enantiomeric, *anti* conformational isomers of **II-27** at low temperature. All three isomers were in a rapid equilibrium at room temperature which resulted in a broad singlet (LB = 24 Hz) for the bridged methylene protons of **II-27**. This rapid equilibrium of *meso (syn)* and enantiomeric (*anti*) conformational isomers of **II-27** demonstrates a fascinating dynamic behavior akin to "*two hands waving*".

Furthermore, we were able to obtain a crystal structure of **II-27** which showed a sandwich structure of the two phenyl rings (*see* Figure 2.10). We noticed that the distance between the two phenyl rings are about 4Å. We thought that this 4Å distance would facilitate sandwiching a transition metal ion inside the two phenyl rings with the help of π-interactions at low temperature. This sandwich X-ray crystal structure corresponded to the *anti*-conformational isomer, **II-27**. Table 2.8 presents the *syn*:*anti* ratio of **II-27** in several deuterated solvents tested at –45°C. Nonetheless, in most of the cases the *syn*-isomer of **II-27** is more favorable in solution than the *anti*-isomer of **II-27**. It is also important to note that only a few deuterated solvents were tested in this study due to poor solubility of **II-27** in other common solvents.

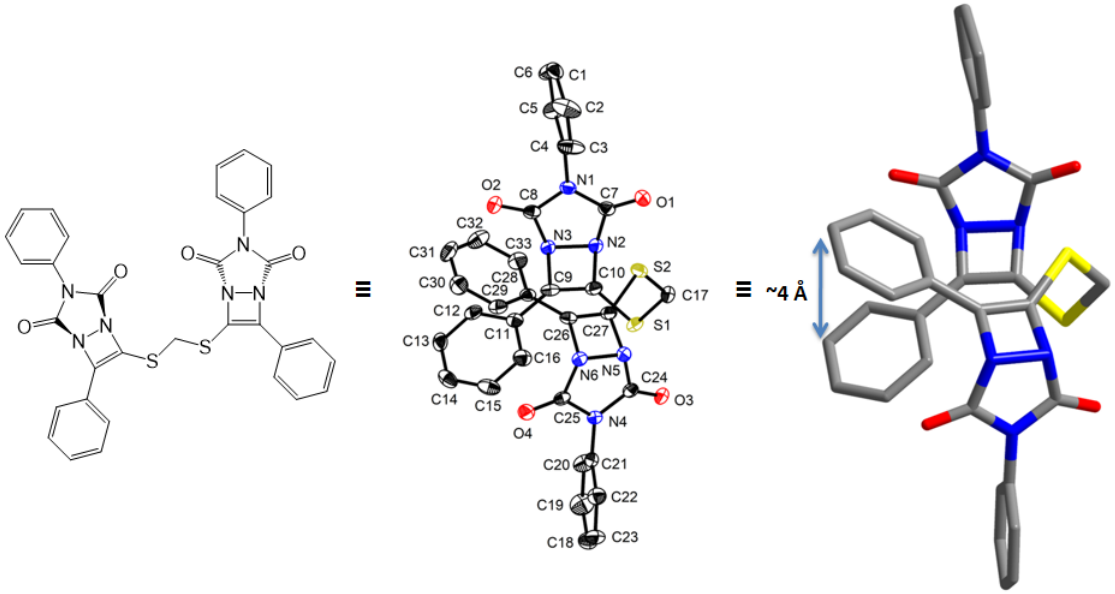

Figure 2.10. Sandwich arrangement of the phenyl rings evident in X-ray crystal structure of the bis-diazacyclobutene.

Table 2.8. *Syn*:*anti* ratio of diazacyclobutene dimer (**II-27**) in several deuterated solvents at –45°C.

Solvent system	***syn* : *anti*** **of II-27 at –45°C**
$CDCl_3$	80 : 20
30% CD_3OD : 70% $CDCl_3$	80 : 20
THF-d8	70 : 30

Further studies to enrich the percentage of the *anti*-diazacyclobutene conformational isomer and enhance the synthetic yield of the **II-27** are in progress. The studies of the diazacyclobutene dimer discussed in this section are unpublished results and further research studies are in progress in order to enhance the synthetic yields of the dimer. Therefore the reader is encouraged to read the future published peer-reviewed articles that the Whitehead group publishes for more details.

2.5 Biological studies of diazacyclobutenes.

N-containing heterocycles have been used as therapeutic agents and this has been reflected by the large number of nitrogen-containing FDA-approved drugs.[71–75] Also, compounds bearing the *vic*-diamine motif have been seen in leading drug candidates.[5,76–81] This information has been discussed extensively in Chapter I. Diazacyclobutenes are four-membered *N*-heterocycles that contain the *vic*-diamine motif. These molecules are rarely found, and there is a lack of biological studies for these molecules. The Whitehead laboratory has begun to study the anti-parasitic behavior of the diazacyclobutenes in collaboration with the Morris Laboratory (CU EPIC).[82,83] In further collaboration with Dr. Kristi Whitehead (CU Biological Sciences), we started to assess the biological activity of diazacyclobutenes and related compounds against gram-positive and gram-negative bacteria.

We have been able to test most of our compounds against parasites and found good potency with submicromolar half maximal effective concentration (EC_{50}). However, we have not seen any microbicidal activity at this point. We also performed cytotoxicity studies with the mammalian cell lines for the most potent diazacyclobutenes and they have showed very low toxicity profiles which are comparable with some of the common over the counter drugs.

Our preliminary biological evaluation results of parasites, bacteria and other cell lines shows that the diazacyclobutenes probably have selective activity against protozoan

parasites. Currently, the Whitehead lab is working on expanding these parasitic studies with other related parasites. The group is generating a library of compounds to test and find more lead compounds based on structure activity relationship (SAR) studies. Also, we are in the progress of claiming this novel antiparasitic diazacyclobutene invention and file the patents. Therefore reader is encouraged to read upcoming patents, peer reviewed articles from Dr. Whitehead laboratory.

2.6 Ongoing and future studies of diazacyclobutenes

In this section, diazacyclobutene synthesis with ynamides and ynamines as well as diazacyclobutene synthesis with 4-substituted 1,2,4-triazoline-2,5-dionesare discussed briefly.

This section also contains unpublished data and this research area is an actively working project in the Whitehead laboratory. Therefore the reader is encouraged to read the upcoming peer reviewed articles that the Whitehead group publishes for further details.

One of the interesting features of the diazacyclobutene scaffold that we synthesized compared to the previously reported diazacyclobutene is; the ability of expanding the substrate scope rapidly. So far it has been shown that the thio- and seleno-electron-rich alkynes can be used to synthesize diazacyclobutenes in good yields. In principle, we can use the ability of changing the chalcogen atom or the electron donor

atom of the electron-rich alkynes to synthesize a broad range of diazacyclobutenes where the electron donor atom can be changed to N, O, P, *etc.* (*see* Scheme 2.10). It is important to note that the electron donor atom is necessary to promote the formal [2+2] cycloaddition to occur based on our initial experiments with commercially available, non-activated terminal alkynes and previous reports.[44,84] We also hypothesized that an electron deficient atom such as boron might be used with the assistance of an electron-rich species to coordinate with boron to pump electron towards the alkyne to perform the [2+2] cycloaddition. So far for the development of this chemistry we have used commercially available cyclic azodicarboxylate 4-phenyl-1,2,4-triazoline-2,5-dione (PTAD). Furthermore, 4-substituted 1,2,4-triazoline-2,5-diones can be prepared by previously reported protocols which can be used to synthesize a wide range of diazacyclobutenes consist of a 4-substituted five-membered urozole ring (Scheme 2.10).

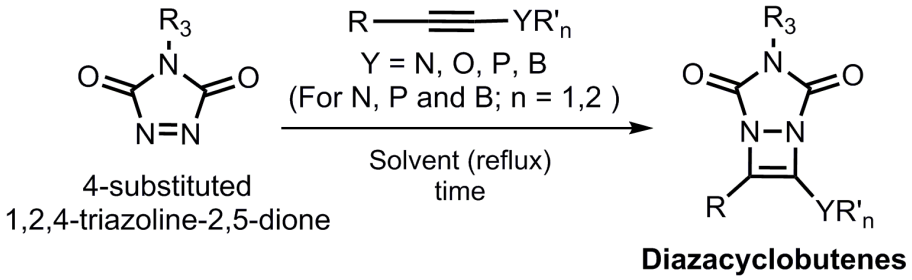

Scheme 2.10. Expanding the diazacyclobutene scope with electron donor atom and *4*-substituted 1,2,4-triazoline-2,5-diones.

2.6.1 Diazacyclobutene synthesis with ynamides and ynamines.

As mentioned in Scheme 2.10 diazacyclobutenes bearing a substituted amide or amine group at the 3rd position of the core ring could be synthesized using ynamides or ynamines. As previously discussed in Chapter I, additional nitrogen in the molecule could significantly change the biological activity of the molecule.[73] To test the possibility of synthesizing these types of diazacyclobutenes, we first synthesized tosyl ynamides.[85–90] We first tried the ynamide synthesis with vinyl dihalides[85,91,92] (Example not shown), however due to the low yield of vinyl dihalide we turned towards the bromoalkyne route[86–90] for the routine attempts in our laboratory. We first synthesized the bromoalkyne **II-29** (in 88% yield) from a terminal alkyne by treating it with *N*-bromosuccinimide (NBS) in the presence of silver nitrate (Scheme 2.11, Eq. 1). Then the bromoalkyne was treated with *N*-tosyl-*N*-methylamine (**II-30**) under reflux conditions with a mild base in the presence of a copper catalyst (Scheme 2.11, Eq. 2) to provide the corresponding ynamide **II-31** in 99% yield.

This ynamide (**II-31**) is then reacted with PTAD (**II-14**) to synthesize the corresponding diazacyclobutene **II-32** (Scheme in Table 2.9). Our initial attempts are highlighted in Table 2.9.

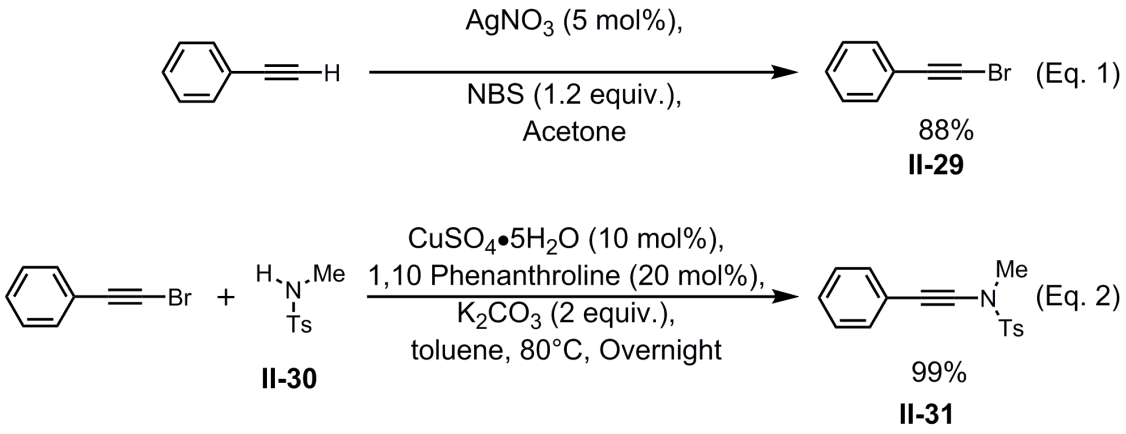

Scheme 2.11. Ynamide synthesis.

Table 2.9. Diazacyclobutene synthesis from ynamides.

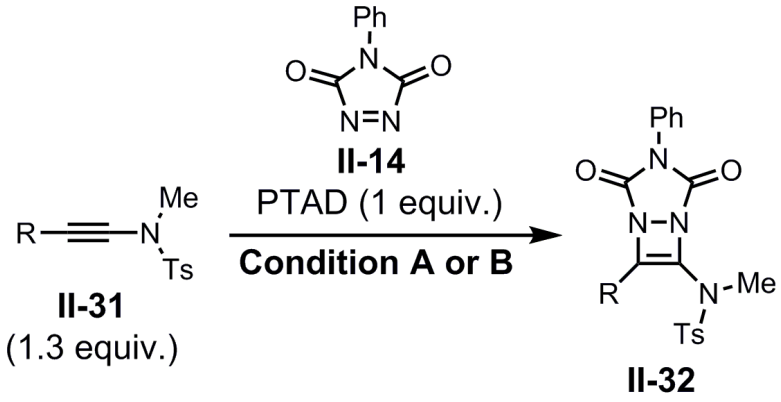

Condition A : Refluxed for 24 h in MeCN
Condition B : Stir with 5 mol% of $AgNTf_2$ catalyst for 24 h in DCM at RT

Entry	R	Condition	Yield% of II-32
1	C_6H_5-	A	20
2	C_6H_5-	B	27
3	C_6H_5-	B, with water work up	13
4	*p*-CF_3-C_6H_4-	A	37
5	*p*-CF_3-C_6H_4-	B	40

In these initial attempts, we used two different reaction conditions. The first condition was our initially optimized acetonitrile reflux protocol (condition A)[84] and the second condition was a catalytic method at room temperature in the presence of silver *N*-triflate (condition B) (Table 2.9). Silver *N*-triflate was found to be active in the [2+2] cycloadditions of siloxyalkynes and α,β-unsaturated ketones in the literature.[48] Also, we used two different ynamide derivatives, R = Ph and R = *p*-CF_3-Ph. As illustrated in Table 2.9; the silver catalyst (condition B) seems to provide better yields compared to our previously optimized thermal condition (condition A) for both ynamide derivatives (Table 2.9, Entry 1-2 and 3-4).

These yields are considered to be moderate or low, which need further optimization. We believe that the low yields result due to the significant electron withdrawing effect of the sulfonyl group on the ynamide. Interestingly, the ynamide bearing R = *p*-CF_3-Ph showed slightly higher yields than the substrate bearing R = Ph. Presumably, the electron withdrawing nature of *p*-CF_3 group is supporting progress of the reaction by offsetting the electron-withdrawal of the sulfonyl group on the alkyne. Furthermore, we noticed that upon aqueous work up, the yields of the diazacyclobutene **II-32** dropped down by half (Table 2.9, Entry 3). We are currently working on further understanding the ynamide-azodicarboxylate chemistry in order to optimize this reaction with different catalytic conditions[93–95] to obtain higher yields of the ynamide-based diazacyclobutenes.

Literature studies have been shown that many metal catalysts such as alkaline earth metals like magnesium (II),[93] transition metal ions such as scandium (III),[96,97] copper (I and II),[95,98] nickel (0),[95] rhodium (I)[94] and post-transition metal ions such as tin (IV),[99] and indium (III)[100] have been used to aid the [2+2] or [4+2] cycloadditions of α, β-unsaturated ketones, imines, nitro alkenes, *etc.* So, we hypothesize that further tuning of the reaction conditions to a milder catalytic condition will provide higher yields as well as a convenient approach to access these diazacyclobutenes at room temperature.

Next, an ynamine was synthesized using a haloalkyne and secondary amine according to the protocol reported by Jeong *et al.*[101] We tested the reactivity of this substrate with azodicarboxylates under our previously optimized thermal conditions (Example not shown).[84,102,103] Unfortunately, there was no significant reactivity seen in the initial attempts. Based on NMR analysis of the crude and purified ynamine; we noticed that the ynamine is highly moisture sensitive. We hypothesized that based on the literature and our experimental analysis, the ynamine can react with water and perform a hydration reaction (Scheme 2.12). As displayed in Scheme 2.12; ynamine **II-33** can undergo protonation by water to produce an intermediate **II-34**. Then, nucleophilic attack of hydroxide on **II-34** will produce the corresponding enol **II-35**. Finally enol **II-35** could convert to the corresponding amide **II-36** via keto-enol tautomerism.[104]

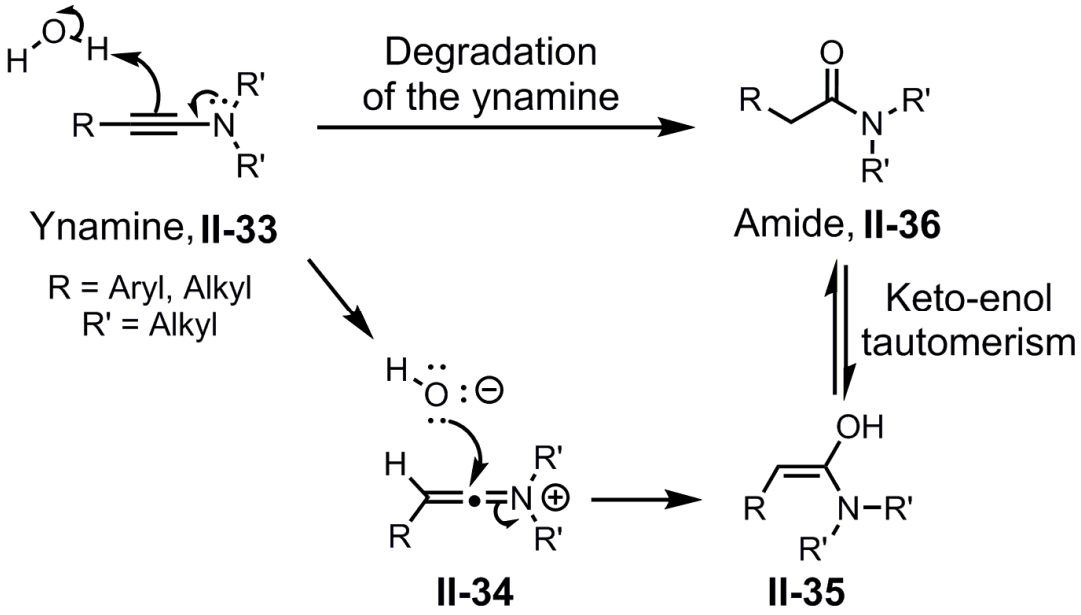

Scheme 2.12. Plausible pathway of ynamine degradation in the presence of moisture.

We believe that due to the moisture sensitivity of the ynamine and the possibility of the ynamine acting as a nucleophile to the azodicarboxylate during the reaction under high temperature, these reaction conditions also need further attention to modify the conditions to milder reaction conditions while preventing the ynamine from converting to the corresponding amide. It has been shown in the literature that magnesium bromide can act as a Lewis acid to perform [2+2] cycloadditions between ynamines and cyclic enones in excellent yields.[93] So we think that we still have a good chance to modify this ynamine-azodicarboxylate chemistry to obtain better yields under catalytic one-pot reaction conditions.

2.6.2 Diazacyclobutene synthesis with 4-substituted 1,2,4-triazoline-2,5-diones (TADs).

As a result of expanding the diazacyclobutene scope, we identified that 4-substitution of the 1,2,4-triazoline-2,5-dione ring will serve as an ideal platform to rapidly access a wide range of diazacyclobutene derivatives.[6] One of the common routes to access 4-substituted 1,2,4-triazoline-2,5-diones (TADs) is via isocyanates by first converting the isocyanates into the corresponding semicarbazide, followed by cyclization to the urozole, followed by oxidation Scheme 2.13, 2.14 and 2.15).[6,105–112]

To begin this study we first synthesized a handful of semicarbazides via isocyanates. Isocyanate **II-38** can be reacted with ethyl carbazate **II-37** under reflux conditions with toluene to obtain the corresponding semicarbazide **II-39** (Scheme 2.13). Semicarbazides **II-39a** and **II-39b** bearing alkyl groups such as *iso*-propyl and *n*-butyl groups at the R position were synthesized in moderate yields (43% and 69%, respectively). Derivatives of semicarbazides bearing chloroalkyl groups such as chloroethyl (**II-39c**), and chloro *n*-butyl (**II-39d**) were also generated in moderate to good yields (49% and 79%, respectively). The importance of these haloalkyl derivatives is that they can be use in late stage modifications of the diazacyclobutenes via further orthogonal chemistry such as nucleophilic substitution reactions, click chemistry, *etc.*[106,113,114]

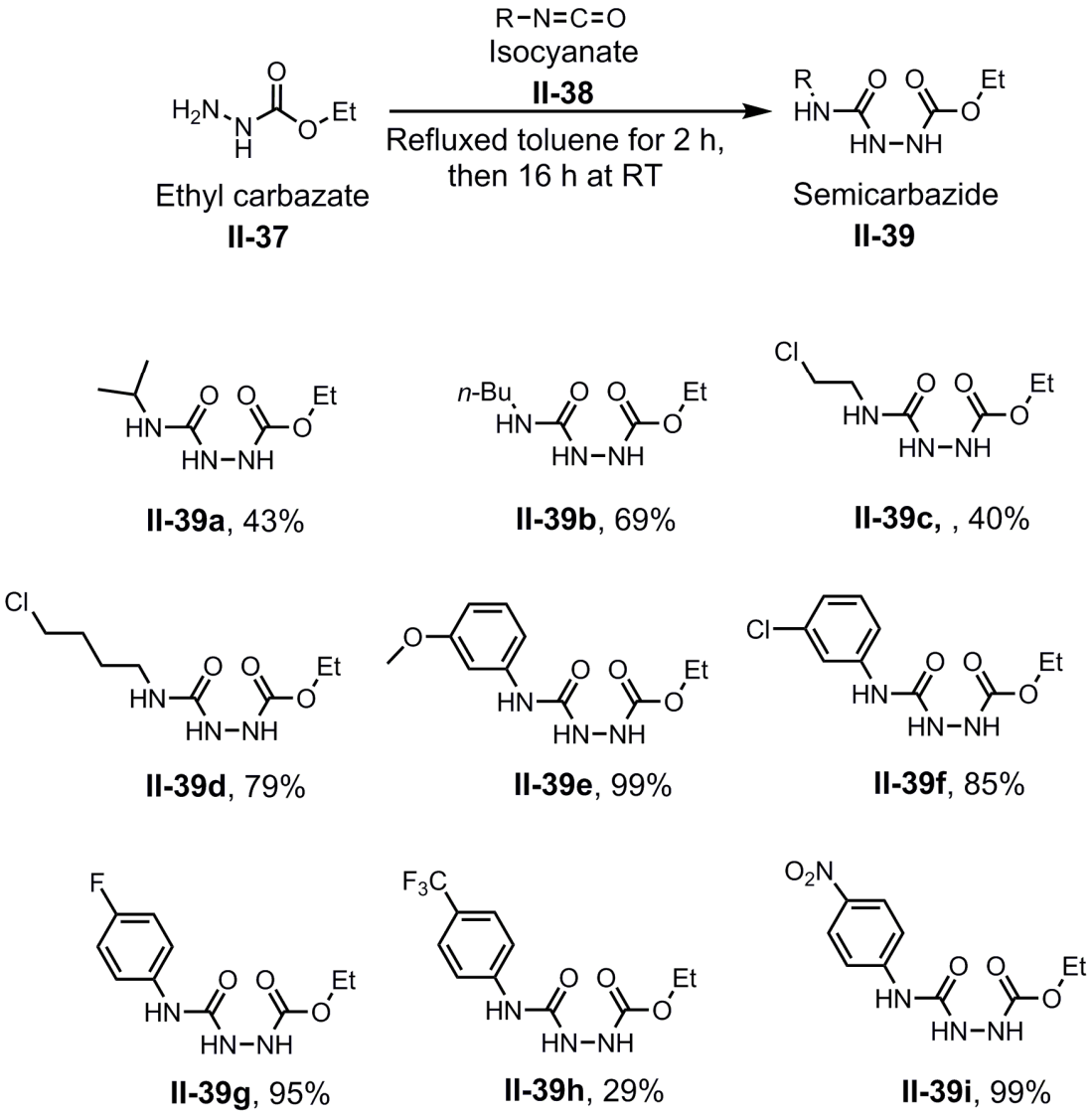

Scheme 2.13. Semicarbazide synthesis and scope.

Semicarbazide derivatives bearing substituted aryl groups at the R position – consisting of both electron-donating and withdrawing groups (*i.e.*, *m*-MeO-C_6H_4-, *m*-Cl-C_6H_4-, *p*-F-C_6H_4-, and *p*-NO_2-C_6H_4- (**II-39e-g and II-39i**) were generated in 85–99% yields. However the corresponding *p*-CF_3-C_6H_4- analog **II-39h** was generated in a lower, 29% yield.

These semicarbazides were then converted to the corresponding urozoles by base-mediated cyclization (Scheme 2.14). Initially the aryl analogs of the semicarbazides (**II-39e-i**) were conveniently converted to their corresponding urozole. Urozole derivatives bearing 4-substituted *m*-MeO-C_6H_4- and *m*-Cl-C_6H_4- were generated in 35% and 44% yields, respectively (**II-40e** and **II-40f**). Urozole analogs bearing *p*-F-C_6H_4-, and *p*-NO_2-C_6H_4- groups such as **II-40g** and **II-40i** were synthesized in moderate to excellent yields (63% and 87% yield, respectively). Again the *p*-CF_3-C_6H_4- urozole analog **II-40h** was isolated in very poor yield (16%). We noticed that the corresponding semicarbazides bearing alkyl groups at the R position were reluctant to cyclize to the urozole and precipitate out during the neutralization work-up step as compared to their aryl congeners.

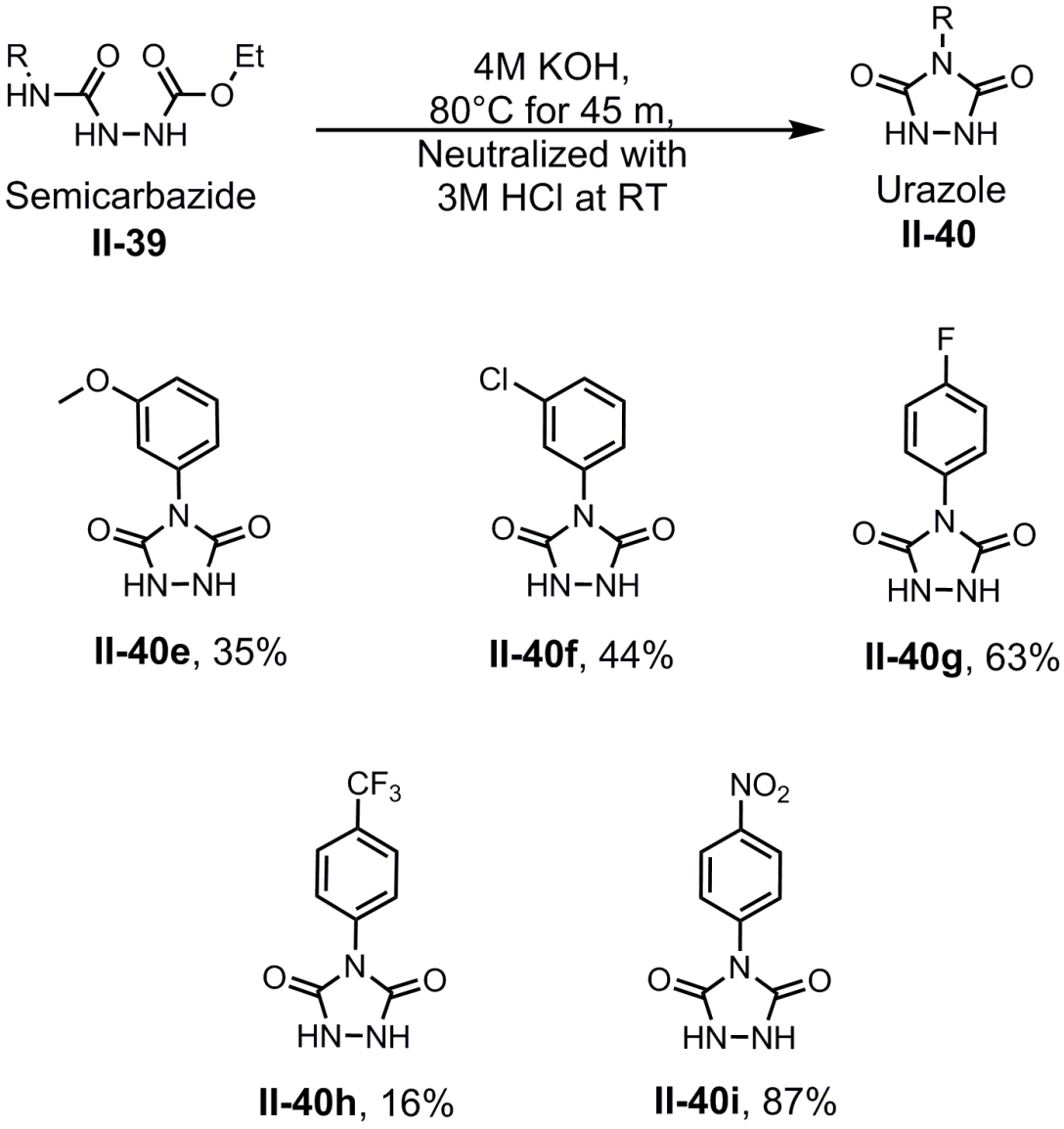

Scheme 2.14. Urozole synthesis and scope.

Then we tried a couple of oxidation methods on the urozole and found that oxidized 4-substituted triazoline-2,5-diones are highly unstable while handling, purification, and processing to the final [2+2] cycloaddition step.[107] Both the iodobenzene diacetate oxidation[108,115–117] and the 1,3-dibromo-5,5-dimethylimidazoline-2,4-dione (DBH) oxidation[107] methods generated the corresponding 4-substituted 1,2,4-triazolind-2,5-dione (TAD) product (Scheme 2.15). However, both methods generated byproducts such as acetic acid and the 5,5-dimethylhydantoin which remained in the final oxidized TAD product. Attempts to remove those byproducts with further purification treatments dropped down the yield of the TAD product and in some cases the TAD degraded while processing further. For example the TAD derivative bearing a *p*-NO_2-C_6H_4- group was completely degraded while removing the solvent.

From a synthetic standpoint, performing the [2+2] cycloaddition to make the dazacyclobutenes after the purification of the oxidized TAD derivative is not productive, due to this higher instability of the oxidized TAD. We then attempted to develop a method which uses the *in situ* oxidation and subsequent [2+2] cycloaddition to avoid the difficulties of the instable TADs (Scheme 2.16).

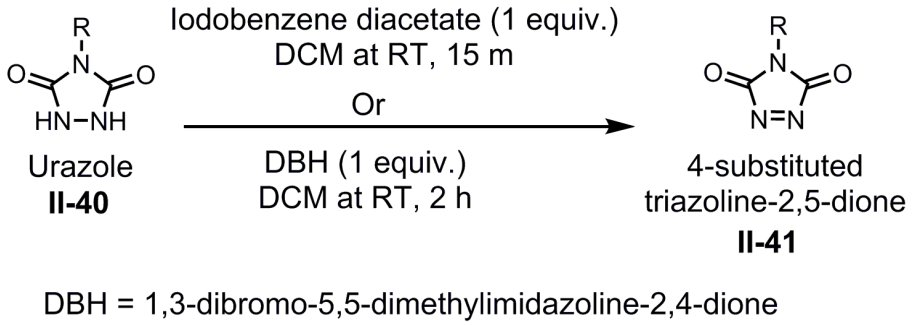

Scheme 2.15. Oxidation of urozole.

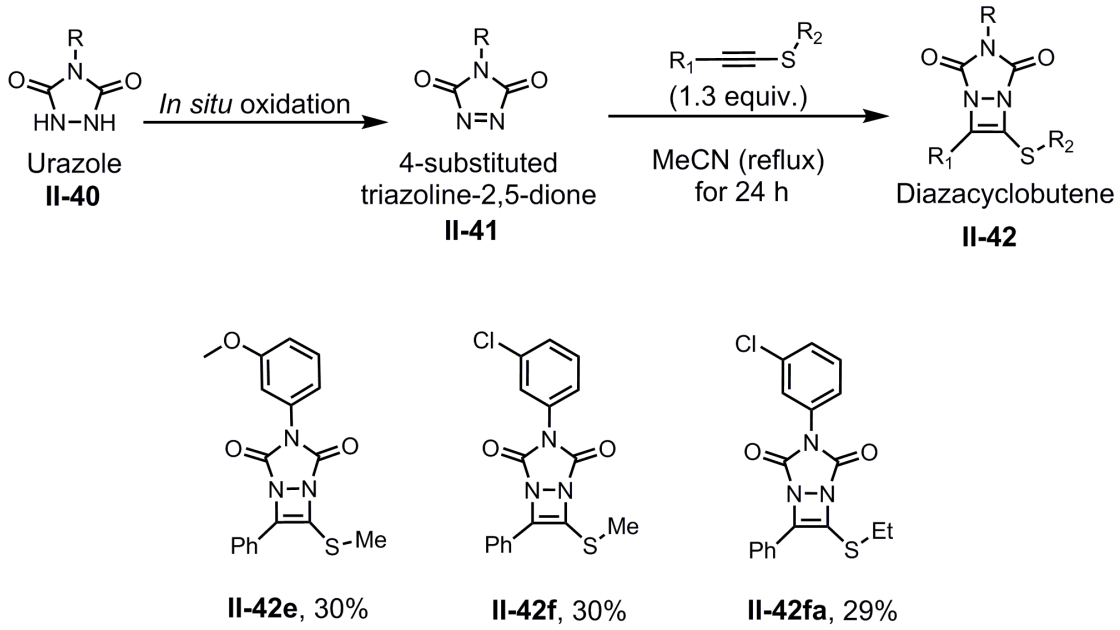

Scheme 2.16. *In situ* oxidation and [2+2] cycloaddition. Note that the final diazacyclobutene yields are based on the unoxidized urozole equivalence.

Initially, a few derivatives of diazacycobutenes were made using in situ prepared TADs bearing *m*-MeO-C_6H_4- and *m*-Cl-C_6H_4-groups (Scheme 2.15, **II-42e**, **II42f**, **II-42fa**). These TADs were made by the *in situ* oxidation of the corresponding urozole and subsequent [2+2] cycloaddition was performed according to the previously optimized conditions after adding the electron-rich alkyne (Scheme 2.16). These new diazacyclobutenes (**II-42e**, **II42f**, **II-42fa)** were generated in rather poor yield (*ca.* 30% based on the unoxidized urozole equivalence).

2.6.3 Development of an in situ catalytic method for [2+2] cycloaddition to provide diazacyclobutenes with 4-substituted 1,2,4-triazoline-2,5-diones (TADs).

This section of the catalytic study contains unpublished data and this part of the study was performed with the collaboration of a fellow colleague, Brock Miller (Clemson University, advisor: Dr. Daniel C. Whitehead). This research area is an actively working project in the Whitehead laboratory. Therefore this part is described in concise manner and the reader is highly encouraged to read the upcoming peer-reviewed articles that the Whitehead group publishes for further details.

Finally, after understanding all these issues, we then attempt to modify our methodology to a milder, one-pot catalytic method to perform the [2+2] cycloaddition at room temperature (Table 2.10). We initially tested a series of catalysts (25 catalysts, 19 metal ions) for this *in situ* oxidation and [2+2] cycloaddition method, such as alkali metal (*e.g.* Li(I)), alkali earth metal (*e.g.* Mg(II)),[93] transition metals (*e.g.* Sc(III),[96,97] Ti(IV),

Co(II), Co (III), Ni (II), Cu (I), Cu (II),[98] Zn (II), Pd (II), Ag (I),[48] Pt (IV), and Au (III)), post-transition metals (*e.g.* Al (III), Sn (II), Sn (IV),[99] and In (III)),[100] lanthanide metal (*e.g.* Yb (III)).[96] In these trials we used a milder oxidation method using calcium hypochlorite (*i.e.*, $Ca(OCl)_2$) and also used a large excess of urozole in order to confirm that sufficient TAD (**II-14**, Table 2.10) had been oxidized in order to perform the follow-on [2+2] cycloaddition. Moreover, the catalytic [2+2] cycloaddition was performed in dichloromethane for 24 h at room temperature. Out of all these trials, the best yielding attempts are summarized in Table 2.10.

The main motivation for the exploration of this extensive catalytic study was that we wanted to see how the metal ions interact with azodicarboxylates more broadly for the [2+2] cycloaddition. Furthermore, at this point in time we had invented a novel reaction to synthesize a biologically relevant five-membered *N*-heterocycle known as tetrahydroindoles using electron-rich alkyne and azodicarboxylate chemistry which also utilizes this [2+2] cycloaddition as the first step. This reaction will be broadly discussed in Chapter III.

Table 2.10. Development of an *in situ* catalytic method for [2+2] cycloaddition.

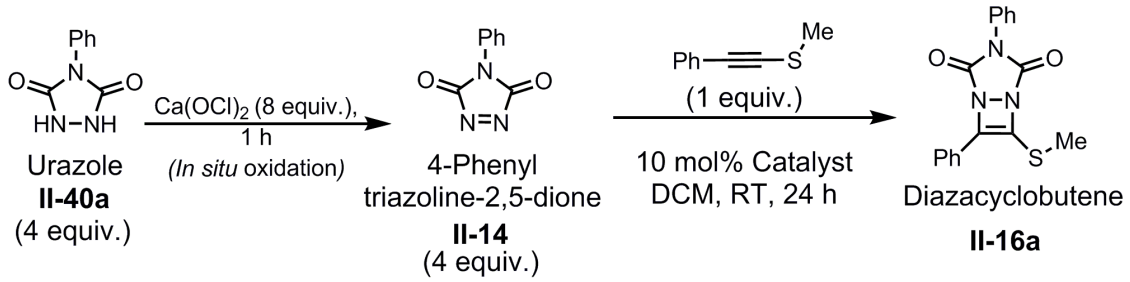

Entry	Catalyst (Lewis Acid)	Isolated Yield%
1	-	28
2	$Sc(OTf)_3$	66
3	AgOTf	60
4	$Cu(OAc)_2$	62
5	TiO_2	71
6	$MgCl_2$	68
7	$SnCl_4$	81 [26][a]
8	$MgCl_2$	98[b]

[a]Sn(IV) gave inconsistent results. [b]Used 30 mol% catalyst, 2 h oxidation time and 3 equiv. of the urozole.

Interestingly, this tetrahydroindole synthesis reaction utilizes an intermediate step similar to the Nazarov cyclization which often uses the assistance of Lewis acids (*See* Chapter III for more details of this reaction). So, we thought that performing a broader catalytic screening for this initial [2+2] cycloaddition with PTAD (**II-14**) might provide a broader understanding of how metal ions interact with azodicarboxylates, which will in return help us to further manipulate and tune our electron-rich alkyne and azodicarboxylate chemistry for other studies such as tetrahydroindole synthesis.

As shown in Table 2.10, the inexpensive phenyl urozole (**II-40a**) was selected for this optimization and a large excess (*i.e.*, 4 equiv.) of the **II-40a** was oxidized with calcium hypochlorite for 1 hour to obtain the oxidized PTAD (**II-14**). This PTAD (**II-14**) was then reacted with the methyl phenylacetylene sulfide (1 equiv.) in DCM for 24 h in the presence of 10 mol% of the catalyst. First, without the catalyst, the reaction underwent relatively poor conversion to yield the diazacyclobutene **II-16a** (28% yield, Table 2.10, Entry 1). Catalytic reactions performed with $Sc(OTf)_3$, AgOTf, $Cu(OAc)_2$, TiO_2, and $MgCl_2$ produced the diazacyclobutene **II-16a** in 60–70% yield (Table 2.10, Entry 2-6). Even though $SnCl_4$ initially gave promising results by providing the desired product in 81% yield, it was later found that $SnCl_4$ was less desirable due to its moisture sensitivity (Table 2.10, Entry 7). It is important to note that water is generated as a byproduct during the oxidation sequence. This moisture could inhibit the action of a catalyst if the catalyst is sensitive to moisture. After several trials, we found that $SnCl_4$ was an ineffective catalyst presumably due to the tendency of reacting with moisture and

perhaps producing HCl fumes, which in turn could protonate or hydrolyze the oxidized TADs. Finally, we further optimized the reaction and found that 30 mol% $MgCl_2$ catalyst with 2 h oxidation time and 3 equiv. of the urozole can produce the diazacyclobutene **II-16a** in 98% yield (Table 2.10, Entry 8).

Currently, more efforts are in progress to expand the substrate scope of this transformation by applying the optimized one-pot catalytic protocol with a broad range of 4-substituted urazoles and electron-rich alkynes. We are also interested in investigating the orthogonal synthetic manipulation (nucleophilic substitution, click chemistry etc.),[106,113] performing late stage modifications, and broadly studying the biological activity[82,83,108,118,119] of this unique class of diazacyclobutenes. Also, further reactions with the double bond of the diazacyclobutenes such as reduction,[58,59] alkene-like reactions[59] as well as hydrolysis[45,120] of the urozole ring, oxidation[121] and desulfurization[122,123] attempts are underway.

2.7 Conclusions.

In summary, by using cyclic azodicarboxylate and electron-rich alkynes, we have successfully developed a convenient route to access a wide range of four-membered *N*-heterocycles containing the *vic*-diamine motif known as diazacyclobutenes (Δ^3-1,2-diazetine). This cycloaddition provides a rapid route to a broad substrate scope (25 examples in this document) of diazacyclobutenes in moderate to good yields.

Almost all the diazacyclobutenes we synthesized are crystalline which is a good fact based on the pharmaceutical standpoint. One of the important features of this diazacyclobutene-core ring is that it formally follows the Hūckel rule for aromaticity. Extensive study of the crystallographic structures by analyzing the 4/5 planar angle between the diazacyclobutene and the urozole ring suggest that our suite of diazacyclobutenes are not aromatic.

Further studies of the dynamic behavior of the diazacyclobutene in solution revealed that, diazacyclobutenes are rapidly isomerizing through the double nitrogen inversion via a near planar transition state ($\Delta G^{\ddagger}_{\text{Inversion (298 K)}}$ = 13.4 ± 0.7 kcal/mol). Theoretically, this near planar transition state is the aromatic analog of the diazacyclobutene and has the most overlap between the lone pair nitrogens and the double bond in the four-membered ring. However, with the evidence of this rapid isomerization in solution, it further suggests that this aromatic analog does not exist as a stable molecule even in solution. Moreover, the diazacyclobutene dimer, which has two

diazacyclobutene units bridged by sulfur-methelene-sulfur linkage, showed a fascinating dynamic behavior akin to “two hands waving” by rapidly equilibrating between *meso*, *anti* and *syn* conformational isomers.

Diazacyclobutene synthesis with ynamines, and ynamides did not proceed in good yields compared to their thio- and seleno- analogs with the optimized thermal conditions. However, the initial catalytic screening studies of the formal [2+2] cycloaddition reaction to provide diazacyclobutenes with *in situ* oxidized 4-substituted 1,2,4-triazoline-3,5-diones showed promising results which could significantly increase the broad utility of these novel compounds.

Additionally, diazacyclobutenes showed excellent antiparasitic activities by showing submicromolar values for the half maximal effective concentration (EC_{50}). Cytotoxicity studies with the mammalian cell lines for the most potent diazacyclobutenes showed very low toxicity profiles.

2.8 Experimental section

2.8.1 General information

All common reagents were obtained from commercially available sources and used without purification. Dry tetrahydrofuran (THF) was prepared by distillation over sodium/benzophenone and dry acetonirtile (MeCN) was prepared by distillation over phosphorous pentoxide. JOEL 500 MHz, Bruker avance 300 MHz/500 MHz NMR spectrometers were used to collect ^{1}H and ^{13}C NMR spectra and chemical shifts were reported in parts per million (ppm). NMR spectra are calibrated and referenced based on the residual solvent peaks. Infrared spectroscopy data were collected using an ATR-FTIR instrument (Shimadzu IRAffinity-1S instrument with MIRacle 10 single reflection ATR accessory) and scanned over the range of 400 to 4000 cm^{-1}. Column chromatography was performed using flash silica gel (32-63 μm). TGA data was collected using TGA instrument SDT Q600 V20.9 Build 20 over the temperature range of 200 – 800˚C, with a ramp rate of 20˚C/min and under the nitrogen flow rate of 100mL/min. All previously known compounds were characterized by ^{1}H and ^{13}C NMR and are in complete agreement with the literature reported data. All novel compounds were characterized by ^{1}H and ^{13}C NMR, ATR-FTIR, XRD (where appropriate), melting point and HRMS.

2.8.2 A typical procedure for the preparation of alkynylthiolate.

Method1 (see Table 2.1)[50]

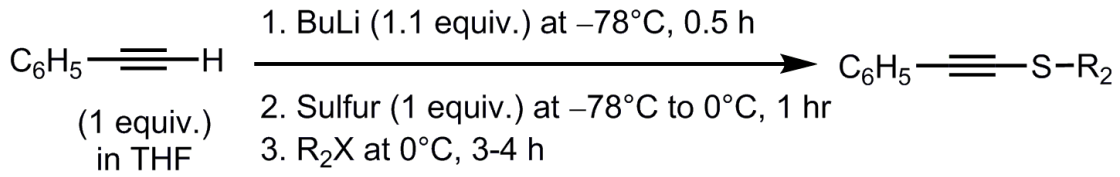

Procedure

A 2-neck round bottom flask was-flame dried, equipped with a stir bar and subsequently fitted with an argon balloon through a rubber septum. Then the flask was heated under argon to flush out any remaining air or moisture. After cooling, 25 mL of THF and the terminal alkyne/phenyl acetylene (5.0 mmol, 1 equiv) was added under argon atmosphere. The solution was then cooled to –78°C and stirred for at least 10 min. Then a solution of *n*-BuLi (5.5 mmol, 1.1 equiv, 1.6 M in hexane) was added and stirred for 15-30 min. After that, finely ground sulfur powder (5.0 mmol, 1 equiv) was added by briefly removing the septum and replacing it quickly. The resulting mixture was stirred at −78°C for 1 h. The mixture was then gradually warmed to 0°C until the sulfur was completely consumed to produce the red color lithium alkynylthiolate. The corresponding alkyl halide (5.0 mmol, 1 equiv) was then added in a dropwise fashion. After 4-6 h, the reaction mixture was quenched with sat.aq. NH_4Cl. The water layer was extracted with diethyl ether (3 x 10 mL).

The combined ether extract was washed with sat. aq. brine. The organic layer was then dried over Na_2SO_4 and the solvent was evaporated under reduced pressure. The crude residue was then purified by flash chromatography (silica gel, hexanes) to afford the alkynyl sulfide (The corresponding yields appear in **Table 2.1** above).

Method 2 (See Table 2.2)[49,51]

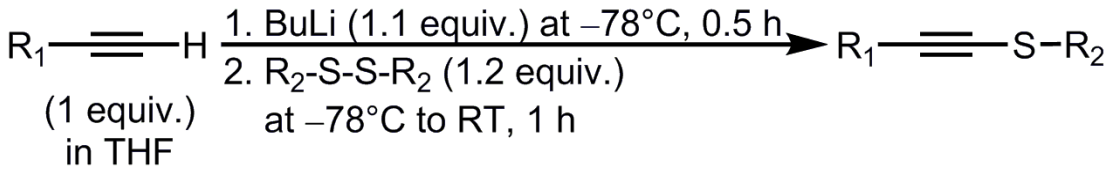

Procedure

A flame-dried round bottom flask, equipped with a magnetic stir bar and a septum, was purged with argon to remove the remaining air and moisture. Then, under the argon atmosphere, 5 mL of THF was added and subsequently a solution of the terminal alkyne (5mmol/1equiv) was added. Then, the solution was cooled to –78˚C and *n*-BuLi (5.5 mmol, 1.1 equiv, 1.6 M in hexane) was added in a dropwise fashion. This solution was stirred for 10-15 min. Dimethyl disulfide (6.0 mmol/1.2 equiv) was then added at –78˚C. The solution was stirred for 1 hr after allowing it to warm to room temperature. Then, the reaction mixture was quenched with sat. aq. NH_4Cl solution. The inorganic layer was extracted with ethyl acetate (3 x 5 mL).

The combined organic layers were dried over anhydrous Na_2SO_4 and the solvent was evaporated under reduced pressure. The crude mixture was purified by flash chromatography (silica gel, hexanes) to yield the corresponding alkynylthiolate. (The corresponding yields appear in **Table 2.2** above).

2.8.3 General procedure for the synthesis of diazacyclobutenes.

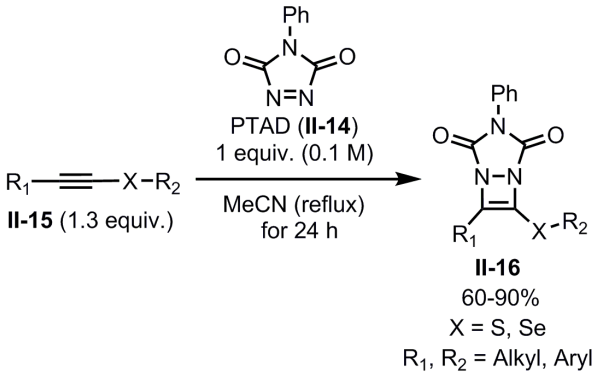

In a flame-dried round bottom flask, equipped with stir bar, were added 4-phenyl-triazoline-3,5-dione (PTAD) (1 mmol, 1 equiv.) and dry acetonitrile (5 mL for 1 mmol of PTAD). To this solution, the previously synthesized electron-rich alkyne (alkynyl sulfide or selenide, **II-15**) was added as a solution in dry acetonitrile (5 mL for 1 mmol of the electron-rich alkyne). The flask was then equipped with water-cooled condenser and the mixture was refluxed for 24 h. The solvent of the resultant mixture was removed under reduced pressure and the residue was subsequently purified via flash chromatography using silica gel and hexane/ethyl acetate eluents. A gradient from 100% hexanes to 80:20 hexanes/ethyl acetate was used to elute the corresponding diazacyclobutene.

2.8.4 Characterization data for alkynyl sulfides and selenides

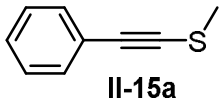

II-15a

Light yellow liquid; Yield: 90%; ^{1}H-NMR (500 MHz, $CDCl_3$) δ 7.48-7.27 (m, 5H), 2.48 (s, 3H); ^{13}C NMR (125 MHz, $CDCl_3$) δ = 131.4, 128.2, 128.0, 123.4, 91.8, 80.9, 19.38.

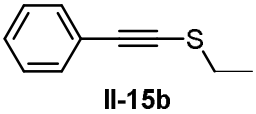

II-15b

Light yellow liquid; Yield: 82%; ^{1}H-NMR (300 MHz, $CDCl_3$) δ 7.45-7.35 (m, 2H), 7.35-7.26 (m, 3H), 2.82 (q, *J* = 7.3 Hz, 2H), 1.46 (t, *J* = 7.3 Hz, 3H); ^{13}C NMR (75 MHz, $CDCl_3$) δ = 131.4, 128.2, 127.9, 123.5, 93.5, 79.2, 29.9, 14.7.

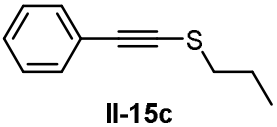

II-15c

Light yellow liquid; Yield: 83%; ^{1}H-NMR (500 MHz, $CDCl_3$) δ 7.50-7.38 (m, 2H), 7.31 (td, *J* = 4.7, 1.7 Hz, 3H), 2.80 (t, *J* = 7.3 Hz, 2H), 1.86 (sext, *J* = 7.3 Hz, 2H), 1.09 (t, *J* = 7.3 Hz, 3H); ^{13}C NMR (125 MHz, $CDCl_3$) δ = 131.3, 128.2, 127.8, 123.5, 92.7, 79.6, 37.7, 22.6, 12.8.

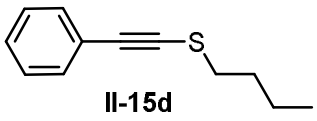

II-15d

Light yellow liquid; Yield: 76%; ^{1}H-NMR (500 MHz, $CDCl_3$) δ 7.50-7.27 (m, 5H), 2.82 (t, *J* = 7.5 Hz, 2H), 1.79 (quint, *J* = 7.5 Hz, 2H), 1.50 (sext, *J* = 7.5 Hz, 2H), 0.97 (t, *J* = 7.5 Hz, 3H); ^{13}C NMR (125 MHz, $CDCl_3$) δ = 131.4, 128.2, 127.9, 123.6, 92.8, 79.7, 35.5, 31.4, 21.4, 13.6.

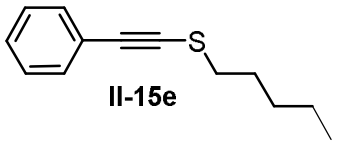

II-15e

Light yellow liquid; Yield: 69%; ^{1}H-NMR (300 MHz, $CDCl_3$) δ 7.70-7.50 (m, 5H), 3.04 (t, *J* = 7.3 Hz, 2H) 2.06 (p, *J* = 7.0 Hz, 2H), 1.66 (m, 4H), 1.19 (t, *J* = 7.0 Hz, 3H); ^{13}C NMR (75 MHz, $CDCl_3$) δ = 90.6, 89.9, 89.8, 88.7, 80.9, 77.7, 66.6, 65.2, 64.9, 63.2, 61.1.

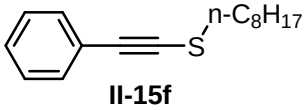

II-15f

Light yellow liquid; Yield: 75%; ^{1}H-NMR (300 MHz, $CDCl_3$) δ 7.70-7.50 (m, 5H), 3.05 (t, *J* = 7.3 Hz, 2H) 2.06 (p, *J* = 7.3 Hz, 2H), 1.71 (broad m, 2H), 1.56 (broad m, 8H), 1.16 (t, *J* = 6.7 Hz, 3H); ^{13}C NMR (75 MHz, $CDCl_3$) δ = 131.3, 128.1, 127.8, 123.5, 92.8, 79.7, 35.7, 31.7, 29.3, 29.1, 29.0, 28.2, 22.6, 14.0.

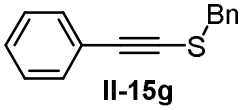

II-15g

Light yellow liquid; Yield: 85%; ^{1}H-NMR (300 MHz, $CDCl_3$) δ 7.60-7.30 (m, 10H), 4.07 (s, 2H); ^{13}C NMR (75 MHz, $CDCl_3$) δ = 136.5, 131.2, 129.0, 128.5, 128.2, 127.9, 127.7, 123.2, 94.5, 79.2, 40.3.

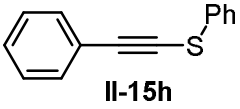

II-15h

Light yellow liquid; Yield: 92%;^{1}H-NMR (300 MHz, $CDCl_3$) δ 7.75-7.55 (m, 4H), 7.5-7.27 (m, 6H); ^{13}C NMR (75 MHz, $CDCl_3$) δ = 136.9, 132.8, 131.6, 129.1, 128.3, 126.4, 126.1, 122.8, 97.86, 75.45.

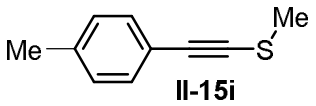

II-15i

Light yellow liquid; Yield: 78%; ^{1}H-NMR (300 MHz, $CDCl_3$) δ 7.35 (d, *J* = 8.0 Hz, 2H), 7.12 (d, *J* = 8.0 Hz, 2H), 2.48 (s, 3H), 2.36 (s, 3H); ^{13}C NMR (75 MHz, $CDCl_3$) δ = 138.1, 131.3, 128.9, 120.2, 91.8, 79.8, 21.3, 19.3.

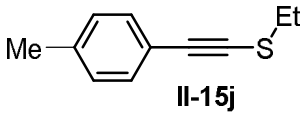

II-15j

Colorless liquid; Yield: 90%, ^{1}H-NMR (300 MHz, $CDCl_3$) δ 7.39 (d, *J* = 8.1 Hz, 2H), 7.14 (d, *J* = 7.9 Hz, 2H), 2.84 (q, *J* = 7.3 Hz, 2H), 2.38 (s, 3H), 1.50 (t, *J* = 7.3 Hz, 2H), ^{13}C NMR (75 MHz, $CDCl_3$) δ = 137.8, 131.9, 128.8, 120.3, 93.4, 78.1, 29.7, 21.2, 14.5.

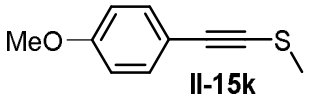

II-15k

Light yellow liquid; Yield: 98%; ^{1}H-NMR (500 MHz, $CDCl_3$) δ 7.37 (d, *J* = 8.7 Hz, 2H), 6.81 (d, *J* = 9.2 Hz, 2H), 3.76 (s, 3H), 2.44 (s, 3H); ^{13}C NMR (125 MHz, $CDCl_3$) δ = 159.4, 133.1, 115.2, 113.7, 91.4, 78.8, 54.9, 19.2.

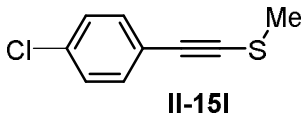

II-15l

Light yellow liquid; Yield: 65%; ^{1}H-NMR (300 MHz, $CDCl_3$) δ 7.35 (d, *J* = 8.8 Hz, 2H), 7.28 (d, *J* = 8.8 Hz, 2H), 2.48 (s, 3H); ^{13}C NMR (75 MHz, $CDCl_3$) δ = 133.8, 132.5, 128.5, 121.7, 90.6, 82.2, 19.2.

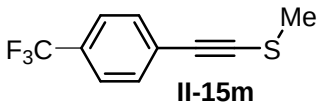

II-15m

Light yellow liquid; Yield: 43%; ^{1}H-NMR (500 MHz, , $CDCl_3$) δ 7.54 (d, *J* = 8.0 Hz, 2H), 7. 47 (d, *J* = 8.0 Hz, 2H), 2.50 (s, 3H); ^{13}C NMR (125 MHz, $CDCl_3$) δ = 131.1, 129.4 (q, $^{2}J_{C\text{-}F}$ = 32.1 Hz) 127.2 (quartet not well resolved, $^{4}J_{C\text{-}F}$ ~ 0.9 Hz), 125.2 (q, $^{3}J_{C\text{-}F}$ = 3.8 Hz), 124.0 (q, $^{1}J_{C\text{-}F}$ = 271.8 Hz), 90.8, 84.4, 19.2.

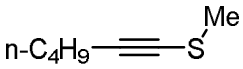

II-15n

Light yellow liquid; Yield: 28%; ^{1}H-NMR (500 MHz, $CDCl_3$) δ 2.28 (s, 3H), 2.23 (t, *J* = 7.0 Hz, 2H), 1.437 (p, *J* = 6.8 Hz, 2H), 1.35 (sext, *J* = 7.4 Hz, 2H), 0.856 (t, *J* = 7.3 Hz, 3H); ^{13}C NMR (125 MHz, $CDCl_3$) δ = 93.0, 69.7, 30.7, 21.8, 19.6, 19.1, 13.4.

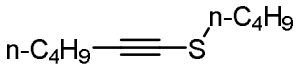

II-15o

Light yellow liquid; Yield: 67%;^{1}H-NMR (300 MHz, $CDCl_3$) δ 2.69 (t, *J* = 7.3 Hz, 2H), 2.32 (t, *J* = 6.8 Hz, 2H), 1.72 (p, *J* = 7.3 Hz, 2H), 1.6-1.35 (m, 6H), 1.00-0.88 (m, 6H); ^{13}C NMR (75 MHz, $CDCl_3$) δ = 94.2, 68.3, 35.2, 31.3, 30.9, 21.9, 21.4, 19.8, 13.6, 13.6.

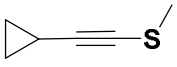

II-15p

Light yellow liquid; Yield: 38%;^{1}H-NMR (300 MHz, $CDCl_3$) δ 2.25 (s, 3H), 1.30-1.15 (m, 1H), 0.77-0.67 (m, 2H), 0.66-0.55 (m, 2H); ^{13}C NMR (75 MHz, $CDCl_3$) δ = 96.7, 65.6, 19.1, 8.6, 0.5.

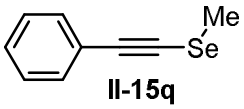

II-15q

Light yellow liquid; Yield: 86%;^{1}H-NMR (300 MHz, $CDCl_3$) δ 7.50-7.43 (m, 2H), 7.40-7.28 (m, 3H), 2.38 (s, 3H); ^{13}C NMR (75 MHz, $CDCl_3$) δ = 131.3, 128.1, 127.9, 123.3, 98.1, 71.3, 9.6.

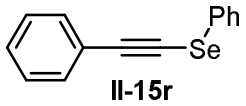

II-15r

Light yellow liquid; Yield: 94%; ^{1}H-NMR (300 MHz, $CDCl_3$) δ 7.70-7.59 (m, 2H), 7.58-7.50 (m, 2H), 7.40-7.28 (s, 6H); ^{13}C NMR (75 MHz, $CDCl_3$) δ = 135.9, 133.4, 131.7, 129.5, 128.9, 128.3, 127.1, 123.1, 102.9, 69.2.

2.8.5Characterization data for diazacyclobutenes (S, Se based examples)

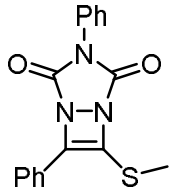

II-16a

Light yellow solid; Yield: 89%; Mp: 98.6-99.6 °C; IR (neat): 2927 (w), 1784 (m), 1732 (s), 1595 (w), 1384 (s), 1220 (s), 696 (s), 686 (s) cm^{-1}; ^{1}H-NMR (500 MHz, $CDCl_3$) δ 8.00-7.78 (m, 2H), 7.67-7.31 (m, 8H), 2.59 (s, 3H); ^{13}C NMR (125 MHz, $CDCl_3$) δ = 156.5, 155.1, 145.3, 130.8, 129.9, 129.3, 129.1, 128.8, 126.3, 125.6, 125.4 (2C, See 2D-HMQC analysis), 17.4; HRMS (ESI^{+}): Calcd for $C_{17}H_{14}N_3O_2S$, $[M+H]^{+}$ 324.0807 Found m/z 324.0822.

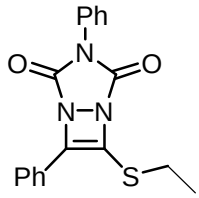

II-16b

Light yellow solid; Yield: 84%; Mp: 90.6-91.2 °C; IR (neat): 3061 (w),2962 (w), 2929 (w), 1793 (m), 1726 (s), 1595 (w), 1386 (s), 1213 (s), 698 (s), 686 (s) cm^{-1}; ^{1}H-NMR (500 MHz, $CDCl_3$) δ 7.92 (d, J = 8.2 Hz, 2H), 7.78-7.29 (m, 8H), 3.06 (q, J = 7.2 Hz, 2H), 1.41 (t, J = 7.3 Hz, 3H); ^{13}C NMR (125 MHz, $CDCl_3$) δ = 156.3, 155.0, 146.9, 130.8, 129.9, 129.3, 129.1, 128.7, 128.1, 126.3, 125.5, 125.4, 29.2, 15.1; HRMS (ESI^+): Calcd for $C_{18}H_{16}N_3O_2S$, $[M+H]^+$ 338.0963 Found m/z 338.0980.

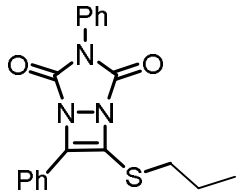

II-16c

Light yellow solid; Yield: 80%;Mp: 85.2-86.2 °C; IR (neat): 3068 (w), 2962 (w), 2929 (w), 2870 (w), 1793 (m), 1728 (s), 1593 (w), 1386 (s), 1213 (s), 700 (s), 686 (s) cm^{-1}; ^{1}H-NMR (500 MHz, $CDCl_3$) δ 8.02-7.80 (m, 2H), 7.64-7.32 (m, 8H), 3.02 (t, J = 6.4 Hz, 2H), 1.77 (q, J = 7.3 Hz, 2H), 1.05 (t, J = 7.3 Hz, 3H); ^{13}C NMR (125 MHz, $CDCl_3$) δ = 156.4, 155.1, 146.5, 130.9, 129.9, 129.3, 129.1, 128.7, 128.5, 126.4, 125.5, 125.4, 36.8, 23.2, 13.0; HRMS (ESI^+): Calcd for $C_{19}H_{18}N_3O_2S$, $[M+H]^+$ 352.1120 Found m/z 352.1129.

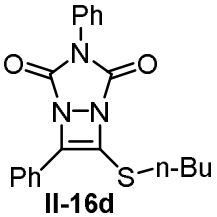

II-16d

Light yellow solid; Yield: 77%; Mp: 60.5-61.7 °C; IR (neat) : 3066 (w),2960 (w), 2931 (w), 2872 (w), 2856 (w), 1788 (m), 1728 (s), 1595 (w), 1388 (s), 1217 (s), 698 (s), 684 (s) cm^{-1}; ^{1}H-NMR (500 MHz, $CDCl_3$) δ 7.88 (d, *J* = 7.5 Hz, 2H) 7.60-7.30 (m, 8H), 3.04 (t, J = 7.5 Hz, 2H), 1.72 (p, *J* = 7.3 Hz, 2H), 1.47 (sext, *J* = 7.3 Hz, 2H), 0.92 (t, *J* = 7.3 Hz, 3H); ^{13}C NMR (125 MHz, $CDCl_3$) δ = 156.4, 155.2, 146.5, 130.9, 129.9, 129.3, 129.1, 128.8, 128.6, 126.4, 125.5, 125.4, 34.6, 31.8, 21.5, 13.5; HRMS (ESI^+): Calcd for $C_{20}H_{20}N_3O_2S$, $[M+H]^+$ 366.1276 Found m/z 366.1286.

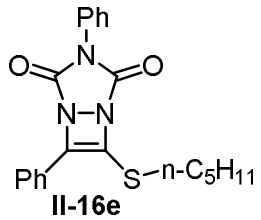

II-16e

Light yellow solid; Yield: 78%; Mp: 70.7-71.2 °C; IR(neat): 3066 (w), 2953 (w), 2927 (w), 2856 (w), 1791 (m), 1730 (s), 1595 (w), 1388 (s), 1213 (s), 698 (s), 684 (s) cm^{-1}; ^{1}H-NMR (500 MHz, $CDCl_3$) δ 7.95-7.85 (m, 2H), 7.6-7.3 (m, 8H), 3.03 (t, *J* = 7.3 Hz, 2H), 1.73 (p, *J* = 7.3 Hz, 2H), 1.5-1.2 (m, 4H), 0.87 (t, *J* = 7.1 Hz, 3H); ^{13}C NMR (125 MHz, $CDCl_3$) δ = 156.3, 155.2, 146.5, 130.9, 129.9, 129.3, 129.1, 128.7, 128.6, 126.4, 125.5, 125.4, 34.9, 30.5, 29.4, 22.1, 13.9; HRMS (ESI^+): Calcd for $C_{21}H_{22}N_3O_2S$, $[M+H]^+$ 380.1433 Found m/z 380.1437.

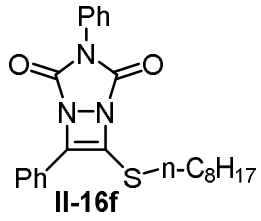

II-16f

Light yellow solid; Yield: 81%;Mp: 36.3-37.3 °C; IR (neat): 3066 (w), 2924 (m), 2852 (w), 1789 (m), 1732 (s), 1595 (w), 1386 (s), 1215 (s), 700 (s), 686 (s) cm^{-1};^{1}H-NMR (300 MHz, $CDCl_3$) δ 7.89 (d, *J* = 6.6 Hz, 2H), 7.6-7.3 (m, 8H), 3.03 (t, *J* = 7.3 Hz, 2H), 1.73 (p, *J* = 7.4 Hz, 2H), 1.56-1.36 (m, 2H), 1.35-1.15 (broad m, 8H), 0.86 (t, *J* = 6.7 Hz, 3H); ^{13}C NMR (75 MHz, $CDCl_3$) δ = 156.4, 155.2, 146.5, 130.9, 129.9, 129.3, 129.1, 128.7, 128.6, 126.4, 125.5, 125.4, 34.9, 31.7, 29.8, 29.1, 29.0, 28.4, 22.6, 14.0; HRMS (ESI^+): Calcd for $C_{24}H_{28}N_3O_2S$, $[M+H]^+$ 422.1902 Found m/z 422.1909.

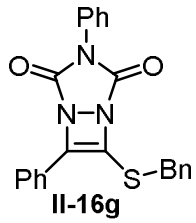

II-16g

Light Pink solid; Yield: 62%;Mp: 92.6-93.8 °C; IR (neat): 3061 (w), 3026 (w), 2929 (w), 2850 (w), 1786 (m), 1735 (s), 1595 (w), 1386 (s), 1224 (s), 694 (s), 682 (s) cm^{-1}; ^{1}H-NMR (300 MHz, $CDCl_3$) δ 7.8-7.1 (m, 15H), 4.21 (s, 2H); ^{13}C NMR (75 MHz, $CDCl_3$) δ = 156.7, 154.9, 148.6, 136.3, 130.8, 130.1, 129.4, 129.2, 129.1, 128.6, 128.5, 127.8, 127.0, 125.9, 125.5, 125.5, 39.2; HRMS (ESI^+): Calcd for $C_{23}H_{18}N_3O_2S$, $[M+H]^+$ 400.1120 Found m/z 400.1136.

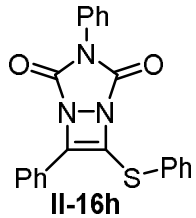

II-16h

White Solid; Yield:85%;Mp: 171.7-172.7 °C ;IR (neat) : 2924 (w), 2850 (w), 1789 (m), 1732 (s), 1593 (w), 1577 (w), 1384 (s), 1215 (s), 1149 (s), 1006 (m), 918 (m), 740 (s) 682 (s) cm^{-1};^{1}H-NMR (300 MHz, $CDCl_3$) δ 7.90-7.80 (m, 2H), 7.60-7.40 (m, 10H), 7.40-7.29 (m, 3H); ^{13}C NMR (75 MHz, $CDCl_3$) δ = 155.6, 154.8, 148.2, 131.8, 130.7, 130.6, 129.7, 129.6, 129.3, 129.1, 128.8, 128.1, 125.9, 125.9, 125.8, 125.4; HRMS (ESI^+): Calcd for $C_{22}H_{16}N_3O_2S$, $[M+H]^+$ 386.0963 Found m/z 386.0978.

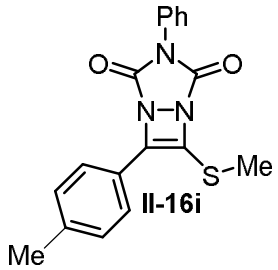

II-16i

White yellow solid; Yield: 92%; Mp: 144.7-145.8 °C; IR (neat): 3072 (w), 3034 (w), 2997 (w), 2926 (w), 2850 (s), 1782 (m), 1724 (s), 1595 (w), 1382 (s), 1217 (s), 690 (s)cm^{-1}; ^{1}H-NMR (300 MHz, $CDCl_3$) δ 7.78 (d, *J* = 8.0 Hz, 2H), 7.6-7.4 (m, 5H), 7.27 (d, *J* = 8.0 Hz, 2H), 2.58 (s, 3H), 2.41 (s, 3H); ^{13}C NMR (75 MHz, $CDCl_3$) δ = 156.7, 155.1, 145.9, 140.4, 130.9, 129.5, 129.3, 129.1, 128.3, 125.6, 125.4, 123.5, 21.6, 17.5; HRMS (ESI^+): Calcd for $C_{18}H_{16}N_3O_2S$, $[M+H]^+$ 338.0963 Found m/z 338.0978.

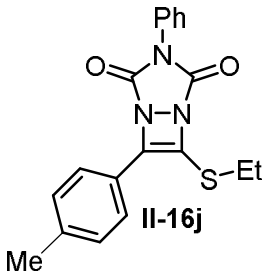

II-16j

White solid; Yield:77%;Mp: 105.3-106.3°C; IR (neat) : 2966 (w), 2931 (w), 2866 (w), 1782 (m), 1728 (s), 1627 (w), 1597 (w), 1496 (m), 1388 (s), 1226 (s), 1145 (s), 1103 (s), 1018 (m), 921 (m), 875 (m), 813 (m), 767 (s), 686 (s) cm^{-1}; ^{1}H-NMR (300 MHz, $CDCl_3$) δ 7.80 (d, *J* = 8.2 Hz, 2H), 7.55-7.37 (m, 5H), 7.26 (d, *J* = 8.01 Hz, 2H), 3.03 (q, *J* = 7.3 Hz, 2H), 2.39 (s, 3H), 1.39 (t, *J* = 7.3 Hz, 3H); ^{13}C NMR (75 MHz, $CDCl_3$) δ = 156.6, 155.1, 147.5, 140.5, 130.8, 129.4, 129.3, 129.1, 127.1, 125.6, 125.4, 123.5, 29.3, 21.6, 15.1; HRMS (ESI^+): Calcd for $C_{19}H_{18}N_3O_2S$, $[M+H]^+$ 352.1120 Found m/z 352.1130.

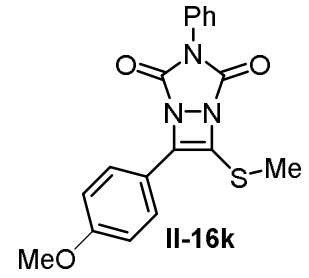

II-16k

White solid; Yield: 74%; Mp: 116.1-116.5 °C; IR (neat): 3070 (w), 3014 (w), 2962 (w), 2927 (w), 2837 (w), 1782 (m), 1724 (s), 1602 (m), 1384 (s), 1257 (s), 1226 (m), 688 (s)cm^{-1};^{1}H-NMR (500 MHz, $CDCl_3$) δ 7.94-7.71 (m, 2H), 7.59-7.34 (m, 5H), 7.02-6.90 (m, 2H), 3.84 (s, 3H), 2.54 (s, 3H); ^{13}C NMR (125 MHz, $CDCl_3$) δ = 160.9, 156.9, 155.2, 145.9, 130.8, 129.2, 129.0, 127.4, 126.9, 125.3, 118.8, 114.2, 55.3, 17.6; HRMS (ESI^+): Calcd for $C_{18}H_{15}N_3O_3S$, $[M+H]^+$ 354.0912 Found m/z 354.0928.

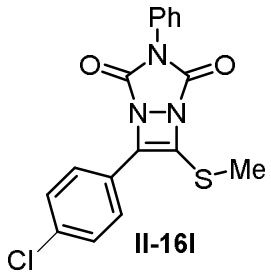

II-16l

White solid; Yield: 85%; Mp: 135.8-136.9 °C; IR (neat): 3091 (w), 3072 (w), 2926 (w), 1784 (m), 1732 (s), 1593 (w), 1381 (s), 825 (s), 686 (s)cm^{-1};^{1}H-NMR (500 MHz, $CDCl_3$) δ 7.80 (d, *J* = 8.7 Hz, 2H), 7.58-7.36 (m, 7H), 2.59 (s, 3H); ^{13}C NMR (125 MHz, $CDCl_3$) δ = 156.2, 155.0, 144.0, 135.8, 130.7, 129.8, 129.4, 129.2, 129.1, 126.8, 125.4, 124.8, 17.3; HRMS (ESI^+): Calcd for $C_{17}H_{13}N_3O_2SCl$, $[M+H]^+$ 358.0417 Found m/z 358.0432.

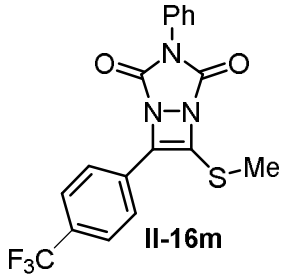

II-16m

White solid; Yield: 83%; Mp: 79.6-81.4 °C; IR (neat): 3068 (w), 3045 (w), 2922 (w), 1788 (m), 1732 (s), 1614 (w), 1388 (s), 1317 (s), 696 (s), 684 (s)cm^{-1}; ^{1}H-NMR (300 MHz, $CDCl_3$) δ 7.94 (d, *J* = 8.2 Hz, 2H), 7.70 (d, *J* = 8.2 Hz, 2H), 7.60-7.40 (m, 5H), 2.63 (s, 3H); ^{13}C NMR (75 MHz, $CDCl_3$) δ = 155.8, 155.0, 142.8, 131.8, 131.1 (q, $^{2}J_{C\text{-}F}$ = 32.9 Hz), 130.7, 129.7 (q, $^{4}J_{C\text{-}F}$ = 1.47 Hz), 129.4, 129.3, 125.8 (q, $^{3}J_{C\text{-}F}$ = 3.8 Hz), 125.6, 125.4, 123.7 (q, $^{1}J_{C\text{-}F}$ = 272.2 Hz), 17.1; HRMS (ESI^+): Calcd for $C_{18}H_{13}N_3O_2SF_3$, $[M+H]^+$ 392.0681 Found m/z 392.0693.

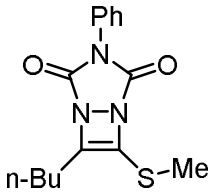

II-16n

White solid; Yield: 61%; Mp: 44.8-45.7°C; IR (neat): 2958 (w), 2927 (w), 2860 (w), 1797 (m), 1739 (s), 1593 (w), 1390 (s), 1211 (m),694 (s) cm^{-1}; ^{1}H-NMR (300 MHz, $CDCl_3$) δ 7.55-7.35 (m, 5H), 2.54 (t, *J* = 7.5 Hz, 2H), 2.44 (s, 3H), 1.70 (p, *J* = 7.5 Hz, 2H), 1.42 (sext, *J* = 7.4 Hz, 2H), 0.95 (t, *J* = 7.3 Hz, 3H); ^{13}C NMR (75 MHz, $CDCl_3$) δ = 156.7, 155.1, 150.5, 132.2, 130.9, 129.2, 128.9, 125.2, 28.0, 25.3, 22.1, 17.8, 13.4; HRMS (ESI^+): Calcd for $C_{15}H_{18}N_3O_2S$, $[M+H]^+$ 304.1120 Found m/z 304.1138.

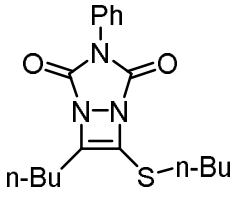

II-16o

Colorless liquid; Yield: 56%; IR (neat) : 2958 (w), 2931 (w), 2870 (w), 1793 (w), 1735 (s), 1597 (w), 1500 (m), 1458 (w), 1377 (s), 1211 (m), 1138 (m), 1072 (m), 999 (m), 921 (m), 748 (m), 690 (m) cm^{-1}; ^{1}H-NMR (300 MHz, $CDCl_3$) δ 7.60-7.35 (m, 5H), 2.87 (bs, 2H), 2.54 (t, J = 7.5 Hz, 2H), 1.80-1.55 (m, 4H), 1.52-1.35 (m, 4H), 1.00-0.85 (m, 6H); ^{13}C NMR (75 MHz, $CDCl_3$) δ = 156.5, 155.2, 151.7, 131.2, 130.9, 129.3, 128.9, 125.3, 34.2, 31.5, 28.1, 25.3, 22.1, 21.3, 13.5 (2C, See 2D-HMQC analysis); HRMS (ESI^+): Calcd for $C_{18}H_{24}N_3O_2S$, $[M+H]^+$ 346.1589 Found m/z 346.1608.

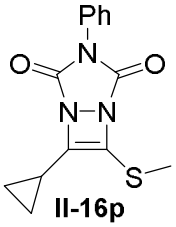

II-16p

White solid; Yield: 94%;Mp: 71.5-72.5°C; IR (neat): 2924 (w), 1793 (w), 1739 (s), 1643 (w), 1593 (w), 1492 (m), 1454 (w), 1427 (w), 1388 (s), 1261 (m), 1215 (s), 1149 (s), 1091 (m), 999 (m), 972 (m), 775 (m), 756 (m), 690 (m) cm^{-1}; ^{1}H-NMR (300 MHz, $CDCl_3$) δ 7.55-7.35 (m, 5H), 2.41 (s, 3H), 1.90-1.60 (m, 1H), 1.40-1.06 (bm, 2H), 1.06-0.90 (bm, 2H); ^{13}C NMR (75 MHz, $CDCl_3$) δ = 156.5, 154.9, 151.2, 130.7, 130.5, 129.1, 128.8, 125.1, 17.8, 6.9, 6.6

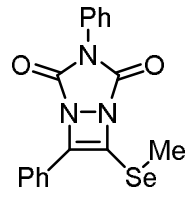

II-16q

White yellow solid; Yield: 80%;Mp:82.6-83.9 °C; IR (neat) : 3066 (w), 3016 (w), 2924 (w), 2850 (w), 1786 (m), 1732 (s), 1631 (w), 1597 (w), 1504 (m), 1489 (m), 1381 (s), 1222 (s), 1141 (s), 1095 (m), 1072 (m), 1018 (s), 758 (m), 744 (m), 682 (s) cm^{-1}; ^{1}H-NMR (300 MHz, $CDCl_3$) δ 7.94-7.84 (m, 2H), 7.56-7.36 (m, 8H), 2.47 (s, 3H); ^{13}C NMR (75 MHz, $CDCl_3$) δ = 156.3, 154.9, 146.5, 130.8, 129.8, 129.3, 129.1, 128.7, 126.4, 125.3, 125.3, 121.3, 8.7; HRMS (ESI^+): Calcd for $C_{17}H_{14}N_3O_2Se$, $[M+H]^+$ 372.0251 Found m/z 372.0269.

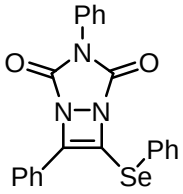

II-16r

White yellow solid; Yield: 93%;Mp: 162-162.8 °C; IR (neat) : 3070 (w), 2924 (w), 2850 (w), 1793 (m), 1735 (s), 1631 (w), 1593 (w), 1573 (w), 1384 (s), 1276 (m), 1215 (s), 1141 (m), 1107 (m), 1068 (m), 995 (m), 918 (m),883 (m), 756 (m), 736 (s), 686 (s) cm^{-1}; ^{1}H-NMR (300 MHz, $CDCl_3$) δ 8.00-7.90 (m, 2H), 7.70-7.60 (m, 2H), 7.53-7.38 (m, 8H), 7.38-7.29 (m, 3H); ^{13}C NMR (75 MHz, $CDCl_3$) δ = 155.7, 154.8, 148.1, 132.2, 130.8, 130.4, 129.8, 129.3, 129.1, 128.8, 128.4, 128.2, 126.1, 125.6, 125.4, 120.7; HRMS (ESI^+): Calcd for $C_{22}H_{16}N_3O_2Se$, $[M+H]^+$ 434.0408 Found m/z 434.0417.

2.8.6 Dynamic NMR Experiments

A small amount (*ca.*100 mg) of the corresponding diazacyclobutene (**II-16b, II-16g** and **II-16s**) was prepared in 0.5 mL of $CDCl_3$. Variable temperature ^1H NMR spectra were collected using a Bruker 300 MHz instrument. Temperature calibration for the instrument was done in advance of the actual experiments. After collecting ^1H NMR spectra for each temperature, a theoretical ^1H NMR spectrum was generated for each temperature by performing a Dynamic NMR (DNMR) line shape analysis. This DNMR analysis was done by means of the Bruker TopSpin 3.5 pl 7 software for AB spin system (*i.e.,* the S-benzyl methylene protons of **II-16g** and **II-16s**) and the WINDNMR-Pro software for the ABX_3 spin system (*i.e.,* the S-ethyl methylene protons of **II-16b**). Figure 2.11 and 2.13 shows the experimental variable temperature (VT) ^1H NMR spectra for **II-16b** and **II-16s** for the labeled protons in the structure displayed in the figure (stacked VT ^1H NMR spectra for **II-16g** was shown earlier in Figure 2.7). Using the DNMR analysis, theoretical spectra were generated and subsequently the exchange rate constants (K_{ex}) were extracted for each temperature (T) for each compound (see Table 2.11**,** 2.12 and 2.13).

In order to extract the thermodynamic parameters for the double-nitrogen inversion of the diazacyclobutenes, the Eyring equation (*i.e.,* $\ln (K_{ex}/T) = -\Delta H^{\ddagger}/RT + \Delta S^{\ddagger}/R + \ln (K_b/h)$, where $\ln (K_b/h) = 23.7600$) was used. Hence, 1000/T vs. $\ln (K_{ex}/T)$ graph was generated for each compound. These graphs are shown in Figure 2.12, and 2.14 (Figure 2.8 has shown the Eyring plot of compound **II-16g**).

Then by using the slope and the intercept extracted from the graph, the enthalpy of activation ($\Delta H^{\ddagger}$) and entropy of activation ($\Delta S^{\ddagger}$) was calculated, respectively. Finally, by applying the equation: $\Delta G^{\ddagger} = \Delta H^{\ddagger} - T\Delta S^{\ddagger}$, the activation energy ($\Delta G^{\ddagger}$) or the standard Gibbs free energy change was calculated for each compound. The error and error propagation of the thermodynamic parameters were calculated based on the reported literature[68,69,124–126] with the help of linear regression statistics in the excel toolpak.[127] These $\Delta H^{\ddagger}$, $\Delta S^{\ddagger}$, and $\Delta G^{\ddagger}$ values are tabulated in Table 2.14 for all compounds tested so far.

Table 2.11. Exchange rate constants for AB spin system in compound **II-16g** for each temperature.

T (K)	**$K_{ex}(s^{-1})$**
295	614
281	231
277	187
273	71
266	38
260	20
254	12
248	6

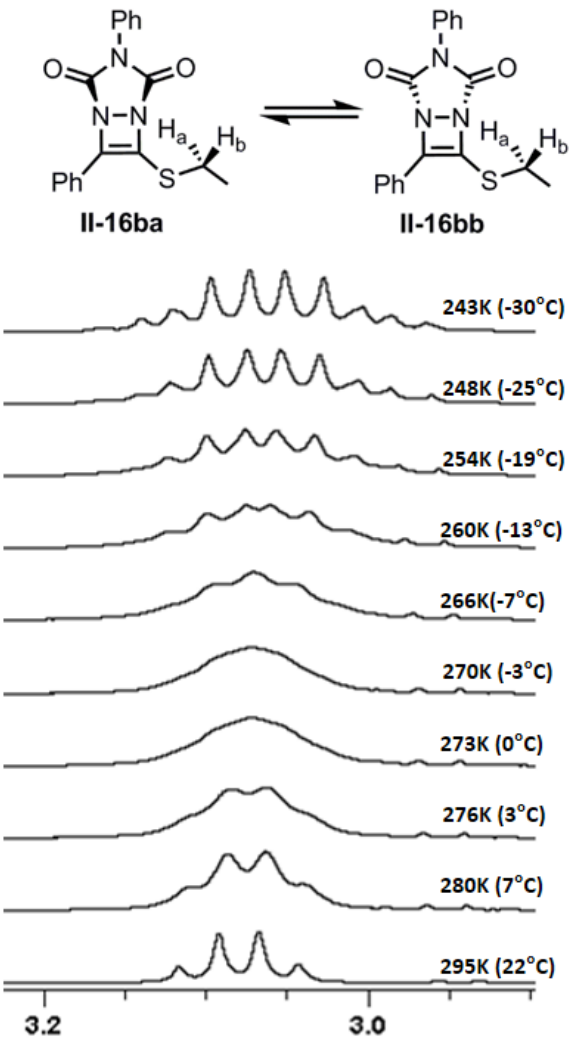

Figure 2.11. Temperature-dependent 300 MHz ^{1}H NMR spectra of the methylene protons of compound **II-16b** in $CDCl_3$.

Table 2.12. Exchange rate constants for ABX_3 spin system in compound **II-16b** for each temperature.

T (K)	$K_{ex}(s^{-1})$
295	480
281	182
277	120
273	79
270	85
266	42
260	23
254	17
248	8
243	3

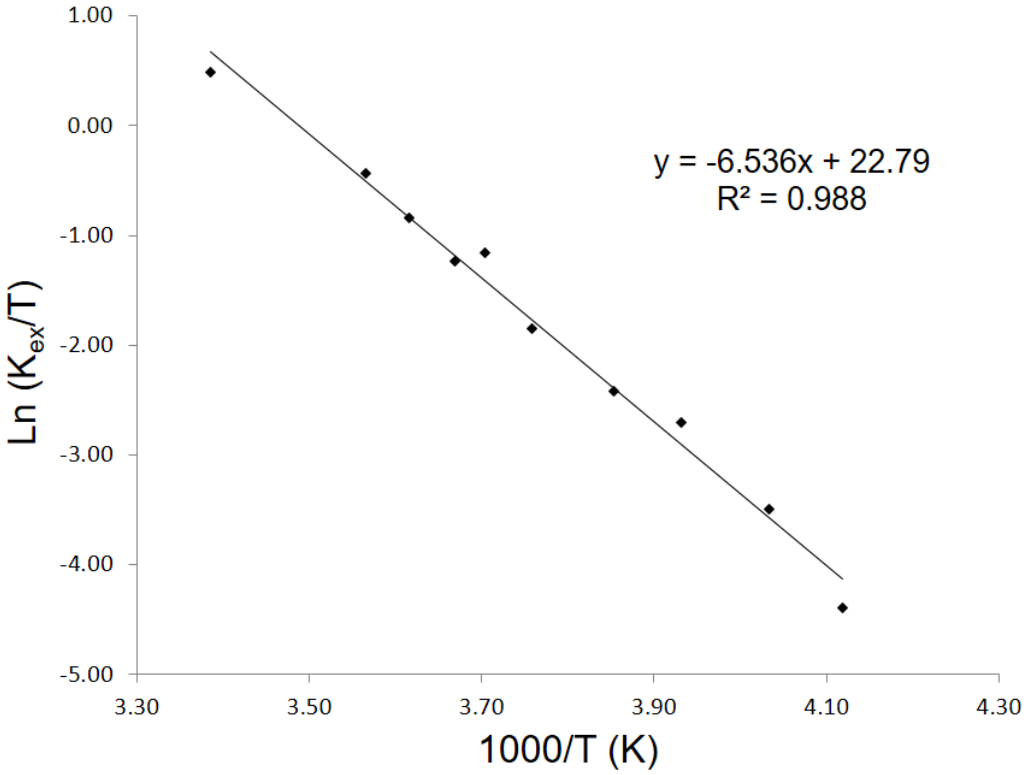

Figure 2.12. Eyring plot originated from simulated spectra for **II-16b** in $CDCl_3$.

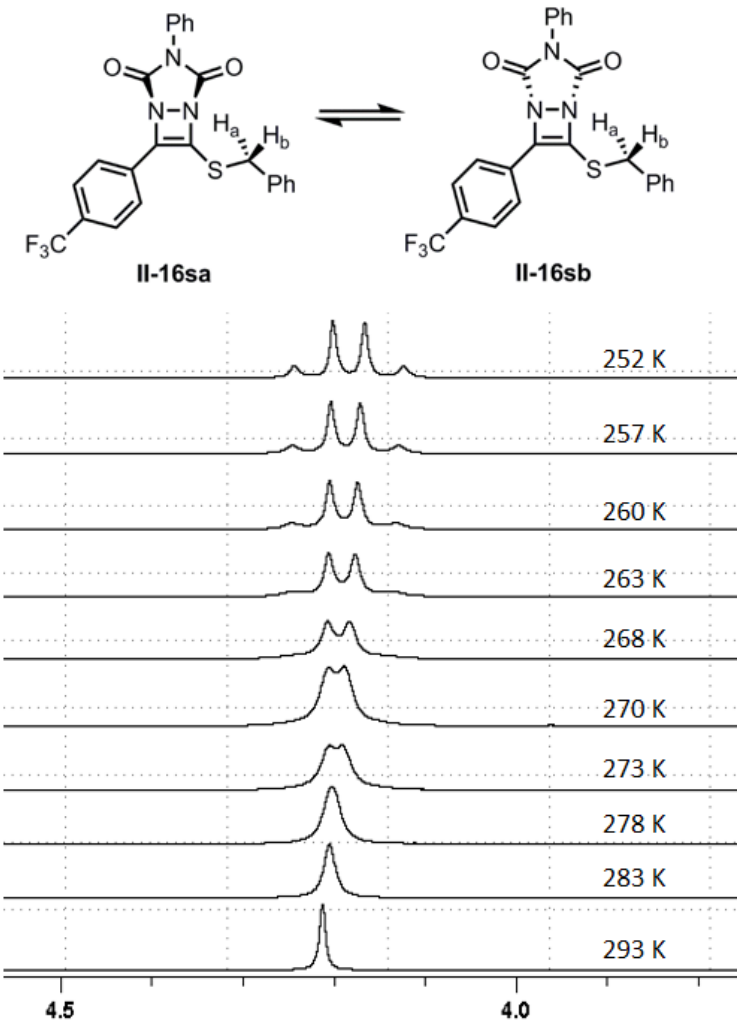

Figure 2.13. Temperature-dependent 300 MHz ^{1}H NMR spectra of the methylene protons of compound **II-16s** in $CDCl_3$.

Table 2.13. Exchange rate constants for AB spin system in compound **II-16s** for each temperature.

T (K)	**$K_{ex}(s^{-1})$**
294	309
281	142
274	96
267	48
263	43
261	27
254	16
251	11
247	8
240	5
234	1

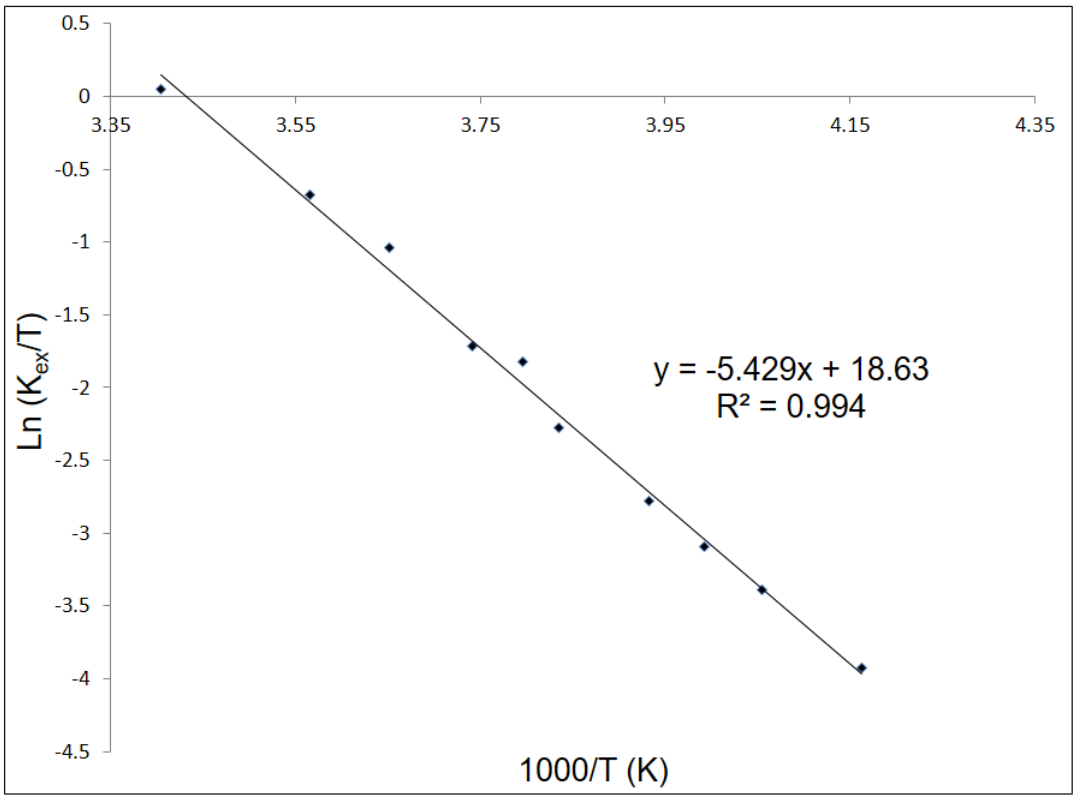

Figure 2.14. Eyring plot originated from simulated spectra for **II-16s** in $CDCl_3$.

Table 2.14. Thermodynamic parameters: $\Delta H^{\ddagger}$, $\Delta S^{\ddagger}$, and $\Delta G^{\ddagger}$ at 298 K (25°C) for the compounds of **II-16g, II-16b** and **II-16s**.

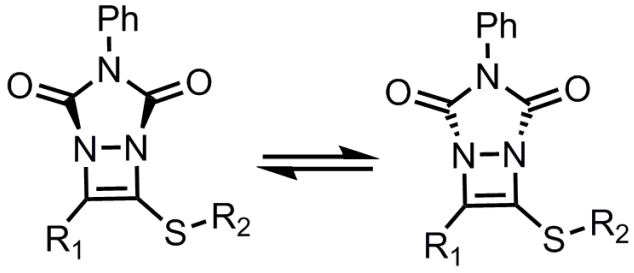

Compound No	R_1	R_2	$\Delta H^{\ddagger}$ (Kcal/mol)	$\Delta S^{\ddagger}$ (Kcal/mol)	$\Delta G^{\ddagger}$ (Kcal/mol) at 298 K
II-16b	C_6H_5-	Et	13.0±0.5	-1.9±1.9	13.6±0.5
II-16g	C_6H_5-	Bn	14.4±0.7	3.2±2.7	13.4±0.7
II-16s	*p*-CF_3-C_6H_4-	Bn	10.8±0.3	-10.2±1.1	13.8±0.3

2.8.7 Generation of single crystals of diazacyclobutenes

In general, about 100 mg of the diazacyclobutene compound was placed in a 3 mL glass vial and subsequently 0.5 mL of chloroform was syringed into the vial. The vial was capped and mixed thoroughly until the diazacyclobutene was dissolved. This solution was layered with 0.5 mL of hexane by syringing hexane along the wall of the glass vial. In order to assist slow evaporation of this solution to create X-ray quality crystals; the vial was covered with paraffin film and subsequently the film was pierced a few times with a needle. This vial was then kept at room temperature overnight. For stubborn compounds which did not yield X-ray quality crystals by this method neat dichloromethane, chloroform or acetone was used without adding hexanes.

2.8.8 X-ray Crystallography Experimental

CCDC 1871105-1871115 contain the supplementary crystallographic data for these diazacyclobutene compounds showed in Figure 2.3 and 2.4.

Structural data on a series of diazacyclobutenes were obtained by single crystal X-ray diffraction. X-ray diffraction data were collected from Bruker D8 Venture diffractometer equipped with Mo Kα radiation (λ = 0.07107 Å) from an IncoatecIμS source and a Photon 100 detector under a cold nitrogen stream. Bruker Apex3 software package was used to control the instrument, data processing (SAINT), and data scaling (SADABS, spherical multi-scan absorption correction).[128] Space group determinations were made based on the systematic absences, and the structures were solved by intrinsic

phasing, then refined on F^2 using full matrix least squares techniques with the SHELXTL software suite.[129] All non-hydrogen atoms were refined anisotropically. Hydrogen atoms were placed in geometrically optimized positions using appropriate riding models. A summary of the crystallographic data and structure refinements are given in Table 2.15, 2.16, 2.17, and 2.18.

Packing diagrams for sulfur-based and selenium based diazacyclobutenes are shown in Figure 2.15 and 2.16, respectively.

Table 2.15: Crystallographic data for sulfur-based diazacyclobutenes.

	II-16a	**II-16b**	**II-16c**
Empirical formula	$C_{17}H_{13}N_3O_2S$	$C_{18}H_{15}N_3O_2S$	$C_{19}H_{17}N_3O_2S$
Formula weight (g/mol)	323.36	337.39	351.41
Crystal system	monoclinic	triclinic	triclinic
Space group, *Z*	$P2_1/c$, 4	*P*-1, 2	*P*-1, 2
Temperature (K)	140	140	140
Crystal size (mm)	0.05 x 0.05 x 0.31	0.10 x 0.11 x 0.24	0.06 x 0.08 x 0.23
a, Å	4.2495(2)	5.5294(3)	5.4355(11)
b, Å	13.0822(8)	12.2824(7)	12.565(3)
c, Å	27.2564(16)	12.3440(6)	12.738(3)
α,°		105.607(2)	101.753(7)
β, °	90.623(2)	99.079(2)	91.504(7)
γ, °		94.064(2)	94.642(7)
Volume ($Å^3$)	1515.17(15)	791.63(7)	848.1(3)
D_{calc} (g/cm^3)	1.418	1.415	1.376
Abs. Coeff. (mm^{-1})	0.227	0.220	0.209
F(000)	672	352	368
T_{max}, T_{min}	1.0000, 0.9369	1.0000, 0.9479	1.0000, 0.9457
Θ range for data	2.73-25.50	2.79-27.51	3.33-26.50
Reflections collected	38600	36079	27872
Data/restraints/parameters	2798 / 0 / 209	3626 / 0 / 218	3506 / 0 / 236
R(int)	0.0526	0.0393	0.0347
Final R [$I > 2\sigma(I)$] R1, wr2	0.0375, 0.0904	0.0325, 0.0779	0.0325, 0.0831
Final R (all data) R1, wr2	0.0441, 0.0947	0.0395, 0.0814	0.0381, 0.0864
Goodness-of-fit on F^2	1.087	1.058	1.046
Larg. Diff. Peak, hole, $eå^{-3}$	0.247, -0.317	0.243, -0.298	0.228, -0.233

Table 2.16: Crystallographic data for sulfur-based diazacyclobutenes cntd.

	II-16h	**II-16j**	**II-16k**
Empirical formula	$C_{22}H_{15}N_3O_2S$	$C_{18}H_{15}N_3O_2S$	$C_{18}H_{15}N_3O_3S$
Formula weight (g/mol)	385.43	337.39	353.39
Crystal system	monoclinic	monoclinic	monoclinic
Space group, *Z*	$P2_1/c$, 4	$P2_1/c$, 8	$P2_1/c$, 4
Temperature (K)	140	140	140
Crystal size (mm)	0.03 x 0.03 x 0.38	0.04 x 0.04 x 0.20	0.03 x 0.04 x 0.26
a, Å	10.835(2)	9.2538(3)	4.2026(6)
b, Å	4.5510(8)	15.6160(6)	23.514(4)
c, Å	36.893(8)	22.1925(9)	16.820(3)
α,°			
β, °	95.936(8)	96.9700(10)	96.362(5)
γ, °			
Volume ($Å^3$)	1809.4(6)	3183.3(2)	1651.9(4)
D_{calc} (g/cm^3)	1.415	1.408	1.421
Abs. Coeff. (mm^{-1})	0.203	0.219	0.219
F(000)	800	1408	736
T_{max}, T_{min}	1.0000, 0.8569	1.0000, 0.9473	1.0000, 0.9093
Θ range for data	2.29-26.00	2.22-25.50	2.44-25.50
Reflections collected	19109	62452	26569
Data/restraints/parameters	3567 / 0 / 253	5915 / 0 / 437	3052 / 0 / 228
R(int)	0.0402	0.0863	0.0431
Final R [$I > 2\sigma(I)$] R1, wr2	0.0408, 0.0924	0.0396, 0.0890	0.0337, 0.0809
Final R (all data) R1, wr2	0.0507, 0.0967	0.0609, 0.0996	0.0404, 0.0851
Goodness-of-fit on F^2	1.079	1.021	1.069
Larg. Diff. Peak, hole, $eå^{-3}$	0.236, -0.264	0.231, -0.317	0.233, -0.271

Table 2.17: Crystallographic data for sulfur-based diazacyclobutenes cntd.

	II-16l	**II-16m**	**II-16p**
Empirical formula	$C_{17}H_{12}ClN_3O_2S$	$C_{18}H_{12}F_3N_3O_2S$	$C_{14}H_{13}N_3O_2S$
Formula weight (g/mol)	357.81	391.37	287.33
Crystal system	monoclinic	triclinic	monoclinic
Space group, *Z*	$P2_1/c$, 8	*P*-1, 4	$P2_1/n$, 8
Temperature (K)	140	140	100
Crystal size (mm)	0.03 x 0.05 x 0.46	0.04 x 0.06 x 0.41	0.10 x 0.14 x 0.29
a, Å	8.9949(8)	4.3570(6)	13.7190(7)
b, Å	15.8185(17)	16.601(2)	12.4361(6)
c, Å	22.177(2)	23.517(3)	16.4246(8)
α,°		84.892(5)	
β, °	96.762(4)	87.991(5)	97.0910(10)
γ, °		87.049(5)	
Volume ($Å^3$)	3133.5(6)	1691.2(4)	2780.8(2)
D_{calc} (g/cm^3)	1.517	1.537	1.373
Abs. Coeff. (mm^{-1})	0.392	0.242	0.237
F(000)	1472	800	1200
T_{max}, T_{min}	1.0000, 0.9245	1.0000, 0.8650	1.0000, 0.9067
Θ range for data	2.28-25.50	2.47-25.24	2.50-25.25
Reflections collected	55874	16063	31474
Data/restraints/parameters	5811 / 0 / 435	5719 / 0 / 489	5021 / 18 / 361
R(int)	0.0672	0.0421	0.0430
Final R [$I > 2\sigma(I)$] R1, wr2	0.0332, 0.0763	0.0881, 0.3108	0.0628, 0.1613
Final R (all data) R1, wr2	0.0459, 0.0832	0.1045, 0.3182	0.0784, 0.1731
Goodness-of-fit on F^2	1.053	1.090	1.092
Larg. Diff. Peak, hole, $eå^{-3}$	0.220, -0.281	0.452, -0.426	1.451, -0.818

Table 2.18. Crystallographic data for Se-based diazacyclobutenes.

	II-16q	**II-16r**
Empirical formula	$C_{17}H_{13}N_3O_2Se$	$C_{22}H_{15}N_3O_2Se$
Formula weight (g/mol)	370.26	432.33
Crystal system	orthorhombic	triclinic
Space group, *Z*	*Fdd*2, 16	*P*-1, 2
Temperature (K)	140	140
Crystal size (mm)	0.06 x 0.06 x 0.38	0.04 x 0.04 x 0.37
a, Å	33.002(3)	5.6338(4)
b, Å	44.669(4)	12.2422(9)
c, Å	4.1629(3)	13.6022(10)
α,°		97.430(3)
β, °		98.791(3)
γ, °		92.491(3)
Volume ($Å^3$)	6136.8(9)	917.42(12)
D_{calc} (g/cm^3)	1.603	1.565
Abs. Coeff. (mm^{-1})	2.461	2.070
F(000)	2976	436
Tmax, Tmin	1.0000, 0.8136	1.0000, 0.8306
Θ range for data	2.47-26.50	2.11-26.00
Reflections collected	65252	32997
Data/restraints/parameters	3145 / 1 / 209	3590 / 0 / 253
R(int)	0.0447	0.0506
Final R [$I > 2\sigma(I)$] R1, wr2	0.0190, 0.0438	0.0258, 0.0547
Final R (all data) R1, wr2	0.0214, 0.0447	0.0326, 0.0570
Goodness-of-fit on F^2	1.106	1.082
Larg. Diff. Peak, hole, $eå^{-3}$	0.175, -0.292	0.289, -0.346

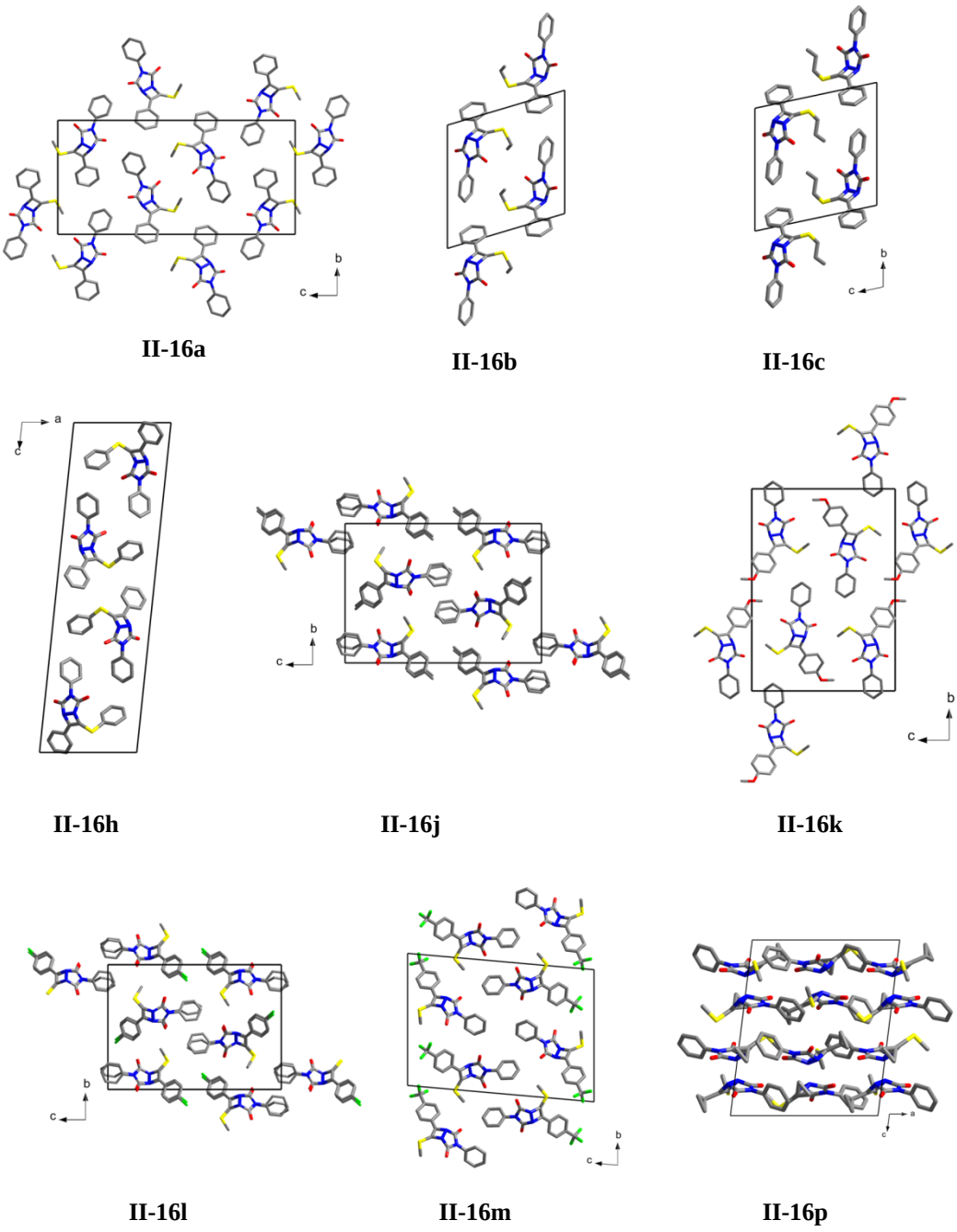

Figure 2.15: Packing diagrams for sulfur-based diazacyclobutenes.

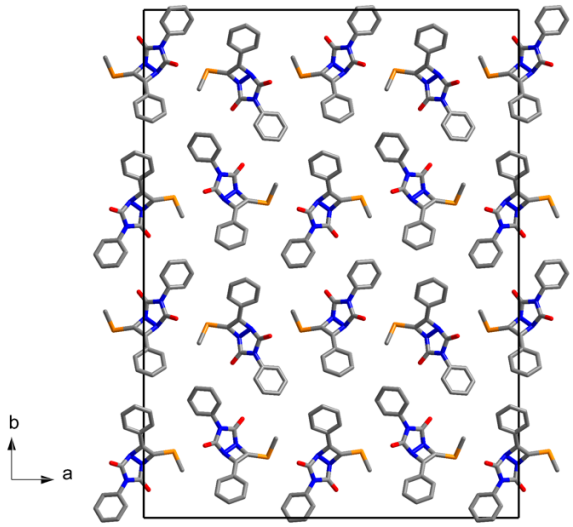

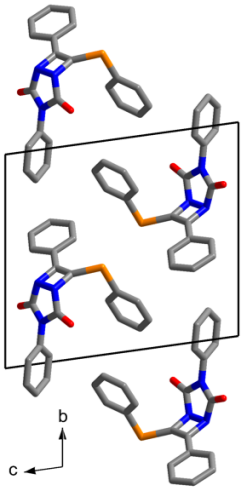

II-16q **II-16r**

Figure 2.16: Packing diagrams for selenium-based diazacyclobutenes.

2.8.9 A typical procedure for the preparation of methanebis(ethynylsulfane)[70]

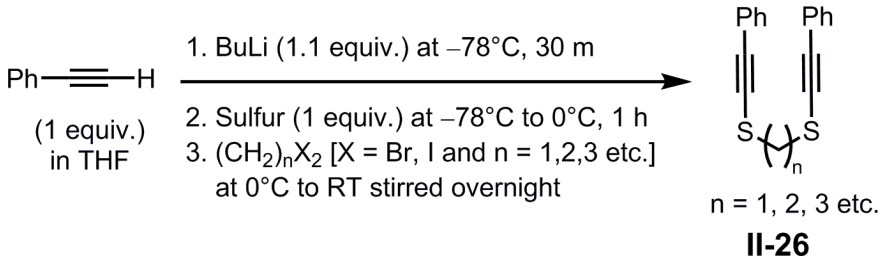

II-26

(Eq. 1)

Procedure

An alkyne thiolate solution was formed using a terminal alkyne (5 mmol, 2.08 equiv) according to the **method 1** which was described earlier. Then the solution was allowed to warm up to the room temperature. To this solution, diiodomethane (2.4 mmol, 1 equiv) was added in a dropwise fashion and the reaction mixture was stirred overnight. Then the reaction mixture was quenched with 25 mL of sat. aq. NH_4Cl. The combined organic layer was washed with 25 mL of sat. aq. brine and dried over anhydrous Na_2SO_4. Then the solvent was evaporated and the crude mixture was purified via flash chromatography with silica gel and hexanes to yield the methanebis(ethynylsulfane) product as a dark yellow oil (**II-26 (n=1)**, 32% yield).

2.8.10 General procedure for the synthesis of diazacyclobutene dimer with methanebis(ethynylsulfane) (II-26 (n=1))

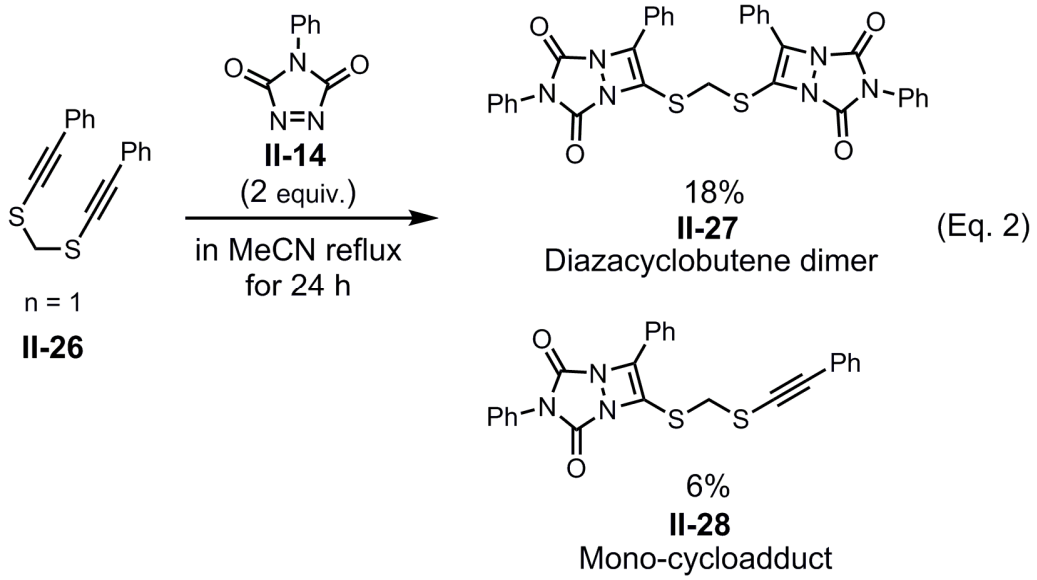

(Eq. 2)

In a flame-dried round bottom flask, equipped with stir bar, were added 4-phenyl-triazoline-3,5-dione (PTAD) (2 mmol, 2equiv) and dry acetonitrile (5 mL for 2 mmol of PTAD). To this solution, the previously synthesized methanebis(ethynylsulfane) (1 mmol, 1 equiv, (**II-26**, n =1)) was added as a solution in dry acetonitrile (5 mL for 1 mmol of the electron-rich alkyne). The RBF was then attached to a water-cooled condenser and the mixture was refluxed for 24 h. Then, the solvent was removed under reduced pressure. The crude reaction mixture was purified via flash chromatography using silica gel and hexane/ethyl acetate (100% hexane to 80:20 hexanes/ethyl acetate) to afford the corresponding diazacyclobutene dimer (18%, **II-27**).

2.8.11 Characterization data for methanebis(ethynylsulfane) and diazacyclobutene dimer (II-26 (n=1))[70]

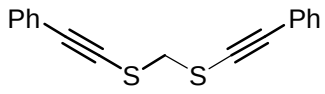

II-26

Light yellow liquid; Yield: 36%; ^{1}H-NMR (300 MHz, $CDCl_3$) δ 7.70-7.45 (m, 4H), 7.45-7.20 (m, 6H), 4.21 (s, 2H); ^{13}C NMR (75 MHz, $CDCl_3$) δ = 131.6, 128.4, 128.2, 122.6, 96.0, 77.1, 43.0.

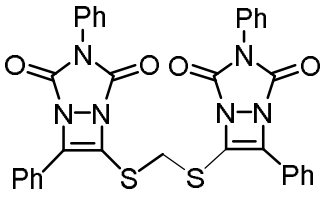

II-28

Light brown solid; Yield: 18%; Mp: 187.8-188.8 °C; IR (neat): 2985 (w), 2924 (w), 2850(w), 1801 (m), 1739 (s), 1631 (w), 1597 (w), 1570 (w), 1496 (s), 1489 (s), 1446 (m), 1377 (s), 1284 (w), 1226 (s), 1203 (s), 1168 (w), 1149 (s), 1103 (s), 1068 (m), 1022 (w), 999 (s), 921 (s), 833 (m), 840 (w), 783 (s), 752 (s), 690 (s), 594 (s) cm^{-1};^{1}H-NMR (300 MHz, $CDCl_3$) δ 8.00-7.30 (m, 14H), 7.25-6.80 (m, 6H), 4.68 (s, 2H); ^{13}C NMR (75 MHz, $CDCl_3$) δ = 156.8, 154.5, 148.9, 130.7, 130.2, 129.4, 129.3, 128.6, 125.53, 125.45, 125.3, 123.9, 37.8.

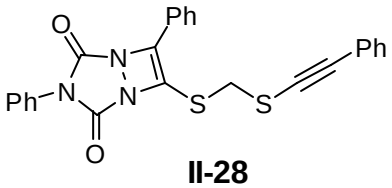

II-28

Mono-cycloadduct

Light brownliquid; Yield: 6%; ^{1}H-NMR (300 MHz, $CDCl_3$) δ 8.10-7.90 (m, 2H), 7.60-7.20 (m, 13H), 4.38 (bs, 2H); ^{13}C NMR (75 MHz, $CDCl_3$) δ = 157.2, 154.7, 150.2, 131.7, 130.8, 130.5, 129.4, 129.3, 128.72, 128.67, 128.4, 126.2, 126.0, 125.6, 124.2, 122.7, 96.4, 76.8, 40.3.

*2.8.12 X-ray crystallographic data for diazacyclobutene dimer (**II-28** (n=1))*

*Crystal Structure Report for **II-28**.*

A specimen of $C_{33}H_{22}N_6O_4S_2$, approximate dimensions 0.167 mm x 0.194 mm x 0.211 mm, was used for the X-ray crystallographic analysis. The X-ray intensity data were measured.

The integration of the data using a monoclinic unit cell yielded a total of 38969 reflections to a maximum θ angle of 26.00° (0.81 Å resolution), of which 5563 were independent (average redundancy 7.005, completeness = 99.7%, R_{int} = 4.49%, R_{sig} = 3.03%) and 4561 (81.99%) were greater than 2σ (F^2). The final cell constants of a = 13.9482(5) Å, b = 13.2287(5) Å, c = 15.4227(5) Å, β = 91.6577(12)°, volume = 2844.55(17) $Å^3$, are based upon the refinement of the XYZ-centroids of reflections above 20 σ(I). The calculated minimum and maximum transmission coefficients (based on crystal size) are 0.9353 and 1.0000.

The structure was solved and refined using the Bruker SHELXTL Software Package, using the space group P 1 21/n 1, with Z = 4 for the formula unit, $C_{33}H_{22}N_6O_4S_2$. The final anisotropic full-matrix least-squares refinement on F^2 with 406 variables converged at R1 = 3.70%, for the observed data and wR2 = 8.83% for all data.

The goodness-of-fit was 1.023. The largest peak in the final difference electron density synthesis was 0.664 $e^-/Å^3$ and the largest hole was -0.355 $e^-/Å^3$ with an RMS deviation of 0.055 $e^-/Å^3$. On the basis of the final model, the calculated density was 1.473 g/cm^3 and F(000), 1304 e^-.

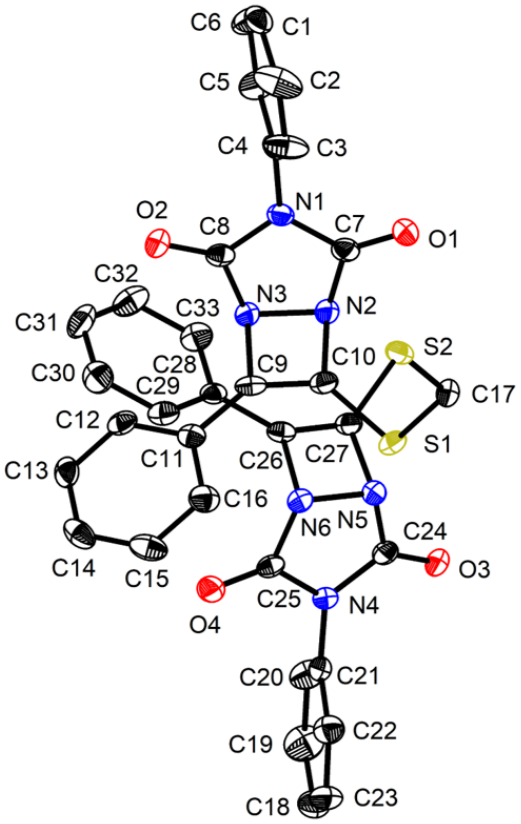

Figure 2.17. Structure of the diazacyclobutene dimer (**II-28** (n=1)) determined by single crystal X-ray diffraction, shown as 50% probability ellipsoids.

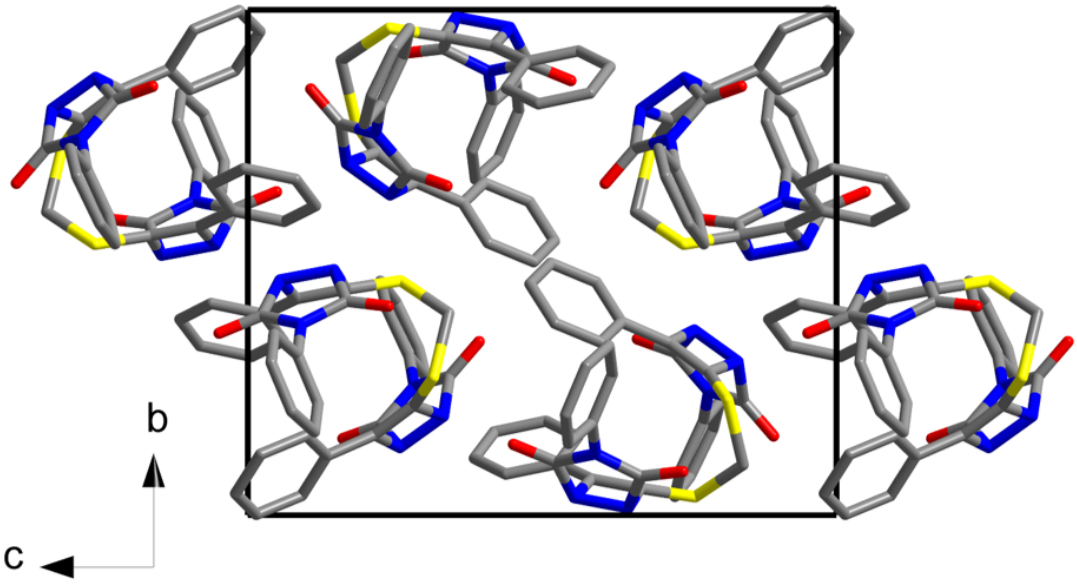

Figure 2.18. Packing diagram of the diazacyclobutene dimer (**II-28** (n=1)).

Table 2.19. Sample and crystal data for **II-28.**

Identification code	Q_0355_CN_V_168_68	
Chemical formula	$C_{33}H_{22}N_6O_4S_2$	
Formula weight	630.68 g/mol	
Temperature	106(2) K	
Wavelength	0.71073 Å	
Crystal size	0.167 x 0.194 x 0.211 mm	
Crystal system	monoclinic	
Space group	P 1 21/n 1	
Unit cell dimensions	a = 13.9482(5) Å	α = 90°
	b = 13.2287(5) Å	β = 91.6577(12)°
	c = 15.4227(5) Å	γ = 90°
Volume	2844.55(17) $Å^3$	
Z	4	
Density (calculated)	1.473 g/cm^3	
Absorption coefficient	0.240 mm^{-1}	
F(000)	1304	

Table 2.20 Data collection and structure refinement for **II-28.**

Theta range for data collection	3.06 to 26.00°	
Index ranges	-17<=h<=17, -16<=k<=16, -18<=l<=19	
Reflections collected	38969	
Independent reflections	5563 [R(int) = 0.0449]	
Max. and min. transmission	1.0000 and 0.9353	
Structure solution technique	direct methods	
Structure solution program	SHELXT-2014 (Sheldrick 2014)	
Refinement method	Full-matrix least-squares on F^2	
Refinement program	SHELXL-2014 (Sheldrick 2014)	
Function minimized	$\Sigma\, w(F_o^2 - F_c^2)^2$	
Data / restraints / parameters	5563 / 0 / 406	
Goodness-of-fit on F^2	1.023	
Δ/σ_{max}	0.001	
Final R indices	4561 data; $I>2\sigma(I)$	R1 = 0.0370, wR2 = 0.0819
	all data	R1 = 0.0502, wR2 = 0.0883
Weighting scheme	$w=1/[\sigma^2(F_o^2)+(0.0354P)^2+2.5132P]$ where $P=(F_o^2+2F_c^2)/3$	
Largest diff. peak and hole	0.664 and -0.355 eÅ^{-3}	
R.M.S. deviation from mean	0.055 eÅ^{-3}	

2.8.13 A typical procedure for the preparation of ynamides.[51,86,130]

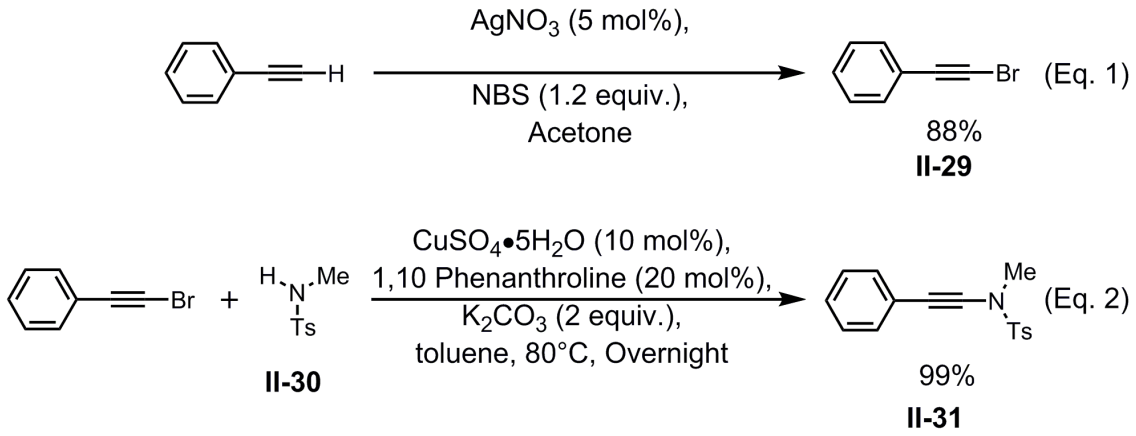

Procedure

Step 1

To a flame-dried round bottom flask, equipped with a stir bar, $AgNO_3$ (5 mol%, 0.25 mmol) and dry acetone (12.5 mL) were added. To this solution, phenylacetylene (5 mmol, 1 equiv) was added and subsequently NBS (6 mmol, 1.2 equiv) was added in portion-wise manner. The mixture was then stirred for 3 h at room temperature. The solvent was removed under reduced pressure. The residue was dissolved in petroleum ether and filtered through a short pad of silica gel. Again, the solvent was removed under the reduced pressure to afford a pale-yellow oil of bromoalkyne (88%, **II-29**).

Step 2

To the above solution of bromoalkyne (2.20 mmol, 1.1 equiv) in 2 mL of anhydrous toluene in a round bottom flask (RBF) were added *N*-methyltoluenesulfonamide (2.00 mmol, 1 equiv (**II-30**)), K_2CO_3 (2 equiv, 4.00 mmol), $CuSO_4 \cdot 5H_2O$ (0.20 mmol, 10 mol%), and 1,10-phenanthroline (0.40 mmol, 20 mol%). Then the flask was capped with a septum and heated in an oil bath at 80˚C overnight under nitrogen atmosphere. After completion of the reaction was confirmed by TLC, the reaction mixture was cooled to room temperature and subsequently diluted with 12 mL of chloroform. This mixture was filtered through a short celite pad, and the filtrate was concentrated under reduced pressure. The crude residue was purified by flash column chromatography using silica gel and hexane/ethyl acetate eluents system. A gradient eluent: 0-20% EtOAc in hexane was used to yield ynamide (99%, **II-31**) as a yellow solid.

2.8.14 A typical procedure for the preparation of ynamines.[101,131]

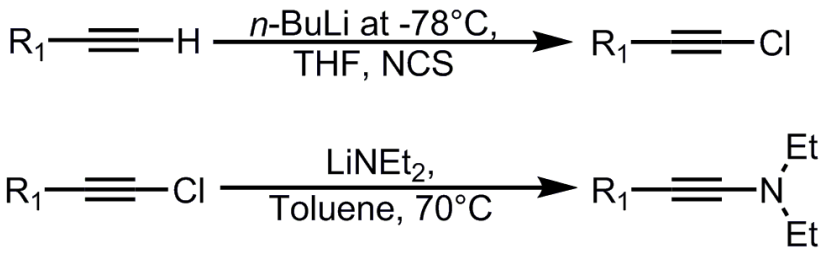

The above procedure was slightly modified from reported procedures.

Procedure

Step 1

A flame-dried flask, equipped with a stir bar, was added a terminal alkyne (5.00 mmol, 1 equiv) and freshly distilled, anhydrous THF (10 mL) under argon. The reaction was cooled to –78˚C and then treated with *n*-butyllithium (1.6 M solution in hexanes, 6.00 mmol, 1.2 equiv). Then the solution was stirred for 15 min and *N*-chlorosuccinimide (6.60 mmol, 1.1 equiv.) was added in one portion-wise manner.

The reaction was then allowed to warm to room temperature and quenched with 15 mL of sat. aq. NH_4Cl. The mixture was then diluted with 30 mL of Et_2O and washed with 20 mL of sat. aq. brine. The aqueous layer was extracted with Et_2O(3 x 30 mL). The combined organic layer was dried over Na_2SO_4, filtered and concentrated under reduced pressure. This crude mixture was then purified by flash column chromatography using silica gel and 100% hexane or petroleum ether afforded the expected chloroalkyne product.

Step 2

A flame dried round bottom flask was charged with a stir bar, equipped with a septum, and flushed with argon while heating to remove remaining air and moisture. Then diethylamine (NEt_2) (2.2 mmol, 1.8 equiv) and 20 mL of anhydrous toluene were added. The mixture was cooled to –78˚C and treated with *n*-butyllithium (1.6 M in hexane, 2.4 mmol, *ca.* 2 equiv). The reaction mixture was stirred for 30 min at –78˚C and allowed to warm to the room temperature. Then the reaction mixture was stirred at room temperature for another 5-10 min and the previously prepared chloroalkyne (1.22 mmol, 1 equiv) was added. The reaction mixture was then heated at 70˚C for 19 h. The reaction mixture was cooled, filtered through a pad of celite, and solvents were removed under reduced pressure. The residue was extracted with hexane, filtered again through a pad of celite, and solvents were removed under reduced pressure to afford the desired ynamine as a red liquid.

2.8.15 General procedure for the synthesis of ynamide based diazacyclobutenes.

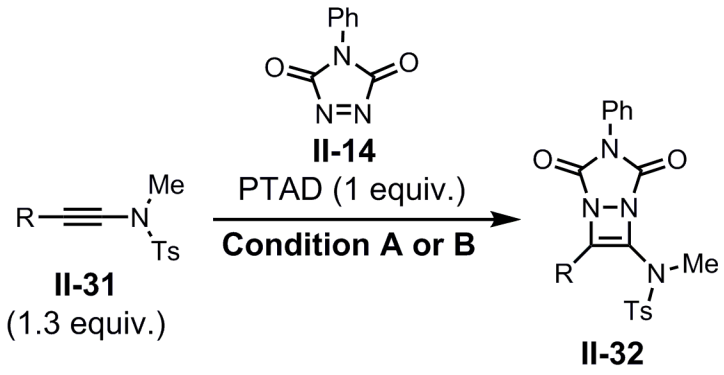

Condition A : Refluxed for 24 h in MeCN
Condition B : Stir with 5 mol% of $AgNTf_2$ catalyst for 24 h in DCM at RT

Condition A

To a flame-dried round bottom flask, equipped with a stir bar, were added 4-phenyl-triazoline-3,5-dione (PTAD) (1 mmol, 1 equiv), and dry acetonitrile (5 mL for 1 mmol of PTAD). Then the corresponding ynamide (1.3 mmol (**II-31**)) was added as a solution in dry acetonitrile (5 mL for 1.3 mmol of ynamide). Then the mixture was refluxed for 24 h. The resultant mixture was concentrated under reduced pressure and purified via flash silica gel column chromatography with a gradient elution using hexane/ethyl acetate eluents system (0-20% ethyl acetate) to afford the corresponding diazacyclobutene (**II-32**).

Condition B

To a flame-dried round bottom flask, equipped with a stir bar, were added 5 mol% $AgNTf_2$ (0.05 mmol), 4-phenyl-triazoline-3,5-dione (PTAD) (1 mmol, 1 equiv), and dry dichloromethane (5 mL for 1 mmol of PTAD). Then the corresponding ynamide (1.3 mmol/ **II-31**) was added as a solution in dry dichloromethane (5 mL for 1.3 mmol of ynamide). Then the mixture was stirred at room temperature for 24 h. The resultant mixture was concentrated under reduced pressure and purified via flash silica gel column chromatography with a gradient elution using hexane/ethyl acetate eluents system (0-20% ethyl acetate) to afford the corresponding diazacyclobutene (**II-32**).

2.8.16 Characterization data for bromoalkynes, ynamides and ynamide based diazacyclobutenes.

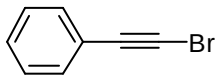

II-29

Colorless liquid; Yield: 88%;^{1}H-NMR (300 MHz, $CDCl_3$) δ 7.60-7.45 (m, 2H), 7.45-7.25(m, 3H); ^{13}C NMR (75 MHz, $CDCl_3$) δ = 131.9, 128.6, 128.3, 122.6, 80.0, 49.8.

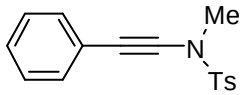

II-31a

Light yellow solid; Yield: 98%;^{1}H-NMR (300 MHz, $CDCl_3$) δ 7.87 (d, *J* = 7.3 Hz, 2H), 7.60-7.33 (m, 4H), 7.33-7.25 (m, 3H), 3.15 (s, 3H), 2.46 (s, 3H); ^{13}C NMR (75 MHz, $CDCl_3$) δ =162.3, 144.8, 133.2, 131.3, 129.8, 128.2, 127.8, 122.6, 83.9, 68.98, 39.26, 21.6.

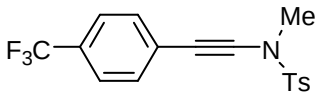

II-31b

Light yellow solid; Yield: 94%; ^{1}H-NMR (300 MHz, $CDCl_3$) δ 7.84 (d, *J* = 8.3 Hz, 2H), 7.60-7.48 (d, *J* = 7.5 Hz, 2H), 7.43 (d, *J* = 8.1 Hz, 2H), 7.38 (d, *J* = 7.9 Hz, 2H), 3.18 (s, 3H), 2.46 (s, 3H); ^{13}C NMR (75 MHz, $CDCl_3$) δ = 145.1, 133.3, 131.0, 129.9, 127.8, 126.8, 125.2 (^{3}J= 3.78 Hz, 1C), 86.5, 68.4, 39.1, 21.6.

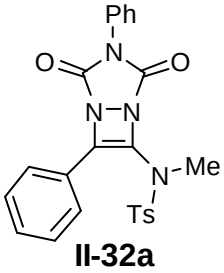

II-32a

Light yellow solid; Yield: 20% (Method-A); Mp: 167.2-168.2°C; IR (neat): 2927 (w), 2854 (w), 1797 (m), 1739 (s), 1693 (m), 1597 (m), 1492 (m), 1450 (m), 1392 (s), 1350 (s), 1292 (w), 1230 (s), 1188 (m), 1149 (s), 1122 (w), 1083 (m), 1045 (w), 1018 (s), 933 (w), 891 (m), 833 (s), 810 (s), 759 (s), 705 (s), 671 (s), 640 9s), 578 (m) cm^{-1}; ^{1}H-NMR (300 MHz, $CDCl_3$) δ 7.80-7.70 (m, 4H), 7.60-7.20 (m, 10H), 3.22 (s, 3H), 2.42 (s, 3H); ^{13}C NMR (75 MHz, $CDCl_3$) δ = 156.1, 155.4, 144.9, 139.7, 133.8, 132.8, 130.7, 130.2, 129.9, 129.2, 129.1, 128.6, 128.2, 126.4, 126.2, 125.3, 36.3, 21.6.

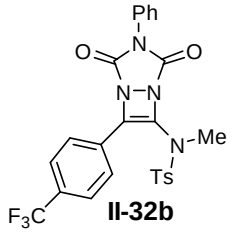

II-32b

Light yellow solid; Yield: 37% (Method-A); Mp: 173.2-174.2°C; IR (neat): 2927(w), 2858 (w), 1801 (w), 1743 (s), 1697 (w), 1616 (w), 1597 (m), 1504 (m), 1458 (m), 1411 (m), 1365 (s), 1350 (s), 1319 (s), 1234 (s), 1157 (s), 1111 (s), 1083 (s), 1064 (s), 1010 (s), 844 (s), 705 (s), 671 (s), 578 (s) cm^{-1};^{1}H-NMR (300 MHz, $CDCl_3$) δ 7.98 (d, *J* = 8.2 Hz, 2H), 7.82 (d, *J* = 8.2 Hz, 2H), 7.70 (d, *J* = 8.3 Hz, 2H), 7.60-7.37 (m, 5H), 7.34 (d, *J* = 8.1 Hz, 2H), 3.24 (s, 3H), 2.41 (s, 3H); ^{13}C NMR (75 MHz, $CDCl_3$) δ = 155.5, 155.4, 145.4, 137.6, 133.5, 131.3, 130.6, 130.1, 129.4, 129.3, 128.8, 128.2, 126.6, 126.8 ($^{1}J_{CF}$ = 272 Hz, 1C), 125.3, 125.7 ($^{3}J_{CF}$ = 3.96 Hz, 1C), 125.3, 36.2, 21.6.

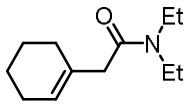

II-36
Hydrated product of the ynamine

Light brown liquid;^{1}H-NMR (500 MHz, $CDCl_3$) δ 5.50-5.40 (m, 1H), 3.34 (q, *J* = 7.1 Hz, 2H), 3.26 (q, *J* = 7.1 Hz, 2H), 2.95 (s, 2H), 2.05-1.90 (m, 4H), 1.65-1.45 (m, 4H), 1.13 (t, *J* = 7.1 Hz, 3H), 1.10 (t, *J* = 7.1 Hz, 3H); ^{13}C NMR (125 MHz, $CDCl_3$) δ = 170.1, 132.2, 123.6, 43.1, 42.1, 39.8, 28.5, 25.2, 22.7, 22.0, 14.2, 12.9.

2.8.17 X-ray crystallographic data for ynamide based diazacyclobutenes.

*Crystal Structure Report for **II-32a**.*

A specimen of $C_{24}H_{20}N_4O_4S$, approximate dimensions 0.056 mm x 0.241 mm x 0.372 mm, was used for the X-ray crystallographic analysis. The X-ray intensity data were measured.

The integration of the data using an orthorhombic unit cell yielded a total of 33874 reflections to a maximum θ angle of 25.50° (0.83 Å resolution), of which 4235 were independent (average redundancy 7.999, completeness = 99.8%, R_{int} = 4.92%, R_{sig} = 2.57%) and 3517 (83.05%) were greater than $2\sigma(F^2)$. The final cell constants of a = 12.2237(4) Å, b = 18.2464(7) Å, c = 20.4324(8) Å, volume = 4557.2(3) $Å^3$, are based upon the refinement of the XYZ-centroids of reflections above 20 σ(I). The calculated minimum and maximum transmission coefficients (based on crystal size) are 0.9417 and 1.0000. The structure was solved and refined using the Bruker SHELXTL Software Package, using the space group P b c a, with Z = 8 for the formula unit, $C_{24}H_{20}N_4O_4S$. The final anisotropic full-matrix least-squares refinement on F^2 with 300 variables converged at R1 = 3.90%, for the observed data and wR2 = 10.31% for all data. The goodness-of-fit was 1.054. The largest peak in the final difference electron density synthesis was 0.199 $e^-/Å^3$ and the largest hole was -0.474 $e^-/Å^3$ with an RMS deviation of 0.049 $e^-/Å^3$. On the basis of the final model, the calculated density was 1.342 g/cm^3 and F(000), 1920 e^-.

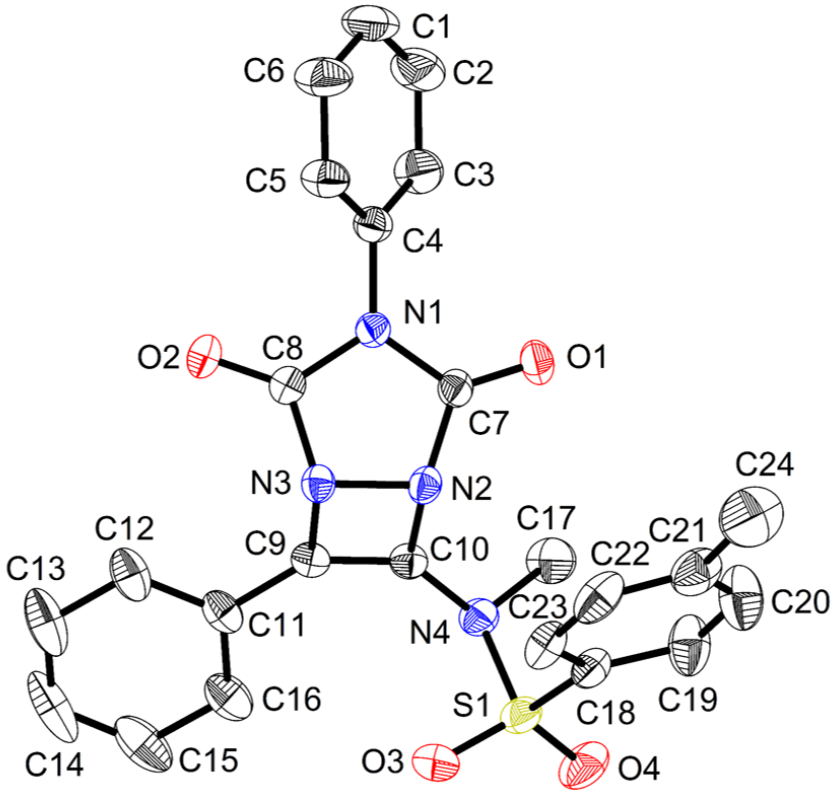

Figure 2.19. Structures of the ynamide-based diazacyclobutenes **II-32a** determined by single crystal X-ray diffraction, shown as 50% probability ellipsoids.

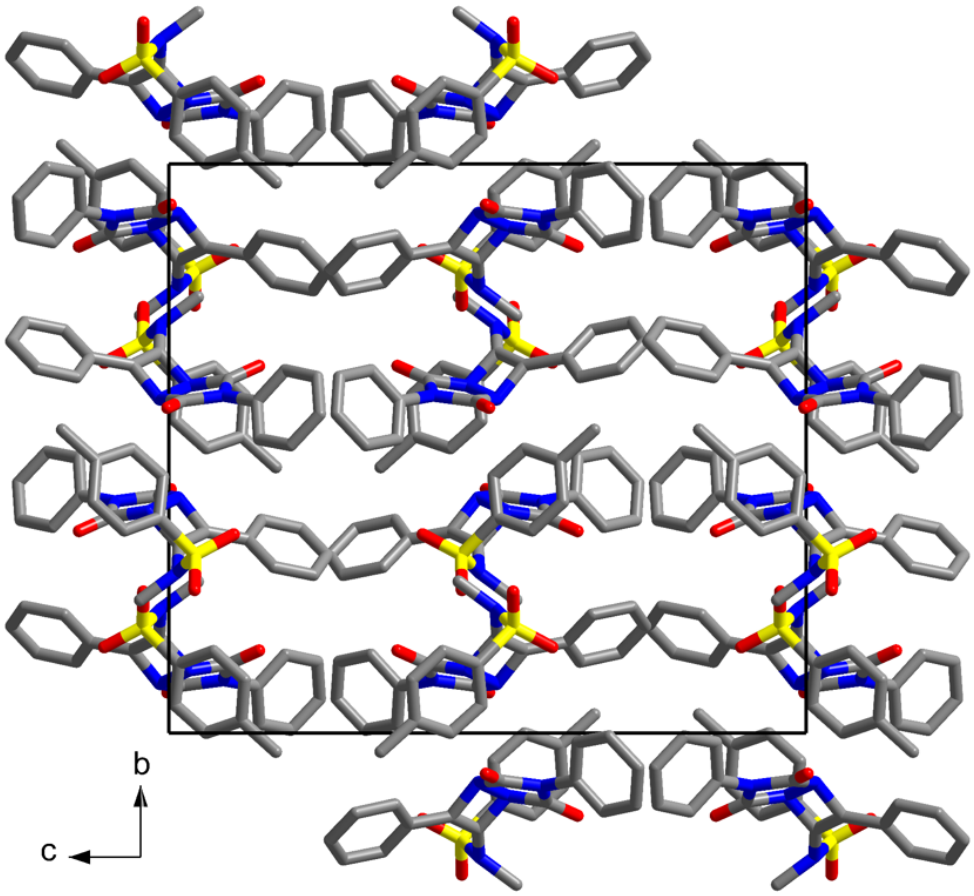

Figure 2.20. Packing diagram of the ynamide-based diazacyclobutenes **II-32a**

Table 2.21. Sample and crystal data for **II-32a.**

Identification code	D8_2823_CN_VI_134_74	
Chemical formula	$C_{24}H_{20}N_4O_4S$	
Formula weight	460.50 g/mol	
Temperature	140(2) K	
Wavelength	0.71073 Å	
Crystal size	0.056 x 0.241 x 0.372 mm	
Crystal system	orthorhombic	
Space group	P b c a	
Unit cell dimensions	a = 12.2237(4) Å	α = 90°
	b = 18.2464(7) Å	β = 90°
	c = 20.4324(8) Å	γ = 90°
Volume	4557.2(3) $Å^3$	
Z	8	
Density (calculated)	1.342 g/cm^3	
Absorption coefficient	0.181 mm^{-1}	
F(000)	1920	

Table 2.22. Data collection and structure refinement for **II-32a.**

Theta range for data collection	2.23 to 25.50°	
Index ranges	-14<=h<=14, -22<=k<=22, -22<=l<=24	
Reflections collected	33874	
Independent reflections	4235 [R(int) = 0.0492]	
Max. and min. transmission	1.0000 and 0.9417	
Structure solution technique	direct methods	
Structure solution program	SHELXT-2014 (Sheldrick 2014)	
Refinement method	Full-matrix least-squares on F^2	
Refinement program	SHELXL-2014 (Sheldrick 2014)	
Function minimized	$\Sigma\, w(F_o^2 - F_c^2)^2$	
Data / restraints / parameters	4235 / 0 / 300	
Goodness-of-fit on F^2	1.054	
Δ/σ_{max}	0.001	
Final R indices	3517 data; $I>2\sigma(I)$	R1 = 0.0390, wR2 = 0.0957
	all data	R1 = 0.0504, wR2 = 0.1031
Weighting scheme	$w=1/[\sigma^2(F_o^2)+(0.0483P)^2+2.1545P]$ where $P=(F_o^2+2F_c^2)/3$	
Largest diff. peak and hole	0.199 and -0.474 eÅ^{-3}	
R.M.S. deviation from mean	0.049 eÅ^{-3}	

*Crystal Structure Report for **II-32b***

A specimen of $C_{26}H_{20}Cl_3F_3N_4O_4S$, approximate dimensions 0.078 mm x 0.087 mm x 0.403 mm, was used for the X-ray crystallographic analysis. The X-ray intensity data were measured.

The integration of the data using a monoclinic unit cell yielded a total of 39210 reflections to a maximum θ angle of 26.00° (0.81 Å resolution), of which 5658 were independent (average redundancy 6.930, completeness = 99.8%, R_{int} = 4.93%, R_{sig} = 2.92%) and 4589 (81.11%) were greater than $2\sigma(F^2)$. The final cell constants of a = 29.839(4) Å, b = 9.6388(12) Å, c = 23.025(3) Å, β = 119.411(6)°, volume = 5768.8(14) $Å^3$, are based upon the refinement of the XYZ-centroids of reflections above 20 σ(I). The calculated minimum and maximum transmission coefficients (based on crystal size) are 0.9021 and 1.0000. The structure was solved and refined using the Bruker SHELXTL Software Package, using the space group C 1 2/c 1, with Z = 8 for the formula unit, $C_{26}H_{20}Cl_3F_3N_4O_4S$. The final anisotropic full-matrix least-squares refinement on F^2 with 428 variables converged at R1 = 4.46%, for the observed data and wR2 = 11.90% for all data. The goodness-of-fit was 1.021. The largest peak in the final difference electron density synthesis was 0.566 $e^-/Å^3$ and the largest hole was -0.421 $e^-/Å^3$ with an RMS deviation of 0.054 $e^-/Å^3$. On the basis of the final model, the calculated density was 1.492 g/cm^3 and F(000), 2640 e^-.

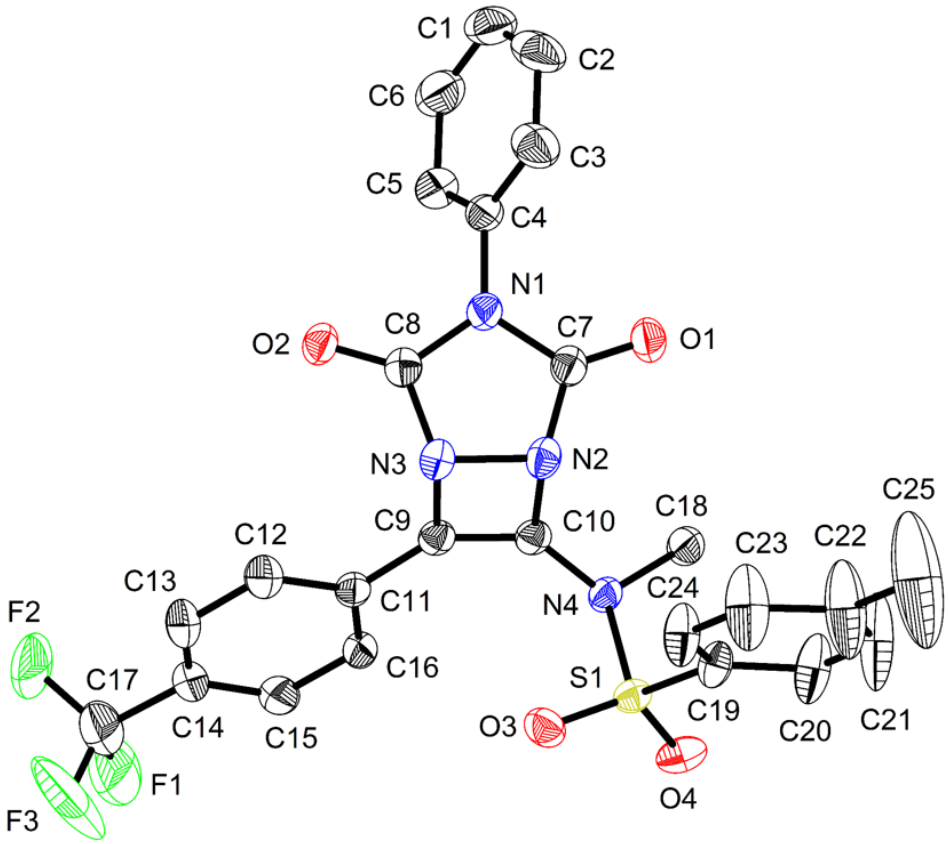

Figure 2.21. Structures of the ynamide-based diazacyclobutenes **II-32b** determined by single crystal X-ray diffraction, shown as 50% probability ellipsoids.

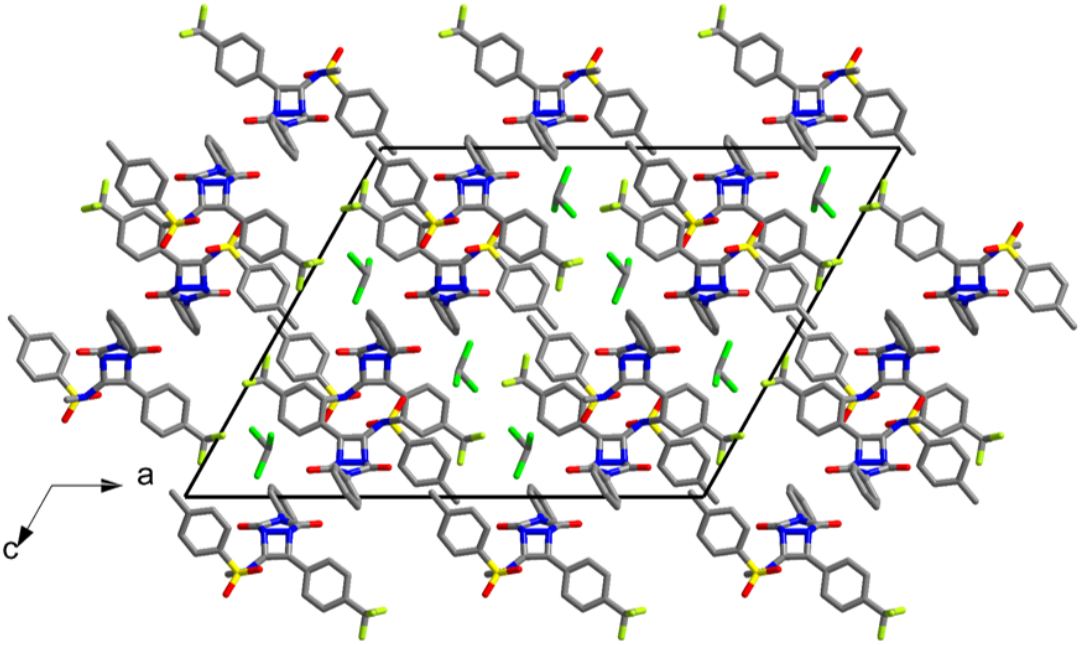

Figure 2.22. Packing diagram of the ynamide-based diazacyclobutenes **II-32b**

Table 2.23 Sample and crystal data for **II-32b.**

Identification code	D8_2662_CN_VI_110_63	
Chemical formula	$C_{26}H_{20}Cl_3F_3N_4O_4S$	
Formula weight	647.87 g/mol	
Temperature	140(2) K	
Wavelength	0.71073 Å	
Crystal size	0.078 x 0.087 x 0.403 mm	
Crystal system	monoclinic	
Space group	C 1 2/c 1	
Unit cell dimensions	a = 29.839(4) Å	α = 90°
	b = 9.6388(12) Å	β = 119.411(6)°
	c = 23.025(3) Å	γ = 90°
Volume	5768.8(14) $Å^3$	
Z	8	
Density (calculated)	1.492 g/cm^3	
Absorption coefficient	0.449 mm^{-1}	
F(000)	2640	

Table 2.24 Data collection and structure refinement for **II-32b.**

Theta range for data collection	2.62 to 26.00°	
Index ranges	-36<=h<=36, -11<=k<=11, -28<=l<=26	
Reflections collected	39210	
Independent reflections	5658 [R(int) = 0.0493]	
Max. and min. transmission	1.0000 and 0.9021	
Structure solution technique	direct methods	
Structure solution program	SHELXT-2014 (Sheldrick 2014)	
Refinement method	Full-matrix least-squares on F^2	
Refinement program	SHELXL-2014 (Sheldrick 2014)	
Function minimized	$\Sigma\, w(F_o^2 - F_c^2)^2$	
Data / restraints / parameters	5658 / 75 / 428	
Goodness-of-fit on F^2	1.021	
Δ/σ_{max}	0.001	
Final R indices	4589 data; $I>2\sigma(I)$	R1 = 0.0446, wR2 = 0.1096
	all data	R1 = 0.0580, wR2 = 0.1190
Weighting scheme	$w=1/[\sigma^2(F_o^2)+(0.0554P)^2+9.1166P]$ where $P=(F_o^2+2F_c^2)/3$	
Largest diff. peak and hole	0.566 and -0.421 eÅ^{-3}	
R.M.S. deviation from mean	0.054 eÅ^{-3}	

2.8.18 A typical procedure for the preparation of semicarbazides.[6,106,108]

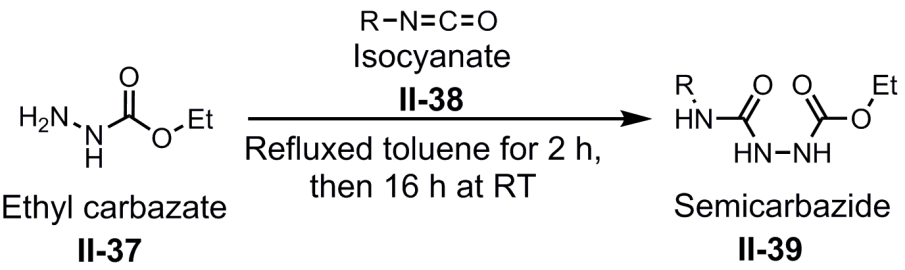

A flame-dried round bottom flask was charged with a stir bar and ethyl carbazate (4 mmol, 1 equiv, (**II-37**)) was added in dry toluene (4 mL). To this solution, was added isocyanate (4 mmol, 1 equiv, (**II-38**)) in dry toluene (4 mL) and the reaction mixture was refluxed at 80˚C for 2 h. Then the mixture was stirred at room temperature overnight (about 16 h). The precipitate that formed was filtered, washed with diethyl ether and dried under air to give the corresponding semicarbazide **II-39**. This compound was used without further purification in the next reaction step.

2.8.19 A typical procedure for the preparation of urozoles.[6,106,107,116]

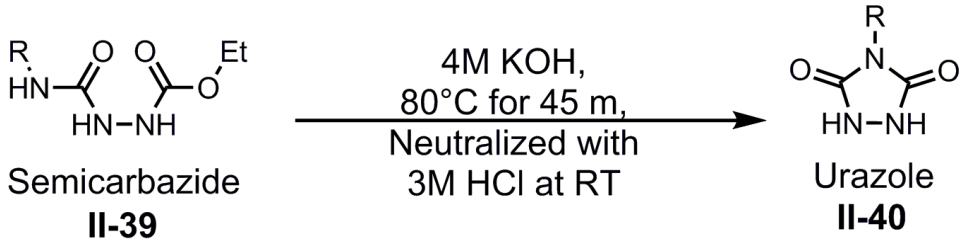

A flame-dried round bottom flask was charged with a stir bar and the semicarbazide **II-39** was added (2 mmol, 1 equiv). This was then reacted with aqueous

4 M KOH solution (4 mmol, 2 equiv), and the flask was placed in a warm water bath at 80˚Cfor 45 min. The reaction mixture was cooled to room temperature and neutralized with 3 M HCl. The formed precipitate was filtered off, washed with cold water, and dried in a vacuum oven at 60°C for 1 h to afford the corresponding 4-substituted urozole **II-40**.

2.8.20 A typical procedure for the oxidation of urozoles.[107,108,115–117]

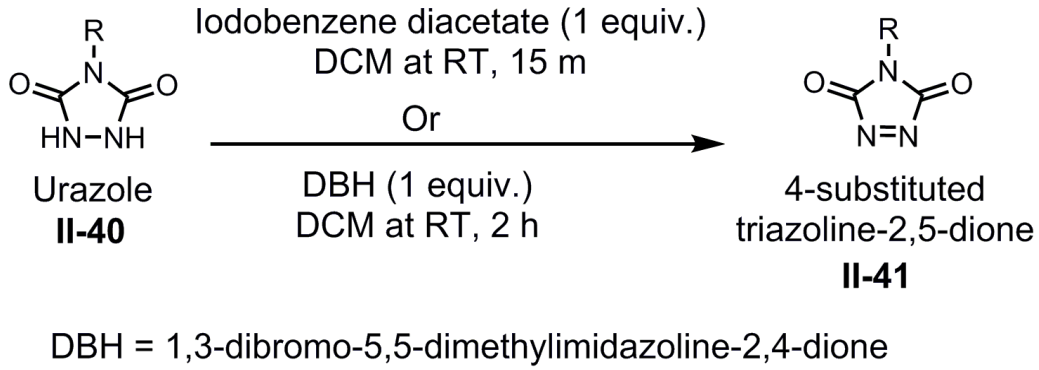

DBH = 1,3-dibromo-5,5-dimethylimidazoline-2,4-dione

DBH oxidation[107]

To a flame-dried round bottom flask were added a stir bar, urozole **II-40**(1 mmol, 1 equiv), dry CH_2Cl_2 (15 mL), and DBH (1 mmol, 1 equiv). The resulting mixture was stirred at room temperature for 2h. To this solution, was added 0.5 g of previously prepared silica sulfuric acid [*i.e.*, prepared by mixing 1 mL of concentrated H_2SO_4 acid to a slurry of silica in ether (10 g in 20 mL of ether) followed by evaporation of solvents and dried at 100˚C for 3 h][132,133] and stirred for 15 min.

The reaction mixture was then filtered and concentrated under reduced pressure to give the red colored 4-substituted-triazoline-3,5-dione (**II-41**). These compounds are very sensitive to heat, so one needs to perform the removal of the solvent carefully without using high temperatures (*i.e.*, >50˚C). Also, these oxidized triazolinediones are sensitive to light, alcohols, ethers, transition metals, and some nucleophiles.

Iodobenzene diacetate ($PhI(OAc)_2$) oxidation[108,115–117]

To a flame-dried round bottom flask were added a stir bar, urozole **II-40** (1 mmol, 1 equiv), dry CH_2Cl_2 (4 mL), and iodobenzene diacetate (1 mmol, 1 equiv). The resulting mixture was stirred at room temperature for 15 min. Then the solvent was removed under reduced pressure, and hexane (8 mL) was added. The slurry was filtered to afford the red colored 4-substituted-triazoline-3,5-dione (**II-41**).

2.8.21 General procedure for the in situ oxidation and following [2+2] cycloaddition to provide diazacyclobutenes with 4-substituted 1,2,4-triazoline-2,5-diones (TADs).

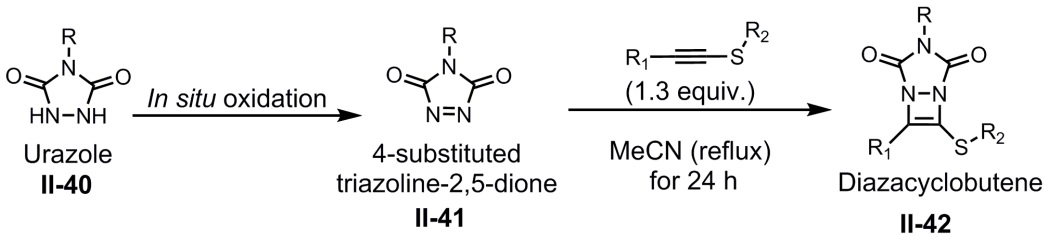

To a flame-dried round bottom flask, was added a stir bar, urozole **II-40** (1 mmol, 1 equiv), oxidant (*i.e.*, DBH or $PhI(OAc)_2$) (1 mmol, 1 equiv), and dry CH_2Cl_2 (10 mL). The resulting mixture was stirred at room temperature for a given period of time. After the oxidation work-up (according to the DBH or iodobenzene diacetate oxidation methods described above) is completed, the *in situ* generated triazolinedione (**II-41**) was directly used without further purification. The triazolinedione (**II-41**) was then reacted with the corresponding alkynyl sulfide (1.3 mmol, 1.3 equiv) in acetonitrile (10 mL) under reflux condition for 24 h. Then the solvent was removed under reduced pressure and the crude mixture was purified using flash silica gel chromatography with a hexane/ethyl acetate solvent system (0 to 20% ethyl acetate) to afford the corresponding diazacyclobutene **II-42**. (Note: Yields were calculated based on the urozole equivalence.)

2.8.22 General procedure for the in situ catalytic method for [2+2] cycloaddition to provide diazacyclobutenes with 4-substituted 1,2,4-triazoline-2,5-diones (TADs).[93,96–100,111]

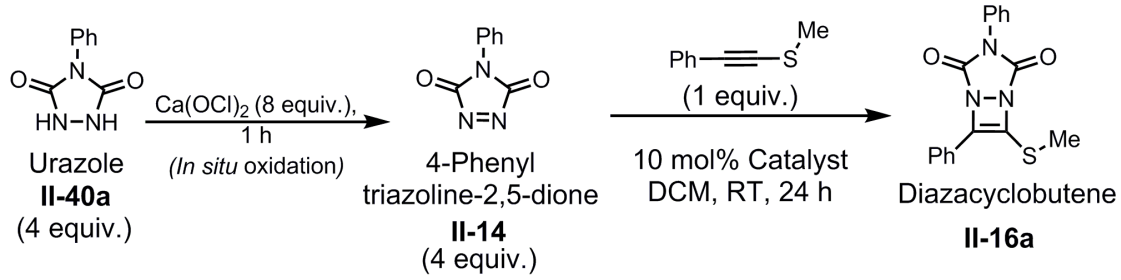

To a flame-dried round bottom flask, was added a stir bar, urozole **II-40a** (4 mmol, 4equiv.), $Ca(OCl)_2$ (8 mmol, 8 equiv.),[111] and dry DCM (10 mL). The resulting mixture was stirred at room temperature for 1 h. After the oxidation is finished, the reaction mixture was filtered, concentrated under reduced pressure, and the residue was used directly without further purification.

To this triazolinedione, was added 10 mol% of the catalyst (0.1 mmol),[93,96–100] and the corresponding alkynyl sulfide (1mmol, 1equiv.) in DCM (10 mL). The resulting mixture was stirred at room temperature for 24 h. Then the solvent was removed under reduced pressure. The crude mixture was purified using flash silica gel chromatography with hexane/ethyl acetate eluents system (0 to 20% ethyl acetate) to afford the diazacyclobutene **II-16a**. Further optimization showed that 3 equiv. of the urozole, 2 h oxidation and 30 mol% of the $MgCl_2$catalyst[93] gave 98% of the diazacyclobutene **II-16a**.

2.8.23 Characterization data for semicarbazides and urozoles

Note: Characterization data for these widely known molecules can be also found in these cited publications[106–108] and they were consistent with this experimental data. Therefore, these characterization data have been limited to ^{1}H NMR or ^{1}H and ^{13}C NMR.

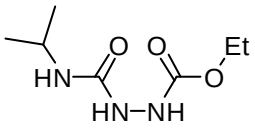

II-39a

White solid; Yield: 43%; ^{1}H-NMR (300 MHz, $CDCl_3$) δ 7.23 (s, 1H), 7.02 (bs, 1H), 5.46 (bs, 1H), 4.16 (*J* = 7.1 Hz, 2H), 4.02-3.78 (bm, 1H), 1.25 (t, *J* = 7.1 Hz, 3H), 1.12 (d, *J* = 6.5 Hz, 6H); ^{13}C NMR (75 MHz, $CDCl_3$) δ = 158.2, 157.5, 62.2, 42.0, 23.0, 14.4.

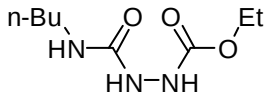

II-39b

White solid; Yield: 69%; ^{1}H-NMR (300 MHz, $CDCl_3$) δ 7.16 (s, 1H), 6.99 (bs, 1H), 5.60 (bs, 1H), 4.17 (q, *J* = 7.1, 2H), 3.18 (t, *J* = 7.1, 2H), 1.56-1.16 (m, 7H), 0.9 (t, *J* = 7.3 Hz, 3H); ^{13}C NMR (75 MHz, $CDCl_3$) δ =.158.9, 157.5, 62.3, 39.8, 32.0, 19.9, 14.4, 13.7.

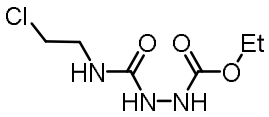

II-39c

White solid; Yield: 40%; ^{1}H-NMR (300 MHz, DMSO-d6) δ 8.8 (s, 1H), 7.9 (s, 1H), 6.6 (s, 1H), 4.0 (q, *J* = 7.1 Hz, 2H), 3.6 (t, *J* = 6.4 Hz, 2H), 3.4-3.2 (m, 2H), 1.17 (t, *J* = 7.1 Hz, 3H);^{13}C NMR (75 MHz, DMSO-d6) δ = 158.4, 157.0, 60.6, 43.9, 41.5, 14.7.

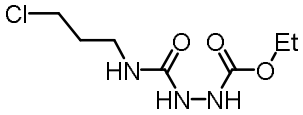

II-39d

White solid; Yield: 40%; ^{1}H-NMR (500 MHz, DMSO-d6) δ 8.76 (s, 1H), 7.73 (s, 1H), 6.53 (s, 1H), 4.02 (q, *J* = 7.0 Hz, 2H), 3.61 (t, *J* = 6.6 Hz, 2H), 3.12 (q, *J* = 6.1 Hz, 2H), 1.83 (pentet, *J* = 6.6 Hz, 2H),1.18 (t, *J* = 6.3 Hz, 3H); ^{13}C NMR (125 MHz, DMSO-d6) δ = 158.9, 157.4, 60.9, 43.5, 37.1, 33.4, 15.0.

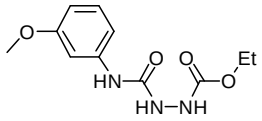

II-39e

White solid; Yield: 99%; ^{1}H-NMR (300 MHz, DMSO-d6) δ 8.92 (s, 1H), 8.72 (s, 1H), 7.99 (s, 1H), 7.5-6.0 (m, 4H), 4.05 (q, *J* = 7.1 Hz, 2H), 3.7 (s, 3H), 1.19 (t, *J* = 6.8 Hz, 3H); ^{13}C NMR (75 MHz, DMSO-d6) δ = 159.6, 156.9, 155.5, 140.9, 129.4, 110.8, 107.3, 104.2, 60.5, 54.9, 14.6.

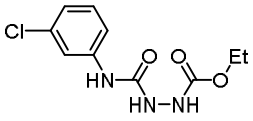

II-39f

White solid; Yield: 85%; ^{1}H-NMR (300 MHz, DMSO-d6) δ 8.97 (s, 2H), 8.17 (s, 1H), 7.69 (s, 1H), 7.35 (s, 1H), 7.25 (t, *J* = 8.0 Hz, 1H), 7.10-6.90 (m, 1H), 4.05 (q, *J* = 7.1 Hz, 2H), 1.19 (t, *J* = 6.9 Hz, 3H); ^{13}C NMR (75 MHz, DMSO-d6) δ = 161.9, 156.9, 155.5, 141.3, 132.9, 130.2, 121.4, 117.9, 60.6, 14.5.

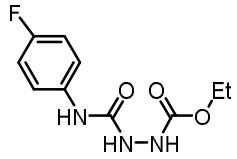

II-39g

White solid; Yield: 95%; ^{1}H-NMR (300 MHz, DMSO-d6) δ 8.92 (s,, 1H), 8.78 (s, 1H), 8.03 (s, 1H), 7.60-7.00 (m, 4H), 4.05 (q, *J* = 7.1 Hz, 2H), 1.19 (t, *J* = 6.9 Hz, 3H)); ^{13}C NMR (75 MHz, DMSO-d6) δ = 157.8 (d, *J* = 237.7 Hz, 1C), 157.5, 156.2, 136.5 (d, *J* = 1.8 Hz, 1C), 120.7, 115.5 (d, *J* = 22.1 Hz, 1C), 61.0, 15.0.

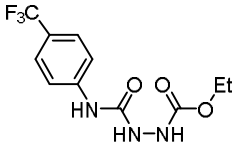

II-39h

White solid; Yield: 29%; ^{1}H-NMR (300 MHz, DMSO-d6) δ 9.19 (s, 1H), 9.00 (s, 1H), 9.00 (s, 1H), 8.23 (s, 1H), 8.00-7.50 (m, 4H), 4.06 (q, *J* = 7.0 Hz, 2H), 1.19 (t, *J* = 6.7 Hz, 3H); ^{13}C NMR (125 MHz, DMSO-d6) δ = 157.0, 155.5, 143.6, 124.6 (q, $^{1}J_{CF}$ = 270.7 Hz, 1C), 126.0, 121.8 (q, $^{1}J_{CF}$ = 31.5 Hz, 1C), 118.2, 60.7, 14.6.

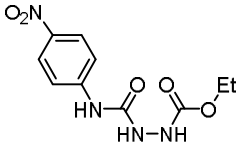

II-39i

White solid; Yield: 99%; ^{1}H-NMR (300 MHz, DMSO-d6) δ 9.54 (s, 1H), 9.06 (s, 1H), 8.41 (s, 1H), 8.16 (d, *J* = 9.2 Hz, 2H), 8.00-7.60 (m, 2H), 4.06 (q, *J* = 7.1 Hz, 2H), 1.20 (t, *J* = 6.8 Hz, 3H); ^{13}C NMR (125 MHz, DMSO-d6:$CDCl_3$ = 5:1) δ =156.9, 155.1, 146.4, 141.1, 124.9, 117.7, 60.7, 14.6.

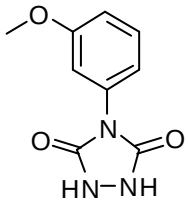

II-40e

White solid; Yield: 35%; ^{1}H-NMR (300 MHz, DMSO-d6) δ10.46 (s, 2H), 7.60-7.20 (m, 1H), 7.20-6.90 (m, 3H), 3.77 (s, 3H); ^{13}C NMR (75 MHz, DMSO-d6) δ = 159.4, 153.3, 129.5, 118.2, 113.2, 111.9, 55.3.

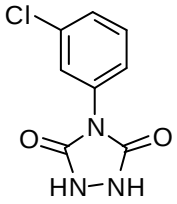

II-40f

White solid; Yield: 44%; ^{1}H-NMR (300 MHz, DMSO-d6) δ 7.70-7.40 (m, 6H); ^{13}C NMR (75 MHz, DMSO-d6) δ = 152.9, 133.5, 132.9, 130.5, 127.6, 125.6, 124.5.

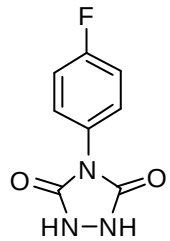

II-40g

White solid; Yield: 63%; ^{1}H-NMR (300 MHz, DMSO-d6) δ10.52 (bs, 2H), 7.60-7.43 (m, 2H), 7.43-7.26 (m, 2H); ^{13}C NMR (75 MHz, DMSO-d6) δ = 161.4 ($^{1}J_{CF}$ = 244.7 Hz, 1C), 153.7, 128.7 ($^{3}J_{CF}$ = 8.8 Hz, 1C), 128.6 ($^{4}J_{CF}$ = 2.9 Hz, 1C), 116.2 ($^{2}J_{CF}$ = 22.8 Hz, 1C).

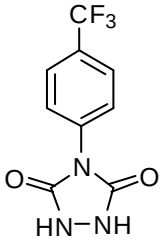

II-40h

White solid; Yield: 16%; ^{1}H-NMR (300 MHz, DMSO-d6) δ10.70 (s, 2H), 7.87 (d, *J* = 8.6 Hz, 2H), 7.78 (d, *J* = 8.6 Hz, 2H).

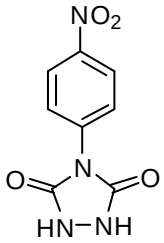

II-40i

White solid; Yield: 87%; ^{1}H-NMR (300 MHz, DMSO-d6) δ8.33 (d, *J* = 8.9 Hz, 2H), 7.86 (d, *J* = 8.9 Hz, 2H); ^{13}C NMR (75 MHz, DMSO-d6) δ = 152.7, 146.0, 138.5, 126.0, 124.6.

2.8.24 Characterization data for the diazacyclobutenes with 4-substituted 1,2,4-triazoline-2,5-diones (TADs).

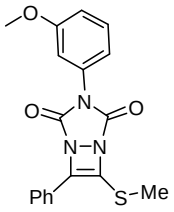

II-42e

Light yellow solid; Yield: 30%; Mp: 113.7-114.7°C; IR (neat): 2924 (w), 2831 (w), 1786 (m), 1732 (s), 1604 (s), 1496 (m), 1388 (s), 1319 (m), 1334 (m), 1261 (s), 1207 (s), 1180 (m), 1145 (m), 1111 (w), 995 (m), 964 (m), 786 (s), 756 (s), 682 (s) cm^{-1}; ^{1}H-NMR (300 MHz, $CDCl_3$) δ 8.00-7.80 (m, 2H), 7.60-7.30 (m,4H), 7.20-6.90 (m, 3H), 3.82 (s, 3H), 2.58 (s, 3H); ^{13}C NMR (125 MHz, $CDCl_3$) δ = 160.2, 156.4, 155.0, 145.3, 131.7, 130.1, 129.9, 129.3, 128.8, 126.3, 125.6, 117.5, 115.3, 110.9, 55.5, 17.4.

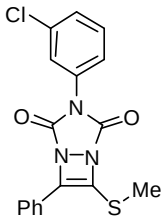

II-42f

Light yellow solid; Yield: 30%; Mp: 126.5-127.5°C; IR (neat): 3082(w), 3055 (w), 3024 (w), 2927 (w), 1786 (m), 1735 (s), 1631 (w), 1589 (m), 1477 (m), 1435 (m), 1381 (s), 1296 (w), 1273 (w), 1230 (s), 1141 (m), 1026 (m), 1002 (m), 945 (w), 867 (m), 783 (s), 748 (s), 682 (s) cm^{-1}; ^{1}H-NMR (300 MHz, $CDCl_3$) δ 7.80-7.30 (m, 9H), 2.58 (s, 3H); ^{13}C NMR (75 MHz, $CDCl_3$) δ = 156.0, 154.6, 145.3, 134.9, 131.8, 130.2, 129.9, 129.4, 129.3, 128.8, 126.1, 125.51, 125.45, 123.3, 17.4.

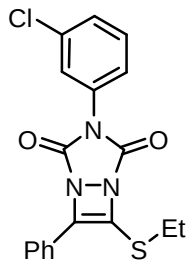

II-42fa

Light yellow solid; Yield: 29%; Mp: 95.5-96.5°C; IR (neat): 3062 (w), 3028 (w), 2966 (w), 2927 (w), 2873 (w), 1793 (w), 1743 (s), 1681 (s), 1593 (m), 1481 (s), 1381 (s), 1261 (w), 1222 (s), 1141 (s), 1076 (m), 1022 (m), 860 (m), 752 (s), 698 (s), 601 (m) cm^{-1}; ^{1}H-NMR (300 MHz, $CDCl_3$) δ 8.00-7.20 (m, 9H), 3.06 (q, *J* = 7.4 Hz, 2H), 1.41 (t, *J* = 7.4 Hz, 3H); ^{13}C NMR (75 MHz, $CDCl_3$) δ = 155.9, 154.7, 147.0, 135.0, 131.9, 130.3, 130.1, 129.6, 129.3, 128.8, 128.6, 126.2, 125.6, 123.4.

2.8.25. ^{1}H NMR spectra and ^{13}C NMR spectra for alkynyl sulfides and selenides

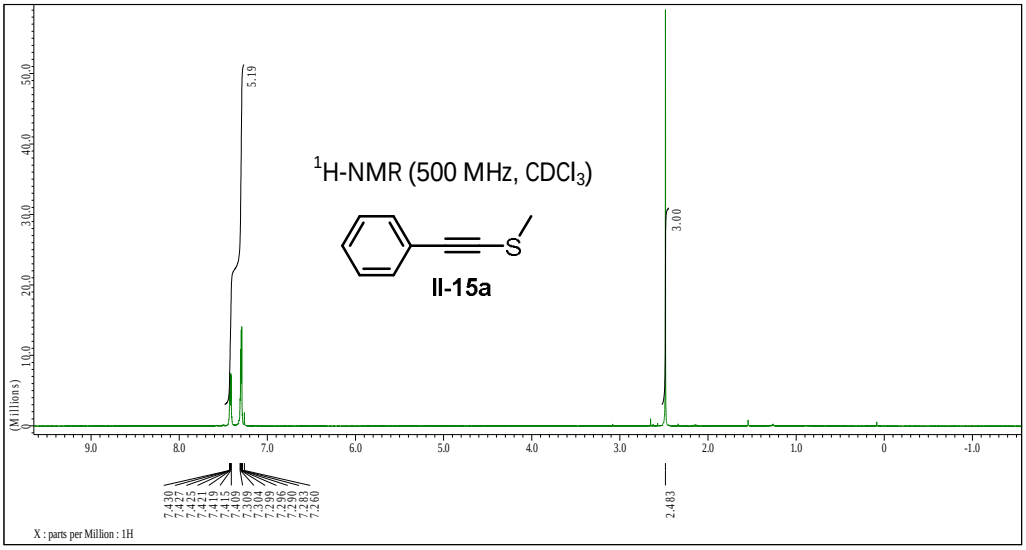

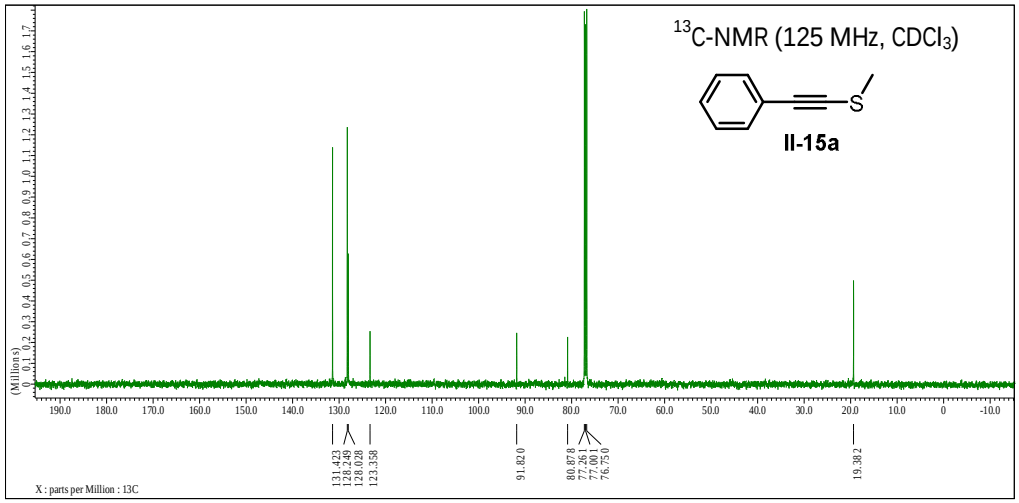

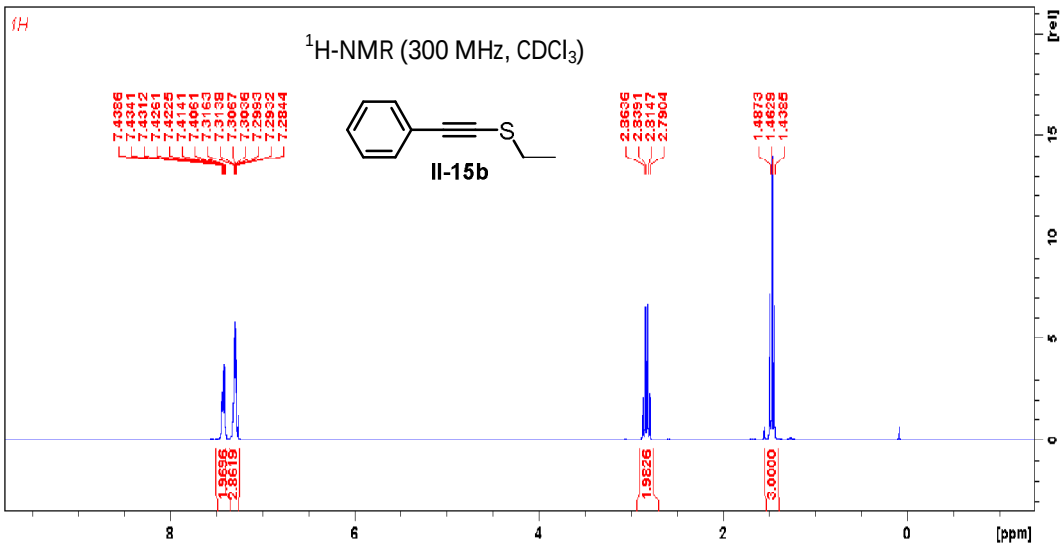
1H
1H-NMR (300 MHz, CDCl3)
II-15b
7.4386
7.4341
7.4312
7.4281
7.4225
7.4141
7.4061
7.3163
7.3138
7.3067
7.3036
7.2953
7.2922
7.2844
2.9636
2.9391
2.9147
2.7904
1.4873
1.4629
1.4385
1.9656
2.8619
1.9526
3.0000
8
6
4
2
0
[ppm]
[rel]

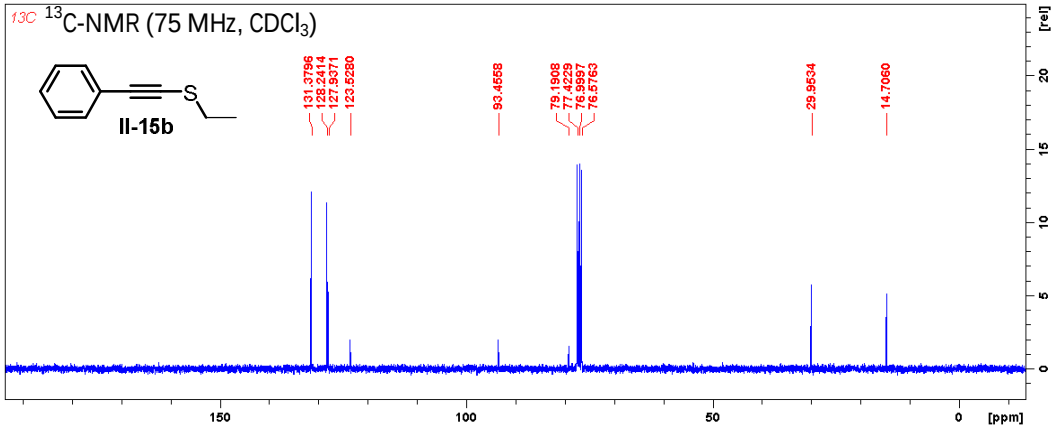
13C
13C-NMR (75 MHz, CDCl3)
II-15b
131.3796
128.2414
127.9371
123.5280
93.4558
79.1908
77.4229
76.8957
76.5763
29.9534
14.7060
150
100
50
0
[ppm]
[rel]

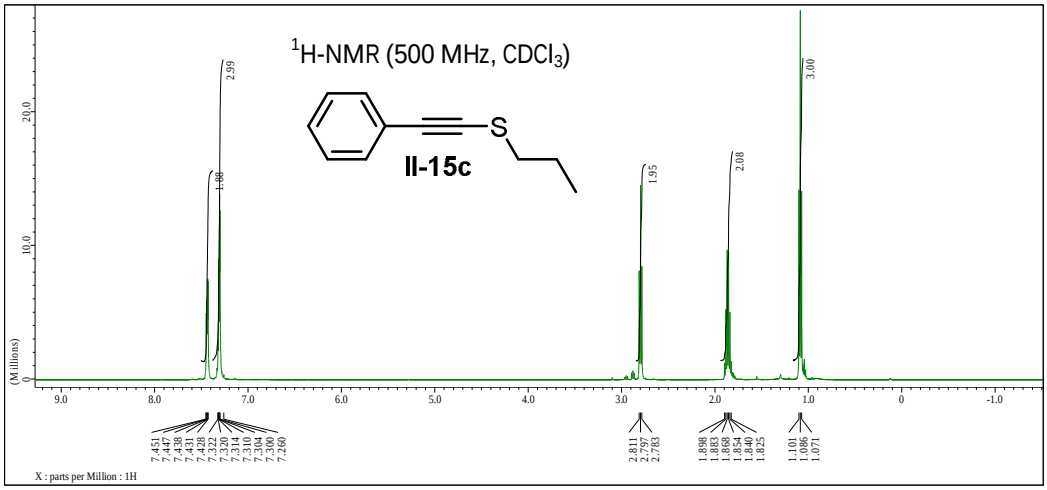
^{1}H-NMR (500 MHz, $CDCl_3$)
II-15c
2.99
1.88
1.95
2.08
3.00
(Millions)
X : parts per Million : 1H

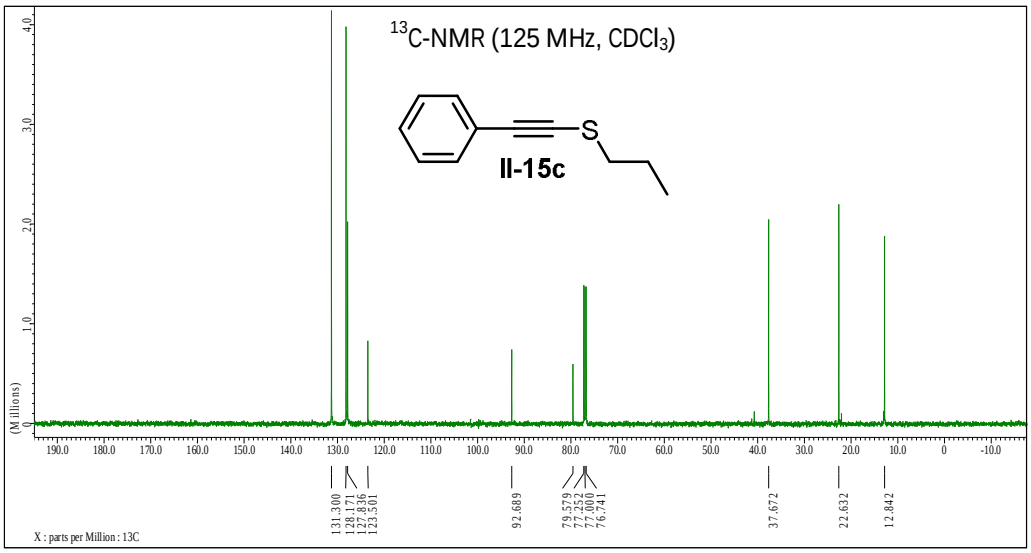
^{13}C-NMR (125 MHz, $CDCl_3$)
II-15c
(Millions)
131.300
128.171
127.836
123.501
92.689
79.579
77.252
77.000
76.741
37.672
22.632
12.842
X : parts per Million : 13C

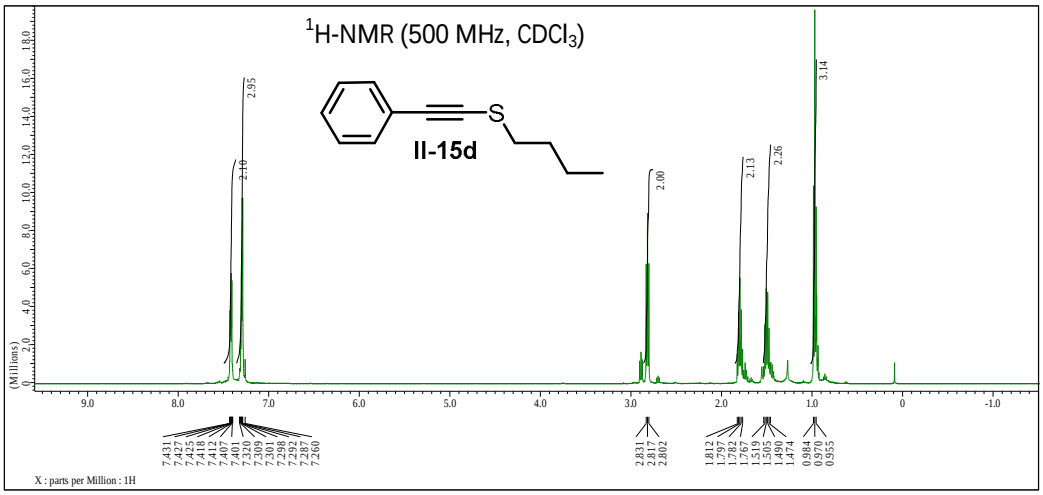
^{1}H-NMR (500 MHz, $CDCl_3$)
II-15d
S
2.95
2.10
2.00
2.13
2.26
3.14
(Millions)
X : parts per Million : 1H

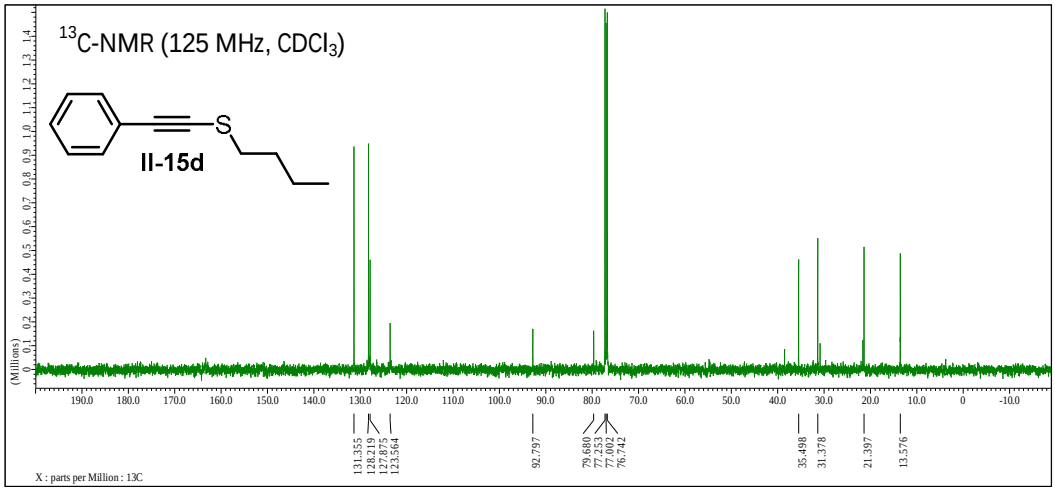
^{13}C-NMR (125 MHz, $CDCl_3$)
II-15d
S
(Millions)
131.355
128.219
127.875
123.564
92.797
79.680
77.353
77.040
76.742
35.498
31.378
21.397
13.576
X : parts per Million : 13C

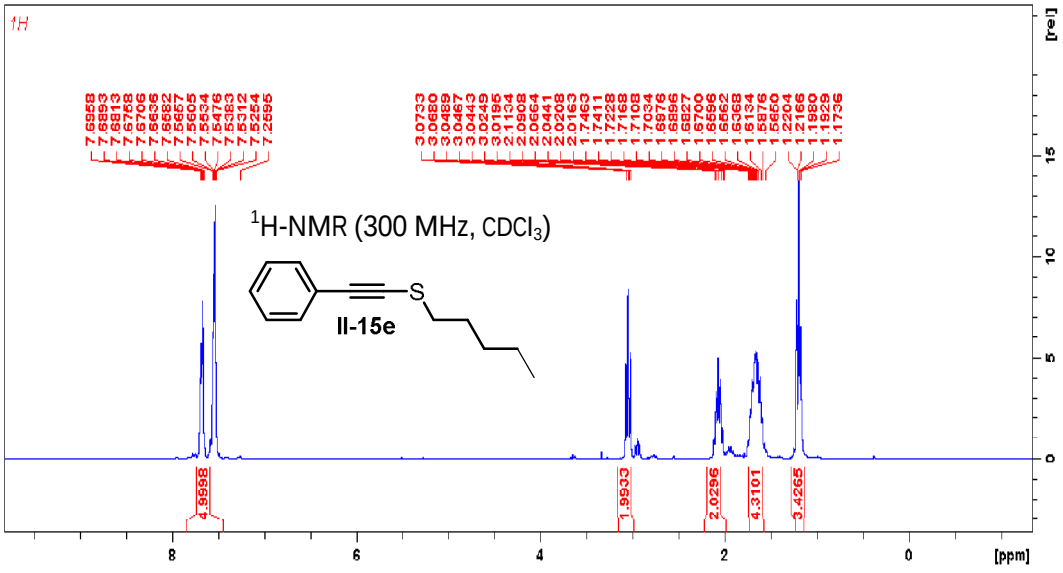
1H
7.6558
7.6493
7.6813
7.6758
7.6706
7.6636
7.6582
7.6667
7.5605
7.5534
7.5476
7.5383
7.5312
7.5254
7.2595
3.0733
3.0680
3.0489
3.0467
3.0443
3.0243
3.0195
2.1134
2.0908
2.0664
2.0441
2.0208
2.0163
1.7463
1.7411
1.7228
1.7168
1.7108
1.7034
1.6976
1.6896
1.6827
1.6700
1.6596
1.6562
1.6368
1.6334
1.5575
1.5550
1.2204
1.2166
1.1980
1.1929
1.1736
[rel]
1H-NMR (300 MHz, CDCl3)
S
II-15e
4.9998
1.9933
2.0296
4.3101
3.4265
8
6
4
2
0
[ppm]

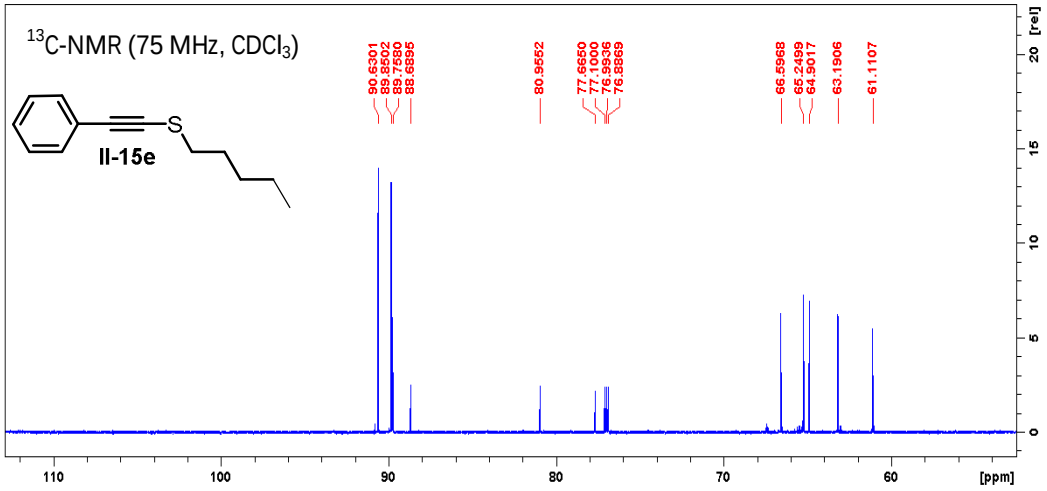
13C-NMR (75 MHz, CDCl3)
S
II-15e
90.6301
89.8502
89.7580
88.6895
80.9552
77.6650
77.1000
76.9336
76.8869
66.5968
65.2499
64.9017
63.1906
61.1107
[rel]
110
100
90
80
70
60
[ppm]

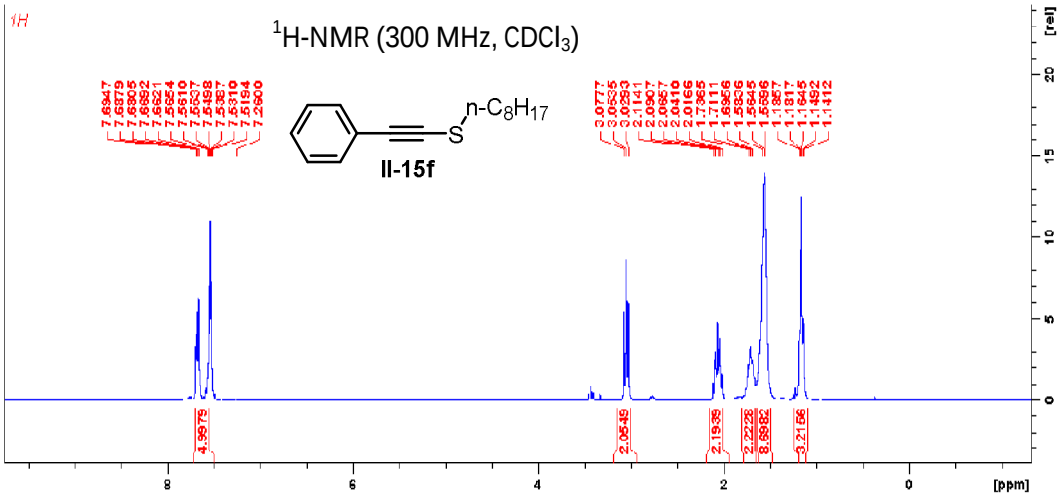
^{1}H-NMR (300 MHz, $CDCl_3$)
n-C_8H_{17}
S
II-15f
[rel]
[ppm]

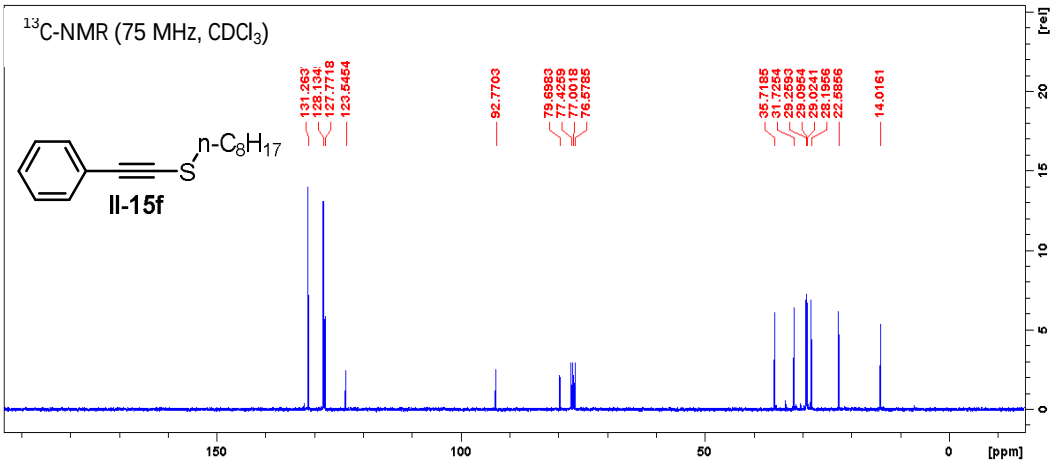
^{13}C-NMR (75 MHz, $CDCl_3$)
n-C_8H_{17}
S
II-15f
[rel]
[ppm]

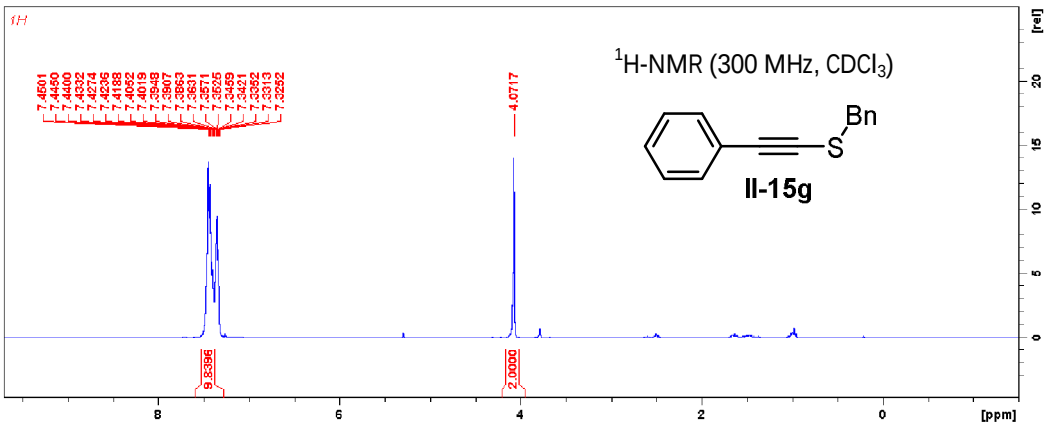
1H
7.4501
7.4450
7.4440
7.4332
7.4274
7.4236
7.4188
7.4062
7.4019
7.3948
7.3907
7.3883
7.3821
7.3571
7.3505
7.3489
7.3421
7.3362
7.3313
7.2252
4.0717
9.2396
2.0000
8
6
4
2
0
[ppm]
[rel]
20
15
10
5
0
1H-NMR (300 MHz, CDCl3)
Bn
S
II-15g

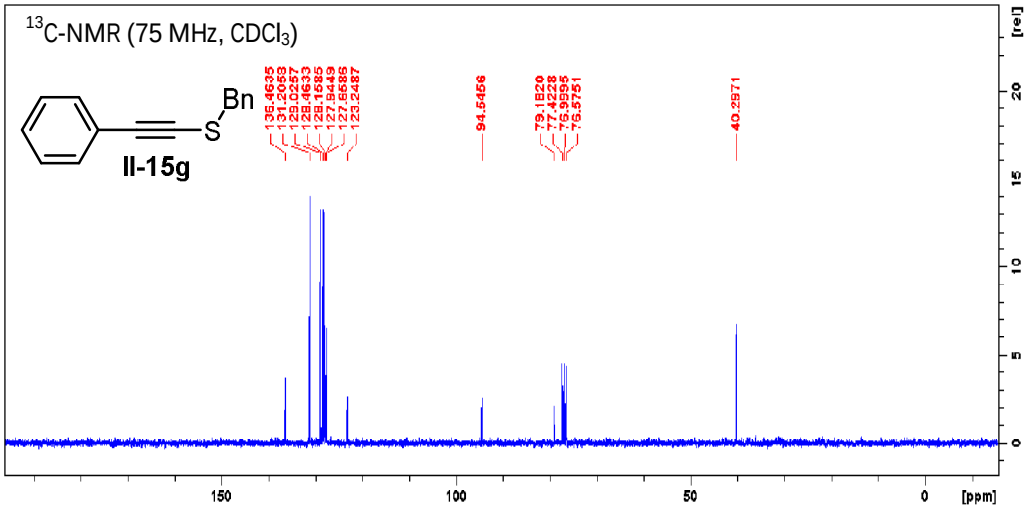
13C-NMR (75 MHz, CDCl3)
Bn
S
II-15g
135.4635
131.2063
129.0257
128.4633
128.1585
127.9449
127.8686
123.2487
94.5456
79.1820
77.4228
75.9926
75.5751
40.2571
150
100
50
0
[ppm]
[rel]
20
15
10
5
0

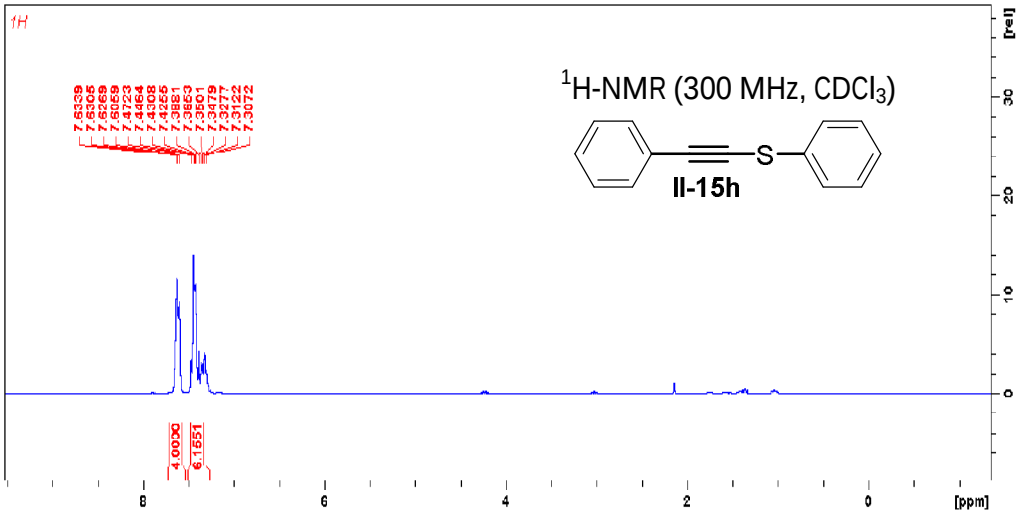
1H
7.6339
7.6305
7.6269
7.6059
7.4723
7.4464
7.4308
7.4255
7.3851
7.3563
7.3501
7.3479
7.3277
7.3122
7.3072
4.0000
6.1551
8
6
4
2
0
[ppm]
[rel]
30
20
10
0
1H-NMR (300 MHz, CDCl3)
S
II-15h

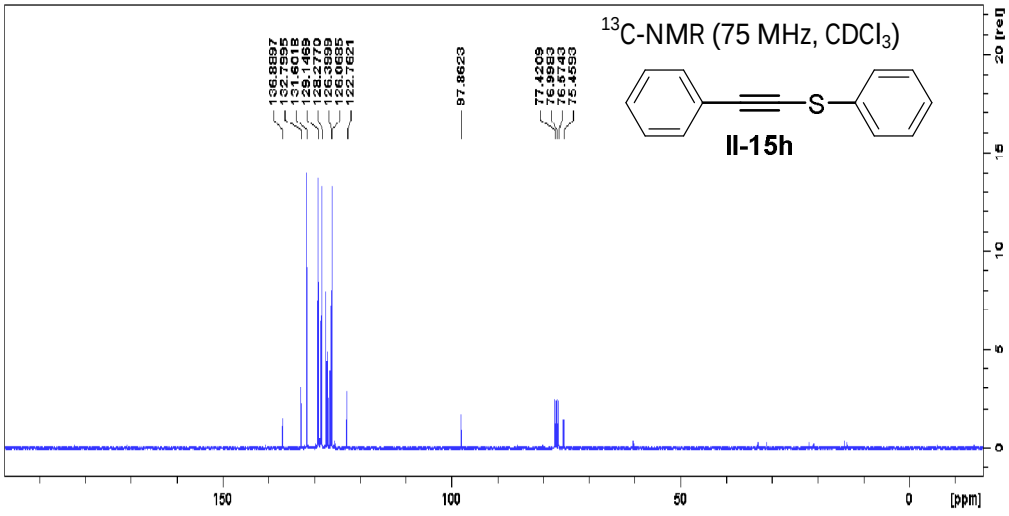
136.8897
132.7595
131.6018
128.1499
128.1270
126.3999
126.0695
122.7621
97.8623
77.4209
76.9983
76.6743
75.4593
150
100
50
0
[ppm]
20 [rel]
15
10
5
0
13C-NMR (75 MHz, CDCl3)
S
II-15h

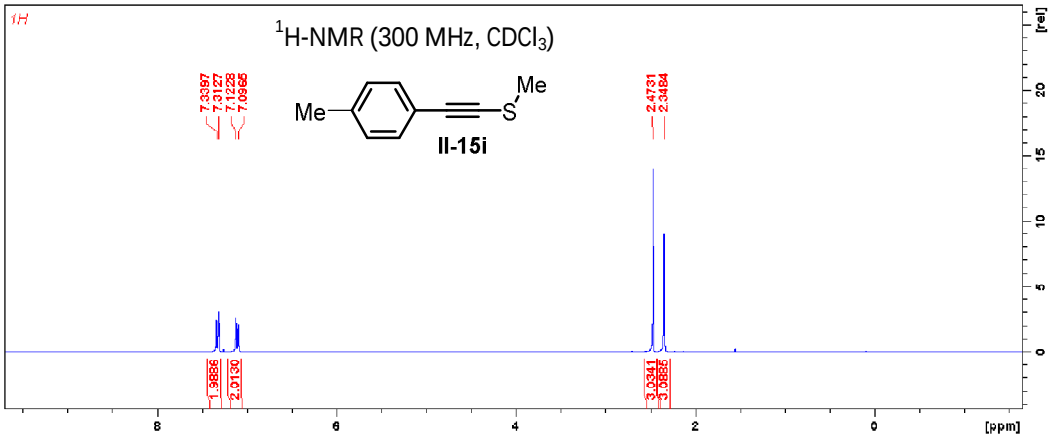
1H
^{1}H-NMR (300 MHz, $CDCl_3$)
7.3397
7.3127
7.1228
7.0985
2.4731
2.3484
1.9856
2.0136
3.0341
3.0000
Me
S
Me
II-15i
[rel]
[ppm]

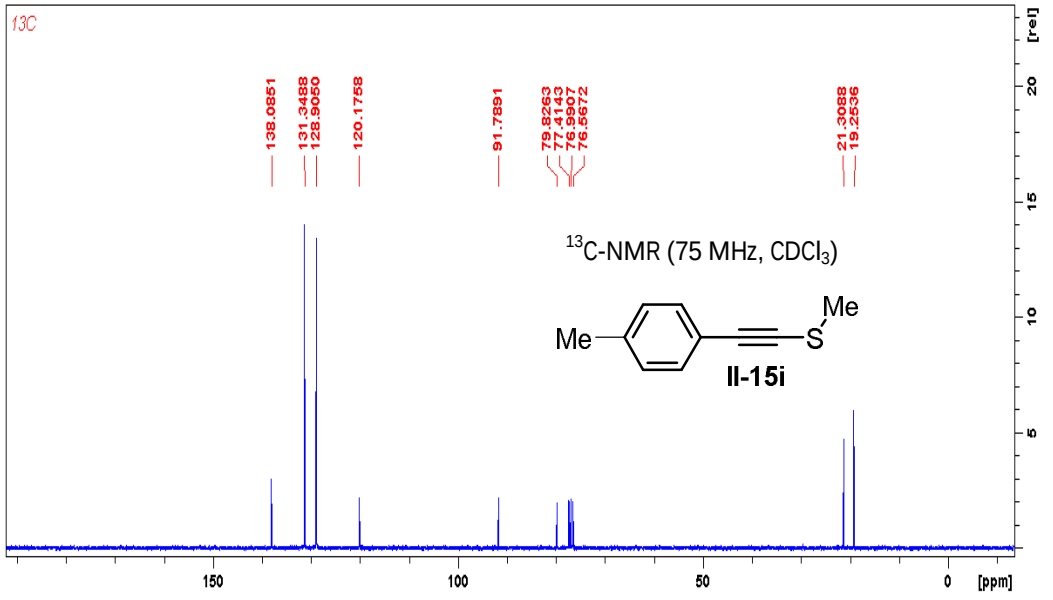
13C
138.0851
131.3488
128.9050
120.1758
91.7891
79.8263
77.4143
76.9907
76.5672
21.3088
19.2536
^{13}C-NMR (75 MHz, $CDCl_3$)
Me
S
Me
II-15i
[rel]
[ppm]

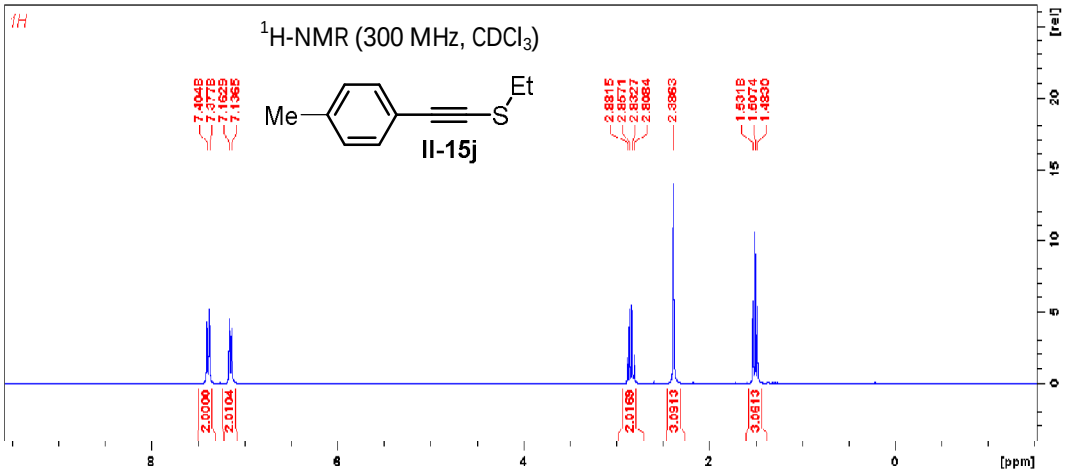
^{1}H-NMR (300 MHz, $CDCl_3$)
Me
S
Et
II-15j
7.4048
7.3778
7.1629
7.1365
2.8815
2.8571
2.8327
2.8084
2.3863
1.5318
1.5074
1.4830
2.0000
2.0104
2.0169
3.0313
3.0613
[rel]
[ppm]

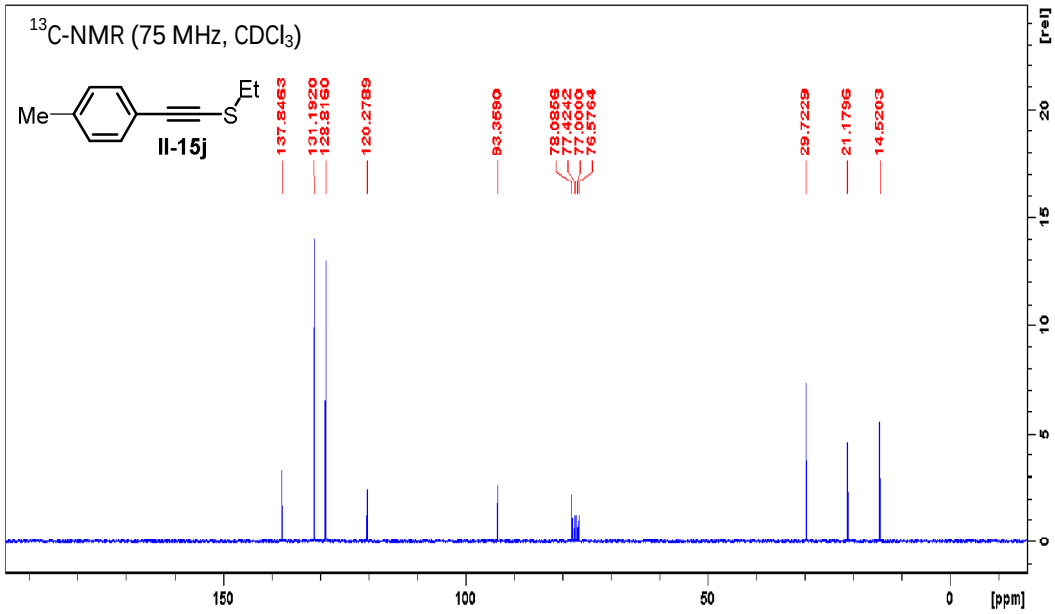
^{13}C-NMR (75 MHz, $CDCl_3$)
Me
S
Et
II-15j
137.8463
131.1920
128.8160
120.2789
93.3590
78.0856
77.4242
77.0000
76.5764
29.7229
21.1796
14.5203
[rel]
[ppm]

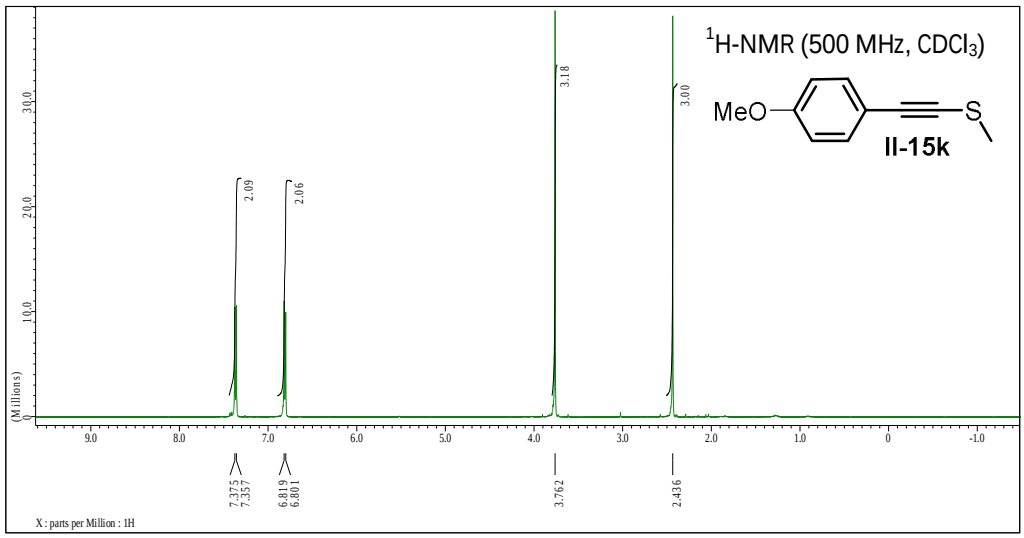
^{1}H-NMR (500 MHz, $CDCl_3$)
MeO
S
II-15k
3.18
3.00
2.09
2.06
7.375
7.357
6.819
6.801
3.762
2.436
X : parts per Million : 1H

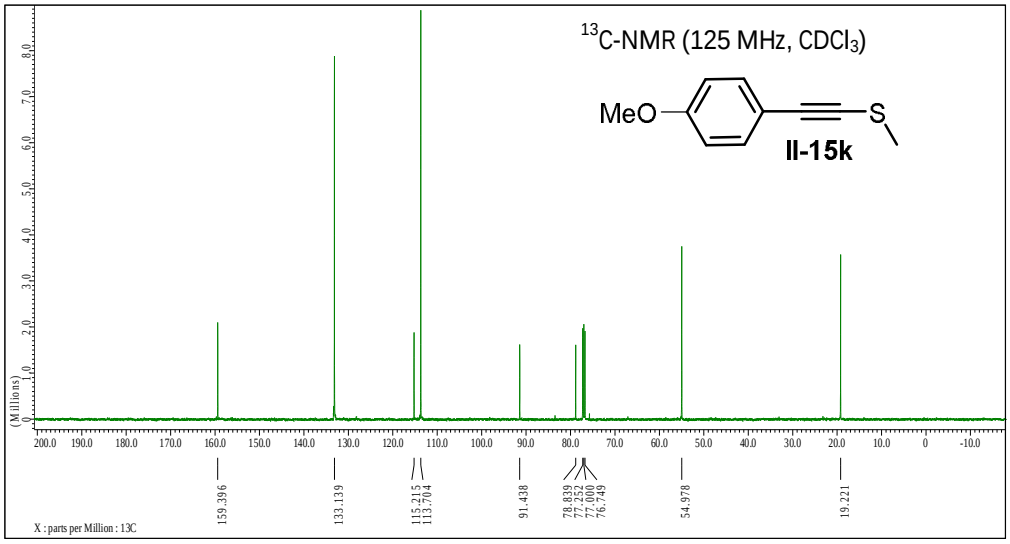
^{13}C-NMR (125 MHz, $CDCl_3$)
MeO
S
II-15k
159.396
133.139
115.215
113.704
91.438
78.839
77.252
77.000
76.749
54.978
19.221
X : parts per Million : 13C

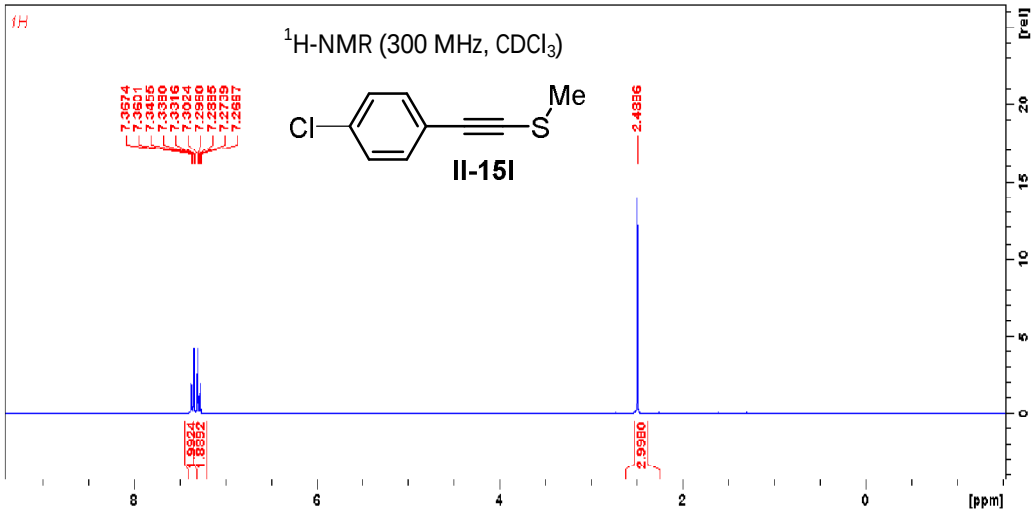
1H
^{1}H-NMR (300 MHz, $CDCl_3$)
7.3674
7.3501
7.3456
7.3380
7.3316
7.3024
7.2960
7.2835
7.2739
7.2687
Cl
S
Me
II-15l
2.4336
1.9824
1.9554
2.9980
8
6
4
2
0
[ppm]
[rel]
20
15
10
5
0

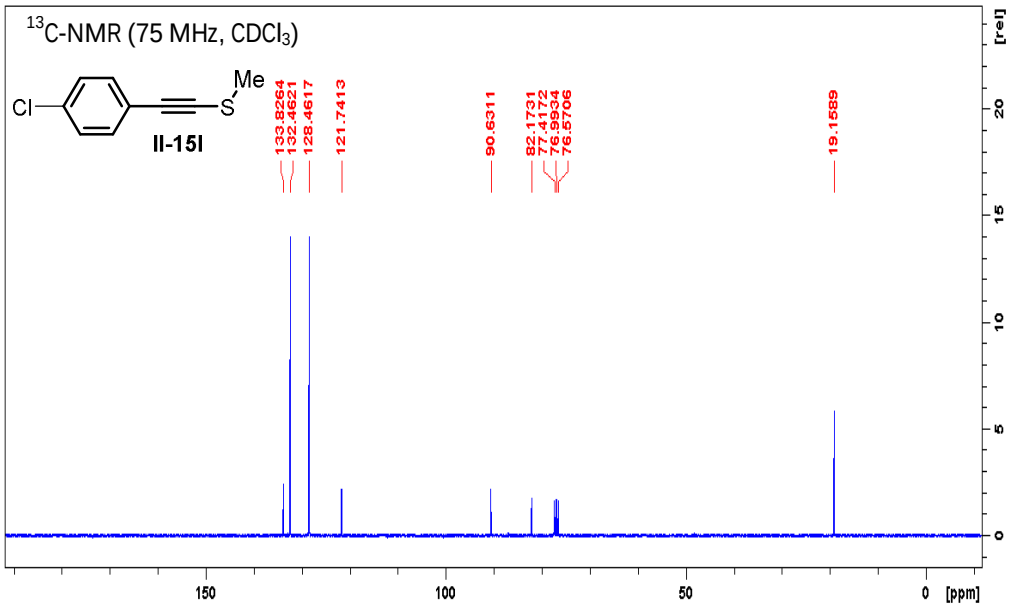
^{13}C-NMR (75 MHz, $CDCl_3$)
Cl
S
Me
II-15l
133.8264
132.4621
128.4617
121.7413
90.6311
82.1731
77.4172
76.9934
76.5706
19.1589
150
100
50
0
[ppm]
[rel]
20
15
10
5
0

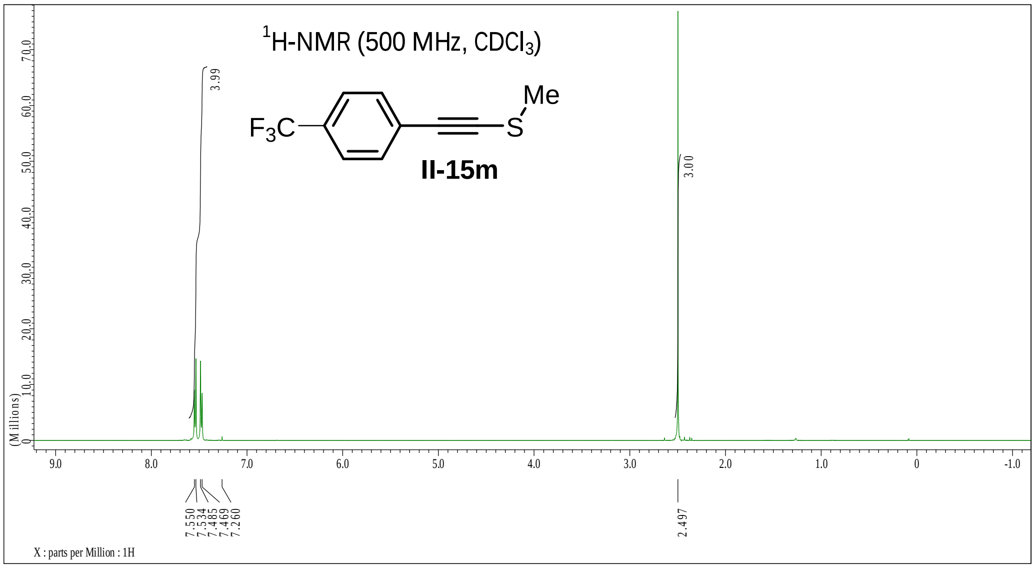

1H-NMR (500 MHz, CDCl3)
F3C
Me
S
II-15m
3.99
3.00
7.550
7.534
7.485
7.469
7.260
2.497
X : parts per Million : 1H

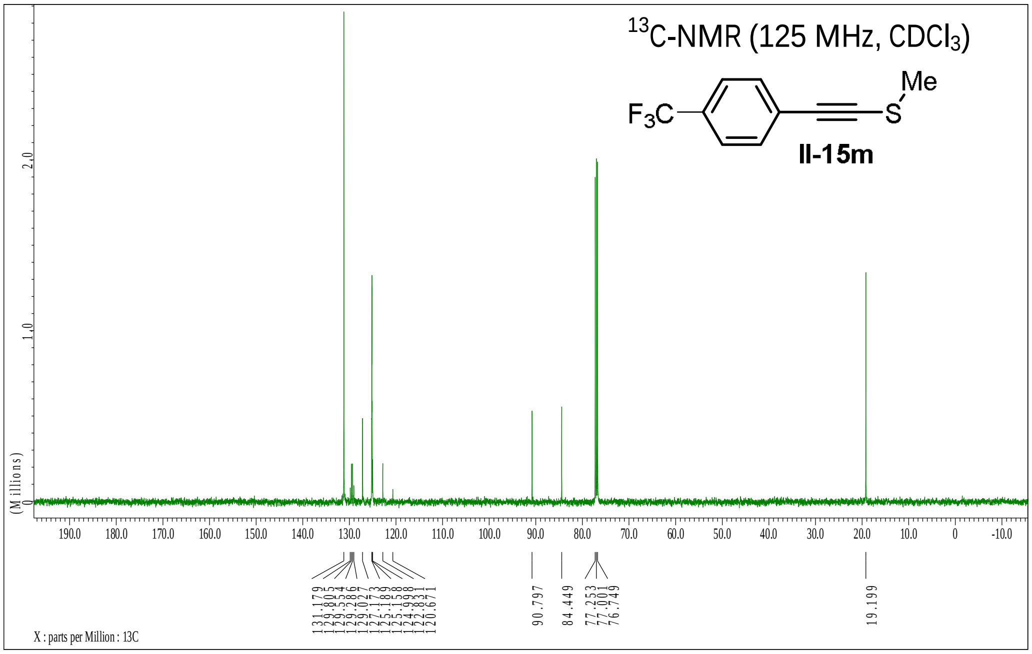

13C-NMR (125 MHz, CDCl3)
F3C
Me
S
II-15m
90.797
84.449
77.253
77.001
76.749
19.199
X : parts per Million : 13C

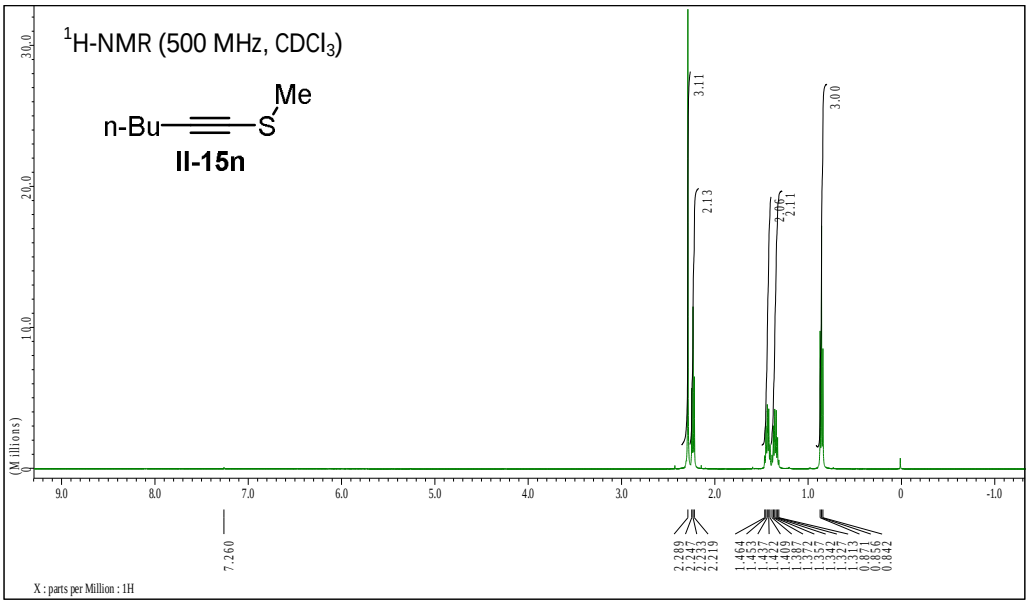
1H-NMR (500 MHz, CDCl3)
n-Bu
Me
S
II-15n
3.11
2.13
2.06
2.11
3.00
7.260
X : parts per Million : 1H

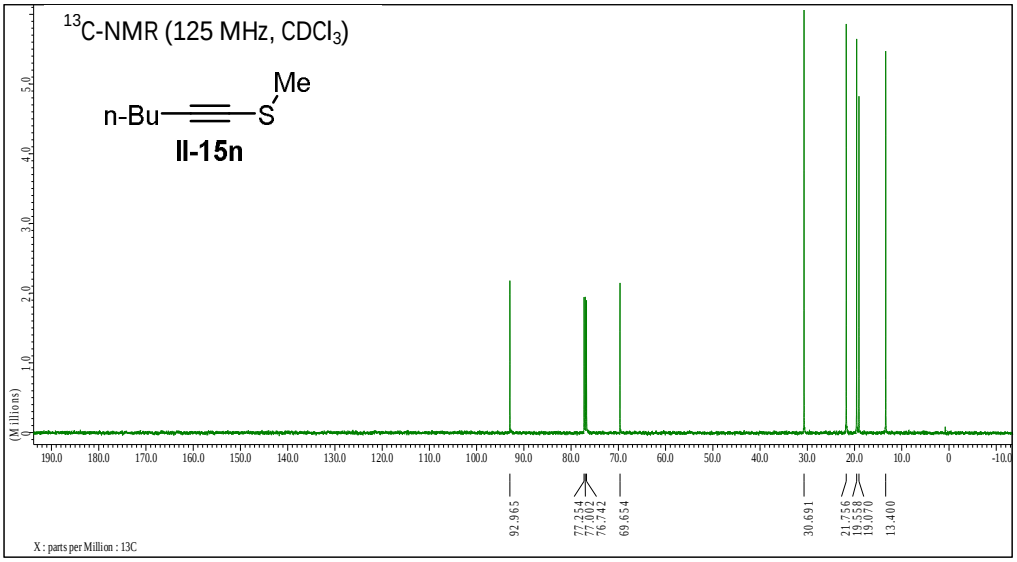
13C-NMR (125 MHz, CDCl3)
n-Bu
Me
S
II-15n
92.965
77.254
77.002
76.742
69.654
30.691
21.756
19.558
19.070
13.400
X : parts per Million : 13C

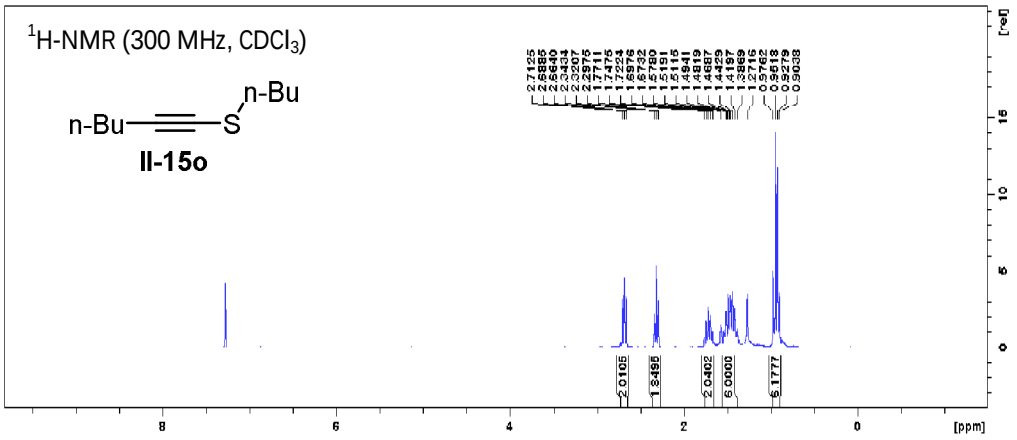
1H-NMR (300 MHz, CDCl3)
n-Bu
n-Bu
S
II-15o
[ppm]
[rel]

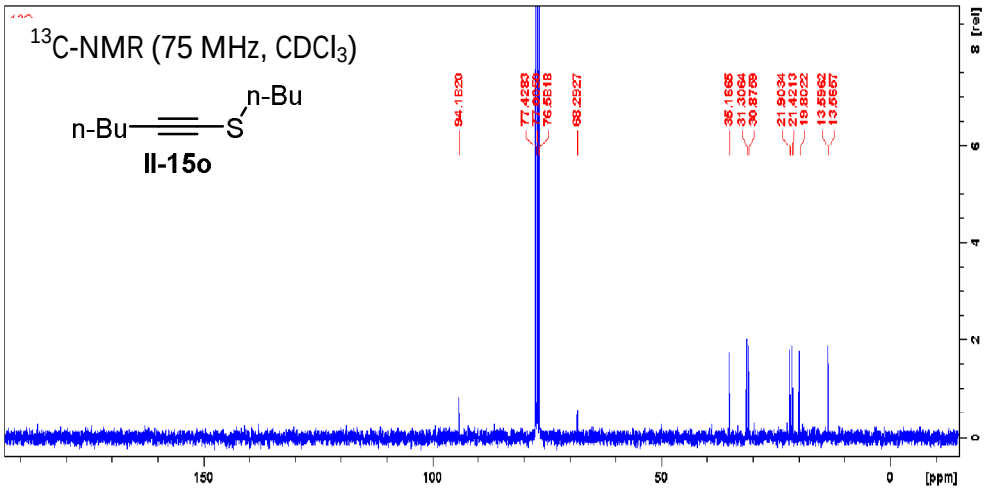
13C-NMR (75 MHz, CDCl3)
n-Bu
n-Bu
S
II-15o
94.1530
77.4823
76.5518
68.2927
35.1685
31.3064
30.8769
21.9034
21.4213
13.8022
13.5562
13.5557
[ppm]
[rel]

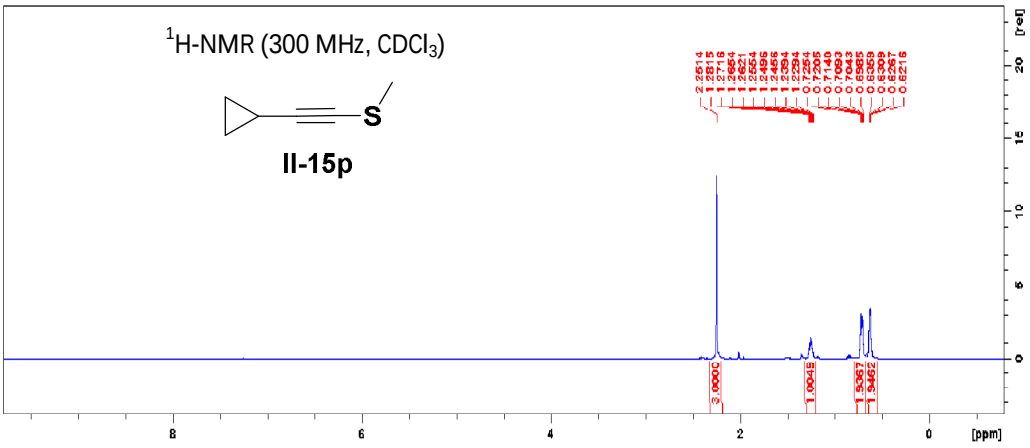
^{1}H-NMR (300 MHz, $CDCl_3$)
II-15p
[rel]
[ppm]

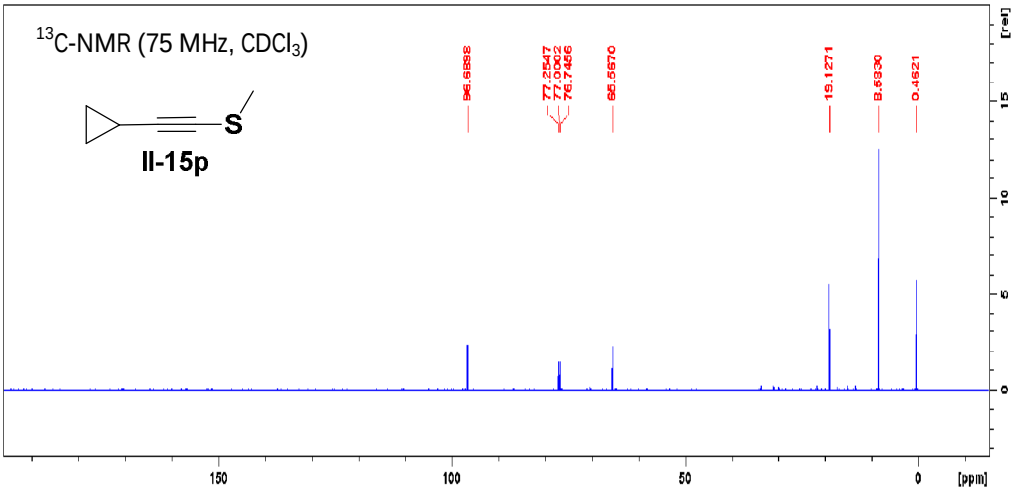
^{13}C-NMR (75 MHz, $CDCl_3$)
II-15p
[rel]
[ppm]

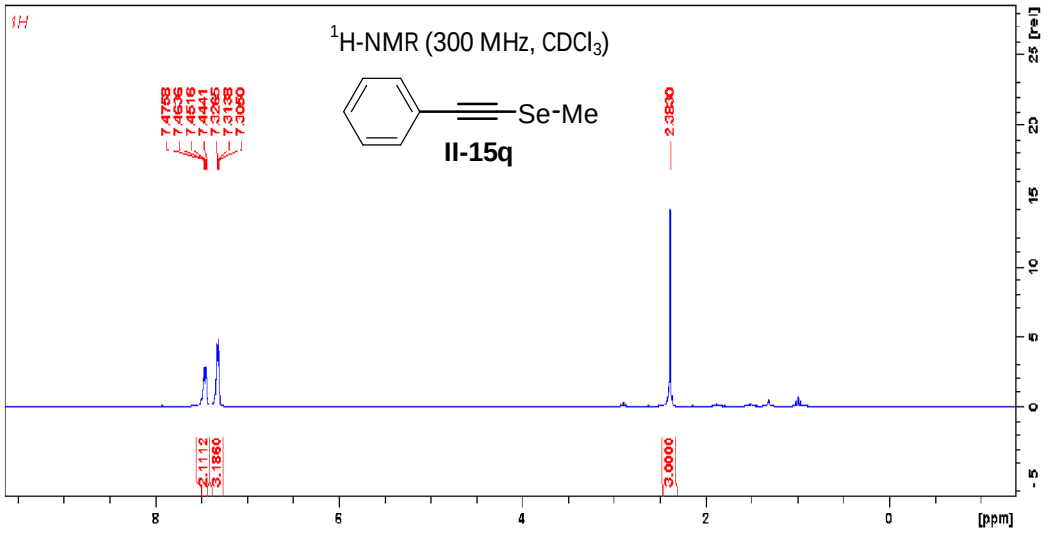
1H
^{1}H-NMR (300 MHz, $CDCl_3$)
Se-Me
II-15q
7.4768
7.4636
7.4516
7.4441
7.4295
7.3138
7.3050
2.3830
2.1112
3.1886
3.0000
[ppm]
[rel]

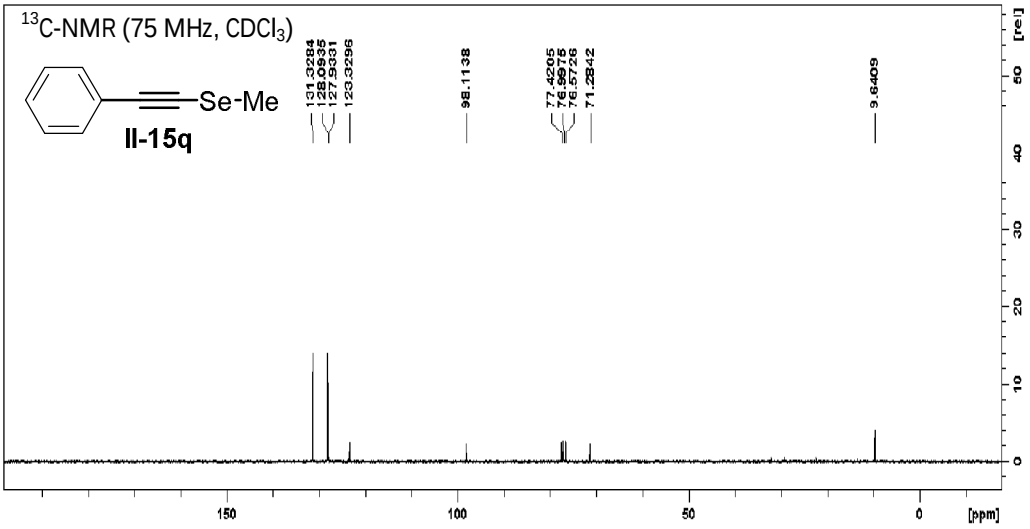
^{13}C-NMR (75 MHz, $CDCl_3$)
Se-Me
II-15q
131.3284
129.0935
127.5331
123.3296
98.1138
77.4205
76.9975
76.5726
71.2842
9.6409
[ppm]
[rel]

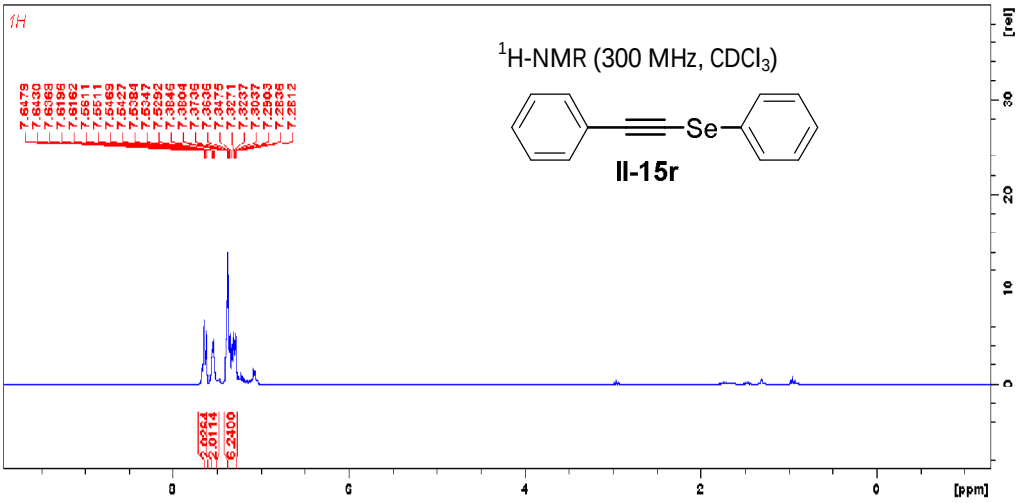
1H
^{1}H-NMR (300 MHz, $CDCl_3$)
Se
II-15r
[rel]
[ppm]

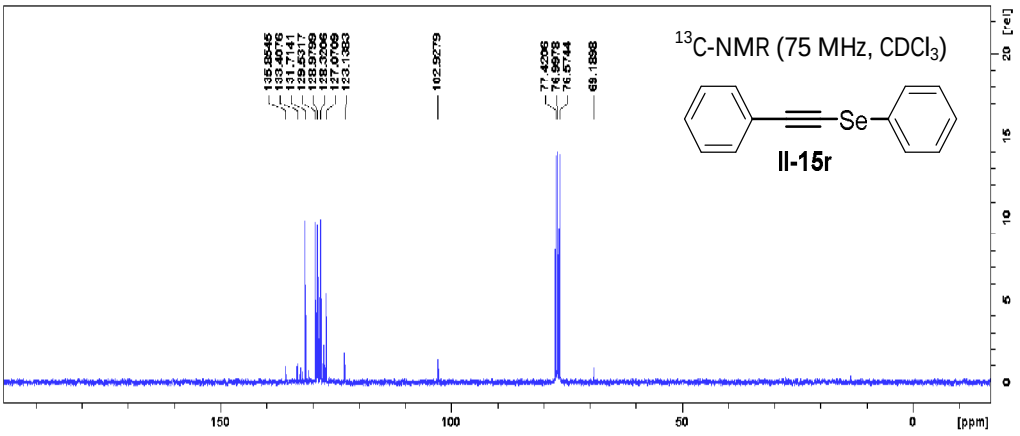
^{13}C-NMR (75 MHz, $CDCl_3$)
Se
II-15r
[rel]
[ppm]

2.8.26. ^{1}H NMR spectra and ^{13}C NMR spectra for diazacyclobutenes

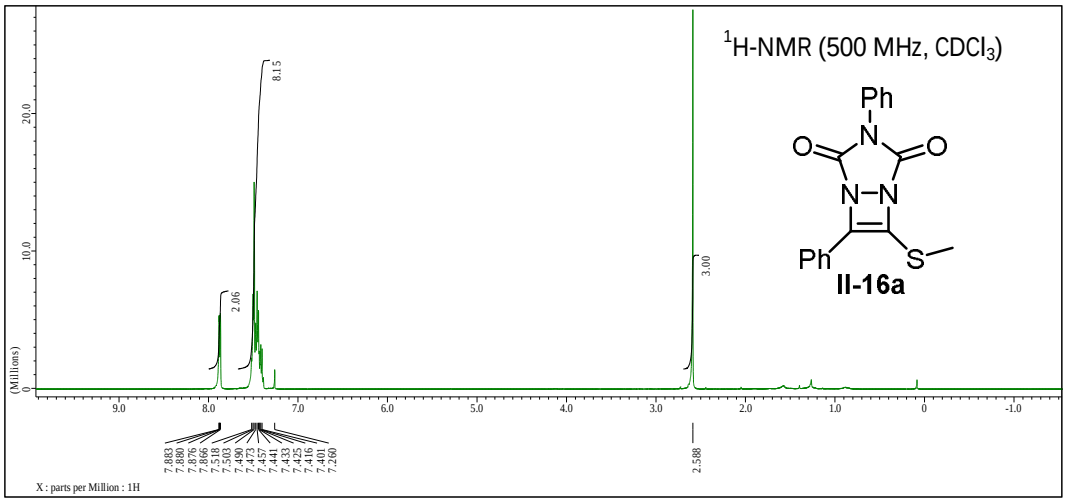

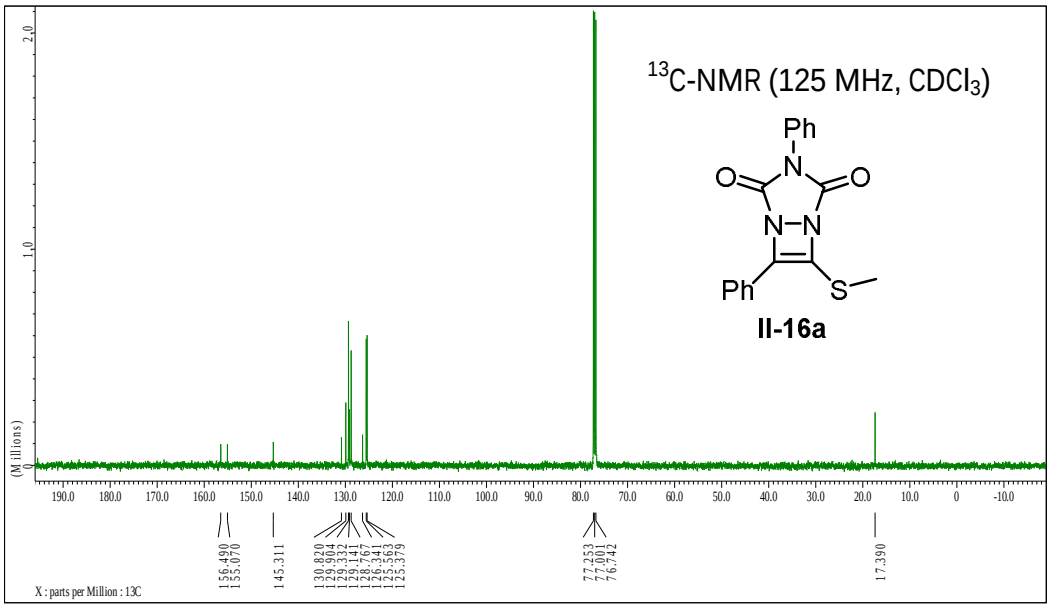

2D-HMQC (F2 = 500 MHz, F1 = 125 MHz, $CDCl_3$) analysis of diazacyclobutene **II-6a**

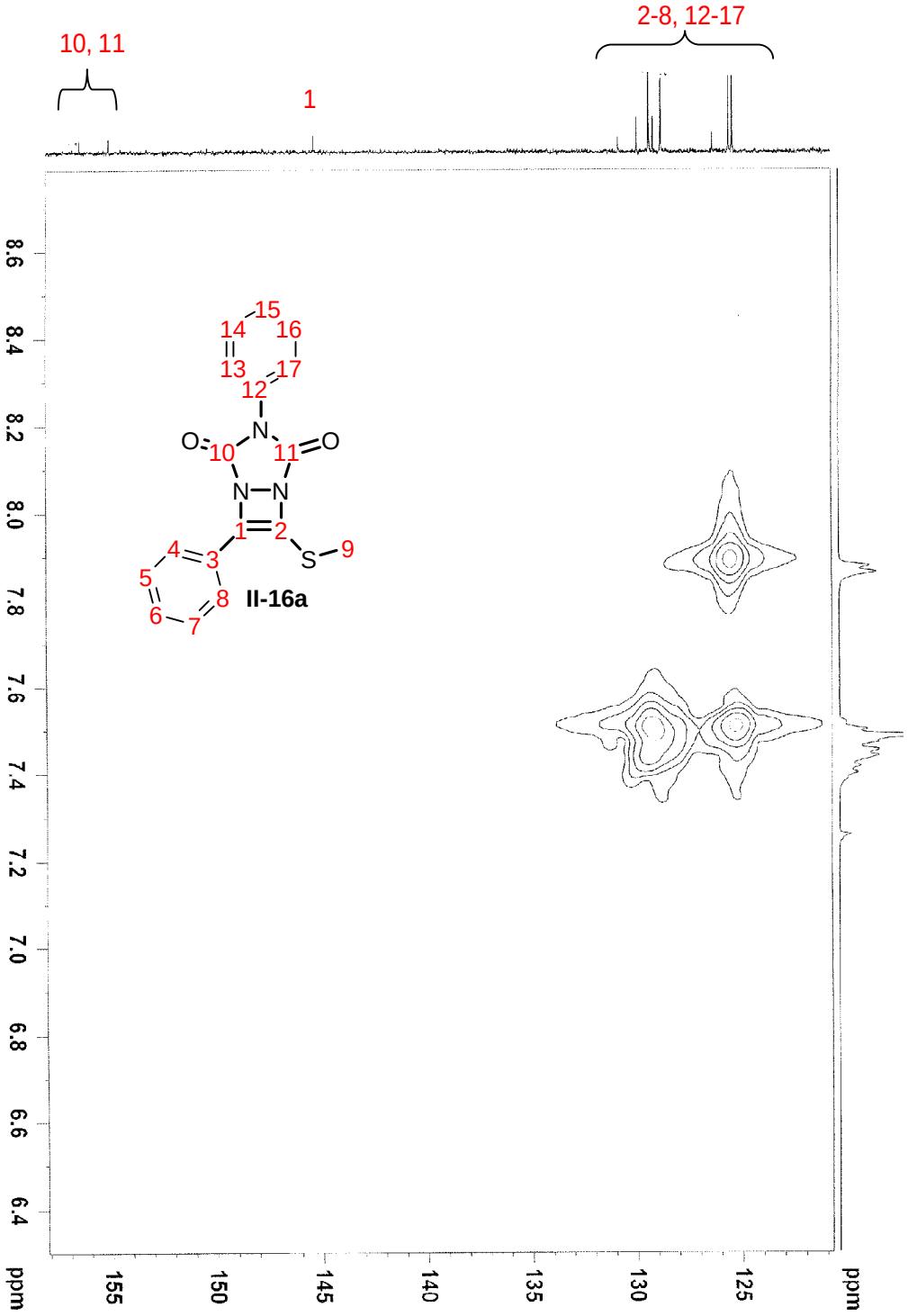

2D-HMQC (F2 = 500 MHz, F1 = 125 MHz, $CDCl_3$) analysis of diazacyclobutene **II-16a** Cntd.

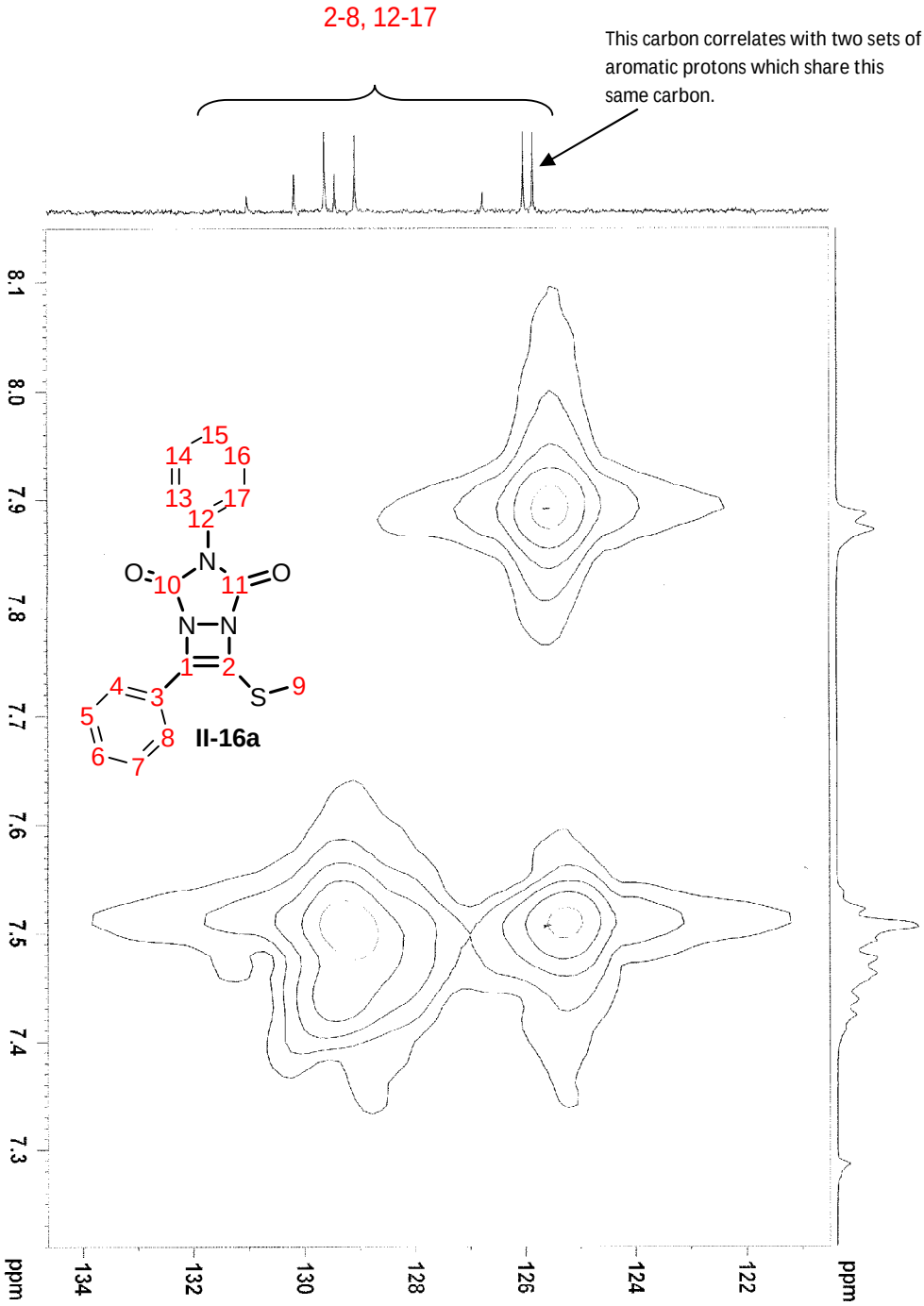

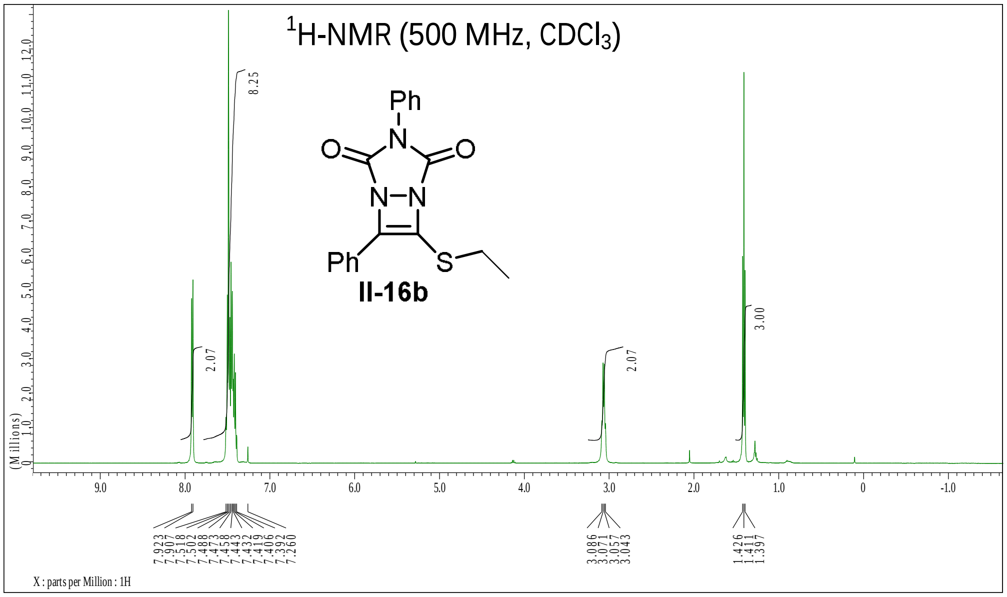

1H-NMR (500 MHz, CDCl3)
Ph
N
O
O
N
N
Ph
S
II-16b
8.25
2.07
2.07
3.00
(Millions)
X : parts per Million : 1H
7.923
7.907
7.518
7.502
7.488
7.473
7.458
7.443
7.432
7.419
7.406
7.392
7.260
3.086
3.071
3.057
3.043
1.426
1.411
1.397

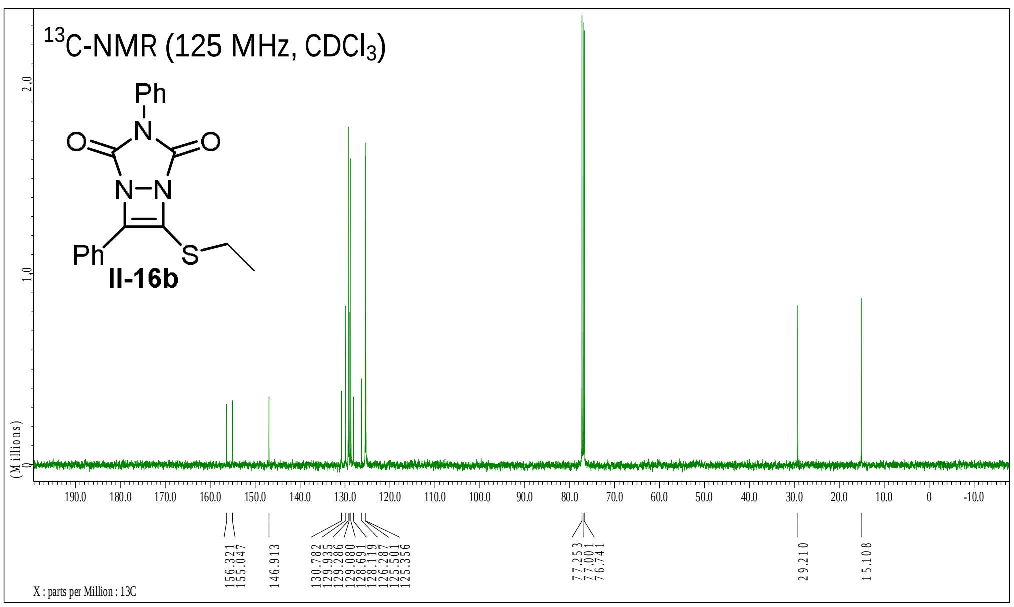

13C-NMR (125 MHz, CDCl3)
Ph
N
O
O
N
N
Ph
S
II-16b
(Millions)
X : parts per Million : 13C
156.321
155.047
146.913
130.782
129.935
129.286
129.080
128.691
126.119
125.787
125.501
125.356
77.253
77.001
76.741
29.210
15.108

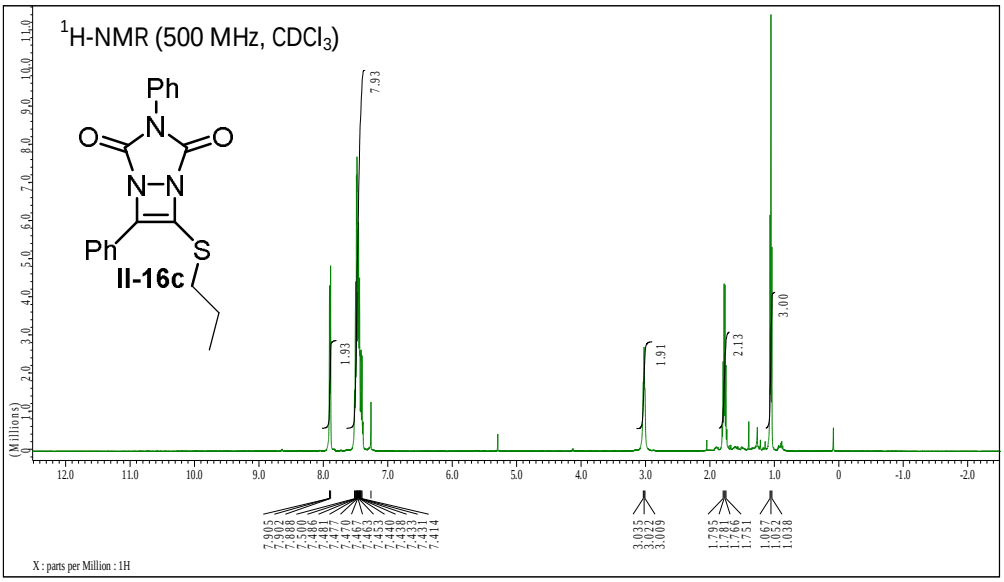
^{1}H-NMR (500 MHz, $CDCl_3$)
Ph
N
O
O
N–N
Ph
S
II-16c
7.93
1.93
1.91
2.13
3.00
(Millions)
X : parts per Million : 1H

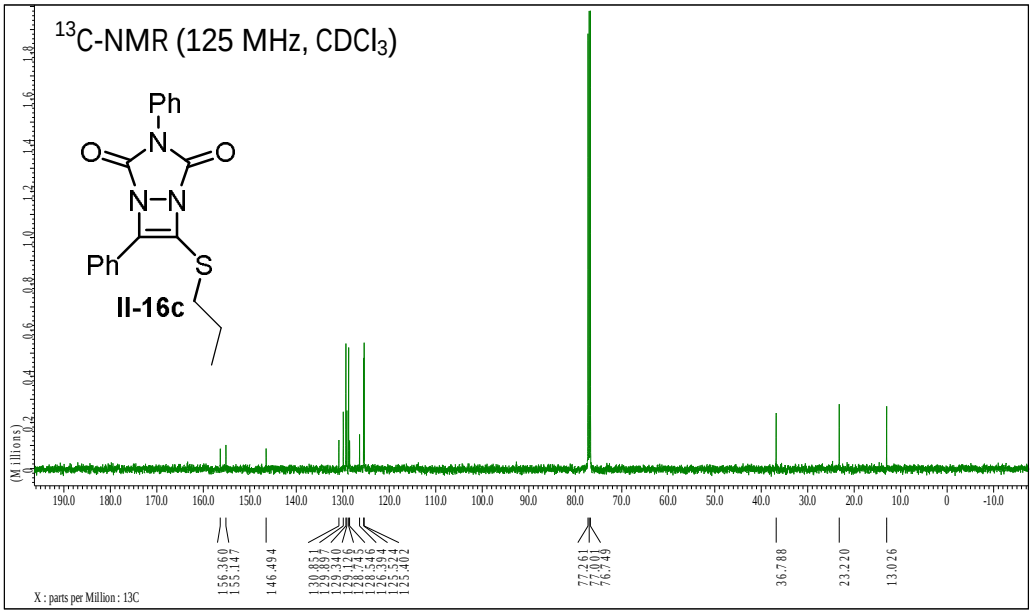
^{13}C-NMR (125 MHz, $CDCl_3$)
Ph
N
O
O
N–N
Ph
S
II-16c
(Millions)
X : parts per Million : 13C

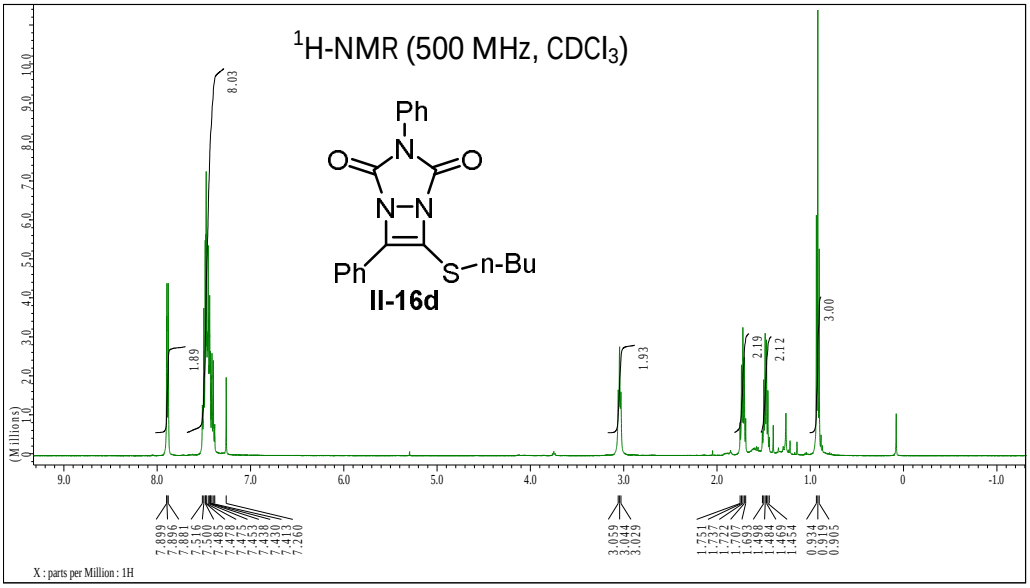
^{1}H-NMR (500 MHz, $CDCl_3$)
Ph
N
O
O
N–N
Ph
S
n-Bu
II-16d
8.03
1.89
1.93
2.19
2.12
3.00
(Millions)
X : parts per Million : 1H

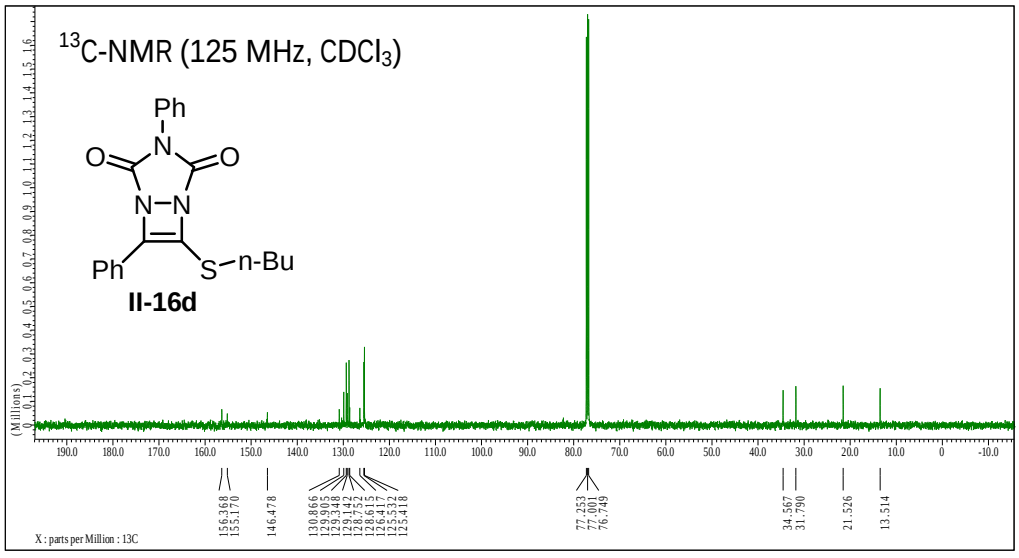
^{13}C-NMR (125 MHz, $CDCl_3$)
Ph
N
O
O
N–N
Ph
S
n-Bu
II-16d
(Millions)
X : parts per Million : 13C

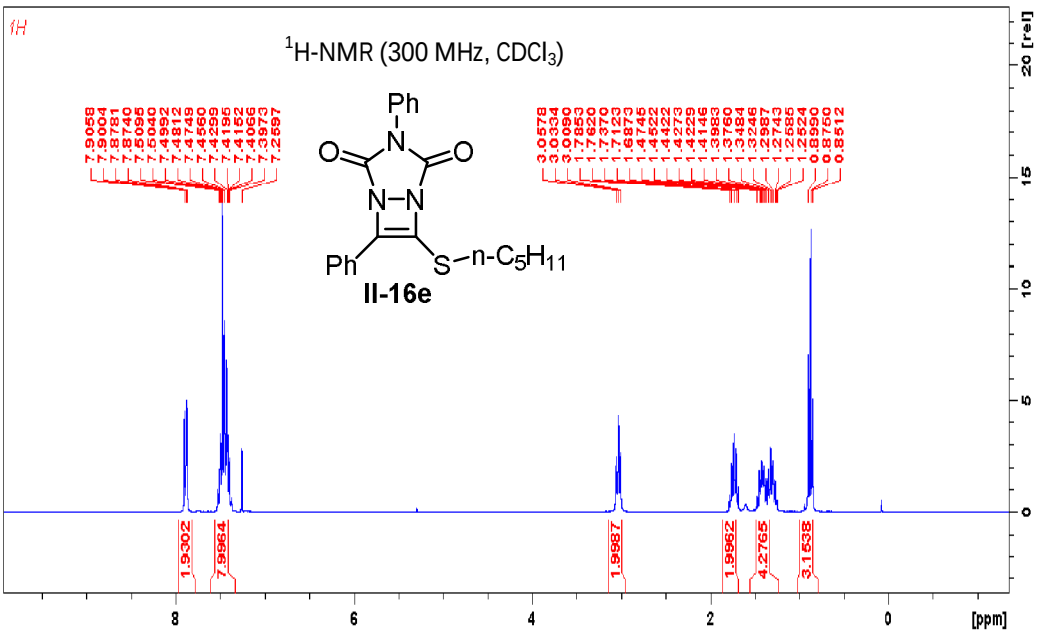
1H
^{1}H-NMR (300 MHz, $CDCl_3$)
Ph
N
O
O
N–N
Ph
S–n-C_5H_{11}
II-16e
7.9058
7.9004
7.8781
7.8740
7.5095
7.5040
7.4892
7.4812
7.4748
7.4560
7.4299
7.4195
7.4152
7.4056
7.3923
7.2897
3.0578
3.0334
3.0090
1.7853
1.7620
1.7370
1.7123
1.6873
1.4745
1.4422
1.4273
1.4229
1.4146
1.3983
1.3760
1.3484
1.3245
1.2887
1.2743
1.2585
1.2524
0.8990
0.8750
0.8512
1.9302
7.9964
1.9987
1.9962
4.2765
3.1638
8
6
4
2
0
[ppm]
20 [rel]
15
10
5
0

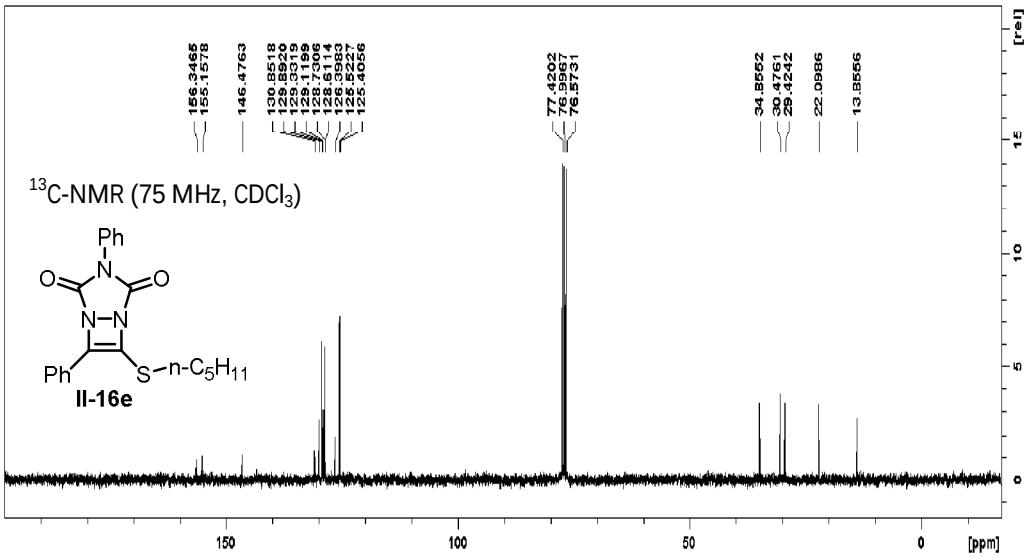
156.3465
155.1578
146.4763
130.8518
129.8929
129.3319
129.1189
128.7306
128.6114
126.3983
125.5227
125.4056
77.4202
76.9967
76.5731
34.8562
30.4761
29.4242
22.0986
13.8556
^{13}C-NMR (75 MHz, $CDCl_3$)
Ph
N
O
O
N–N
Ph
S–n-C_5H_{11}
II-16e
150
100
50
0
[ppm]
[rel]
15
10
5
0

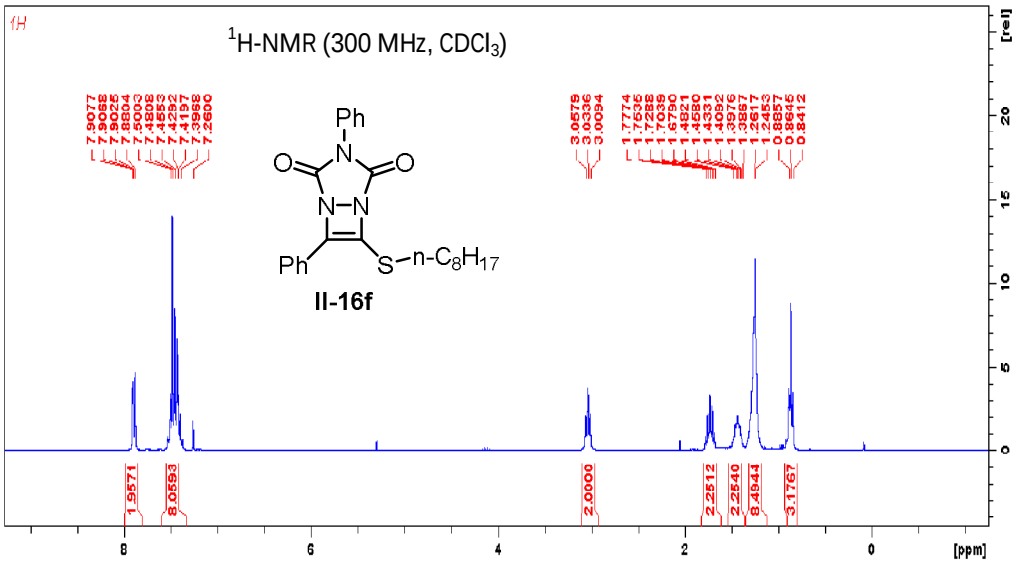
1H
^{1}H-NMR (300 MHz, $CDCl_3$)
Ph
N
O
O
N–N
Ph
S–n-C_8H_{17}
II-16f
[rel]
[ppm]

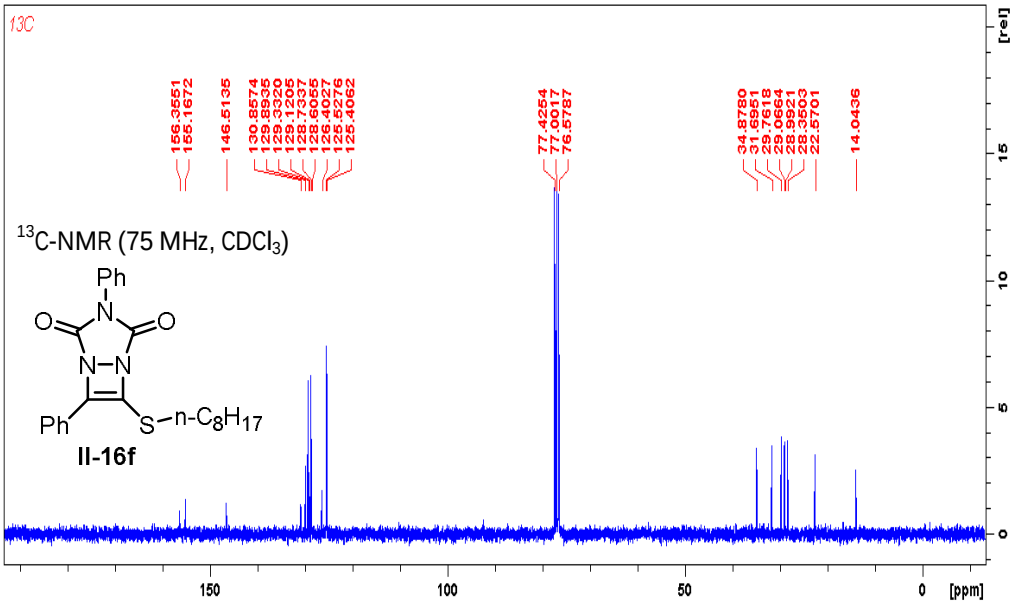
13C
^{13}C-NMR (75 MHz, $CDCl_3$)
Ph
N
O
O
N–N
Ph
S–n-C_8H_{17}
II-16f
[rel]
[ppm]

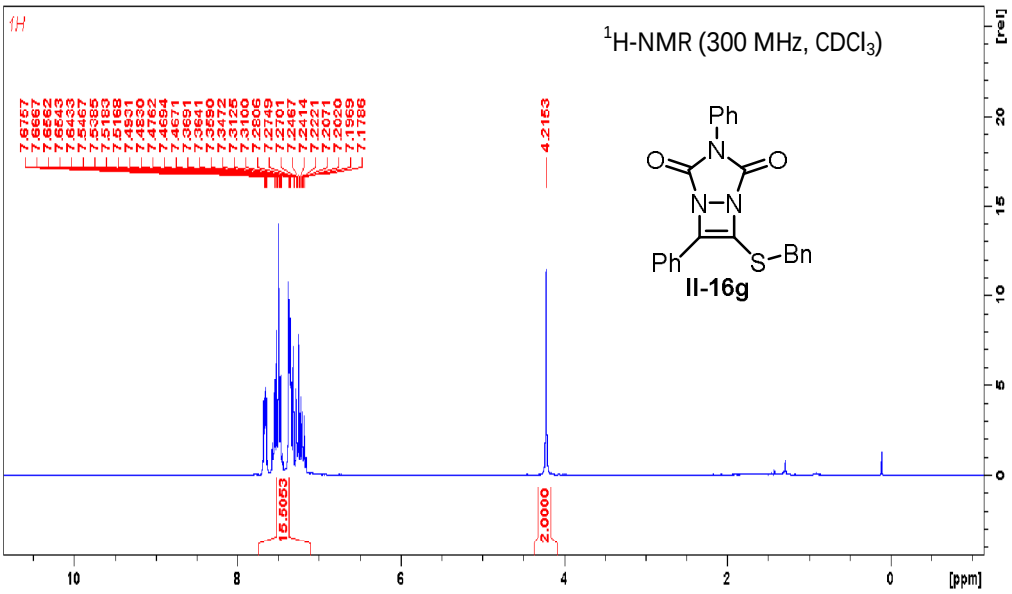
1H
^{1}H-NMR (300 MHz, CDCl$_3$)
7.6757
7.6667
7.6552
7.6443
7.6433
7.5467
7.5385
7.5183
7.5168
7.4831
7.4830
7.4762
7.4694
7.4671
7.3931
7.3691
7.3590
7.3472
7.3125
7.3100
7.2946
7.2703
7.2701
7.2467
7.2414
7.2221
7.2171
7.2020
7.1969
7.1786
4.2153
15.6053
2.0000
Ph
N
O
O
N–N
Ph
S–Bn
II-16g
10
8
6
4
2
0
[ppm]
[rel]
20
15
10
5
0

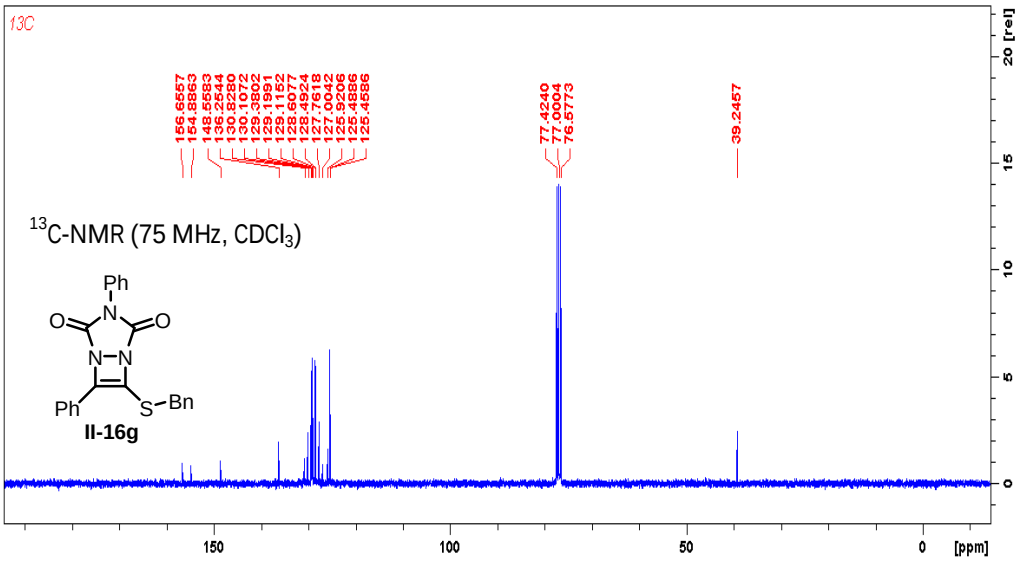
13C
156.6557
154.8563
148.5563
136.2544
130.8280
130.1072
129.3802
129.1991
129.1152
128.6077
128.4824
127.7618
127.0042
125.9206
125.4886
125.4586
77.4240
77.0004
76.5773
39.2457
^{13}C-NMR (75 MHz, CDCl$_3$)
Ph
N
O
O
N–N
Ph
S–Bn
II-16g
150
100
50
0
[ppm]
20 [rel]
15
10
5
0

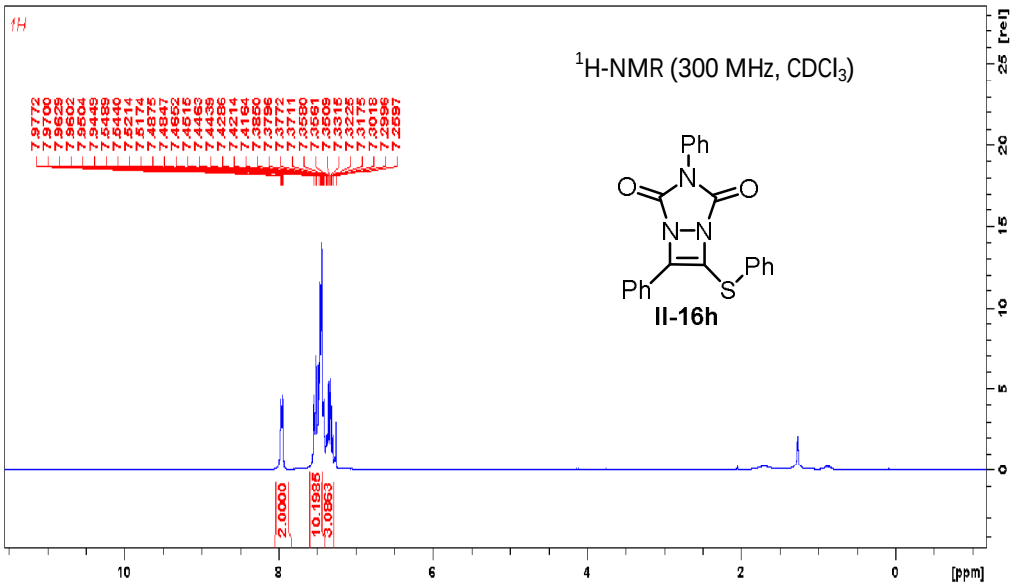
1H
^{1}H-NMR (300 MHz, $CDCl_3$)
Ph
N
O
O
N–N
Ph
S
Ph
II-16h
2.0000
10.1986
3.0863
10
8
6
4
2
0
[ppm]
[rel]

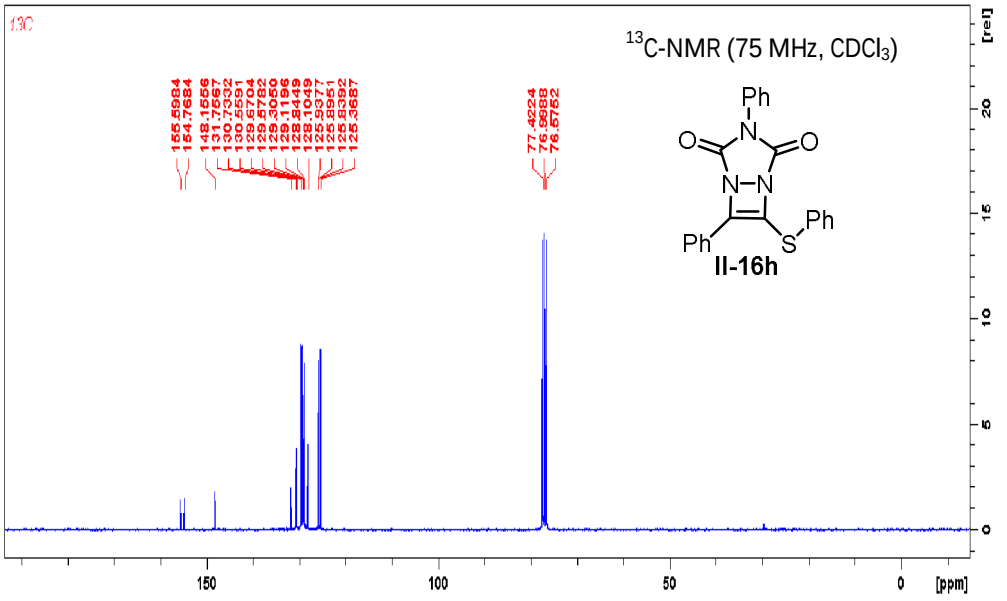
13C
^{13}C-NMR (75 MHz, $CDCl_3$)
155.5924
154.7884
148.1556
131.7567
130.7332
130.5591
129.6704
129.4082
129.3060
129.1196
128.8449
128.1049
125.9377
125.8361
125.8392
125.3687
77.4224
76.9888
76.5552
Ph
N
O
O
N–N
Ph
S
Ph
II-16h
150
100
50
0
[ppm]
[rel]

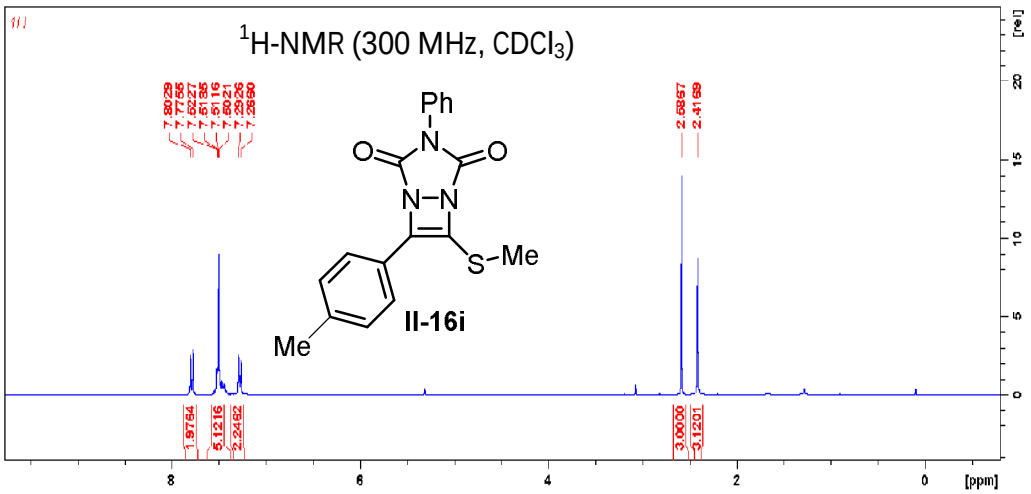
1H-NMR (300 MHz, CDCl3)
Ph
N
O
O
N–N
S–Me
Me
II-16i
[ppm]
[rel]

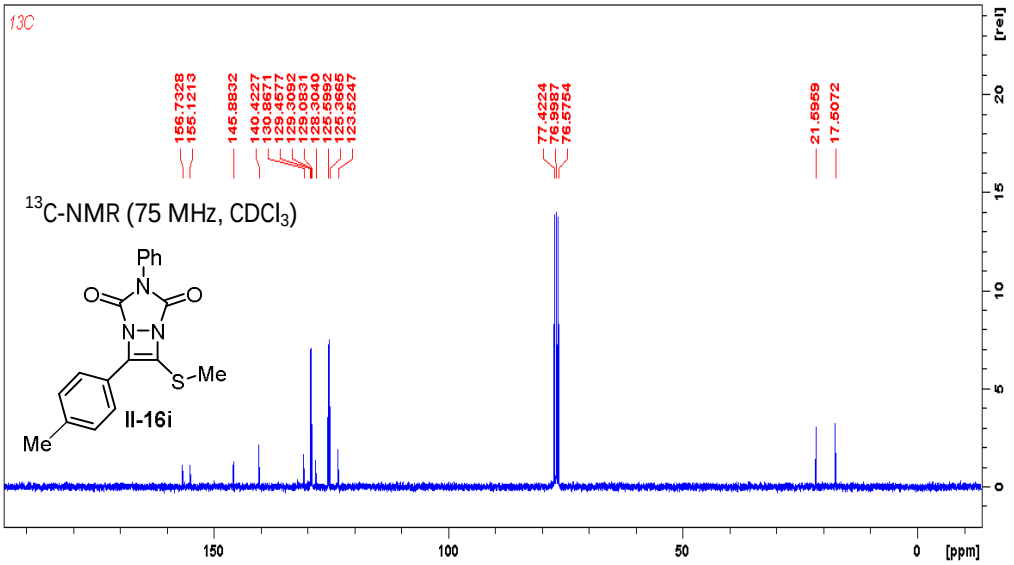
13C
13C-NMR (75 MHz, CDCl3)
Ph
N
O
O
N–N
S–Me
Me
II-16i
[ppm]
[rel]

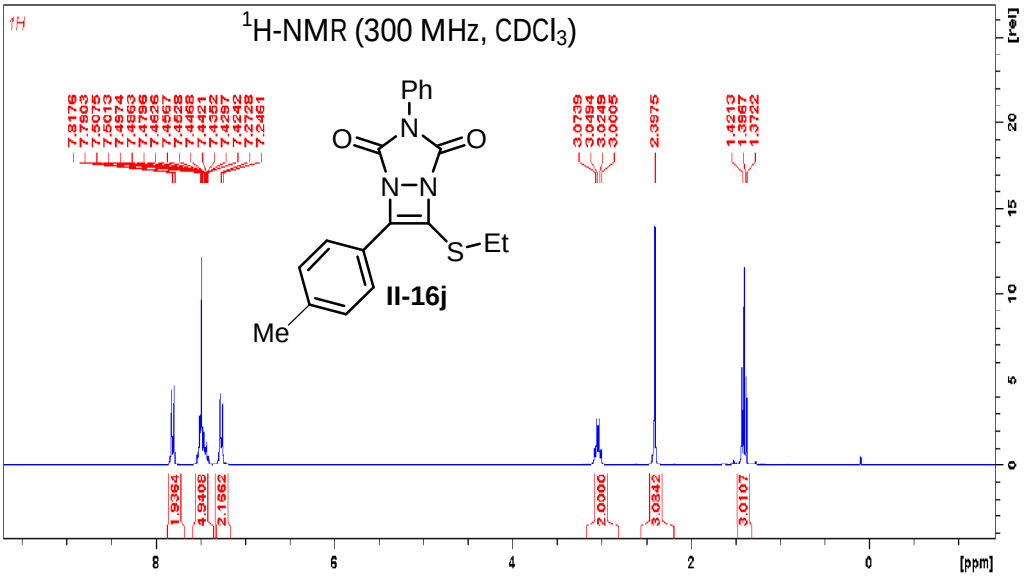
1H
^{1}H-NMR (300 MHz, $CDCl_3$)
Ph
N
O
O
N–N
S–Et
Me
II-16j
7.8176
7.7903
7.5175
7.5013
7.4974
7.4863
7.4796
7.4626
7.4527
7.4487
7.4468
7.4421
7.4352
7.4297
7.4232
7.4128
7.2461
3.0739
3.0494
3.0249
3.0005
2.3975
1.4213
1.3867
1.3722
1.9364
4.9405
2.1662
2.0000
3.0342
3.0107
8
6
4
2
0
[ppm]
[rel]

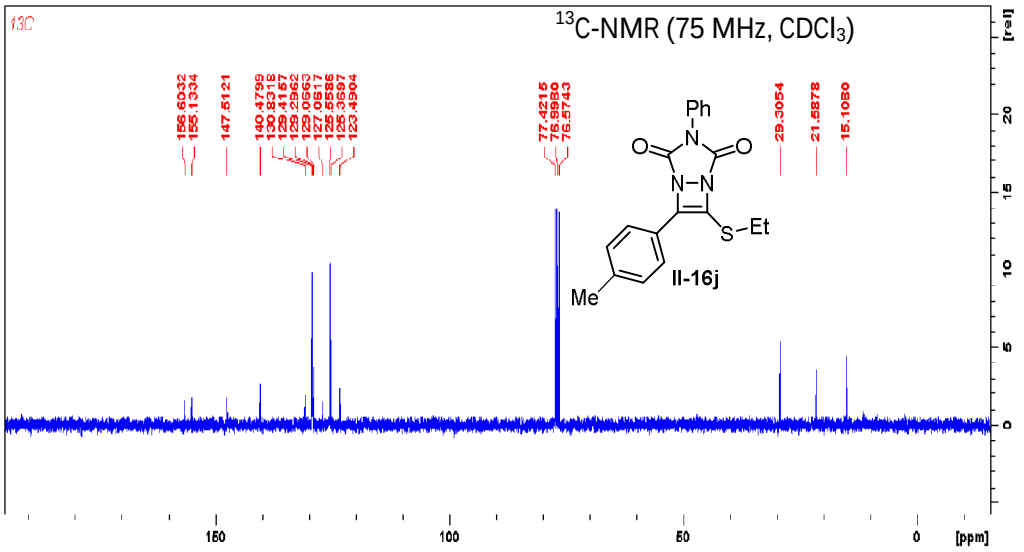
13C
^{13}C-NMR (75 MHz, $CDCl_3$)
156.6032
155.1334
147.5121
140.4799
130.8318
129.4157
129.2962
127.0963
126.0617
125.5586
125.3597
123.4904
77.4215
76.9930
76.5743
29.3054
21.5878
15.1080
Ph
N
O
O
N–N
S–Et
Me
II-16j
150
100
50
0
[ppm]
[rel]

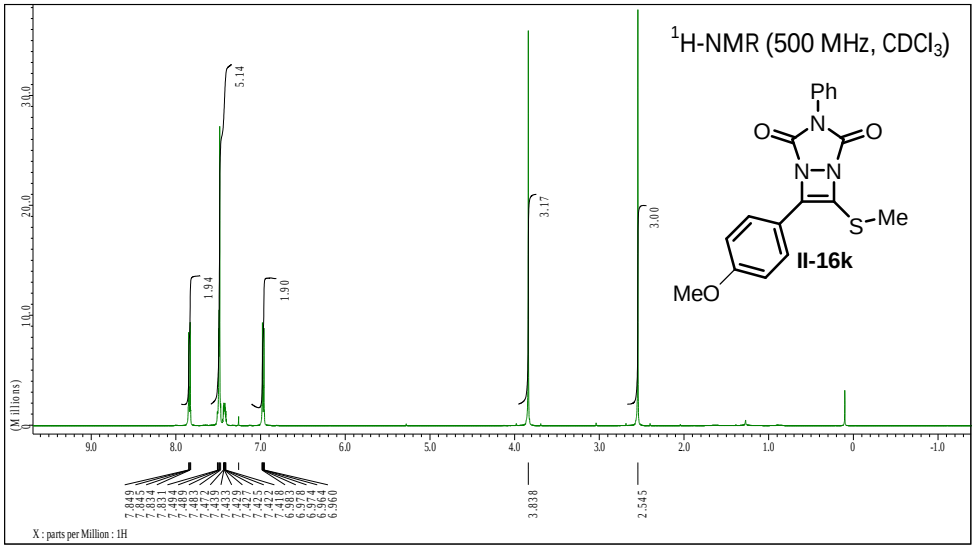
1H-NMR (500 MHz, CDCl3)
Ph
N
O
O
N–N
S–Me
MeO
II-16k
5.14
3.17
3.00
1.94
1.90
(Millions)
9.0
8.0
7.0
6.0
5.0
4.0
3.0
2.0
1.0
0
-1.0
3.838
2.545
X : parts per Million : 1H

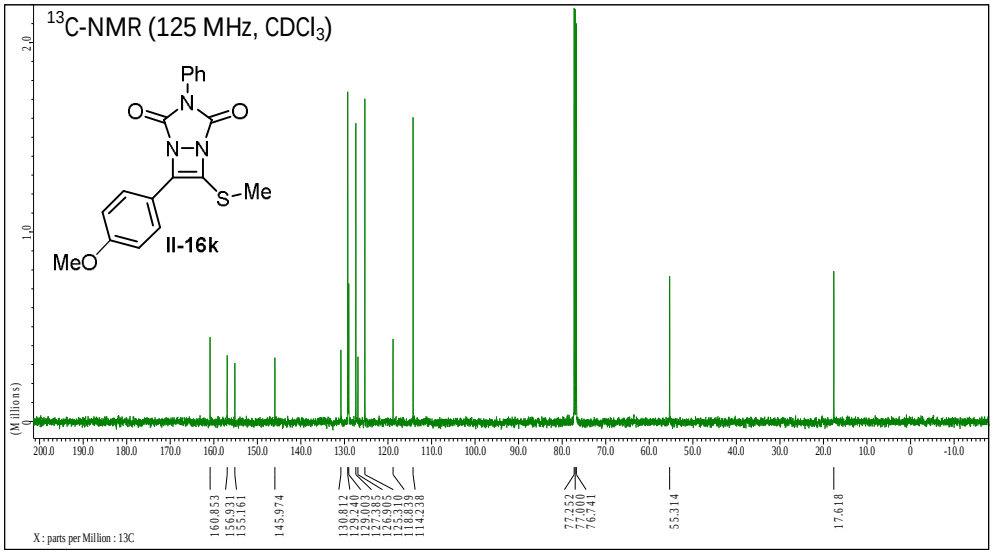
13C-NMR (125 MHz, CDCl3)
Ph
N
O
O
N–N
S–Me
MeO
II-16k
(Millions)
200.0
190.0
180.0
170.0
160.0
150.0
140.0
130.0
120.0
110.0
100.0
90.0
80.0
70.0
60.0
50.0
40.0
30.0
20.0
10.0
0
-10.0
160.853
156.931
155.161
145.974
130.812
129.240
127.403
127.385
126.905
125.310
114.838
114.238
77.252
77.000
76.741
55.314
17.618
X : parts per Million : 13C

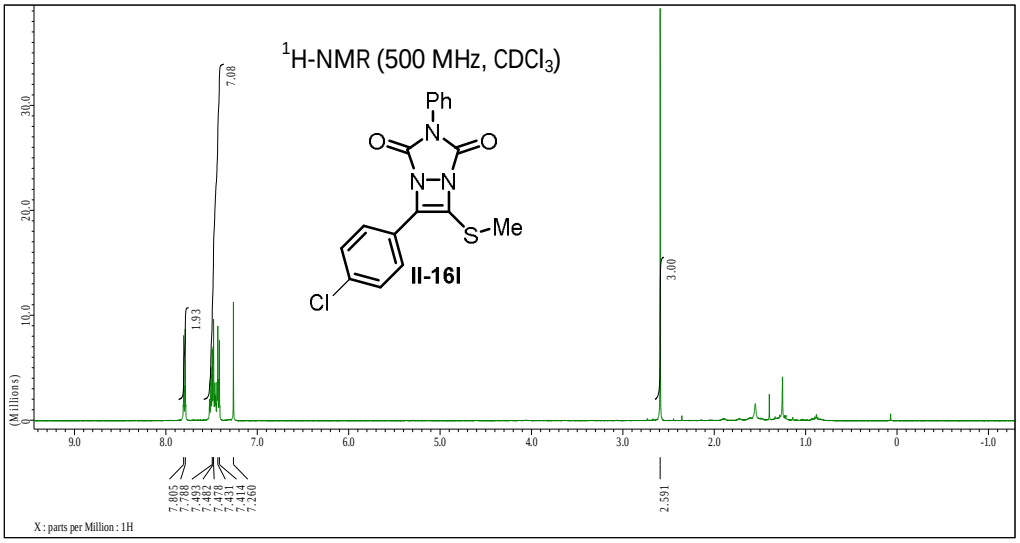
^{1}H-NMR (500 MHz, $CDCl_3$)
Ph
N
O
O
N–N
S–Me
Cl
II-16l
7.08
1.93
3.00
(Millions)
9.0
8.0
7.0
6.0
5.0
4.0
3.0
2.0
1.0
0
-1.0
7.805
7.788
7.493
7.492
7.431
7.414
7.260
2.591
X : parts per Million : 1H

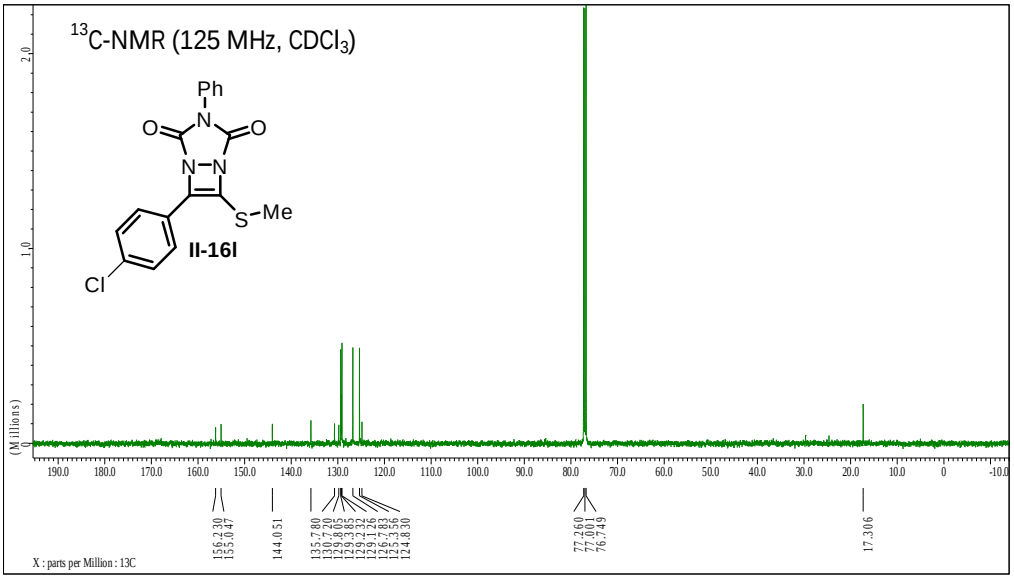
^{13}C-NMR (125 MHz, $CDCl_3$)
Ph
N
O
O
N–N
S–Me
Cl
II-16l
(Millions)
190.0
180.0
170.0
160.0
150.0
140.0
130.0
120.0
110.0
100.0
90.0
80.0
70.0
60.0
50.0
40.0
30.0
20.0
10.0
0
-10.0
156.230
153.047
144.051
135.780
130.720
129.865
129.385
129.232
129.146
125.383
125.356
124.830
77.260
77.001
76.749
17.306
X : parts per Million : 13C

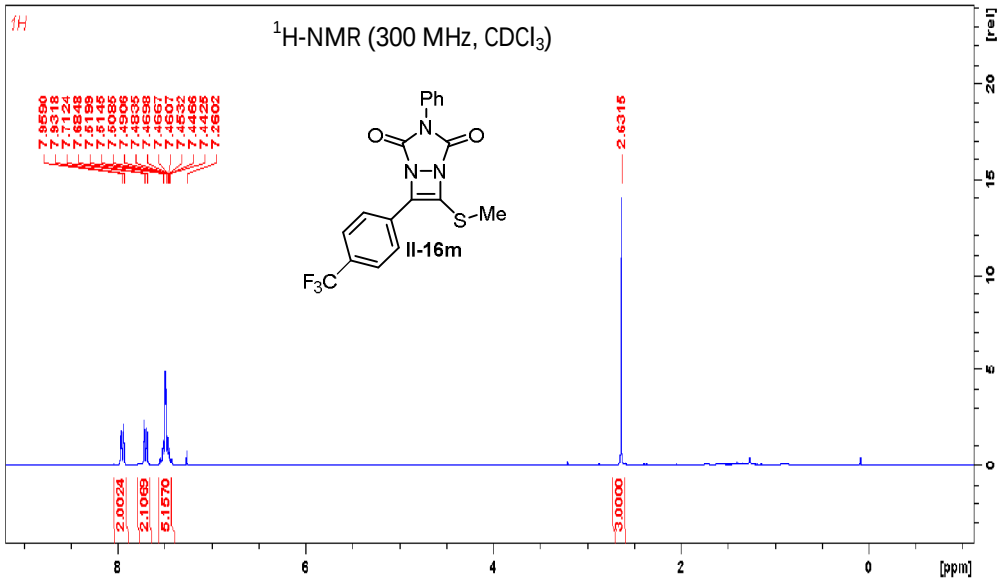
1H
^{1}H-NMR (300 MHz, CDCl$_3$)
7.9590
7.9318
7.7124
7.6848
7.5149
7.5146
7.5085
7.4906
7.4835
7.4638
7.4607
7.4532
7.4466
7.4425
7.2602
Ph
N
O
O
N–N
S–Me
II-16m
F$_3$C
2.6315
2.0024
2.1069
5.1570
3.0000
8
6
4
2
0
[ppm]
[rel]

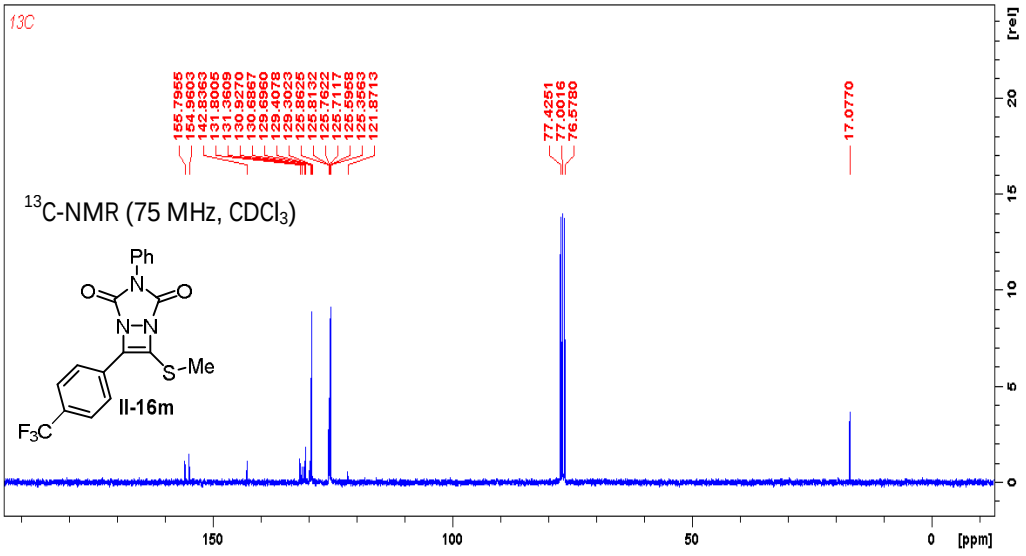
13C
155.7955
154.9603
142.8363
131.8006
131.3909
131.3270
130.6867
129.6960
129.4078
129.3023
125.8625
125.8132
125.7972
125.7117
125.5958
125.3563
121.8713
77.4251
77.0016
76.5780
17.0770
^{13}C-NMR (75 MHz, CDCl$_3$)
Ph
N
O
O
N–N
S–Me
II-16m
F$_3$C
150
100
50
0
[ppm]
[rel]

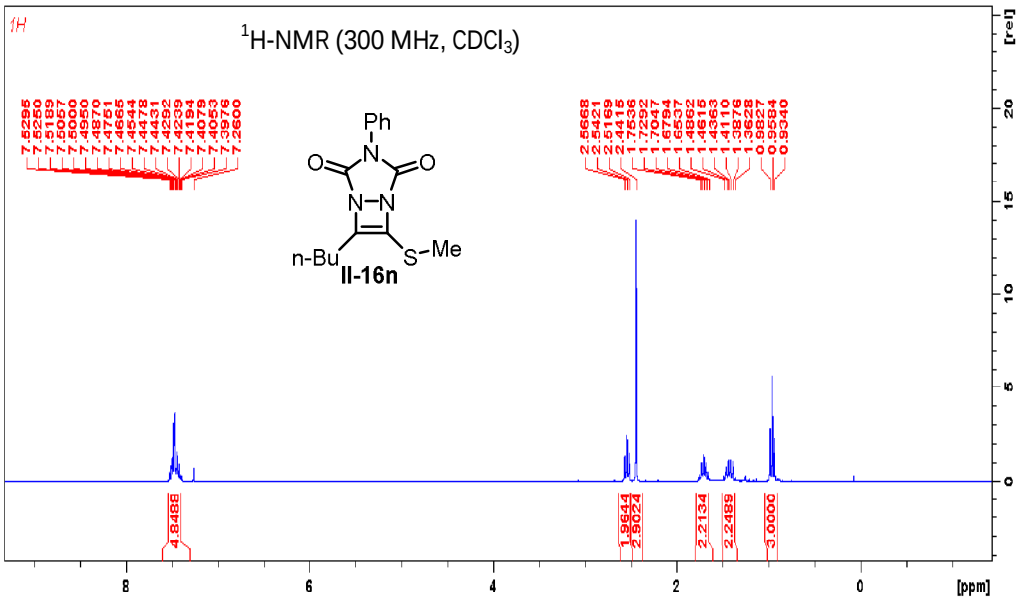
1H
1H-NMR (300 MHz, CDCl3)
Ph
n-Bu
S-Me
II-16n
[rel]
[ppm]

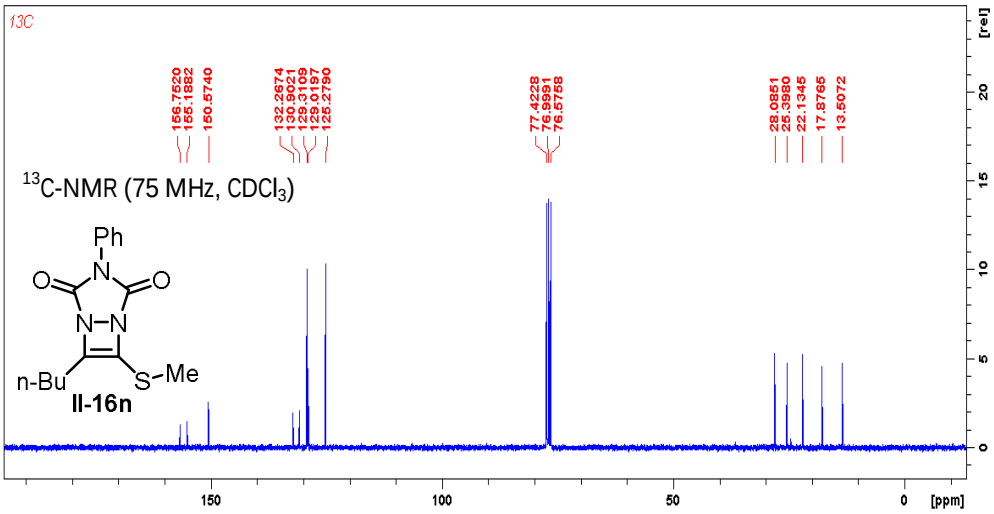
13C
13C-NMR (75 MHz, CDCl3)
Ph
n-Bu
S-Me
II-16n
[rel]
[ppm]

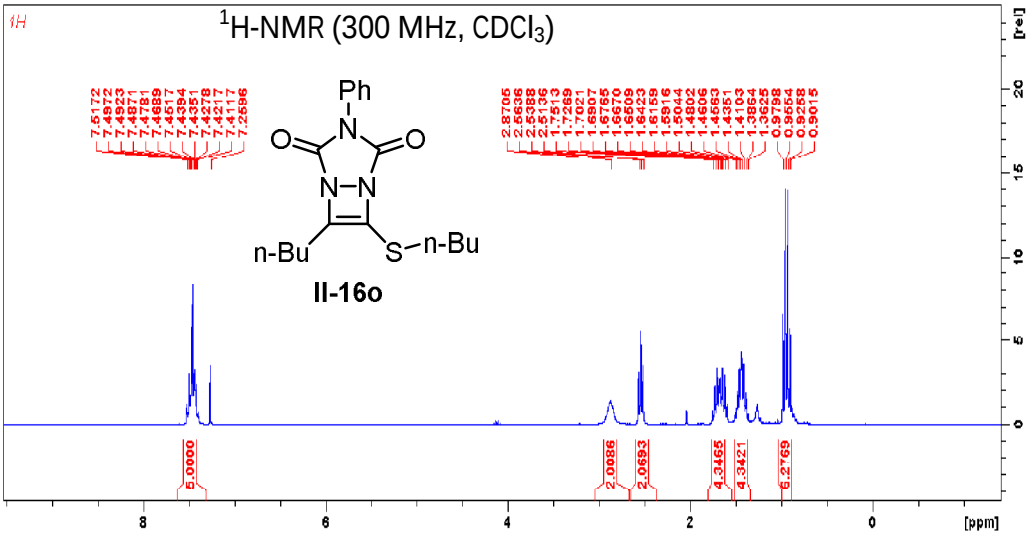
1H
^{1}H-NMR (300 MHz, $CDCl_3$)
Ph
n-Bu
S
n-Bu
II-16o
[ppm]
[rel]

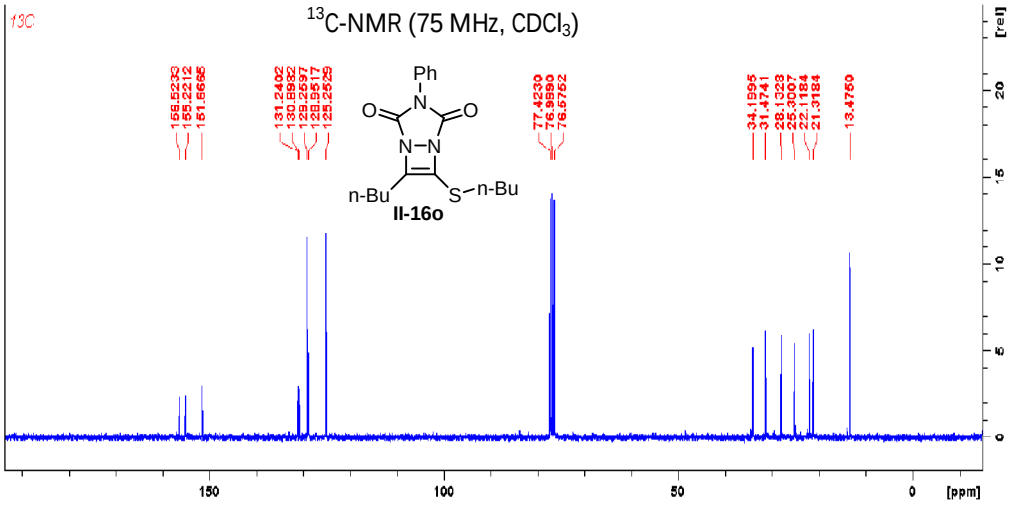
13C
^{13}C-NMR (75 MHz, $CDCl_3$)
Ph
n-Bu
S
n-Bu
II-16o
[ppm]
[rel]

2D-HMQC (F2= 300 MHz, F1 = 75 MHz, $CDCl_3$) analysis of diazacyclobutene **II-16o**

(Carbons were denoted in numbers and hydrogens were denoted in letters in the chemical structure and the spectrum)

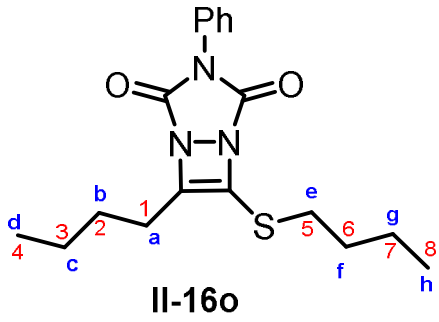

II-16o

The two overlapping ^{1}H signals from H_d and H_h correlate to a single ^{13}C resonance resulting from accidental degeneracy of the resonances from C4 and C8.

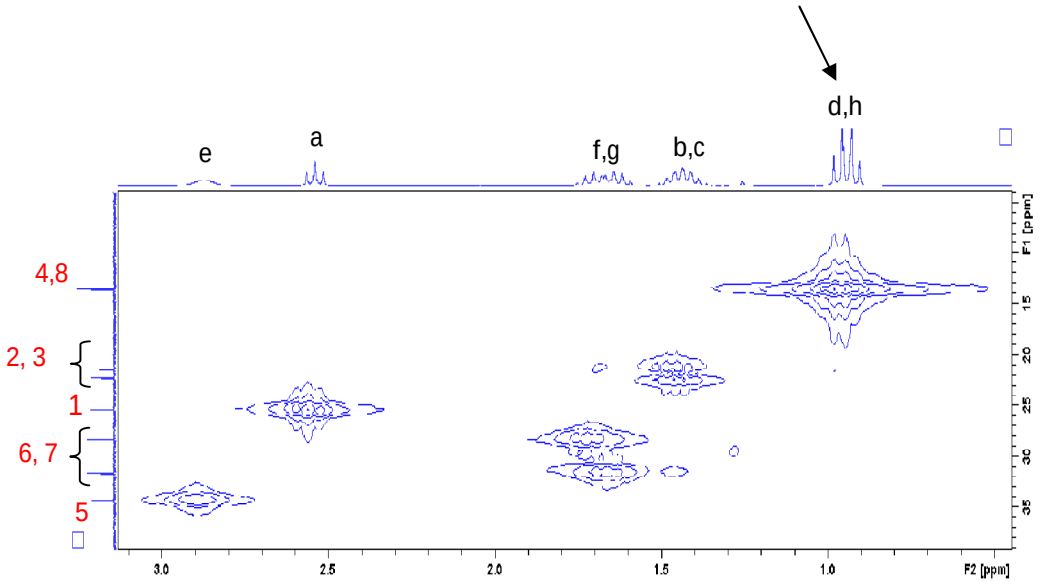

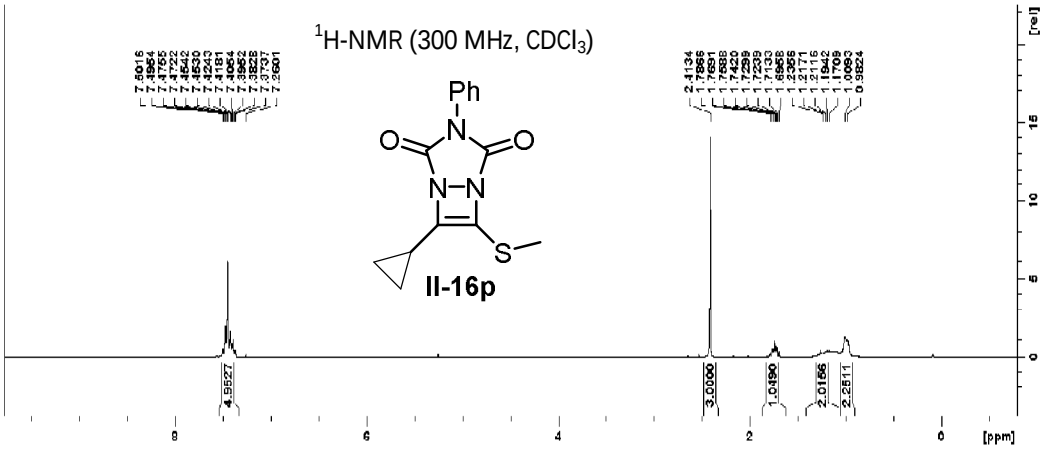
^{1}H-NMR (300 MHz, $CDCl_3$)
Ph
N
O
O
N–N
S
II-16p
4.9527
3.0000
1.0490
2.0156
2.2811
[ppm]
[rel]

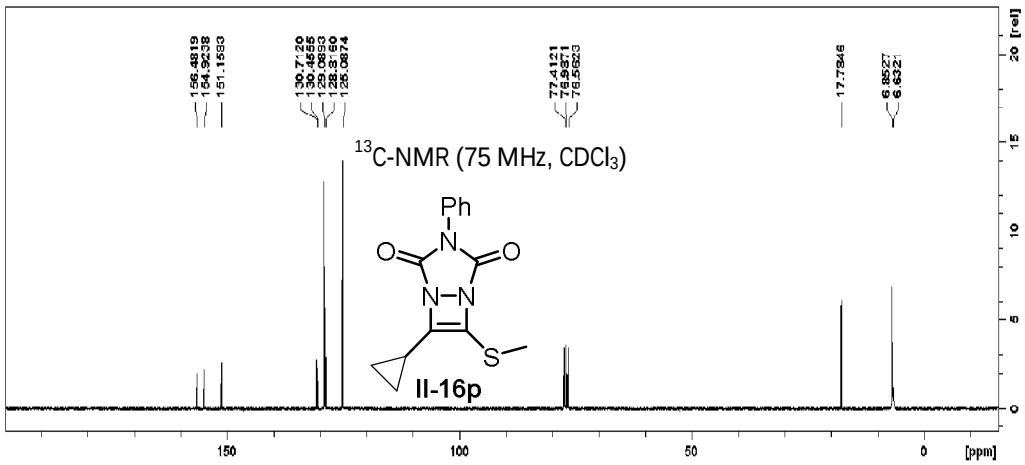
^{13}C-NMR (75 MHz, $CDCl_3$)
Ph
N
O
O
N–N
S
II-16p
156.4819
154.9238
151.1583
130.7120
130.4855
129.0693
128.3750
125.0674
77.4121
76.9871
76.5623
17.7846
6.8527
6.8321
[ppm]
[rel]

2D-HMQC (F2= 300 MHz, F1 = 75 MHz, $CDCl_3$) analysis of diazacyclobutene **II-16p**

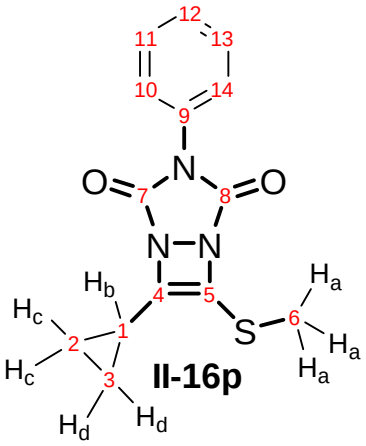

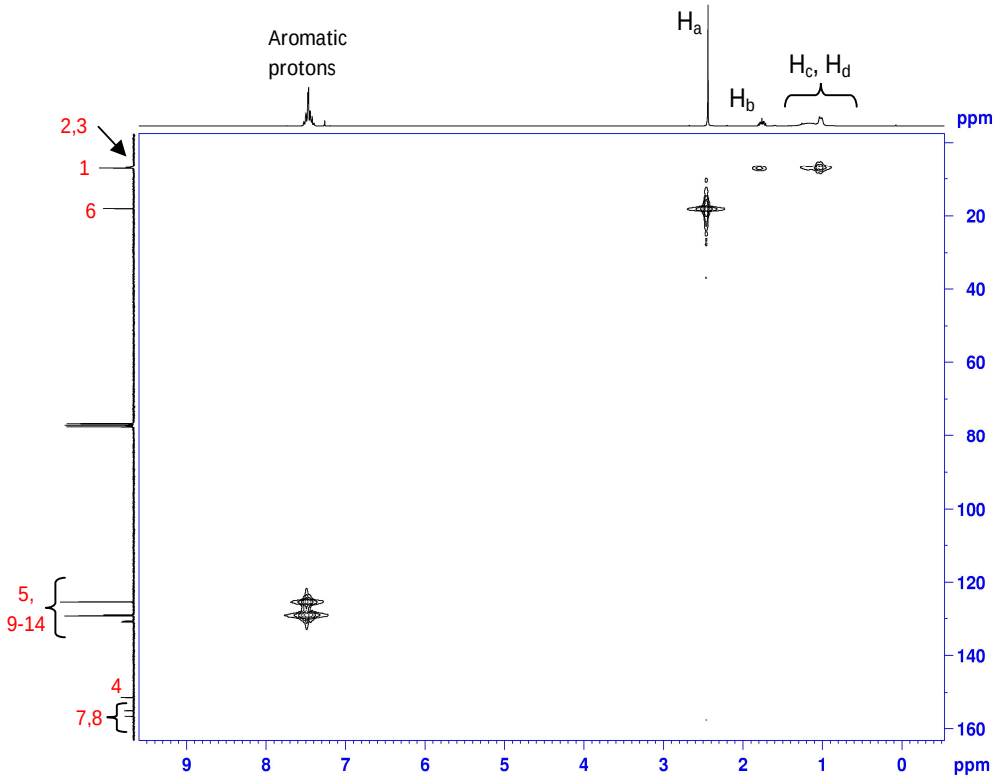

2D-HMQC (F2= 300 MHz, F1 = 75 MHz, $CDCl_3$) analysis of diazacyclobutene **II-16p** Cntd.

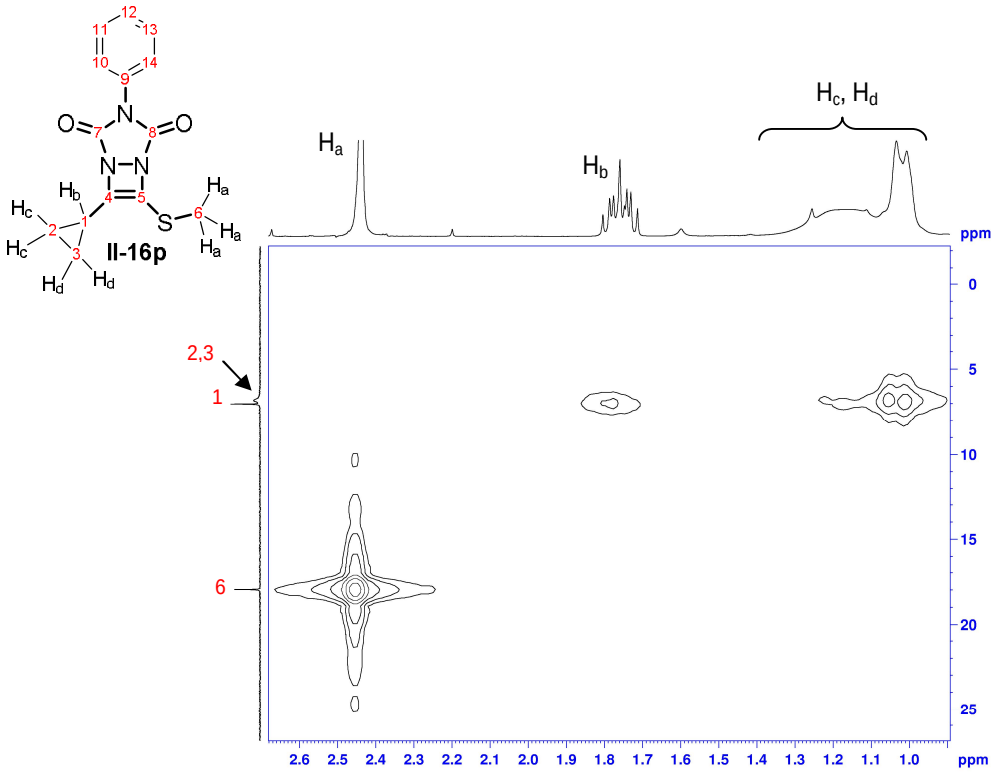

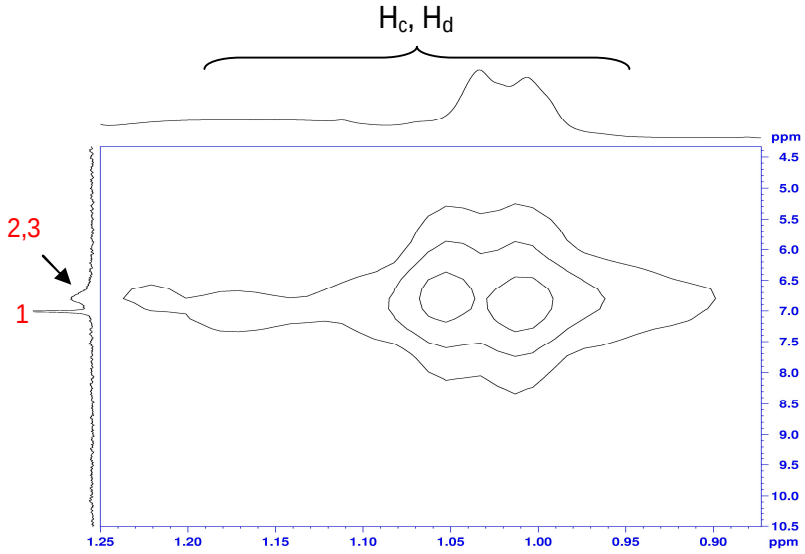

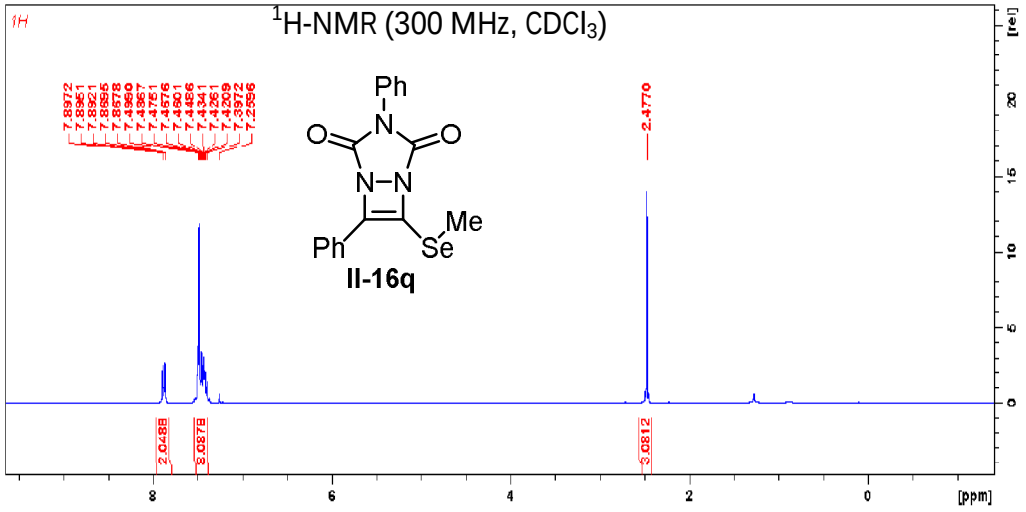
1H
^{1}H-NMR (300 MHz, $CDCl_3$)
7.8972
7.8951
7.8921
7.8895
7.8878
7.4360
7.4357
7.4351
7.4576
7.4501
7.4486
7.4341
7.4261
7.4179
7.3972
7.2596
2.4770
Ph
N
O
O
N–N
Ph
Me
Se
II-16q
2.0488
3.0278
3.0612
8
6
4
2
0
[ppm]
[rel]

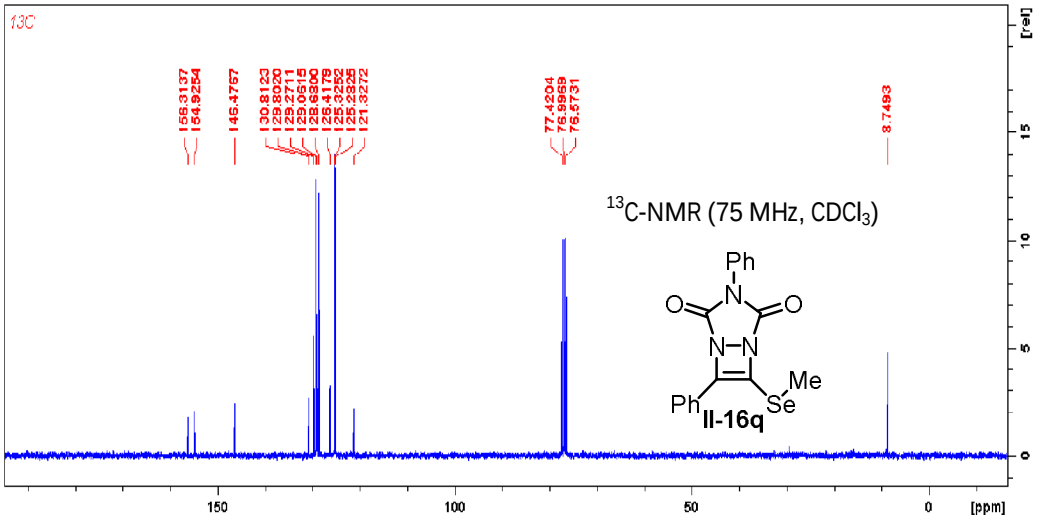
13C
156.3137
154.9254
145.4767
130.8123
129.8020
129.2711
128.9514
128.7300
126.4175
125.3252
125.2325
121.3272
77.4204
76.9959
76.5731
8.7493
^{13}C-NMR (75 MHz, $CDCl_3$)
Ph
N
O
O
N–N
Ph
Me
Se
II-16q
150
100
50
0
[ppm]
[rel]

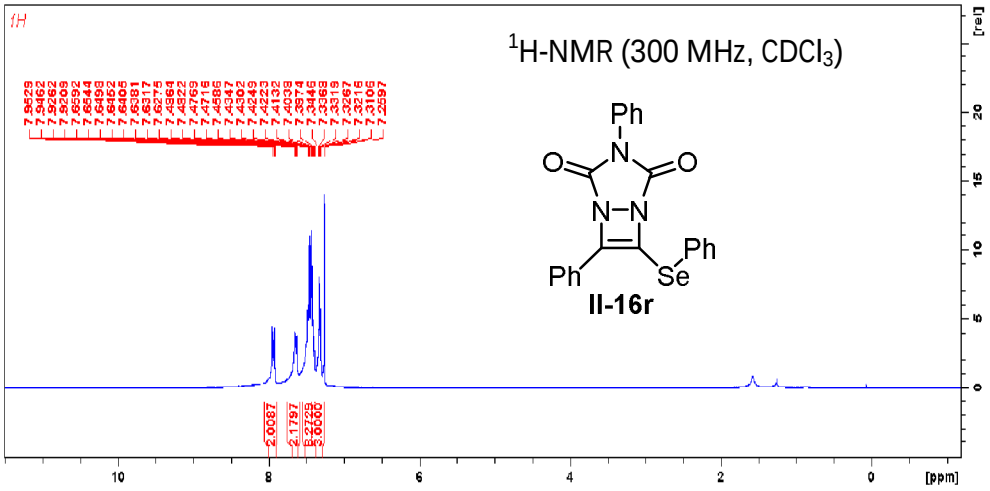
1H
^{1}H-NMR (300 MHz, $CDCl_3$)
Ph
N
O
O
N–N
Ph
Ph
Se
II-16r
[rel]
[ppm]

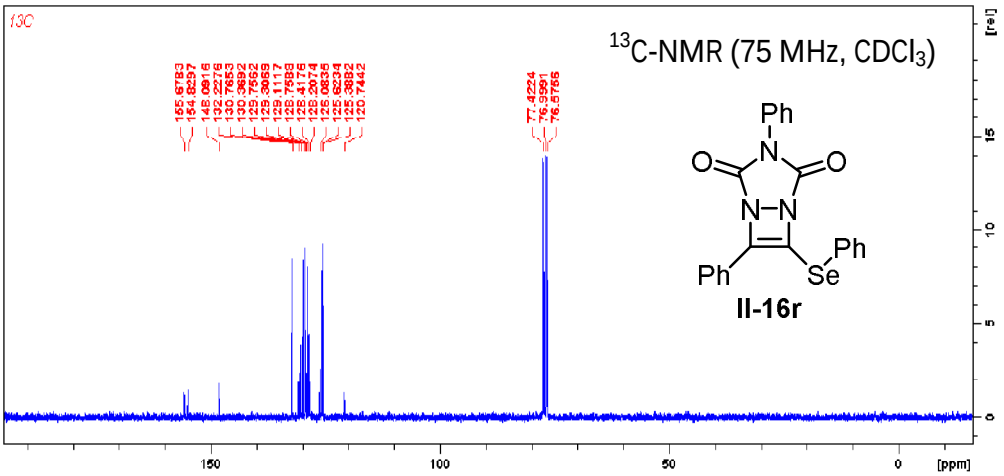
13C
^{13}C-NMR (75 MHz, $CDCl_3$)
Ph
N
O
O
N–N
Ph
Ph
Se
II-16r
[rel]
[ppm]

2.8.27. ^{1}H NMR and ^{13}C NMR spectra for methanebis(ethynylsulfane) and diazacyclobutene dimer (II-26 (n=1))

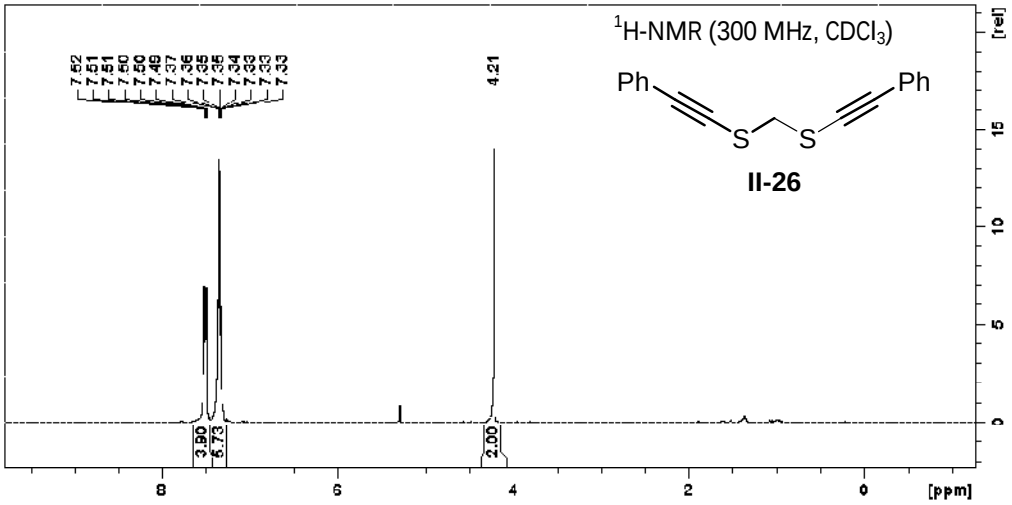

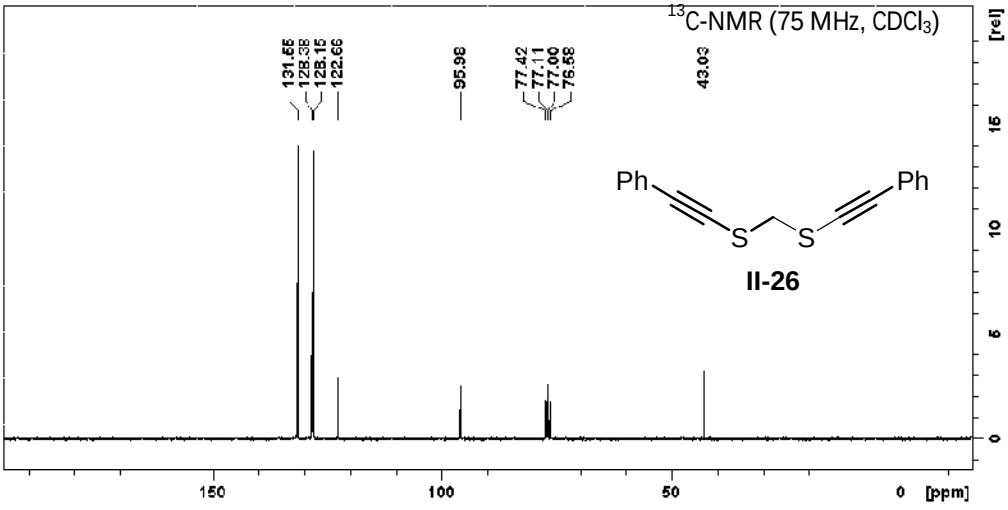

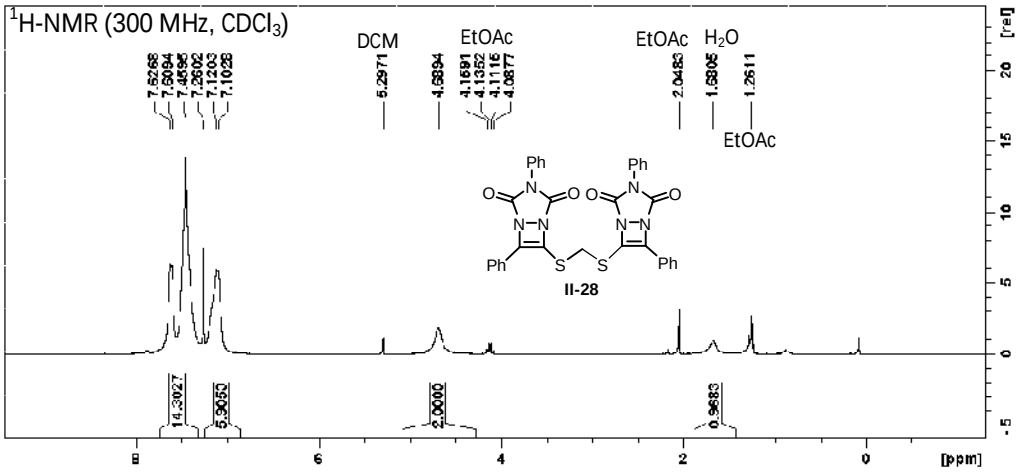
1H-NMR (300 MHz, CDCl3)
DCM
EtOAc
EtOAc
H2O
EtOAc
II-28
[ppm]

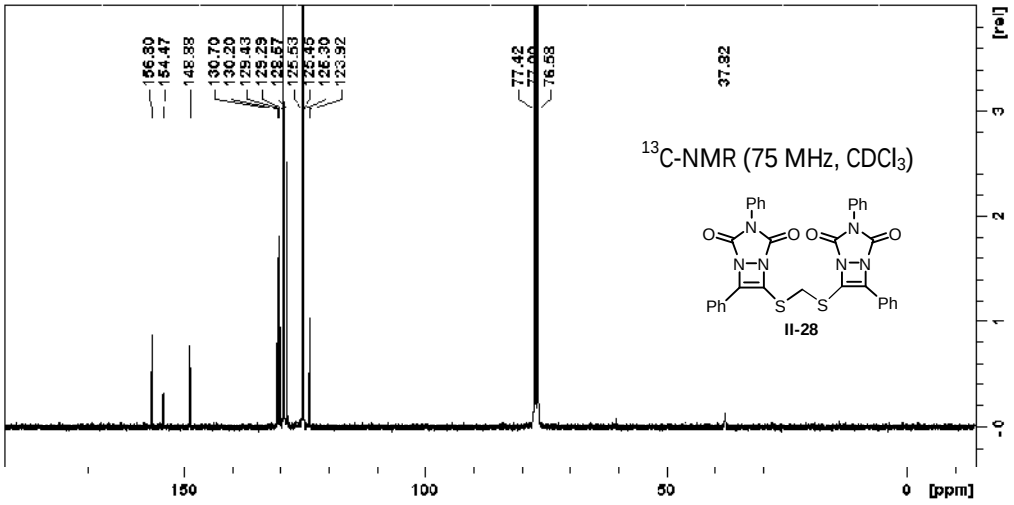
13C-NMR (75 MHz, CDCl3)
II-28
[ppm]

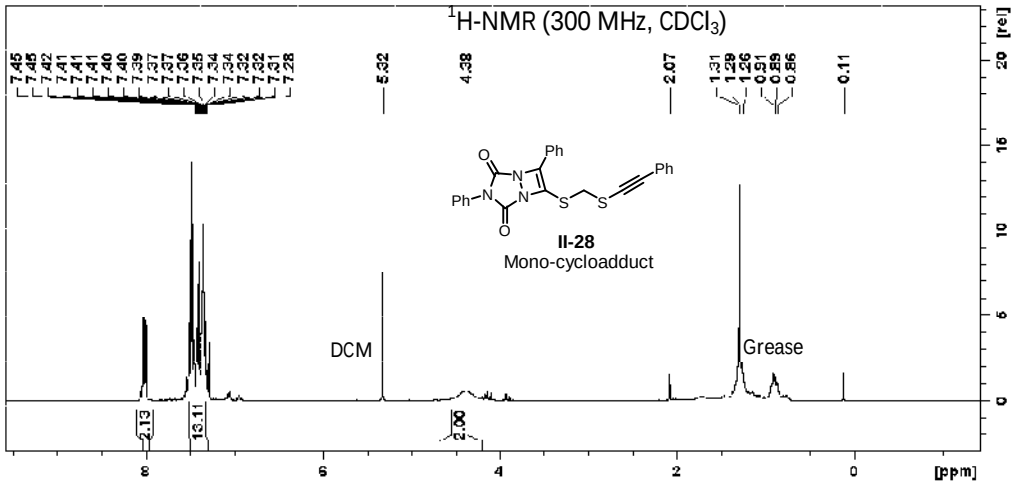
1H-NMR (300 MHz, CDCl3)
7.45
7.45
7.42
7.41
7.41
7.41
7.40
7.40
7.39
7.37
7.37
7.36
7.35
7.34
7.34
7.32
7.32
7.31
7.28
5.32
4.38
2.07
1.31
1.29
1.26
0.91
0.89
0.86
0.11
Ph
O
N
N
Ph
O
S
S
Ph
II-28
Mono-cycloadduct
DCM
Grease
2.13
13.11
2.00
8
6
4
2
0
[ppm]
[rel]

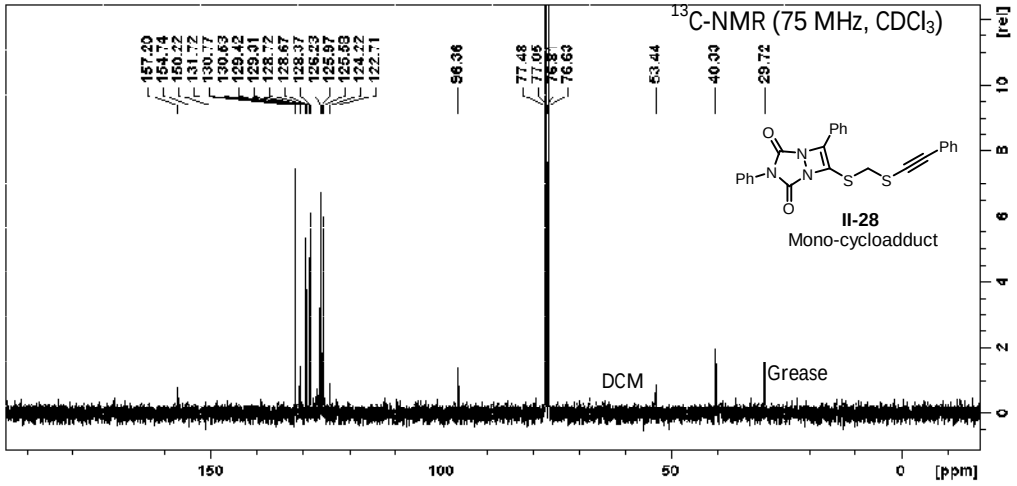
13C-NMR (75 MHz, CDCl3)
157.20
154.74
150.22
131.72
130.77
130.63
129.42
129.31
128.72
128.67
128.37
126.23
125.97
125.63
124.22
122.71
56.36
77.48
77.05
76.63
53.44
40.33
29.72
Ph
O
N
N
Ph
O
S
S
Ph
II-28
Mono-cycloadduct
DCM
Grease
150
100
50
0
[ppm]
[rel]

2.8.28. ^{1}H NMR and ^{13}C NMR spectra for bromoalkynes, ynamides and ynamide based diazacyclobutenes.

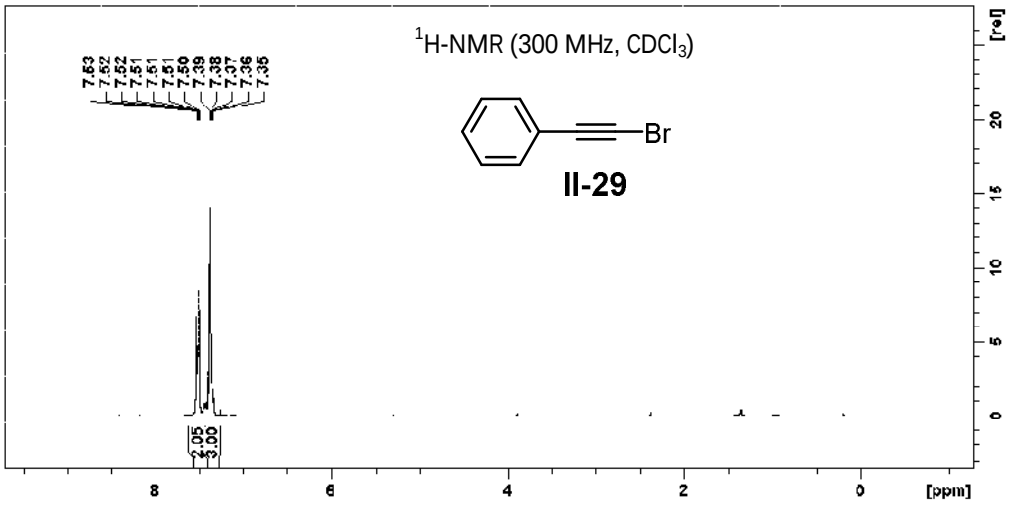

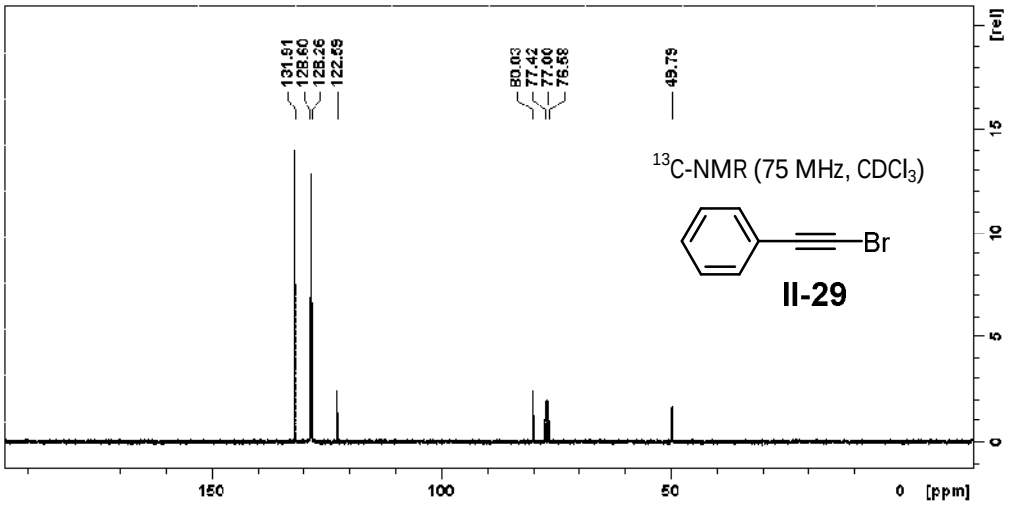

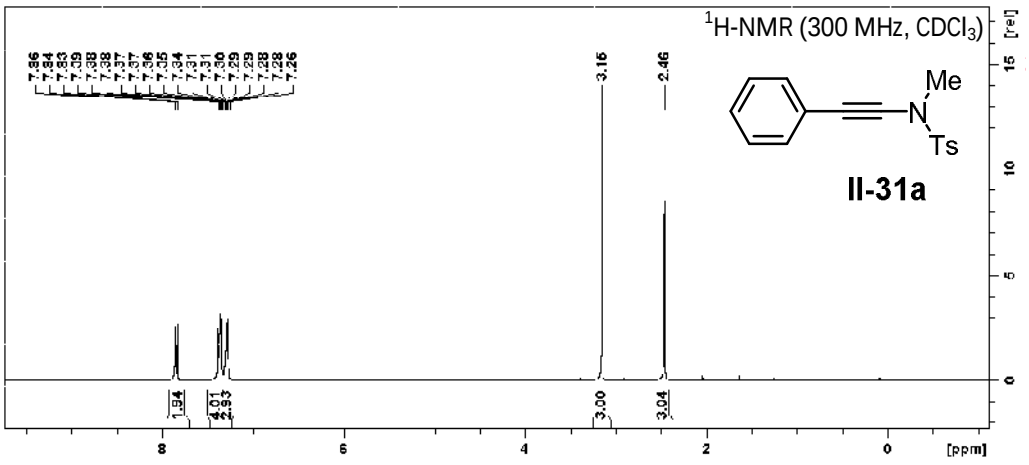
^{1}H-NMR (300 MHz, $CDCl_3$)
7.86
7.84
7.83
7.39
7.38
7.38
7.37
7.37
7.36
7.35
7.34
7.31
7.31
7.30
7.29
7.29
7.28
7.28
7.26
3.16
2.46
Me
N
Ts
II-31a
1.94
4.01
2.93
3.00
3.04
8
6
4
2
0
[ppm]
[rel]

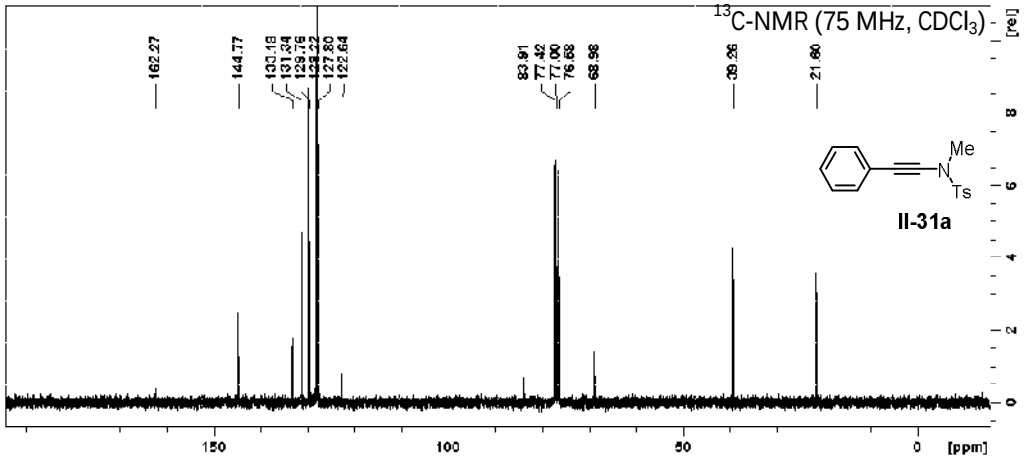
^{13}C-NMR (75 MHz, $CDCl_3$)
162.27
144.77
133.18
131.34
129.75
128.22
127.80
122.64
83.91
77.42
77.00
76.68
68.96
29.26
21.60
Me
N
Ts
II-31a
150
100
50
0
[ppm]
[rel]

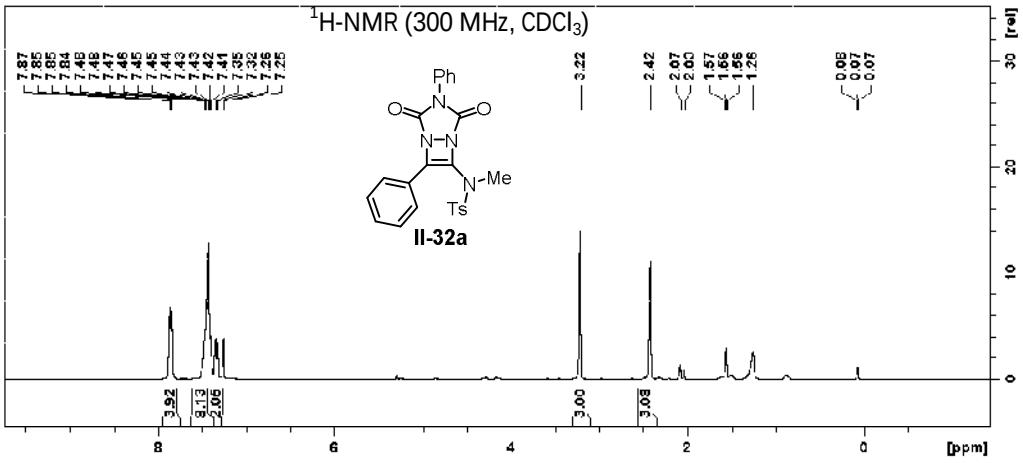
^{1}H-NMR (300 MHz, $CDCl_3$)
Ph
N-Me
Ts
II-32a
[ppm]
[rel]

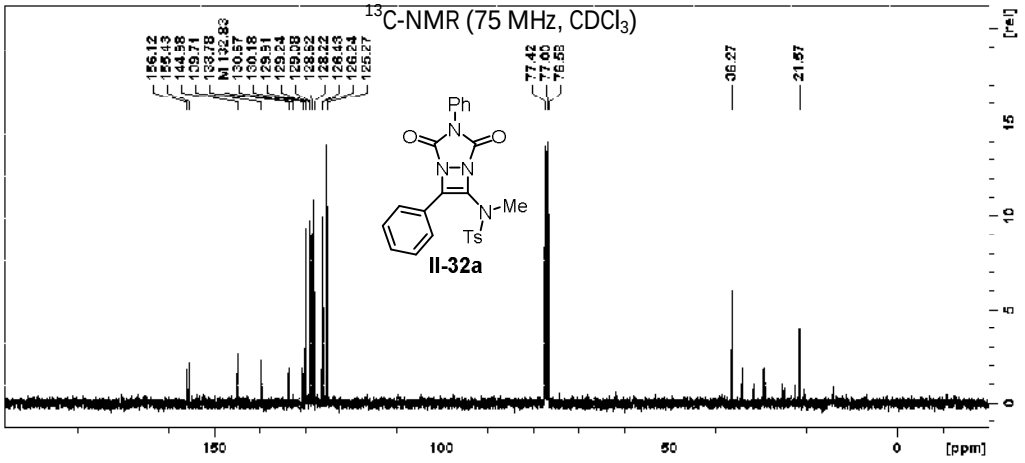
^{13}C-NMR (75 MHz, $CDCl_3$)
Ph
N-Me
Ts
II-32a
[ppm]
[rel]

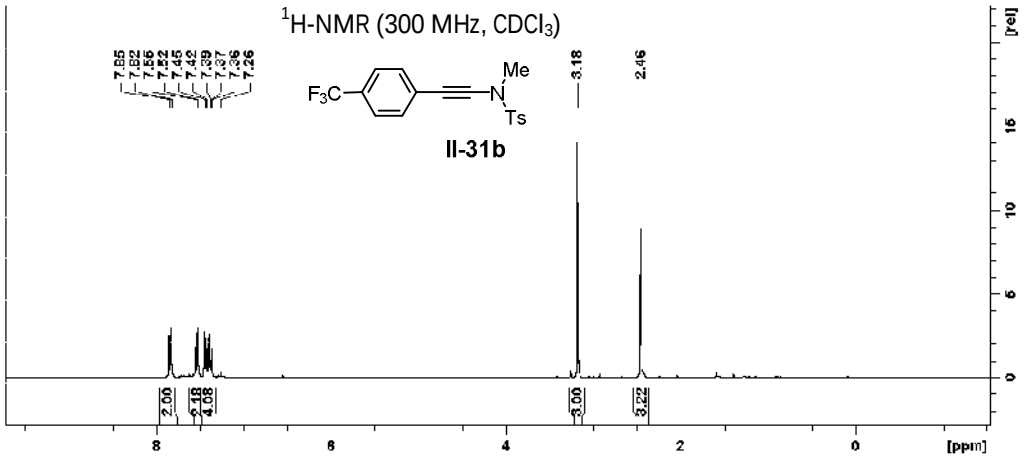
1H-NMR (300 MHz, CDCl3)
7.85
7.82
7.56
7.52
7.45
7.42
7.39
7.37
7.36
7.26
F3C
Me
N
Ts
II-31b
3.18
2.46
2.00
2.16
4.08
3.00
3.22
8
6
4
2
0
[ppm]
[rel]

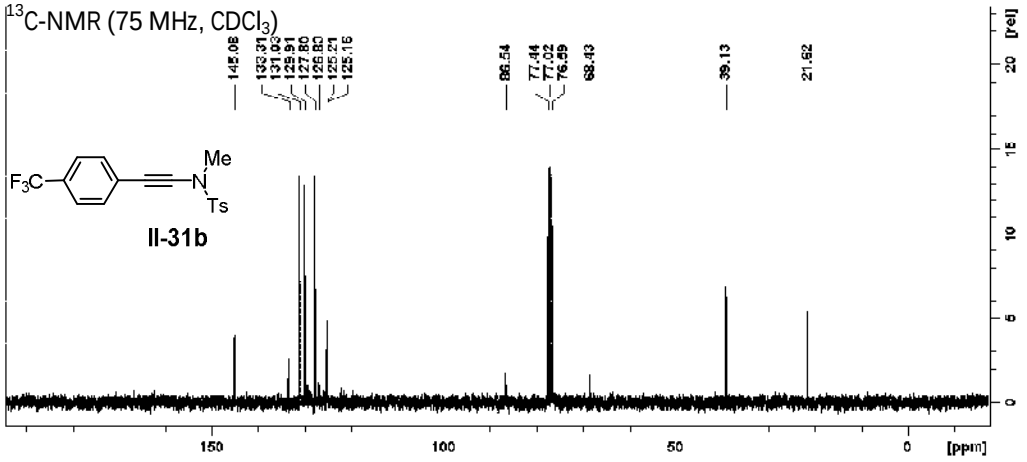
13C-NMR (75 MHz, CDCl3)
145.08
133.31
131.03
129.91
127.80
126.80
125.21
125.16
86.54
77.44
77.02
76.59
68.43
39.13
21.62
F3C
Me
N
Ts
II-31b
150
100
50
0
[ppm]
[rel]

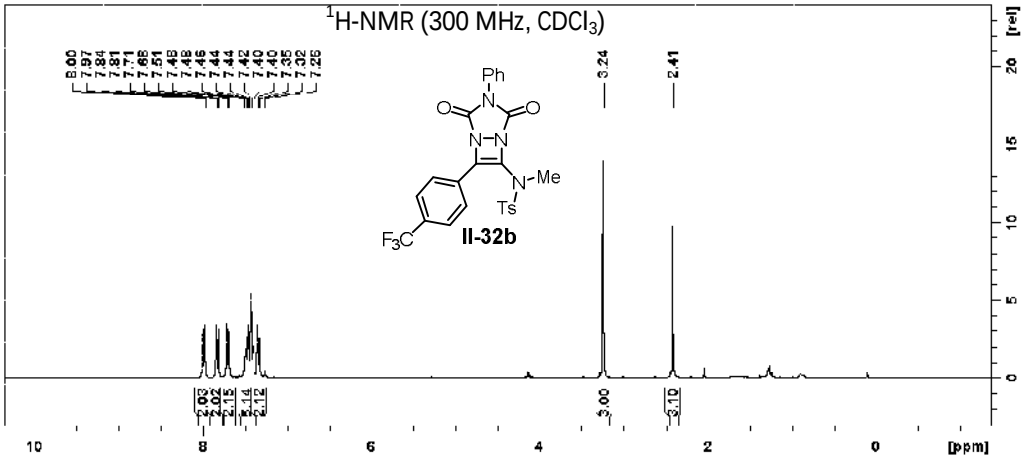
^{1}H-NMR (300 MHz, $CDCl_3$)
8.00
7.97
7.84
7.81
7.71
7.68
7.51
7.48
7.46
7.44
7.42
7.40
7.35
7.32
7.25
3.24
2.41
Ph
N
O
O
N–N
N-Me
Ts
F_3C
II-32b
2.03
2.02
2.15
3.14
2.12
3.00
3.10
10
8
6
4
2
0
[ppm]
[rel]

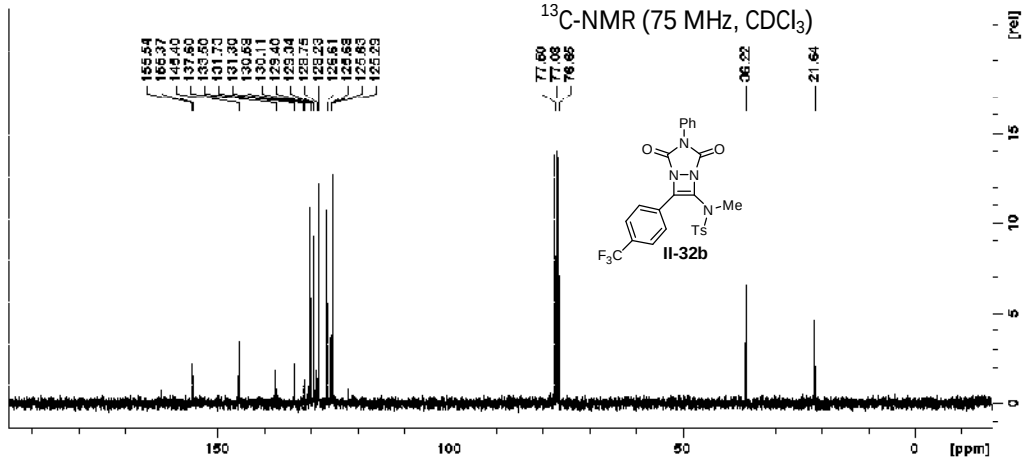
^{13}C-NMR (75 MHz, $CDCl_3$)
155.54
155.37
145.40
137.60
133.50
131.70
131.30
130.88
130.11
129.40
129.34
128.75
128.23
126.61
125.68
125.63
125.29
77.60
77.08
76.85
36.22
21.64
Ph
N
O
O
N–N
N-Me
Ts
F_3C
II-32b
150
100
50
0
[ppm]
[rel]

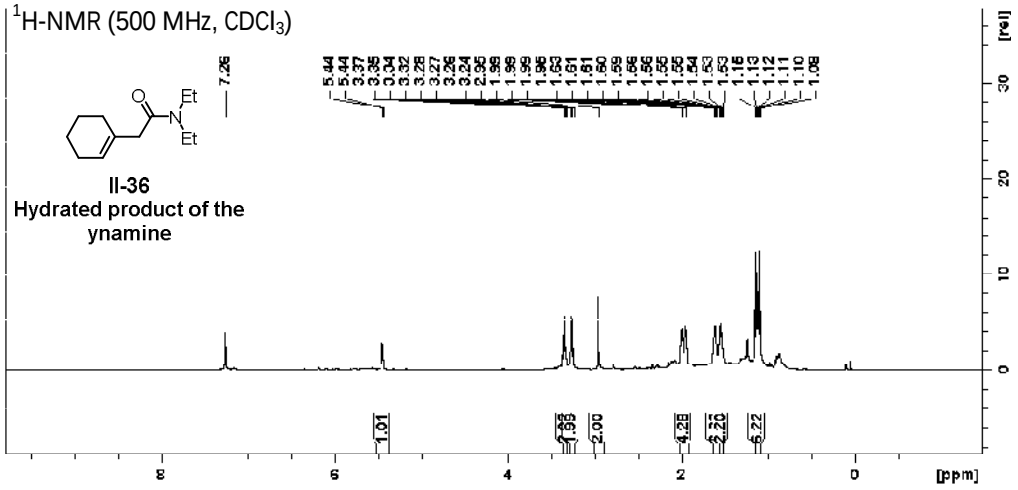
^{1}H-NMR (500 MHz, $CDCl_3$)
II-36
Hydrated product of the ynamine
[ppm]
[rel]

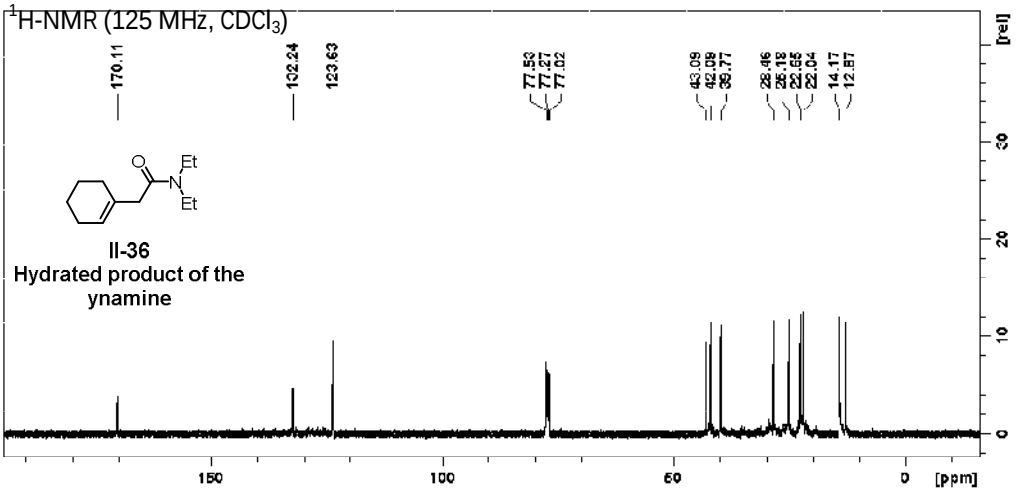
^{1}H-NMR (125 MHz, $CDCl_3$)
II-36
Hydrated product of the ynamine
[ppm]
[rel]

2.8.29. ^{1}H NMR and ^{13}C NMR spectra for semicarbazides and urozoles

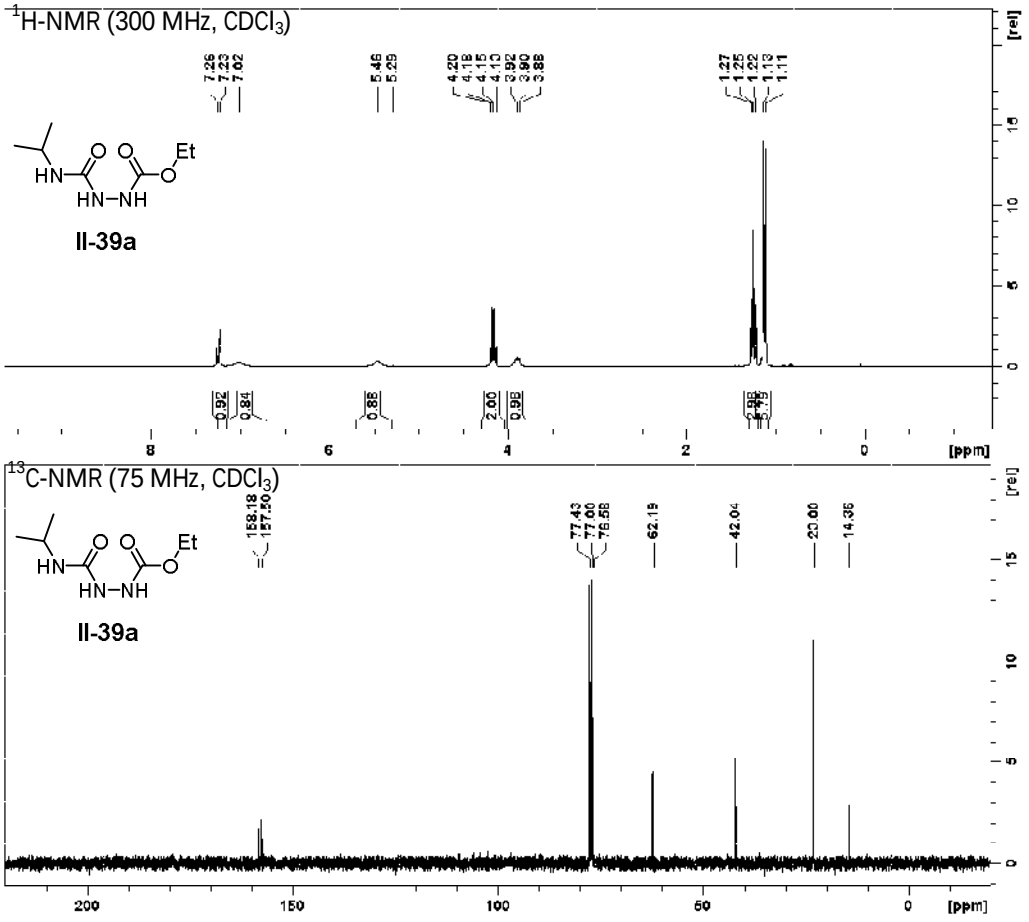

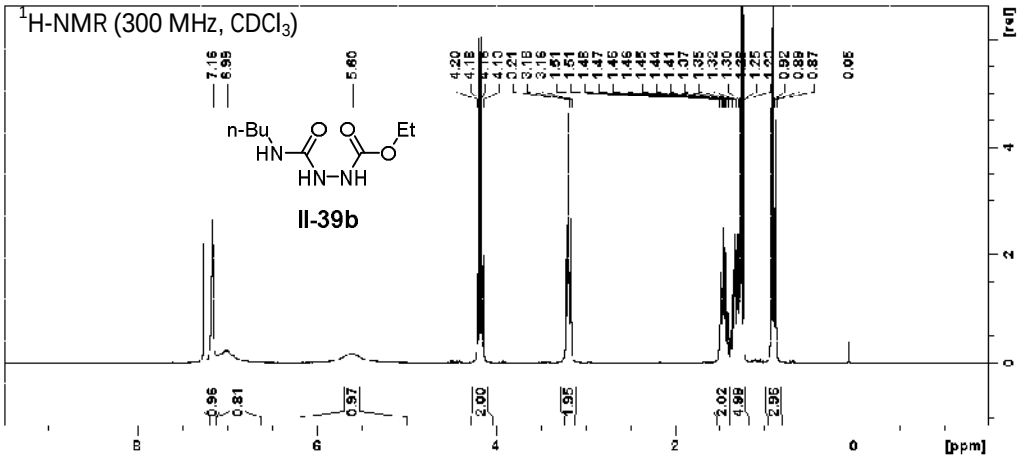
^{1}H-NMR (300 MHz, $CDCl_3$)
n-Bu
HN
HN–NH
Et
II-39b
[ppm]

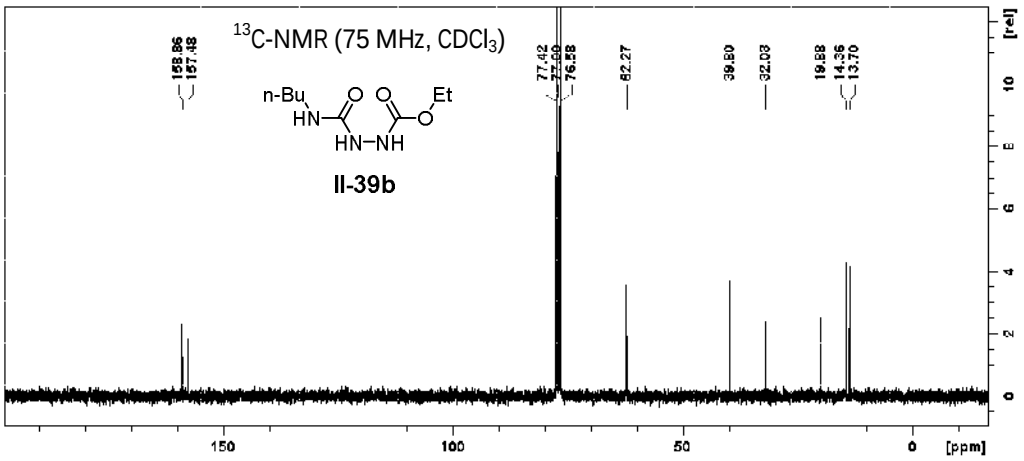
^{13}C-NMR (75 MHz, $CDCl_3$)
n-Bu
HN
HN–NH
Et
II-39b
[ppm]

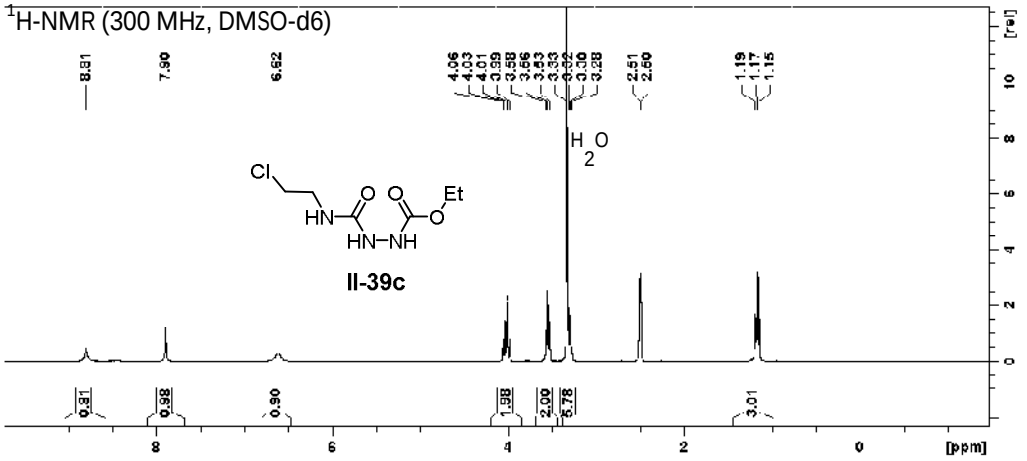
1H-NMR (300 MHz, DMSO-d6)
8.81
7.90
6.62
4.06
4.03
4.01
3.99
3.58
3.56
3.53
3.33
3.02
3.00
2.98
2.51
2.50
1.19
1.17
1.15
H2O
Cl
HN
O
O
Et
HN–NH
II-39c
0.91
0.98
0.90
1.98
2.00
5.78
3.01
8
6
4
2
0
[ppm]
[rel]

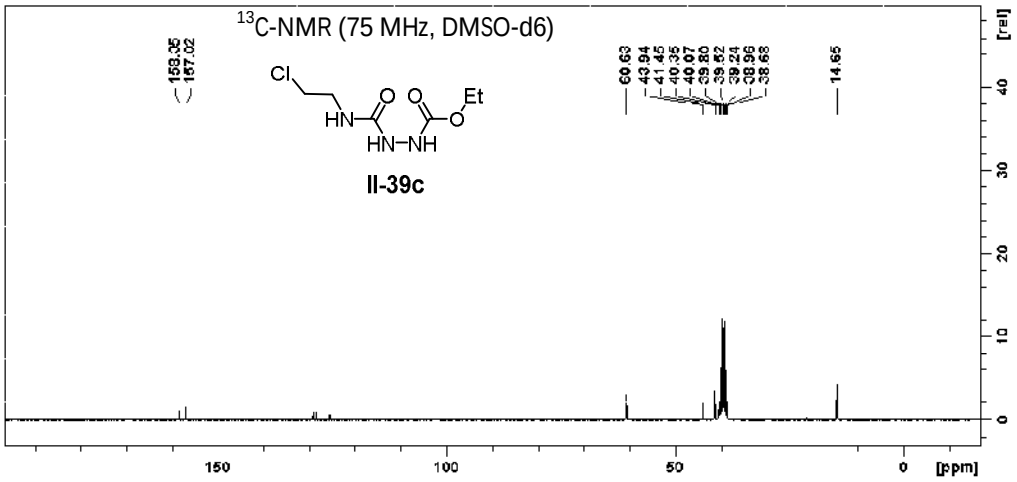
13C-NMR (75 MHz, DMSO-d6)
153.05
157.02
60.63
43.94
41.45
40.35
40.07
39.80
39.52
39.24
38.96
38.68
14.65
Cl
HN
O
O
Et
HN–NH
II-39c
150
100
50
0
[ppm]
[rel]

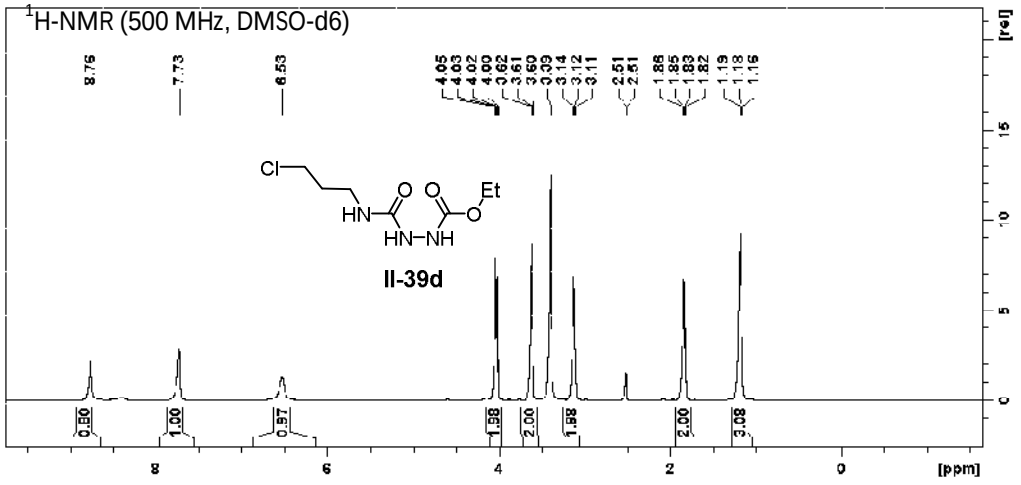
1H-NMR (500 MHz, DMSO-d6)
8.76
7.73
6.53
4.05
4.03
4.02
4.00
3.62
3.61
3.60
3.39
3.14
3.12
3.11
2.51
2.51
1.88
1.85
1.83
1.82
1.19
1.18
1.16
Cl
HN
HN–NH
O
O
O
Et
II-39d
0.50
1.00
0.97
1.58
2.00
1.88
2.00
3.08
8
6
4
2
0
[ppm]
[rel]

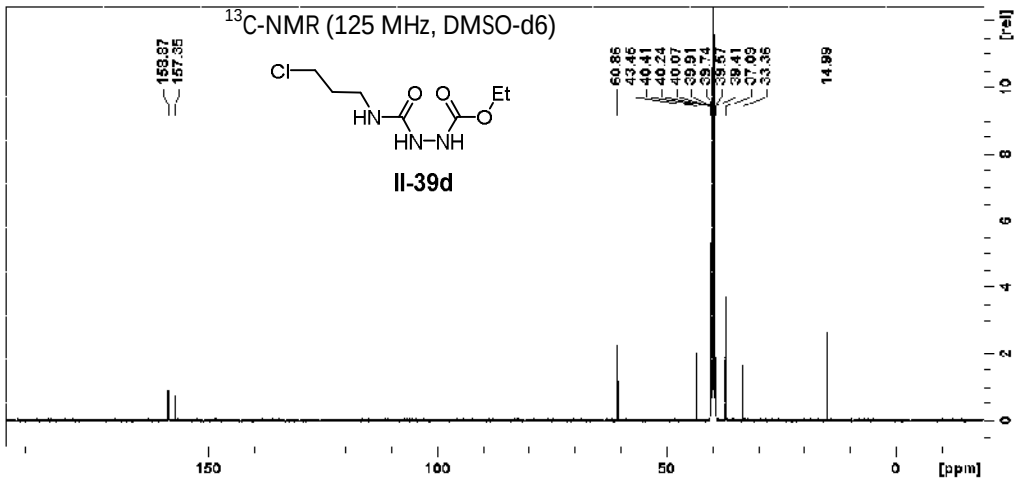
13C-NMR (125 MHz, DMSO-d6)
159.87
157.35
60.86
43.46
40.41
40.24
40.07
39.91
39.74
39.57
39.41
37.09
33.36
14.99
Cl
HN
HN–NH
O
O
O
Et
II-39d
150
100
50
0
[ppm]
[rel]

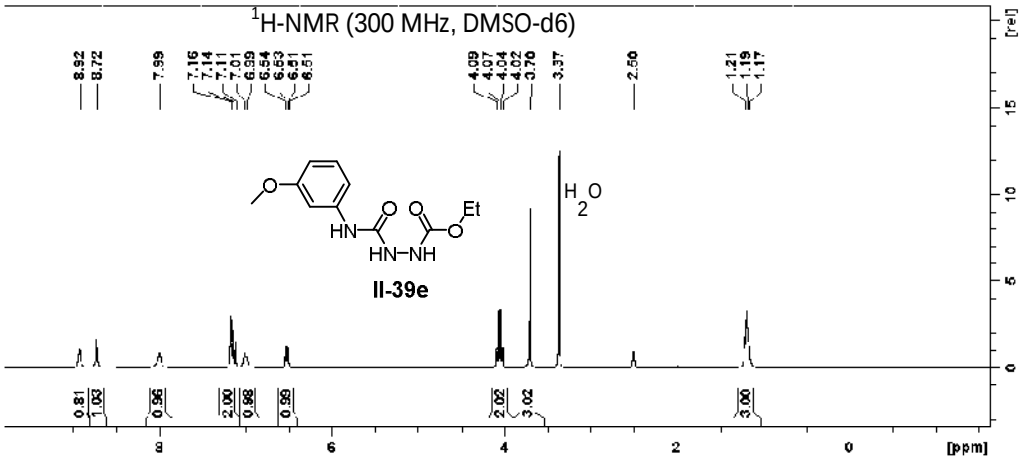
1H-NMR (300 MHz, DMSO-d6)
8.92
8.72
7.99
7.16
7.14
7.11
7.01
6.99
6.54
6.53
6.51
6.51
4.09
4.07
4.04
4.02
3.76
3.37
2.50
1.21
1.19
1.17
H2O
HN
HN–NH
Et
II-39e
0.81
1.03
0.96
2.00
0.98
0.99
2.02
3.02
3.00
[rel]
[ppm]

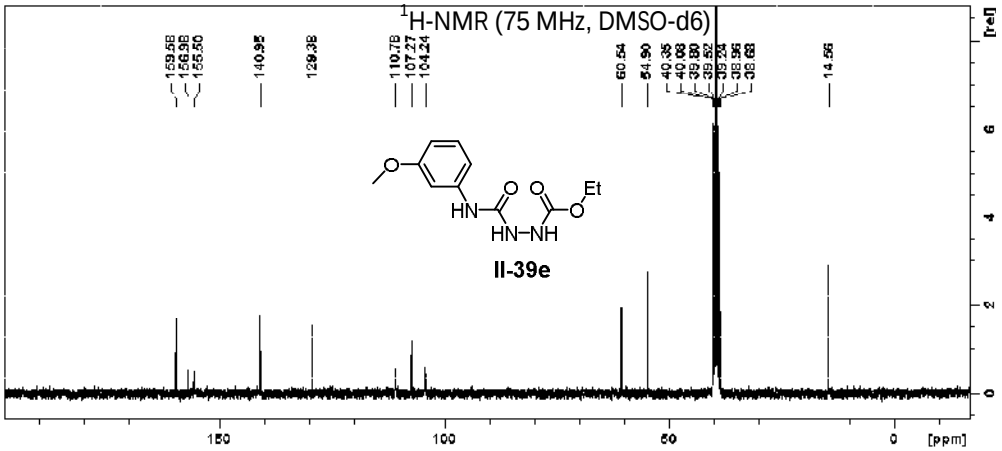
1H-NMR (75 MHz, DMSO-d6)
159.58
156.98
155.50
140.95
129.38
110.78
107.27
104.24
60.54
54.90
40.35
40.08
39.80
39.53
39.26
38.99
38.68
14.56
HN
HN–NH
Et
II-39e
[rel]
[ppm]

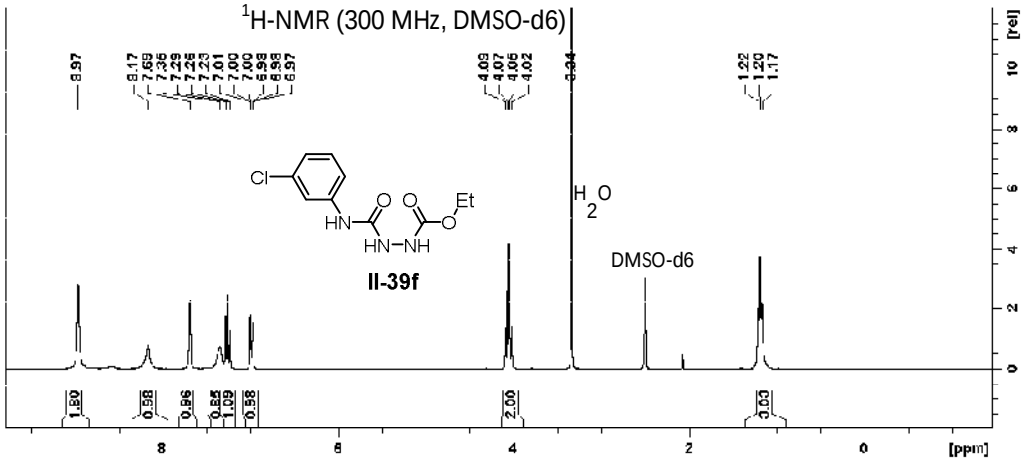
1H-NMR (300 MHz, DMSO-d6)
8.97
8.17
7.69
7.36
7.29
7.26
7.23
7.01
7.00
7.00
6.98
6.97
4.09
4.07
4.06
4.02
3.34
1.22
1.20
1.17
H2O
DMSO-d6
Cl
HN
O
O
O
Et
HN–NH
II-39f
1.00
0.58
0.96
0.85
1.09
0.58
2.06
3.03
8
6
4
2
0
[ppm]
[rel]

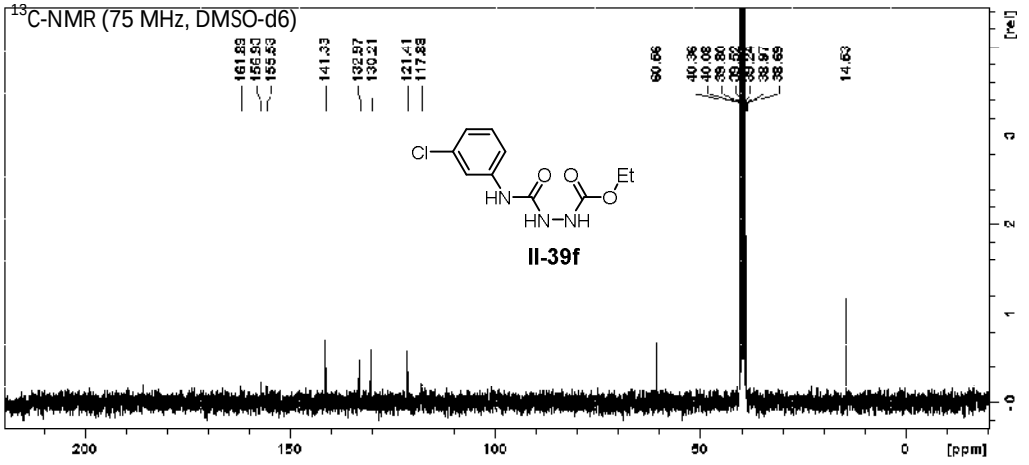
13C-NMR (75 MHz, DMSO-d6)
161.89
156.50
155.53
141.33
132.87
130.21
121.41
117.28
60.66
40.36
40.08
38.97
38.69
14.63
Cl
HN
O
O
O
Et
HN–NH
II-39f
200
150
100
50
0
[ppm]
[rel]

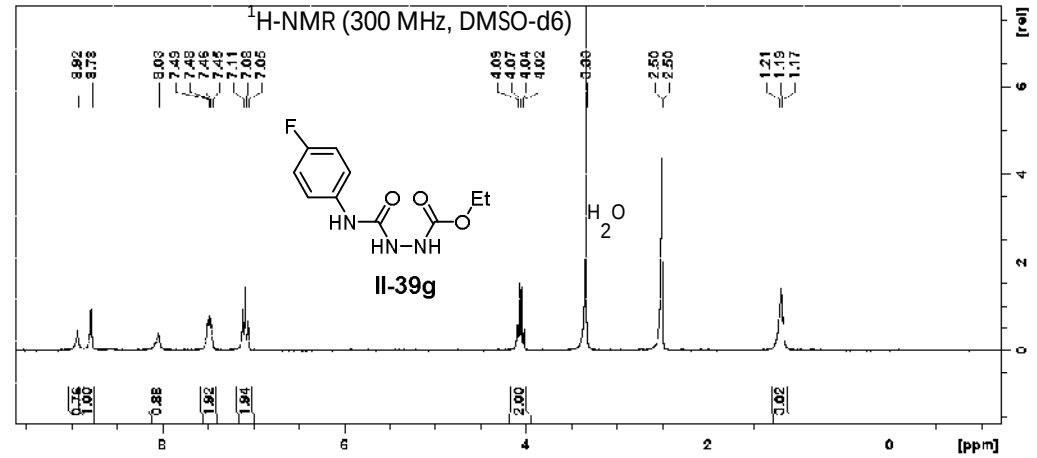
1H-NMR (300 MHz, DMSO-d6)
F
HN
O
O
Et
HN–NH
II-39g
H2O
[ppm]

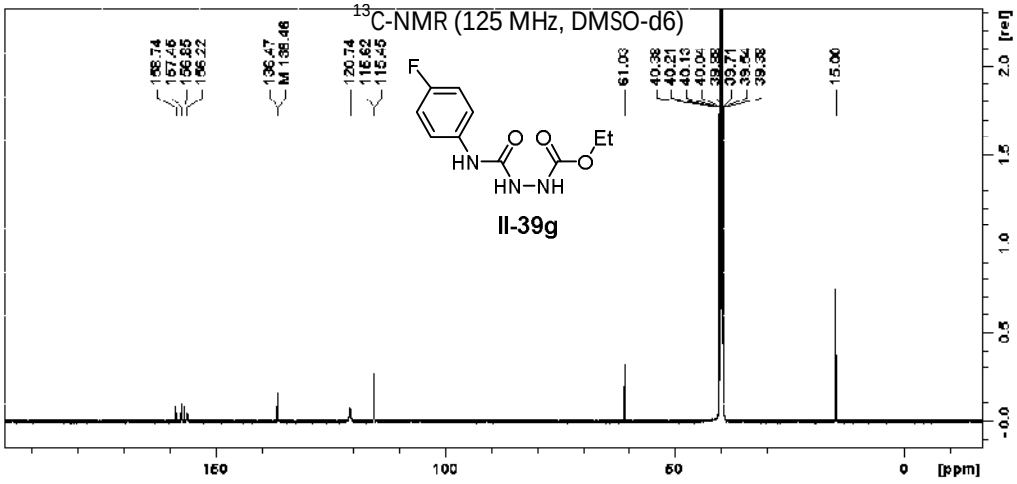
13C-NMR (125 MHz, DMSO-d6)
F
HN
O
O
Et
HN–NH
II-39g
[ppm]

^{1}H-NMR (300 MHz, DMSO-d6)

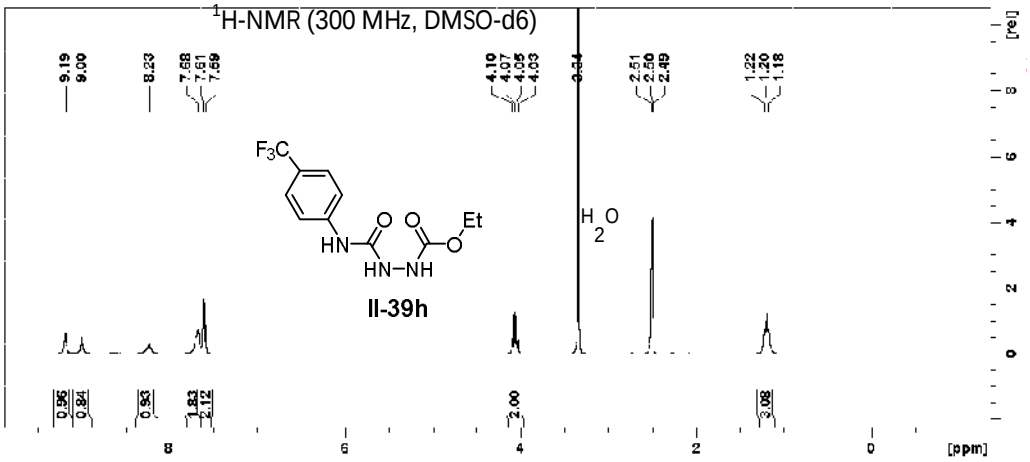

^{13}C-NMR (125 MHz, DMSO-d6)

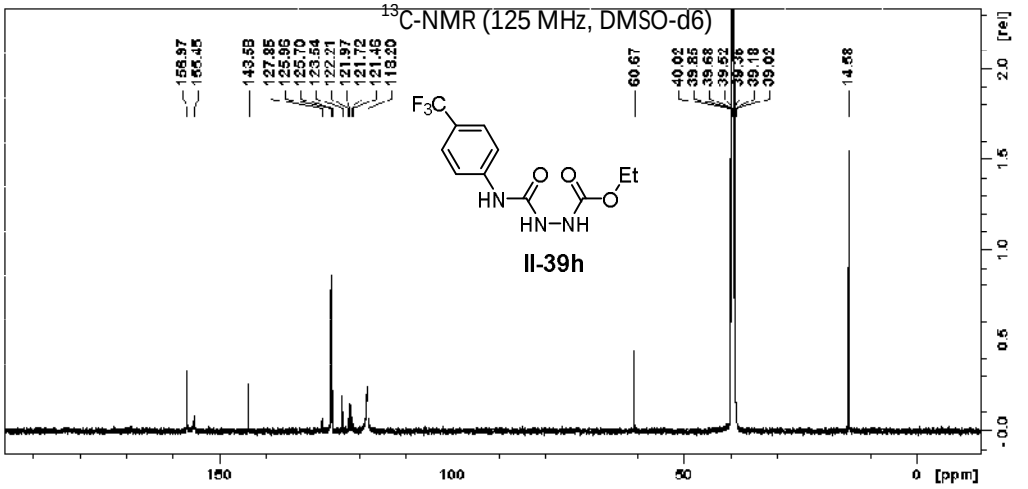

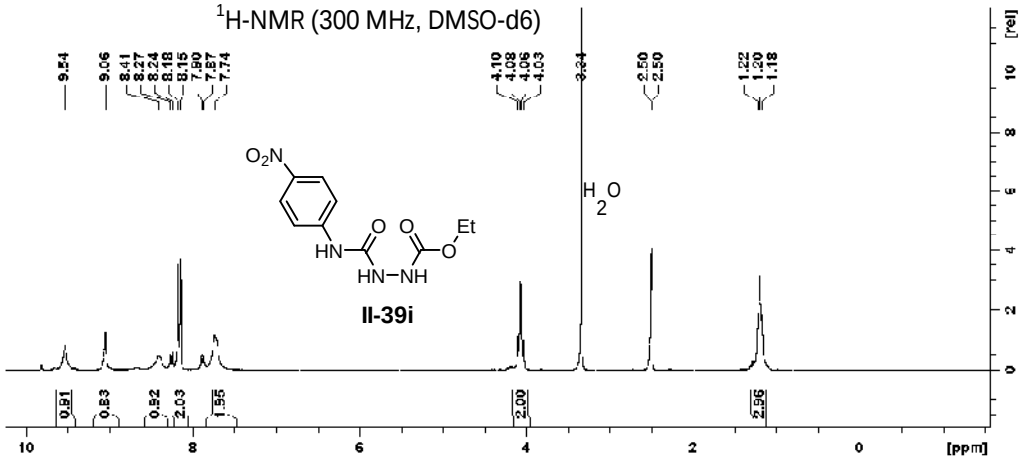
1H-NMR (300 MHz, DMSO-d6)
9.54
9.06
8.41
8.27
8.24
8.18
8.15
7.90
7.87
7.74
4.10
4.08
4.06
4.03
3.34
2.50
2.50
1.22
1.20
1.18
H2O
O2N
HN
O
O
Et
HN–NH
II-39i
0.91
0.83
0.52
2.03
1.55
2.00
2.96
10
8
6
4
2
0
[ppm]
[rel]

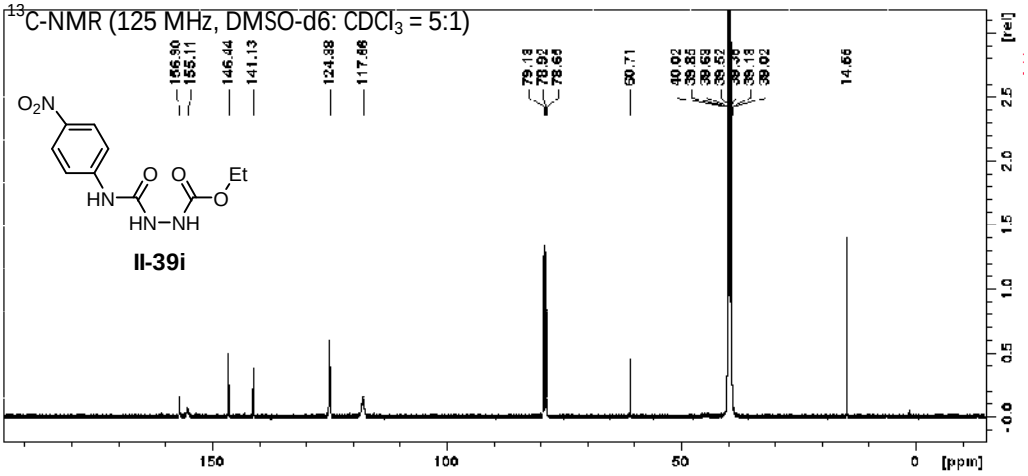
13C-NMR (125 MHz, DMSO-d6: CDCl3 = 5:1)
156.90
155.11
146.44
141.13
124.38
117.66
79.13
78.92
78.65
60.71
40.02
39.85
39.63
39.52
39.36
39.13
39.02
14.66
O2N
HN
O
O
Et
HN–NH
II-39i
150
100
50
0
[ppm]
[rel]

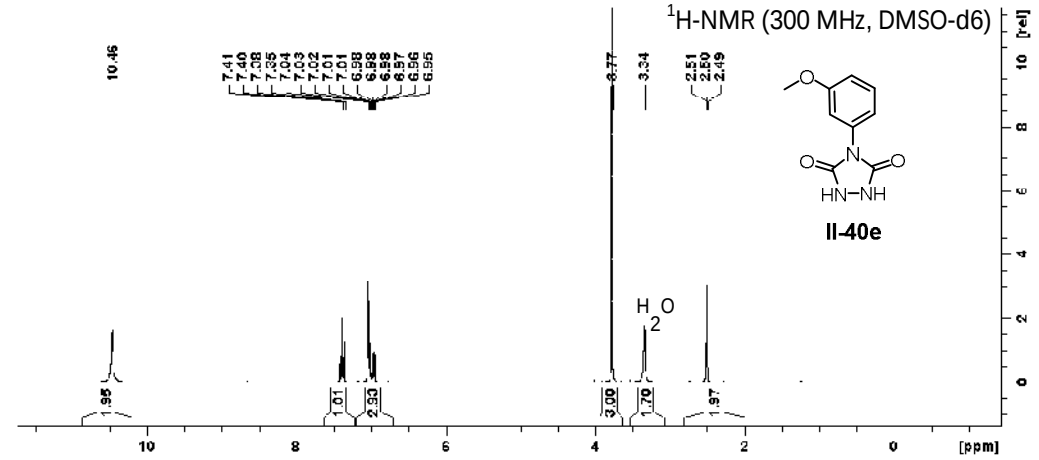
1H-NMR (300 MHz, DMSO-d6)
10.46
7.41
7.40
7.38
7.35
7.04
7.03
7.02
7.01
7.01
6.98
6.98
6.98
6.97
6.96
6.95
8.77
3.34
2.51
2.50
2.49
H2O
1.95
1.01
2.93
3.00
1.70
1.97
HN–NH
II-40e
10
8
6
4
2
0
[ppm]
[rel]

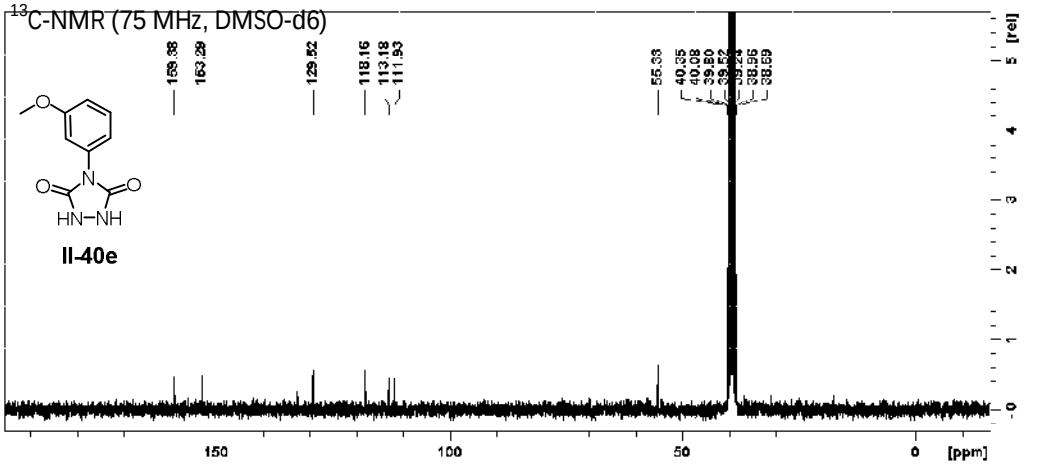
13C-NMR (75 MHz, DMSO-d6)
159.38
153.29
129.52
118.16
113.18
111.93
55.33
40.35
40.08
39.80
39.52
39.24
38.96
38.69
HN–NH
II-40e
150
100
50
0
[ppm]
[rel]

^{1}H-NMR (300 MHz, DMSO-d6)

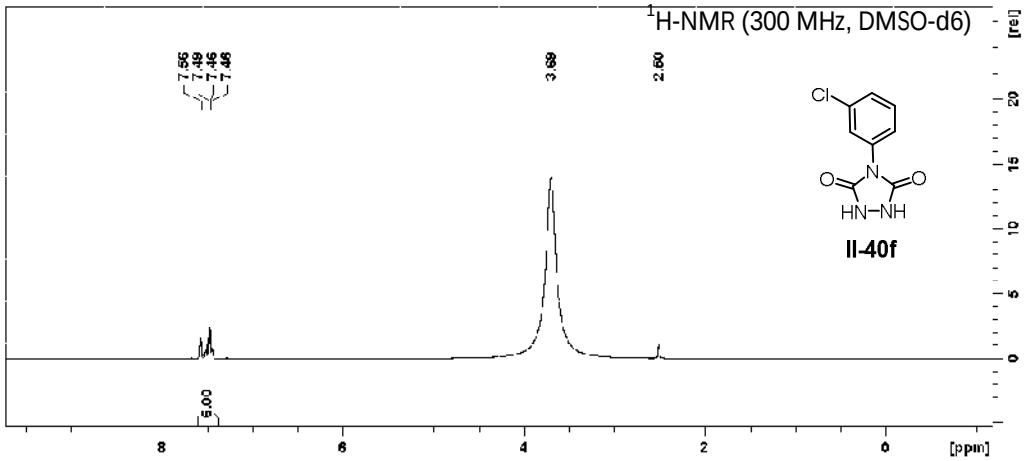

^{13}C-NMR (75 MHz, DMSO-d6)

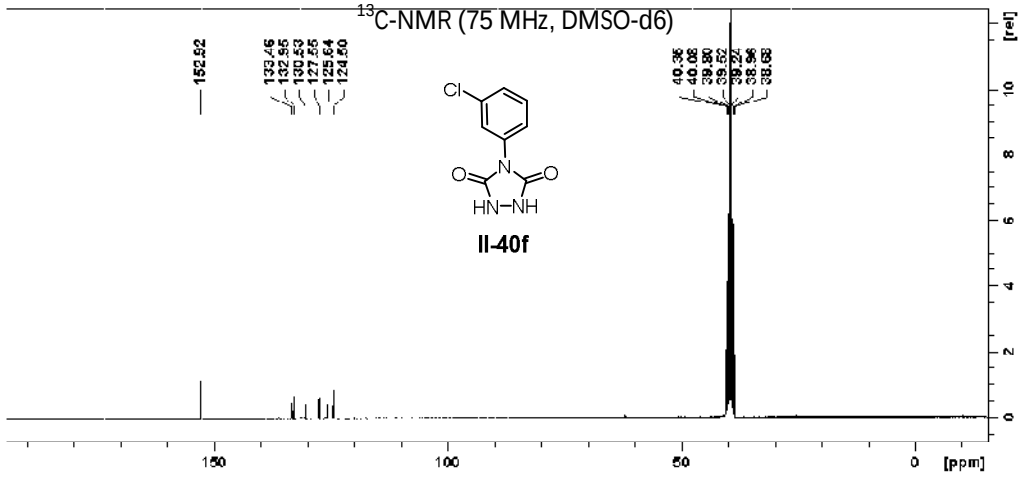

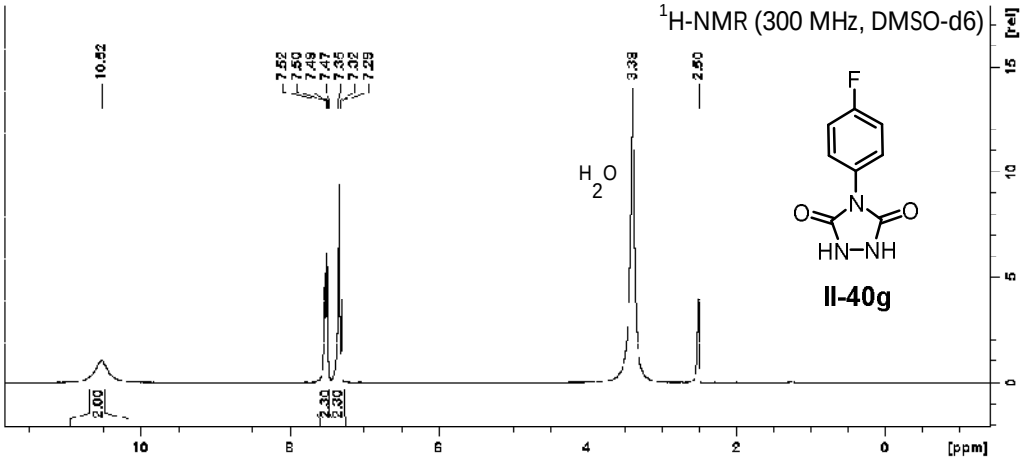
1H-NMR (300 MHz, DMSO-d6)
10.62
7.52
7.50
7.49
7.47
7.36
7.32
7.29
3.38
2.50
H2O
F
O
N
O
HN–NH
II-40g
2.00
2.30
2.00
10
8
6
4
2
0
[ppm]
[rel]

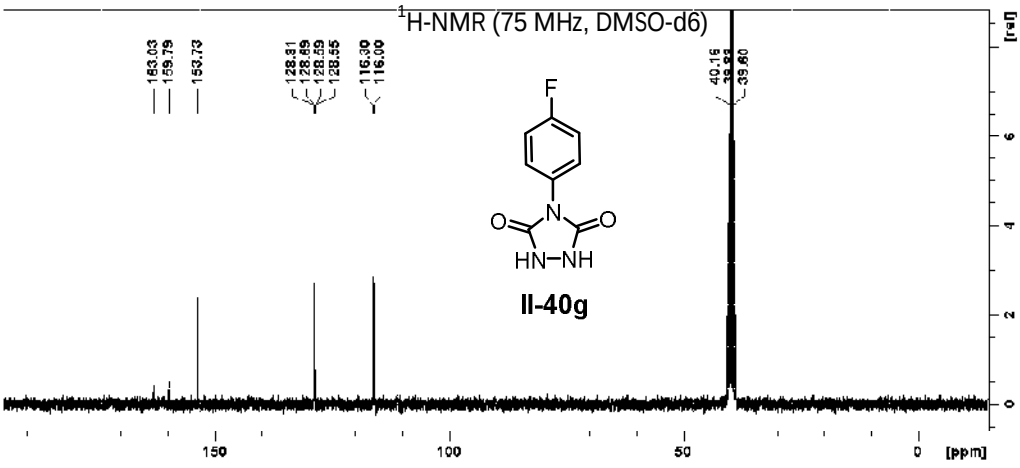
1H-NMR (75 MHz, DMSO-d6)
163.03
159.79
153.73
128.31
128.49
128.59
128.55
116.30
116.00
40.16
39.80
F
O
N
O
HN–NH
II-40g
150
100
50
0
[ppm]
[rel]

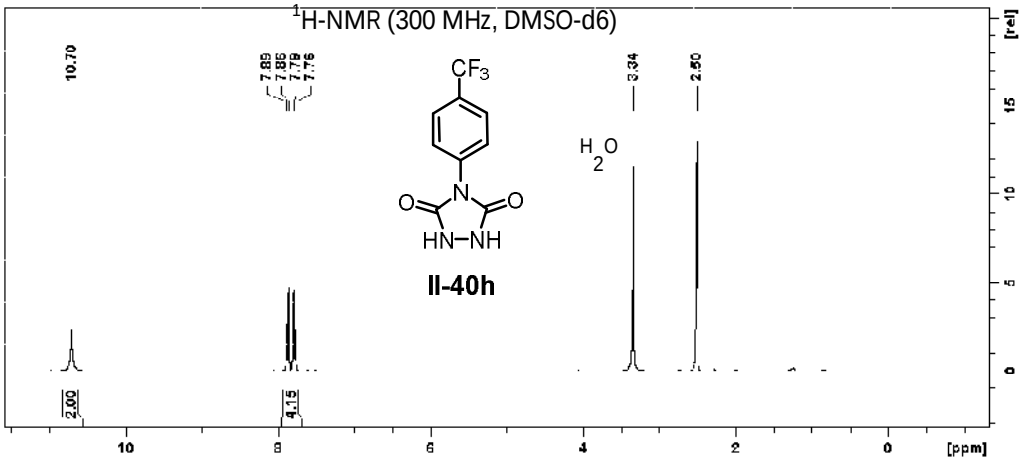
1H-NMR (300 MHz, DMSO-d6)
10.70
7.89
7.85
7.79
7.76
3.34
2.50
H2O
CF3
N
O
O
HN–NH
II-40h
2.00
4.15
10
8
6
4
2
0
[ppm]
[rel]

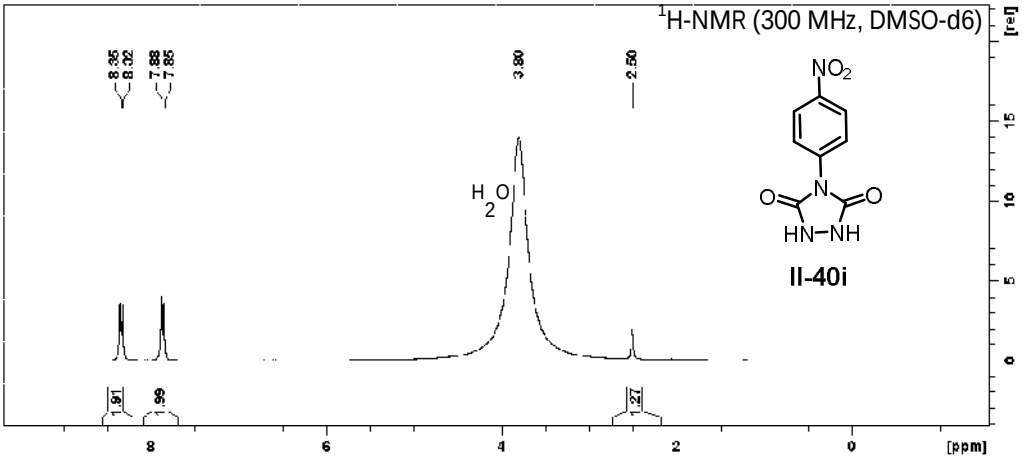
1H-NMR (300 MHz, DMSO-d6)
8.35
8.32
7.88
7.85
3.80
2.50
H2O
NO2
O
N
O
HN–NH
II-40i
1.91
1.99
1.27
8
6
4
2
0
[ppm]
[rel]

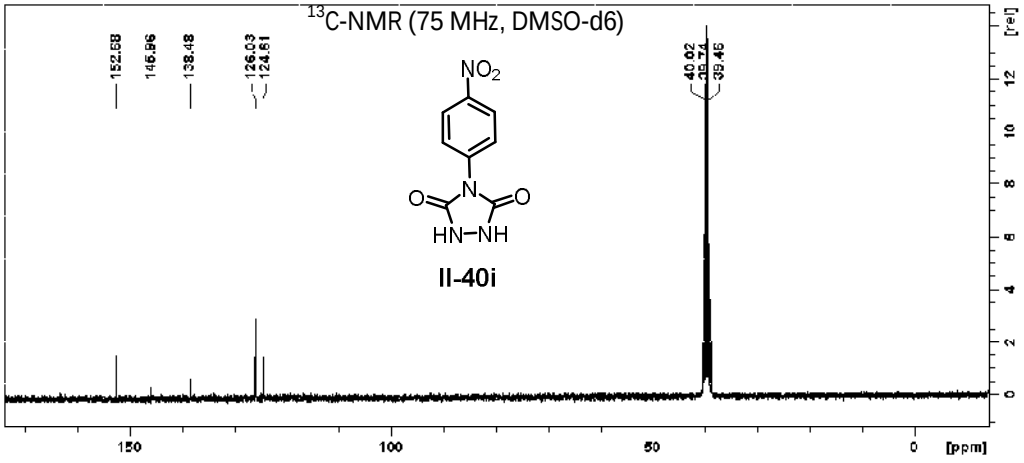
13C-NMR (75 MHz, DMSO-d6)
152.68
146.96
138.48
126.03
124.61
40.02
39.74
39.46
NO2
O
N
O
HN–NH
II-40i
150
100
50
0
[ppm]
[rel]

2.8.30. ^{1}H NMR and ^{13}C NMR spectra the diazacyclobutenes with 4-substituted 1,2,4-triazoline-2,5-diones (TADs).

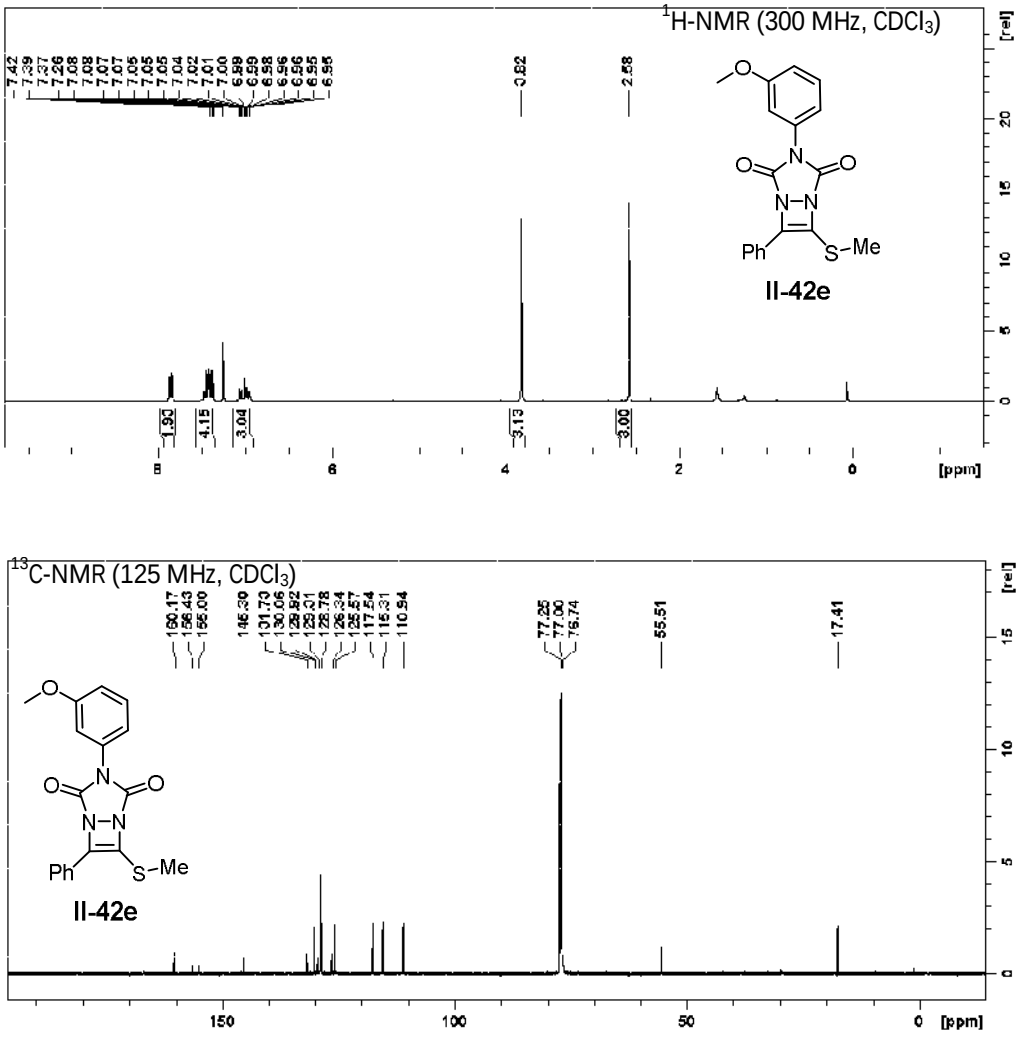

^{1}H-NMR (300 MHz, $CDCl_3$)

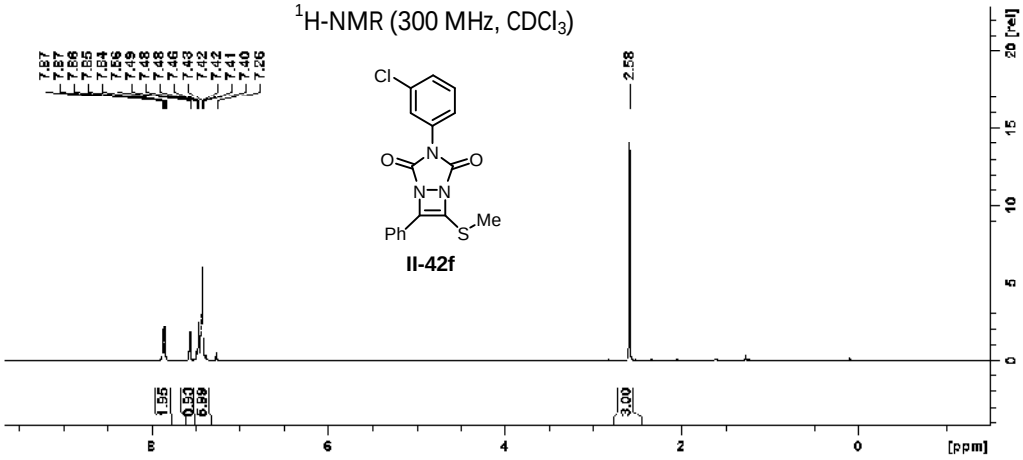

II-42f

^{13}C-NMR (75 MHz, $CDCl_3$)

II-42f

^{1}H-NMR (300 MHz, $CDCl_3$)

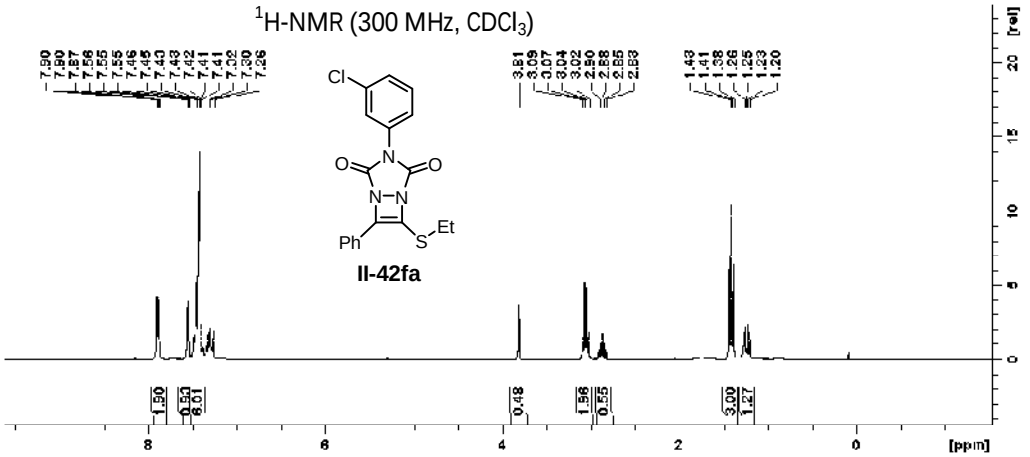

^{13}C-NMR (75 MHz, $CDCl_3$)

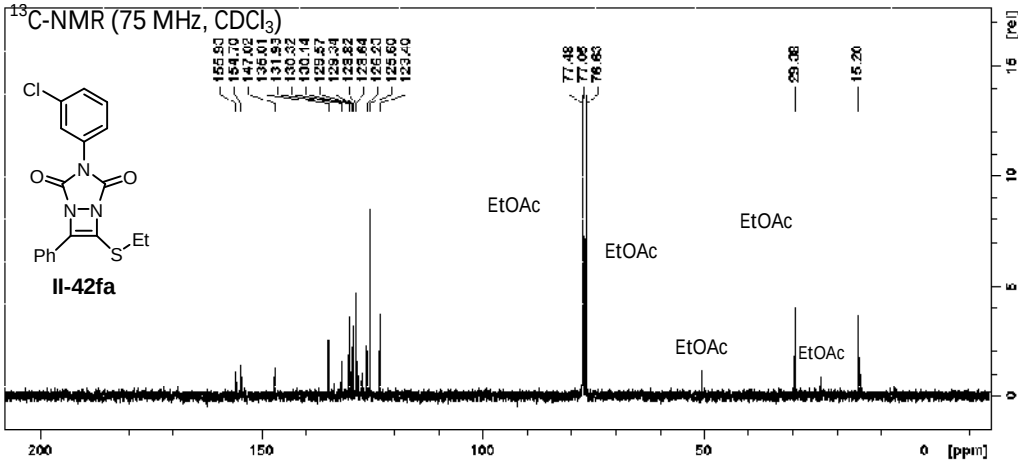

2.9 References

(1) Kolb, H. C.; VanNieuwenhze, M. S.; Sharpless, K. B. Catalytic Asymmetric Dihydroxylation. *Chem. Rev.* **1994**, *94* (8), 2483–2547. https://doi.org/10.1021/cr00032a009.

(2) O'Brien, P. Sharpless Asymmetric Aminohydroxylation: Scope, Limitations, and Use in Synthesis. *Angewandte Chemie International Edition* **1999**, *38* (3), 326–329. https://doi.org/10.1002/(SICI)1521-3773(19990201)38:3<326::AID-ANIE326>3.0.CO;2-T.

(3) Katsuki, T. Chiral Metallosalen Complexes: Structures and Catalyst Tuning for Asymmetric Epoxidation and Cyclopropanation. *Advanced Synthesis & Catalysis* **2002**, *344* (2), 131–147. https://doi.org/10.1002/1615-4169(200202)344:2<131::AID-ADSC131>3.0.CO;2-T.

(4) Wong, O. A.; Shi, Y. Organocatalytic Oxidation. Asymmetric Epoxidation of Olefins Catalyzed by Chiral Ketones and Iminium Salts. *Chem. Rev.* **2008**, *108* (9), 3958–3987. https://doi.org/10.1021/cr068367v.

(5) Cardona, F.; Goti, A. Metal-Catalysed 1,2-Diamination Reactions. *Nature Chem* **2009**, *1* (4), 269–275. https://doi.org/10.1038/nchem.256.

(6) De Bruycker, K.; Billiet, S.; Houck, H. A.; Chattopadhyay, S.; Winne, J. M.; Du Prez, F. E. Triazolinediones as Highly Enabling Synthetic Tools. *Chem. Rev.* **2016**, *116* (6), 3919–3974. https://doi.org/10.1021/acs.chemrev.5b00599.

(7) Kanzian, T.; Mayr, H. Electrophilic Reactivities of Azodicarboxylates. *Chemistry – A European Journal* **2010**, *16* (38), 11670–11677. https://doi.org/10.1002/chem.201001598.

(8) Nair, V.; Biju, A. T.; Mathew, S. C.; Babu, B. P. Carbon–Nitrogen Bond-Forming Reactions of Dialkyl Azodicarboxylate: A Promising Synthetic Strategy. *Chemistry – An Asian Journal* **2008**, *3* (5), 810–820. https://doi.org/10.1002/asia.200700341.

(9) Ciganek, E. Electrophilic Amination of Carbanions, Enolates, and Their Surrogates. In *Organic Reactions*; John Wiley & Sons, Inc., Ed.; John Wiley & Sons, Inc.: Hoboken, NJ, USA, 2009; pp 1–366. https://doi.org/10.1002/0471264180.or072.01.

(10) Huang, H.; Kang, J. Y. Mitsunobu Reaction Using Basic Amines as Pronucleophiles. *J. Org. Chem.* **2017**, *82* (13), 6604–6614. https://doi.org/10.1021/acs.joc.7b00622.

(11) Beveridge, R. E.; Batey, R. A. Terminal Alkyne Addition to Diazodicarboxylates: Synthesis of Hydrazide Linked Alkynes (Ynehydrazides). *Org. Lett.* **2012**, *14* (2), 540–543. https://doi.org/10.1021/ol2031608.

(12) Shi, M.; Zhao, G.-L. Aza-Baylis–Hillman Reactions of Diisopropyl Azodicarboxylate or Diethyl Azodicarboxylate with Acrylates and Acrylonitrile. *Tetrahedron* **2004**, *60* (9), 2083–2089. https://doi.org/10.1016/j.tet.2003.12.059.

(13) Dadwal, M.; M. Mobin, S.; N. Namboothiri, I. N. Highly Efficient Hydrazination of Conjugated Nitroalkenes via Imidazole or DMAP Mediated Morita–Baylis–Hillman Reaction. *Organic & Biomolecular Chemistry* **2006**, *4* (13), 2525–2528. https://doi.org/10.1039/B604899D.

(14) Mane, V.; Pandey, J.; Ayyagari, N.; Dey, C.; Kale, R.; N. Namboothiri, I. N. Synthesis of Hydrazinoheterocycles from Morita–Baylis–Hillman Adducts of Nitroalkenes with Azodicarboxylates. *Organic & Biomolecular Chemistry* **2016**, *14* (8), 2427–2438. https://doi.org/10.1039/C5OB02656C.
(15) Nair, V.; Biju, A. T.; Abhilash, K. G.; Menon, R. S.; Suresh, E. Reaction of Diaryl-1,2-Diones with Triphenylphosphine and Diethyl Azodicarboxylate Leading to N,N-Dicarboethoxy Monohydrazones via a Novel Rearrangement. *Org. Lett.* **2005**, *7* (11), 2121–2123. https://doi.org/10.1021/ol050403+.
(16) Nair, V.; Mathew, S. C.; Biju, A. T.; Suresh, E. A Novel Reaction of the "Huisgen Zwitterion" with Chalcones and Dienones: An Efficient Strategy for the Synthesis of Pyrazoline and Pyrazolopyridazine Derivatives. *Angewandte Chemie International Edition* **2007**, *46* (12), 2070–2073. https://doi.org/10.1002/anie.200604025.
(17) Moody, C. J. Azodicarbonyl Compounds in Heterocyclic Synthesis. In *Advances in Heterocyclic Chemistry*; Katritzky, A. R., Ed.; Academic Press, 1982; Vol. 30, pp 1–45. https://doi.org/10.1016/S0065-2725(08)60024-0.
(18) Uemura, T.; Yamaguchi, M.; Chatani, N. Amination of Arylboronic Compounds via the Copper-Catalyzed Addition of Arylboronic Esters to Azodicarboxylates. *Synthesis* **2015**, *47* (23), 3746–3750. https://doi.org/10.1055/s-0035-1560468.
(19) Xu, C.; Zhang, L.; Luo, S. Asymmetric Enamine Catalysis with β-Ketoesters by Chiral Primary Amine: Divergent Stereocontrol Modes. *J. Org. Chem.* **2014**, *79* (23), 11517–11526. https://doi.org/10.1021/jo502152w.
(20) Mamone, M.; Morvan, E.; Milcent, T.; Ongeri, S.; Crousse, B. Electrophilic Amination of Fluoroalkyl Groups on Azodicarboxylate Derivatives. *J. Org. Chem.* **2015**, *80* (3), 1964–1971. https://doi.org/10.1021/jo502638y.
(21) Yamashita, Y.; Ishitani, H.; Kobayashi, S. Silver-Catalyzed Asymmetric Amination of Silyl Enol Ethers. *Can. J. Chem.* **2000**, *78* (6), 666–672. https://doi.org/10.1139/v00-023.
(22) Yanagisawa, A.; Miyake, R.; Yoshida, K. Asymmetric α-Amination Reaction of Alkenyl Trifluoroacetates Catalyzed by a Chiral Phosphine–Silver Complex. *Organic & Biomolecular Chemistry* **2014**, *12* (12), 1935–1941. https://doi.org/10.1039/C3OB42111B.
(23) Vilaivan, T.; Bhanthumnavin, W. Organocatalyzed Asymmetric α-Oxidation, α-Aminoxylation and α-Amination of Carbonyl Compounds. *Molecules* **2010**, *15* (2), 917–958. https://doi.org/10.3390/molecules15020917.
(24) Hall, J. H.; Jones, M. L. Reactions of Azodiones with Electron-Rich Alkenes. 1,2,4-Triazoline-3,5-Diones and Vinyl Ethers. *J. Org. Chem.* **1983**, *48* (6), 822–826. https://doi.org/10.1021/jo00154a014.
(25) Huebner, C. F.; Strachan, P. L.; Donoghue, E. M.; Cahoon, N.; Dorfman, L.; Margerison, R. B.; Wenkert, E. Diels-Alder Reactions of Indene. *J. Org. Chem.* **1967**, *32* (4), 1126–1130. https://doi.org/10.1021/jo01279a060.
(26) Seymour, C. A.; Greene, F. D. Mechanism of Triazolinedione-Olefin Reactions. Ene and Cycloaddition. *J. Am. Chem. Soc.* **1980**, *102* (20), 6384–6385. https://doi.org/10.1021/ja00540a054.

(27) Zhang, H.; Ma, C.; Sun, R.; Liao, X.; Wu, J.; Xie, M. Sustainable Elastomer of Triazolinedione-Modified Eucommia Ulmoides Gum with Enhanced Elasticity and Shape Memory Capability. *Polymer* **2019**, *184*, 121904. https://doi.org/10.1016/j.polymer.2019.121904.
(28) Lai, Y. C.; Mallakpour, S. E.; Butler, G. B.; Palenik, G. J. Diels-Alder and Ene Reactions of 4-Substituted 1,2,4-Triazoline-3,5-Diones and Some Substituted Styrenes. *J. Org. Chem.* **1985**, *50* (22), 4378–4381. https://doi.org/10.1021/jo00222a036.
(29) Kiriazis, A.; Rüffer, T.; Jäntti, S.; Lang, H.; Yli-Kauhaluoma, J. Stereoselective Aza Diels−Alder Reaction on Solid Phase: A Facile Synthesis of Hexahydrocinnoline Derivatives. *J. Comb. Chem.* **2007**, *9* (2), 263–266. https://doi.org/10.1021/cc060125l.
(30) Mondal, P.; Jana, G.; Kumar Behera, P.; Kumar Chattaraj, P.; K. Singha, N. A New Healable Polymer Material Based on Ultrafast Diels–Alder 'Click' Chemistry Using Triazolinedione and Fluorescent Anthracyl Derivatives: A Mechanistic Approach. *Polymer Chemistry* **2019**, *10* (37), 5070–5079. https://doi.org/10.1039/C9PY00499H.
(31) Schué, E.; Kopyshev, A.; Lutz, J.; Börner, H. G. Molecular Bottle Brushes with Positioned Selenols: Extending the Toolbox of Oxidative Single Polymer Chain Folding with Conformation Analysis by Atomic Force Microscopy. *Journal of Polymer Science* **2020**, *58* (1), 154–162. https://doi.org/10.1002/pola.29496.
(32) Moriarty, R.; Prakash, I. Amination of PTAD with Silyl Enol Ethers. *Synth. Commun.* **1985**, *15* (7), 649–655.
(33) Okumura, M.; Nakamata Huynh, S. M.; Pospech, J.; Sarlah, D. Arenophile-Mediated Dearomative Reduction. *Angewandte Chemie* **2016**, *128* (51), 16142–16146. https://doi.org/10.1002/ange.201609686.
(34) Chaminda Lakmal, H. H.; Xu, J. X.; Xu, X.; Ahmed, B.; Fong, C.; Szalda, D. J.; Ramig, K.; Sygula, A.; Webster, C. E.; Zhang, D.; Cui, X. Synthesis of C-Unsubstituted 1,2-Diazetidines and Their Ring-Opening Reactions via Selective N–N Bond Cleavage. *J. Org. Chem.* **2018**, *83* (16), 9497–9503. https://doi.org/10.1021/acs.joc.8b01223.
(35) Hall, J. H.; Bigard, W. S. 1,2-Diazetidine Conformation. Double Nitrogen Inversion. *J. Org. Chem.* **1978**, *43* (14), 2785–2788. https://doi.org/10.1021/jo00408a009.
(36) Brown, M. J.; Clarkson, G. J.; Inglis, G. G.; Shipman, M. Synthesis and Functionalization of 3-Alkylidene-1,2-Diazetidines Using Transition Metal Catalysis. *Org. Lett.* **2011**, *13* (7), 1686–1689. https://doi.org/10.1021/ol200193n.
(37) Ghosh, A. K.; Brindisi, M. Organic Carbamates in Drug Design and Medicinal Chemistry. *J. Med. Chem.* **2015**, *58* (7), 2895–2940. https://doi.org/10.1021/jm501371s.
(38) Ghosh, A. K.; Brindisi, M. Urea Derivatives in Modern Drug Discovery and Medicinal Chemistry. *J. Med. Chem.* **2020**, *63* (6), 2751–2788. https://doi.org/10.1021/acs.jmedchem.9b01541.

(39) Effenberger, F.; Maier, R. Cycloaddition of Azosulfones and Sulfonylimines. *Angew. Chem. Int. Ed. Engl.* **1966**, *5* (4), 416–417. https://doi.org/10.1002/anie.196604162.
(40) Staudinger, H. *Die ketene*; F. Enke, 1912.
(41) Richter, R.; Ulrich, H. Four-Membered Rings Containing Two Nitrogenc Heteroatoms. In *Chemistry of Heterocyclic Compounds*; John Wiley & Sons, Ltd, 2008; pp 443–545. https://doi.org/10.1002/9780470187197.ch3.
(42) Tandon, V. K.; Chhor, R. B. Metal Mediated Dechlorination - A New Route to Nitriles http://www.ingentaconnect.com/contentone/ben/loc/2004/00000001/00000001/art00010 (accessed Mar 26, 2020). https://doi.org/info:doi/10.2174/1570178043488680.
(43) Nunn, E. E.; Warrener, R. N. Dimethyl Δ3-1,2-Diazetine-1,2-Dicarboxylate: A New Four-Membered 6π-Ring System. *J. Chem. Soc., Chem. Commun.* **1972**, No. 14, 818–819. https://doi.org/10.1039/C39720000818.
(44) Cheng, C. C.; Greene, F. D.; Blount, J. F. Reaction of Triazolinediones with Acetylenes. Electrophilic Addition. *J. Org. Chem.* **1984**, *49* (16), 2917–2922. https://doi.org/10.1021/jo00190a015.
(45) Breton, G. W.; Shugart, J. H.; Hughey, C. A.; Perala, S. M.; Hicks, A. D. Synthesis of Δ1-1,2-Diazetines via a Diels−Alder Cycloaddition Approach. *Org. Lett.* **2001**, *3* (20), 3185–3187. https://doi.org/10.1021/ol0164942.
(46) DeKorver, K. A.; Li, H.; Lohse, A. G.; Hayashi, R.; Lu, Z.; Zhang, Y.; Hsung, R. P. Ynamides: A Modern Functional Group for the New Millennium. *Chem. Rev.* **2010**, *110* (9), 5064–5106. https://doi.org/10.1021/cr100003s.
(47) Muller, M.; Forster, W.-R.; Holst, A.; Kingma, A. J.; Schaumann, E.; Adiwidjaja, G. Synthesis of 4-Silylcyclobut-2-Enethiones and Their Use in Cyclobutadiene Generation. *Chemistry – A European Journal* **1996**, *2* (8), 949–956.
(48) Sweis, R. F.; Schramm, M. P.; Kozmin, S. A. Silver-Catalyzed [2 + 2] Cycloadditions of Siloxy Alkynes. *Journal of the American Chemical Society* **2004**, *126* (24), 7442–7443. https://doi.org/10.1021/ja048251l.
(49) Melzig, L.; Metzger, A.; Knochel, P. Pd- and Ni-Catalyzed Cross-Coupling Reactions of Functionalized Organozinc Reagents with Unsaturated Thioethers. *Chemistry – A European Journal* **2011**, *17* (10), 2948–2956. https://doi.org/10.1002/chem.201002850.
(50) Zheng, W.; Zheng, F.; Hong, Y.; Hu, L. A One-Pot Synthesis of Alkynyl Sulfides from Terminal Alkynes. *Heteroatom Chemistry* **2012**, *23* (1), 105–110. https://doi.org/10.1002/hc.20744.
(51) Xie, L.-G.; Niyomchon, S.; Mota, A. J.; González, L.; Maulide, N. Metal-Free Intermolecular Formal Cycloadditions Enable an Orthogonal Access to Nitrogen Heterocycles. *Nature Communications* **2016**, *7* (1), 1–9. https://doi.org/10.1038/ncomms10914.
(52) Hückel, E. Quantentheoretische Beiträge zum Benzolproblem. *Z. Phys.* **1931**, *70*, 204–286.

(53) Hückel, E. Quantentheoretische Beiträge zum Problem der aromatischen und ungesättigten Verbindungen. III. *Z. Physik* **1932**, *76* (9), 628–648. https://doi.org/10.1007/BF01341936.
(54) Budzelaar, P. H. M.; Cremer, D.; Wallasch, M.; Wuerthwein, E. U.; Schleyer, P. v. R. Dioxetenes and Diazetines: Nonaromatic 6.Pi.-Systems in Four-Membered Rings. *Journal of the American Chemical Society* **1987**, *109* (21), 6290–6299. https://doi.org/10.1021/ja00255a011.
(55) Mó, O.; Yáñez, M.; Elguero, J. A MO Analysis of the Aromaticity of Some Nitrogen Heterocyclic Compounds. *Journal of Molecular Structure: THEOCHEM* **1989**, *201*, 17–37. https://doi.org/10.1016/0166-1280(89)87059-9.
(56) Bachrach, S. M.; Liu, M. Ab Initio Study of the Conrotatory Ring Opening of Phospha- and Azacyclobutenes. 2. Diphospha- and Diazacyclobutenes. *The Journal of Organic Chemistry* **1992**, *57* (7), 2040–2047. https://doi.org/10.1021/jo00033a026.
(57) Vol'pin, M. E. NON-BENZENOID AROMATIC COMPOUNDS AND THE CONCEPT OF AROMATICITY. *Russ. Chem. Rev.* **1960**, *29* (3), 129. https://doi.org/10.1070/RC1960v029n03ABEH001224.
(58) Warrener, R. N.; Nunn, E. E.; Paddon-Row, M. N. The Synthesis and Properties of Dimethyl 1,2-Diazetine-1,2-Dicarboxylate, a Potentially Aromatic Molecule. *Aust. J. Chem.* **1979**, *32* (12), 2659–2674. https://doi.org/10.1071/ch9792659.
(59) Breton, G. W.; Martin, K. L. Are 1,2-Dihydrodiazetes Aromatic? An Experimental and Computational Investigation. *J. Org. Chem.* **2002**, *67* (19), 6699–6704. https://doi.org/10.1021/jo026082m.
(60) Krespan, C. G.; McKusick, B. C.; Cairns, T. L. Dithietene and Bicycloöctatriene Ring Systems from Bis-(Fluoroalkyl)-Acetylenes. *J. Am. Chem. Soc.* **1960**, *82* (6), 1515–1516. https://doi.org/10.1021/ja01491a072.
(61) Nyulászi, L. Aromaticity of Phosphorus Heterocycles. *Chem. Rev.* **2001**, *101* (5), 1229–1246. https://doi.org/10.1021/cr990321x.
(62) Mattmann, E.; Mathey, F.; Sevin, A.; Frison, G. De-Aromatizing Phosphole. *J. Org. Chem.* **2002**, *67* (4), 1208–1213. https://doi.org/10.1021/jo0108156.
(63) Garratt, P. J.; Zahler, R. The Dianion of Dimethyl Cyclobut-3-Ene-1,2-Dicarboxylate. Aromaticity vs. Coulombic Repulsion. *J. Am. Chem. Soc.* **1978**, *100* (24), 7753–7754. https://doi.org/10.1021/ja00492a066.
(64) Boche, G.; Etzrodt, H.; Marsch, M.; Thiel, W. Das Dianion 1,2,3,4-Tetraphenylcyclobutadiendiid. *Angewandte Chemie* **1982**, *94* (2), 141–142. https://doi.org/10.1002/ange.19820940221.
(65) Balci, M.; McKee, M. L.; Schleyer, P. von R. Theoretical Study of Tetramethyl- and Tetra-Tert-Butyl-Substituted Cyclobutadiene and Tetrahedrane. *J. Phys. Chem. A* **2000**, *104* (6), 1246–1255. https://doi.org/10.1021/jp9922054.
(66) Sekiguchi, A.; Matsuo, T.; Watanabe, H. Synthesis and Characterization of a Cyclobutadiene Dianion Dilithium Salt: Evidence for Aromaticity. *J. Am. Chem. Soc.* **2000**, *122* (23), 5652–5653. https://doi.org/10.1021/ja0004175.

(67) Frahm, J. J. Sandström: Dynamic NMR Spectroscopy, Academic Press, London 1982. 226 Seiten, Preis: £ 19.20/$ 39.50. *Berichte der Bunsengesellschaft für physikalische Chemie* **1982**, *86* (9), 873–873. https://doi.org/10.1002/bbpc.19820860926.
(68) Tafazzoli, M.; Ziyaei-Halimjani, A.; Ghiasi, M.; Fattahi, M.; Saidi, M. R. Dynamic NMR Studies of N-Benzoyl Pyrrolidine and N-Benzoyl Piperidine Derivatives. *Journal of Molecular Structure* **2008**, *886* (1), 24–31. https://doi.org/10.1016/j.molstruc.2007.01.019.
(69) Bain, A. D.; Duns, G. J.; Ternieden, S.; Ma, J.; Werstiuk, N. H. The Barrier to Internal Rotation and Chemical Exchange in N-Acetylpyrrole. A Study on NMR Methods and Molecular Modeling. *The Journal of Physical Chemistry* **1994**, *98* (31), 7458–7463. https://doi.org/10.1021/j100082a012.
(70) Smela, M. P.; Hoye, T. R. A Traceless Tether Strategy for Achieving Formal Intermolecular Hexadehydro-Diels–Alder Reactions. *Organic Letters* **2018**, *20* (17), 5502–5505. https://doi.org/10.1021/acs.orglett.8b02473.
(71) G. de la Torre, B.; Albericio, F. The Pharmaceutical Industry in 2018. An Analysis of FDA Drug Approvals from the Perspective of Molecules. *Molecules* **2019**, *24* (4), 809. https://doi.org/10.3390/molecules24040809.
(72) de la Torre, B. G.; Albericio, F. The Pharmaceutical Industry in 2019. An Analysis of FDA Drug Approvals from the Perspective of Molecules. *Molecules* **2020**, *25* (3), 745. https://doi.org/10.3390/molecules25030745.
(73) Pennington, L. D.; Moustakas, D. T. The Necessary Nitrogen Atom: A Versatile High-Impact Design Element for Multiparameter Optimization. *J. Med. Chem.* **2017**, *60* (9), 3552–3579. https://doi.org/10.1021/acs.jmedchem.6b01807.
(74) Research, C. for D. E. and. Novel Drug Approvals for 2019. *FDA* **2020**.
(75) Das, P.; Delost, M. D.; Qureshi, M. H.; Smith, D. T.; Njardarson, J. T. A Survey of the Structures of US FDA Approved Combination Drugs. *J. Med. Chem.* **2019**, *62* (9), 4265–4311. https://doi.org/10.1021/acs.jmedchem.8b01610.
(76) Rosenberg, B.; Vancamp, L.; Trosko, J. E.; Mansour, V. H. Platinum Compounds: A New Class of Potent Antitumour Agents. *Nature* **1969**, *222* (5191), 385–386. https://doi.org/10.1038/222385a0.
(77) Lucet, D.; Gall, T. L.; Mioskowski, C. The Chemistry of Vicinal Diamines. *Angewandte Chemie International Edition* **1998**, *37* (19), 2580–2627. https://doi.org/10.1002/(SICI)1521-3773(19981016)37:19<2580::AID-ANIE2580>3.0.CO;2-L.
(78) Kotti, S. R. S. S.; Timmons, C.; Li, G. Vicinal Diamino Functionalities as Privileged Structural Elements in Biologically Active Compounds and Exploitation of Their Synthetic Chemistry. *Chemical Biology & Drug Design* **2006**, *67* (2), 101–114. https://doi.org/10.1111/j.1747-0285.2006.00347.x.
(79) Shvarts, G.; Grigor'ev, N.; Severina, I.; Ryaposova, I.; Lapitskaia, A.; Volodarskii, L.; Tikhonov, A.; Kurbnikova, I.; Mazhukin, D.; Granik, V. Derivatives of 1,2-Diazetine-1,2-Dioxide: A New Class of Nitric Oxide Generators Exhibiting Vasodilator Activity. *Pharmaceutical Chemistry Journal* **1994**, *28*, 261–266. https://doi.org/10.1007/BF02219799.

(80) Kirilyuk, I. A.; Utepbergenov, D. I.; Mazhukin, D. G.; Fechner, K.; Mertsch, K.; Khramtsov, V. V.; Blasig, I. E.; Haseloff, R. F. Thiol-Induced Nitric Oxide Release from 3-Halogeno-3,4-Dihydrodiazete 1,2-Dioxides. *J. Med. Chem.* **1998**, *41* (7), 1027–1033. https://doi.org/10.1021/jm960737s.
(81) Breton, G. W.; Oliver, L. H.; Nickerson, J. E. Synthesis of a Stereochemically Defined 1,2-Diazetine N,N‘-Dioxide and a Study of Its Thermal Decomposition. *J. Org. Chem.* **2007**, *72* (4), 1412–1416. https://doi.org/10.1021/jo062357c.
(82) Gordhan, H. M.; Patrick, S. L.; Swasy, M. I.; Hackler, A. L.; Anayee, M.; Golden, J. E.; Morris, J. C.; Whitehead, D. C. Evaluation of Substituted Ebselen Derivatives as Potential Trypanocidal Agents. *Bioorganic & Medicinal Chemistry Letters* **2017**, *27* (3), 537–541. https://doi.org/10.1016/j.bmcl.2016.12.021.
(83) M. Gordhan, H.; E. Milanes, J.; Qiu, Y.; E. Golden, J.; A. Christensen, K.; C. Morris, J.; C. Whitehead, D. A Targeted Delivery Strategy for the Development of Potent Trypanocides. *Chemical Communications* **2017**, *53* (62), 8735–8738. https://doi.org/10.1039/C7CC03378H.
(84) Narangoda, C. J.; Lex, T. R.; Moore, M. A.; McMillen, C. D.; Kitaygorodskiy, A.; Jackson, J. E.; Whitehead, D. C. Accessing the Rare Diazacyclobutene Motif. *Org. Lett.* **2018**, *20* (24), 8009–8013. https://doi.org/10.1021/acs.orglett.8b03590.
(85) Tu, Y.; Zeng, X.; Wang, H.; Zhao, J. A Robust One-Step Approach to Ynamides. *Organic Letters* **2018**, *20* (1), 280–283. https://doi.org/10.1021/acs.orglett.7b03665.
(86) Gao, Y.; Wu, G.; Zhou, Q.; Wang, J. Palladium-Catalyzed Oxygenative Cross-Coupling of Ynamides and Benzyl Bromides by Carbene Migratory Insertion. *Angewandte Chemie International Edition* **2018**, *57* (10), 2716–2720. https://doi.org/10.1002/anie.201712795.
(87) Cao, W.; Chen, P.; Wang, L.; Wen, H.; Liu, Y.; Wang, W.; Tang, Y. A Highly Regio- and Stereoselective Syntheses of α-Halo Enamides, Vinyl Thioethers, and Vinyl Ethers with Aqueous Hydrogen Halide in Two-Phase Systems. *Org. Lett.* **2018**, *20* (15), 4507–4511. https://doi.org/10.1021/acs.orglett.8b01809.
(88) Alcaide, B.; Almendros, P.; Lázaro-Milla, C. Regioselective Synthesis of Heteroatom-Functionalized Cyclobutene-Triflones and Cyclobutenones. *Advanced Synthesis & Catalysis* **2017**, *359* (15), 2630–2639. https://doi.org/10.1002/adsc.201700492.
(89) Murakami, K.; Imoto, J.; Matsubara, H.; Yoshida, S.; Yorimitsu, H.; Oshima, K. Copper-Catalyzed Extended Pummerer Reactions of Ketene Dithioacetal Monoxides with Alkynyl Sulfides and Ynamides with an Accompanying Oxygen Rearrangement. *Chemistry – A European Journal* **2013**, *19* (18), 5625–5630. https://doi.org/10.1002/chem.201204072.
(90) Mukherjee, A.; Dateer, R. B.; Chaudhuri, R.; Bhunia, S.; Karad, S. N.; Liu, R.-S. Gold-Catalyzed 1,2-Difunctionalizations of Aminoalkynes Using Only N- and O-Containing Oxidants. *J. Am. Chem. Soc.* **2011**, *133* (39), 15372–15375. https://doi.org/10.1021/ja208150d.

(91) Rao, M. L. N.; Jadhav, D. N.; Dasgupta, P. Pd-Catalyzed Domino Synthesis of Internal Alkynes Using Triarylbismuths as Multicoupling Organometallic Nucleophiles. *Org. Lett.* **2010**, *12* (9), 2048–2051. https://doi.org/10.1021/ol1004164.
(92) Rao, M. L. N.; Dasgupta, P. A Concise Route to Functionalized Benzofurans Directly from Gem-Dibromoalkenes and Phenols. *RSC Adv.* **2015**, *5* (80), 65462–65470. https://doi.org/10.1039/C5RA13213D.
(93) Ficini, J.; Krief, A.; Guingant, A.; Desmaele, D. Influence of Magnesium Bromide on the Regioselectivity of the Cycloaddition of Ynamines with Cyclenones: Difference in Reactivity between Cyclohexenones and Cyclopentenones. *Tetrahedron Letters* **1981**, *22* (8), 725–728. https://doi.org/10.1016/0040-4039(81)80134-7.
(94) Smith, D. L.; Chidipudi, S. R.; Goundry, W. R.; Lam, H. W. Rhodium-Catalyzed [2 + 2] Cycloaddition of Ynamides with Nitroalkenes. *Org. Lett.* **2012**, *14* (18), 4934–4937. https://doi.org/10.1021/ol302259v.
(95) Sumaria, C. S.; Türkmen, Y. E.; Rawal, V. H. Non-Precious Metals Catalyze Formal [4 + 2] Cycloaddition Reactions of 1,2-Diazines and Siloxyalkynes under Ambient Conditions. *Org. Lett.* **2014**, *16* (12), 3236–3239. https://doi.org/10.1021/ol501254h.
(96) Ishitani, H.; Nagayama, S.; Kobayashi, S. A New Reaction of Imines with Alkynyl Sulfides Affording α,β-Unsaturated Thioimidates. *J. Org. Chem.* **1996**, *61* (6), 1902–1903. https://doi.org/10.1021/jo951924l.
(97) Ma, Y.; Qian, C. [2+2] Cycloaddition Reactions of Imines with Alkynyl Selenides Catalyzed by Scandium Triflate. *Tetrahedron Letters* **2000**, *41* (6), 945–947. https://doi.org/10.1016/S0040-4039(99)02178-4.
(98) Qin, Y.; Lv, J.; Luo, S.; Cheng, J.-P. Direct Intramolecular Conjugate Addition of Simple Alkenes to α,β-Unsaturated Carbonyls Catalyzed by Cu(OTf)2. *Org. Lett.* **2014**, *16* (19), 5032–5035. https://doi.org/10.1021/ol502373u.
(99) Matsuo, J.; Sasaki, S.; Hoshikawa, T.; Ishibashi, H. Tin(IV) Chloride Catalyzed Cycloaddition Reactions between 3-Ethoxycyclobutanones and Allylsilanes. *Org. Lett.* **2009**, *11* (17), 3822–3825. https://doi.org/10.1021/ol901329c.
(100) Shen, L.; Zhao, K.; Doitomi, K.; Ganguly, R.; Li, Y.-X.; Shen, Z.-L.; Hirao, H.; Loh, T.-P. Lewis Acid-Catalyzed Selective [2 + 2]-Cycloaddition and Dearomatizing Cascade Reaction of Aryl Alkynes with Acrylates. *Journal of the American Chemical Society* **2017**, *139* (38), 13570–13578. https://doi.org/10.1021/jacs.7b07997.
(101) Jeong, H.; von Kugelgen, S.; Bellone, D.; Fischer, F. R. Regioselective Termination Reagents for Ring-Opening Alkyne Metathesis Polymerization. *J. Am. Chem. Soc.* **2017**, *139* (43), 15509–15514. https://doi.org/10.1021/jacs.7b09390.
(102) Viehe, H. G. Synthesis and Reactions of the Alkynylamines. *Angewandte Chemie International Edition in English* **1967**, *6* (9), 767–778. https://doi.org/10.1002/anie.196707671.

(103) Wu, W.; Jiang, H. Haloalkynes: A Powerful and Versatile Building Block in Organic Synthesis. *Acc. Chem. Res.* **2014**, *47* (8), 2483–2504. https://doi.org/10.1021/ar5001499.
(104) Kim, J.; Stahl, S. S. Cu-Catalyzed Aerobic Oxidative Three-Component Coupling Route to N-Sulfonyl Amidines via an Ynamine Intermediate. *J. Org. Chem.* **2015**, *80* (4), 2448–2454. https://doi.org/10.1021/jo5029198.
(105) 4-PHENYL-1,2,4-TRIAZOLINE-3,5-DIONE. *Org. Synth.* **1971**, *51*, 121. https://doi.org/10.15227/orgsyn.051.0121.
(106) H. Hassall, C.; Kröhn, A.; J. Moody, C.; Anthony Thomas, W. The Design and Synthesis of New Triazolo, Pyrazolo-, and Pyridazo-Pyridazine Derivatives as Inhibitors of Angiotensin Converting Enzyme. *Journal of the Chemical Society, Perkin Transactions 1* **1984**, *0* (0), 155–164. https://doi.org/10.1039/P19840000155.
(107) Zolfigol, M. A.; Nasr-Isfahani, H.; Mallakpour, S.; Safaiee, M. Oxidation of Urazoles with 1,3-Dihalo-5,5-Dimethylhydantoin, Both in Solution and under Solvent-Free Conditions. *Synlett* **2005**, *2005* (05), 0761–0764. https://doi.org/10.1055/s-2005-863706.
(108) Alakurtti, S.; Heiska, T.; Kiriazis, A.; Sacerdoti-Sierra, N.; Jaffe, C. L.; Yli-Kauhaluoma, J. Synthesis and Anti-Leishmanial Activity of Heterocyclic Betulin Derivatives. *Bioorganic & Medicinal Chemistry* **2010**, *18* (4), 1573–1582. https://doi.org/10.1016/j.bmc.2010.01.003.
(109) Mallakpour, S.; Rafiee, Z. A Novel One-Pot Synthesis of 4-Substituted 1,2,4-Triazolidine-3,5-Diones. *Synlett* **2007**, *2007* (08), 1255–1256. https://doi.org/10.1055/s-2007-977413.
(110) Pitucha, M.; Matysiak, J.; Senczyna, B. Synthesis and RP HPLC Studies of Biologically Active Semicarbazides and Their Cyclic Analogues 1,2,4-Triazol-3-Ones. *Monatsh Chem* **2012**, *143* (4), 657–667. https://doi.org/10.1007/s00706-011-0715-z.
(111) Zolfigol, M. A.; Mallakpour, S.; Khazaiae, A.; Vaghaie, R. G.; Torabi, M. Ca(OCl)2 as an Efficient Oxidizing Agent for the Oxidation of Urazoles under Mild and Heterogeneous Conditions. *Bull. Korean Chem. Soc.* **2004**, *25* (8), 1251–1252.
(112) Bausch, M. J.; David, B.; Dobrowolski, P.; Guadalupe-Fasano, C.; Gostowski, R.; Selmarten, D.; Prasad, V.; Vaughn, A.; Wang, L. H. Proton-Transfer Chemistry of Urazoles and Related Imides, Amides, and Diacyl Hydrazides. *J. Org. Chem.* **1991**, *56* (19), 5643–5651. https://doi.org/10.1021/jo00019a034.
(113) Meng, G.; Guo, T.; Ma, T.; Zhang, J.; Shen, Y.; Sharpless, K. B.; Dong, J. Modular Click Chemistry Libraries for Functional Screens Using a Diazotizing Reagent. *Nature* **2019**, *574* (7776), 86–89. https://doi.org/10.1038/s41586-019-1589-1.
(114) Sokolova, N. V.; Latyshev, G. V.; Lukashev, N. V.; Nenajdenko, V. G. Design and Synthesis of Bile Acid–Peptide Conjugates Linked Viatriazole Moiety. *Org. Biomol. Chem.* **2011**, *9* (13), 4921–4926. https://doi.org/10.1039/C0OB01188F.

(115) Park, J.; Koh, M.; Koo, J. Y.; Lee, S.; Park, S. B. Investigation of Specific Binding Proteins to Photoaffinity Linkers for Efficient Deconvolution of Target Protein. *ACS Chem. Biol.* **2016**, *11* (1), 44–52. https://doi.org/10.1021/acschembio.5b00671.
(116) Ogawa, S.; Kittaka, H.; Nakata, A.; Komatsu, K.; Sugiura, T.; Satoh, M.; Nomura, F.; Higashi, T. Enhancing Analysis Throughput, Sensitivity and Specificity in LC/ESI–MS/MS Assay of Plasma 25-Hydroxyvitamin D3 by Derivatization with Triplex 4-(4-Dimethylaminophenyl)-1,2,4-Triazoline-3,5-Dione (DAPTAD) Isotopologues. *Journal of Pharmaceutical and Biomedical Analysis* **2017**, *136*, 126–133. https://doi.org/10.1016/j.jpba.2016.11.030.
(117) Moriarty, R. M.; Prakash, I.; Penrnasta, R. An Improved Synthesis of Ethyl Azodicarboxylate and 1,2,4-Triazoline-3,5-Diones Using Hypervalent Iodine Oxidation. *Synthetic Communications* **1987**, *17* (4), 409–413. https://doi.org/10.1080/00397918708063918.
(118) Frearson, J. A.; Wyatt, P. G.; Gilbert, I. H.; Fairlamb, A. H. Target Assessment for Antiparasitic Drug Discovery. *Trends in Parasitology* **2007**, *23* (12), 589–595. https://doi.org/10.1016/j.pt.2007.08.019.
(119) Mitra, A. K.; Mawson, A. R. Neglected Tropical Diseases: Epidemiology and Global Burden. *Trop Med Infect Dis* **2017**, *2* (3). https://doi.org/10.3390/tropicalmed2030036.
(120) Das, U. K.; Kumar, A.; Ben-David, Y.; Iron, M. A.; Milstein, D. Manganese Catalyzed Hydrogenation of Carbamates and Urea Derivatives. *J. Am. Chem. Soc.* **2019**, *141* (33), 12962–12966. https://doi.org/10.1021/jacs.9b05591.
(121) Taylor, E. C.; Macor, J. E. Synthesis of Pyridines by Diels-Alder Reactions of Hetero-Substituted 1,2,4-Triazines with Enamines and an Enaminone. *J. Org. Chem.* **1989**, *54* (6), 1249–1256. https://doi.org/10.1021/jo00267a007.
(122) Herrera, A.; Martínez-Alvarez, R.; Ramiro, P.; Molero, D.; Almy, J. New Easy Approach to the Synthesis of 2,5-Disubstituted and 2,4,5-Trisubstituted 1,3-Oxazoles. The Reaction of 1-(Methylthio)Acetone with Nitriles. *J. Org. Chem.* **2006**, *71* (8), 3026–3032. https://doi.org/10.1021/jo052619v.
(123) Barbero, N.; Martin, R. Ligand-Free Ni-Catalyzed Reductive Cleavage of Inert Carbon–Sulfur Bonds. *Org. Lett.* **2012**, *14* (3), 796–799. https://doi.org/10.1021/ol2033306.
(124) MASSART, D. L. Chemometrics: A Textbook. *Data Handling in Science and Technology* **1988**, *2*, 53.
(125) Brown, S. D. Chemometrics: A Textbook. D. L. Massart. B. G. M. Vandeginste, S. N. Deming, Y. Michotte, and L. Kaufman, Elsevier, Amsterdam, 1988. ISBN 0-444-42660-4. Price Dfl 175.00. *Journal of Chemometrics* **1988**, *2* (4), 298–299. https://doi.org/10.1002/cem.1180020409.
(126) Box, G. E. P.; Hunter, W. G.; Hunter, J. S. *Statistics for Experimenters: An Introduction to Design, Data Analysis, and Model Building*; Wiley series in probability and mathematical statistics; Wiley: New York, 1978.
(127) Liengme, B. *A Guide to Microsoft Excel 2007 for Scientists and Engineers*; Academic Press, 2008.

(128) APEX3 suite for crystallographic software - single crystal X-ray diffraction https://www.bruker.com/products/x-ray-diffraction-and-elemental-analysis/single-crystal-x-ray-diffraction/sc-xrd-software/apex3.html (accessed May 1, 2020).
(129) Sheldrick, G. M. Crystal Structure Refinement with SHELXL. *Acta Cryst C* **2015**, *71* (1), 3–8. https://doi.org/10.1107/S2053229614024218.
(130) Zhang, Y.; Hsung, R. P.; Tracey, M. R.; Kurtz, K. C. M.; Vera, E. L. Copper Sulfate-Pentahydrate-1,10-Phenanthroline Catalyzed Amidations of Alkynyl Bromides. Synthesis of Heteroaromatic Amine Substituted Ynamides. *Org. Lett.* **2004**, *6* (7), 1151–1154. https://doi.org/10.1021/ol049827e.
(131) Bai, Y.-B.; Luo, Z.; Wang, Y.; Gao, J.-M.; Zhang, L. Au-Catalyzed Intermolecular [2+2] Cycloadditions between Chloroalkynes and Unactivated Alkenes. *J. Am. Chem. Soc.* **2018**, *140* (17), 5860–5865. https://doi.org/10.1021/jacs.8b01813.
(132) Mukhopadhyay, B. Sulfuric Acid Immobilized on Silica: An Efficient Promoter for One-Pot Acetalation–Acetylation of Sugar Derivatives. *Tetrahedron Letters* **2006**, *47* (26), 4337–4341. https://doi.org/10.1016/j.tetlet.2006.04.118.
(133) Pal, K. B.; Verma, P. R.; Gupta, T.; Mukhopadhyay, B. Synthesis of the Trisaccharide Repeating Unit of the Lipopolysaccharide from Moritella Viscosa Strain M2-226. *Journal of Carbohydrate Chemistry* **2015**, *34* (4), 173–182. https://doi.org/10.1080/07328303.2015.1021476.

CHAPTER THREE

SUBSTRATE DEPENDENT AND DIVERGENT REACTIVITY OF AZODICARBOXYLATES IN [2+2] CYCLOADDITION WITH ELECTRON-RICH ALKYNES

3.1 Cyclic vs. acyclic azodicarboxylates in [2+2] cycloaddition with electron-rich alkynes

In chapter II of this dissertation, the synthesis of stable diazacyclobutene derivatives (**III-2**) by means of a formal [2+2] cycloaddition of 4-phenyl-1,2,4-triazolinedione (PTAD) and electron-rich alkynyl sulfides (*eg:* **III-1**) or selenides was described (Scheme 1, eq. 1).[1] The resulting bicyclic diazacyclobutenes exhibit excellent thermal stability up to >200 ˚C (*see* also Chapter I, Figure 2.2), significantly higher compared to the previously studied monocyclic diazacyclobutenes.[1–8] These results are also in good agreement with the studies done by Breton and co-workers.[9,10] Apparently, this enhanced thermal stability is due to the fused second ring (*i.e.*, the 5-membered urozole ring), which prevents the 4π conrotatory cycloreversion of the initially formed diazacyclobutene **III-2** to produce a rather strained (1*Z*,3*E*)-cycloheptadienyl heterocyclic ring **III-3** (Scheme 3.1, eq. 1).[9] This information has been further discussed in Chapter II, section 2.3. Warrener showed that the monocyclic diazacyclobutene that they made, dimethyl Δ^3-1,2-diazetine-1,2-dicarboxylate (**III-4**),was thermally unstable (*i.e.*, $t_{1/2}$ (20 ˚C) = 6.9 h; $t_{1/2}$ (34 ˚C) = 1.8 h) and isomerized into ring open-product **III-5** even at ambient temperatures (Scheme 1.3, eq. 2).[2]

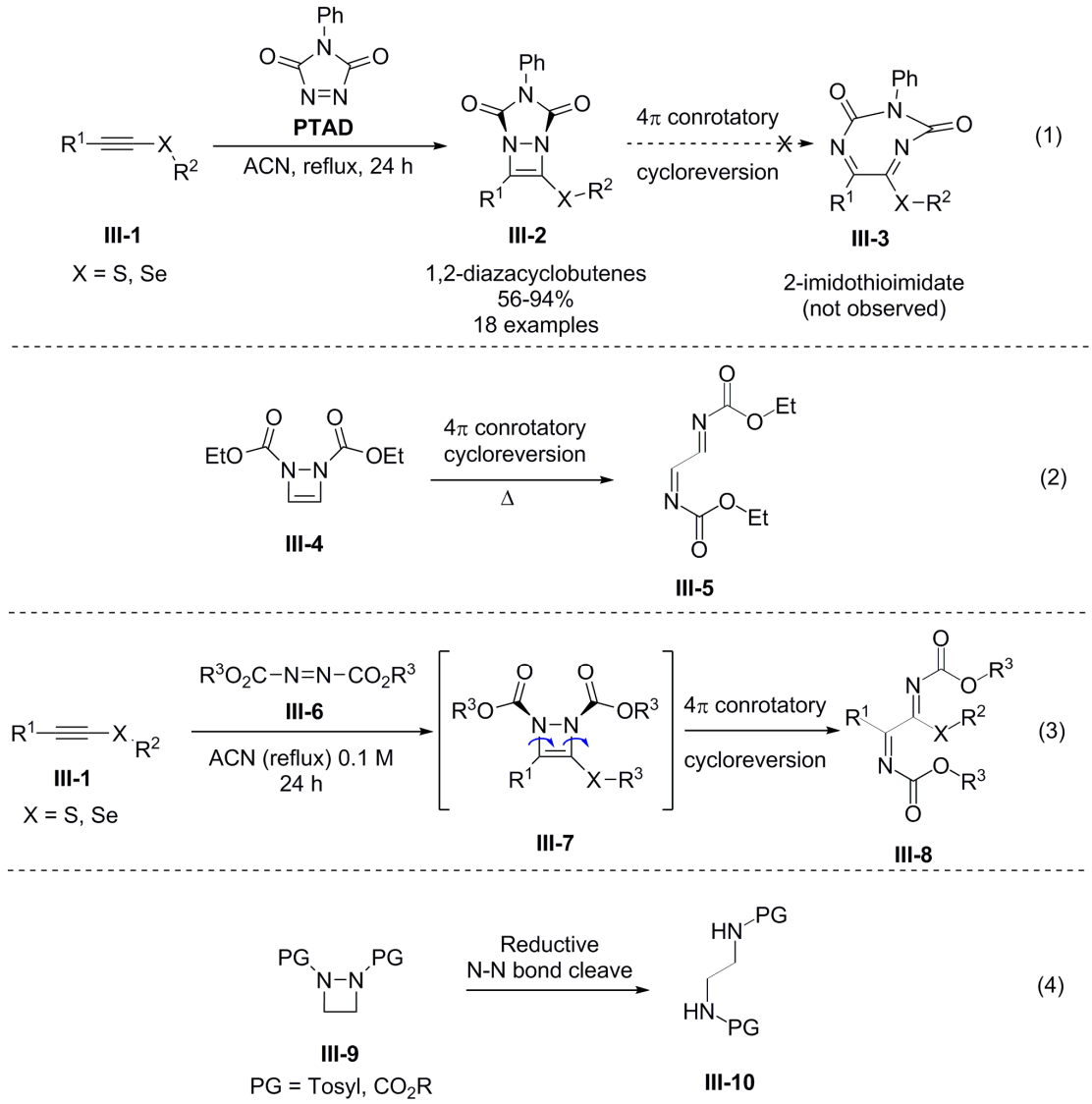

Scheme 3.1. Straightforward approach to synthesize the *vic*-diamine motif containing acyclic 2-iminothioimidates.

Nevertheless, this protocol has not been broadly utilized to synthesize the *vic*-diamine motif due to certain drawbacks including the impracticality of larger scale reactions, the requirement for non-commercial precursors, and tedious synthetic protocols.[2] Inspired by the previous literature,[2,3,9,10] we assumed that reacting electron rich alkynes with acyclic azodicarboxylates (**III-6**) instead of cyclic azodicarboxylates (*e.g.* PTAD), would provide a straightforward approach to synthesize a new class of compounds known as *N*,*N*-dicarbamoyl 2-iminothioimidates (**III-8**). In this approach, the monocyclic diazacyclobutene **III-7** was initially formed via an analogous formal [2+2] cycloaddition with alkynyl sulfide **III-1** and subsequently undergoes facile 4π conrotatory cycloreversion to provide the *N*,*N*-dicarbamoyl 2-iminothioimidates **III-8** (Scheme 3.1, eq. 3).[11]

2-iminothioimidates are rarely reported compounds in the literature.[2] Interestingly this molecular architecture consists of an oxidized variant of the *vic*-diamine motif, and the synthesis of these molecules only requires one synthetic operation from an electron-rich alkyne precursor. Previous methods for the synthesis of acyclic 1,2-diamines from the four-membered 1,2-diazetidine heterocycles (**III-9**) would require a reductive N-N bond cleavage step to form the acyclic *vic*-diamine motif containing compound **III-10** (Scheme 3.1, eq. 4).[12–15] However, it is important to note that the new protocol of 2-iminothioimidate synthesis does not require this step due to the inherent strain of the diazacyclobutene **III-7** leveraging the N-N bond cleaving step (Scheme 3.1, eq. 3).

It is apparent that further treatments are required to access the diamine motif from the molecule **III-8**; however we hope that this molecular scaffold could be a broadly useful template in organic synthesis apart from accessing vicinal diamines.

According to best of our knowledge, there are no examples in literature for the direct synthesis of the 2-iminothioimidate molecular scaffold. Nevertheless, a few related scaffolds that bear α-oxidized functionality such as α-keto (**III-11**), α-oximo (**III-12**), and α-hydrazono (**III-13)** analogs have been encountered in literature (Figure 3.1).[16–25] In addition, α-oxidized thioimidates have a wide range of applications such as precursors for the synthesis of dyes,[18] as metal-binding ligands,[16,17] significance in Maillard flavors in cooked food,[26] intermediates for heterocycle syntheses,[19] and fungicides and pesticides.[25,27,28]

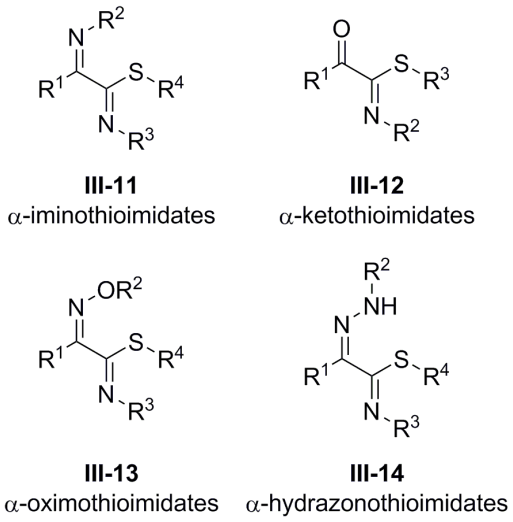

Figure 3.1. α-oxidized thioimidate scaffolds.

Based on literature studies, these 2-iminothioimidate compounds may be useful building blocks for diverse applications. These applications further encouraged us to investigate the validity of this protocol as a general method to access these compounds.

3.1.1 Synthesis of acyclic N,N-dicarbamoyl 2-iminothioimidates.

We first synthesized a set of phenyl alkynyl sulfides as our electron-rich alkynes from the previously developed *n*-butyl lithium protocol. These alkynyl sulfides (**III-1**, where X = S) were then reacted with diethyl azodicarboxylate (DEAD, **III-6**) under the previously optimized conditions[1] (*i.e.*, refluxing acetonitrile for 24 h) to provide the corresponding *N*,*N*-dicarbamoyl 2-imidothioimidates **III-8** (Scheme 3.2). The first series of the *N*,*N*-dicarbamoyl 2-imidothioimidates were prepared by varying the length of the alkyl chain (R^2) resident on the sulfur atom. The *N*,*N*-dicarbamoyl 2-imidothioimidates bearing shorter *n*-alkyl chains at R^2 such as methyl, ethyl, *n*-propyl, and *n*-butyl were successfully prepared in good to excellent yields (**III-8a**−**III-8d** in 73−99% yields). The 2-imidothioimidate derivatives **III-8e** and **III-8f** bearing *n*-pentyl and *n*-octyl groups at R^2 position were provided 80% and 73% yields, respectively. .

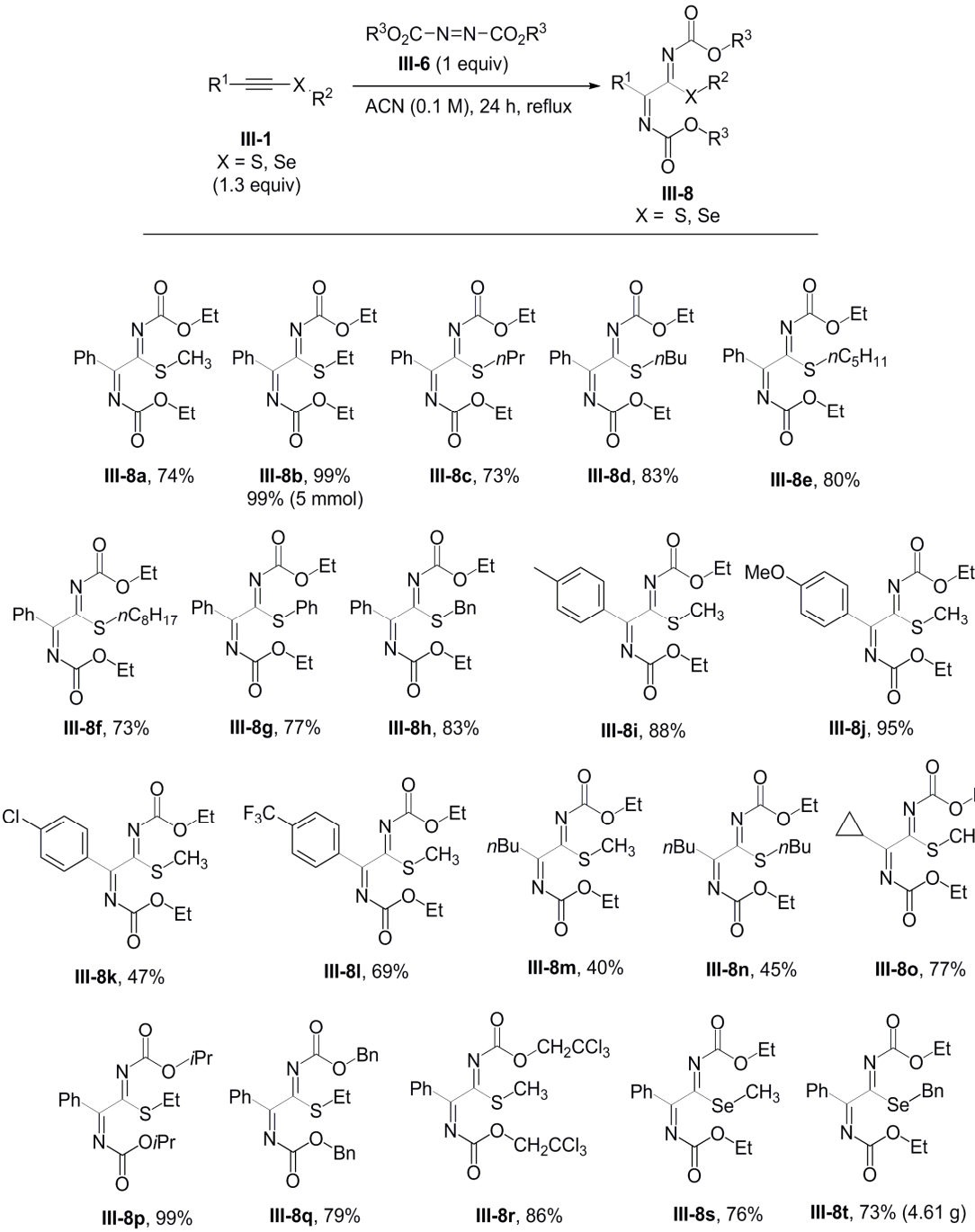

Scheme 3.2. Substrate scope of *N*,*N*-dicarbamoyl 2-imidothioimidates.

Incorporating aryl groups at the R^2 position such as phenyl and benzyl groups yielded the corresponding 2-iminothioimidates **III-8g** and **III-8h** in 77% and 83% yields, respectively.

Then we examined the reactivity of alkynyl sulfides bearing aryl groups at the R^1 position with both electron donating and deficient substituents. First, 2-iminothioimidates bearing *para*-substituted electron donating groups such as *para*-methyl or *para*-methoxy at the R^1 position were synthesized in 88% and 95%yields (**III-8i** and **III-8j**, respectively). In contrast, electron deficient aryl substituents at R^1 such as *para*-chloro (**III-8k**) and *para*-trifluoromethyl (**III-8l**) yielded their corresponding 2-iminothioimidate products in low to moderate yields (47% and 69% respectively).

Then we turned towards assessing the yields of alkyl analogs of the 2-iminothioimidates. The 2-iminothioimidates **III-8m** (Where R^1 = *n*-butyl and R^2 = methyl) and **III-8n** (Where R^1 = *n*-butyl and R^2 = *n*-butyl) were isolated in moderate yields (40% for **III-8m** and 47% for **III-8n**). We noticed that these alkyl analogs are not stable and tends to decompose after isolation. This is presumably due to the presence of α–protons at the R^1 group in these alkyl analogs which can undergo tautomerism into a corresponding enamine and consequently decay into other by-products. In contrast to linear alkyl groups at R^1 position, the product bearing a cyclopropyl group (**III-8o**) was found to be stable and was isolated in a 77% yield. This is probably due to the ring strain

resulting from the cyclopropyl group which prevents the formation of the corresponding enamine by product.

Then we decided to evaluate this reaction with other commercially available, symmetric azodicarboxylates (*i.e.*, exploring variations at the R^3 position). As a result of this, 2-iminothioimidates derived from azodicarboxylates bearing diisopropyl, dibenzyl, and bis(2,2,2-trichloroethyl) groups were generated in very good yields (**III-8p-r**, 79-99% yield). In addition, the chalcogen atom of the 2-iminothioimidates was changed to selenium by reacting alkynyl selenides with DEAD. Consequently, the corresponding 2-iminoselenoimidates were generated in very good yields (76% for **III-8s** where R^1 = phenyl and R^2 = methyl, and 73% for **III-8t** where R^1 = phenyl and R^2 = benzyl). Moreover, this 2-iminothioimidate synthesis was able to be performed at gram scale, resulting in very high yields. Sulfur analog **III-8b** was generated in 99% yield at a 5 mmol scale and the synthesis of selenium analog **III-8t** proceeded smoothly to provide 4.61 g of the desired product.

3.1.2 Mechanistic investigations for the [2+2] cycloaddition of the alkynyl sulfide and diethyl azodicarboxylate (DEAD)

We hypothesized that the formal [2+2] cycloaddition between alkynyl sulfide and diethyl azodicarboxylates could follow two main pathways (*path a* and *b*, Scheme 3.3). It is apparent that regardless of whether the reaction proceeds through *path a* or *path b* initially, both will form a thermally unstable monocyclic diazacyclobutene **III-7b** which will undergo facile 4π conrotatory ring opening to provide the corresponding 2-iminothioimidate **III-8b**.[2,3] However, the only noticeable difference between *path a* vs. *path b* is that *path a* undergoes a concerted [2+2] cycloaddition and in contrast *path b* undergoes a stepwise [2+2] cycloaddition.

As a result of the formation of ketene type intermediate **III-15b** (Scheme 3.3) from the minor resonance contributor of the alkynyl sulfide, we envisioned that a concerted [2+2] cycloaddition could be possible to generate the monocyclic diazacyclobutene intermediate.[29,30] Ketenes are well known precursors for [2+2] cycloaddition in the literature.[31–33] On the other hand, if the reaction follows *path b*, it will first form a 1,5-dipole intermediate **III-16b**, and thus will cyclize back by attack of the negatively charged nitrogen nucleophile onto the most reactive ketene-type carbon atom within the 1,5-dipole, thus forming the monocyclic diazacyclobutene **III-7b**.

Previous work of mechanistic investigations of the reactions between vinyl ethers and 4-phenyl-1,2,4-triazoline-3,5-dione (PTAD) revealed that these reactions proceed via a dipole intermediate.[34,35] Therefore, we were equally interested that our reaction could also proceed via a 1,5-dipole intermediate according to *path b* (Scheme 3.3).

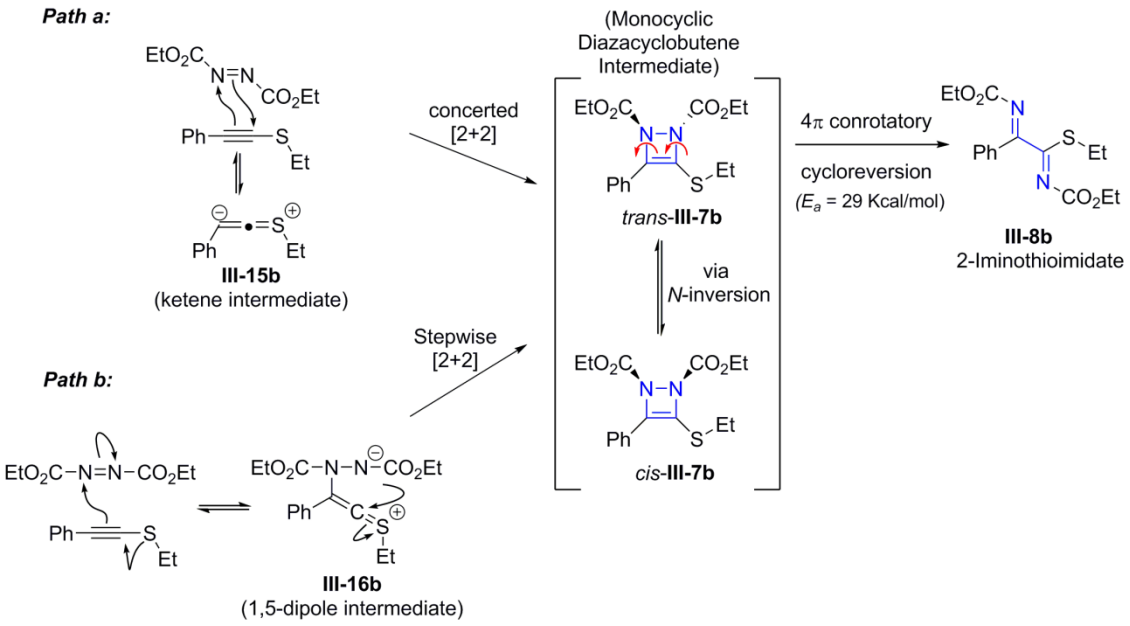

Scheme 3.3. Plausible mechanistic paths for the formation of 2-iminothioimidate.

In order to gain more insights about the mechanism, we then began to thoroughly investigate this reaction by means of variable temperature NMR studies, react-IR, computational modeling. According to Werrener's and Breton's previous studies, we recognized that this reaction proceeds via a monocyclic diazacylcobutene intermediate.[2,3,9] To probe this question, we isolated the monocyclic diazacyclobutene intermediate **III-7b** (Figure 3.2) by preparative TLC and confirmed its structure with ^{1}H, ^{13}C NMR, and FTIR spectroscopy. The quaternary carbon at the 4th position of the diazacyclobutene ring resonates at 140 ppm which serves as a fingerprint peak to show the presence of the diazacyclobutene ring (**III-7b**), whereas the two imine ^{13}C NMR peaks of the 2-iminothioimidate product (**III-8b**) appear between 160-175 ppm.

Next, we performed a variable temperature NMR study for **III-7b** at different temperatures ranging from –35°C to 50˚C (238–323 K) in acetonitrile-d3 while monitoring the quartet generating from the S-methylene protons (**x** and **y**) of **III-7b** and **III-8b** (Figure 3.2). Note that the reaction arrow has been drawn from right to left in the Figure in order to coincide that with the corresponding **x** and **y** quartets of the stacked ^{1}H NMR spectra.

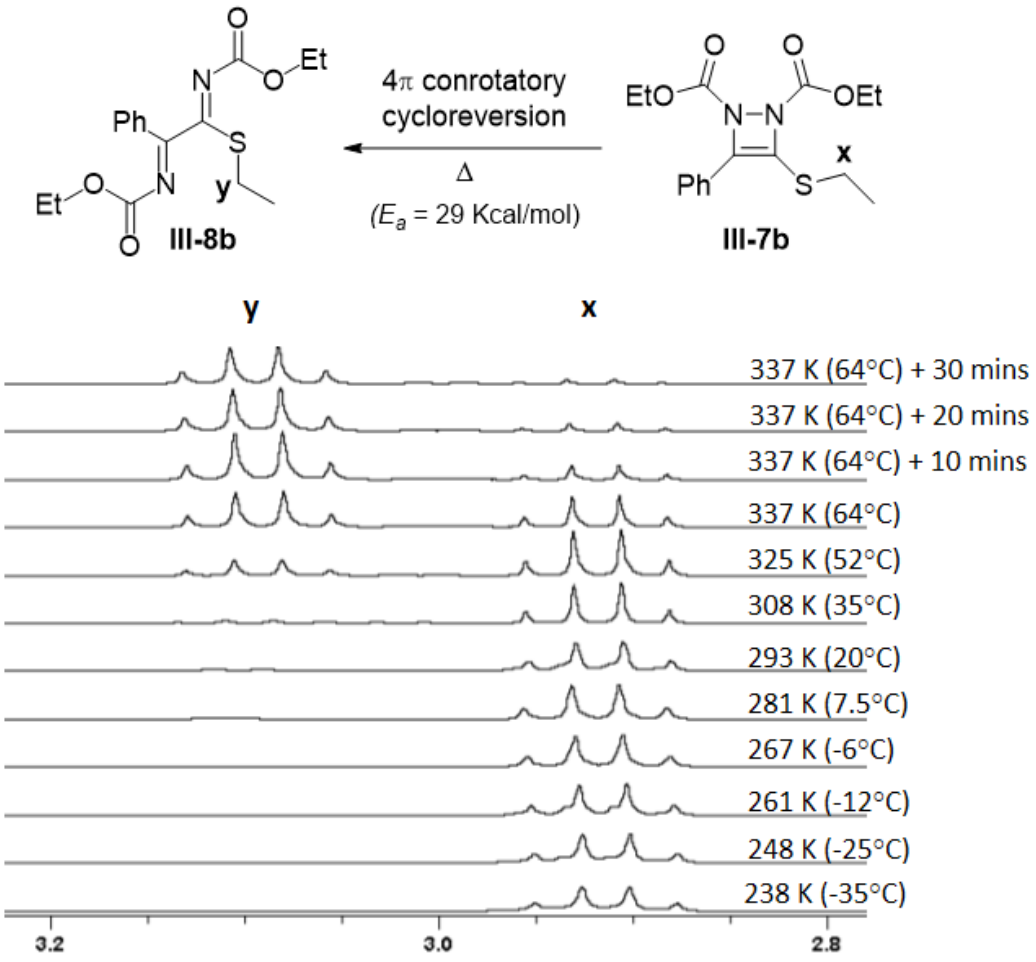

Figure 3.2. Variable temperature ^{1}H NMR spectra of **III-7b** recorded at different temperatures in the range of –35˚C to 50˚C (238–323 K) in acetonitrile-d3.

These variable temperature NMR results suggest that at higher temperatures (>45˚C) the monocyclic diazacyclobutene **III-7b** undergoes facile cycloreversion due to its lower thermal stability compared to the 2-iminothioimidate products.[2,3,9]

The next question that we wanted to probe was which isomer of the monocyclic diazacyclobutene *cis*-**III-7b** or *trans*-**III-7b** provides the 2-iminothioimidate **III-8b** from the conrotatory ring open process (Scheme 3.3). Since the imine geometry (E/Z) of the 2-iminothioimidate is dependent on which isomer (*cis* or *trans* of **III-7b**) is undergoing the ring open process, this could provide more information about the mechanism.

In addition, monocyclic diazacyclobutene **III-7b**, which was isolated for variable temperature NMR, also exhibits diastereotopicity at lower temperatures exchange process from S-methylene protons (**x**) which can be accomplished via *cis-trans* inter-conversion shown in Scheme 3.3 through nitrogen inversion. This is also an analogous process that we saw in the double-nitrogen inversion of 4,5 bicyclic diazacyclobutene (**III-2**, Scheme 3.1). This process was clearly described in our recent work and in Chapter II.[1] However, in this case, when **III-7b** was cooled down, no further splitting of the S-methylene quartet (**x**) was seen which indicates that no diastereotopicity was observed at lower temperatures. This was attributed to a very low energy barrier for this *cis-trans* inter-conversion of **III-7b** which is also in good agreement with Warrener's previous work (*i.e.*, ~7.5 kcal/mol) (Scheme 3.3).[3] This suggests that monocyclic diazacyclobutene **III-7b** undergoes rapid *cis-trans* isomerization under the reaction conditions.

Nonetheless, based on conventional molecular orbital symmetry arguments the *cis* analog of the **III-7b** would have a higher energy barrier during the conrotatory ring open process compared to the *trans*-**III-7b**.[3,8,11] So, we can speculate that the 4π-conrotatory ring open process presumably proceeds via *trans*-**III-7b**.

Furthermore, we analyzed the integration data for the electrocyclic ring opening of **III-7b** to provide **III-8b** at 373 and 298 K and found that this process follows first-order decay and subsequently extracted the rate constants k of 7.3(1) × 10^{-4} and 3(1) × 10−6 s^{-1} for 373 and 298 K, respectively. By applying these two data sets into the Arrhenius equation, the activation energy (E_a) for the ring open process was calculated to be 29 ± 4 kcal/mol (see the Experimental section for more details). This value was also in good agreement with the calculated barrier of 29.4 kcal/mol for the ring open process by using computational simulations.[11]

The next question that we probed was to identify which pathway –*path a* or *path b*– was operative (Scheme 3.3). It is apparent that *path b* proceeds via 1,5-dipole intermediate which could be further trapped by an appropriate electrophile.[34,35] With the hope of examining the formation of possible dipole intermediate (**III-16b**, Scheme 3.3), we then performed experiments to trap the dipole intermediate of the reaction between alkynylsulfides with PTAD and DEAD separately, in the presence of excess aldehydes and ketones as an electrophilic solvent.[34,35] These experiments were unsuccessful with PTAD due to the very fast cyclization to the diazacyclobutene. On the other hand,

reactions with DEAD tend to give α or β-carbonyl hydrazine esters through hydrogen abstraction from the corresponding aldehyde or ketone which was confirmed by crude NMR analysis.[36–38]

3.1.3. In situ react-IR studies

We then moved onto react-IR experiments of the reaction between phenylethynyl sulfide with PTAD and DEAD at room temperature and reflux conditions in dichloromethane to see whether there was any evidence of the formation of C=S stretching during the reaction.[34,35,39–41] If the [2+2] cycloaddition follows *path b* it might be evident from the C=S stretch arising from the C=S group in the 1,5-dipole intermediate (**III-16b**, Scheme 3.3). We analyzed the IR spectral region from 1300-2000 cm^{-1} while running these reactions to find any evidence of the intermediate species.[39–41] In-situ react-IR stacked spectra for the reaction of phenylethynyl sulfide with DEAD is shown in Figure 3.3. These results did not show any significant evidence for the C=S stretching for a possible 1,5-dipole intermediate (**III-16b**, Scheme 3.3).

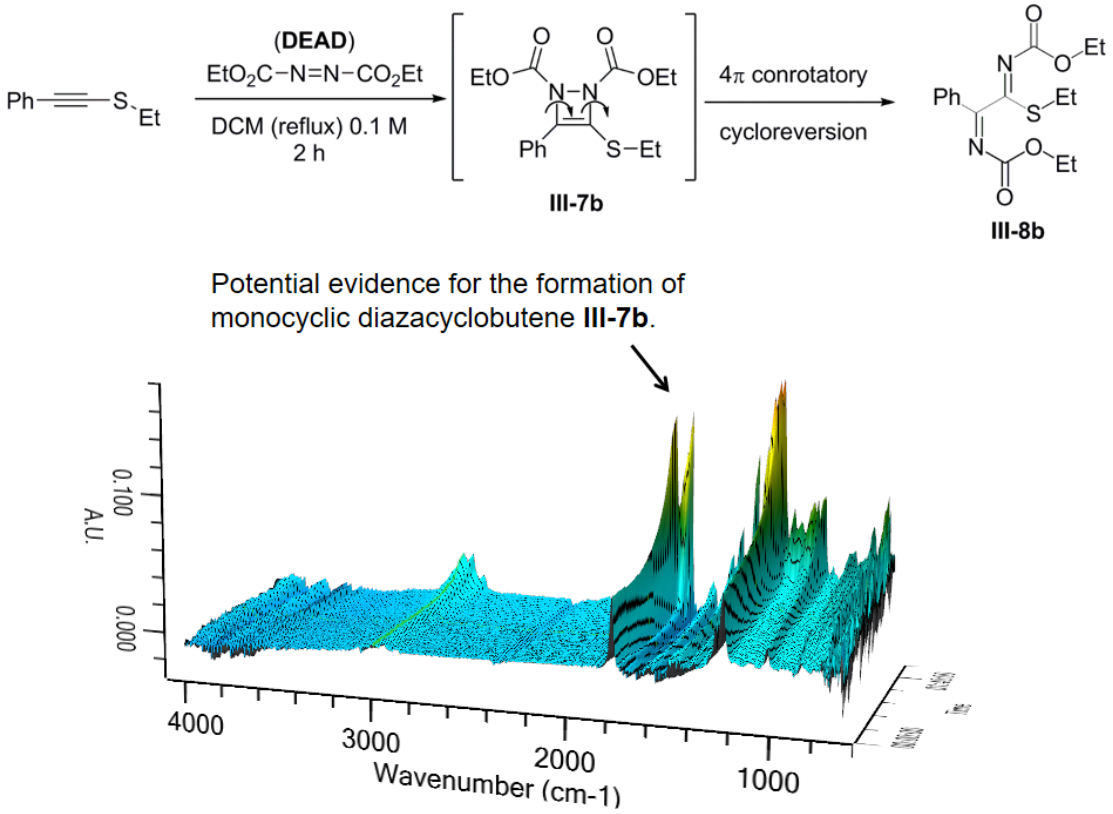

Figure 3.3. *In situ* react-IR stacked spectra for alkynyl sulfide and diethyl azodicarboxylate (DEAD) reaction.

Nevertheless, when we carefully looked at the react-IR spectra, the carbonyl region (~1600-1800 cm^{-1}) of the stacked IR spectra showed a gradual increase in the intensity and followed by a sudden drop and again an increase over the course of the reaction. We believe that this "zig-zag" behavior in the intensity could be a manifestation of the formation and accumulation of the monocyclic diazacyclobutene **III-7b** and then facile ring opening of the **III-7b** (Figure 3.3).

In contrast, the *in situ* react-IR stacked spectra of the reaction of phenylethynyl sulfide with PTAD has no evidence of any intermediate species other than a sudden drop of the carbonyl stretching intensity of PTAD and the increase of the product carbonyl stretching intensity, followed by a saturation as expected (shown in Figure 3.4).

Finally, we turned towards a computational simulation of this reaction. These simulations revealed that the reaction likely proceeds through a highly asynchronous [2+2] cycloaddition to form the monocyclic diazacyclobutene. This means that *path a* and *path b* both could be operative in this reaction mechanism.[11]

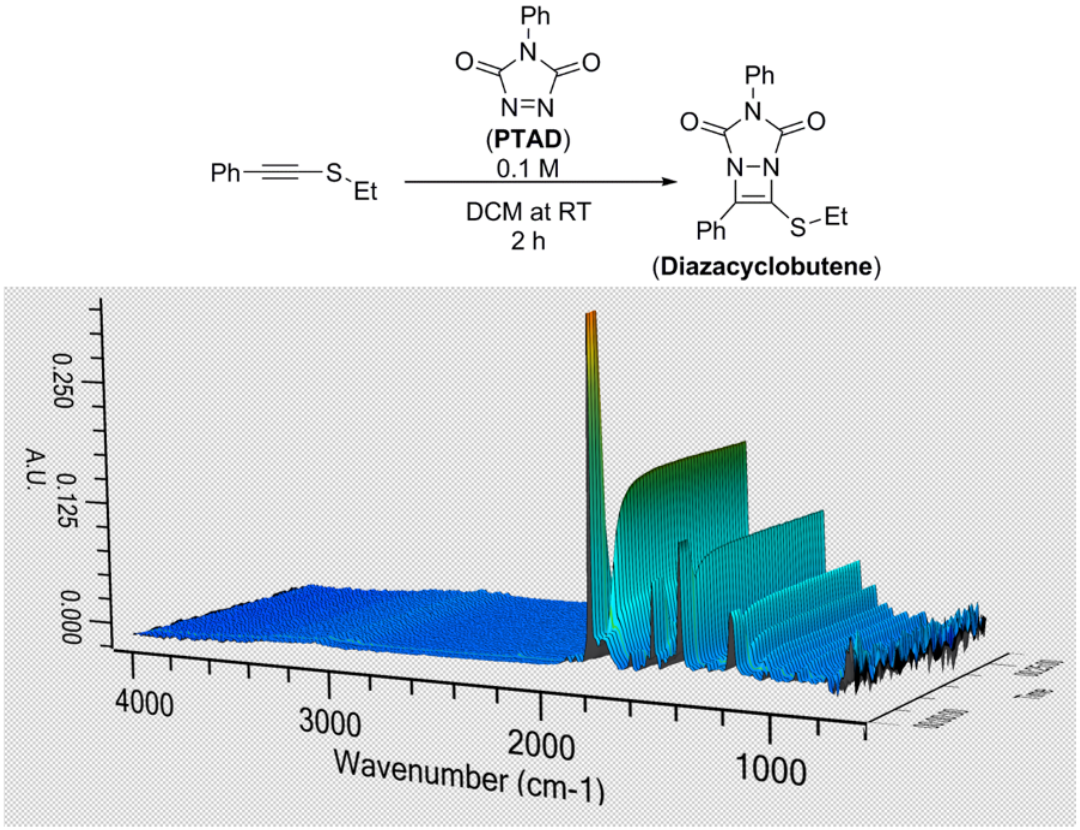

Figure 3.4. *In situ* react-IR stacked spectra for alkynyl sulfide and 4-phenyl-triazoline-3,5-dione (PTAD) reaction.

Then we wished to further analyze the geometry of the 2-iminothioimidate **III-8b** since the geometry of **III-8b** might also provide more information about the conrotatory ring opening event. We further analyzed the final 2-iminothioimidate products by means of 2D-NOESY, low temperature NMR; X-ray crystallographic data, and computational simulations in order to identify the possible isomers of the 2-iminothioimidate product.

2D-NOESY was unable to provide any direct evidence of the imine/thioimidate geometries. The low temperature NMR studies showed that 2-iminothioimidate rapidly isomerizes at room temperature. These results are extensively discussed in section 3.1.4. We were also able to generate single crystals of the 2-iminothioimidate **III-8g** (Where R^1 = Phenyl, R^2 = Phenyl and X = S, *see* Experimental section 3.5.9 for more information), and we found that **III-8g** has a solid state geometry of (*Z*)-imine, (*Z*)-thioimidate. (This (*Z*)-imine, (*Z*)-thioimidate geometry has been drawn for the all the 2-iminothioimidate structures shown in Scheme 3.2 by analogy).

Lastly, computational analysis also suggested that these 2-iminothioimidates rapidly interconvert between *Z*/*E* isomers at ambient temperature.[11] The detailed energy analysis for all the possible conformers of **III-8** were performed computationally and found that (*Z*)-imine, (*E*)-thioimidate or the *Z*/*E* isomer is the lowest energy form of **III-8**.[11] The difference of the geometry in crystalline **III-8g** (*Z*/*Z*) appears to be an artifact of the crystal packing forces due to π stacking. Further calculations revealed that the energy difference of the crystallized conformer **III-8g** ($E_{(Z/Z)}$ = +0.3 kcal/mol) is rather small

compared to the absolute lowest energy geometry (E(*Z*/*E*) = 0.0 kcal/mol). It is not surprising that the crystalline **III-8g** compensates such a small energy change by crystal packing forces to prefer Z/*Z* geometry rather than *Z*/*E*. In conclusion, due to the rapid isomerization of the 2-iminothioimidate, we found that it is difficult to assign which isomer is first formed during the reaction by means of the electrocyclic ring opening of the diazacyclobutene intermediate.

Based on overall experimental data and literature studies, we believe that, the [2+2] cycloaddition between alkynyl sulfide and azodicarboxylates proceeds by process at the interface between *path a* and *path b* to form the monocyclic diazacyclobutene **III-7**, which isomerizes rapidly between *cis*- **III-7** and *trans*- **III-7**. Since the *trans*- **III-7** is more stable than the *cis* analog, this intermediate probably undergoes the 4π-conrotatory cycloreversion to form the *Z*/*E* conformer of the 2-iminothioimidate **III-8** followed by a rapid *Z*/*E* isomerization at room temperature (Scheme 3.3).[3,11]

3.1.4. Dynamic NMR studies of 2-iminothioimidates

The 2-iminothioimidate **III-8q** (R^1 = Ph, R^2 = Et, R^3 = Bn, X = S in Scheme 3.2) was chosen for low temperature NMR studies due to the possible diastereotopicity of the benzyl methylene protons at the R^3 position and the sulfur methylene protons at the R^2 position. Initial variable temperature NMR results with imidothioimidate **III-8q** were surprising to us. We observed two different proton exchange rates for the two benzyl methylene protons of the imine carbamoyl groups with one being an AB doublet of doublets owing to the diastereotopic exchange present in one of the benzyl methylene protons due to slow exchange (see 4.5–5.5 ppm in Figure 3.5).

Moreover, the S-methylene protons of **III-8q** also showed multiplets, possibly due to the diastereotopic effect (see 2.5–3.5 ppm in Figure 3.5). In order to further confirm that these S-methylene multiplets are arising from a diastereotopicity rather than from different isomers or rotomers that shows different chemical shifts; we decoupled the adjacent methyl protons of the S-ethyl group and observed the low temperature spectra. We found that the observed spectra arise solely from a diastereotopic exchange process by obtaining an AB doublet of doublet for this decoupled spectrum (*see* 2.8– 3.2 ppm in Figure 3.6).

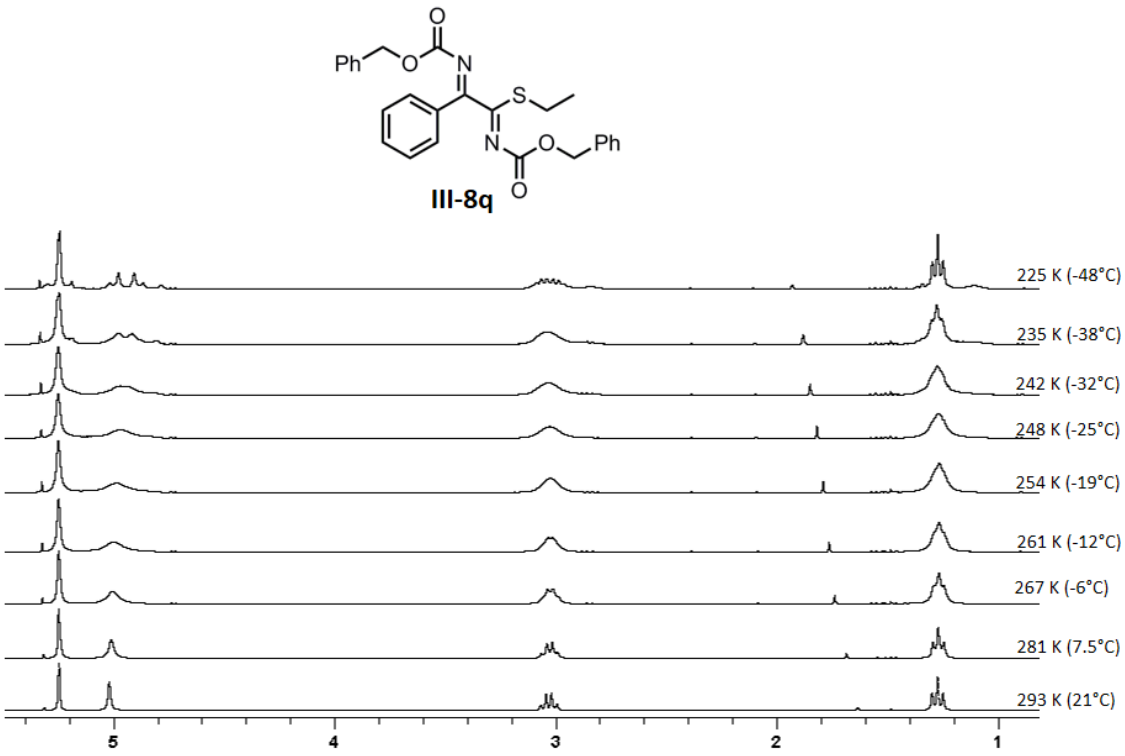

Figure 3.5. Variable temperature ^{1}H NMR spectra of **III-8q** recorded at different temperatures in the range of 21°C to –48˚C (293 –225 K) in $CDCl_3$.

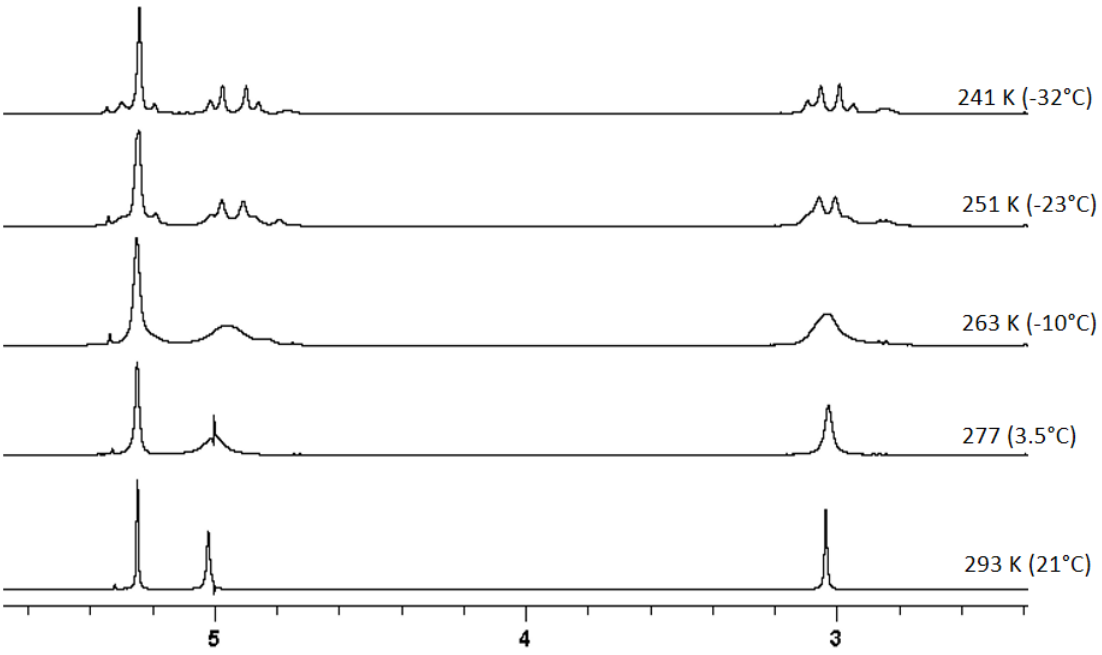

Figure 3.6. Variable temperature homodecoupled (at methyl protons) ^{1}H NMR spectra of **III-8q** recorded at different temperatures over the range of 21˚C to –32˚C (293 – 225 K) in $CDCl_3$.

Theoretically, there are three major ways these S-methelene protons and benzyl methylene protons can exhibit diastereotopicity at lower temperatures. If the lower temperatures slow the rotation about the C-C single bond in-between the two imine moieties beyond the NMR timescale, two more stable, chiral atropisomers (staggered-1 and 2) may appear, out of four major rotomers (staggered and eclipsed, *see* Scheme 3.4).

Another possible explanation might be the out-of-plane imine N-inversion (*i.e.,* with respect to the imine double bond plane), which would result in four diastereomers which will be a pair of non-superimposable mirror images for any of the rotomers in Scheme 3.4. However, it is apparent that the out-of-plane N-inversion in **III-8q** is a geometrically restricted process due to the perpendicular imine pi bond. Therefore, another possible N-inversion pathway is the in-plane N-inversion via sp^2-sp-sp^2 hybridization change of the nitrogen. The in-plane imine N-inversion would not produce an instance of diastereotopicity unless it arises from a non-eclipsed rotomer with slowed rotation beyond the NMR time scale (*i.e.*, any other rotomer than eclipsed in Scheme 3.4). Finally, rotation about imino nitrogen-carbamoyl carbon bond could also lead to chiral species.[42–45]

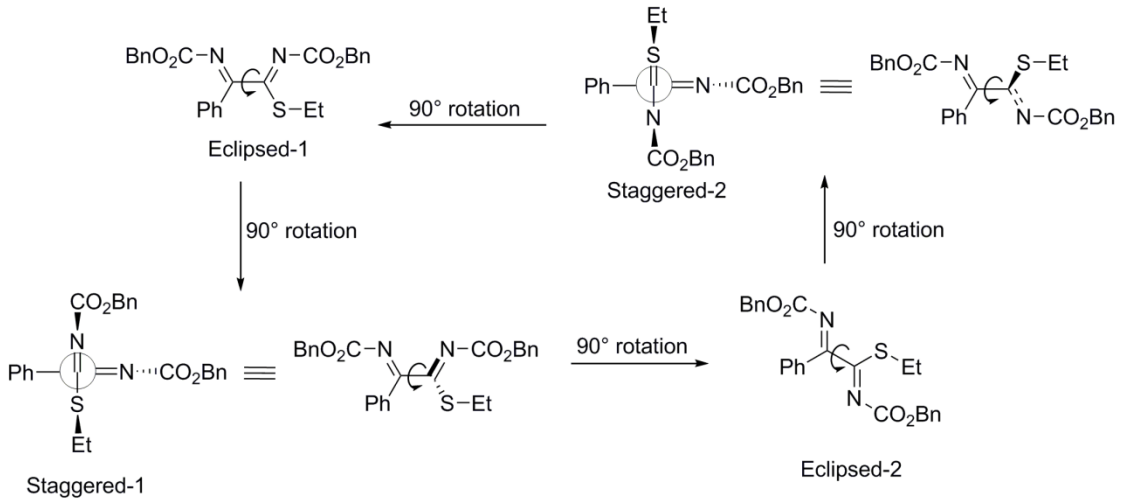

Scheme 3.4. Major atropisomers possible via slowed C-C rotation between two imine moieties for **III-8q** (In-plane imine N-inversion has not been considered here.)

We then set out to determine what are the major isomers present in a sample of 2-iminothioimidate **III-8q** at very low temperature. We used THF-d8 to access temperatures as low as –58˚C in the spectrometer. Unexpectedly, in THF-d8, we saw both benzyl methylene protons of the imine carbamoyl groups are showing slow exchange (Figure 3.7). In addition, we saw an AB doublet of doublet and three singlets in between 5.1-5.4 ppm (*see* Figure 3.7) at low temperature in THF-d8, suggesting that there could be chiral and achiral species in the mixture at very low temperature.

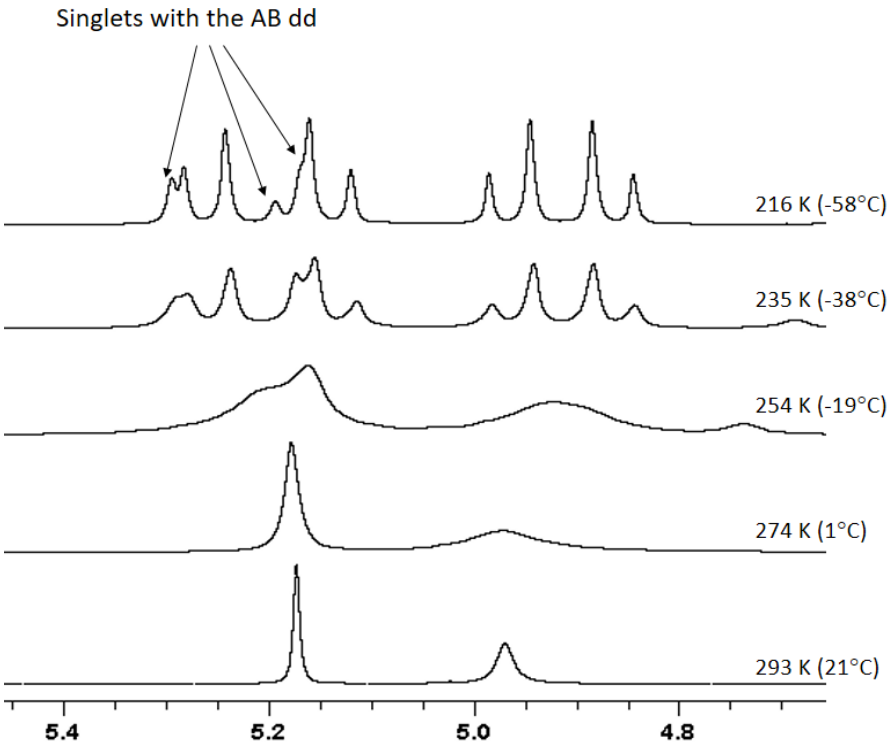

Figure 3.7. Variable temperature ^{1}H NMR spectra of **III-8q** recorded at different temperatures over the range of 21˚C to –58˚C (293–216 K) in THF-d8.

The achiral components of the mixture might be explained by considering eclipsed rotational isomers. Chiral species can be achieved by rotation about the imino nitrogen-carbamoyl carbon bond or atropisomers arising from slowed rotation of the central C-C bond. One of the important questions we had at this point is to find out whether N-inverison (in-plane) is slower than the hindered C-C rotation between the sp^2 carbons or imino N-carbamoyl carbon rotation.

In order to understand the rotational energy barrier of the C-C joining two sp^2 Cs; the dihedral angle vs. energy of the conformer **III-8b** in gas phase was graphed. The energies of the conformers were computed at 6-31G*/B3LYP (d,p) level, as implemented in the Gaussian 09 program.[46,47] These results are shown in Figure 3.8.

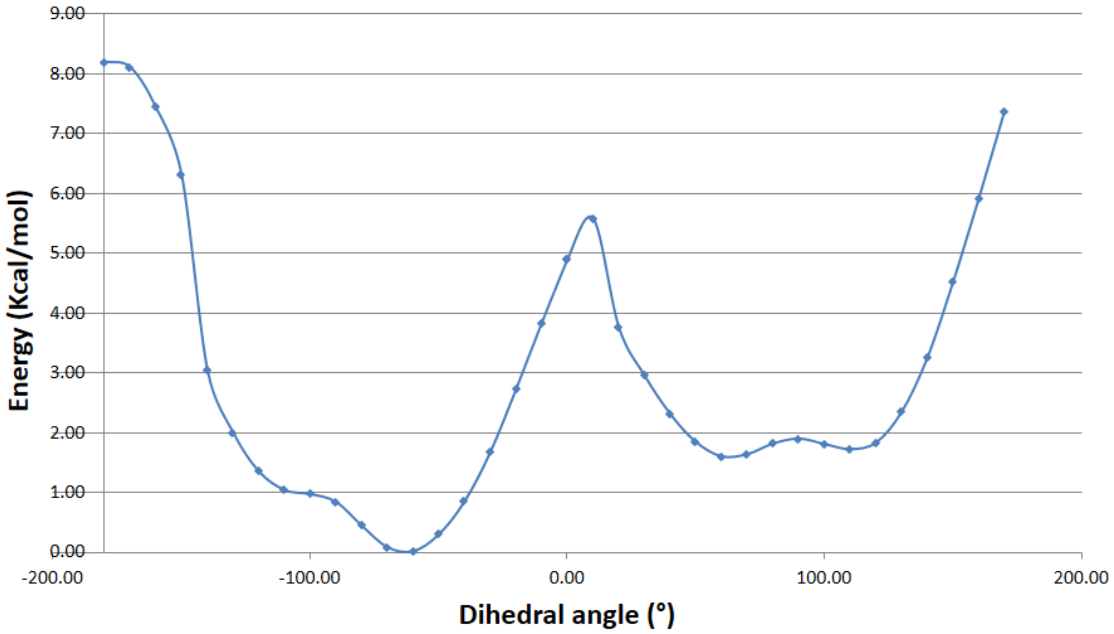

Figure 3.8. Dihedral angle vs. potential energy of **III-8b** [DFT 6-31G*/B3LYP (d,p)]

(Note: Dihedral angle was taken through imine nitrogen to thioimidate nitrogen and +ve values are anti clockwise rotation whereas –ve values are clockwise rotation)

The highest energy conformer of **III-8b** in the gas phase was +8 kcal/mol and thus shows a very lower energy barrier for imine C-C rotation. These results suggest that imine C-C rotation is more likely a fast process on the NMR time scale.

In addition, when we carefully investigate the experimental observations of the two different proton exchange rates in $CDCl_3$ (Figure 3.5) vs. THF-d8 (where both imine N-inversions showed slow exchange, *see* Figure 3.7); it is apparent that this experimental evidence are in good agreement with the sp^2-sp-sp^2 imine N-inversion since the hindered rotation and the rotation between imino nitrogen and carbamoyl carbon are less likely to be influenced by the solvent polarity. Furthermore, these two different rates suggest that the transition state (TS) energy of the sp^2-sp-sp^2 N-inversions of the imine moiety and the imidate moiety are different. This is possibly due to fact that the N-inversion TS of the imine moiety has more nonpolar character compared to the TS of the imidate N-inversion. Typically, if there are chiral isomers evidences in ^1H NMR via slow N-inversion at low temperature; this means that the energy barrier of the N-inversion is very high at that particular temperature. In this case, compared to $CDCl_3$ (Figure 3.5), THF-d8 (Figure 3.7) increases the transition state energy of one of the N-inversion by changing the dipole moment (Chloroform = 1.04 debye, THF = 1.75 debye).[48] Since the imine moiety has more nonpolar character than the imidate moiety, THF-d8 presumably increases the TS energy of the more nonpolar TS which corresponds to the imine moiety. Therefore, we speculate that, further downfield slow exchange of the benzyl methylene protons are arising from the imine moiety which is sensitive to polar solvents. This is also

reflected in the Mulliken charge distribution of the lowest energy conformer of **III-8b** which was computed at6-31G*/B3LYP (d,p)] DFT method in gas phase. These Mulliken charges are tabulated below in Table 3.1. Table 3.1 clearly shows that the atomic charge difference of the C=N and C=O groups are high in the thioimidate moiety compared to the imine moiety. This is presumably due to electron pushing from the electron donor atom (sulfur) adjacent to the C=N group of the thioimidate moiety which is absent in the imine moiety.

Since the rotation between imino nitrogen and carbamoyl carbon is also less likely to occur, we can eliminate the contribution from those processes to generate these low temperature 2-iminothioimidate isomers. Taken together, we can speculate that these isomers at low temperature are most probably arising by a combination of in-plane N-inversion and hindered rotation at very low temperature. However, little can be said at present about the correct mode of this diastereotopic exchange process than speculating the most possible mode of diastereotopic exchange with the current experimental and computational results. But more studies are needed in order to validate these experimental results and investigate the correct mode of the diastereotopic exchange process at low temperature.

Table 3.1. Mulliken charges of **III-8b** computed at 6-31G*/B3LYP (d,p) level in gas phase. (Note: Imine moiety is in blue color and thioimidate moiety is in red color in the chemical structure).

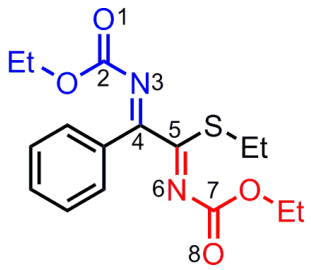

Atom number	Imine moiety	Imidate moeity
1	–0.191	-
2	–0.119	-
3	0.109	-
4	–0.202	-
5	-	–0.369
6	-	0.363
7	-	0.026
8	-	–0.222

Overall, these low temperature NMR studies show that 2-iminothioimidates are rapidly isomerizing at room temperature. Also, it is important to note that the N-inversion of the imine nitrogen and the imidate nitrogen of the same 2-iminothioimidate molecule **III-8q** has a solvent effect which is evident when comparing the stacked spectra in Figure 3.5 and 3.7 ($CDCl_3$ vs. THF-d8). It would be interesting to study this behavior in detail with more solvents with different dipole moments to identify the effects on the transition state of this dynamic process. More experimental studies by synthesizing different 2-iminothioimidates with asymmetric azodicarboxylates[49] and computational studies with implementing different methods (*e.g.* by considering solvation models and non-covalent interactions)[1,11,50] are underway in order to further investigate this dynamic process more accurately.

3.1.5. Conclusions

In conclusion, we have showed a convenient route to access synthetically useful *N*,*N*-dicarbamoyl 2-iminothioimidates by means of the [2+2] cycloaddition of alkynylsulfides and selenides with commercially available acyclic azodicarboxylates to form a monocyclic diazacyclobutene intermediate followed by 4π-conrotatory cycloreversion. This reaction served as the first reaction to make this new class of compounds according to best of our knowledge. Also, these 2-iminothioimidates may provide access to acyclic *vic*-diamines which could be obtained by one synthetic operation. Thorough investigations of the mechanism of this reaction with the help of variable temperature NMR, react-IR, and computational studies suggested that the

reaction could either proceed via a concerted [2+2] cycloaddition or via a 1,5-dipole intermediate to form the monocyclic diazacyclobutene followed by 4π-conrotatory cycloreversion to form the corresponding 2-iminothioimidate.

Additionally, low temperature NMR studies and computational studies predicted that 2-iminothioimidate exists as a mixture of isomers at very low temperature. Low temperature NMR and homodecoupled NMR further suggest that the imine N-inversion of the 2-iminothioimidate is a diastereomeric process and more likely occurring through a combination effect of in-plane N-inversion with the hindered rotation. In addition, low temperature studies with different solvents with different dipole moments revealed that the N-inversion of imine moiety and the imidate moiety has different transition state (TS) natures. Therefore this N-inversion is in good agreement with the sp^2-sp-sp^2 imine N-inversion since the solvent polarity has less effect on the hindered rotation and the rotation between imino nitrogen and carbamoyl carbon. This study further showed that the TS of the N-inversion of the imine moiety have a nonpolar character. More experimental and computational studies are underway in order to further prove these arguments.

3.2. [2+2] vs. Ene reaction competition for the reaction between electron-rich alkynes and acyclic azodicarboxylates and the synthesis of five-membered N-heterocycle: Tetrahydroindoles.

3.2.1 Introduction

With the hope of exploring this chemistry even further, we wished to investigate the competition between our initially developed [2+2] cycloaddition and the traditional ene reaction. A typical ene reaction is a reaction between an ene component (*eg:* alkene, alkyne, C-heteroatom bond) and the enophile (*eg:* C=C, C=O, C=N, N=N) to form the ene product while breaking and forming bonds in a concerted fashion (Scheme 3.5, Eq. 1).

In previous studies, particularly acyclic azodicarboxylates have shown ene reactions with acyclic olefins, cyclic mono-olefins, and cyclic di-olefins.[51–55] For example Bis(2,2,2-trichloroethyl) azodicarboxylate (**III-6d**) formed the ene product with cyclic mono olefins such as cyclohexene (**III-18**) under thermal conditions (Scheme 3.5, Eq. 2).[53] Furthermore, under catalytic conditions such as in the presence of $SnCl_4$ at cryogenic temperatures, cyclohexene (**III-18**) and diethyl azodicarboxylate (**III-6a**) were found to rapidly form the corresponding ene product (**III-20**) (Scheme 3.5, Eq. 3).[52]

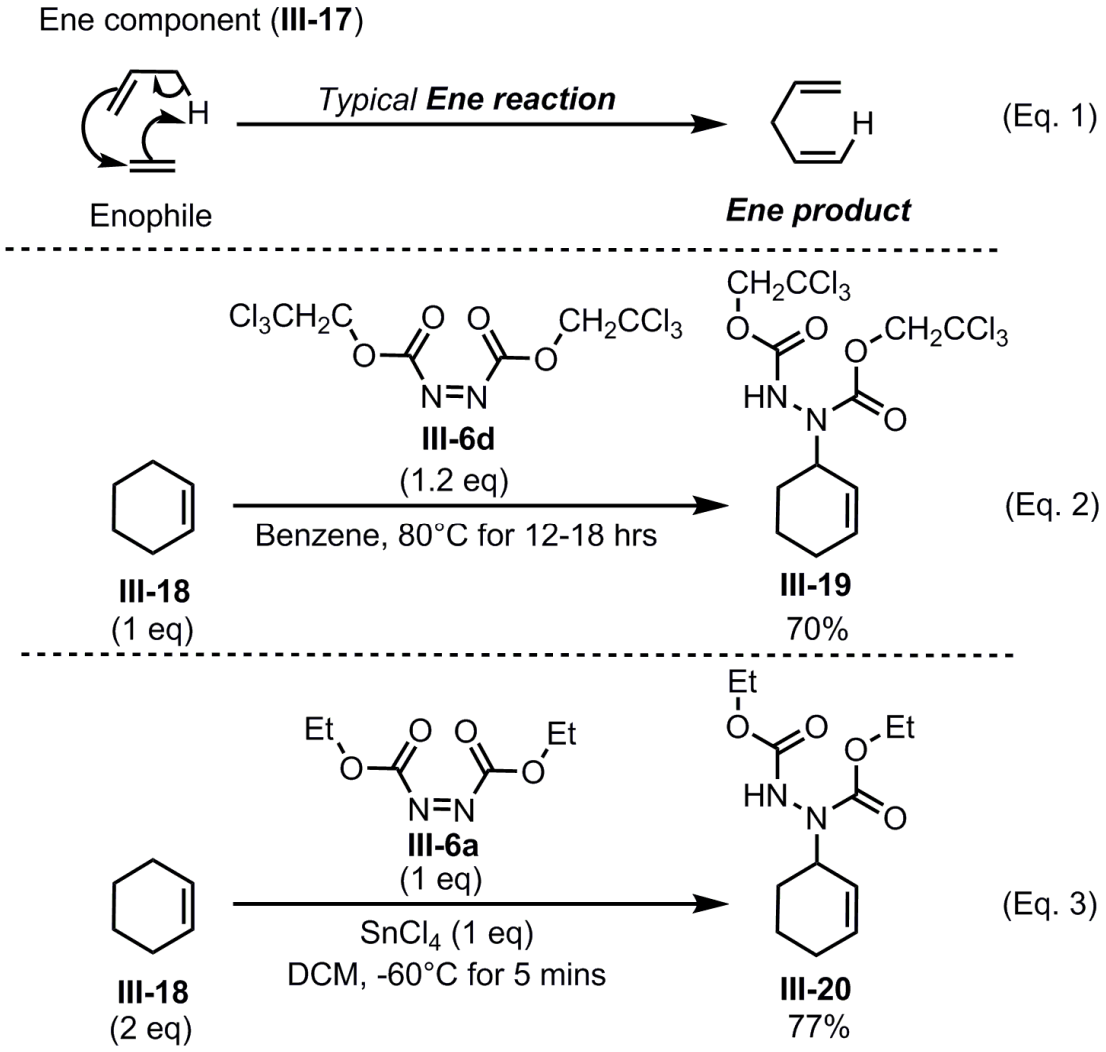

Scheme 3.5. Related examples of the formal ene reaction of azodicarboxylates.

These previous ene reaction examples of the acyclic azodicarboxylates inspired us to evaluate whether the ene reaction might compete with our previously developed [2+2] cycloaddition reaction. In order to study this competition, we selected a model compound, cyclohexenyl sulfide **III-26**, which bear cyclic olefin functionality with allylic hydrogens that could in principle undergo competing ene reaction along with required electron rich alkyne functionality to perform the [2+2] cycloaddition (Scheme 3.6).

3.2.2 Testing the Ene reaction competition with a model compound

In order to start these studies we first selected a couple of acyclic azodicarboxylates (*i.e.*, **III-6a** (DEAD), **III-6d** (TCEAD)) and reacted them with the model compound **III-26** under reflux conditions using common solvents such as dichloromethane, acetonitrile, and toluene. If the substrate undergoes an ene reaction, it could possibly form two different ene products due to the presence of two different allylic positions on the model compound **III-26** (Scheme 3.6).[51–54] However, if the reaction predominantly follows the [2+2] cycloaddition route, it will first form the monocyclic diazacyclobutene (**III-7u**) and then it will convert into the corresponding 2-iminothioimidate (**III-8u**) via 4π-conrotatory ring opening similar to what we have discussed earlier in this chapter (Section 3.1).[11] Interestingly, we saw that the thermal reaction between the cyclic enyne sulfides (**III-26**) and acyclic azodicarboxylates predominantly follow the [2+2] cycloaddition pathway, without any detectable amounts of ene products.

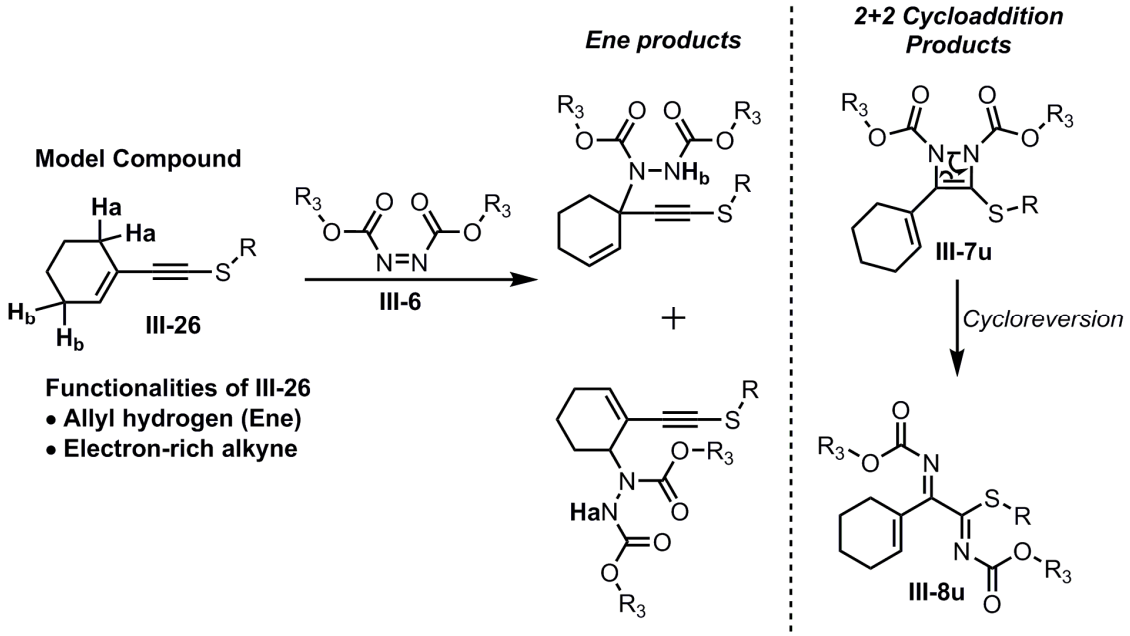

Scheme 3.6. Competition between the formal ene reaction and the initially developed [2+2] cycloaddition.

In order to understand this competition even better, it is important to know the possible reaction pathways of the thermal ene reaction of cyclic olefins and acyclic azodicarboxylates. In previous studies, researchers have broadly investigated the thermal ene reaction between acyclic azodicarboxylates with cyclic mono-olefins and cyclic dienes.[56–58]

Moreover, literature studies suggest that "ene reaction" of cyclic mono-olefins with acyclic azodicarboxylates follows more likely a stepwise (*i.e.,* diradical) pathway, as the principle mode of reaction due to the entropic or energetic favorability (Scheme 3.7).[56] If acyclic mono-olefin **III-17** follows a radical pathway during the ene reaction with acyclic azodicarboxylates, in the propagation step, it will react with a radical intermediate **III-21** and form the diradical **III-22** (Scheme 3.7, Eq. 1). During this process, **III-17** will lose the rotation around the C-C single bond which will lead to an unfavorable entropy change between the ground state **III-17** and the transition state of the process. Due to this phenomenon, acyclic mono-olefins are unlikely to follow a diradical pathway during this ene raction. In contrast, cyclic mono-olefins such as cyclohexene **III-18** will not have such an entropy change to form the diradical **III-24** due to the restricted geometry in the ground state (Scheme 3.7, Eq. 2). Thus cyclic mono-olefins favor the diradical or the stepwise pathway during this ene reaction.[56]

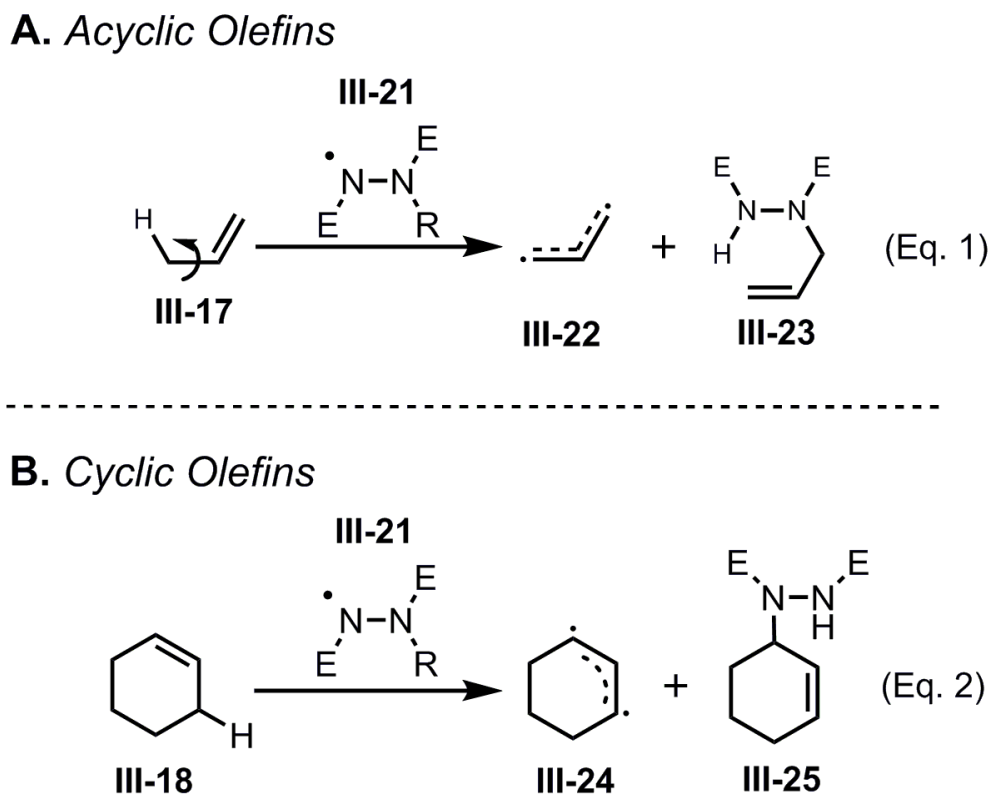

Scheme 3.7. Comparison of the plausible mechanism of formal ene reaction between acyclic and cyclic mono-olefins with azodicarboxylates.

On the other hand, the [2+2] cycloaddition between electron rich alkynes and the azodicarboxylates is a highly asynchronous process and it could either be accomplish via a concerted or stepwise manner.[11] Therefore, we believe that the [2+2] cycloaddition is an energetically favorable process in this competitive reaction compared to the stepwise diradical pathway under thermal conditions.

3.2.3. Substrate dependency and temperature dependency

When we further explore these ene vs. [2+2] cycloaddition competition reactions, we found an interesting substrate dependent and temperature dependent reactivity of the alkyl cyclohexenyl sulfides **III-26a** and the acyclic azodicarboxylates **III-6a** and **III-6d** (Scheme 3.8).When the alkyl cyclohexenyl sulfide **III-26** was reacted with diethyl azodicarboxylate (**III-6a**, DEAD) under the previously optimized thermal conditions (*i.e.*, refluxing acetonitrile, 24 h), the corresponding 2-iminothioimidate **III-8v** (R_2 = Me) and **III-8w** (R_2 = Et) was formed in good yields (66% and 68% respectively) (Reaction 1, Scheme 3.8). In contrast, when the same reaction condition was used with cyclohexenyl sulfide **III-26a** while changing the azodicarboxylate substrate to a more electrophillic bis(2,2,2-trichloroethyl) azodicarboxylate (**III-6d**, TCEAD), the 2-iminothioimidate (**III-8x**) was generated in 33% yield, and another new compound, tetrahydroindole (**III-27a**) was isolated in 12% yield (Reaction 2, Condition B, Scheme 3.8). This substrate dependency of the reaction surprised us. In addition, when the same reaction was performed at dichloromethane reflux condition, it was only provided the 2-iminothioimidate product in 36% yield (Reaction 2, Condition A, Scheme 3.8).

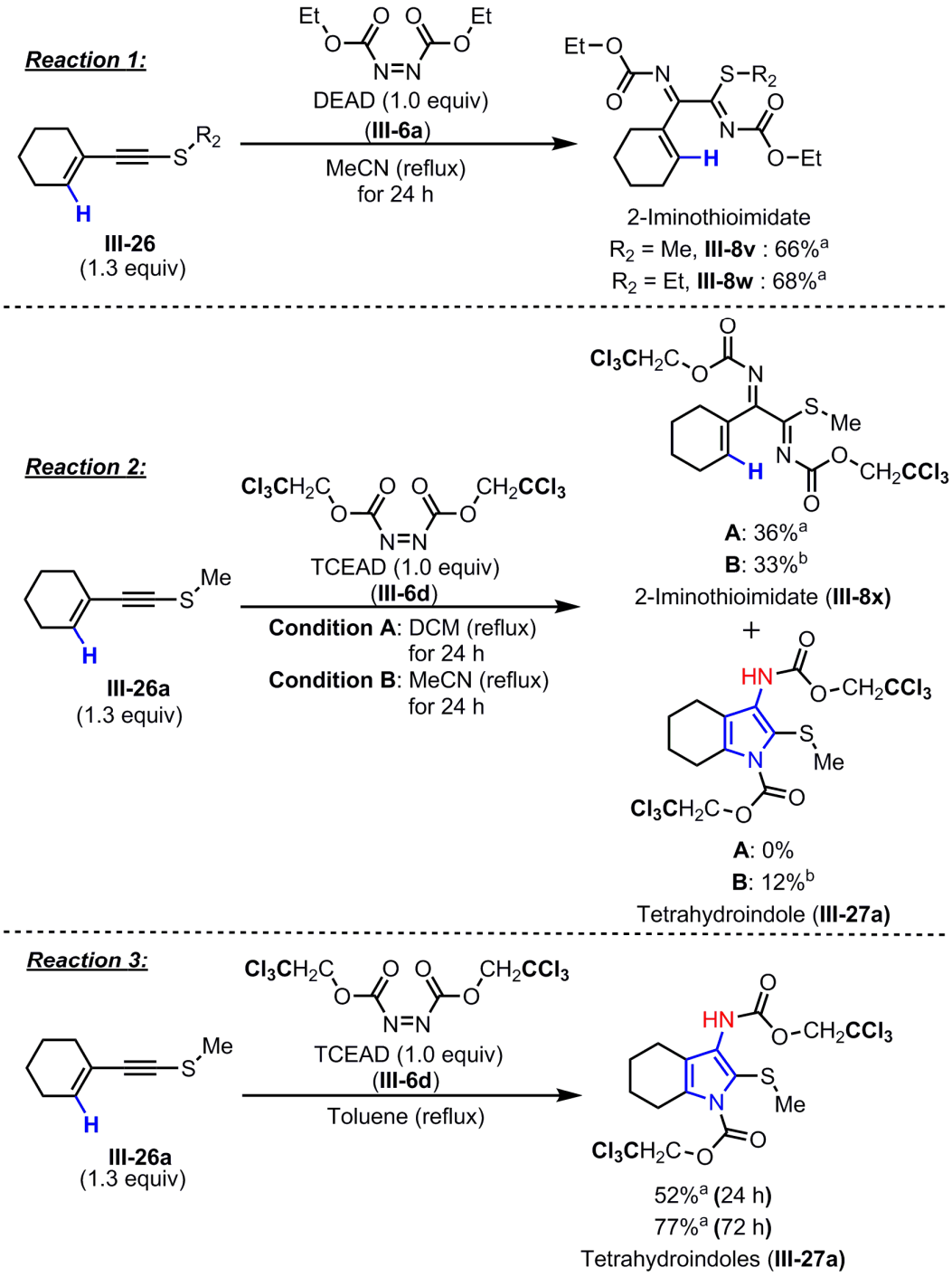

Scheme 3.8. Substrate dependency and different solvent reflux studies of the tetrahydroindole synthesis. (Note: a = isolated yields, b = ^{1}H NMR integration ratio of the crude product)

Furthermore, upon performing the reaction with TCEAD at a higher temperature in refluxing toluene, it provided 52% of the tetrahydroindole **III-27a** in 24 hours and 77% of the tetrahydroindole **III-27a** in 72 hours with no evidence of the 2-iminothioimidate product (Reaction 3, Scheme 3.8). One of the disadvantages we observed in the ^{1}H NMR spectrum is that the signals for the vinyl hydrogen of the corresponding 2-iminothioimidate and the hydrogen of the NH group of tetrahydroindole product (**III-27a**) both comes around the same chemical shift as a broad singlet which makes it difficult to distinguish these products.

However, we were able to confirm the two different products generated with DEAD and TCEAD by means of 2D-HMQC analysis (Figure 3.9 and 3.10). Figure 3.9 shows the 2D-HMQC analysis of the 2-iminothioimidate **III-8v**, and Figure 3.10 shows the 2D-HMQC analysis of thetetrahydroindole **III-27a**. It is important to note that the 2-iminothioimidate **III-8v** has a vinyl hydrogen directly attached to a vinyl carbon whereas in the tetrahydroindole product **III-27a**, that vinylic proton no longer exists due to the fused six and five membered rings. This is evidently seen in the 2D-HMQC analysis where the 2-iminothioimidate (**III-8v**) has a cross peak which is directly correlated to a carbon at 146 ppm (Figure 3.9) whereas tetrahydroindole (**III-27a**) does not have any cross peaks in the 2D-HMQC spectrum suggesting that the hydrogen is no longer attached to the carbon (Figure 3.10). Furthermore, the inset of the Figure 3.9 shows evidence for the characteristic isomerization process of the 2-iminothioimidate **III-8v** for the vinyl hydrogen signal in the ^{1}H NMR at very low temperature in $CDCl_3$.

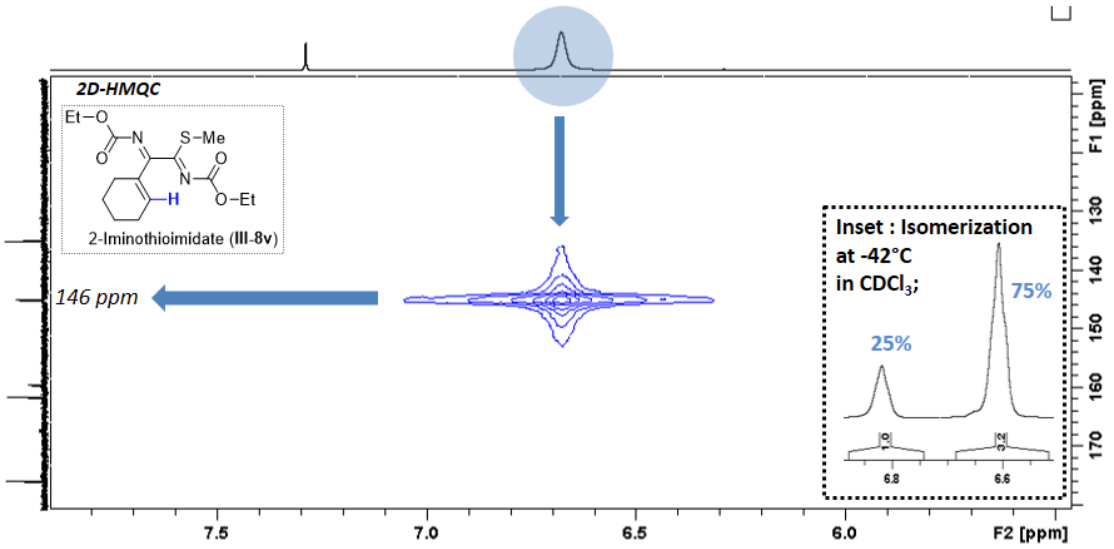

Figure 3.9. 2D-HMQC analysis of 2-iminothioimidate **III-8v**.

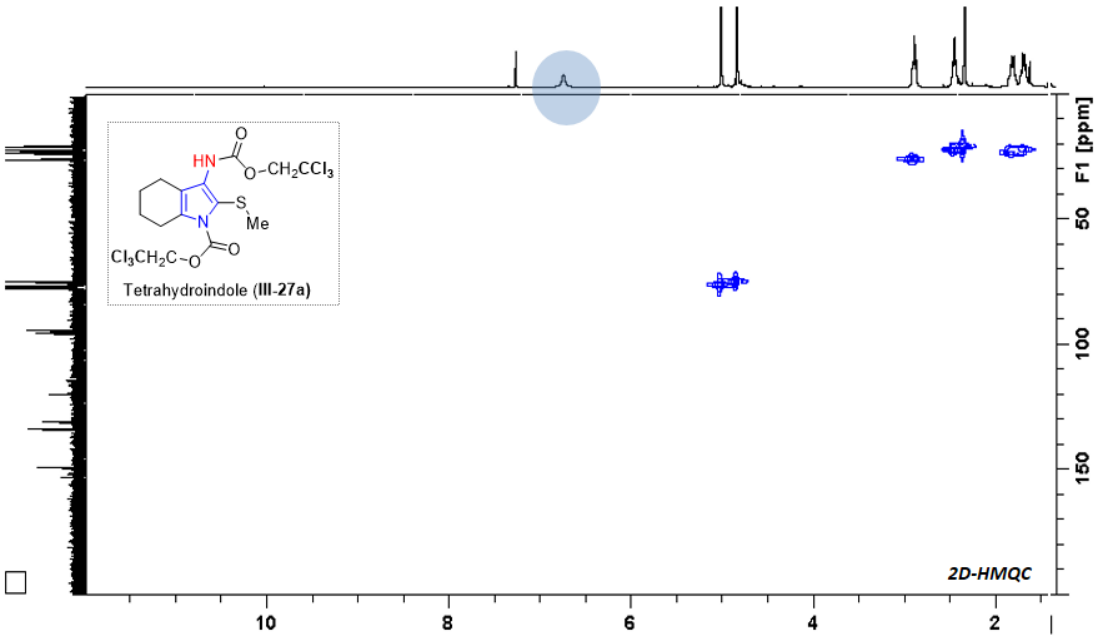

Figure 3.10. 2D-HMQC analysis of tetrahydroindole **III-27a**.

Additionally, the same scenario of the formation of 2-iminothioimidate was proved with an additional cyclohexenyl thio-alkyne substrate bearing an S-Ethyl group as well as with an azodicarboxylate substrate; di-isopropyl azodicarboxylate (DIAD). These results further confirm the substrate dependency and the temperature dependency of this tetrahydroindole synthesis with cyclohexenyl sulfides and acyclic azodicarboxylates.

3.2.4. Mechanism of the tetrahydroindole synthesis

Based on our initial understanding of this [2+2] cycloaddition reaction[1,3,9,11] and the experimental evidence, we proposed a mechanism for the synthesis of tetrahydroindoles which is outlined in Scheme 3.9. First, the alkyl cyclohexenyl sulfide can perform the [2+2] cycloaddition with the bis(2,2,2-trichloroethyl) azodicarboxylate (TCEAD) to form the monocyclic diazacyclobutene intermediate. As we described earlier, this diazacyclobutene intermediate is rather unstable and forms the corresponding 2-iminothioimidate via facile cycloreversion. Now this particular 2-iminothioimidate generated from the enyne sulfide and TCEAD will have two distinct electronic regions in the same molecule which have been color coded in red and green in Scheme 3.9. α,β–unsaturated imine portion of the molecule which is indicated in red is more electrophilic and could act as a Michael acceptor whereas the imidate portion of the molecule highlighted in green could act as a Michael donor. Due to the two distinct electronic environments, this 2-iminothioimidate might undergo intramolecular aza-Michael addition to form intermediate **III-28**, followed by hydrogen transfer and aromatization to form the final tetrahydroindole product.

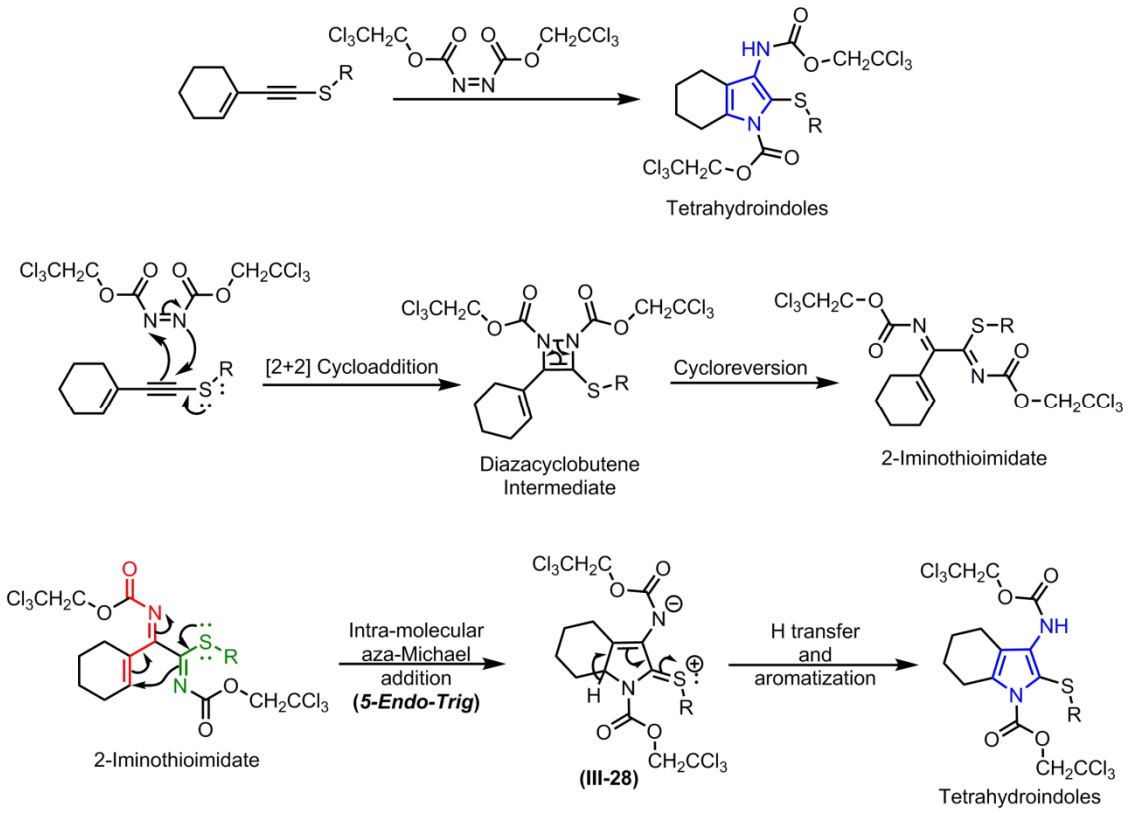

Scheme 3.9. Plausible mechanism of the tetrahydroindole synthesis.

It is interesting to note that the trichloroethyl groups in the TCEAD (**III-6d**) appear to provide sufficient electron withdrawing properties to the Michael acceptor portion of the molecule to facilitate the cyclization whereas DEAD (**III-6a**) evidently does not promote the cyclization to the tetrahydoindole. Intriguingly, according to Baldwin rules of cyclization, this particular transformation of intra-molecular aza-Michael addition to form the fused tetrahydroindole motif can be categorized under the 5-endo-trig cyclization which is well documented as a disfavored ring closure.[59–64] However, we believe that the 5-membered aromatic pyrrole ring that forms at the end of the transformation is governing this reaction to a thermodynamic sink which tips the balance in favor of tetrahydroindole formation.

We performed radical scavenger experiments in the presence of styrene or 1,1-diphenylethylene while running the same experiment for the tetrahydroindole synthesis and analyzed the GC-MS data in order to find any evidence of whether or not this reaction proceeds via radical intermediate.[65] However, these experiments failed to provide any evidence of radical intermediate during the reaction. Nevertheless, the precise mechanism of the 5-endo-trig cyclization is still vague and yet to be fully understood. Further experiments to understand this mechanism are currently underway.[66,67]

3.2.5. Biological importance and previous studies of the tetrahydroindoles.

In addition to the mechanistic interest, we are delighted about the synthesis of tetrahydroindoles due to their biological importance. A few examples highlighting the biological importance of the tetrahydroindoles and related motifs known as tetrahydrocyclopenta[b]pyrroles are highlighted in Figure 3.11.

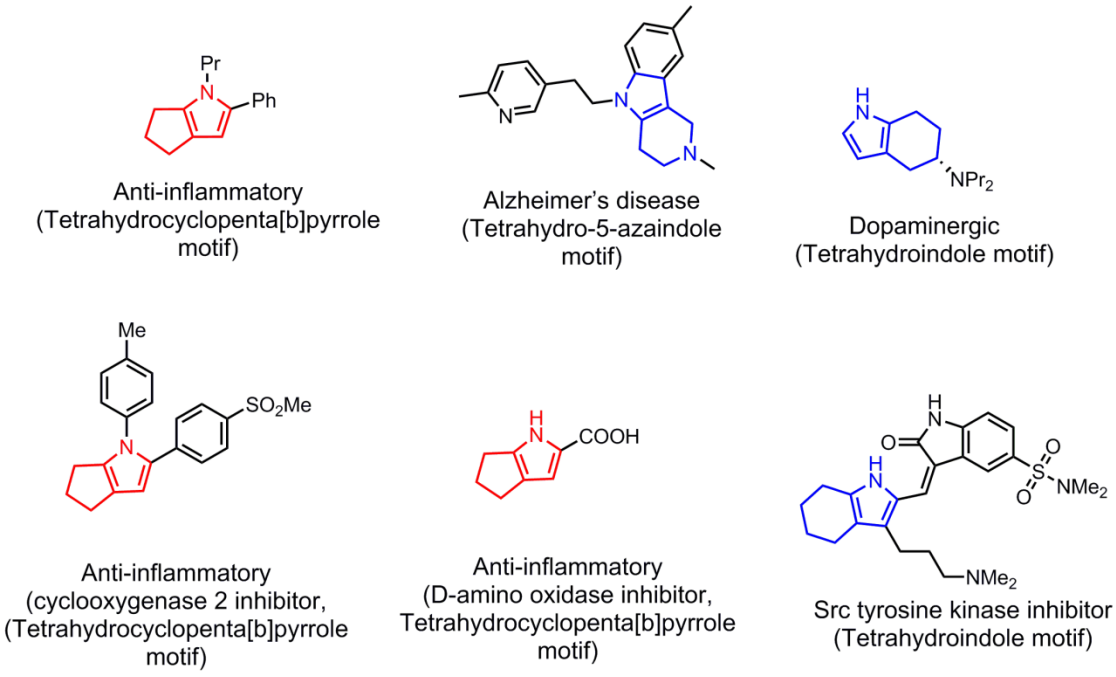

Figure 3.11. Biological importance of the tetrahydroindoles and tetrahydrocyclopenta[*b*]pyrroles.

These motifs are found in pharmacophores that serve as anti-inflammatory agents,[68] therapeutic agents of Alzheimer's disease,[69–71] dopaminergic drugs,[72] or inhibitors for cyclooxygenase 2,[73] D-amino oxidase[74] and Src tyrosine kinase.[75]

There are multiple different synthetic strategies that have been developed to synthesize tetrahydroindole derivatives in the past.[73,76–91] These reactions often involve pyrolysis,[76] olefin metathesis,[88] catalytic hydrogenation and dehydrogenation strategies,[82,83,90] cascade reactions[77,81,84–87] with substitution, addition and rearrangements. Some of the recent and frequently used strategies are outlined in the Scheme 3.10. One of the common approaches used to produce tetrahydroindoles is converting cyclic mono or di-ketones to the corresponding tetrahydroindole derivative via cyclic oximes or enamines.[77,78,81,84–87,91] This approach has been recently utilized in a one-pot synthetic operation to obtain 44% of the tetrahydroindole (**III-31**) via cyclohexanone (**III-30**) (Scheme 3.10 Eq. 1).[87]

Another divergent method has been used to synthesize tetrahydroindole derivatives via the catalytic ring expansion of propargylic aziridines (**III-33**) (Scheme 3.10 Eq. 2).[79] However this method required multiple steps to produce the propargylic aziridine precursor prior to the synthesis of tetrahydroindoles. A majority of protocols have employed catalytic and thermal 5-endo-dig cyclizations to form the tetrahydroindole motif. For example amino propargylic alcohols such as **III-35** are often used as the key starting material to produce tetrahydroindoles (Scheme 3.10 Eq. 3).[80]

Recently, a [2+2+1] annulation reaction has been developed by Malone *et al.* with cyclic α-hydroxy silylenol ethers (*eg:***III-37**) by reacting that with silylenol ethers (*eg:* **III-38**) and primary amine nucleophiles to obtain a diverse array of tetrahydroindole and tetrahydrocyclopenta[b]pyrroles derivatives in moderate to excellent yields (Scheme 3.10 Eq. 4).[73]

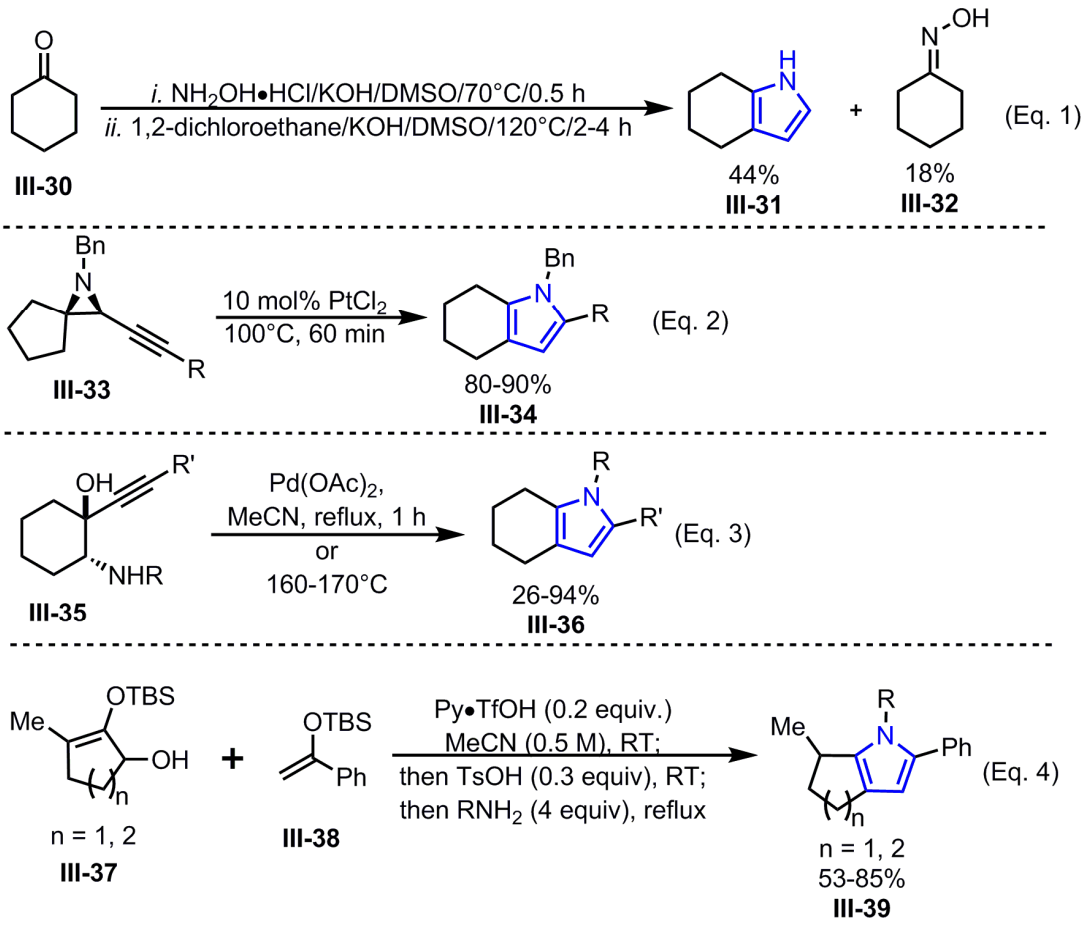

Scheme 3.10. Recent examples of the synthesis of tetrahydroindoles.

3.2.6. Optimization and the scope of tetrahydroindoles.

Regardless of the previous attempts on synthesizing tetrahydroindoles, we believe that the methodology that is described here is a unique strategy to form highly substituted tetehydroindoles with an interesting and unprecedented 5-endo-trig cyclization mechanism. Furthermore, it is interesting to note that in literature studies, highly substituted tetrahydroindoles (*eg:* **III-27a** in Scheme 3.8) are scarce.

Thus, we set out experiments to optimize the reaction conditions for the tetrahydroindole synthesis with methyl cyclohexenyl sulfide (**III-26a**) and bis(2,2,2-trichloroethyl) azodicarboxylate (**III-6d**) (Table 3.2). We first used our previously optimized conditions (*i.e.*, MeCN reflux for 24 h and 1:1.3 equiv of TCEAD: thio-alkyne) to provide the corresponding tetrahydroindole **III-27a** (entry 1,Table 3.2). We found that even after isolation via flash silica gel chromatography, there was some remaining 2-iminothioimidate (**III-8x**) left over in the product. This is presumably due to the similar polarities of both 2-iminothioimidate (**III-8x**) and the tetrahydroindole (**III-27a**), causing them to elute at the same time. Since both compounds (**III-8x** and **III-27a**) have the same molecular weight, we determined that 12% of the tetrahydroindole product **III-27a** was formed based on the weight of the isolated crude product and the ^{1}H NMR integration ratio analysis.

Because both 2-iminothioimidate **III-8v** and the tetrahydroindole **III-27a** have a tendency to elute at the same time and because the ^{1}H NMR signals for the vinyl

hydrogen of **III-8v** and the hydrogen for the NH group of **III-27a** both appear at the same ppm, all of the optimization experiments were further confirmed with 2D-HMQC analysis and ^{13}C NMR in order to distinguish these two compounds. Thus, the acetonitrile reflux time of the reaction was lengthened to 72 h and 21% yield of the tetrahydroindole product **III-27a** was isolated (entry 2, Table 3.2). Next, the reaction was refluxed with toluene for 24, 48 and 72 h and these attempts provided the tetrahydroindole product in 52%, 80% and 77% yields, respectively (entry 3-5).

Later, it was found that the results of the 48 h attempt had minor impurities of the 2-iminothioimidate (**III-8x**). However, isolation of the tetrahydroindole **III-27a** after 72 h resulted in a clean product presumably due to the longer reaction time provided for a thermal clean-up of the remaining 2-iminothioimidate intermediate by converting it to the final product.

In order to see whether the reaction time could be shortened with a catalyst, the reaction was refluxed in toluene for a shorter period of time such as for 24 h in the presence of a Lewis acid such as 10 mol% $MgCl_2$, which resulted 64% of the **III-27a** (entry 6). The selection of the $MgCl_2$ as a catalyst was decided after performing this reaction with a variety of different potential catalysts which will be described later in this discussion. Then the gradual decrease of the equivalence of the methyl cyclohexenyl sulfide **III-26a** resulted in significant drop in yield from 80% to about 40% yield (entry 7-9). It is important to note that optimization efforts under reflux conditions with higher

boiling solvents such as DMSO and DMF did not show any evidence of the tetrahydroindole product.

Table 3.2. Optimization of the tetrahydroindole synthesis.

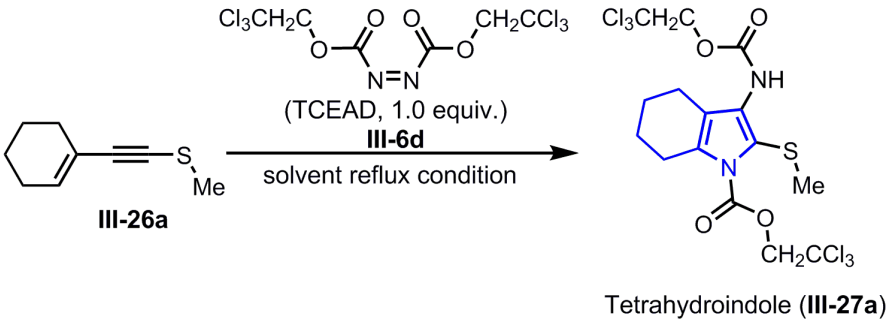

Entry	Solvent	Reflux time (h)	Equiv. of the Thio-alkyne	Yield%[a]
1	MeCN	24	1.3	12[b]
2	MeCN	72	1.3	21
3	Toluene	24	1.3	52
4	Toluene	48	1.3	80[b]
5	**Toluene**	**72**	**1.3**	**77**
6[c]	Toluene	24	1.3	64
7	Toluene	72	1.2	72
8	Toluene	72	1.1	32
9	Toluene	72	1.0	45

a = Isolated yields, b = isolation and NMR integration ratio, c = 10 mol% $MgCl_2$ was used.

Next, we screened this reaction with different additives and catalysts at room temperature and reflux conditions with lower boiling solvents, in order to see the possibility of performing this reaction at milder conditions than the vigorous thermal conditions for a longer period. In all of these screening attempts, the crude mixture was carefully analyzed by ^{1}H NMR and 2D-HMQC to verify the evidence of the tetrahydroindole product prior to the purification step in order to facilitate a rapid catalytic screening.

We initially tested additives such as weak bases and Lewis bases (*eg.*. K_2CO_3, triphenylphosphine, and triethylamine) and found that these bases inhibit the reaction by quickly reacting with the azodicarboxylate (**III-6d**, TCEAD). Then we tested a series of Lewis acid catalysts such as alkali earth metal (Mg(II)),[92] metalloids (BF_3•Et_2O), transition metals (Sc(III),[93,94] Ti(IV), Cu(II),[95] Zn(II), Ag(I)), post-transition metals (Al (III), Sn(IV),[96] In (III)),[97] and none of them provided the tetrahydroindole product.

Furthermore, since the *5-endo-trig* cyclization from the 2-iminothioimidate to tetrahydroindole (*see* **Scheme 3.9**) is similar to Nazarov cyclization, we employed several Nazarov reaction conditions to see this approach facilitated the reaction. However, the Nazarov reaction conditions with catalytic amounts of *para*-toluenesulfonic acid, triflic acid, and camphor sulfonic acid were unable to produce any evidence of the tetrahydroindole product.[98–104] Interestingly, 10 mol% of $MgCl_2$ in DCM for 72 h at room temperature resulted 41% of the clean 2-iminothioimidate product. In recent catalytic

combination studies, for instance Mg(II) coupled with Cu(II) was able to produce trace evidence of the tetrahydroindole product. These results gave us optimism to further explore a new catalytic system to synthesize tetrahydroindoles in a more convenient fashion. Further catalytic attempts are an active area of study in our laboratory.

Nevertheless, based on all these observations so far, we settled on the conditions in entry 5 (highlighted in bold in Table 3.2) as our current optimized reaction conditions to explore the substrate scope limits of the tetrahydroindole synthesis. To begin, we first synthesized a standard series of enyne sulfides (**III-26**) by changing the R_2 group (Scheme 3.11). We used the same *n*-butyl lithium protocols to perform this synthesis which was described earlier (in Chapter 2, Section 2.2, Tables 2.1 and 2.2).[105–107] Using this established protocol, a set of alkyl cyclohexenyl sulfides bearing shorter and longer alkyl chains or aryl groups (*eg:* benzyl group) at the R_2 position were synthesized in moderate to excellent yields (**III-26a-g**, Scheme 3.11). In addition, by changing the chalcogen atom from sulfur to selenium; two cyclohexenyne selenides (**III-26h** and **III-26i**) were also synthesized in excellent yields (*i.e.,* 93% and 94% yield, respectively). Moreover, methanebis(cyclohexenynlsulfane) **III-26j** was also synthesized which consist of two cyclohexenynl units bridged by sulfur-methelene-sulfur linkage in rather low yield (*i.e.,* 24%).

Furthermore, with the hope synthesizing the corresponding pyrroles by utilizing the same *5-endo-trig* cyclization reaction with acyclic enyne sulfides, two additional

analogues of the enyne sulfide **III-29a-b** were prepared from 3-buten-1-yne by applying the established *n*-butyl lithium protocols (Scheme 3.11). However, these acyclic enyne sulfides **III-29a-b** were used as crude products due to their high volatility. Due to the volatility of **III-29a-b**; another enyne sulfide **III-29c** was synthesized which consist of an S-benzyl group in 71% yield.

We then employed the optimized conditions (*i.e.*, refluxing toluene, 72 h) to synthesize our first series of tetrahydroindoles bearing different S-alkyl or aryl groups (Scheme 3.12). Cyclohexenyl sulfides bearing shorter S-alkyl chains such as methyl, ethyl, *n*-propyl, and *n*-butyl were successfully converted into their corresponding tetrahydroindoles **III-27a-d** in 72-79% yields. Substrates bearing long S-alkyl chains (*i.e.*, *n*-pentyl, *n*-octyl) afforded tetrahydroindoles **III-27e-f** in 77% and 83% yields, respectively.

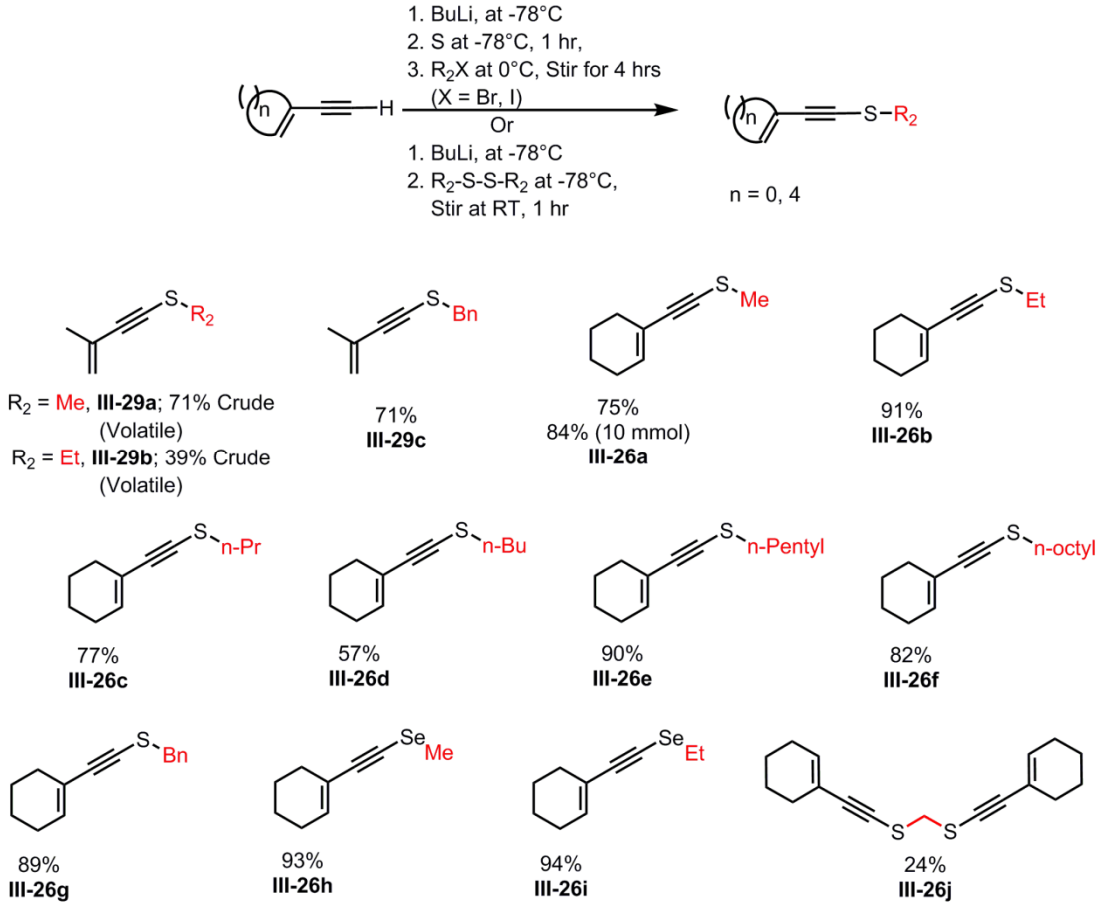

Scheme 3.11. Enyne sulfide synthesis.

In contrast, the S-benzyl analogue of the tetrahydroindole derivative **III-27g** was formed in a rather poor yield (29%). This lower yield resulted presumably due to the less tolerance of the S-benzyl group bearing cyclohexenyl sulfide **III-26g** to a longer reflux time in toluene at very high temperature (*ca.* 110˚C). This was evident by TLC analysis that indicated the absence of the cyclohexenyl sulfide after the reaction was completed. Also, by performing the reaction with the cyclohexenyl selenides the analogous selenium derivative of the tetrahydroindole **III-27i** was formed in lower yield (31%). However, the tetrahydroindole resulted from the methyl cyclohexenyl selenide (**III-26h**) showed some minor evidence of the 2-iminothioimidate intermediate in the NMR even after the purification due to the co-elution of the tetrahydroindole and the 2-iminothioimidate intermediate. Moreover, a gram scale preparation of **III-27a** was able to provide 1.01 g (64%) of the tetrahydroindole under the thermally optimized conditions.

On the other hand, the volatile enyne sulfides (**III-29a-b**) and the S-benzyl analog **III-29c** synthesized from 3-buten-1-yne were failed to provide the corresponding pyrrole product presumably due to the less tolerance to the 72 hrs toluene reflux conditions. This reaction failure was also reflected in the reaction with methanebis(cyclohexenynlsulfane) **III-26j**. We believe that the sulfur-methelene-sulfur linkage of **III-26j** is less tolerance to the toluene reflux conditions. Synthesizing more derivatives of these tetrahydroindole compounds is currently underway.

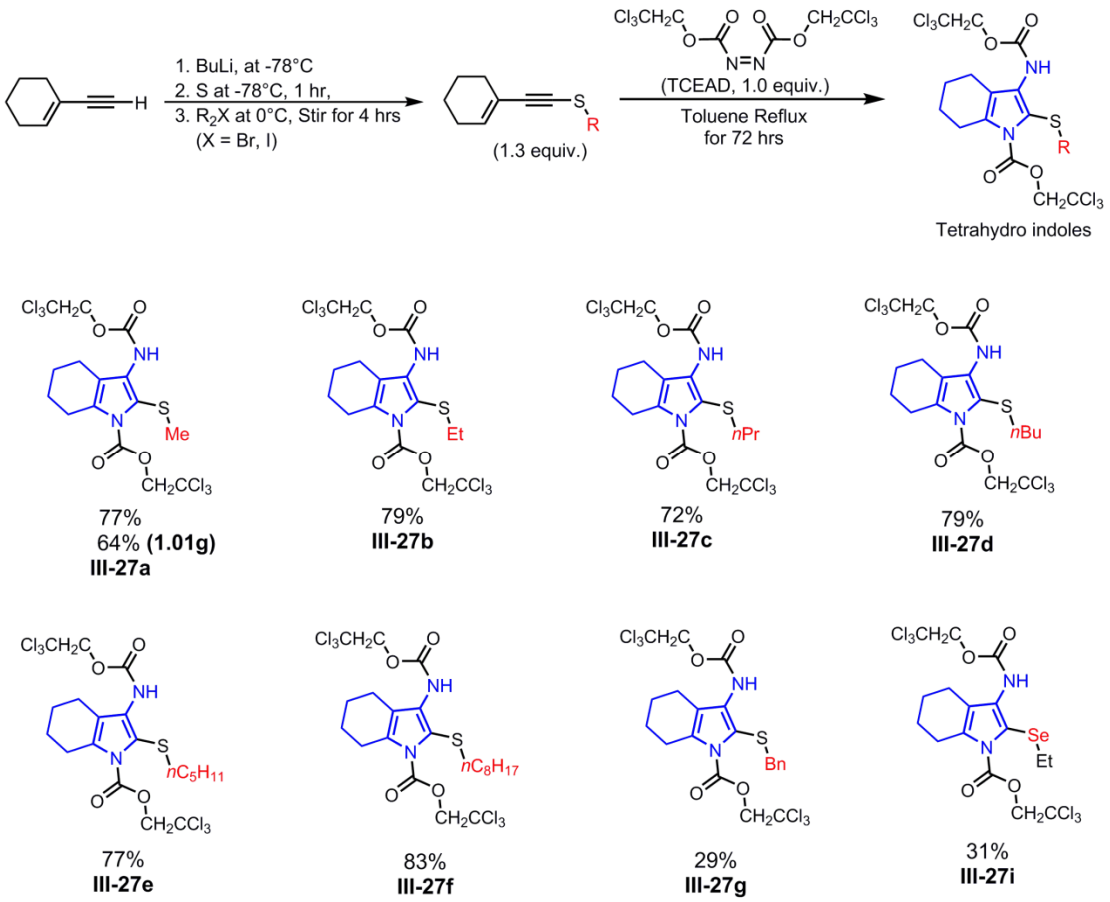

Scheme 3.12. Scope of the tetrahydroindoles.

3.2.7. Ongoing and future work of the tetrahydroindole synthesis

We then turned towards synthesizing different tetrahydroindoles starting with cyclic ketones which could allow us to change the cyclohexene side of the final product. However, changing the cyclohexene side of the molecule is not trivial compared to changing the R group at the chalcogen atom. One of the convenient strategies that we can follow is to start from a cyclic ketone such as **III-33** and form the corresponding tetrahydroindole in 5 synthetic steps (Scheme 3.13). First we can convert the cyclic ketone such as **III-33** into the corresponding vinyl triflate **III-34** and then synthesize the silyl protected alkyne **III-35** via Sonagashira coupling. Then by deprotection of the silyl group of **III-35** to obtain **III-36** followed by applying the *n*-butyl lithium chemistry to synthesize the corresponding cyclohexenyl sulfide **III-37** will allow us to perform the tetrahydroindole synthesis with TCEAD under the optimized conditions (Scheme 3.13).[79,108–111]

A similar strategy can be utilized to synthesize the corresponding pyrroles by starting from commercially available acyclic ketones which is illustrated in Scheme 3.14.[109,112–114]

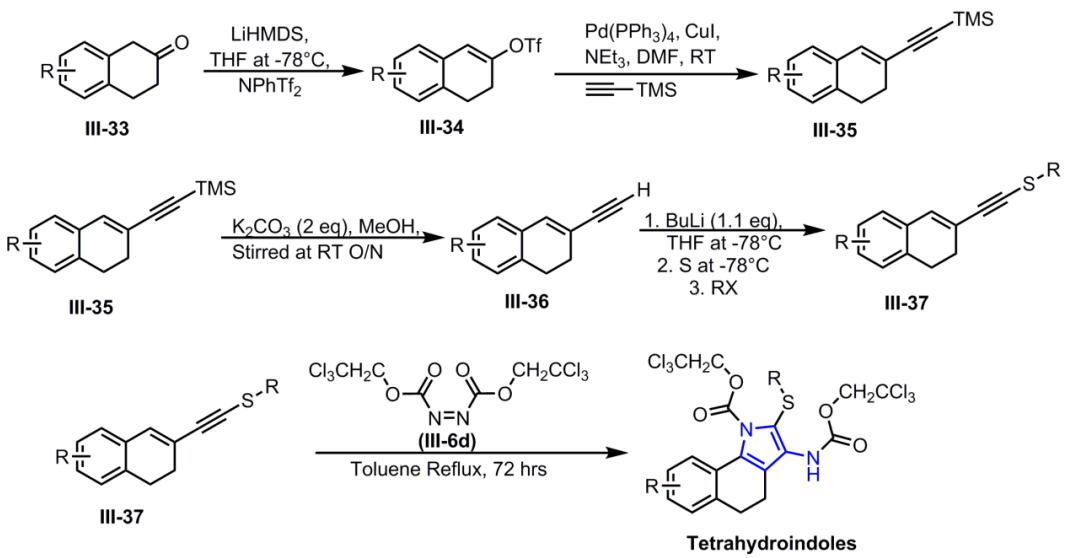

Scheme 3.13. Synthesis of the tetrahydroindoles using cyclic ketones.

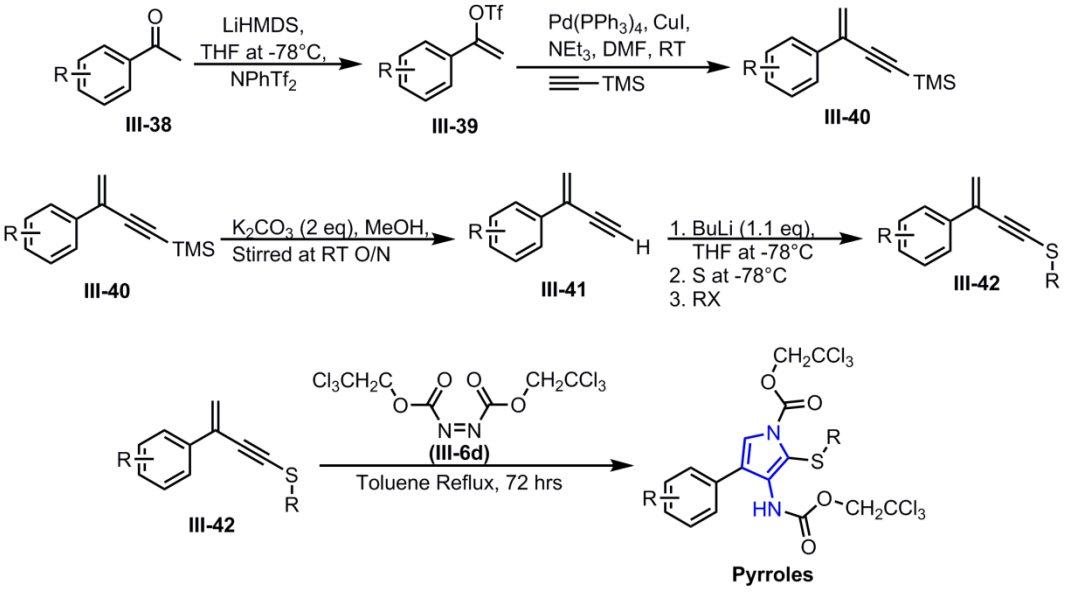

Scheme 3.14. Synthesis of pyrroles using acyclic ketones.

3.2.8. Conclusions

The analysis of the products from the competition between the Ene reaction and the initially developed [2+2] cycloaddition resulted an unprecedented reaction pathway to produce novel compounds known as tetrahydroindoles. We successfully designed a model reaction with alkyl cyclohexenyl sulfide and azodicarboxylates under thermal conditions to analyze the competition between the Ene reaction and the [2+2] cycloaddition.

This tetrahydroindole synthesis reaction deserves a special mention about the remarkable dependency of the reaction route based upon the nature of the azodicarboxylates that are employed. If the cyclohexenyl sulfide reacts with diethyl azodicarboxylate (DEAD), it will only form the 2-iminothioimidate whereas when the bis(2,2,2-trichloroethyl) azodicarboxylate (TCEAD) was used, it performs an extra step to form the tetrahydroindole product via *5-endo-trig* cyclization.

Intriguingly, this *5-endo-trig* cyclization is an *anti*-Baldwin pathway and little can be said at present about the actual reaction pathway. However, based on the initial radical scavenging experiments and the temperature dependency of the reaction, we believe that this reaction presumably going via an ionic intermediate similar to the Nazarov type intermediate and the aromatic pyrrole ring in the final product is facilitating the reaction to go through a thermodynamic sink to produce the most stable tetrahydroindole product.

Nevertheless, further mechanistic investigations are needed in order to elucidate the transition states and the driving force of this interesting *anti*-Baldwin cyclization.

We successfully synthesized the first series of the tetrahydroindole derivatives using different alkyl cyclohexenyl sulfides and the bis(2,2,2-trichloroethyl) azodicarboxylate (TCEAD) by applying the newly optimized thermal conditions (*i.e.*, refluxing toluene reflux for 72 h with 1.3 equiv. of the cyclohexenyl sulfide). Interestingly, the same synthetic approach can be applied to the synthesis of the pyrroles from acyclic alkenyl sulfides. Attempts to synthesize more derivatives of the tetrahydroindoles and pyrroles from acyclic and cyclic ketones are currently underway. With the inspiration from the initial catalytic screening studies, further work is also directed towards developing a one-pot tetrahydroindole and pyrrole synthesis at milder conditions under catalytic environment and these extensive catalytic screenings are currently underway in our laboratory.

3.3 Divergent reactivity in the presence of catalysts: Synthesis of six-membered 1,3,4-oxadiazin-2-ones.

As a result of extensive exploration of the chemistry between electron-rich alkynes and azodicarboxylates; we were able to uncover another novel reaction to synthesize a 6-membered *N*-heterocycle known as 1,3,4-oxadiazin-2-one with divergent reactivity of azodicarboxylates. When we treated a less reactive azodicarboxylate such as di-*tert*-butylazodicarboxylate (DTBAD, **III-6e**) with the phenylacetylene sulfide (**III-15b**), in the presence of 10 mol% of the AgOTf, a 6-membered 1,3,4-oxadiazin-2-one derivative **III-43** was isolated in 27% yield (*See* **Scheme 3.15**).[115] This interesting new class of oxadiazinone compound brought our attention to optimize and explore the scope limits of this synthesis.

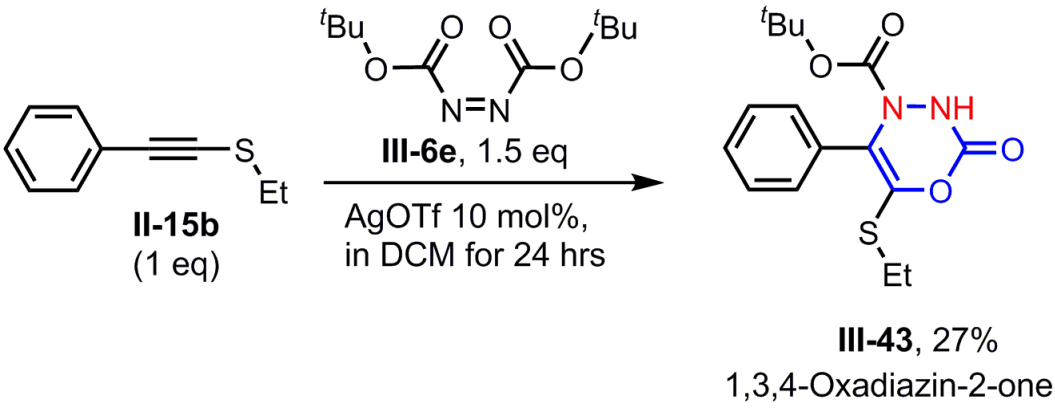

Scheme 3.15. Synthesis of 1,3,4-oxadiazin-2-one.

3.3.1. Oxadiazinones

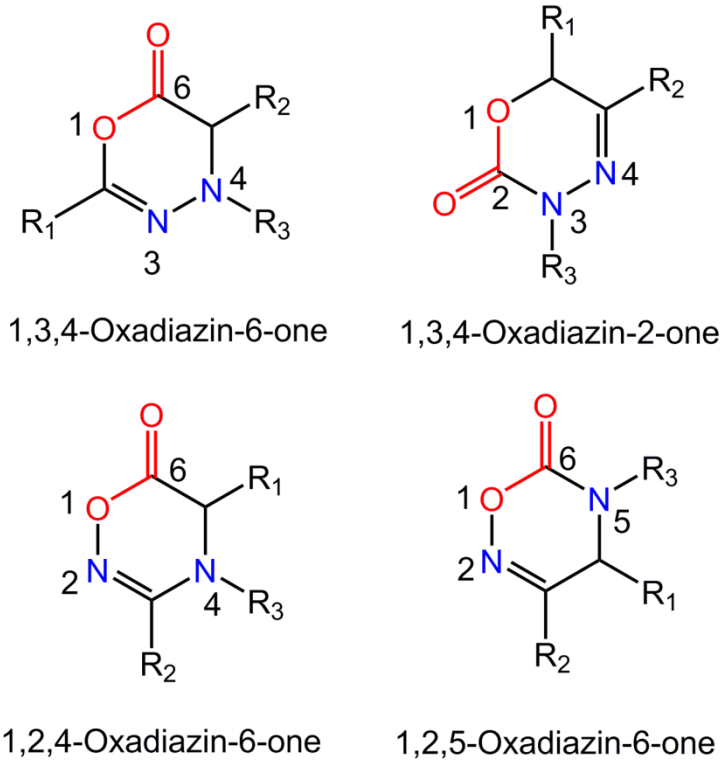

Figure 3.12. Various types of oxadiazinones.

Oxadiazinones are 6-membered heterocycles which contain oxygen, two nitrogens and carbonyl functionality. Depending on the position of these functionalities, the compounds are named differently (*See* **Figure 3.12**). Taken together, the oxadiazinones represent a highly useful scaffold because of a broad range of bioactivity such as antibacterial, antiviral, antiparasatic, antiflammatory, antifungal, *etc*.[116]

In 1977 Berkowitz *et. al.* examined a series of 1,2,4-oxadiazin-3-ones (**III-44**) and most of them showed evidence of antimicrobial and antifungal activity (**Figure 3.13**).[117] Dekeyser and co-workers reported biphenyl substituted 1,3,4-oxadiazin-5-ones (**III-45**) which showed good anti-parasatic activities such as miticidal and nematocidal properties.[118]

In addition, the Khan group synthesized 1,3,4-oxadiazin-5-one derivatives (**III-46**) bearing substituted phenyl and nitrile functionality. These structures have exhibited antibacterial and monamine oxidase inhibition.[119] In 2010, Sun and co-workers evaluated the insecticidal activity of 1,3,4-oxadiazin-5-ones (**III-47**) which were derivatized from cinnamic acid. These compounds have shown significant insecticidal activity and caused mortality of the *Culex pipiens* mosquito which is a vector of Japanese encephalitis disease.[120]

As a result of versatile pharmaceutical activity of this oxadiazinone moiety, most of the medicinal chemistry researchers have focused on investigating new synthetic protocols to access different derivatives of oxadiazinones and discover new biological activities related to these molecules.

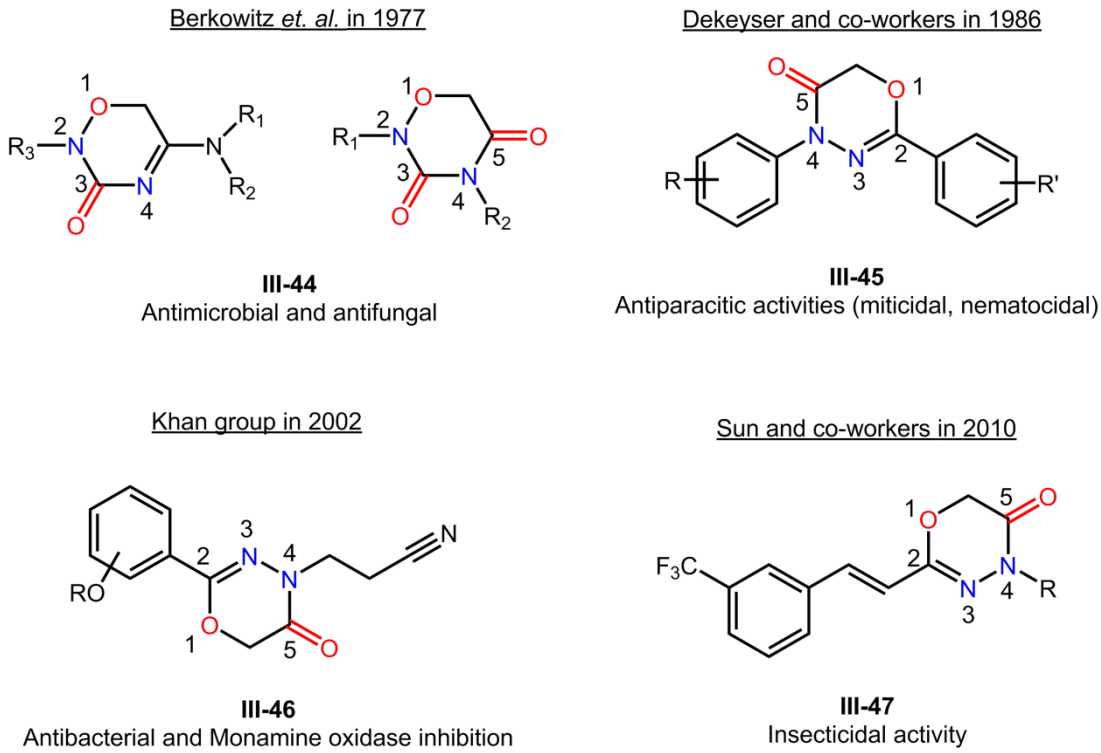

Figure 3.13. Examples of the versatile bioactivity of oxadiazinone derivatives.

3.3.2. Mechanistic investigations of the 1,3,4-oxadiazin-2-one synthesis

In order to understand the anomalous behavior of the di-*tert*-butylazodicarboxylate (DTBAD, **III-6e**) with the phenylacetylene sulfide (**III-15b**) in the presence of AgOTf, we started to perform mechanistic investigations. We hypothesized that this reaction could proceed via 2 possible pathways (*path a* and *path b*, Scheme 3.16). It is possible to envision that the Lewis acid, Ag(I), first interact with the DTBAD (**III-6e)** to form an ionic intermediate **III-48** which is comprised of a thioketene and silver carboxylate functionality. This intermediate **III-48** can then undergo *6-exo-di*g cyclization, followed by elimination of Ag(I) ion to form an unstable anti-aromatic intermediate **III-49**. Finally, this anti-aromatic intermediate **III-49**, could cleave off a *tert*-butyl group to produce the stable 1,3,4-oxadiazin-2-one **III-43**. This mechanistic route was assigned as *path a* in Scheme 3.16.

In order to assess the possibility of *path a*, DTBAD (**III-6e)** was treated with different amounts of catalyst (*i.e.*, AgOTf (0 mol%, 20 mol%, and 100 mol%) in $CDCl_3$ and, we acquired stacked ^1H NMR spectra (Figure 3.14). This evidently showed that upon increasing the loading of AgOTf, an extra shoulder of signal for the *tert*-butyl methyl protons started to appear and gradually increased its intensity upon increasing the amount of catalyst.

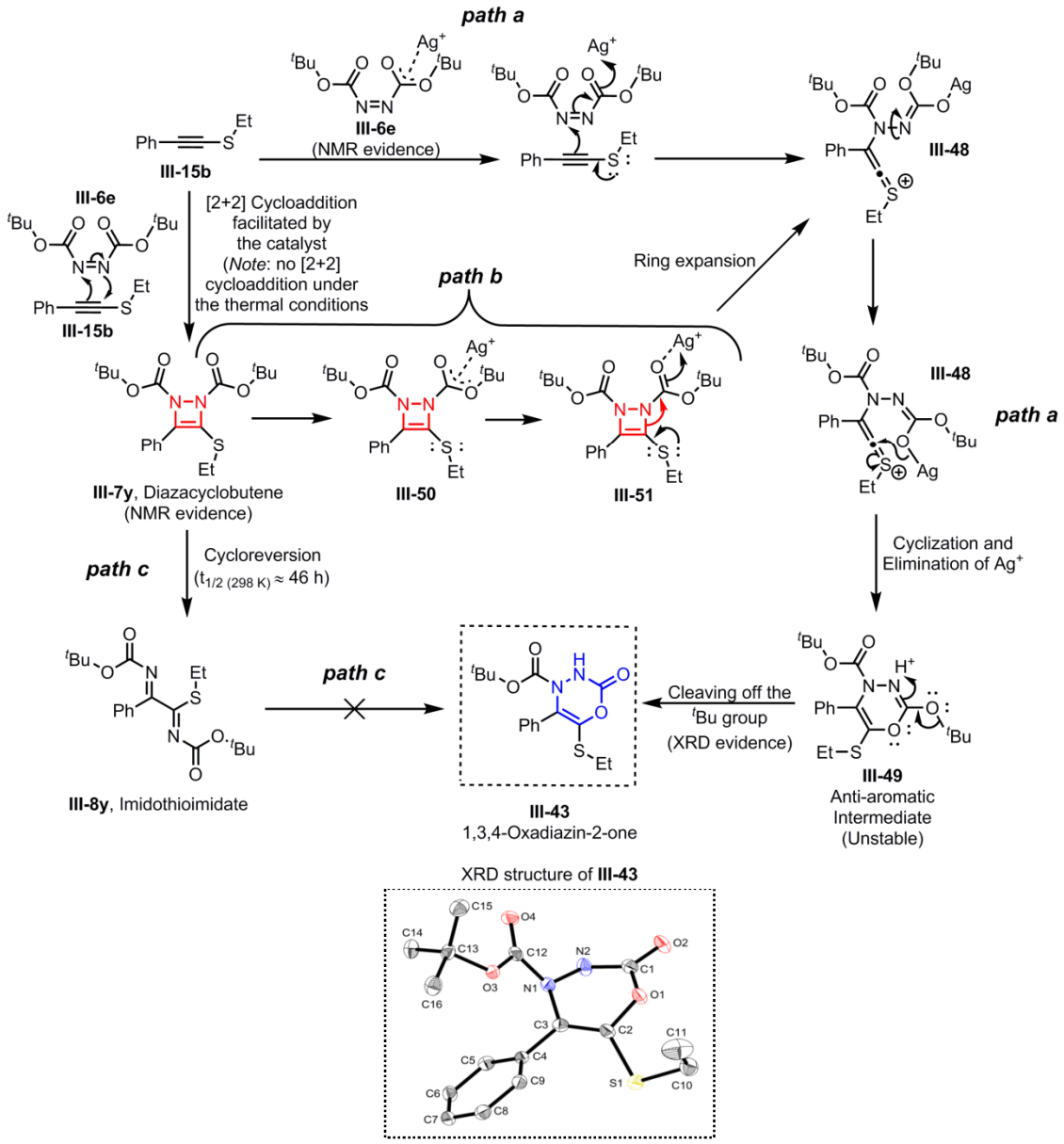

Scheme 3.16. Possible mechanism of the 1,3,4-oxadiazin-2-one **III-43** synthesis.

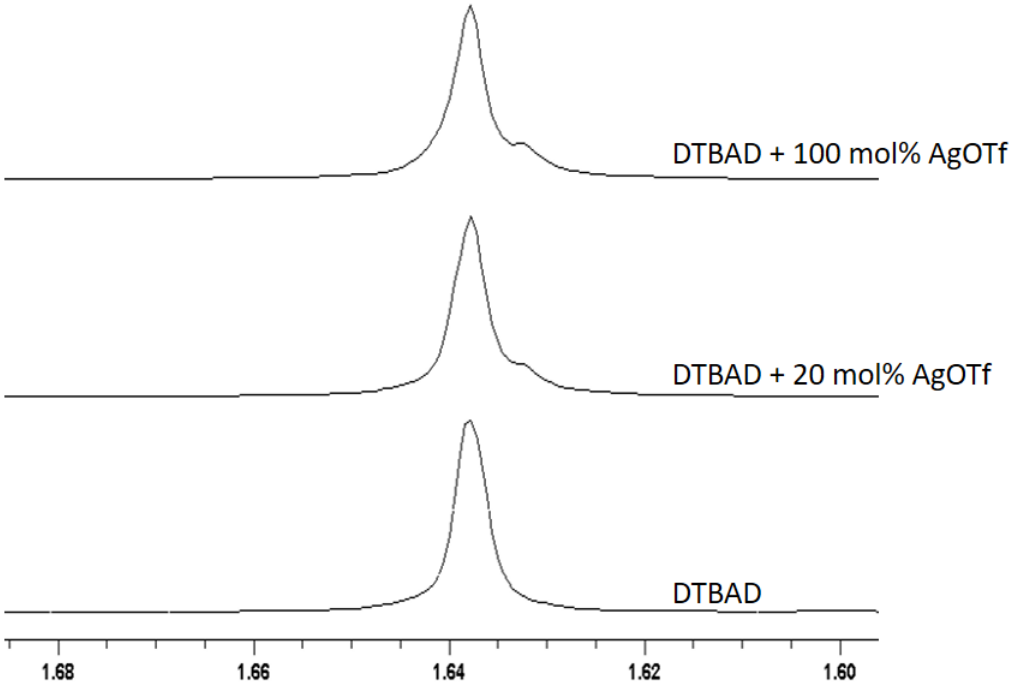

Figure 3.14. ^{1}H NMR stacked spectra of the *tert*-butyl methyl proton signal of di-*tert*-butyl azodicarboxylate (DTBAD, **III-6e**) under the different amounts of AgOTf in $CDCl_3$ at room temperature.

These results show the ability of the Lewis acid catalyst to interact with the DTBAD. Taking together the possibility of the formation of a thioketene dipole intermediate during the previously discussed [2+2] cycloaddition and the interaction of the Lewis acid, we can now assume that this reaction might first form a dipole intermediate **III-48** via the attack from the alkynyl sulfide onto the azo bond of the DTBAD and the simultaneous interaction of the Lewis acid.

The next key steps in this *path a* are the *6-exo-dig* cyclization which is a Baldwin-allowed transformation to form the *anti*-aromatic **III-49**, followed by cleaving off the *tert*-butyl group to form the final product. Even though the *tert*-butyl scavenging experiments to follow the *tert*-butyl cleavage step did not produce any evidence, we were able to find an indirect XRD evidence of a *tert*-butyl cleaved product **III-52** while performing the same reaction under reflux in toluene (Scheme 3.17). This product **III-52** is an *N-tert*-butyl substituted molecule of DTBAD, which indirectly proves the possibility of the *tert*-butyl cleaving step in *path a*.[121,122]

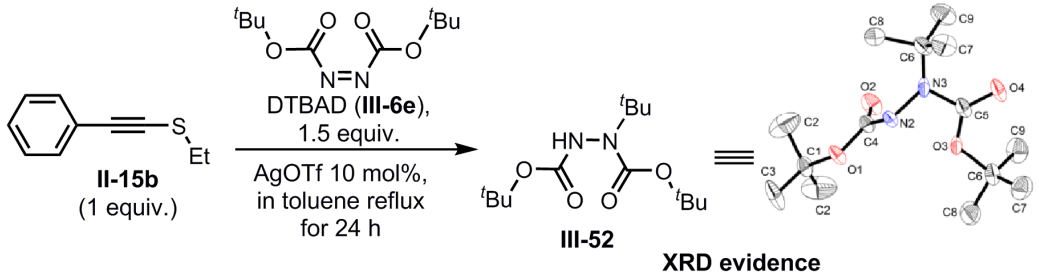

Scheme 3.17. Evidence of the *tert*-butyl cleaved product.

In addition, the final product: 1,3,4-oxadiazin-2-one **III-43** was further characterized by X-ray crystallography and returned consistent NMR data with the proposed, isolated product (Scheme 3.16).

On the other hand we are equally interested in *path* b, where the first step is the formation of previously known [2+2] cycloadduct **III-7y** followed by the interaction of **III-7y** with the Lewis acid to perform a ring expansion. This ring expansion pathway will form the intermediate **III-48**, which will consequently follow the consecutive steps in the same manner as *path a*. Compared to *path a* and *path b*, we can directly eliminate *path c*, which is the formation of the final product via 2-iminothioimidate **III-8y** due to the already cleaved N-N bond in the 2-iminothioimidate.

During the byproduct analysis of the Ag (I) catalyzed 1,3,4-oxadiazin-2-one synthesis reaction; we were able to isolate diazacyclobutene **III-7y** in very poor yield (<6%) which was readily identified by its fingerprint ^{13}C NMR peak at around 140 ppm. In contrast to the Ag(I) catalyzed reaction; we did not observe any of **III-7y** and **III-8y** under our previously optimized thermal conditions (*i.e.*, refluxing acetonitrile, 24 h), presumably due to the steric hindrance arising from the *tert*-butyl group which could inhibit the direct [2+2] cycloaddition under thermal conditions. In addition, since the half-life of the cycloreversion of the diazacyclobutene **III-7y** to 2-iminothioimidate **III-8y** is about 46 hrs; we can hypothesize that Ag (I) have enough time to perform a ring expansion reaction to activate the *path b* (Scheme 3.16). These observations suggest that

Ag (I) catalyzed [2+2] cycloaddition is also operative in this reaction and the validity of investigating the possibility of the ring expansion pathway (*path b*, Scheme 3.16). Attempting to obtain the 1,3,4-oxadiazin-2-one via slightly higher reflux temperatures than room temperature (*ca.* 40˚C) in the presence of the silver catalyst also failed to result in any improvements. This indirect evidence suggests that we were unable to favor *path b* under thermal conditions. We believe that *path a* and *path b* both are viable routes to form the final 1,3,4-oxadiazin-2-one product. However, further experimental and computational studies are underway in order to extract more information of this interesting reaction mechanism.

3.3.3. Optimization of the reaction conditions for 1,3,4-oxadiazin-2-one synthesis

In order to achieve synthetically useful yields of the 1,3,4-oxadiazin-2-one (**III-43**) product and to identify the optimum azodicarboxylate for this silver catalyzed reaction, we initially screened an electron-rich alkylacetylenesulfide such as ethyl phenylacetylene sulfide (**II-15b**) against a panel of common, commercially available azodicarboxylates such as diethyl azodicarboxylates (DEAD), di-*iso*-propyl azodicarboxylates (DIAD), di-*tert*-butyl azodicarboxylates (DTBAD), and dibenzyl azodicarboxylate (DBnAD) in the presence of 10 mol% of AgOTf catalyst.[115] As mentioned earlier, our initial screening of these experiments revealed that this reaction is also highly substrate dependent and DTBAD is required for this 1,3,4-oxadiazin-2-one synthesis.

Then we screened a series of Lewis acid catalysts that we identified from our previous catalytic studies for the reaction of ethyl phenylacetylene sulfide (**II-15b**) with DTBAD. We found that the experiments with Mg(II), Sn(IV), Ti(IV) did not show any evidence of the 1,3,4-oxadiazin-2-one product, however, Cu(II), Zn(II), Sc(III) and Ag(I) showed evidence of product **III-43**. The reaction of ethyl phenylacetylene sulfide with DTBAD in the presence of 10 mol% of the $Sc(OTf)_3$ provided 7% of the 1,3,4-oxadiazin-2-one **III-43** (entry 1, Table 3.3). Attempting to remove the catalyst by performing a work up step with saturated aqueous sodium bicarbonate and NH_4Cl resulted no evidence of the 1,3,4-oxadiazin-2-one product on TLC in the $Cu(OTf)_2$ trials. It was found that the isolated yields from Cu (II) and Zn (II) were also very poor (*i.e.*, <6% yield; entry 2 and 3, Table 3.3). It has been found that the reaction seems to be facilitated by silver triflate (AgOTf) compared to the other catalysts that were screened.

Next, we increased the AgOTf catalyst loading and found that above 25 mol% catalyst loading, the formation of the 1,3,4-oxadiazin-2-one is inhibited. Furthermore, the reaction with 10 mol% of AgOTf and 1.0 equivalence of the DTBAD (**III-6e**) at room temperature for 18 h resulted in a 16% yield of the 1,3,4-oxadiazin-2-one **III-43** (entry 4, Table 3.3). Attempts to perform this reaction over a longer period of time (*i.e.*, 48 h) resulted in an enhanced yield of 27% (entry 5). Since the byproduct of this reaction, the *tert*-butyl cleaved product **III-52**, was evident in the TLC analysis and crude NMR spectrum, we decided to keep the equivalence of the DTBAD to a higher value (*i.e.*, 1.5 equiv) with the hope of improving the product yield. However, this reaction provided

27% of the 1,3,4-oxadiazin-2-one without any improvement of the yield, but within a shorter reaction time of 24 h (entry 6). Since the *tert*-butyl cleaving step is decreasing the effective amount of DTBAD in the reaction; the reaction was next performed with *tert*-butyl scavenging agents such as methanol and anisole to see whether this approach enhanced the product yield. The reaction with methanol did not show any evidence of the product. However, conducting the reaction in the presence of 1 equivalence of anisole provided a slightly higher 34% yield of the product (entry 7). It is also important to note that this *tert*-butyl cleaving step could also occur via intra-molecular retro-ene rearrangement similar to the rearrangements commonly known in literature for the *tert*-butyl ethers.[122] The inability for enhancing the product yields significantly by the *tert*-butyl scavenging agents could be explained by this intra-molecular retro-ene rearrangement phenomenon.

Table 3.3. Optimization of the 1,3,4-oxadiazin-2-one **III-43** synthesis.

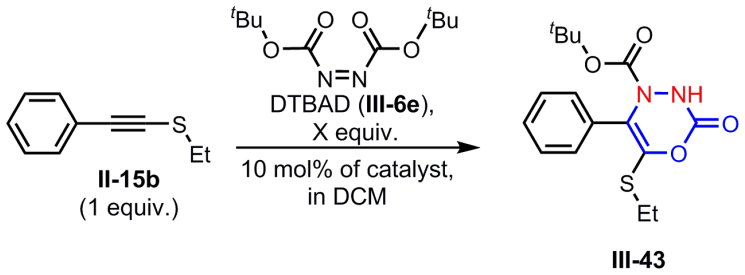

III-43

Entry	Equivalence of DTBAD	Catalyst	Additive	Temperature	Time (h)	Yield[a]
1	1.0	$Sc(OTf)_3$	-	RT	24	7
2	1.5	$Cu(OTf)_2$	-	RT	24	<6
3	1.5	$Zn(OTf)_2$	-	RT	24	<6
4	1.0	AgOTf	-	RT	18	16
5	1.0	AgOTf	-	RT	48	27
6	1.5	AgOTf	-	RT	24	27
7	1.5	AgOTf	Anisole (1 equiv.)	RT	24	34
8	1.5	AgOTf	Anisole (1 equiv.)	40°C	45	29
9	1.5	$AgNO_3$	-	RT	137	<3
10	1.5	AgOTs	-	RT	137	9

Note: RT = room temperature, a = Isolated yields

In order to investigate whether this reaction can be forced to proceed via *path b* (Scheme 3.16) which was described earlier, the same reaction was performed in refluxing DCM (*ca.* 40°C) with 10 mol% AgOTf and 1 equivalence of anisole which provided 29% of the product **III-43** (entry 8,Table 3.3). This indirectly suggests that *path b* is less likely to be forced by thermal conditions. Also, further attempts to perform this reaction at higher temperatures (*i.e.,* refluxing toluene, 24 h) provided the *tert*-butyl cleaved product **III-52**, which suggests that higher temperatures are less favorable for this reaction.[121]

Further optimization of the reaction was carried out with different silver catalysts (10 mol %) bearing different organic and inorganic ligands such as $AgNO_3$, Ag_2O, Ag_2SO_4 and AgOTs with 1.5 equivalence of the DTBAD (**III-6e**) and 1.0 equivalence of the thio-alkyne **II-15b** for about 5-6 days at room temperature. Even though, $AgNO_3$ and AgOTs showed the evidence of the oxadiazinone product on TLC; attempting to isolate the product yielded very poor yields (*i.e.,* <3% and 9% respectively; entry 9 and 10, Table 3.3). It is important to note that the isolation of the product from the reaction with AgOTs was co-eluted diazacyclobutene **III-7y** and di-*tert*-butyl azodicarboxylate (**III-6e)**. Later, it was found that the diazacyclobutene **III-7y** has produced in AgOTs reaction for about 19% yield based on the isolated amount and the NMR integration analysis. These results also suggest the possibility of regio-divergence reactivity of this oxadiazinone synthesis reaction where the triflate ligand (*i.e.,* OTf) promote the 1,3,4-oxadiazinone synthesis and on the other hand other ligands such as bulky tosylate (OTs) ligand facilitate the [2+2] cycloaddition to form the diazacyclobutene. For future

studies; use of other Ag (I) triflates such as $AgNTf_2$, combination of Lewis acids coupled with Ag (I), or with different *tert*-butyl scavenging agents will be performed. More experimental and computational work towards studying the mechanism of this reaction to understand the feasibility of *path a* or *path b* are also expected to carry out in near future. After the final optimization trials are completed, we are planning on synthesizing a library of these compounds to understand the scope and limitations of this reaction. Further transformation of **III-43** by possible alkylation and acylation of the NH group is another potential future work which could allow for the incorporation of a more functional handle of this molecule.[123] Lastly, the testing of these 1,3,4-oxadiazin-2-one derivatives for their antimicrobial and anti-parasitic activity are also in progress.

3.4 Overall conclusions

The most remarkable feature of the observed reactivity between electron-rich alkynes and the azodicarboxylates was the diverse outcomes arising from exploring different azodicarboxylates under different conditions Scheme 3.18 Eq. 1-2 and Scheme 3.19 Eq. 3-4).

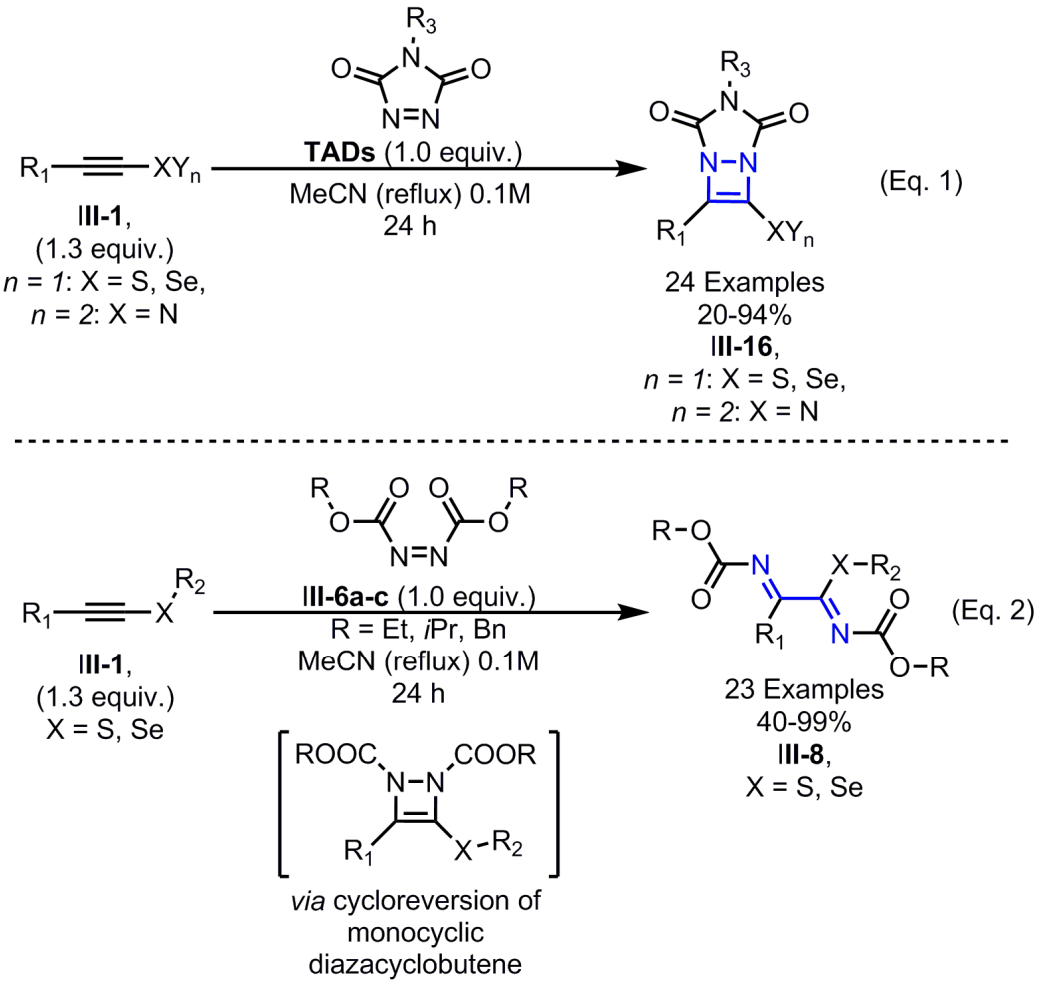

Scheme 3.18. Diverse reactivity patterns of azodicarboxylates with alkylacetylene sulfides.

As we mentioned earlier in the Chapter III, Section 3.1 and 3.2, the reaction of electron-rich alkynes with a cyclic azodicarboxylate such as PTAD forms the diazacyclobutenes whereas an acyclic azodicarboxylate, such as diethylazodicarboxylate (DEAD), provides the corresponding 2-iminothioimidate via an analogous, monocyclic diazacyclobutene intermediate (Scheme 3.18 Eq. 1 and Eq. 2). Further, it was found that the second fused ring is required to make a stable diazacyclobutene ring. The bicyclic diazacyclobutenes that were synthesized in this project were found to be non-aromatic and conformationally fluxional at room temperature via double nitrogen inversion. Extensive variable temperature NMR studies suggest that the 2-iminothioimidates are also rapidly isomerizing (Z/E) at room temperature, most likely via in-plane (with respect to the C=N bond plane) sp^2-sp-sp^2 nitrogen inversion.

Interestingly, the cyclohexenyl sulfide with a more electron-deficient, acyclic azodicarboxylate such as bis(2,2,2-trichloroethyl) azodicarboxylate (TCEAD) provided novel tetrahydroindoles (Scheme 3.19 Eq. 3). Apparently, the tetrahydroindole ring was formed via an unprecedented *5-endo-trig* cyclization at reflux temperatures. We also confirmed the substrate and temperature dependency of the tetrahydroindole synthesis via 2D-HMQC and low temperature NMR.

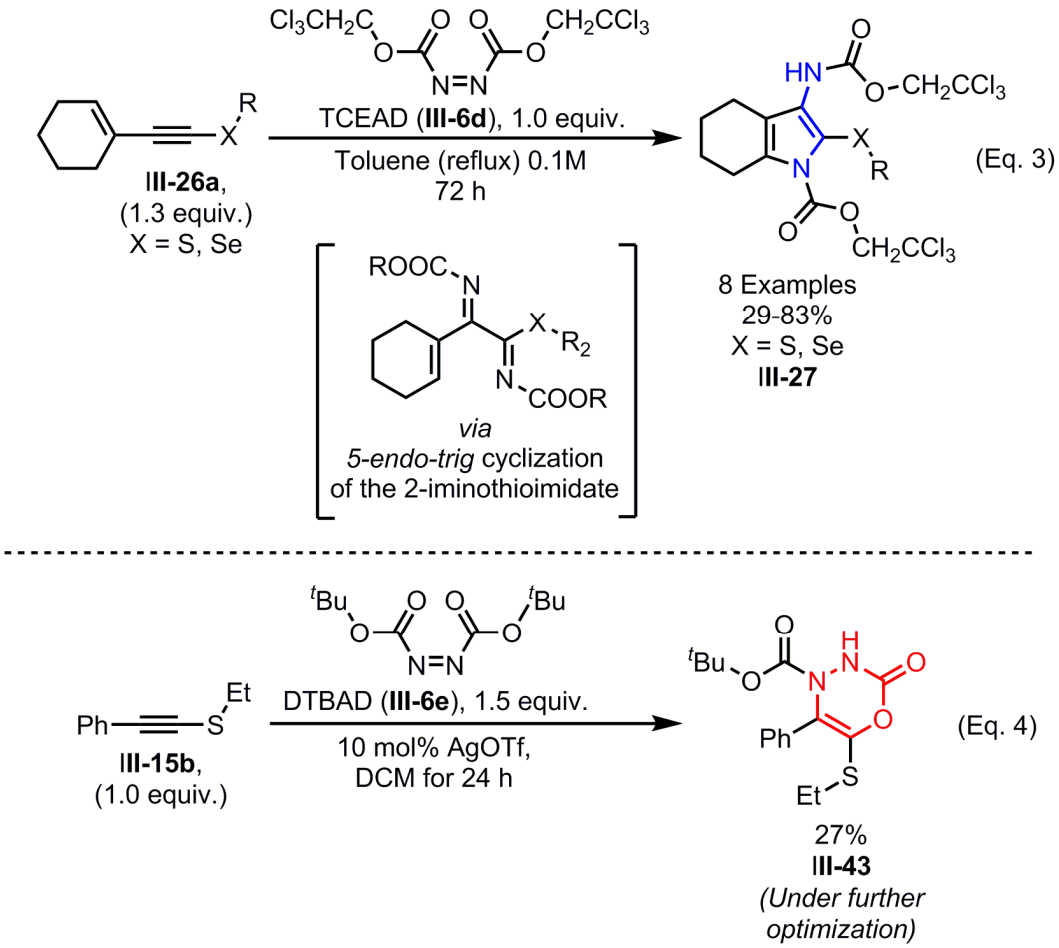

Scheme 3.19. Diverse reactivity patterns of azodicarboxylates with alkylacetylene sulfides.

In contrast to reactions described above, the less reactive di-*tert*-butyl azodicarboxylates and alkynyl sulfides showed a divergent reactivity in the presence of catalytic silver to provide 1,3,4-oxadiazin-2-ones (Scheme 3.19 Eq. 4).

This chemistry has opened up multiple avenues of synthetic organic and medicinal chemistry. We believe that this chemistry has a huge potential for further expansion. Further work is underway in order to further evaluate the chemistry between electron-rich alkynes and azodicarboxylates to synthesize novel and biologically relevant N-heterocycles such as pyrroles, indoles.

3.5 Experimental section

3.5.1. General information

All reagents were purchased from commercially available sources and used without further purification. THF and acetonitrile were dried before use by distillation over sodium/benzophenone and phosphorous pentoxide, respectively. ^{1}H and ^{13}C NMR spectra were collected using Bruker 300 MHz, 500 MHz NMR spectrometers using deuterated solvents ($CDCl_3$, CD_3CN). NMR chemical shifts are reported in parts per million (ppm). NMR spectra are calibrated based on residual solvent peaks. Infrared spectroscopy data were collected using IRAffinity-1S instrument (with MIRacle 10 single reflection ATR accessory). Flash chromatography was performed using silica gel (40-63 μm). All known compounds were characterized by ^{1}H and ^{13}C NMR and are in complete agreement with samples reported elsewhere. All new compounds were characterized by ^{1}H and ^{13}C NMR, ATR-FTIR, HRMS, XRD, and melting point (where appropriate).

3.5.2 General Procedure for the synthesis of N,N-dicarbamoyl 2-iminothioimidates

A flame dried round bottom flask (RBF) was charged with a stir bar, a solution of azodicarboxylates (1 mmol/1 equiv) and 5 mL of dry acetonitrile. To this stirring solution was added a solution of alkynyl sulfide (1.3mmol, 1.3 equiv) in 5 mL of dry acetonitrile in a dropwise fashion. The RBF was then equipped with a water-cooled condenser and refluxed for 24 h. The resultant crude mixture was concentrated by rotary evaporation and purified via flash silica gel chromatography with hexane/ethyl acetate as eluent (0 to 20% ethyl acetate) to afford the corresponding α-imidothioimidate derivative.

3.5.3 Characterization data for alkynyl sulfides and selenides

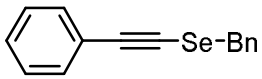

II-15t

Light yellow liquid; Yield: 84% (4.46 g); ^{1}H-NMR (300 MHz, $CDCl_3$) δ = 7.6-7.28 (m, 10H), 4.16 (s, 2H); ^{13}C NMR (75 MHz, $CDCl_3$) δ = 137.4, 131.35, 129.0, 128.5, 128.2, 128.1, 127.5, 123.4, 101.2, 71.0, 33.0.

3.5.4 Characterization data for N,N-dicarbamoyl 2-iminothioimidates

Methyl N-(Ethoxycarbonyl)-2-((ethoxycarbonyl)imino)-2-phenylethanimidothioate ***(III-8a)***

Colorless liquid; Yield: 74% (239 mg); IR (neat): 2981 (w), 2931 (w), 1716 (s), 1627 (m), 1577 (m), 1446 (m), 1365 (m), 1207 (s), 1091 (m), 1033 (m), 864 (w), 690 (m) cm^{-1}; ^{1}H-NMR (300 MHz, $CDCl_3$) δ = 7.83 (d, *J* = 6.6 Hz, 2H), 7.52 (t, *J* = 7.4 Hz, 1H), 7.42 (t, *J* = 7.3 Hz, 2H), 4.27 (q, *J* = 7.1 Hz, 2H), 4.08 (q, *J* = 6.8 Hz, 2H), 2.47 (s, 3H), 1.30 (t, *J* = 7.1 Hz, 3H), 1.15 (t, *J* = 7.1 Hz, 3H); ^{13}C NMR (75 MHz, $CDCl_3$) δ = 175.6, 166.2, 160.8, 159.2, 133.0, 132.4, 128.7, 128.7, 63.0 (2C, see 2D-HMQC), 14.3, 14.1, 14.0; HRMS (ESI^{+}): Calcd for $C_{15}H_{19}N_2O_4S$, $[M+H]^{+}$ 323.1066 Found m/z 323.1087.

*Ethyl N-(Ethoxycarbonyl)-2-((ethoxycarbonyl)imino)-2-phenylethanimidothioate **(III-8b)***

Colorless liquid; Yield: ≥99% (334 mg); ; IR (neat): 2981 (w), 2931 (w), 2870 (w), 1716 (s), 1627 (m), 1577 (m), 1446 (m), 1365 (m), 1207 (s), 1091 (m), 1033 (m), 864 (m), 690 (m) cm^{-1}; ^{1}H-NMR (300 MHz, $CDCl_3$) δ = 7.76 (d, *J* = 6.5 Hz, 2H), 7.44 (t, *J* = 7.3 Hz, 1H), 7.34 (t, *J* = 7.4 Hz, 2H), 4.19 (q, *J* = 7.1 Hz, 2H), 3.99 (q, *J* = 6.9 Hz, 2H), 3.02 (q, *J* = 7.3 Hz, 2H), 1.23 (t, *J* = 7.3 Hz, 6H, see 2D HMQC), 1.05 (t, *J* = 7.1 Hz, 3H); ^{13}C NMR (75 MHz, $CDCl_3$) δ = 174.6, 166.0, 160.4, 158.8, 132.7, 132.1, 128.5, 128.4, 62.6 (2C), 25.6, 13.8, 13.5, 12.9; HRMS (ESI^+): Calcd for $C_{16}H_{21}N_2O_4S$, $[M+H]^+$ 337.1222 Found m/z 337.1242.

*Propyl N-(Ethoxycarbonyl)-2-((ethoxycarbonyl)imino)-2-phenylethanimidothioate **(III-8c)***

Colorless liquid; Yield: 73% (256 mg); ; IR (neat): 2970 (w), 2931 (w), 1716 (s), 1627 (m), 1577(m), 1446 (w), 1365 (m), 1284 (w), 1207 (s), 1091 (m), 1033 (m), 864 (w), 729 (m), 690 (m) cm^{-1}; ^{1}H-NMR (300 MHz, $CDCl_3$) δ = 7.82 (d, *J* = 7.1 Hz, 2H), 7.52 (t, *J* = 7.3 Hz, 1H), 7.42 (t, *J* = 7.3 Hz, 2H), 4.27 (q, *J* = 7.1 Hz, 2H), 4.06 (q, *J* = 7.1 Hz, 2H), 3.07 (q, *J* = 7.2 Hz, 2H), 1.69 (sextet, *J* = 7.3 Hz, 2H), 1.31 (t, *J* = 7.1 Hz, 3H), 1.13 (t, *J* = 7.1 Hz, 3H), 0.98 (t, *J* = 7.4 Hz, 3H); ^{13}C NMR (75 MHz, $CDCl_3$) δ = 175.0, 166.5, 160.7, 159.1, 132.9, 132.5, 128.8, 128.6, 62.9 (2C), 33.3, 21.5, 14.1, 13.8, 13.2; HRMS (ESI^+): Calcd for $C_{17}H_{23}N_2O_4S$, $[M+H]^+$ 351.1379 Found m/z 351.1398.

*Butyl N-(Ethoxycarbonyl)-2-((ethoxycarbonyl)imino)-2-phenylethanimidothioate **(III-8d)***

Colorless liquid; Yield: 83% (303 mg); IR (neat) : 2958 (w), 2931 (w), 2870 (w), 1716 (s), 1627 (m), 1577 (m), 1446 (m), 1365 (m), 1207 (s), 1091 (m), 1033 (m), 864 (w), 783 (m), 729 (m), 690 (m) cm^{-1}; ^{1}H-NMR (300 MHz, $CDCl_3$) δ = 7.79 (d, *J* = 7.2 Hz, 2H), 7.48 (t, *J* = 7.3 Hz, 1H), 7.38 (t, *J* = 7.5 Hz, 2H), 4.24 (q, *J* = 7.1 Hz, 2H), 4.03 (q, *J* = 7.1 Hz, 2H), 3.06 (t, *J* = 7.3 Hz, 2H), 1.60 (p, *J* = 7.3 Hz, 2H), 1.5-1.2 (m, 5H), 1.10 (t, *J* = 7.1 Hz, 3H), 0.86 (t, *J* = 7.3 Hz, 3H); ^{13}C NMR (75 MHz, $CDCl_3$) δ = 174.7, 166.3, 160.6, 159.0, 132.8, 132.5, 128.7, 128.5, 62.8 (2C), 31.1, 29.9, 21.7, 14.0, 13.7, 13.2; HRMS (ESI^+): Calcd for $C_{18}H_{25}N_2O_4S$, $[M+H]^+$ 365.1535 Found m/z 365.1556.

Pentyl N-(Ethoxycarbonyl)-2-((ethoxycarbonyl)imino)-2-phenylethanimidothioate

(III-8e)

Colorless liquid; Yield: 80% (303 mg); IR (neat): 2954 (w), 2931 (w), 2858 (w), 1720 (s), 1627 (m), 1577 (m), 1446 (m), 1365 (m), 1280 (w), 1207 (s), 1091 (m), 1033 (m), 783 (m), 729 (m), 690 (m) cm^{-1}; ^{1}H-NMR (300 MHz, $CDCl_3$) δ = 7.76 (d, *J* = 6.54 Hz, 2H), 7.44 (t, *J* = 7.3 Hz, 1H), 7.34 (t, *J* = 7.5 Hz, 2H), 4.20 (q, *J* = 7.1 Hz, 2H), 4.00 (q, *J* = 6.90 Hz, 2H), 3.02 (t, *J* = 7.2 Hz, 2H), 1.58 (p, *J* = 7.0 Hz, 2H), 1.4-1.15(m, 7H), 1.05 (t, *J* = 7.1 Hz, 3H), 0.79 (t, *J* = 6.9 Hz, 3H); ^{13}C NMR (75 MHz, $CDCl_3$) δ = 174.6, 166.1, 160.4, 158.8, 132.7, 132.2, 128.5, 128.3, 62.6 (2C), 31.1, 30.4, 27.4, 21.7, 13.8, 13.5, 13.4; HRMS (ESI^+): Calcd for $C_{19}H_{27}N_2O_4S$, $[M+H]^+$ 379.1692 Found m/z 379.1710.

*Octyl N-(Ethoxycarbonyl)-2-((ethoxycarbonyl)imino)-2-phenylethanimidothioate **(III-8f)***

Light yellow liquid; Yield: 73% (307 mg); IR (neat): 2924 (m), 2854 (w), 1720 (s), 1627 (m), 1577 (m), 1446 (m), 1365 (m), 1207 (s), 1091 (m), 1033 (m), 910 (m), 783 (m), 729 (m), 688 (m) cm^{-1}; ^{1}H-NMR (300 MHz, $CDCl_3$) δ = 7.77 (d, *J* = 6.63 Hz, 2H), 7.45 (t, *J* = 7.3 Hz, 1H), 7.36 (t, *J* = 7.4 Hz, 2H), 4.21 (q, *J* = 7.1 Hz, 2H), 4.00 (q, *J* = 7.0 Hz, 2H), 3.03 (t, *J* = 7.2 Hz, 2H), 1.59 (p, *J* = 7.1 Hz, 2H), 1.4-1.12 (m, 13H), 1.07 (t, *J* = 7.1 Hz, 3H), 0.79 (t, *J* = 6.4 Hz, 3H); ^{13}C NMR (75 MHz, $CDCl_3$) δ = 175.0, 166.4, 160.7, 159.1, 132.9, 132.5, 128.8, 128.6, 62.9, 62.8, 31.6, 31.5, 28.9, 28.8, 28.6, 27.9, 22.4, 14.1, 13.9, 13.8; HRMS (ESI^+): Calcd for $C_{22}H_{33}N_2O_4S$, $[M+H]^+$ 421.2161 Found m/z 421.2161.

*Phenyl N-(Ethoxycarbonyl)-2-((ethoxycarbonyl)imino)-2-phenylethanimidothioate **(III-8g)***

Light yellow solid; Yield: 77% (296 mg); Mp: 70-71 °C; IR (neat) : 2981 (w), 1724 (s), 1712 (s), 1631 (m), 1612 (m), 1577 (w), 1477 (m), 1442 (m), 1207 (s), 1095 (w), 1022 (m), 968 (m), 860 (w), 752 (s), 686 (s) cm^{-1}; ^{1}H-NMR (300 MHz, $CDCl_3$) δ = 7.54 (d, J = 7.4 Hz, 2H), 7.50-7.20 (m, 6H), 7.15 (t, *J* = 7.5 Hz, 2H), 4.38 (q, *J* = 7.1 Hz, 2H), 4.28 (broad q, *J* = 7.1 Hz, 2H), 1.41 (t, *J* = 7.1 Hz, 3H), 1.35 (t, *J* = 7.1 Hz, 3H); ^{13}C NMR (125 MHz, $CDCl_3$) δ = 173.9, 165.5, 161.3, 159.6, 135.8, 133.2, 132.5, 130.3, 129.0, 128.4, 128.2, 126.1, 63.23, 63.16, 14.2, 14.1; HRMS (ESI^+): Calcd for $C_{20}H_{21}N_2O_4S$, $[M+H]^+$ 385.1222 Found m/z 385.1240.

Benzyl N-(Ethoxycarbonyl)-2-((ethoxycarbonyl)imino)-2-phenylethanimidothioate

(III-8h)

Colorless liquid; Yield: 83% (330 mg); IR (neat): 2978 (w), 1716 (s), 1627 (w), 1577 (m), 1492 (w), 1450 (w), 1207 (s), 1087 (m), 1026 (m), 910 (w), 729 (w), 690 (w) cm^{-1}; ^{1}H-NMR (300 MHz, $CDCl_3$) δ = 7.81 (d, *J* = 6.2 Hz, 2H), 7.51 (t, *J* = 7.0 Hz, 1H), 7.40 (t, *J* = 7.7 Hz, 2H), 7.35-7.16 (m, 5H), 4.34 (s, 2H), 4.23 (q, *J* = 7.1 Hz, 2H), 4.10 (q, *J* = 7.1 Hz, 2H), 1.27 (t, *J* = 7.1 Hz, 3H), 1.15 (t, *J* = 7.1 Hz, 3H); ^{13}C NMR (75 MHz, $CDCl_3$) δ = 174.2, 165.9, 160.6, 158.9, 134.6, 132.9, 132.3, 130.4, 129.1, 128.7, 128.5, 127.7, 62.88, 62.86, 35.8, 14.0, 13.7; HRMS (ESI^+): Calcd for $C_{21}H_{23}N_2O_4S$, $[M+H]^+$ 399.1379 Found m/z 399.1391.

Methyl N-(Ethoxycarbonyl)-2-((ethoxycarbonyl)imino)-2-(p-tolyl)ethanimidothioate

(III-8i)

Colorless liquid; Yield: 88% (296 mg); IR (neat): 2978 (w), 2927 (w), 1716 (s), 1627 (m), 1600 (m), 1462 (w), 1446 (w), 1411 (w), 1388 (w), 1365 (m), 1292 (m), 1207 (s), 1180 (m), 1091 (s), 1033 (s), 914 (m), 821 (w), 775 (w), 729 (s) cm^{-1}; ^{1}H-NMR (300 MHz, $CDCl_3$) δ = 7.71 (d, *J* = 7.26 Hz, 2H), 7.21 (d, *J* = 7.9 Hz, 2H), 4.24 (q, *J* = 7.1 Hz, 2H), 4.07 (q, *J* = 6.74 Hz, 2H), 2.44 (s, 3H), 2.35 (s, 3H), 1.28 (t, *J* = 7.1 Hz, 3H), 1.14 (t, *J* = 7.0 Hz, 3H); ^{13}C NMR (75 MHz, $CDCl_3$) δ = 175.7, 166.0, 160.8, 159.1, 144.0, 129.6, 129.3, 128.7, 62.79, 62.77, 21.5, 14.2, 14.0, 13.7; HRMS (ESI^+): Calcd for $C_{16}H_{21}N_2O_4S$, $[M+H]^+$ 337.1222 Found m/z 337.1241.

*Methyl N-(Ethoxycarbonyl)-2-((ethoxycarbonyl)imino)-2-(4-methoxyphenyl)ethanimidothioate (**III-8j**)*

Colorless liquid; Yield: 95% (335 mg); IR (neat): 2978 (w), 2931 (w), 2839 (w), 1716 (s), 1593 (s), 1570 (w), 1508 (m), 1462 (w), 1442 (w), 1207 (s), 1168 (s), 1091 (m), 1026 (s), 910 (m), 840 (m), 729 (s) cm^{-1}; ^{1}H-NMR (300 MHz, $CDCl_3$) δ = 7.77 (d, *J* = 8.4 Hz, 2H), 6.87 (d, *J* = 8.9 Hz, 2H), 4.22 (q, *J* = 7.1 Hz, 2H), 4.06 (q, *J* = 7.0 Hz, 2H), 3.79 (s, 3H), 2.42 (s, 3H), 1.27 (t, *J* = 7.1 Hz, 3H), 1.13 (t, *J* = 7.0 Hz, 3H); ^{13}C NMR (75 MHz, $CDCl_3$) δ = 175.6, 165.3, 163.6, 160.9, 159.1, 130.9, 124.7, 114.0, 62.8, 62.7, 55.3, 14.1, 14.0, 13.7; HRMS (ESI^+): Calcd for $C_{16}H_{21}N_2O_5S$, $[M+H]^+$ 353.1171 Found m/z 353.1185.

*Methyl 2-(4-Chlorophenyl)-N-(ethoxycarbonyl)-2-((ethoxycarbonyl)imino)ethanimidothioate (**III-8k**)*

Colorless liquid; Yield: 47% (168 mg); IR (neat): 2978 (w), 2927 (w), 1716 (s), 1627 (m), 1589 (m), 1400 (w), 1365 (w), 1207 (s), 1087 (s), 1029 (s), 864 (w), 783 (w), 725 (m) cm^{-1}; ^{1}H-NMR (300 MHz, $CDCl_3$) δ = 7.77 (d, *J* = 8.0 Hz, 2H), 7.40 (d, *J* = 8.6 Hz, 2H), 4.26 (q, *J* = 7.1 Hz, 2H), 4.10 (q, *J* = 7.1 Hz, 2H), 2.47 (s, 3H), 1.30 (t, *J* = 7.1 Hz, 3H), 1.17 (t, *J* = 7.1 Hz, 3H); ^{13}C NMR (75 MHz, $CDCl_3$) δ = 175.4, 165.4, 160.6, 159.0, 139.5, 130.9, 130.0, 129.0, 63.1 (2C), 14.3, 14.1, 13.8; HRMS (ESI^+): Calcd for $C_{15}H_{18}ClN_2O_4S$, $[M+H]^+$ 357.0676 Found m/z 357.0686.

*Methyl N-(Ethoxycarbonyl)-2-((ethoxycarbonyl)imino)-2-(4-(trifluoromethyl)phenyl)ethanimidothioate (**III-8l**)*

Colorless liquid; Yield: 69% (270 mg); IR (neat): 2981 (w), 1724 (s), 1631 (w), 1577 (w), 1411 (w), 1323 (s), 1211 (s), 1168 (m), 1126 (m), 1064 (s), 1033 (w), 1014 (w), 848 (m), 771 (w), 748 (w) cm^{-1}; ^{1}H-NMR (300 MHz, $CDCl_3$) δ = 7.95 (d, *J* = 7.4 Hz, 2H), 7.68 (d, *J* = 8.4 Hz, 2H), 4.27 (q, *J* = 7.1 Hz, 2H), 4.09 (q, *J* = 6.9 Hz, 2H), 2.49 (s, 3H), 1.30 (t, *J* = 7.1 Hz, 3H), 1.16 (t, *J* = 7.1 Hz, 3H); ^{13}C NMR (75 MHz, $CDCl_3$) δ = 175.5, 165.5, 160.4, 159.1, 135.8, 134.3 (q, $^{2}J_{CF}$ = 32.8 Hz, 1C), 129.1, 125.7 (q, $^{3}J_{CF}$ = 3.7 Hz, 1C), 123.5 (q, $^{1}J_{CF}$ = 272.7 Hz), 63.33, 63.25, 14.3, 14.1, 13.9; HRMS (ESI^+): Calcd for $C_{16}H_{18}F_3N_2O_4S$, $[M+H]^+$ 391.0939 Found m/z 391.0963.

*Methyl N-(Ethoxycarbonyl)-2-((ethoxycarbonyl)imino)hexanimidothioate (**III-8m**)*

Light yellow liquid; Yield: 40% (121 mg) ; IR (neat): 2958 (w), 2931 (w), 1716 (s), 1662 (w), 1608 (w), 1500 (w), 1465 (w), 1365 (w), 1215 (s), 1095 (w), 1033 (m), 948 (w), 914 (w), 732 (m) cm^{-1}; ^{1}H-NMR (300 MHz, $CDCl_3$) δ = 4.4-4.1 (m, 4H), 2.48 (t, *J* = 7.8 Hz, 2H), 2.41 (s, 3H), 1.56 (p, *J* = 7.6 Hz, 2H), 1.40-1.23 (m, 8H), 0.86 (t, *J* = 7.3 Hz, 3H); ^{13}C NMR (75 MHz, $CDCl_3$) δ = 171.2, 161.7, 160.6, 159.7, 62.9, 62.8, 27.8, 23.3, 15.1, 14.1, 14.0, 13.7, 13.5; HRMS (ESI^+): Calcd for $C_{13}H_{22}N_2O_4SNa$, $[M+Na]^+$ 325.1198 Found m/z 325.1210.

*Butyl N-(Ethoxycarbonyl)-2-((ethoxycarbonyl)imino)hexanimidothioate (**III-8n**)*

Light yellow liquid; Yield: 45% (155 mg); IR (neat): 2958 (w), 2931 (w), 2870 (w), 1724 (s), 1662 (w), 1604 (m), 1462 (w), 1365 (w), 1215 (s), 1095 (w), 1037 (m), 948 (w), 914 (w), 779 (w), 732 (w) cm^{-1}; ^{1}H-NMR (300 MHz, $CDCl_3$) δ = 4.19 (m, 4H), 2.99 (t, *J* = 7.3 Hz, 2H), 2.47 (t, *J* = 7.6 Hz, 2H), 1.7-1.48 (m, 4H), 1.48-1.22 (m, 10H), 1.00-0.80 (m, 6H); ^{13}C NMR (75 MHz, $CDCl_3$) δ = 171.4, 161.0, 160.5, 159.8, 62.8, 62.7, 30.6, 30.0, 29.5, 27.7, 22.3, 21.8, 14.1, 14.0, 13.4, 13.3; HRMS (ESI^+): Calcd for $C_{16}H_{29}N_2O_4S$, $[M+H]^+$ 345.1848 Found m/z 345.1862.

*Methyl 2-Cyclopropyl-N-(ethoxycarbonyl)-2-((ethoxycarbonyl)imino)ethanimidothioate (**III-8o**)*

Colorless liquid; Yield: 99% (361 mg); IR (neat): 2978 (w), 2931 (w), 2873 (w), 1716 (s), 1627 (w), 1577 (m), 1450 (w), 1373 (w), 1215 (s), 1180 (w), 1145 (w), 1099 (s), 983 (m), 937 (w), 786 (w), 729 (m), 686 (m) cm^{-1}; ^{1}H-NMR (300 MHz, $CDCl_3$) δ = 7.82 (d, *J* = 5.6 Hz, 2H), 7.55-7.44 (m, 1H), 7.44-7.33 (m, 2H), 5.03 (septet, *J* = 6.2 Hz, 1H), 4.89-466 (bm, 1H), 3.06 (q, *J* = 7.1 Hz, 2H), 1.41-1.17 (bm, 9H), 1.08 (d, *J* = 5.64 Hz, 6H); ^{13}C NMR (75 MHz, $CDCl_3$) δ = 173.8, 165.6, 160.2, 158.5, 132.8, 132.5, 128.7, 128.5, 70.9, 70.8, 25.8, 21.6, 21.3, 13.1; HRMS (ESI^+): Calcd for $C_{18}H_{25}N_2O_4S$, $[M+H]^+$ 365.1535 Found m/z 365.1548.

*Ethyl N-(Isopropoxycarbonyl)-2-((isopropoxycarbonyl)imino)-2-phenylethanimidothioate **(III-8p)***

Colorless liquid; Yield: 79% (364 mg); IR (neat): 2962 (w), 2927 (w), 1716 (s), 1627 (w), 1577 (m), 1450 (m), 1373 (m), 1195 (s), 1095 (m), 1002 (w), 910 (w), 732 (w), 694 (m) cm^{-1}; ^{1}H-NMR (300 MHz, $CDCl_3$) δ = 7.82 (d, *J* = 5.6 Hz, 2H), 7.60-7.48 (m, 1H), 7.48-7.20 (m, 12H), 5.26 (s, 2H), 5.03 (s, 2H), 3.04 (q, *J* = 7.4 Hz, 2H), 1.27 (t, *J* = 7.4 Hz, 3H); ^{13}C NMR (75 MHz, $CDCl_3$) δ = 175.1, 166.4, 160.5, 158.9, 135.0, 134.9, 133.0, 132.2, 132.1, 128.7, 128.6, 128.5, 128.4, 128.3, 128.2, 128.1, 68.6, 68.5, 25.8, 13.0; HRMS (ESI^+): Calcd for $C_{26}H_{25}N_2O_4S$, $[M+H]^+$ 461.1535 Found m/z 461.1545.

*Ethyl N-((Benzyloxy)carbonyl)-2-(((benzyloxy)carbonyl)imino)-2-phenylethanimidothioate **(III-8q)***

Colorless liquid; Yield: 86% (455 mg); IR (neat): 2954 (w), 1732 (s), 1627 (w), 1593 (w), 1577 (w), 1369 (m), 1276 (w), 1176 (s), 1033 (m), 906 (m), 806 (m), 721 (s), 686 (m) cm^{-1}; ^{1}H-NMR (300 MHz, $CDCl_3$) δ = 7.86 (d, *J* = 8.0 Hz, 2H), 7.56 (t, *J* = 7.4 Hz, 1H), 7.45 (t, *J* = 7.5 Hz, 2H), 4.84 (s, 2H), 4.66 (s, 2H), 2.53 (s, 3H); ^{13}C NMR (75 MHz, $CDCl_3$) δ = 178.0, 167.2, 158.9, 157.3, 133.8, 131.6, 129.0, 128.9, 94.14, 94.07, 75.9, 75.7, 14.7; HRMS (ESI^+): Calcd for $C_{15}H_{13}N_2O_4SCl_6$, $[M+H]^+$ 526.8727 Found m/z 526.8739.

Methyl 2-Phenyl-N-((2,2,2-trichloroethoxy)carbonyl)-2-(((2,2,2-trichloroethoxy)carbonyl)imino)ethanimidothioate ***(III-8r)***

Colorless liquid; Yield: 77% (220 mg); IR (neat): 2981 (w), 2931 (w), 1716 (s), 1651 (m), 1583 (m), 1444 (w), 1382 (w), 1365 (m), 1219 (s), 1193 (s), 1028 (s), 995 (m), 862 (m), 775 (m) 731 (m) cm^{-1}; ^{1}H-NMR (300 MHz, $CDCl_3$) δ = 4.25 (q, *J* = 7.1 Hz, 2H), 4.21 (q, *J* = 7.1 Hz, 2H), 2.45 (s, 3H), 2.10-1.70 (m, 1H), 1.33 (t, *J* = 6.3 Hz, 3H), 1.28 (t, *J* = 6.3 Hz, 3H) 1.26-1.05 (m, 4H); ^{13}C NMR (75 MHz, $CDCl_3$) δ = 176.1, 175.0, 160.6, 159.3, 63.0, 62.7, 17.2, 13.9, 12.4.

Methyl N-(Ethoxycarbonyl)-2-((ethoxycarbonyl)imino)-2-phenylethanimidoselenoate ***(III-8s)***

Light yellow liquid; Yield: 76% (280 mg); IR (neat): 2981 (w), 2935 (w), 1716 (s), 1597 (s), 1573 (w), 1446 (w), 1369 (w), 1330 (w), 1292 (w), 1211 (s), 1095 (w), 1026 (m), 898 (w), 864 (w), 771 (w), 732 (w), 690 (m), 528 (w) cm^{-1}; ^{1}H-NMR (300 MHz, $CDCl_3$) δ = 7.88 (d, *J* = 7.4 Hz, 2H), 7.60-7.47 (m, 1H), 7.47-7.30 (m, 2H), 4.23 (q, *J* = 6.9 Hz, 2H), 2.19 (s, 3H), 1.45 (m, 6H); ^{13}C NMR (75 MHz, $CDCl_3$) δ = 179.9, 165.0, 160.8, 160.4, 133.1, 132.3, 128.7, 128.5, 63.1, 62.8, 14.0, 13.9, 8.3; HRMS (ESI^+): Calcd for $C_{15}H_{19}N_2O_4Se$, $[M+H]^+$ 371.0510 Found m/z 371.0528.

*Benzyl N-(Ethoxycarbonyl)-2-((ethoxycarbonyl)imino)-2-phenylethanimidoselenoate **(III-8t)***

Light yellow liquid; Yield: 81% (361 mg); IR (neat): 2981 (w), 2931 (w), 1716 (s), 1689 (m), 1627 (m), 1577 (w), 1554 (w), 1494 (m), 1448 (m) 1365 (m), 1207 (s), 1180 (s), 1093 (m), 1024 (s), 970 (w), 904 (m), 732 (m), 694 (s) cm^{-1}; ^{1}H-NMR (300 MHz, $CDCl_3$) δ = 7.96 (d, *J* = 6.6 Hz, 2H), 7.70-7.00 (m, 8H), 4.32 (q, *J* = 7.1 Hz, 2H), 4.27-4.15 (m, 4H), 1.33 (t, *J* = 7.1 Hz, 3H), 1.30 (t, *J* = 7.1 Hz, 3H); ^{13}C NMR (75 MHz, $CDCl_3$) δ = 179.0, 165.3, 161.0, 160.2, 135.1, 133.1, 132.1, 129.0, 128.7, 128.6, 128.5, 127.3, 63.2, 62.9, 32.3, 14.0, 13.8.

*Diethyl 3-(Ethylthio)-4-phenyl-1,2-diazete-1,2-dicarboxylate (**III-7b**)*

Colorless liquid; Isolated by Prep TLC (2 mg); IR (in $CHCl_3$): 2927 (w), 2849 (w), 1721 (s), 1561 (w), 1463 (s), 1382 (m), 1222 (s), 1095 (m), 1029 (w), 567 (m) cm^{-1}; ^{1}H-NMR (500 MHz, $CDCl_3$) δ = 7.85-7.70 (m, 2H), 7.40-7.27 (m, 3H), 4.35 (q, *J* = 7.1 Hz, 2H), 4.24 (q, *J* = 7.1 Hz, 2H), 2.93 (q, *J* = 7.4 Hz, 2H), 1.42-1.34 (m, 6H), 1.26 (t, *J* = 7.1 Hz, 3H); ^{13}C NMR (125 MHz, $CDCl_3$) δ = 154.54, 154.45, 143.7, 128.8, 128.0, 127.0, 124.4, 63.4, 63.1, 29.8, 29.7, 14.9, 14.4, 14.1

*Di-tert-butyl 3-(Ethylthio)-4-phenyl-1,2-diazete-1,2-dicarboxylate (**III-7y**)*

White sticky paste; Yield: 6% (24 mg); IR (in $CHCl_3$): 2981 (w), 2935 (w), 1782 (s), 1539 (s), 1477 (m), 1450 (w), 1369 (m), 1253 (m), 1157 (s), 1126 (m), 1059 (w), 968 (m) cm^{-1}; ^{1}H-NMR (300 MHz, $CDCl_3$) δ = 7.70 (d, *J* = 8.1 Hz, 2H), 7.50-7.00 (m, 3H), 2.93 (q, *J* = 7.4 Hz, 2H), 1.58 (s, 9 H), 1.46 (s, 9H), 1.38 (t, *J* = 7.4 Hz, 3H); ^{13}C NMR (75 MHz, $CDCl_3$) δ = 153.0, 143.3, 128.4, 127.8, 127.2, 123.8, 83.6, 83.2, 29.7, 28.1, 27.9, 14.8.

*Methyl 2-Cyclohexenyl-N-(ethoxycarbonyl)-2-((ethoxycarbonyl)imino)ethanimidothioate **(III-8v)***

Colorless liquid; Yield: 66% (217 mg); ^{1}H-NMR (500 MHz, $CDCl_3$) δ = 6.65 (s), 4.25-4.10 (m, 4H), 2.43 (s, 3H), 2.34-2.20 (bm, 4H), 1.70-1.55 (m, 4H), 1.27 (q, *J* = 7.3 Hz, 6H); ^{13}C NMR (125 MHz, $CDCl_3$) δ = 175.8, 167.2, 161.5, 159.4, 144.9, 134.9, 62.9, 62.8, 26.7, 23.3, 21.8, 21.5, 14.5, 14.2, 14.2. *see* 2D-HMQC for more details.

Ethyl 2-Cyclohexenyl-N-(ethoxycarbonyl)-2-((ethoxycarbonyl)imino)ethanimidothioate ***(III-8w)***

Colorless liquid; Yield: 68% (1041 mg); ^{1}H-NMR (300 MHz, $CDCl_3$) δ = 6.55 (s, 1H), 4.09 (sextet, *J* = 7.3 Hz, 4H), 2.95 (q, *J* = 7.4 Hz, 2H), 2.30-2.00 (bm, 4H), 1.65-1.40 (bm, 4H), 1.25-1.10 (m, 9H); ^{13}C NMR (75 MHz, $CDCl_3$) δ = 174.4, 167.0, 161.0, 158.9, 144.4, 134.5, 62.4, 62.3, 26.3, 25.5, 23.0, 21.4, 21.1, 13.84, 13.79, 12.9.

Methyl 2-Cyclohexenyl-N-((2,2,2-trichloroethoxy)carbonyl)-2-(((2,2,2-trichloroethoxy)carbonyl)imino)ethanimidothioate ***(III-8x)***

Colorless liquid; Yield: 41% (61 mg); ^{1}H-NMR (500 MHz, $CDCl_3$) δ = 6.78 (s, 1H, *2D-HMQC* cross spot at 146 ppm), 4.81 (s, 2H), 4.77 (s, 2H), 2.51 (s, 3H), 2.40-2.12 (bm, 4H), 1.80-1.50 (bm, 4H), ; ^{13}C NMR (125 MHz, $CDCl_3$) δ = 178.5, 168.0, 159.6, 157.5, 146.8, 135.0, 94.42, 94.39, 76.0, 75.8, 26.9, 23.3, 21.6, 21.3, 14.8.

3.5.5 General React IR Procedure

The react IR experiments were performed in order to obtain mechanistic insights of the reaction between azodicarboxylates and alkynyl sulfides and to obtain any further evidence of the possible intermediates during the reaction.

In situ IR data was collected on a Mettler-Toledo IC 10 React IR instrument with a silicon ATR probe. A flame dried, three-neck 250 mL round bottom flask (RBF) was charged with a stir bar and equipped with a water cooled reflux condenser. Under the nitrogen atmosphere, the silicon probe was inserted into the RBF and the background IR spectrum of the air was collected for the empty flask and followed by a solvent background after the addition of dichloromethane (10 mL). Dichloromethane was selected as the solvent due to the less overlap from the solvent IR peaks on the observing IR range. Next, the corresponding azodicarboxylate (1.0 mmol) was added via syringe at room temperature. Then the background of the azodicarboxylate in dichloromethane was also collected. The IR instrument parameters were adjusted to scan every 5 seconds for a total of 2 hours per experiment. Then the IR data collection was initiated at t=0 time point and after 2 minutes of data collection, the alkynyl sulfide (1.3 mmol) was quickly added via syringe to start the reaction. The reaction mixture was either kept at room temperature throughout the reaction or kept under reflux conditions depending on specific substrate conditions. The formations of the products were further monitored via TLC during these experiments. In order to find absorbance plots showing the formation and depletion of species; the dichloromethane or azodicarboxylate in dichloromethane background

spectrum was subtracted from the each experimental spectrum by using Mettler-Toledo's ConcIRT software over the course of the reaction. The spectral region from 1300-2000 cm^{-1} was then analyzed to find any evidence of the intermediate species.

3.5.6 Reaction conditions for alkynyl sulfide and diethyl azodicarboxylate (DEAD).

To a flame dried 250 mL round bottom flask was added a stir bar, 10 mL of dichloromethane and 0.436 g of diethyl azodicarboxylate (DEAD) (1 mmol). The in situ IR data collection was started and 0.211 g of alkynyl sulfide (1.3 mmol) was added. The reaction temperature was then gradually increased to the reflux temperature and the in situ IR experiment scans were collected for about 2 h. IR data was processed by subtracting the dichloromethane background and analyzed in the range of 1377-1985 cm^{-1}.[41] (*Note:* The in-situ IR experiments of the 4-phenyltriazoline-3,5-dione (PTAD) was performed in the similar fashion as above, however instead of reflux condition, the data was collected at room temperature since the reaction rate is much faster than the reaction with DEAD).

3.5.7 General procedure for the variable temperature NMR study

First, a reaction between alkynyl sulfide and diethyl azodicarboxylate (DEAD) according to the general procedure described earlier in section **3.5.2** was initiated using DCM as the solvent instead of acetonitrile and the reaction was performed for 2 h at reflux conditions. Less reaction time was used in order to produce enough of the intermediate monocyclic diazacyclobutene **III-7b**.After the reaction, diazacyclobutene **III-7b** was isolated by means of preparative TLC. Variable-temperature ^{1}H NMR spectra for diazacyclobutene **III-7b** were collected using Bruker 300 MHz with CD_3CN in the temperature range of −35°C to 64°C.

Low temperature NMR experiment

First, the NMR dewar was filled with about 24 L of liquid nitrogen (about 80%). Then the white teflon cap from the N_2 evaporator was removed and the evaporator was gently inserted into the dewar. Then the evaporator was clamped to the dewar and the pressure in the dewar was allowed to drop. Next, the glass ball joint of the N_2 evaporator transfer probe (located at the other end of the N_2 evaporator) was lubricated. Then the regular air transfer line was removed from the NMR instrument and replaced with the N_2evaporator transfer probe. Then the teflon cap of the N_2 evaporator was replaced in order to allow cold nitrogen to flow to the NMR probe in the NMR instrument. The temperature control was started by entering “edte” command in the XWIN-NMR command line of the Topspin software version 2.1. Then the cooling function was turned on and the cooling power was increased gradually (10% at each time) in order to reach a

certain temperature. After changing the cooling power, we waited for several minutes and changed it again if the temperature did not reach the targeted temperature. The target temperature was set based on the low temperature calibration curve for the NMR instrument (temperature calibration was performed prior to the actual experiment). Temperature change was performed in small increments in order to avoid substantial thermal gradient which could led to the damage of the instrument. Therefore after reaching to a certain temperature, the machine was kept there for at least 15-20 min before going to the next temperature. Once the temperature was stabilized; the sample was allowed to equilibrate for 5 min before collecting the ^{1}H NMR spectrum. After the experiment is completed, the temperature of the NMR machine was gradually brought to room temperature. Then, the cooling function was turned off. The teflon cap was removed from the N_2 evaporator and we gently disconnected the N_2 evaporator transfer probe from the cold N_2 transfer joint and replaced it with the regular air line. Then the N_2 evaporator was removed from the dewar and the dewar was capped. Lastly, the N_2 evaporator was allowed to warm up to room temperature.

High temperature NMR experiment

In this experiment, the temperature of the spectrometer was changed using same procedure described above. However, the regular air line was not removed and the NMR probe heater was used to increase the temperature. The heater function in the "edte" command box was turned on and the air flow was adjusted between 400-700 L/h. The target temperature was set based on the high temperature calibration curve for the NMR instrument. The target temperature was reached by adjusting the heating power with a method similar to that described earlier. Once the temperature was stabilized; the sample was allowed to equilibrate for 5 min before the ^{1}H NMR spectrum was collected. After the experiment is completed, the temperature of the NMR machine was gradually brought to the room temperature. Then the heating function was turned off.

*3.5.8 Reaction order determination and activation energy barrier calculation for the ring opening of **III-7b** to **III-8b** using half-life and Arrhenius equations*

First, the monocyclic diazacyclobutene intermediate **III-7b** was isolated through preparative TLC and dissolved in 0.5 mL of CD_3CN. Then, the ^1H NMR spectra was taken at different time intervals at two different temperatures (298 K and 337 K). Integration of the sulfur methylene protons of the diazacyclobutene intermediate and the 2-iminothioimidate product were normalized with an internal standard. Acetonitrile (CD_3CN) residual peak integration was unchanged during the experiment and was taken as the internal standard in these experiments for normalizing the other integrations. The half-life ($t_{1/2}$) of the ring opening reaction was extracted from the graph of the normalized integration of the S-methylene protons of the diazacyclobutene intermediate vs time.

Theoretically, the half-life of a first order reaction is constant (*i.e.*, ln 2/k, where k is the reaction rate constant) where as for a zero order reaction, the half-life is dependent on the initial concentration. The reaction rate constants were then calculated based on the half-life values at each temperature. Finally, the energy barrier for the ring opening process was calculated from the Arrhenius equation. A stepwise guide for the energy barrier calculation is given below.

*Reaction Order Determination for the Ring Opening of **III-7b** to **III-8b** Using Half-life and Arrhenius Equations*

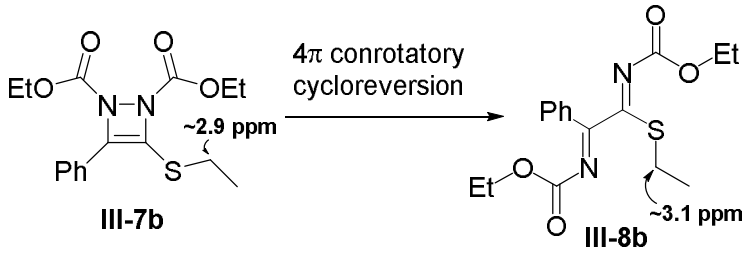

*At 373K (64°C) integration analysis of **III-7b** over time (Spectra recorded in Bruker-300 MHz NMR Instrument at 337K in CD_3CN)*

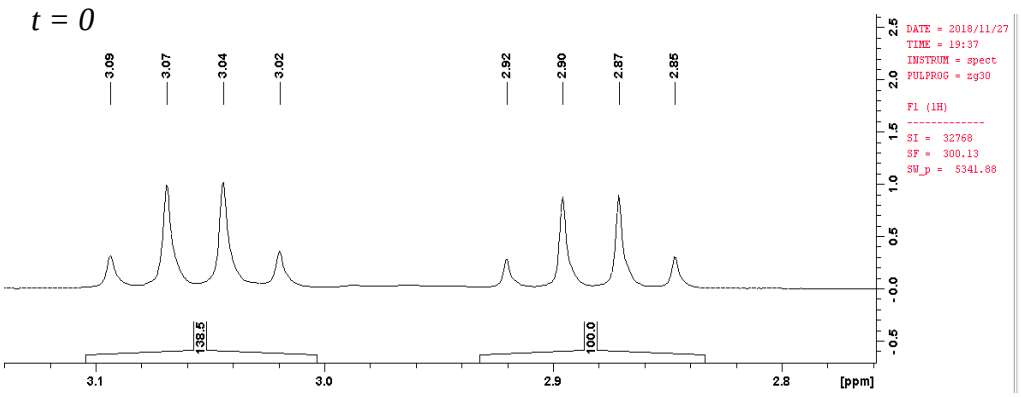

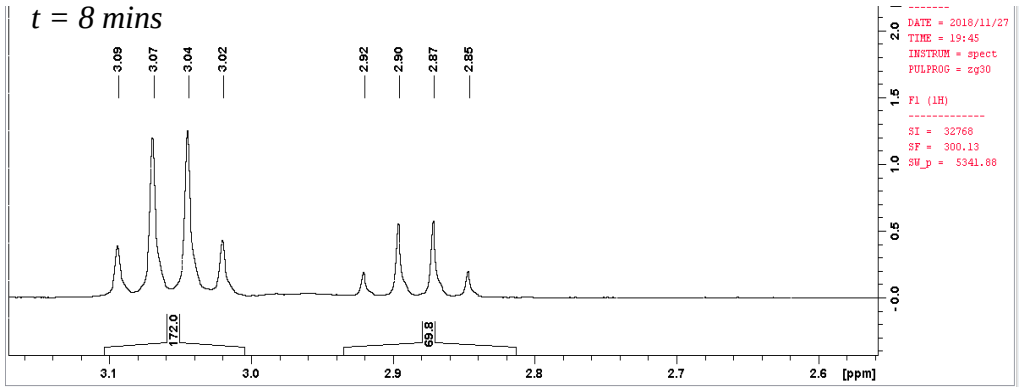

t = 16 mins

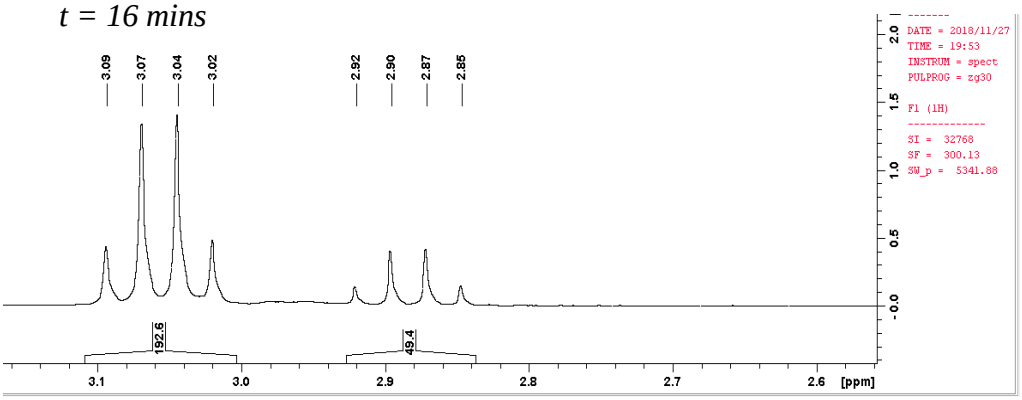

t = 20 mins

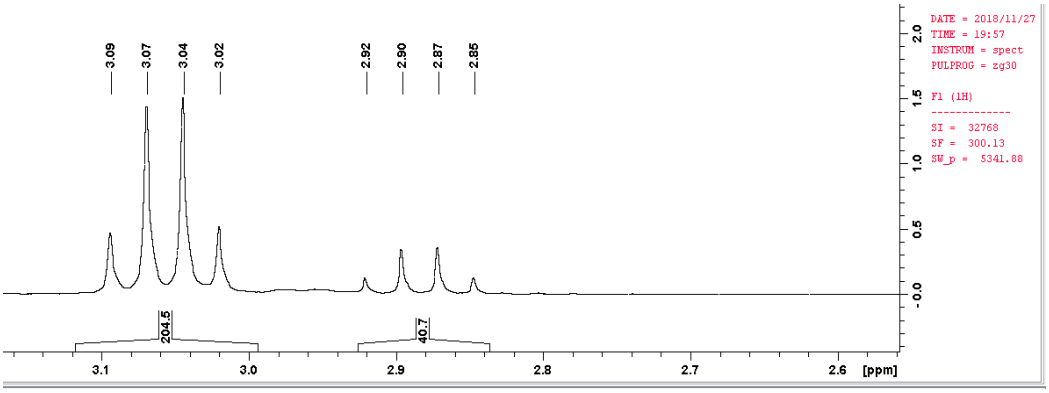

t = 25 mins

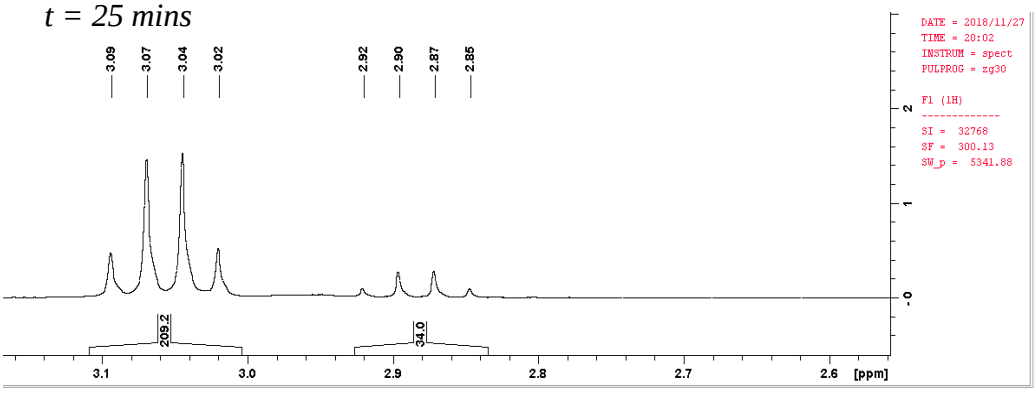

t = 30 mins

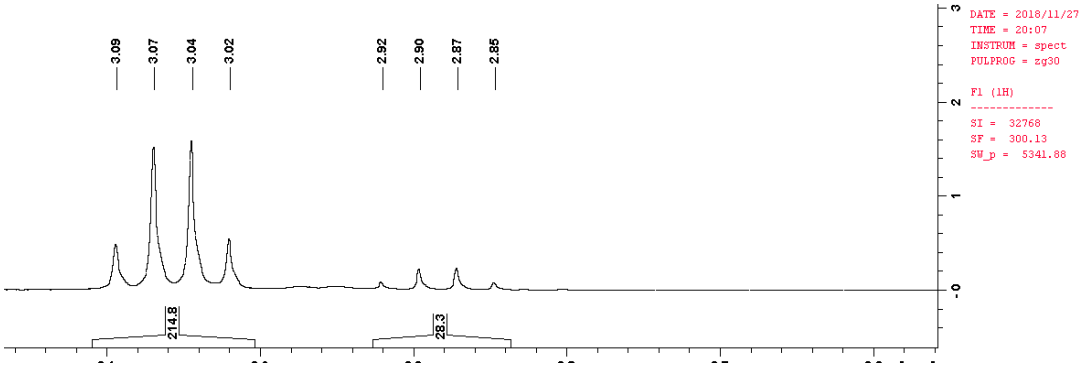

t = 35 mins

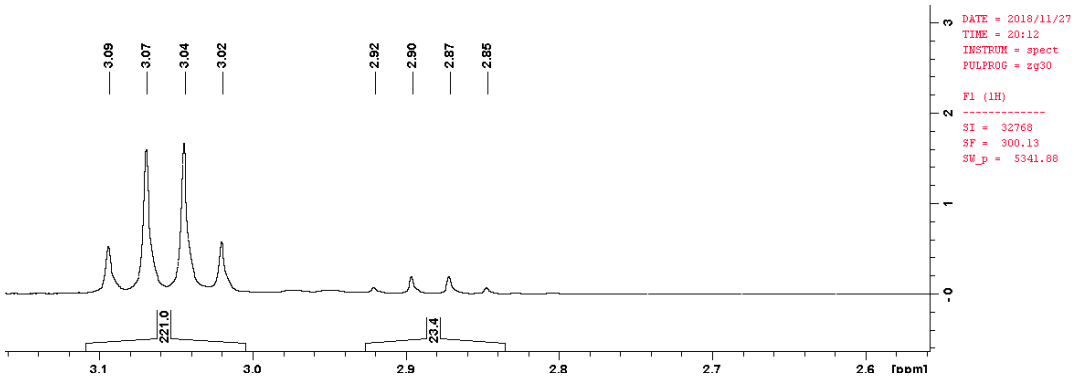

Table 3.4. Normalized integration of the 2.9 ppm quartet of **III-7b** over time at 337 K

Time (min)	Integration of III-7b
0	100
8	70
16	49
20	41
25	34
30	28
35	23

Figure 3.15. Rate of the consumption (normalized integration of the 2.9 ppm quartet) of **III-7b** over time at 373 K

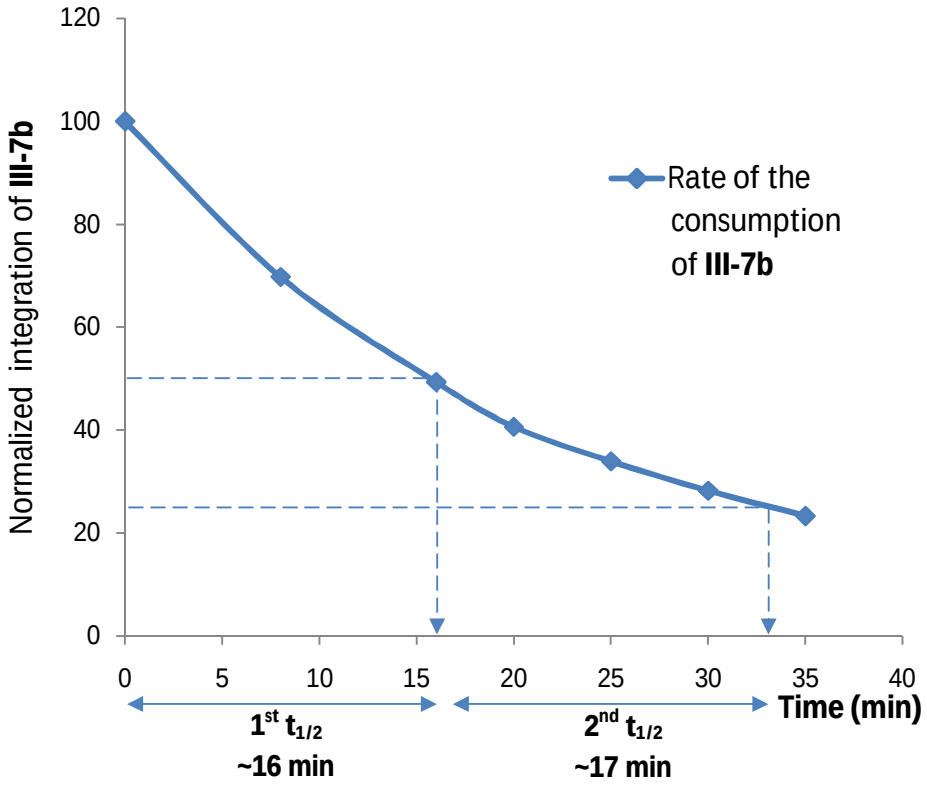

Table 3.5. Approximately estimated half-lives of **III-7b** from the above graph at 373 K

Half-life	**Time (min)**
1^{st} $t_{1/2}$	16 min
2^{nd} $t_{1/2}$	17 min

The non-linear behavior of the plot in **Figure 3.15** and the similarity of the two consecutive half-lives suggest that the electrocyclic ring opening of **III-7b** is following first order kinetics. Hence, the average $t_{1/2}$ at 337 K is 16.5 min (990 s), and by applying the first order kinetics ($t_{1/2}$ = ln 2 / k), the rate constant, k is found to be 7.0 x 10^{-4} sec^{-1}.These data were more formally fitted to an exponential decay function using Excel and more accurate rate constant value was found to be 7.3(1) x 10^{-4} sec^{-1} for this 337 K temperature data.

The rate of the ring opening at ambient temperature was similarly obtained from NMR spectra obtained over two days (shown below) and the rate constant is found to be 3(1) x 10^{-6} sec^{-1}. The large uncertainty in this rate constant was caused by the uncertain values of measurement times and room temperature fluctuations. Finally, by applying higher temperature and room temperature rate constants into a two-point Arrhenius analysis (see below for calculations), the energy barrier of the ring opening reaction, E_a was roughly estimated to be 28 ± 4 kcal/mol.

*At 298 K integration analysis of **III-7b** over time (Spectra recorded in NEO-500 MHz Avance NMR Instrument in $CDCl_3$)*

Approximate half-life is 46 hours (165600 s) at 298 K.

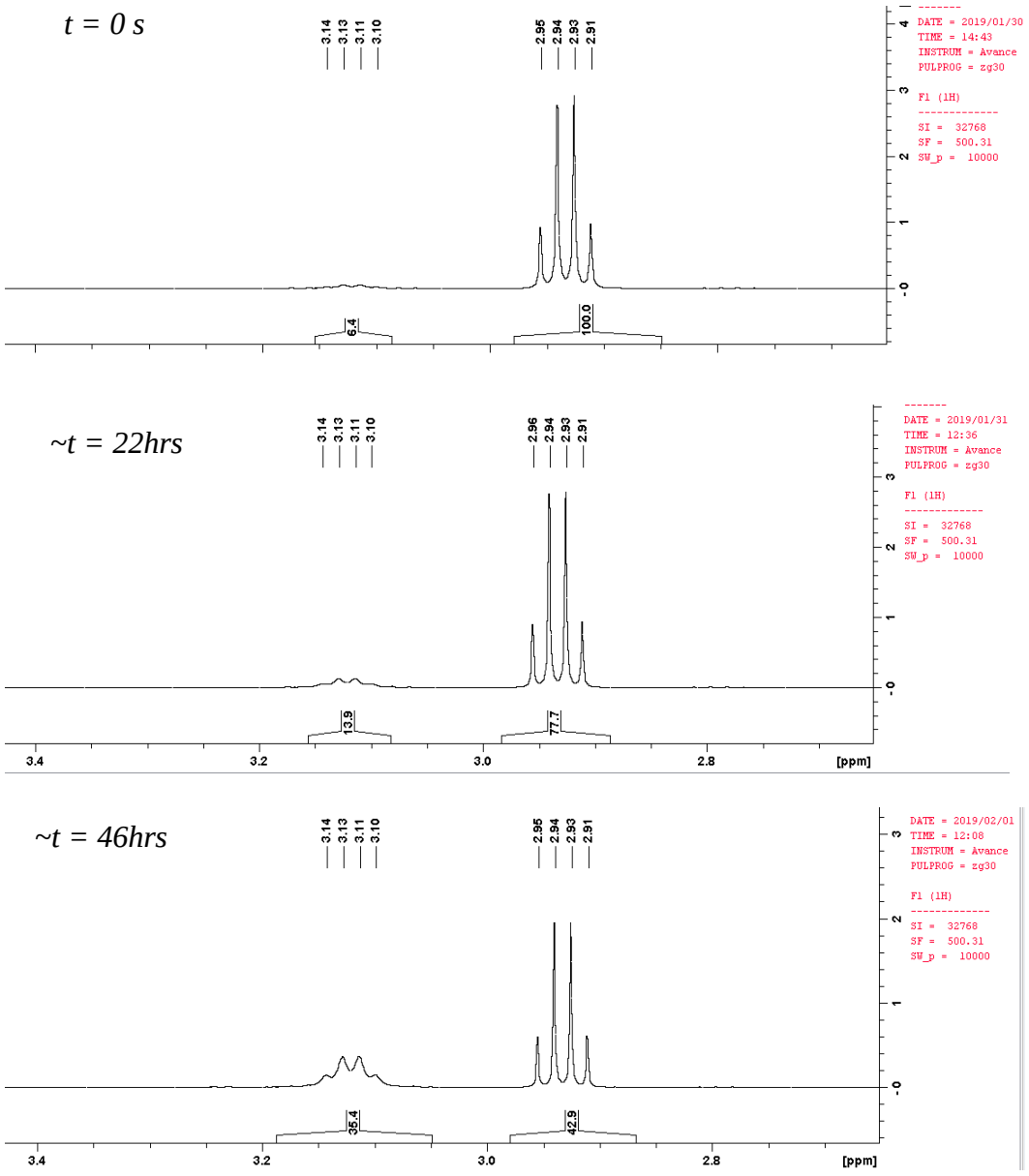

*Activation energy barrier calculation for the ring opening of **III-7b** to **III-8b** using half-life and Arrhenius equations*

Using the half-life at different temperatures of **III-7b** and first order kinetics;

$$t_{1/2} = \frac{ln\,2}{k} \qquad (eq.1)$$

In which $t_{1/2}$ and k are half-life of the reaction and rate constants respectively. Thus, from eq. 1, rate constants at 298 and 337 K can be calculated shown as

$$k_{298} = \frac{0.693}{165{,}600}s^{-1},\ k_{337} = \frac{0.693}{990}s^{-1}$$

Using rate constants at two temperatures, theactivation energy can be calculated via the Arrhenius equation:

$$k = A \times e^{-\frac{E_a}{RT}} \qquad (eq.2)$$

In which $k, A, E_a, R,$ and$T$ are rate constant, pre-exponential factor, activation energy, universal gas constant, and temperature, respectively.

$$\ln\left(\frac{k_{337}}{k_{298}}\right) = 5.5 = \frac{E_a}{R}\left(\frac{1}{298} - \frac{1}{337}\right), R = 0.001987\frac{cal}{molK} \rightarrow \boldsymbol{E_a = 28.1 kcal/mol}$$

So, the activation energy barrier (E_a) for the ring opening of **III-7b** to **III-8b** is approximately 28 kcal/mol**.**

*3.5.9. X-ray crystallography data Phenyl N-(Ethoxycarbonyl)-2-((ethoxycarbonyl)imino)-2-phenylethanimidothioate (**III-8g**)*

Single crystal X-ray diffraction data were accumulated using Bruker D8 Venture and Bruker D8 Quest diffractometers with Mo Kα radiation (λ = 0.07107 Å) and a Photon 100 detector. Data were acquired using phi and omega scans with the oscillations of 0.5°. Bruker Apex3 software package was used for the instrument control, data processing (SAINT), and data scaling (SADABS).[124] Space group were determined by the systematic absences, and intrinsic phasing (SHELXT) was used to solve the structures, subsequently refined on F^2 from full matrix least squares techniques (SHELXL).[125] Anisotropic refinements were used for non-hydrogen atoms. Appropriate riding models were used to place the hydrogen atoms in geometrically optimized positions. The location of the hydrogen atom attached to the nitrogen atom N2 of **III-8g** was able to confirm by the difference electron density map. The crystallographic data for **III-8g** has provided in Table 3.6.

Table 3.6. Crystallographic data.

	III-8g
Empirical formula	$C_{20}H_{20}N_2O_4S$
Formula weight (g/mol)	384.44
Crystal system	monoclinic
Space group, *Z*	$P2_1/c$, 4
Temperature (K)	140
Crystal size (mm)	0.09 x 0.15 x 0.24
a, Å	9.6872(9)
b, Å	12.2430(12)
c, Å	16.6225(15)
β, °	102.063(3)
volume ($Å^3$)	1927.9(3)
D_{calc} (g/cm^3)	1.324
Abs. Coeff. (mm^{-1})	0.196
F(000)	808
T_{max}, T_{min}	1.0000, 0.9635
Θ range for data (°)	3.56-26.50
Reflections collected	37901
Data/restraints/parameters	3982 / 0 / 244
R(int)	0.0328
Final R [$I > 2\sigma(I)$] R1, wr2	0.0331, 0.0763
Final R (all data) R1, wr2	0.0395, 0.0800
Goodness-of-fit on F^2	1.080
Larg. Diff. Peak, hole, $eå^{-3}$	0.275, -0.267

The molecular structure and packing arrangement of compound **III-8g** is shown in Figure 3.16. The C1-N1 and C2-N2 bond lengths are of imine bonds, while the remaining bonds to C1 and C2 (C1-C9, C1-C2, C2-S1) are consistent with typical single bonds. The packing of molecules seems to be mainly governed by H···pi interactions between the phenyl rings of neighboring molecules (H12···Cg = 2.974 Å), while weak C-H···N and C-H···O interactions (H···A = 2.43-2.68 Å; D···A = 3.243(2)-3.596(2) Å; D-H···A = 135.6-156.3°) are providing an additional support.

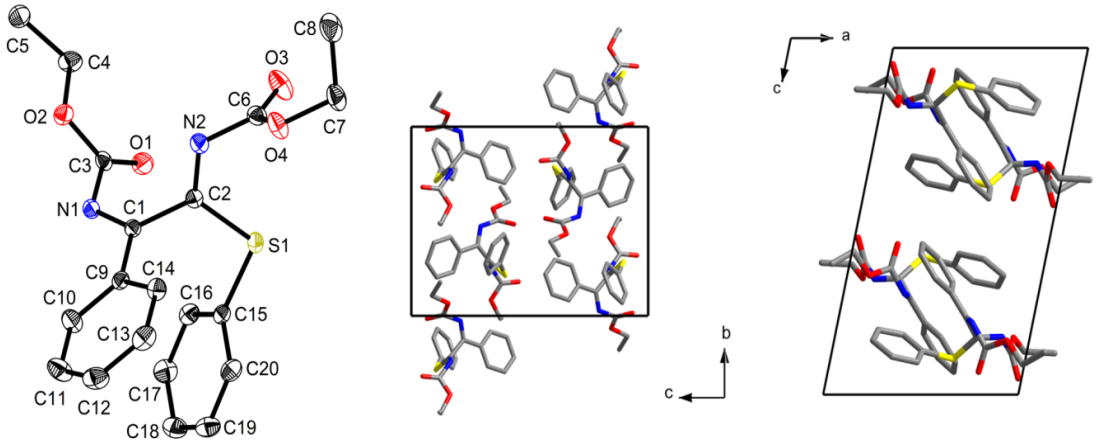

Figure 3:16. Molecular structure (left) and molecular packing (center, right) of **III-8g**.

3.5.10 Characterization data for the enyne sulfides and the compounds related to enyne synthesis.

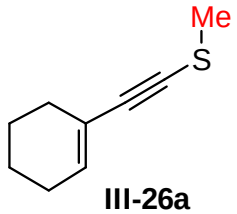

III-26a

Light yellow liquid; Yield: 75% (571 mg), 84% (10 mmol, 1.278 g); ^{1}H-NMR (300 MHz, $CDCl_3$) δ =6.00 (pentet, *J* = 2.0 Hz, 1H), 2.31 (s, 3H), 2.20-1.90 (m, 4H), 1.70-1.40 (m, 4H); ^{13}C NMR (75 MHz, $CDCl_3$) δ =134.5, 120.6, 93.4, 77.3, 28.9, 25.4, 22.1, 21.2, 19.2.

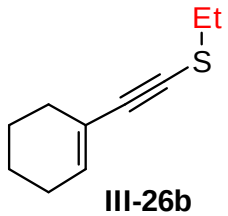

III-26b

Light yellow liquid; Yield: 91% (756 mg); ^{1}H-NMR (300 MHz, $CDCl_3$) δ =6.04 (pentet, *J* = 2.0 Hz, 1H), 2.69 (q, *J* = 7.3 Hz, 2H), 2.20-2.00 (m, 4H), 1.70-1.45 (m, 4H), 1.35 (t, *J* = 7.3 Hz, 3H); ^{13}C NMR (75 MHz, $CDCl_3$) δ =134.4, 120.8, 95.2, 75.5, 29.8, 29.1, 25.5, 22.2, 21.4, 14.5.

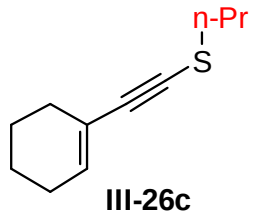

III-26c

Light yellow liquid; Yield: 77% (694 mg); ^{1}H-NMR (500 MHz, $CDCl_3$) δ =6.02 (bs, 1H), 2.64 (t, *J* = 7.1 Hz, 2H), 2.20-2.00 (m. 4H), 1.73 (sextet, *J* = 7.1 Hz, 2H), 1.65-1.45 (m, 4H), 0.98 (t, *J* = 7.3 Hz, 3H); ^{13}C NMR (125 MHz, $CDCl_3$) δ =134.2, 120.9, 94.5, 75.9, 37.6, 29.1, 25.5, 22.4, 22.2, 21.4, 12.8.

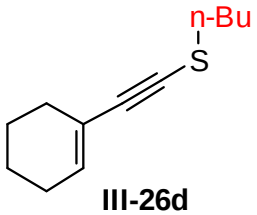

III-26d

Light yellow liquid; Yield: 57% (554 mg); ^{1}H-NMR (300 MHz, $CDCl_3$) δ =6.04 (pentet, *J* = 2.0 Hz, 1H), 2.68 (t, *J* = 7.3 Hz, 2H), Hz, .20-2.00 (m, 4H), 1.69 (pentet, *J* = 7.4 Hz, 2H), 1.64-1.50 (m, 4H), 1.42 (sextet, *J* = 7.4 Hz, 2H), 0.91 (t, *J* = 7.3 Hz, 3H); ^{13}C NMR (75 MHz, $CDCl_3$) δ =134.3, 120.9, 94.6, 76.1, 35.4, 31.2, 29.1, 25.6, 22.2, 21.4, 21.3, 13.5.

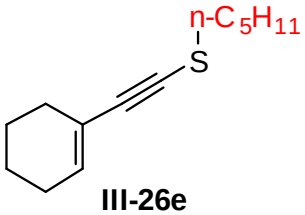

III-26e

Light yellow liquid; Yield: 90% (938 mg); ^{1}H-NMR (500 MHz, $CDCl_3$) δ =6.10-6.00 (m, 1H), 2.70 (t, *J* = 7.3 Hz, 2H), 2.20-2.00 (m, 4H), 1.73 (pentet, *J* = 7.3 Hz, 2H), 1.65-1.50 (m, 4H), 1.45-1.28 (m, 4H), 2.70 (t, *J* = 7.3 Hz, 3H); ^{13}C NMR (125 MHz, $CDCl_3$) δ =134.4, 121.0, 94.7, 76.1, 35.8, 30.4, 29.2, 28.9, 25.6, 22.3, 22.2, 21.4, 13.9.

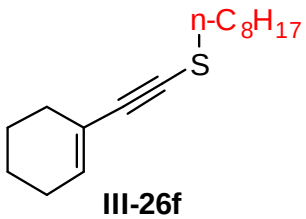

III-26f

Light yellow liquid; Yield: 82% (1027 mg); ^{1}H-NMR (300 MHz, $CDCl_3$) δ =6.07 (pentet, *J* = 2.0 Hz, 1H), 2.70 (t, *J* = 7.3 Hz, 2H), 2.20-2.00 (m, 4H), 1.72 (pentet, *J* = 7.3 Hz, 2H), 1.67-1.50 (m, 4 H), 1.47-1.20 (m, 10H), 0.88 (t, *J* = 6.6 Hz, 3H); ^{13}C NMR (75 MHz, $CDCl_3$) δ =134.5, 121.0, 94.7, 76.1, 35.8, 31.8, 29.21, 29.18, 29.13, 29.1, 28.2, 25.6, 22.6, 22.3, 21.5, 14.1.

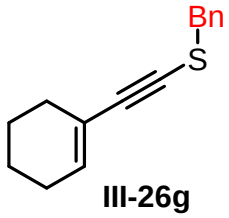

III-26g

Light yellow liquid; Yield: 89% (1016 mg); ^{1}H-NMR (300 MHz, $CDCl_3$) δ =7.50-7.30 (m, 5H), 6.08 (pentet, *J* = 2.0 Hz, 1H), 3.96 (s, 2H), 2.20-2.05 (m, 4H), 1.75-1.50 (m, 4H); ^{13}C NMR (75 MHz, $CDCl_3$) δ =136.6, 134.4, 128.9, 128.3, 127.4, 120.7, 96.4, 75.7, 40.3, 28.9, 25.5, 22.1, 21.3.

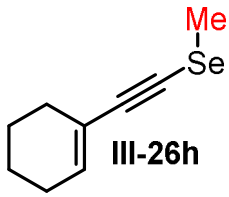

III-26h

Light yellow liquid; Yield: 93% (908 mg); ^{1}H-NMR (500 MHz, $CDCl_3$) δ = 6.20-6.00 (m, 1H), 2.28 (s, 3H), 2.20-2.00 (m, 4H), 1.70-1.50 (m, 4H); ^{13}C NMR (75 MHz, $CDCl_3$) δ = 135.0, 121.0, 100.1, 67.7, 29.2, 25.7, 22.3, 21.5, 9.8.

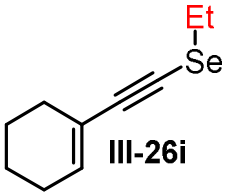

III-26i

Light yellow liquid; Yield: 94% (1000 mg); ^{1}H-NMR (300 MHz, $CDCl_3$) δ = 6.07 (pentet, *J* = 2.0 Hz, 1H), 2.77 (q, *J* = 7.4 Hz, 2H), 2.20-2.00 (m, 4H), 1.70-1.57 (m, 4H), 1.53 (t, *J* = 7.4 Hz, 3H); ^{13}C NMR (75 MHz, $CDCl_3$) δ = 134.5, 121.0, 101.8, 66.3, 29.1, 25.5, 22.8, 22.2, 21.4, 15.5.

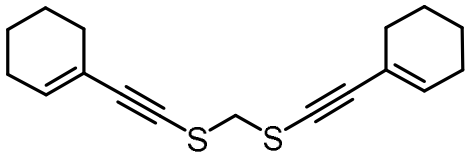

III-26j

Light yellow liquid; Yield: 24% (346 mg); ^{1}H-NMR (500 MHz, $CDCl_3$) δ = 6.15 (heptet, *J* = 1.87 Hz, 2H), 4.00 (s, 2H), 2.20-2.00 (m, 8H), 1.70-1.50 (m, 8H); ^{13}C NMR (125 MHz, $CDCl_3$) δ = 136.1, 120.7, 97.7, 73.9, 43.4, 29.0, 25.7, 22.2, 21.4.

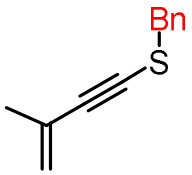

III-29c

Light yellow liquid; Yield: 71% (401 mg); ^{1}H-NMR (300 MHz, $CDCl_3$) δ = 7.42-7.26 (m, 5H), 5.22-5.17 (m, 1H), 5.17-5.11 (m, 1H), 3.95 (s, 2H), 1.90-1.80 (m, 3H); ^{13}C NMR (75 MHz, $CDCl_3$) δ = 136.6, 129.1, 128.6, 127.8, 126.7, 120.5, 96.4, 78.3, 40.4, 23.2.

*3.5.11 General procedure for the synthesis of tetrahydroindoles (**III-27**)*

To a flame dried round bottom flask (RBF), was added a stir bar, bis(2,2,2-trichlorethyl) azodicarboxylate (1 mmol, 1 equiv.) and 5 mL of dry toluene. To this reaction mixture, the corresponding alkynyl sulfide (1.3 mmol, 1.3 equiv.) in a solution of dry toluene (5 mL) was added in dropwise fashion. Then the RBF was equipped with a water cooled condenser and refluxed for 72 h under a nitrogen atmosphere while maintaining the volume of toluene throughout the experiment (Note: in order to maintain the same reaction volume; 5-6 mL of fresh toluene was added into the reaction mixture in between every 24 hrs as needed). Next, the crude reaction mixture was concentrated by rotary evaporation and purified via flash silica gel chromatography with hexane/ethyl acetate (0 to 20% ethyl acetate) to provide the corresponding tetrahydroindole **III-27**.

*3.5.12. Characterization data for tetrahydroindoles (**III-27**)*

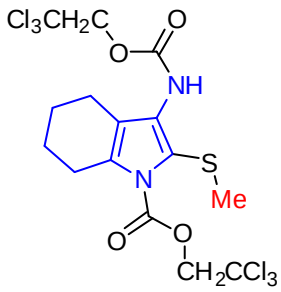

III-27a

Light yellow solid; Yield: 77% (373 mg), 64% (1.01 g);Mp: 130.4-131.4°C; IR(neat): 3298 (m), 2951 (m), 2927 (m), 2854 (m), 1720 (s), 1612 (m), 1550 (m), 1471 (m), 1438 (w), 1377 (s), 1342 (w), 1319 (s), 1280 (m), 1222 (m), 1203 (m), 1180 (s), 111 (s), 1068 (w), 1041 (w), 1026 (m), 709 (s), 570 (s) cm^{-1}; ^{1}H-NMR (300 MHz, $CDCl_3$) δ =6.74 (bs, 1H), 5.00 (s, 2H), 4.83 (s, 2H), 2.89 (t, *J* = 6.1 Hz, 2H), 2.45 (t, *J* = 5.9 Hz, 2H), 2.34 (s, 3H), 1.90-1.75 (m, 2H), 1.75-1.65 (m, 2H); ^{13}C NMR (75 MHz, $CDCl_3$) δ = 152.7, 149.1, 133.7, 130.7, 119.6, 116.5, 95.4, 94.1, 76.0, 74.7, 25.9, 23.1, 22.0 (2C, *see* 2D HMQC analysis), 20.7.

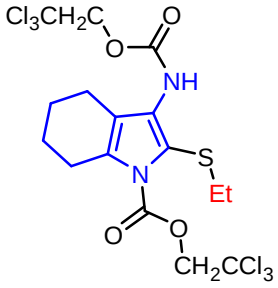

III-27b

Light yellow solid; Yield: 91% (498 mg); Mp: 114.6-115.6°C; IR (neat):3259 (bm), 2924 (m), 2854 (m), 1751 (s), 1712 (s), 1616 (s), 1558 (s), 1492 (s), 1442 (s), 1384 (s), 1357 (w), 1338 (w), 1315 (s), 1261 (w), 1238 (m), 1203 (m), 1180 (s), 1118 (s), 1064 (m), 1026 (s), 810 (s), 709 (s), 567 (m) cm^{-1}; ^{1}H-NMR (300 MHz, $CDCl_3$) δ =6.80 (bs, 1H), 4.99 (s, 2H), 4.82 (s, 2H), 2.89 (t, *J* = 6.2 Hz, 2H), 2.77 (q, *J* = 7.4 Hz, 2H), 2.45 (t, *J* = 6.0 Hz, 2H), 1.90-1.76 (m, 2H), 1.76-1.60 (m, 2H), 1.18 (t, *J* = 7.4 Hz, 3H); ^{13}C NMR (75 MHz, $CDCl_3$) δ =152.7, 149.2, 134.0, 132.2, 119.6, 113.9, 95.4, 94.1, 76.0, 74.7, 31.0, 26.0, 23.1, 22.2, 22.1, 14.6.

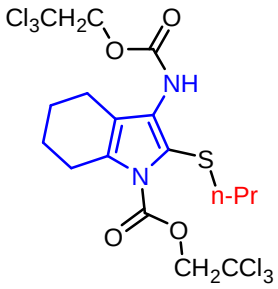

III-27c

Light yellow solid; Yield: 72% (404 mg); Mp: 110.4-111.4°C; IR (neat):3259 (m), 2962 (w), 2939 (m), 2854 (w), 1751 (s), 1712 (s), 1612 (s), 1558 (s), 1492 (s), 1442 (s), 1381 (s), 1338 (w), 1257 (m), 1234 (m), 1203 (m), 1180 (s), 1120 (s), 1056 (m), 1029 (s), 995 (w), 871 (w), 840 (s), 810 (s), 708 (s), 563 (s) cm^{-1}; ^{1}H-NMR (500 MHz, $CDCl_3$) δ =6.79 (bs, 1H), 5.00 (s, 2H), 4.82 (s, 2H), 2.89 (t, *J* = 6.3 Hz, 2H), 2.71 (t, *J* = 7.4 Hz, 2H), 2.47 (t, *J* = 6.1 Hz, 2H),1.90-1.76 (m, 2H), 1.76-1.64 (m, 2H), 1.54 (sextet, *J* = 7.4 Hz, 2H), 0.96 (t, *J* = 7.3 Hz, 3H); ^{13}C NMR (125 MHz, $CDCl_3$) δ =152.6, 149.2, 133.9, 131.9, 119.5, 114.2, 95.4, 94.1, 76.0, 74.7, 39.1, 26.0, 23.1, 22.8, 22.2, 22.1, 13.3.

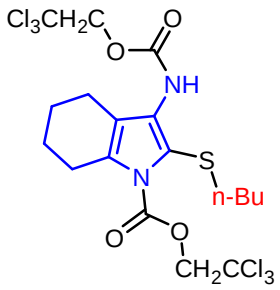

III-27d

Light yellow solid; Yield: 79% (454 mg); Mp: 120.6-121.6°C; IR (neat): 3255 (bm), 2931 (m), 2850 (w), 1743 (s), 1708 (s), 1612 (s), 1550 (s), 1485 (s), 1442 (s), 1381 (s), 1315 (s), 1238 (s), 1207 (w), 1180 (s), 1114 (s), 1064 (w), 1049 (w), 1029 (s), 995 (w), 740 (m), 709 (s), 567 (s)cm^{-1}; ^{1}H-NMR (500 MHz, $CDCl_3$) δ =6.79 (bs, 1H), 5.00 (s, 2H), 4.82 (s, 2H), 2.89 (t, *J* = 6.1 Hz, 2H), 2.74 (t, *J* = 7.5 Hz, 2H), 2.47 (t, *J* = 5.9 Hz, 2H), 1.90-1.76 (m, 2H), 1.76-1.60 (m, 2H), 1.50 (pentet, *J* = 7.4 Hz, 2H), 1.38 (sextet, *J* = 7.4 Hz, 2H), 0.87 (t, *J* = 7.3 Hz, 3H); ^{13}C NMR (125 MHz, $CDCl_3$) δ =152.6, 149.2, 133.9, 131.9, 119.5, 114.3, 95.4, 94.1, 76.0, 74.7, 36.8, 31.5, 26.0, 23.1, 22.2, 22.1, 21.9, 13.7.

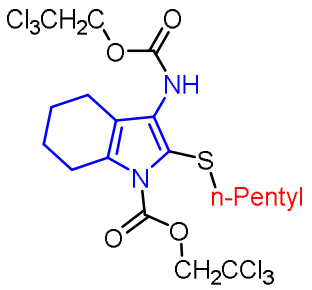

III-27e

Light yellow solid; Yield: 77% (453 mg); Mp: 112.7-113.7°C; IR (neat):3259 (bm), 2924 (m), 2854 (w), 1747 (s), 1708 (s), 1612 (s), 1550 (s), 1485 (s), 1442 (s), 1381 (s), 1315 (s), 1238 (s), 1176 (s), 1114 (s), 1053 (w), 1026 (s), 790 (m), 713 (s), 567 (s) cm^{-1}; ^{1}H-NMR (500 MHz, $CDCl_3$) δ =6.78 (bs, 1H), 4.99 (s, 2H), 4.81 (s, 2H), 2.89 (t, *J* = 6.3 Hz, 2H), 2.74 (t, *J* = 7.5 Hz, 2H), 2.46 (t, *J* = 6.1 Hz, 2H), 1.90-1.75 (m, 2H), 1.75-1.65 (m, 2H), 1.53 (pentet, *J* = 7.4 Hz, 2H), 1.40-1.20 (m, 4H), 0.87 (t, *J* = 7.2 Hz, 3H); ^{13}C NMR (125 MHz, $CDCl_3$) δ =152.6, 149.1, 133.9, 131.9, 119.5, 114.4, 95.4, 94.1, 76.0, 74.7, 37.1, 30.9, 29.1, 26.0, 23.1, 22.3, 22.2, 22.1, 14.0.

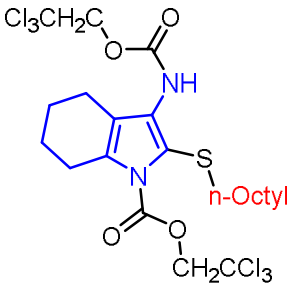

III-27f

Light yellow solid; Yield: 83% (524 mg); Mp: 53.3-54.3°C; IR (neat):3325 (m), 2927 (s), 2854 (m), 1755 (s), 1728 (s), 1608 (s), 1550 (s), 1477 (m), 1446 (m), 1392 (s), 1319 (s), 1273 (w), 1211 (s), 1176 (s), 1111 (s), 1064 (w), 1049 (w), 1026 (s), 960 (m), 837 (m), 798 (s), 725 (s), 570 (s) cm^{-1}; ^{1}H-NMR (300 MHz, $CDCl_3$) δ =6.78 (bs, 1H), 4.99 (s, 2H), 4.81 (s, 2H), 2.89 (t, *J* = 6.0 Hz, 2H), 2.73 (t, *J* = 7.5 Hz, 2H), 2.46 (t, *J* = 5.8 Hz, 2H), 1.90-1.76 (m, 2H), 1.76-1.60 (m, 2H), 1.60-1.44 (m, 2H), 1.40-1.15 (m, 10H), 0.87 (t, *J* = 6.7 Hz, 3H); ^{13}C NMR (75 MHz, $CDCl_3$) δ =152.6, 149.1, 133.8, 131.8, 119.5, 114.4, 95.4, 94.1, 76.0, 74.7, 37.1, 31.8, 29.5, 29.2 (2C, *see* 2D-HMQC), 28.8, 26.0, 23.1, 22.6, 22.2, 22.1, 14.1.

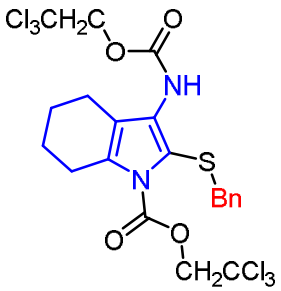

III-27g

Light yellow solid; Yield: 29% (177 mg); Mp: 89.6-90.7°C; IR (neat): 3298 (bm), 2927 (m), 2850 (w), 1751 (s), 1716 (s), 1608 (s), 1550 (s), 1481 (s), 1442 (s), 1381 (s), 1315 (s), 1234 (s), 1176 (s), 1114 (m), 1095 (m), 1064 (w), 1049 (w), 1026 (s), 906 (w), 802 (s), 709 (s), 659 (m), 563 (w) cm^{-1}; ^{1}H-NMR (500 MHz, $CDCl_3$) δ =7.40-7.22 (m, 3H), 7.20-7.10 (m, 2H), 5.93 (bs, 1H), 5.02 (s, 2H), 4.69 (s, 2H), 3.91 (s, 2H), 2.90 (t, *J* = 6.3 Hz, 2H), 2.36 (t, *J* = 6.1 Hz, 2H), 1.90-1.75 (m, 2H), 1.75-1.60 (m, 2H); ^{13}C NMR (125 MHz, $CDCl_3$) δ =152.2, 149.2, 138.5, 134.3, 133.1, 128.9, 128.6, 127.2, 119.4, 113.0, 95.4, 94.1, 76.1, 74.6, 41.7, 25.9, 23.0, 22.0 (2C, *see* 2D-HMQC).

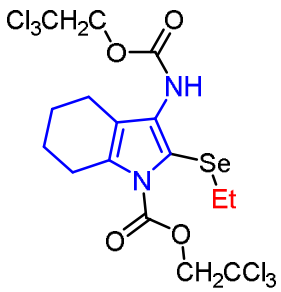

III-27i

Light yellow solid; Yield: 31% (172 mg); Mp: 92.0-93.0°C; IR (neat): 3317 (s), 3012 (w), 2939(s), 2854 (w), 1743 (s), 1712 (s), 1612 (s), 1554 (s), 1485 (m), 1435 (s), 1388 (s), 1323 (s), 1219 (s), 1199 (s), 1180 (s), 1107 (s), 1064 (m), 1022 (s), 906 (s), 798 (m), 759 (m), 709 (s), 567 (s) cm^{-1}; ^{1}H-NMR (500 MHz, $CDCl_3$) δ =6.74 (bs, 1H), 4.99 (s, 2H), 4.82 (s, 2H), 2.90 (t, *J* = 6.3 Hz, 2H), 2.80 (q, *J* = 7.4 Hz, 2H), 2.46 (t, *J* = 6.0 Hz, 2H), 1.90-1.75 (m, 2H), 1.75-1.60 (m, 2H), 1.32 (t, *J* = 7.5 Hz, 3H); ^{13}C NMR (125 MHz, $CDCl_3$) δ =152.8, 149.4, 134.2, 132.1, 120.1, 108.0, 95.4, 94.1, 76.0, 74.7, 26.0, 24.1, 23.1, 22.10, 22.06, 15.4.

*3.5.13. XRD data for tetrahydroindoles (**III-27**)*

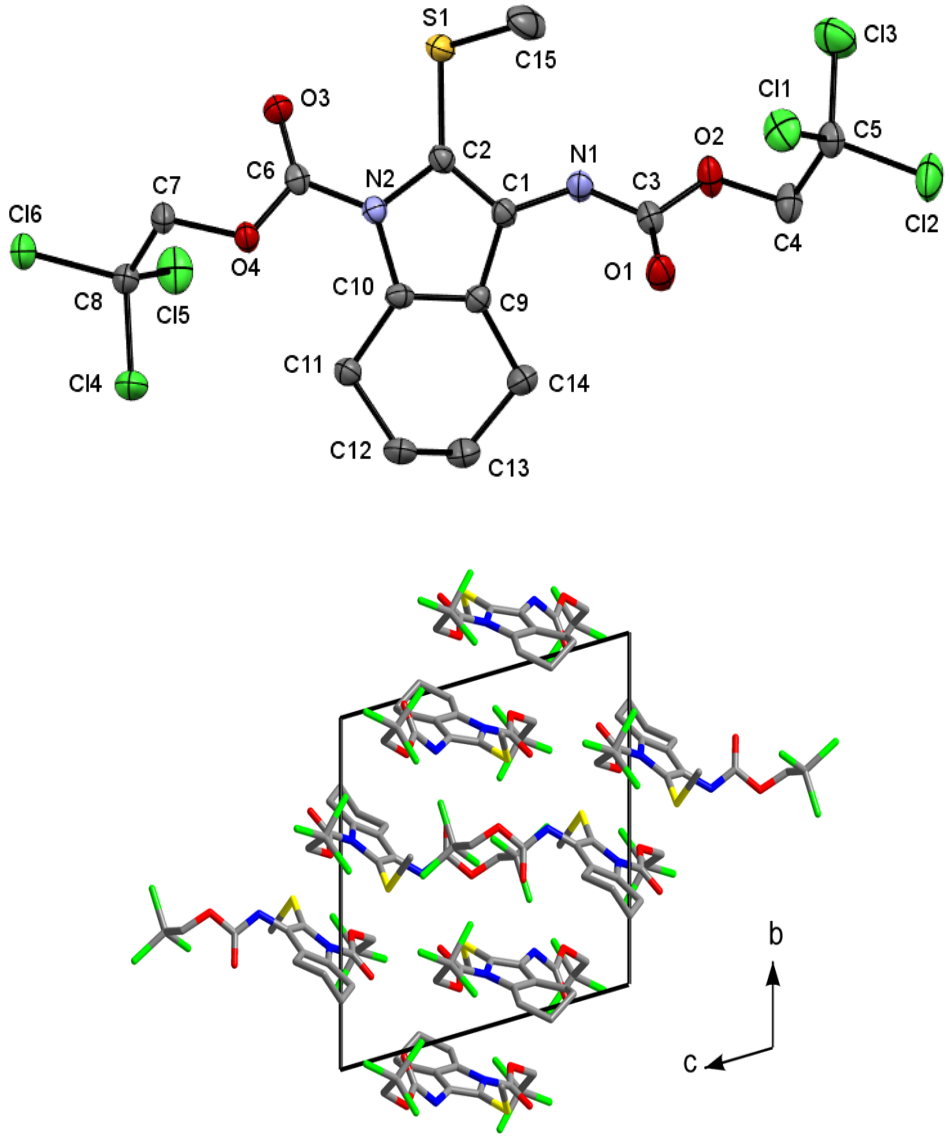

Figure 3.17. XRD structure (top) and the packing diagram (bottom) of the tetrahydroindole (**III-27a**).

Table 3.7 Sample and crystal data for **III-27a**.

Identification code	Q_1325_CN_IV_147_89	
Chemical formula	$C_{15}H_{16}Cl_6N_2O_4S$	
Formula weight	533.06 g/mol	
Temperature	173(2) K	
Wavelength	0.71073 Å	
Crystal size	0.145 x 0.152 x 0.214 mm	
Crystal system	triclinic	
Space group	P -1	
Unit cell dimensions	a = 12.3731(8) Å	α = 95.196(2)°
	b = 13.8691(9) Å	β = 112.586(2)°
	c = 14.4046(9) Å	γ = 108.206(2)°
Volume	2104.6(2) $Å^3$	
Z	4	
Density (calculated)	1.682 g/cm^3	
Absorption coefficient	0.941 mm^{-1}	
F(000)	1080	

Table 3.8. Data collection and structure refinement for **III-27a**.

Theta range for data collection	3.19 to 26.50°	
Index ranges	-15<=h<=15, -17<=k<=17, -18<=l<=18	
Reflections collected	37523	
Independent reflections	8541 [R(int) = 0.0396]	
Max. and min. transmission	1.0000 and 0.9053	
Structure solution technique	direct methods	
Structure solution program	SHELXT 2014/5 (Sheldrick, 2014)	
Refinement method	Full-matrix least-squares on F^2	
Refinement program	SHELXL-2016/6 (Sheldrick, 2016)	
Function minimized	$\Sigma\, w(F_o^2 - F_c^2)^2$	
Data / restraints / parameters	8541 / 0 / 507	
Goodness-of-fit on F^2	1.035	
Δ/σ_{max}	0.001	
Final R indices	6407 data; $I>2\sigma(I)$	R1 = 0.0391, wR2 = 0.0849
	all data	R1 = 0.0607, wR2 = 0.0940
Weighting scheme	$w=1/[\sigma^2(F_o^2)+(0.0369P)^2+1.7101P]$ where $P=(F_o^2+2F_c^2)/3$	
Largest diff. peak and hole	0.789 and -0.640 eÅ^{-3}	
R.M.S. deviation from mean	0.068 eÅ^{-3}	

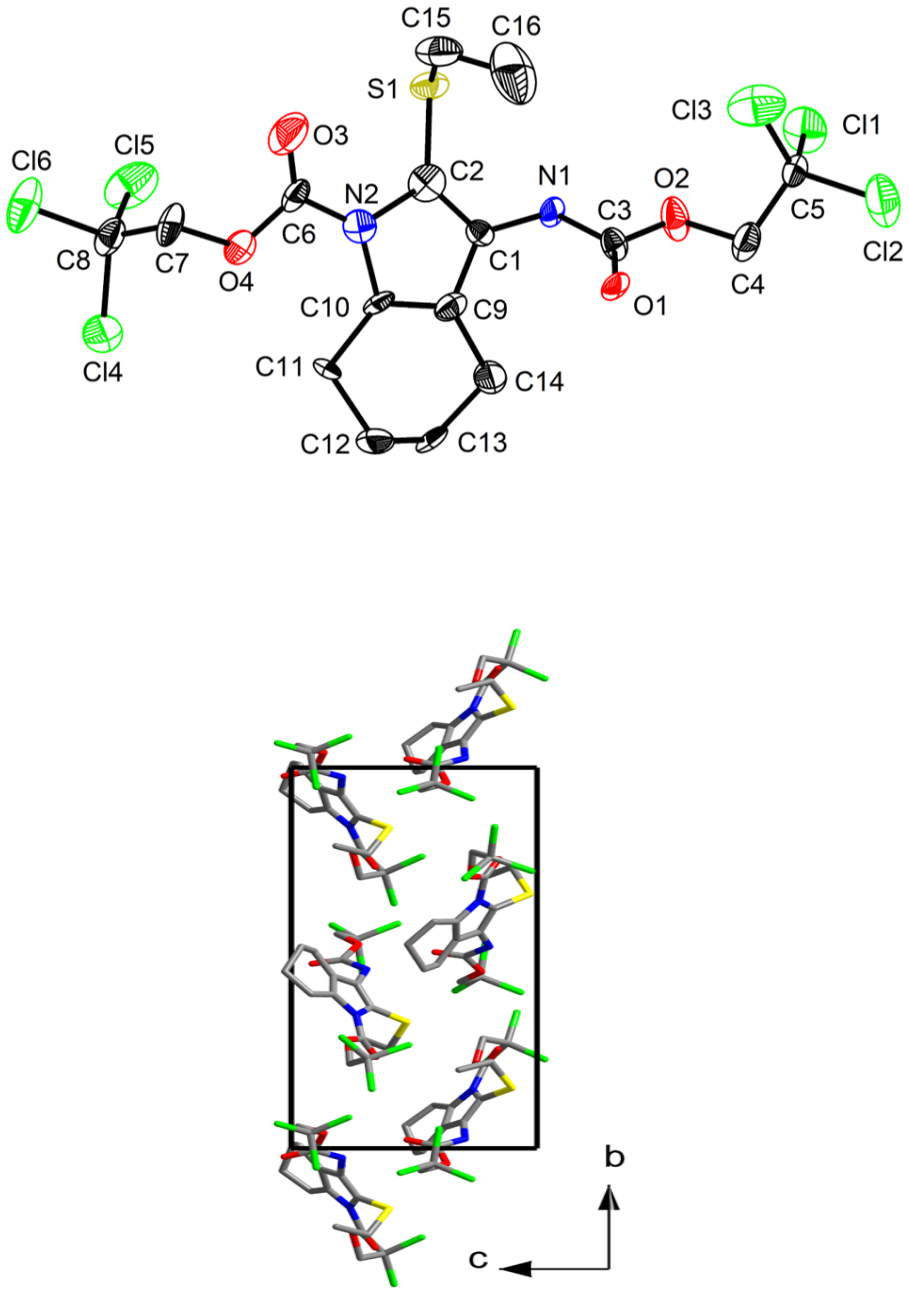

Figure 3.18. XRD structure (top) and the packing diagram (bottom) of the tetrahydroindole (**III-27b**).

Table 3.9 Sample and crystal data for **III-27b**.

Identification code	Q_0752_CN_IV_160_58	
Chemical formula	$C_{16}H_{18}Cl_6N_2O_4S$	
Formula weight	547.08 g/mol	
Temperature	140(2) K	
Wavelength	0.71073 Å	
Crystal size	0.059 x 0.087 x 0.214 mm	
Crystal system	monoclinic	
Space group	P c	
Unit cell dimensions	a = 12.5120(17) Å	α = 90°
	b = 19.393(3) Å	β = 96.051(4)°
	c = 9.6223(13) Å	γ = 90°
Volume	2321.8(5) $Å^3$	
Z	4	
Density (calculated)	1.565 g/cm^3	
Absorption coefficient	0.855 mm^{-1}	
F(000)	1112	

Table 3.10 Data collection and structure refinement for **III-27b**.

Theta range for data collection	3.30 to 25.25°	
Index ranges	-15<=h<=15, -23<=k<=23, -11<=l<=11	
Reflections collected	20840	
Independent reflections	8056 [R(int) = 0.0476]	
Max. and min. transmission	1.0000 and 0.8421	
Structure solution technique	direct methods	
Structure solution program	SHELXT 2014/5 (Sheldrick, 2014)	
Refinement method	Full-matrix least-squares on F^2	
Refinement program	SHELXL-2016/6 (Sheldrick, 2016)	
Function minimized	$\Sigma\, w(F_o^2 - F_c^2)^2$	
Data / restraints / parameters	8056 / 20 / 524	
Goodness-of-fit on F^2	1.107	
Final R indices	6876 data; $I>2\sigma(I)$	R1 = 0.0866, wR2 = 0.2180
	all data	R1 = 0.0991, wR2 = 0.2263
Weighting scheme	$w=1/[\sigma^2(F_o^2)+(0.1065P)^2+14.4015P]$ where $P=(F_o^2+2F_c^2)/3$	
Absolute structure parameter	0.14(18)	
Largest diff. peak and hole	1.448 and -0.627 eÅ^{-3}	
R.M.S. deviation from mean	0.150 eÅ^{-3}	

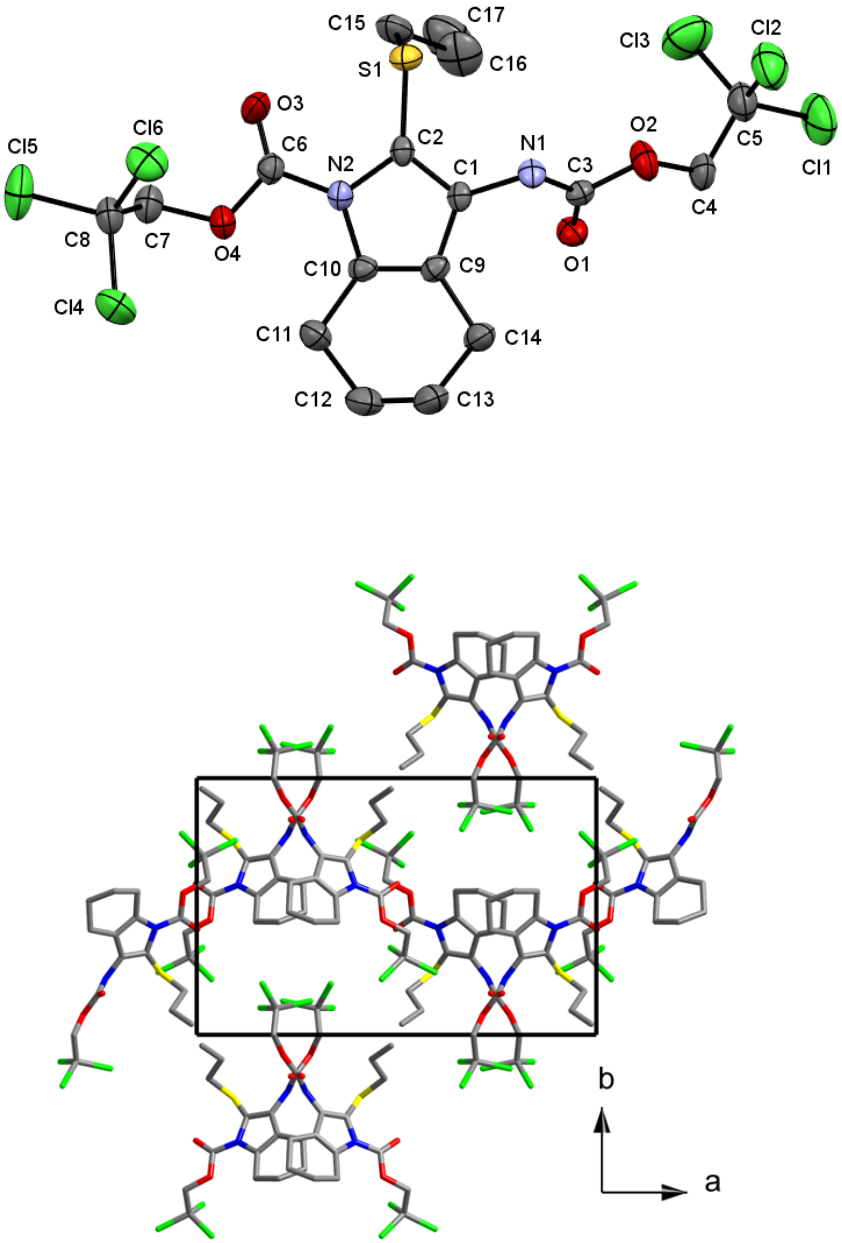

Figure 3.19. XRD structure (top) and the packing diagram (bottom) of the tetrahydroindole (**III-27c**).

Table 3.11. Sample and crystal data for **III-27c**.

Identification code	D8_3847_CN_III_32_16	
Chemical formula	$C_{17}H_{20}Cl_6N_2O_4S$	
Formula weight	561.11 g/mol	
Temperature	298(2) K	
Wavelength	0.71073 Å	
Crystal size	0.024 x 0.024 x 0.187 mm	
Crystal system	orthorhombic	
Space group	P c a 21	
Unit cell dimensions	a = 20.017(2) Å	α = 90°
	b = 12.8682(15) Å	β = 90°
	c = 9.6796(10) Å	γ = 90°
Volume	2493.3(5) $Å^3$	
Z	4	
Density (calculated)	1.495 g/cm^3	
Absorption coefficient	0.798 mm^{-1}	
F(000)	1144	

Table 3.12. Data collection and structure refinement for **III-27c**

Theta range for data collection	2.82 to 25.25°	
Index ranges	-24<=h<=24, -15<=k<=15, -11<=l<=10	
Reflections collected	16616	
Independent reflections	4339 [R(int) = 0.0785]	
Max. and min. transmission	1.0000 and 0.8395	
Structure solution technique	direct methods	
Structure solution program	SHELXT 2014/5 (Sheldrick, 2014)	
Refinement method	Full-matrix least-squares on F^2	
Refinement program	SHELXL-2016/6 (Sheldrick, 2016)	
Function minimized	$\Sigma\, w(F_o^2 - F_c^2)^2$	
Data / restraints / parameters	4339 / 1 / 272	
Goodness-of-fit on F^2	1.045	
Final R indices	2801 data; $I>2\sigma(I)$	R1 = 0.0605, wR2 = 0.1045
	all data	R1 = 0.1023, wR2 = 0.1179
Weighting scheme	$w=1/[\sigma^2(F_o^2)+(0.0383P)^2+1.1424P]$ where $P=(F_o^2+2F_c^2)/3$	
Absolute structure parameter	0.00(5)	
Largest diff. peak and hole	0.217 and -0.203 eÅ^{-3}	
R.M.S. deviation from mean	0.046 eÅ^{-3}	

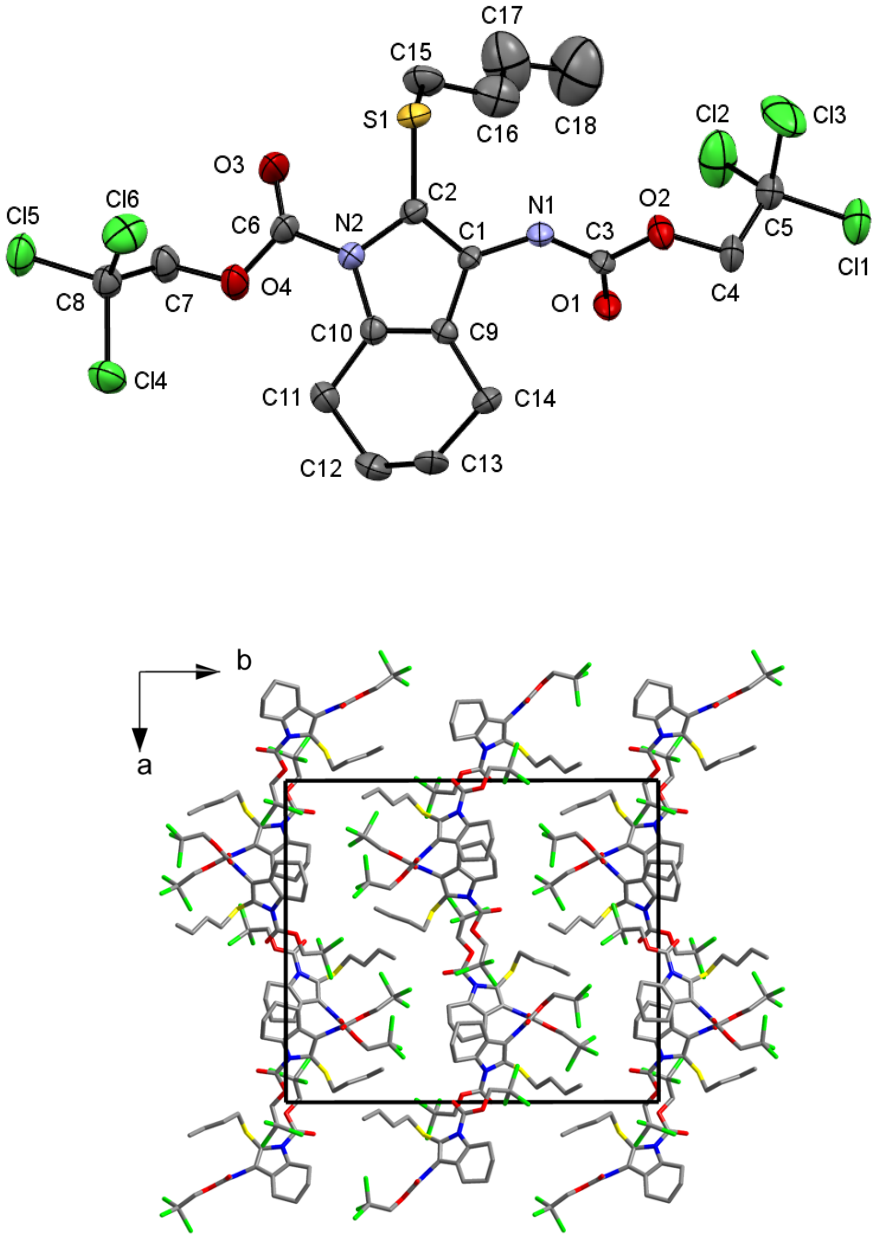

Figure 3.20. XRD structure (top) and the packing diagram (bottom) of the tetrahydroindole (**III-27d**).

Table 3.13. Sample and crystal data for **III-27d**

Identification code	D8_3851_CN_III_61_40	
Chemical formula	$C_{18}H_{22}Cl_6N_2O_4S$	
Formula weight	575.13 g/mol	
Temperature	298(2) K	
Wavelength	0.71073 Å	
Crystal size	0.036 x 0.041 x 0.210 mm	
Crystal system	orthorhombic	
Space group	P n a 21	
Unit cell dimensions	a = 21.206(5) Å	α = 90°
	b = 24.547(5) Å	β = 90°
	c = 9.891(2) Å	γ = 90°
Volume	5148.7(19) $Å^3$	
Z	8	
Density (calculated)	1.484 g/cm^3	
Absorption coefficient	0.775 mm^{-1}	
F(000)	2352	

Table 3.14. Data collection and structure refinement for **III-27d**.

Theta range for data collection	2.22 to 25.25°	
Index ranges	-25<=h<=25, -29<=k<=29, -11<=l<=11	
Reflections collected	56004	
Independent reflections	9274 [R(int) = 0.1012]	
Max. and min. transmission	1.0000 and 0.7978	
Structure solution technique	direct methods	
Structure solution program	SHELXT 2014/5 (Sheldrick, 2014)	
Refinement method	Full-matrix least-squares on F^2	
Refinement program	SHELXL-2016/6 (Sheldrick, 2016)	
Function minimized	$\Sigma\, w(F_o^2 - F_c^2)^2$	
Data / restraints / parameters	9274 / 50 / 608	
Goodness-of-fit on F^2	1.071	
Final R indices	6724 data; $I>2\sigma(I)$	R1 = 0.0746, wR2 = 0.1653
	all data	R1 = 0.1037, wR2 = 0.1802
Weighting scheme	$w=1/[\sigma^2(F_o^2)+(0.0782P)^2+4.3833P]$ where $P=(F_o^2+2F_c^2)/3$	
Absolute structure parameter	-0.02(4)	
Largest diff. peak and hole	0.601 and -0.355 eÅ^{-3}	
R.M.S. deviation from mean	0.062 eÅ^{-3}	

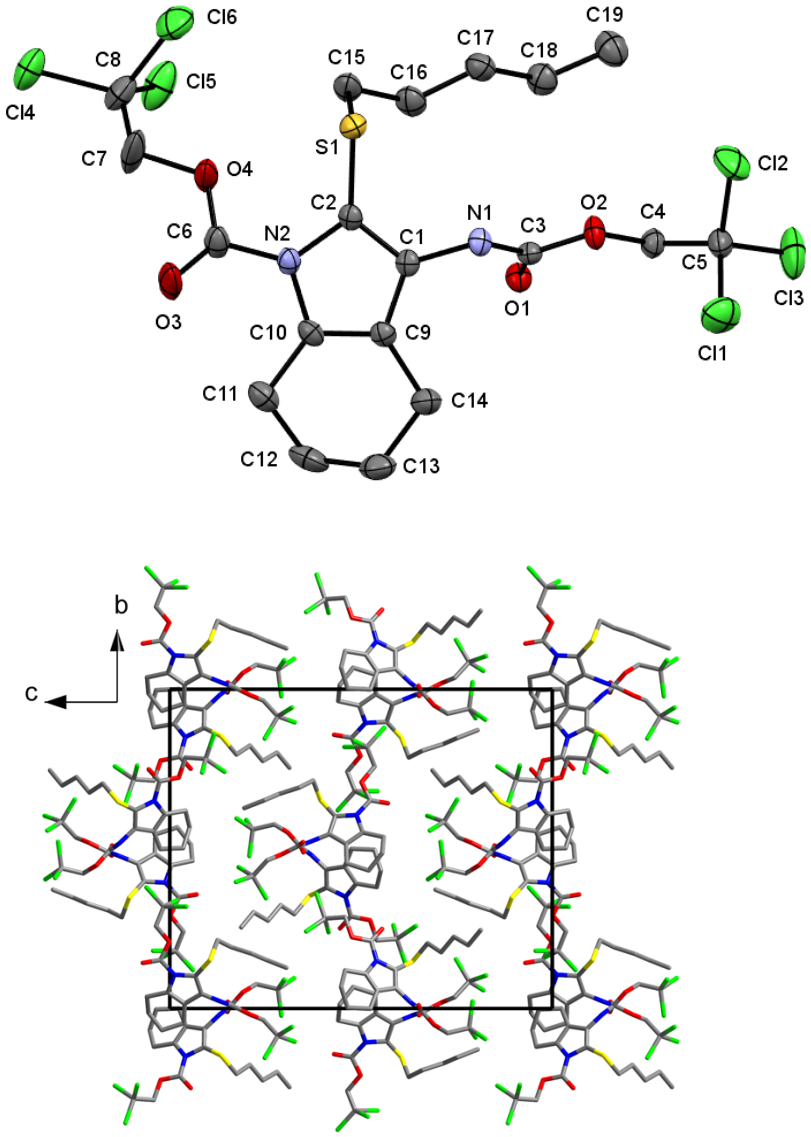

Figure 3.21. XRD structure (top) and the packing diagram (bottom) of the tetrahydroindole (**III-27e**).

Table 3.15. Sample and crystal data for **III-27e**.

Identification code	D8_3846_CN_III_62_41	
Chemical formula	$C_{19}H_{24}Cl_6N_2O_4S$	
Formula weight	589.16 g/mol	
Temperature	298(2) K	
Wavelength	0.71073 Å	
Crystal size	0.033 x 0.037 x 0.212 mm	
Crystal system	orthorhombic	
Space group	P 21 21 21	
Unit cell dimensions	a = 9.9256(4) Å	α = 90°
	b = 21.0135(10) Å	β = 90°
	c = 25.1872(12) Å	γ = 90°
Volume	5253.3(4) $Å^3$	
Z	8	
Density (calculated)	1.490 g/cm^3	
Absorption coefficient	0.762 mm^{-1}	
F(000)	2416	

Table 3.16. Data collection and structure refinement for **III-27e**.

Theta range for data collection	2.10 to 25.36°	
Index ranges	-11<=h<=11, -25<=k<=25, -30<=l<=30	
Reflections collected	67709	
Independent reflections	9585 [R(int) = 0.0766]	
Max. and min. transmission	1.0000 and 0.9338	
Structure solution technique	direct methods	
Structure solution program	SHELXT 2014/5 (Sheldrick, 2014)	
Refinement method	Full-matrix least-squares on F^2	
Refinement program	SHELXL-2016/6 (Sheldrick, 2016)	
Function minimized	$\Sigma\, w(F_o^2 - F_c^2)^2$	
Data / restraints / parameters	9585 / 79 / 633	
Goodness-of-fit on F^2	1.054	
Δ/σ_{max}	0.001	
Final R indices	7507 data; $I>2\sigma(I)$	R1 = 0.0547, wR2 = 0.1045
	all data	R1 = 0.0751, wR2 = 0.1125
Weighting scheme	$w=1/[\sigma^2(F_o^2)+(0.0382P)^2+3.8484P]$ where $P=(F_o^2+2F_c^2)/3$	
Absolute structure parameter	0.03(2)	
Largest diff. peak and hole	0.314 and -0.286 eÅ^{-3}	
R.M.S. deviation from mean	0.048 eÅ^{-3}	

3.5.14 General procedure for the synthesis of 6-membered 1,3,4-oxadiazinone-3-one ***(III-43)***

To a flame dried round bottom flask equipped with a stir bar, were added 10 mol% of silver triflate (AgOTf, 0.1 mmol), di-*tert*-butyl azodicarboxylate (DTBAD) (1.5 mmol, 1.5 equiv.), and 5 mL of dry DCM. Then the corresponding alkynyl sulfide (1 mmol, 1 equiv.) was added in 5 mL of DCM. Then the mixture was stirred under nitrogen atmosphere at room temperature for 24 h. The resultant mixture was concentrated under reduced pressure and purified via flash silica gel column chromatography with a gradient elution using hexane/ethyl acetate (0-20% ethyl acetate) to afford the corresponding 1,3,4-oxadiazin-3-one (**III-43)**.

*3.5.15. Characterization data for Di-tert-butyl 3-(Ethylthio)-4-phenyl-1,2-diazete-1,2-dicarboxylate (III-5u) and oxadiazinone-3-one (**III-43**)*

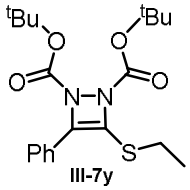

III-7y

White sticky paste; Yield: 6% (24 mg); IR (in $CHCl_3$): 2981 (w), 2935 (w), 1782 (s), 1539 (s), 1477 (m), 1450 (w), 1369 (m), 1253 (m), 1157 (s), 1126 (m), 1059 (w), 968 (m) cm^{-1}; ^{1}H-NMR (300 MHz, $CDCl_3$) δ = 7.70 (d, *J* = 8.1 Hz, 2H), 7.50-7.00 (m, 3H), 2.93 (q, *J* = 7.4 Hz, 2H), 1.58 (s, 9 H), 1.46 (s, 9H), 1.38 (t, *J* = 7.4 Hz, 3H); ^{13}C NMR (75 MHz, $CDCl_3$) δ = 153.0, 143.3, 128.4, 127.8, 127.2, 123.8, 83.6, 83.2, 29.7, 28.1, 27.9, 14.8.

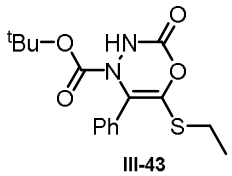

III-43

Light yellow solid; Yield: 27% (90 mg); Mpt: 122.8-123.8°C; IR (neat): 3275 (bw), 2978 (w), 2927 (w), 1766 (s), 1732 (s), 1670 (w), 1627 (w), 1597 (w), 1446 (m), 1365 (s), 1292 (s), 1253 (s), 1149 (s), 1080 (s), 1056 (s), 999 (m), 968 (w), 929 (w), 891 (m), 856 (s), 786 (m), 763 (s), 725 (s), 694 (s) cm^{-1}; ^{1}H-NMR (500 MHz, $CDCl_3$) δ = 7.94 (s, 1H), 7.50-7.30 (m, 5H), 2.85 (q, *J* = 7.4 Hz, 2H), 1.23 (t, *J* = 7.4 Hz, 3H), 1.14 (s, 9H) ; ^{13}C NMR (125 MHz, $CDCl_3$) δ = 152.9, 152.4, 138.9, 132.3, 128.64, 128.55, 128.2, 127.9, 84.2, 27.5, 26.5, 14.6.

*3.5.16 XRD data of 6-membered oxadiazinone-3-one **(III-43)***

Table 3.17. Crystallographic data.

Empirical formula	$C_{16}H_{20}N_2O_4S$
Formula weight (g/mol)	336.40
Crystal system	monoclnic
Space group, *Z*	*C*2/*c*, 8
Temperature (K)	100
Crystal size (mm)	0.04 x 0.04 x 0.20
a, Å	28.733(3)
b, Å	5.9310(5)
c, Å	21.2717(19)
β, °	116.127(3)
Volume ($Å^3$)	3254.6(5)
D_{calc} (g/cm^3)	1.373
Abs. coeff. (mm^{-1})	0.221
F(000)	1424
T_{max}, T_{min}	1.0000, 0.9334
Θ range for data (°)	2.93-25.25
Reflections collected	23296
Data/restraints/parameters	2732 / 0 / 208
R(int)	0.0600
Final R [$I > 2\sigma(I)$] R1, wR2	0.0455, 0.0994
Final R (all data) R1, wR2	0.0585, 0.1062
Goodness-of-fit on F^2	1.122
Larg. diff. peak, hole, $eÅ^{-3}$	0.589, -0.319

The molecular structure and packing arrangement of compound **III-43** is shown in Figure 3.22. Here, the bond lengths from the X-ray structure indicate single bonds of N1-N2, N1-C12, N1-C3, N2-C1, C1-O1, C2-O1, C2-S1, and C3-C4. The C2-C3 bond length (1.323(3) Å) is characteristic of a double bond within the ring, as is the C1-O2 bond (1.200(3) Å)extending from the ring. The N2 atom is protonated and participates in strong N-H···O hydrogen bonding between neighboring molecules along the *b*-axis (H2···O2 = 1.98 Å; N2···O2 = 2.811(3) Å; N2-H2···O2 = 156.7°). Weaker C-H···O (H15B···O4 = 2.68 Å; C15···O4 = 3.594(3) Å; C15-H15B···O4 = 155.4°) and C-H···pi (H8···Cg = 2.753 Å; C-H···Cg = 127.6°) interactions may play an assisting role. The N1-N2-C1-O1-C2-C3 ring takes on a slight twist-boat conformation.

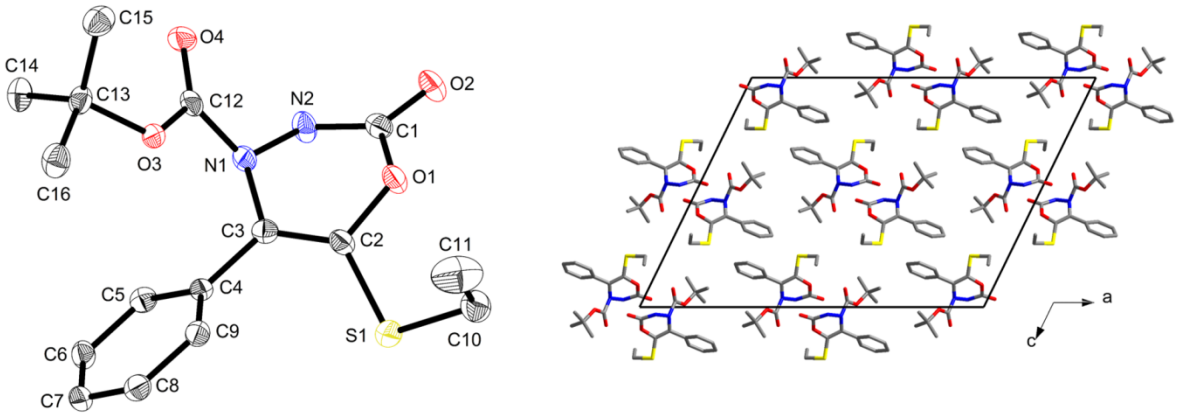

Figure 3.22. Molecular structure (left) and molecular packing (right) of **III-43**.

3.5.17. XRD data of the ^{t}Bu group cleaved product **III-52** *from the di-tert-butyl azodicarboxylate ($C_{14}H_{28}N_2O_4$)*

Crystal Structure Report for ***(III-52)***

A specimen of $C_{14}H_{28}N_2O_4$, approximate dimensions 0.067 mm x 0.074 mm x 0.288 mm, was used for the X-ray crystallographic analysis. The X-ray intensity data were measured.The integration of the data using an orthorhombic unit cell yielded a total of 14667 reflections to a maximum θ angle of 25.38° (0.83 Å resolution), of which 1671 were independent (average redundancy 8.777, completeness = 99.7%, R_{int} = 5.05%, R_{sig} = 2.57%) and 1505 (90.07%) were greater than $2\sigma(F^2)$. The final cell constants of a = 16.3046(13) Å, b = 10.5513(13) Å, c = 10.1600(8) Å, volume = 1747.9(3) Å^3, are based upon the refinement of the XYZ-centroids of reflections above 20 σ(I). The calculated minimum and maximum transmission coefficients (based on crystal size) are 0.8986 and 1.0000.

The structure was solved and refined using the Bruker SHELXTL Software Package, using the space group C m c 21, with Z = 4 for the formula unit, $C_{14}H_{28}N_2O_4$. The final anisotropic full-matrix least-squares refinement on F^2 with 128 variables converged at R1 = 3.57%, for the observed data and wR2 = 8.63% for all data. The goodness-of-fit was 1.085. The largest peak in the final difference electron density synthesis was 0.127 e^-/Å^3 and the largest hole was -0.137 e^-/Å^3 with an RMS deviation of 0.032 e^-/Å^3. On the basis of the final model, the calculated density was 1.096 g/cm^3 and F(000), 632 e^-.

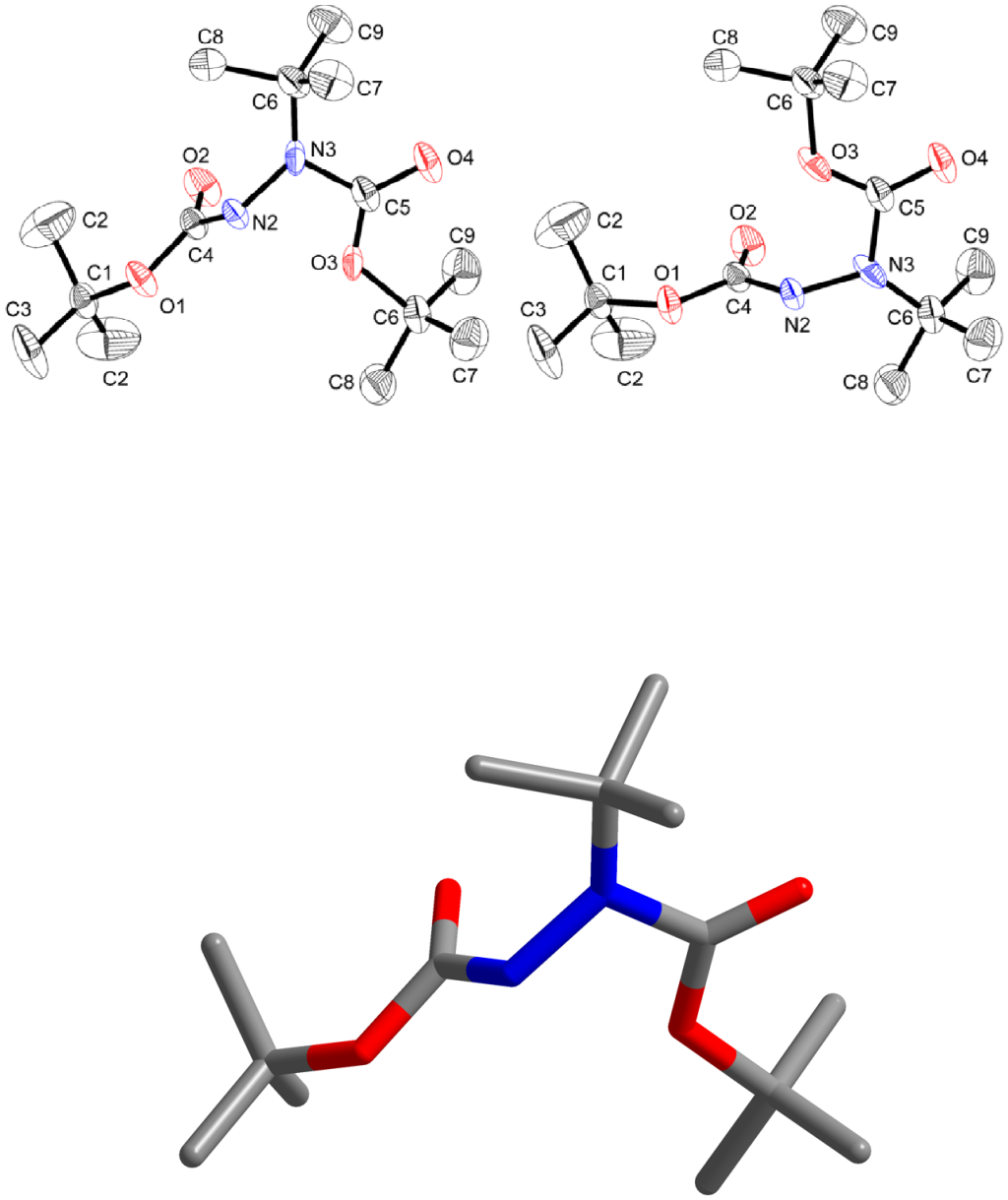

Figure 3.23. XRD structure of *tert*-butyl cleaved product **III-52**.

Table 3.18. Sample and crystal data for **III-52**

Identification code	D8_1602_CN_6C_118_83A	
Chemical formula	$C_{14}H_{28}N_2O_4$	
Formula weight	288.38 g/mol	
Temperature	120(2) K	
Wavelength	0.71073 Å	
Crystal size	0.067 x 0.074 x 0.288 mm	
Crystal system	orthorhombic	
Space group	C m c 21	
Unit cell dimensions	a = 16.3046(13) Å	α = 90°
	b = 10.5513(13) Å	β = 90°
	c = 10.1600(8) Å	γ = 90°
Volume	1747.9(3) $Å^3$	
Z	4	
Density (calculated)	1.096 g/cm^3	
Absorption coefficient	0.080 mm^{-1}	
F(000)	632	

Table 3.19. Data collection and structure refinement for **III-52**

Theta range for data collection	2.30 to 25.38°	
Index ranges	-19<=h<=19, -12<=k<=12, -12<=l<=12	
Reflections collected	14667	
Independent reflections	1671 [R(int) = 0.0505]	
Max. and min. transmission	1.0000 and 0.8986	
Structure solution technique	direct methods	
Structure solution program	SHELXT-2014 (Sheldrick 2014)	
Refinement method	Full-matrix least-squares on F^2	
Refinement program	SHELXL-2014 (Sheldrick 2014)	
Function minimized	$\Sigma\, w(F_o^2 - F_c^2)^2$	
Data / restraints / parameters	1671 / 2 / 128	
Goodness-of-fit on F^2	1.085	
Final R indices	1505 data; $I>2\sigma(I)$	R1 = 0.0357, wR2 = 0.0821
	all data	R1 = 0.0423, wR2 = 0.0863
Weighting scheme	$w=1/[\sigma^2(F_o^2)+(0.0459P)^2+0.3565P]$ where $P=(F_o^2+2F_c^2)/3$	
Absolute structure parameter	-0.4(19)	
Largest diff. peak and hole	0.127 and -0.137 eÅ^{-3}	
R.M.S. deviation from mean	0.032 eÅ^{-3}	

3.5.18. ^{1}H NMR spectra and ^{13}C NMR spectra for alkynyl sulfides and selenides

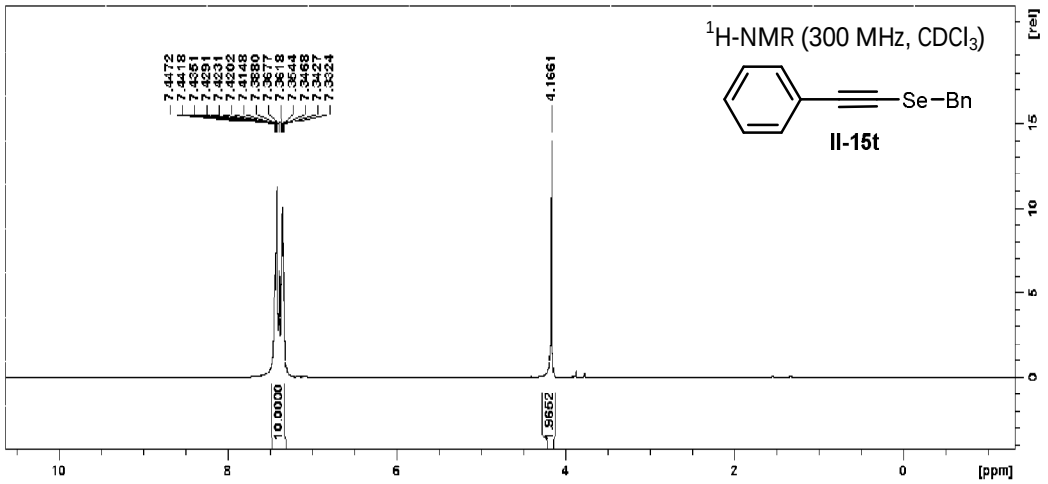

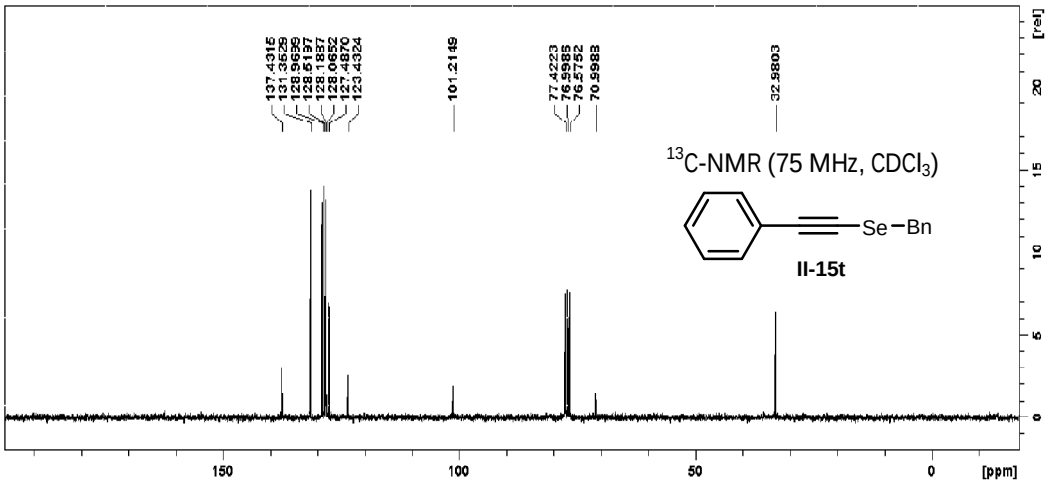

3.5.19. ^{1}H NMR and ^{13}C NMR spectra for N,N-dicarbamoyl 2-iminothioimidates

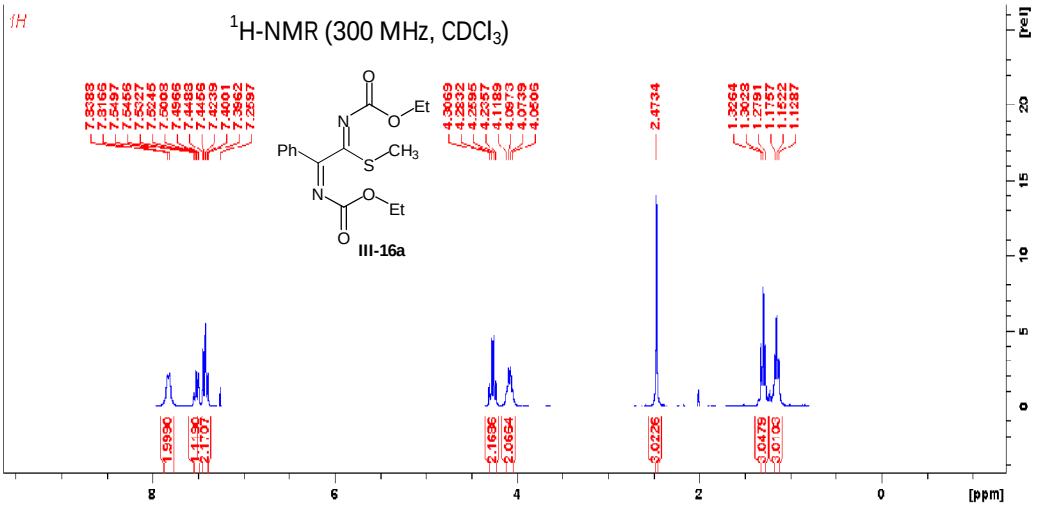

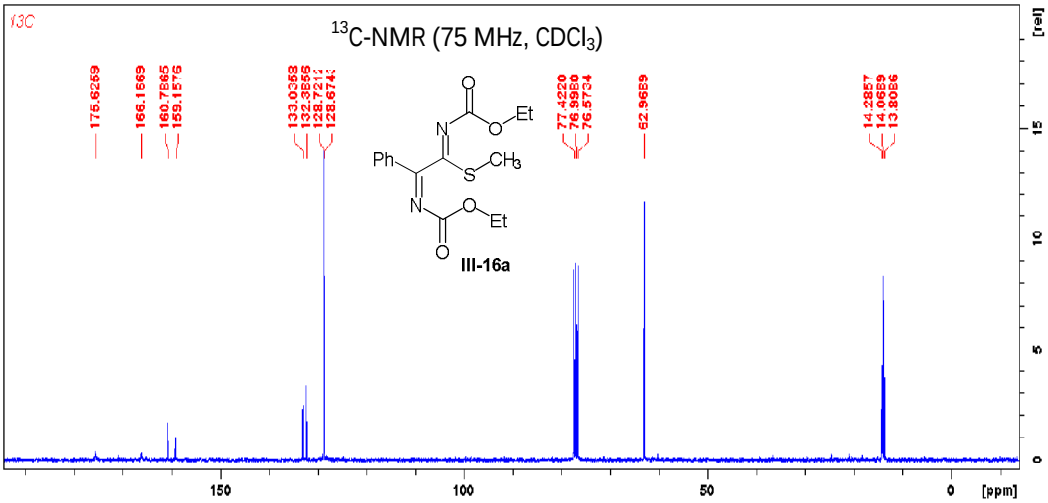

2D-HMQC (F2 = 300 MHz, F1 = 75 MHz, $CDCl_3$) analysis of 2-iminothioimidate **III-16a**

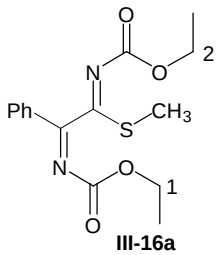

III-16a

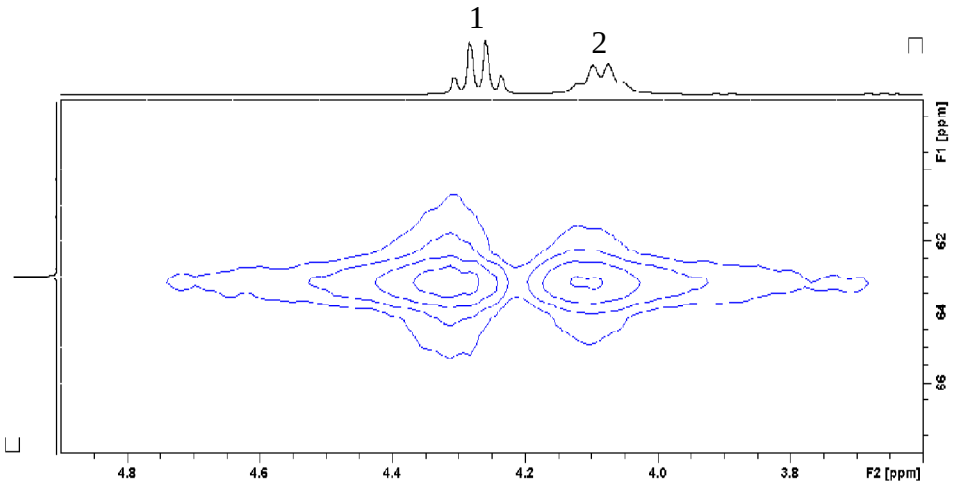

Carbamate methylene protons 1 and 2 share the same carbon signal.

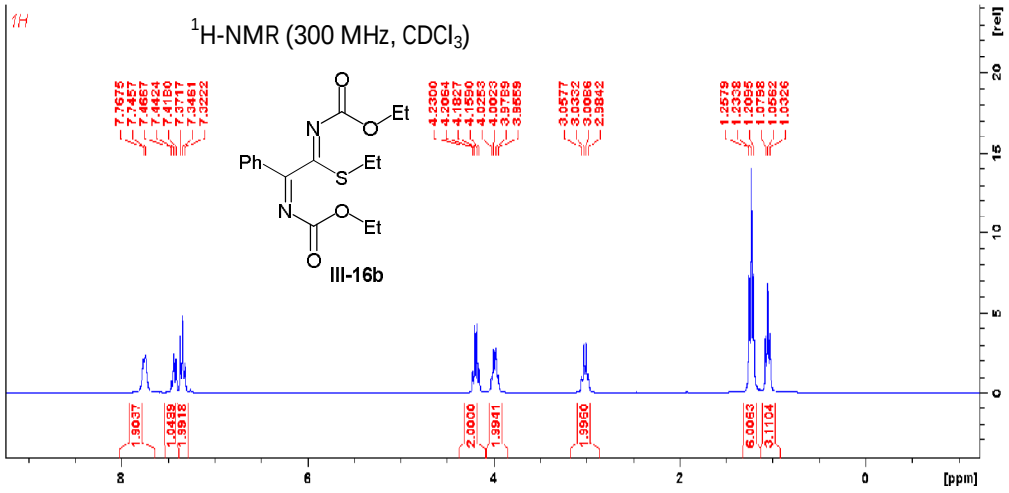

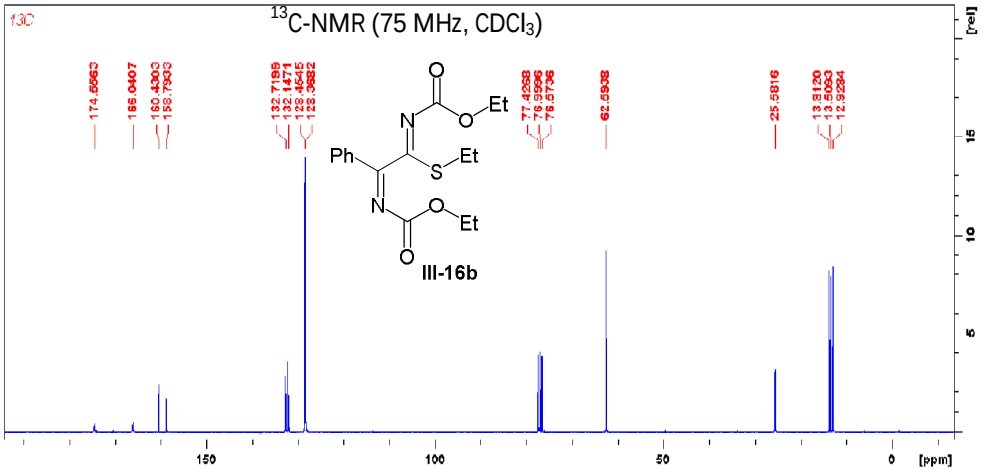

Carbamate methylene protons share the same carbon signal.

2D-HMQC (F2 = 300 MHz, F1 = 75 MHz, $CDCl_3$) analysis of 2-imidothioimidate **III-16b**

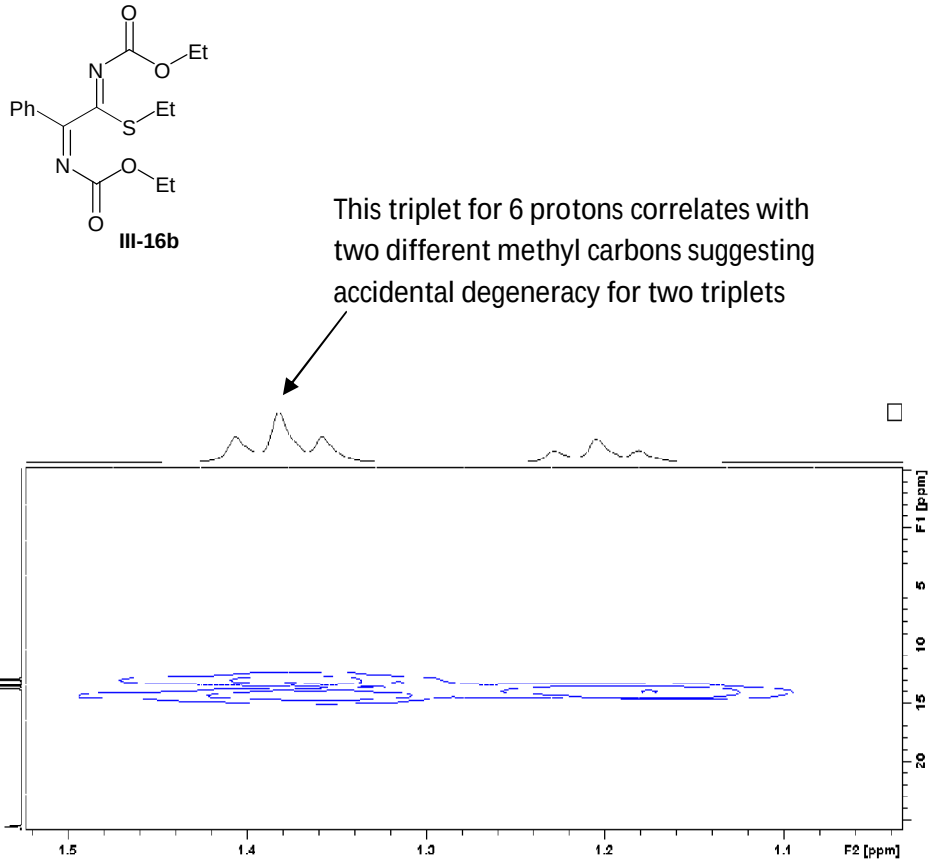

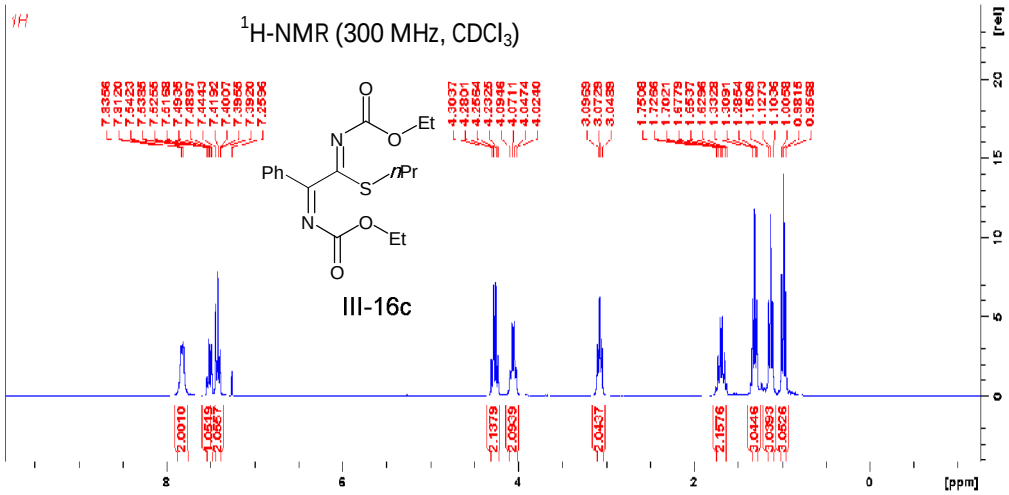

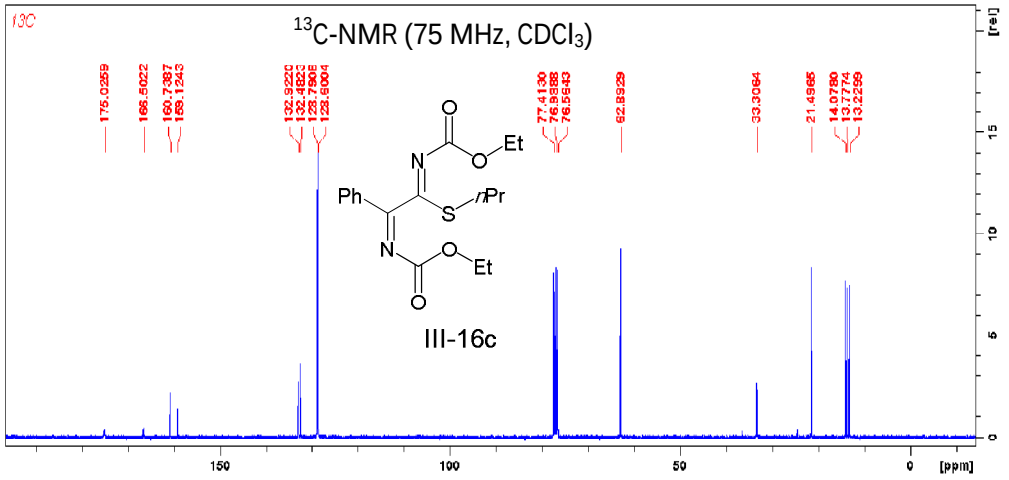

Carbamate methylene protons share the same carbon signal.

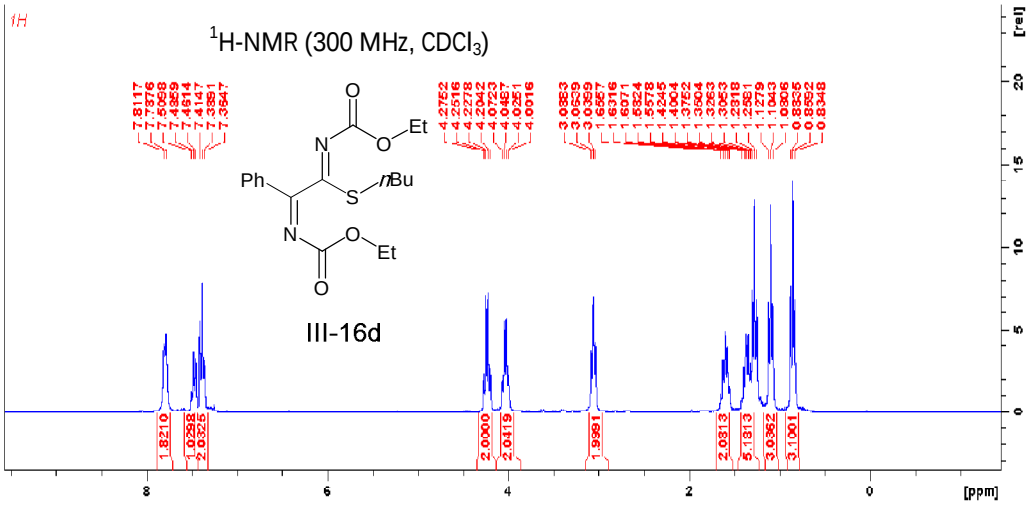

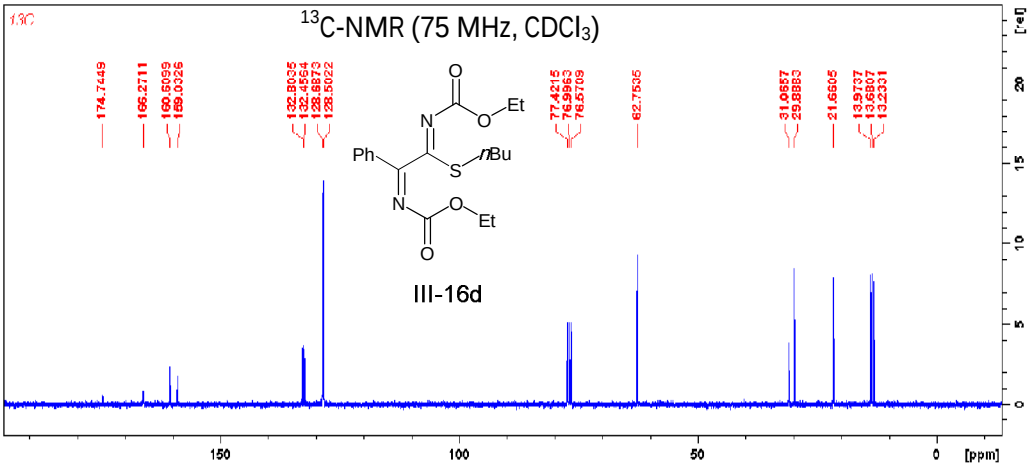

Carbamate methylene protons share the same carbon signal.

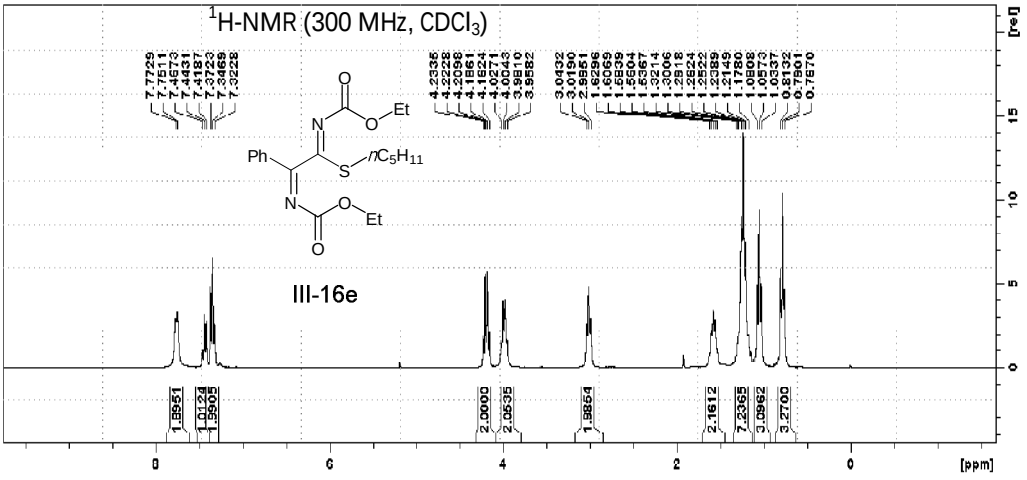

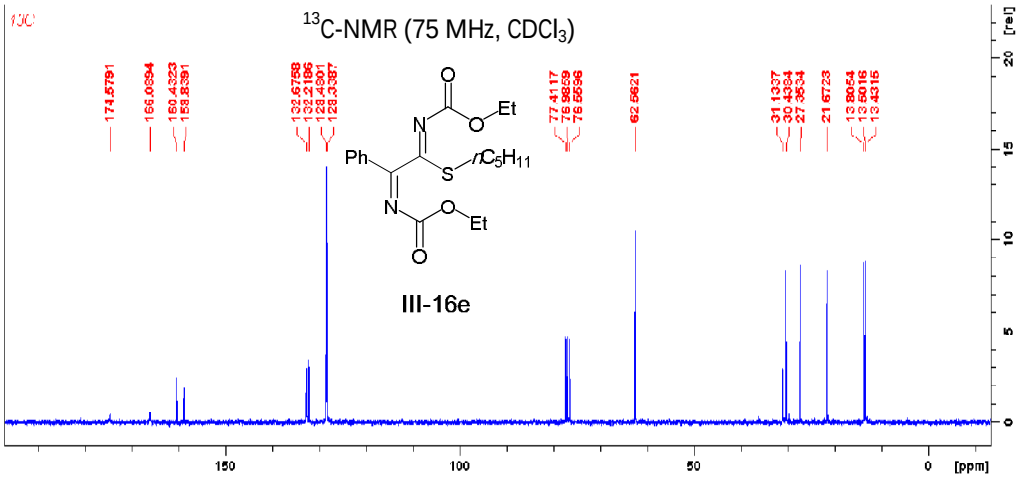

Carbamate methylene protons share the same carbon signal.

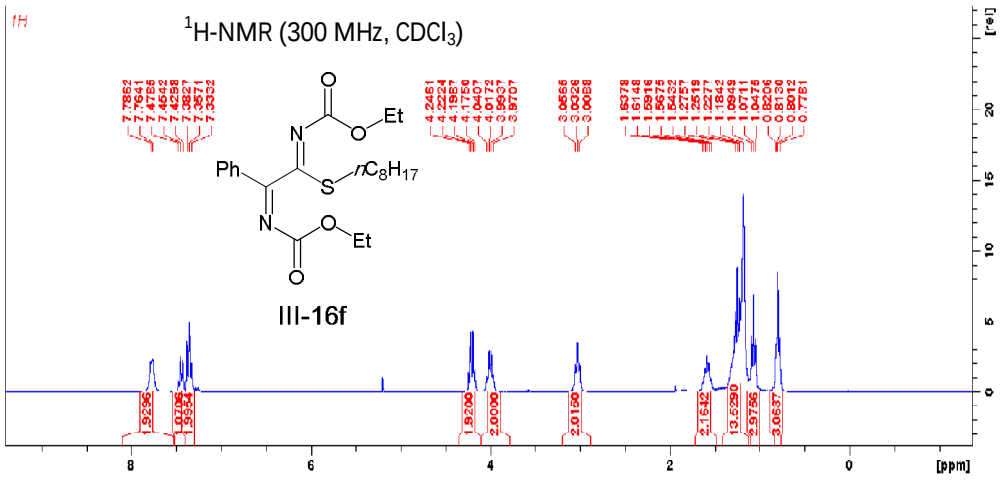
1H-NMR (300 MHz, CDCl3)
III-16f
[ppm]
[rel]

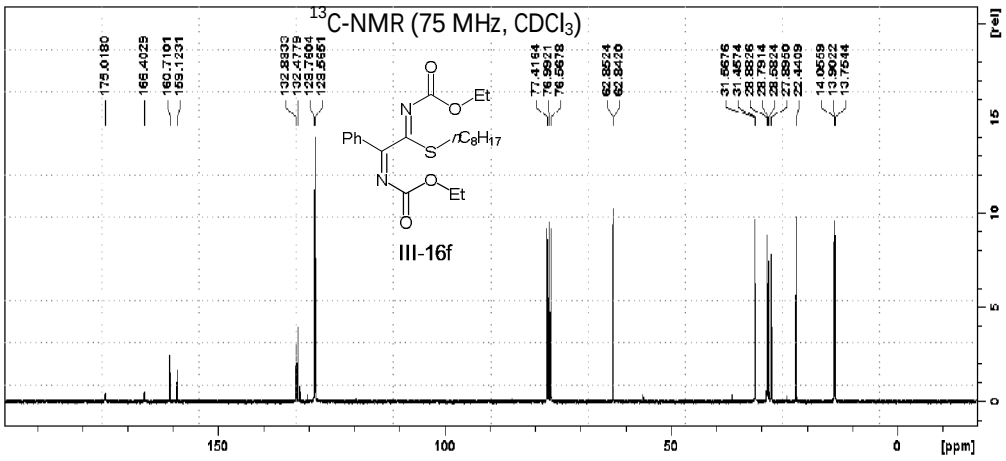
13C-NMR (75 MHz, CDCl3)
III-16f
[ppm]
[rel]

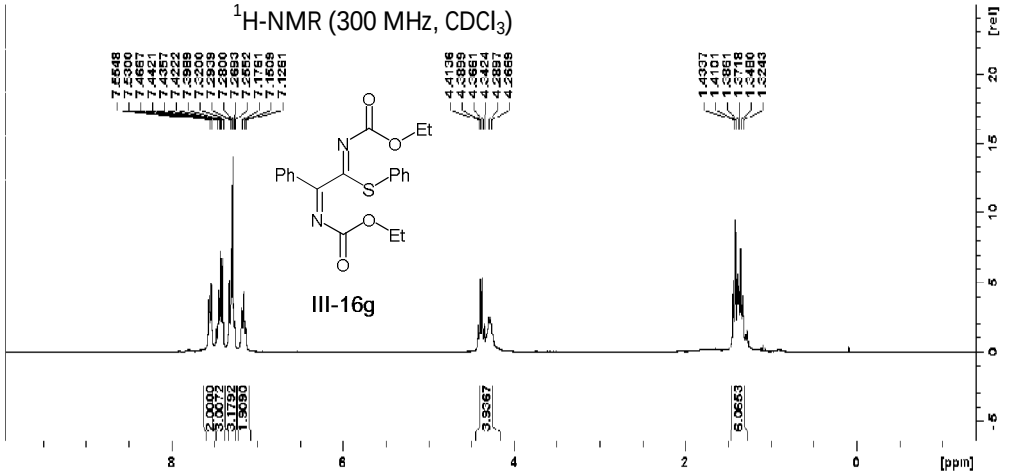
^{1}H-NMR (300 MHz, $CDCl_3$)
III-16g
[ppm]

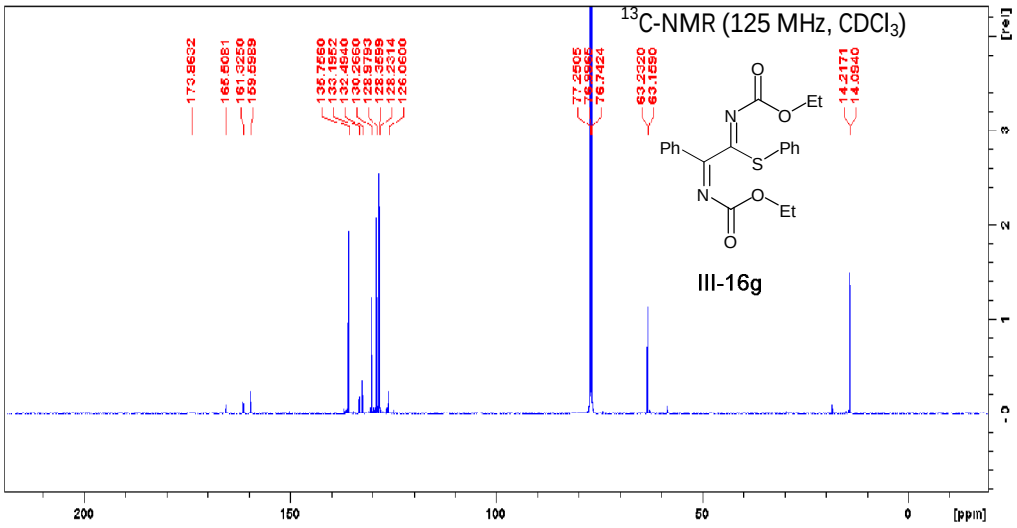
^{13}C-NMR (125 MHz, $CDCl_3$)
III-16g
[ppm]

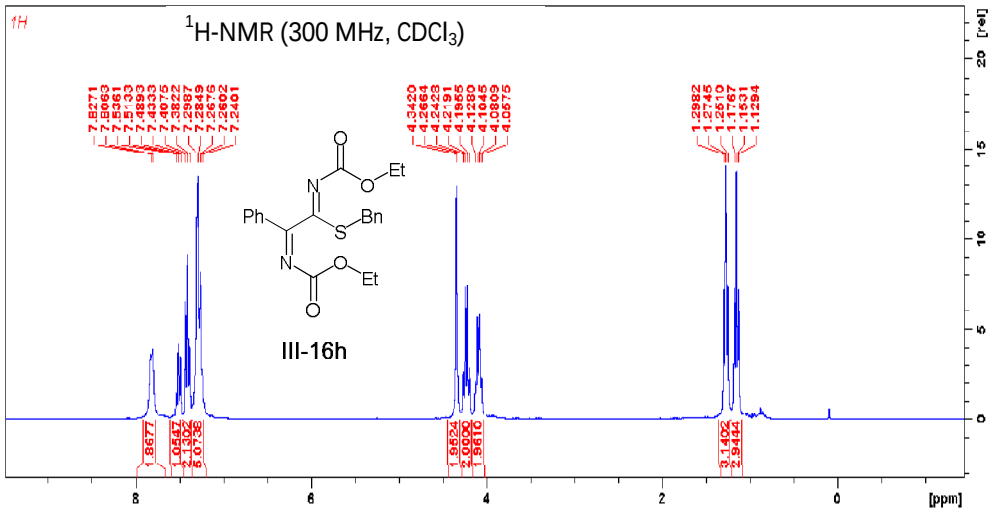
1H-NMR (300 MHz, CDCl3)
III-16h
[ppm]

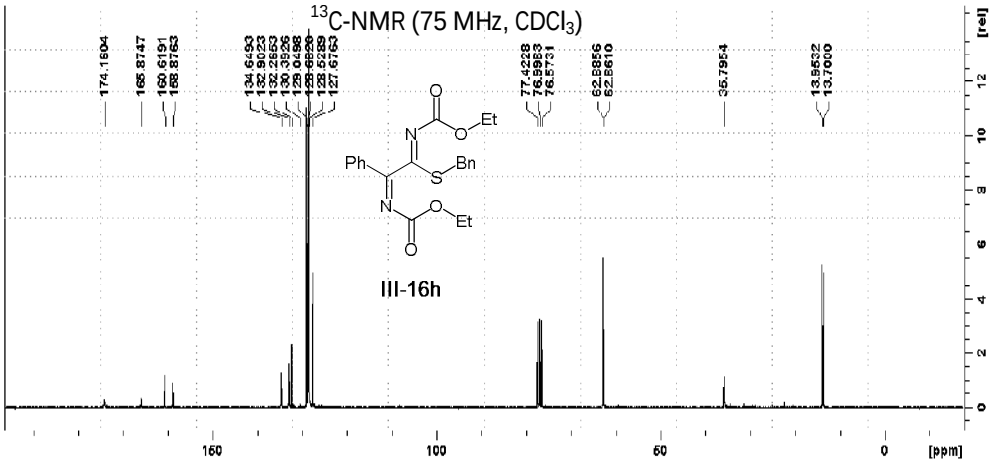
13C-NMR (75 MHz, CDCl3)
III-16h
[ppm]

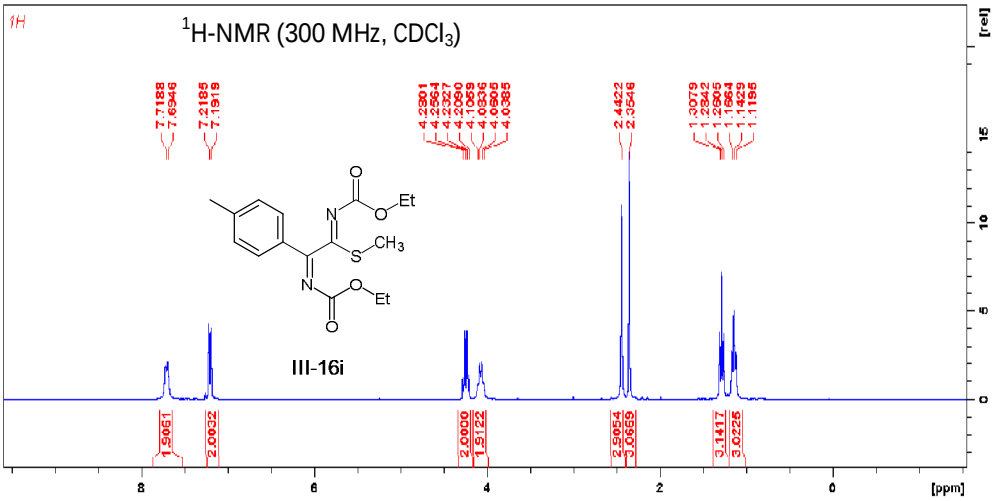
1H
^{1}H-NMR (300 MHz, $CDCl_3$)
7.7188
7.6946
7.2185
7.1919
4.2301
4.2264
4.2227
4.2090
4.1059
4.0536
4.0295
4.0035
2.4422
2.3546
1.3079
1.2942
1.2805
1.1964
1.1429
1.1195
Et
CH_3
S
N
O
III-16i
1.9061
2.0032
2.0000
1.9122
2.9054
3.0669
3.1417
3.0226
[rel]
[ppm]

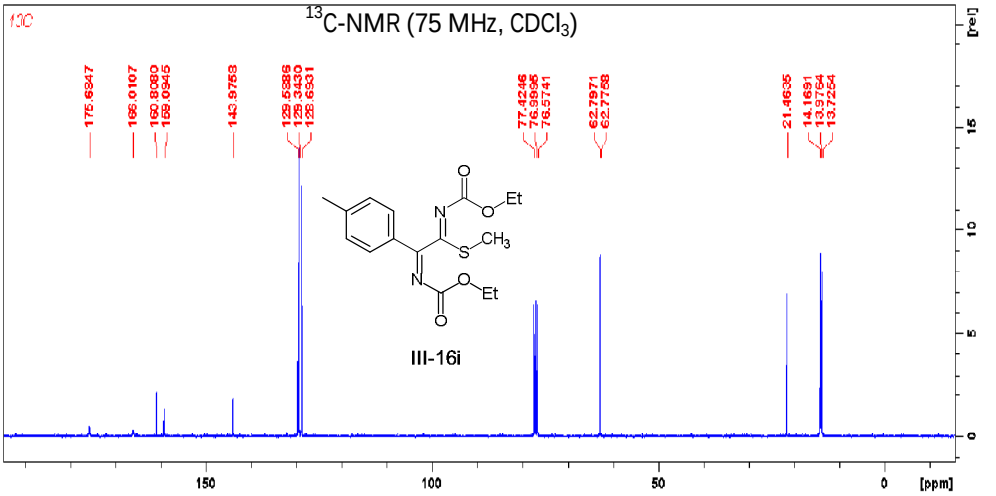
13C
^{13}C-NMR (75 MHz, $CDCl_3$)
175.6947
166.0107
160.8080
159.0945
143.9763
129.5395
128.4470
126.6331
77.4246
76.3996
76.5741
62.7971
62.7758
21.4635
14.1691
13.9764
13.7254
Et
CH_3
S
N
O
III-16i
[rel]
[ppm]

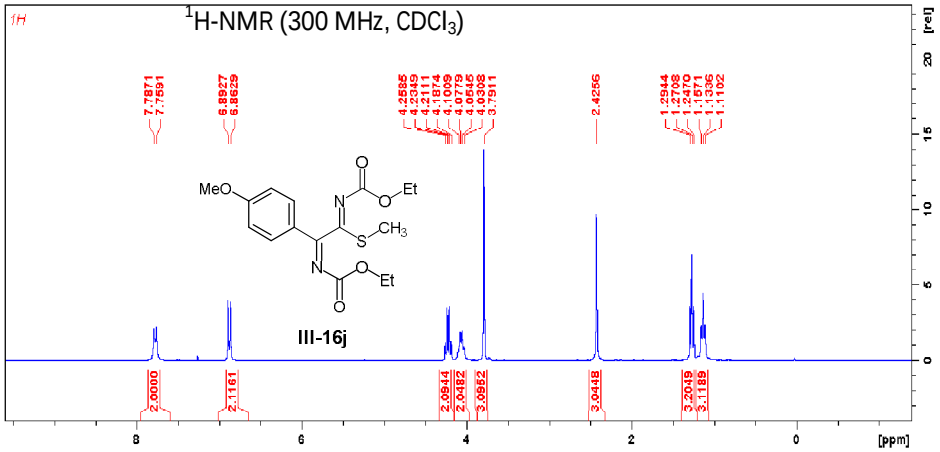
1H
^{1}H-NMR (300 MHz, $CDCl_3$)
7.7871
7.7591
6.8927
6.8629
4.2585
4.2349
4.2111
4.1874
4.1638
4.0779
4.0545
4.0308
3.7911
2.4256
1.2944
1.2708
1.2470
1.1671
1.1336
1.1102
MeO
O
N
O
Et
S
CH3
N
O
Et
O
III-16j
2.0000
2.1161
2.0944
2.0482
3.0952
3.0418
3.2045
3.1189
8
6
4
2
0
[ppm]
[rel]

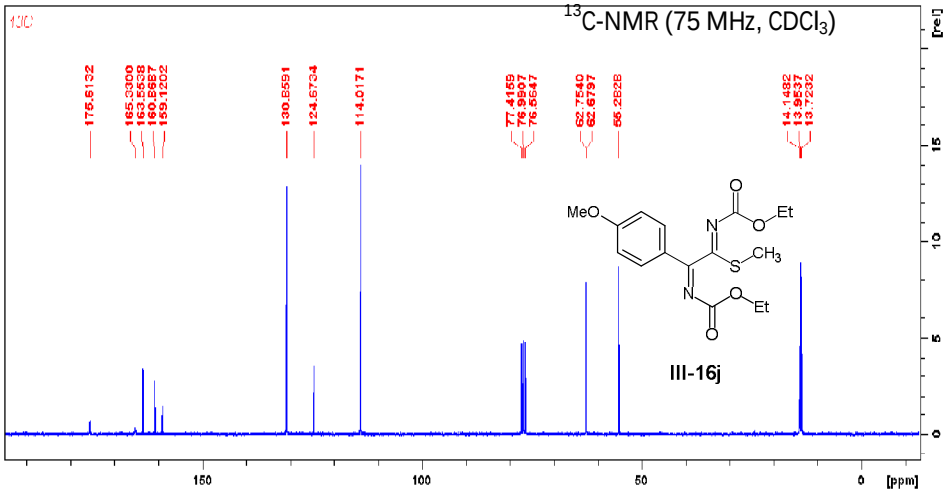
13C
^{13}C-NMR (75 MHz, $CDCl_3$)
175.6132
165.2300
163.5538
160.8687
159.1202
130.8591
124.6734
114.0171
77.4155
76.9907
76.5647
62.7549
62.6797
55.2828
14.1432
13.9537
13.7232
MeO
O
N
O
Et
S
CH3
N
O
Et
O
III-16j
150
100
50
0
[ppm]
[rel]

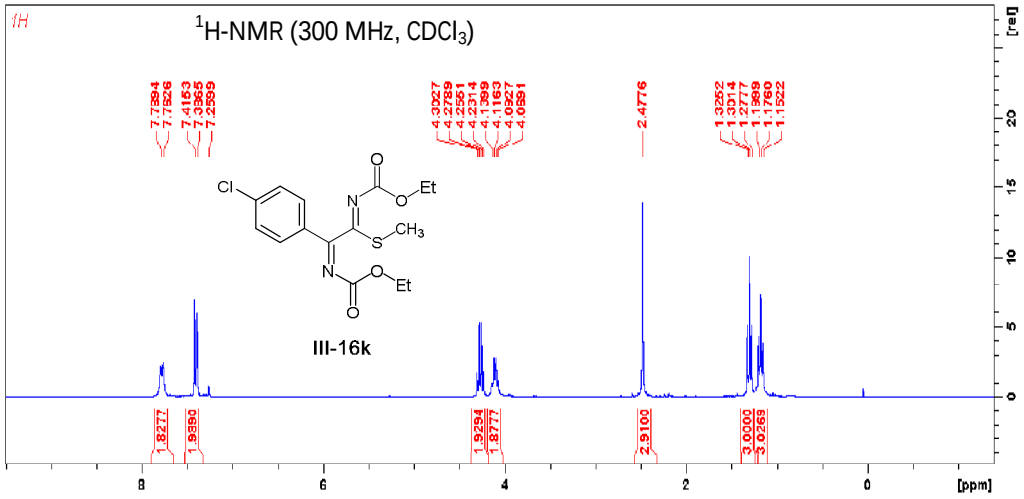

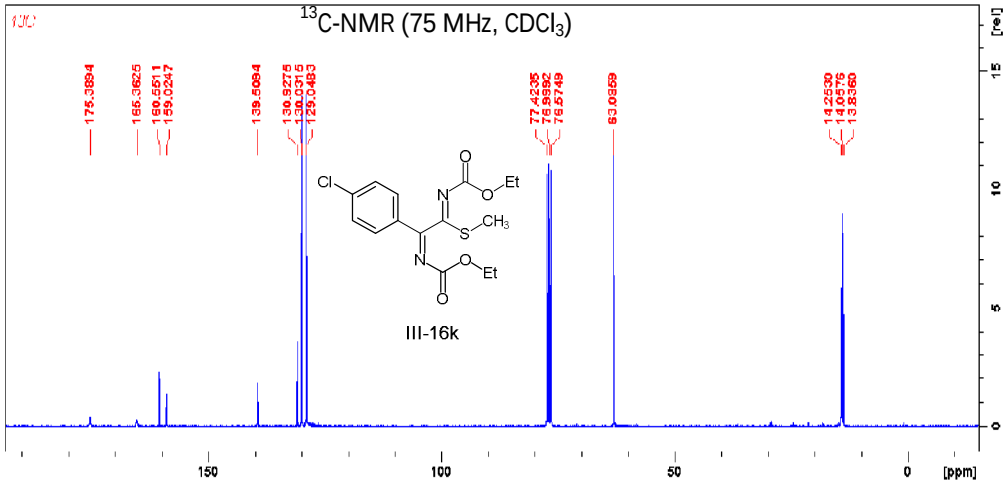

Carbamate methylene protons share the same carbon signal.

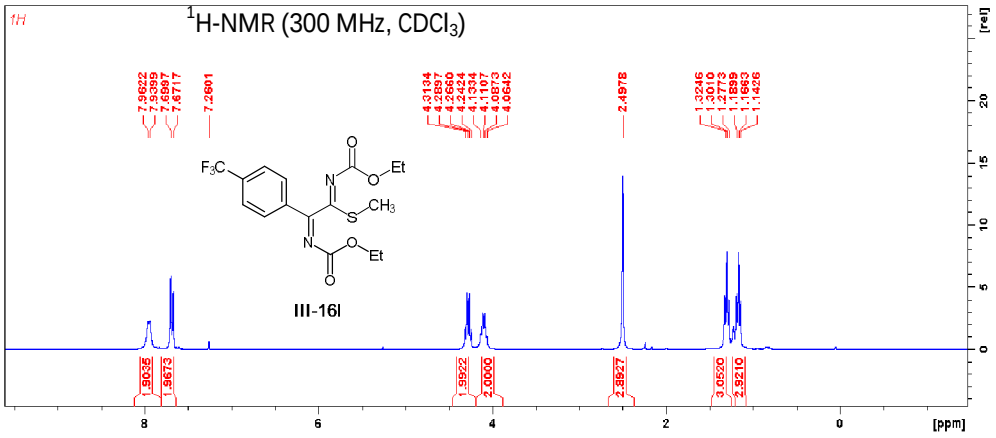
1H
1H-NMR (300 MHz, CDCl3)
7.9622
7.9399
7.6987
7.6717
7.2601
4.3134
4.2897
4.2660
4.2424
4.1334
4.1107
4.0873
4.0642
2.4978
1.3246
1.3010
1.2773
1.1899
1.1663
1.1426
F3C
N
O
Et
S
CH3
III-16l
1.9035
1.9673
1.9922
2.0000
2.8927
3.0520
2.9210
[rel]
[ppm]

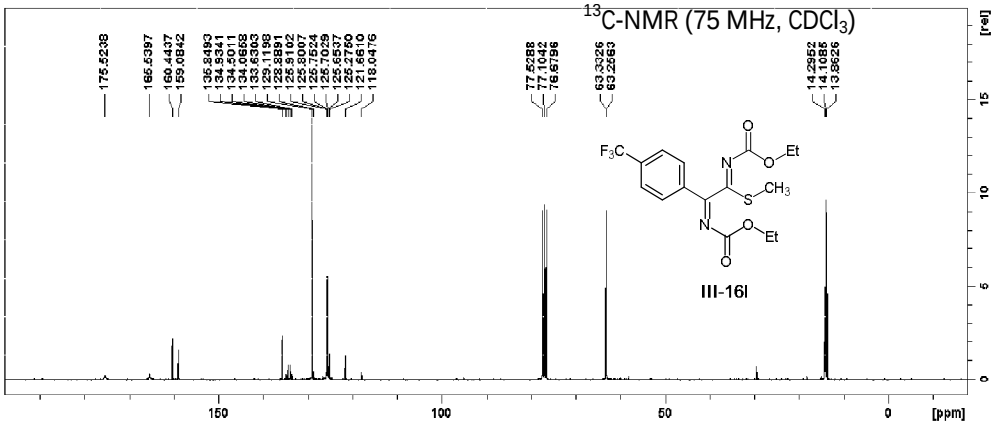
13C-NMR (75 MHz, CDCl3)
175.5238
165.5397
160.4437
159.0842
135.8493
134.5411
134.5011
134.0668
133.6363
129.1198
128.8891
125.8102
125.6007
125.7524
125.7029
125.6537
125.2750
121.6610
118.0475
77.5688
77.1042
76.6598
63.3326
63.2563
14.2952
14.1088
13.8626
F3C
III-16l
[rel]
[ppm]

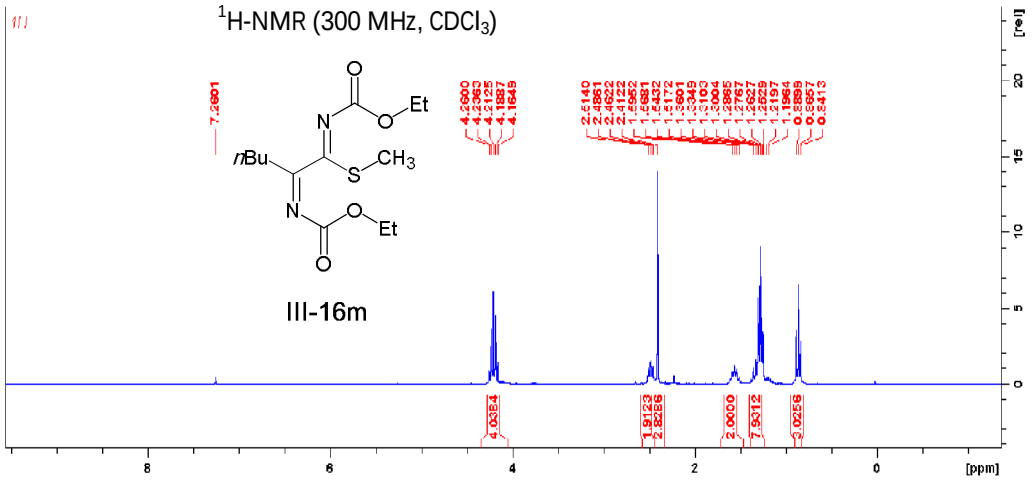
^{1}H-NMR (300 MHz, $CDCl_3$)
III-16m
[ppm]

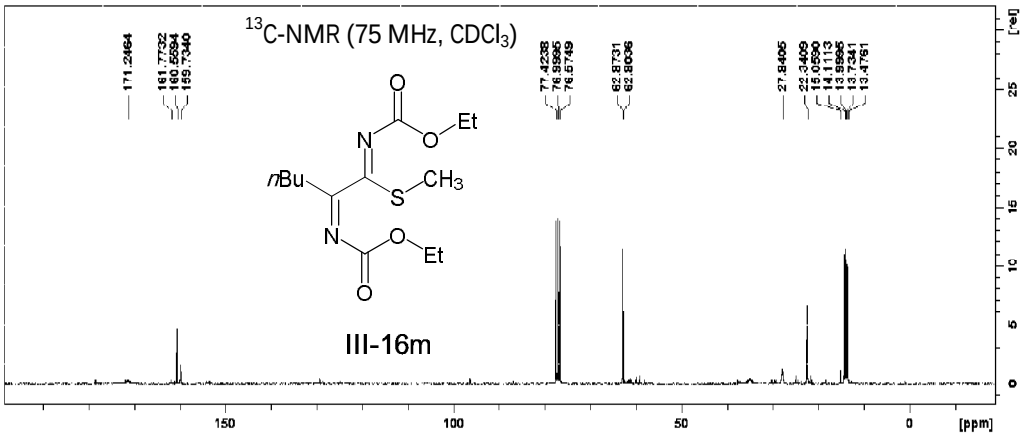
^{13}C-NMR (75 MHz, $CDCl_3$)
III-16m
[ppm]

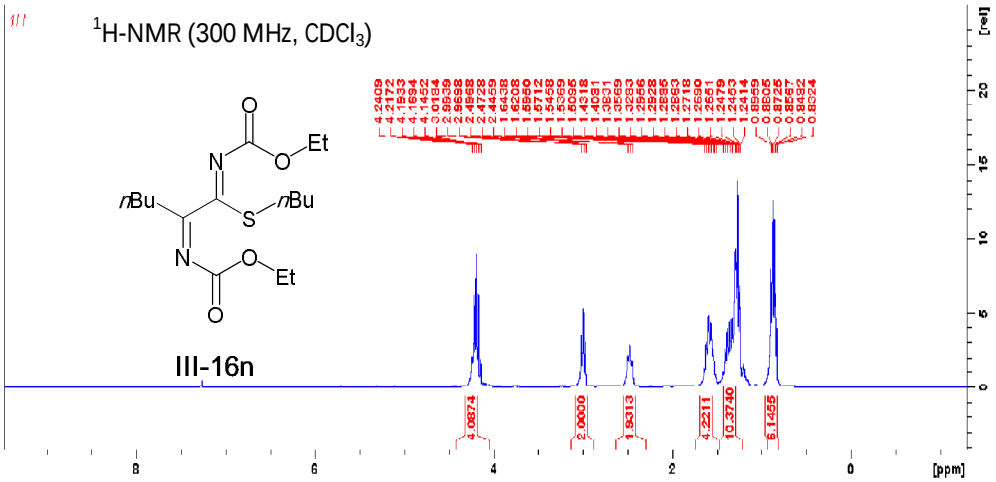
^{1}H-NMR (300 MHz, $CDCl_3$)
III-16n
[ppm]
[rel]

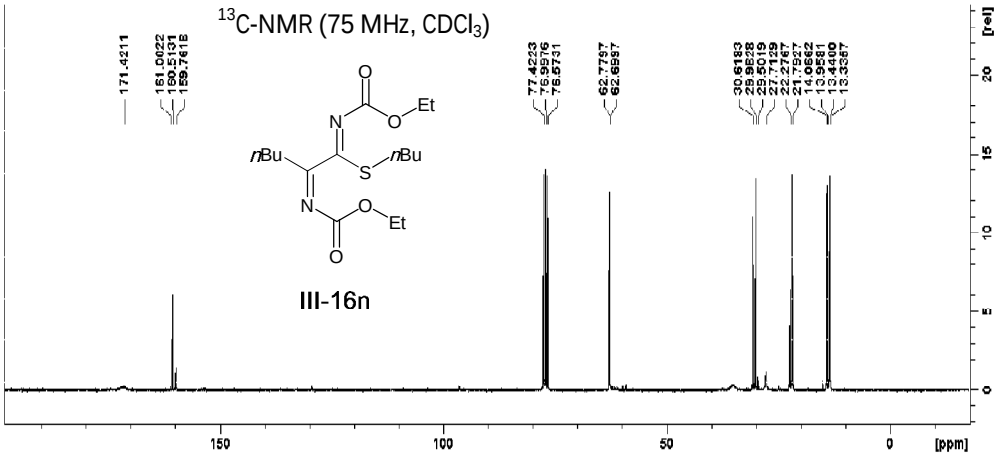
^{13}C-NMR (75 MHz, $CDCl_3$)
III-16n
[ppm]
[rel]

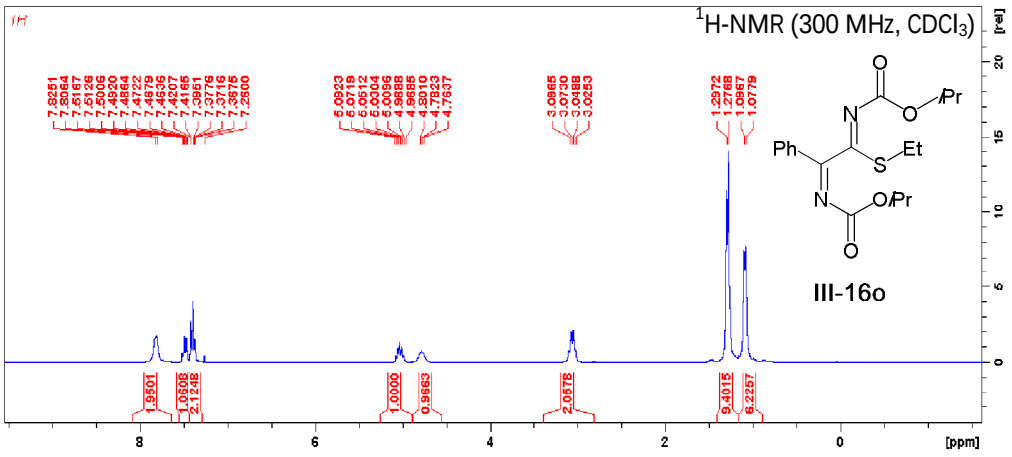
1H
^{1}H-NMR (300 MHz, $CDCl_3$)
III-16o
[ppm]

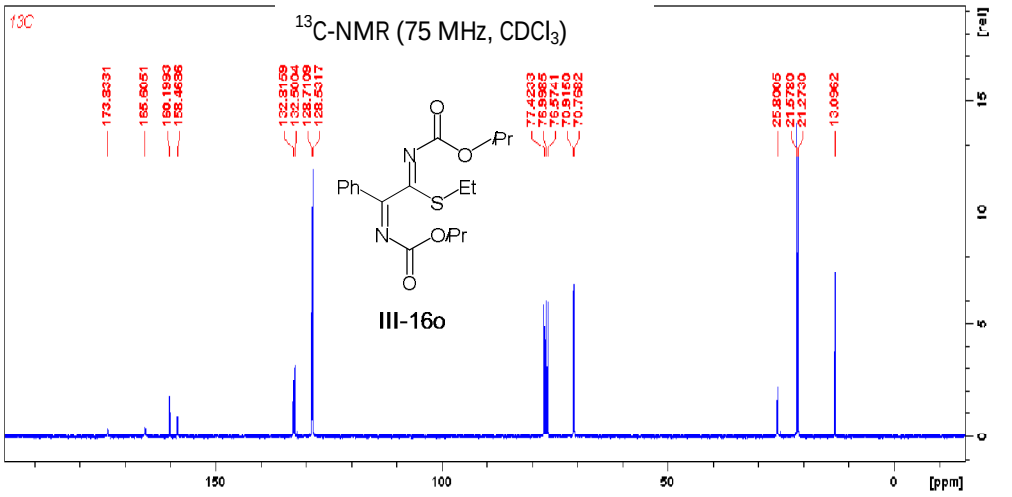
13C
^{13}C-NMR (75 MHz, $CDCl_3$)
III-16o
[ppm]

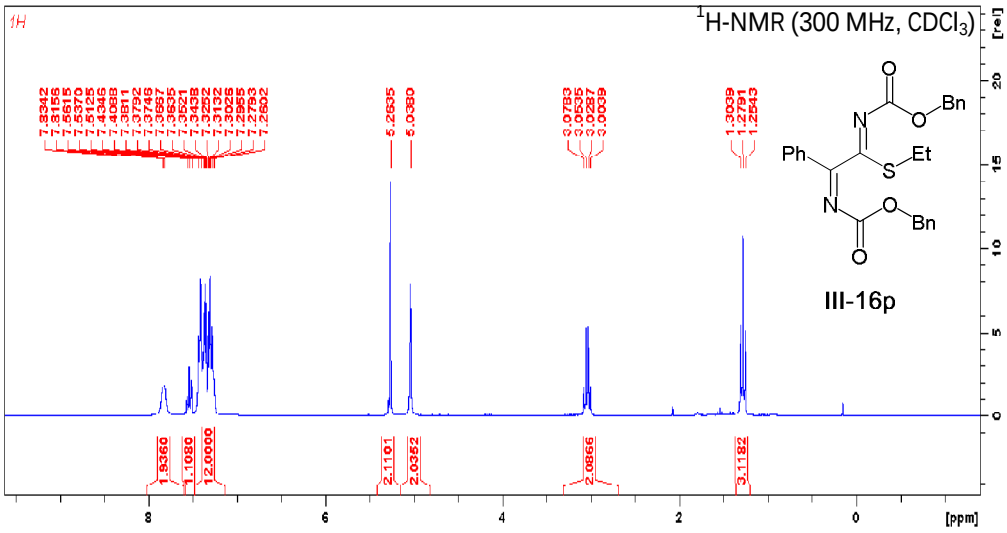
1H
^{1}H-NMR (300 MHz, CDCl$_3$)
7.3342
7.3156
7.5615
7.5370
7.5125
7.4346
7.4093
7.3911
7.3792
7.3746
7.3697
7.3635
7.3521
7.3438
7.3252
7.3132
7.3026
7.2955
7.2793
7.2692
5.2535
5.0380
3.0793
3.0535
3.0237
3.0039
1.3039
1.2791
1.2543
1.9360
1.1080
12.0000
2.1101
2.0352
2.0866
3.1182
8
6
4
2
0
[ppm]
[rel]
Ph
N
O
Bn
S
Et
III-16p

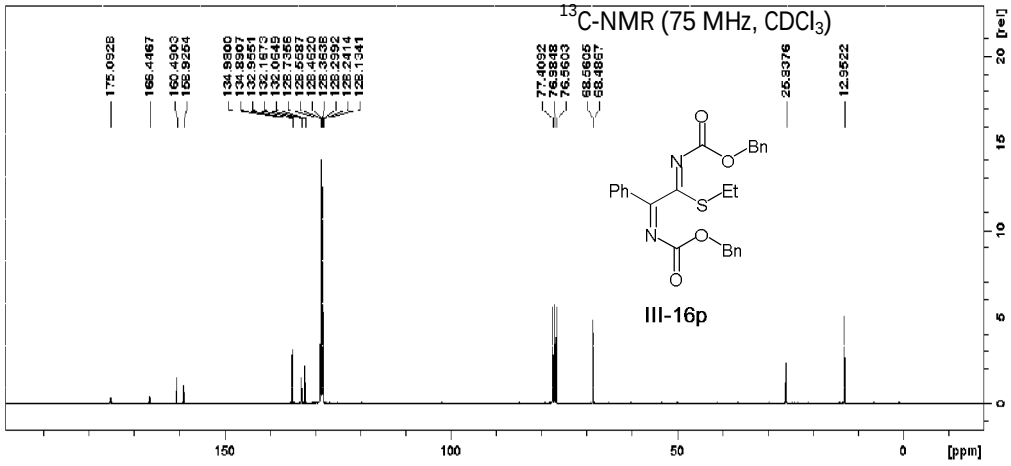
^{13}C-NMR (75 MHz, CDCl$_3$)
175.0928
166.4467
160.4903
158.9264
134.9300
134.8907
132.9551
132.1673
132.0645
128.7386
128.6587
128.4620
128.4438
128.2992
128.2414
128.1341
77.4092
76.3848
76.5603
68.5605
68.4867
25.9376
12.9522
150
100
50
0
[ppm]
[rel]
Ph
N
O
Bn
S
Et
III-16p

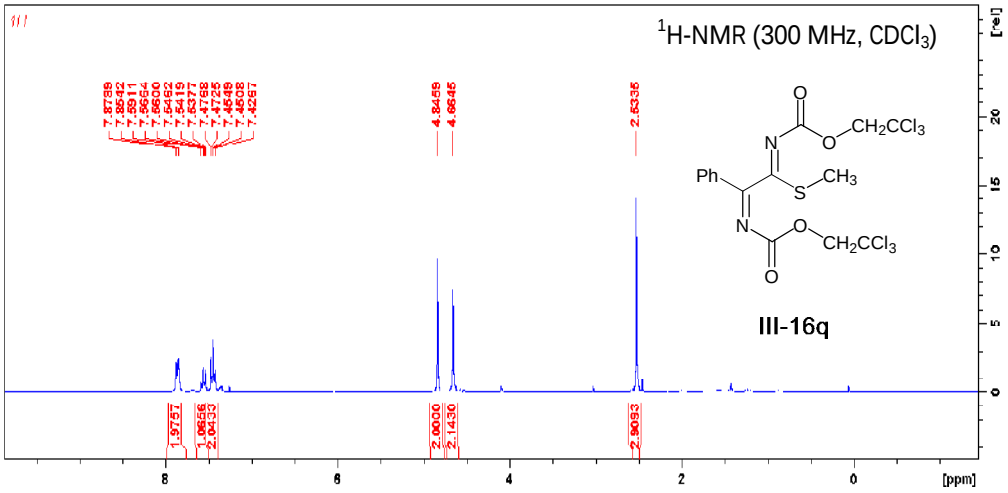
^{1}H-NMR (300 MHz, $CDCl_3$)
III-16q
[ppm]

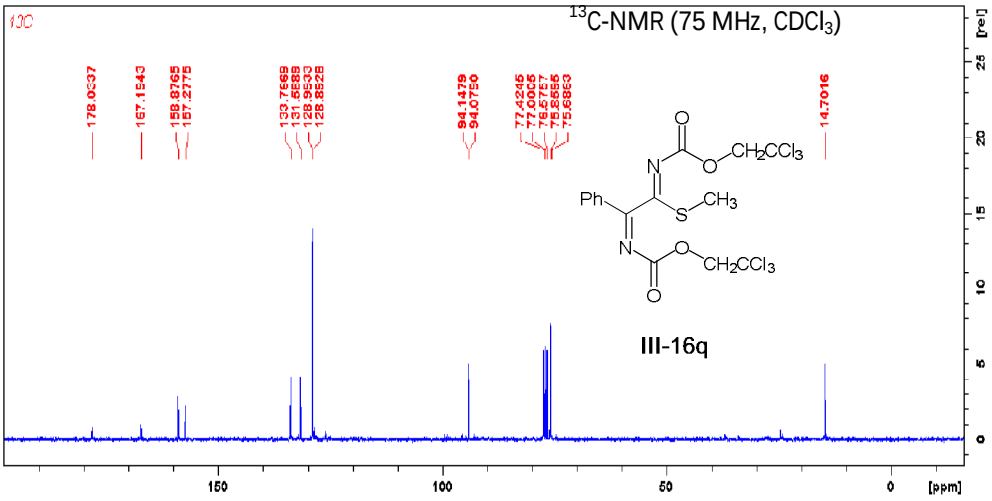
^{13}C-NMR (75 MHz, $CDCl_3$)
III-16q
[ppm]

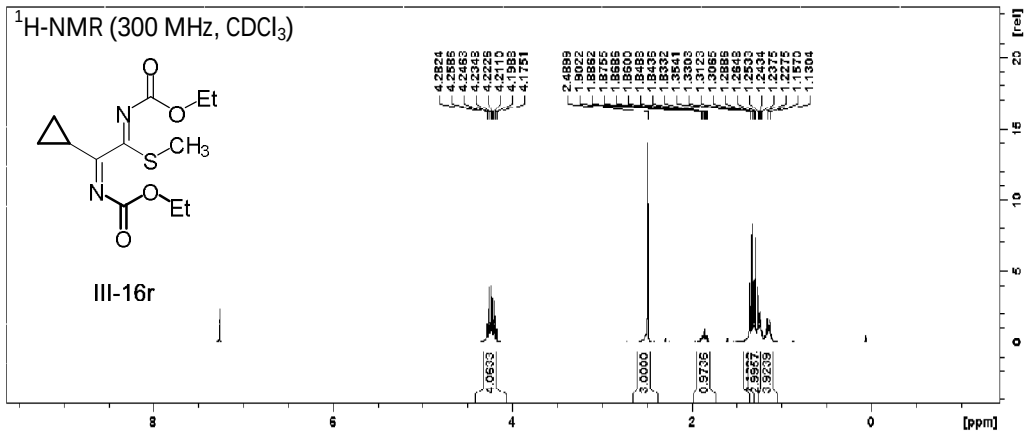
^{1}H-NMR (300 MHz, $CDCl_3$)
III-16r
[ppm]
[rel]

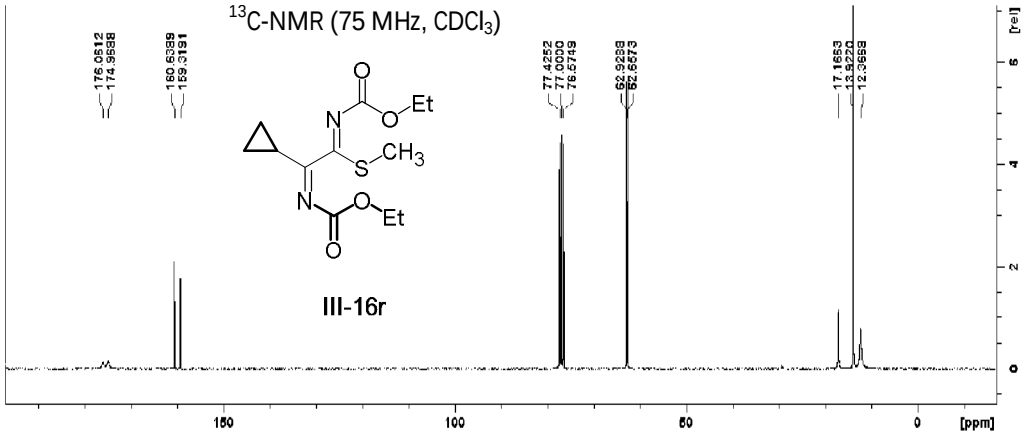
^{13}C-NMR (75 MHz, $CDCl_3$)
III-16r
[ppm]
[rel]

2D-HMQC (F2 = 300 MHz, F1 = 75 MHz, $CDCl_3$) analysis of 2-iminothioimidate **III-16r**

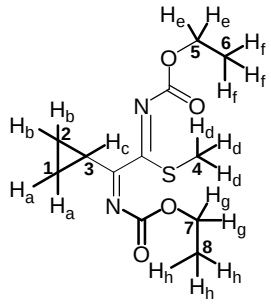

III-16r

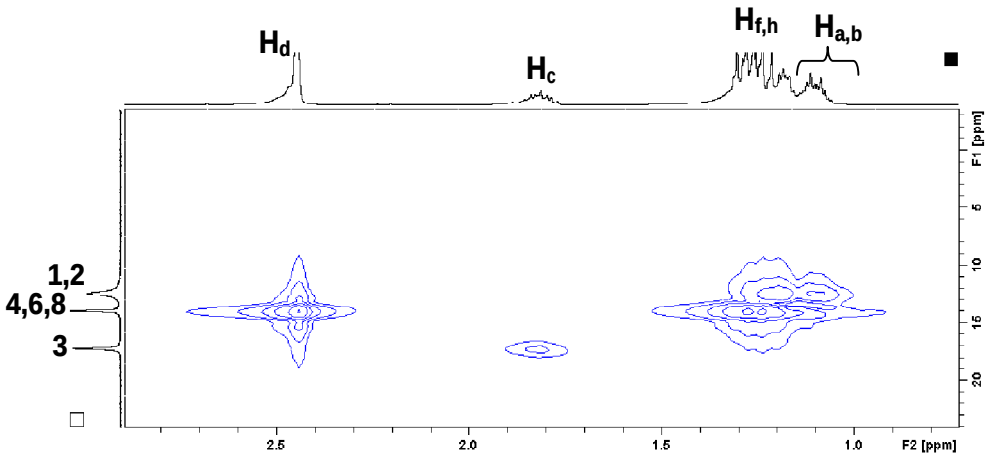

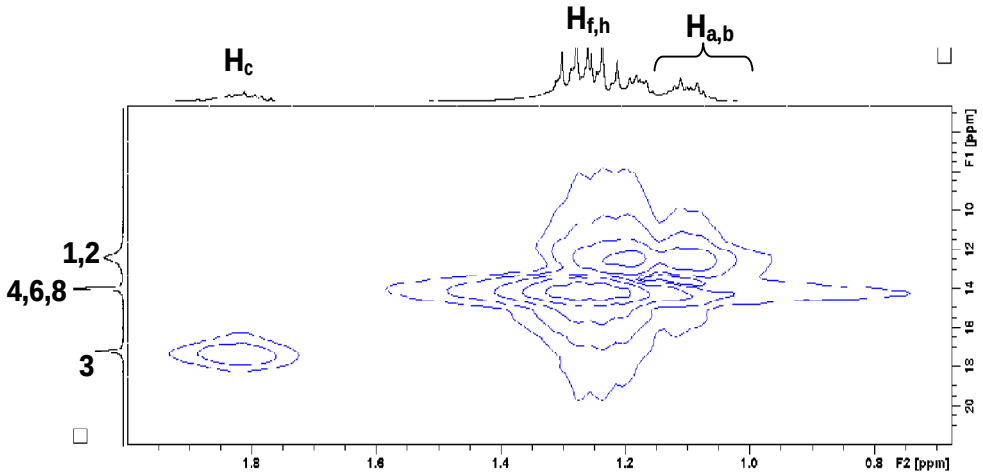

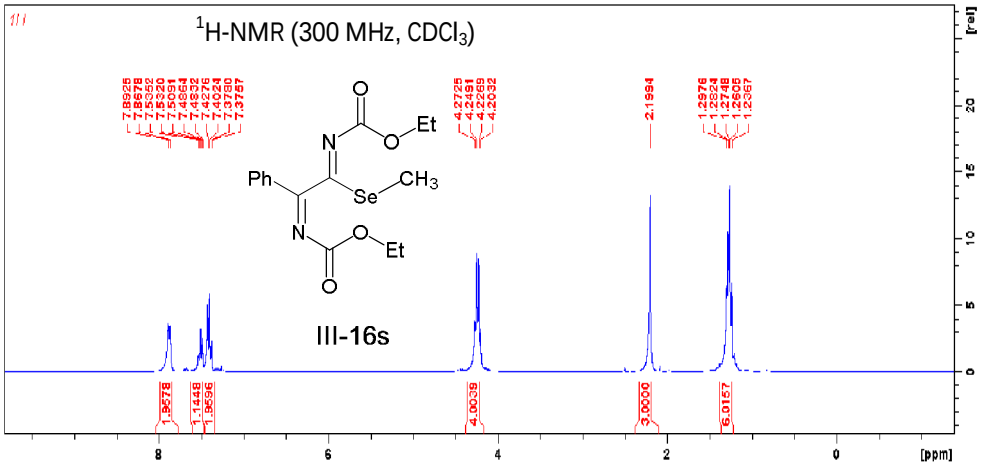
1H-NMR (300 MHz, CDCl3)
III-16s
[ppm]
[rel]

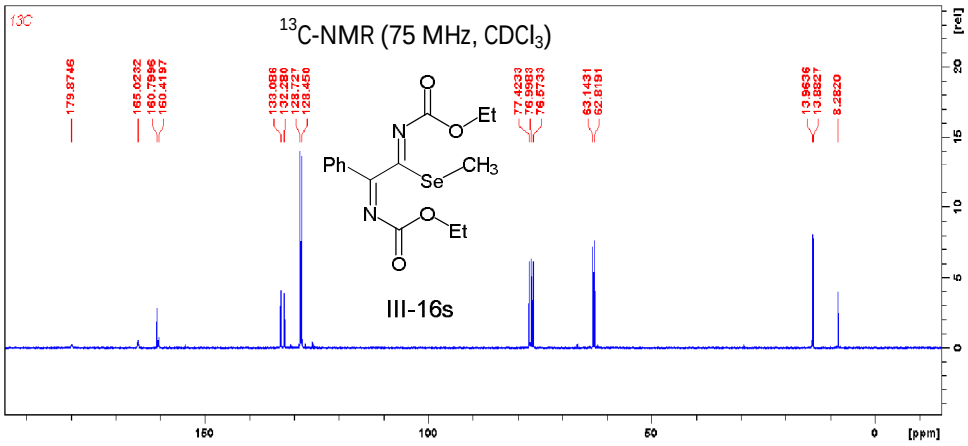
13C-NMR (75 MHz, CDCl3)
III-16s
[ppm]
[rel]

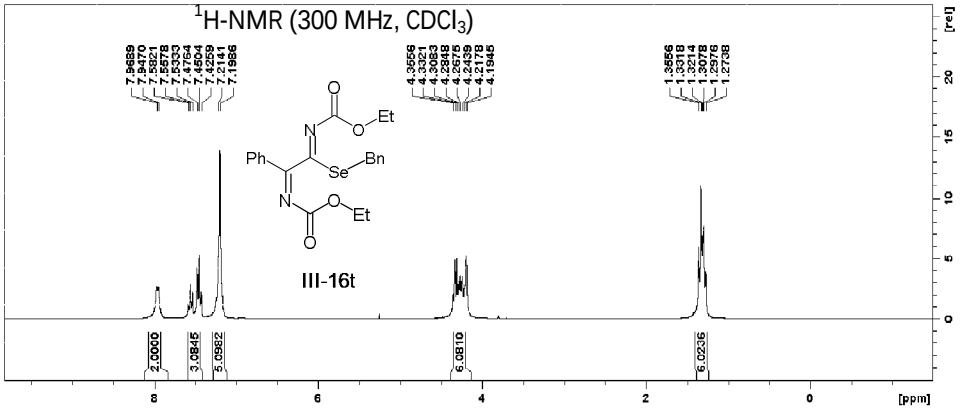
^{1}H-NMR (300 MHz, CDCl$_3$)
7.9689
7.9470
7.5821
7.5573
7.5373
7.4764
7.4504
7.4259
7.2141
7.1956
4.3556
4.3321
4.3083
4.2848
4.2735
4.2439
4.2178
4.1945
1.3856
1.3713
1.3214
1.3078
1.2976
1.2738
Ph
Se
Bn
Et
III-16t
2.0000
3.0845
5.0592
6.0810
6.0236
[rel]
[ppm]

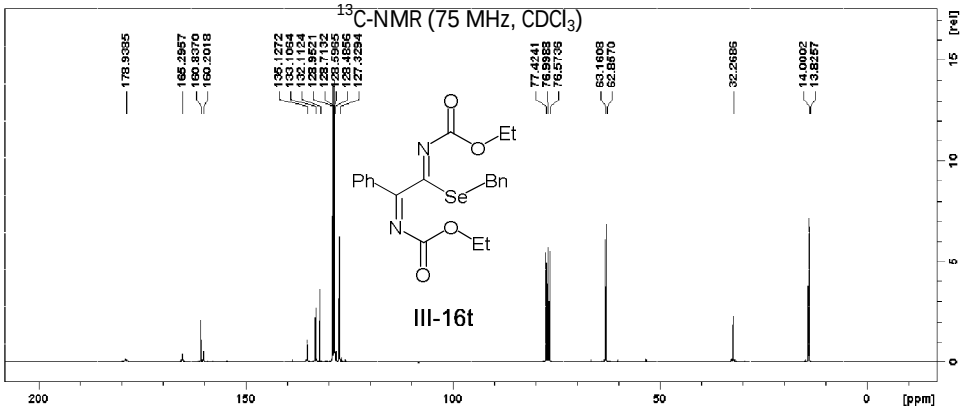
^{13}C-NMR (75 MHz, CDCl$_3$)
178.9385
165.2957
160.8370
160.2018
135.1272
133.0654
132.1124
128.9521
128.7132
128.5595
128.4856
127.9284
77.4241
76.9988
76.5736
63.1603
62.8870
32.2686
14.0002
13.8257
Ph
Se
Bn
Et
III-16t
[rel]
[ppm]

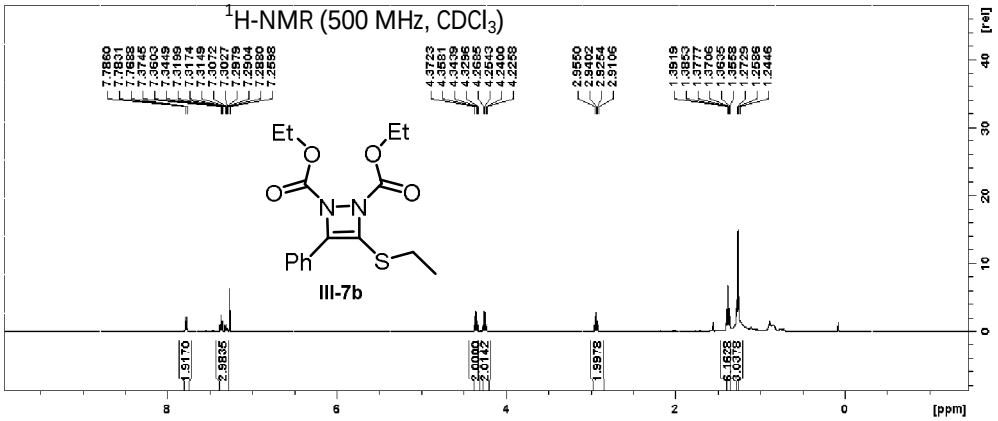
^{1}H-NMR (500 MHz, $CDCl_3$)
Et
O
O
Et
O
O
N–N
Ph
S
III-7b
[ppm]
[rel]

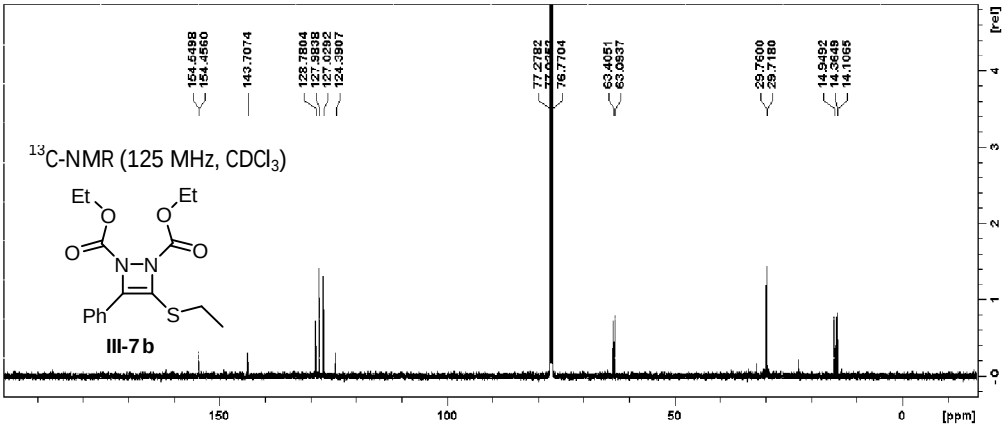
^{13}C-NMR (125 MHz, $CDCl_3$)
Et
O
O
Et
O
O
N–N
Ph
S
III-7b
[ppm]
[rel]

3.5.20. ^{1}H NMR and ^{13}C NMR spectra for cyclohexenyl derivatives of N,N-dicarbamoyl 2-iminothioimidates

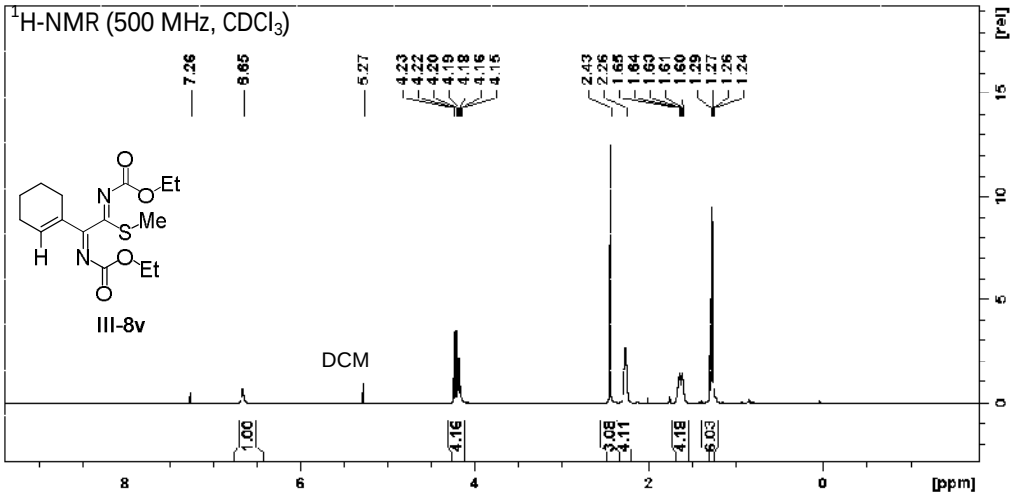

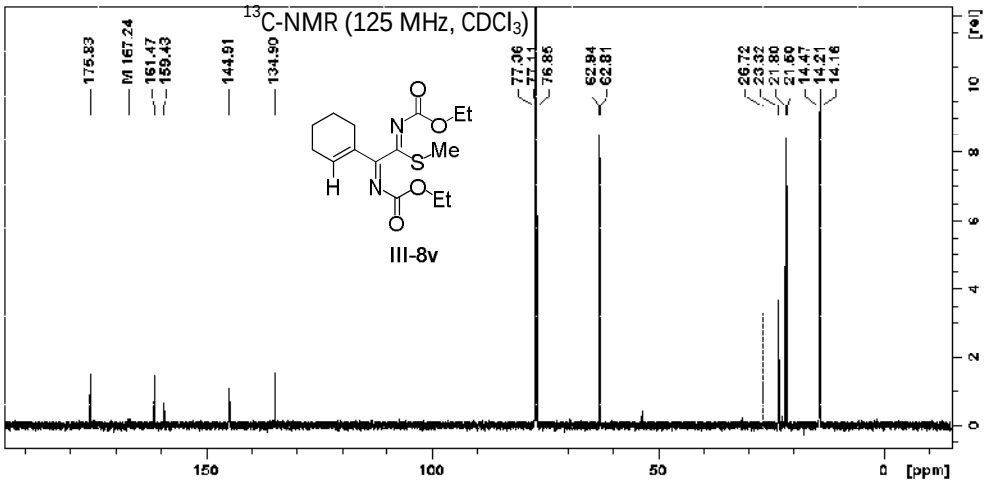

2D-HMQC (F2 = 500 MHz, F1 = 125 MHz, $CDCl_3$) analysis of 2-iminothioimidate **III-8v**

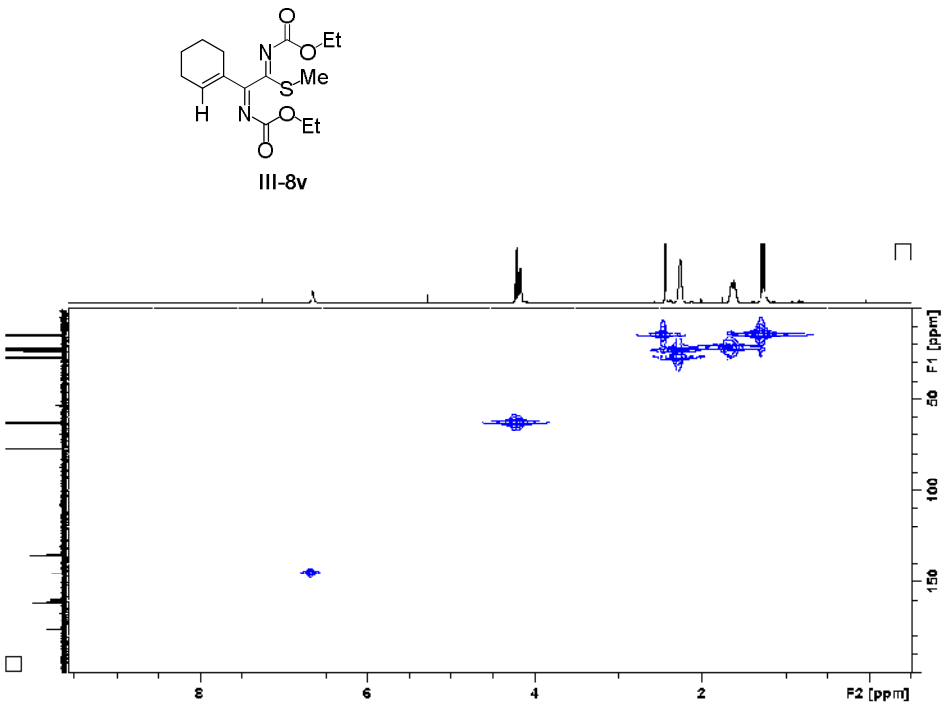

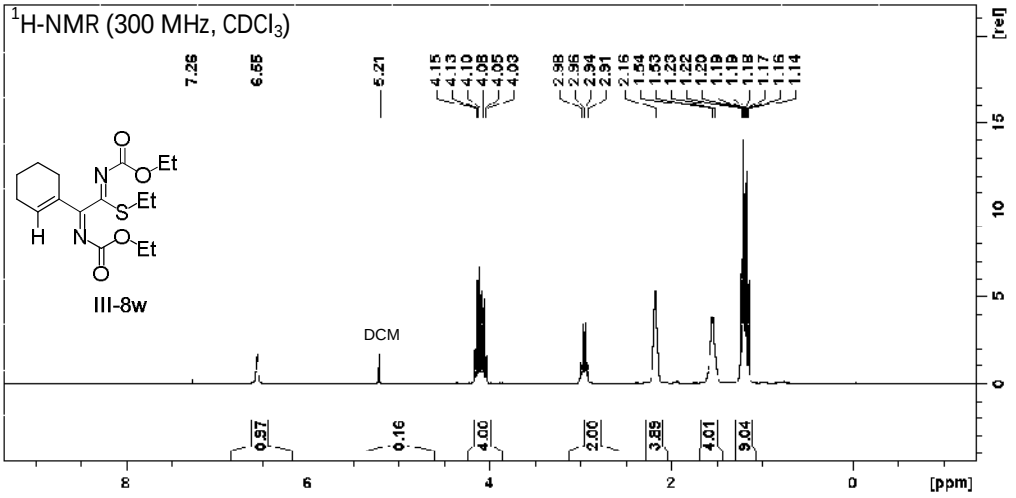
1H-NMR (300 MHz, CDCl3)
7.26
6.55
5.21
4.15
4.13
4.10
4.08
4.05
4.03
2.98
2.96
2.94
2.91
2.16
1.54
1.53
1.23
1.22
1.20
1.19
1.18
1.17
1.16
1.14
Et
N
O
Et
S
Et
H
N
O
Et
O
III-8w
DCM
0.97
0.16
4.00
2.00
3.89
4.01
9.04
8
6
4
2
0
[ppm]
[rel]
15
10
5
0

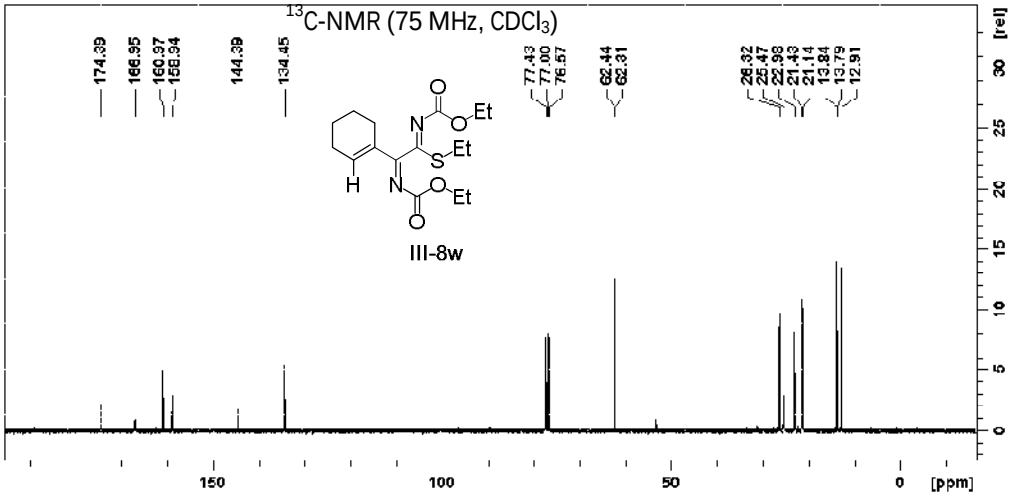
13C-NMR (75 MHz, CDCl3)
174.39
166.95
160.97
158.94
144.39
134.45
77.43
77.00
76.57
62.44
62.31
28.32
25.47
22.98
21.43
21.14
13.84
13.79
12.91
Et
N
O
Et
S
Et
H
N
O
Et
O
III-8w
150
100
50
0
[ppm]
[rel]
30
25
20
15
10
5
0

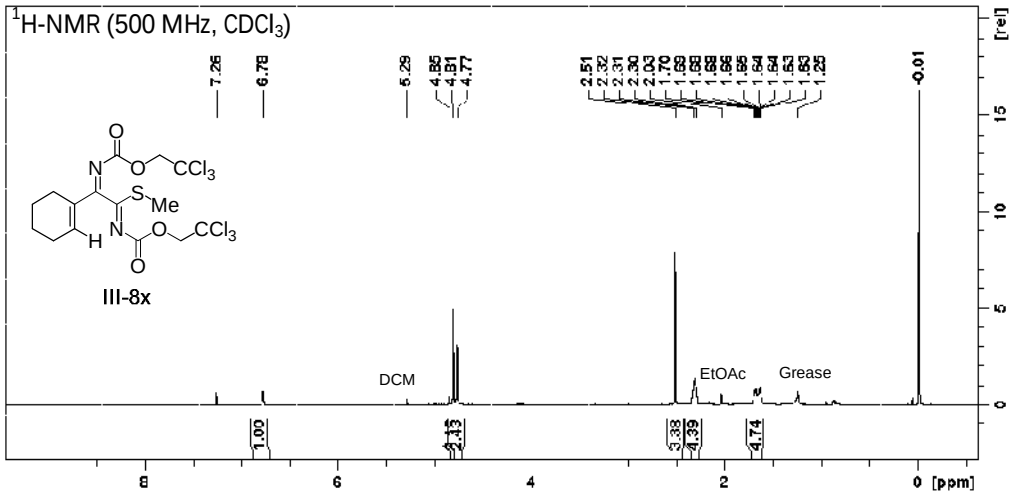
1H-NMR (500 MHz, CDCl3)
7.26
6.78
5.29
4.85
4.81
4.77
2.51
2.32
2.31
2.30
2.03
1.70
1.69
1.68
1.68
1.66
1.65
1.64
1.64
1.63
1.63
1.25
-0.01
DCM
EtOAc
Grease
1.00
2.13
3.38
4.39
4.74
III-8x
[rel]
[ppm]

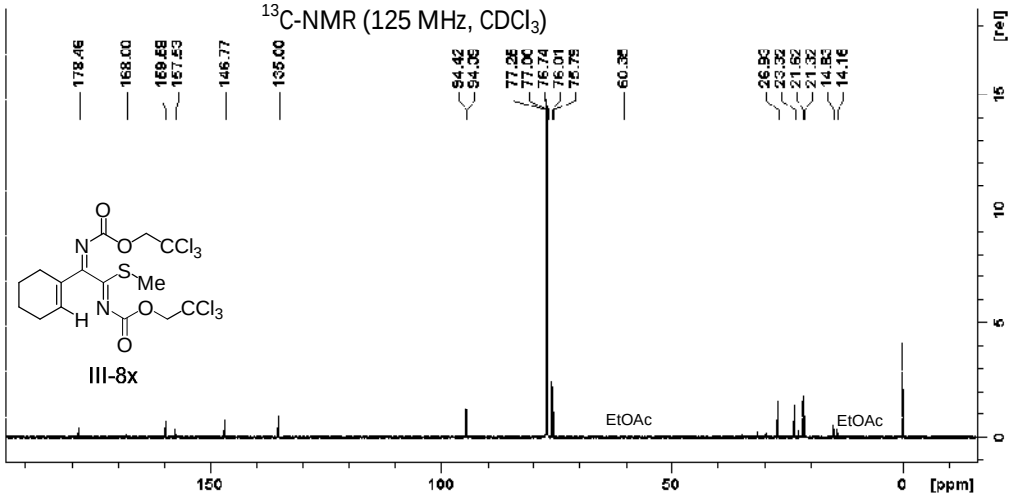
13C-NMR (125 MHz, CDCl3)
178.46
168.00
159.58
157.53
146.77
135.00
94.42
94.36
77.25
77.00
76.74
76.01
75.75
60.38
26.90
23.32
21.62
21.32
14.83
14.16
EtOAc
EtOAc
III-8x
[rel]
[ppm]

2D-HMQC (F2 = 500 MHz, F1 = 125 MHz, $CDCl_3$) analysis of tetrahydroindole **III-8x**

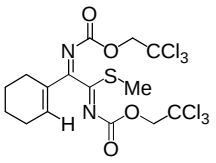

III-8x

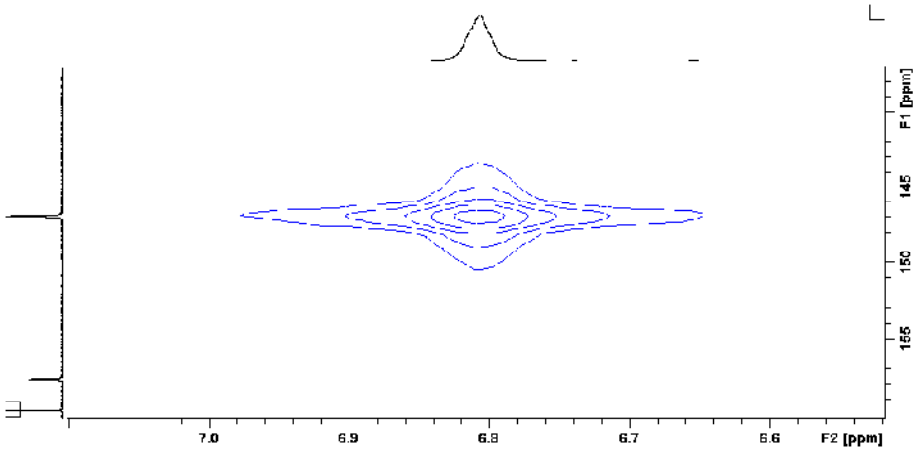

3.5.21. ^{1}H and ^{13}C NMR spectra for characterization data for enynes (III-26)

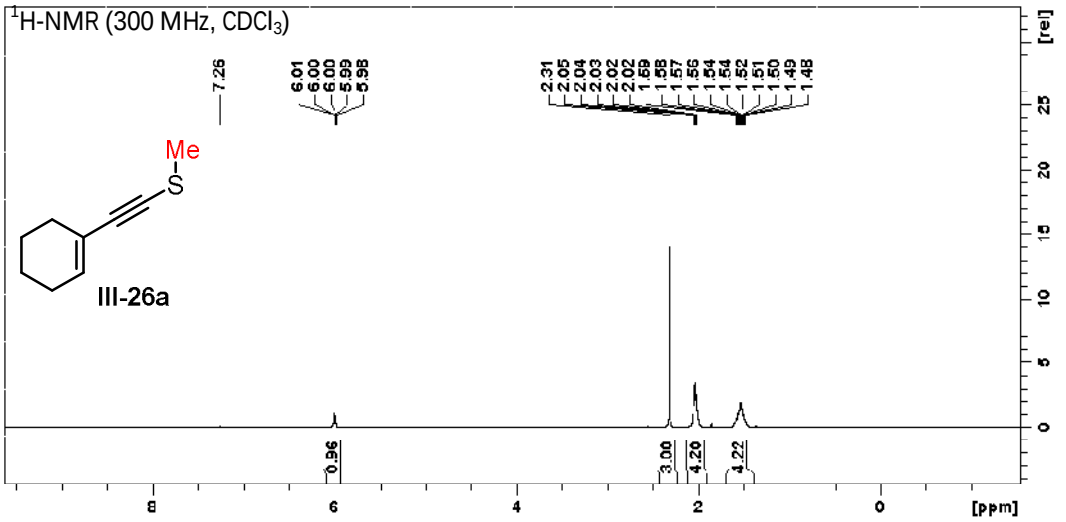

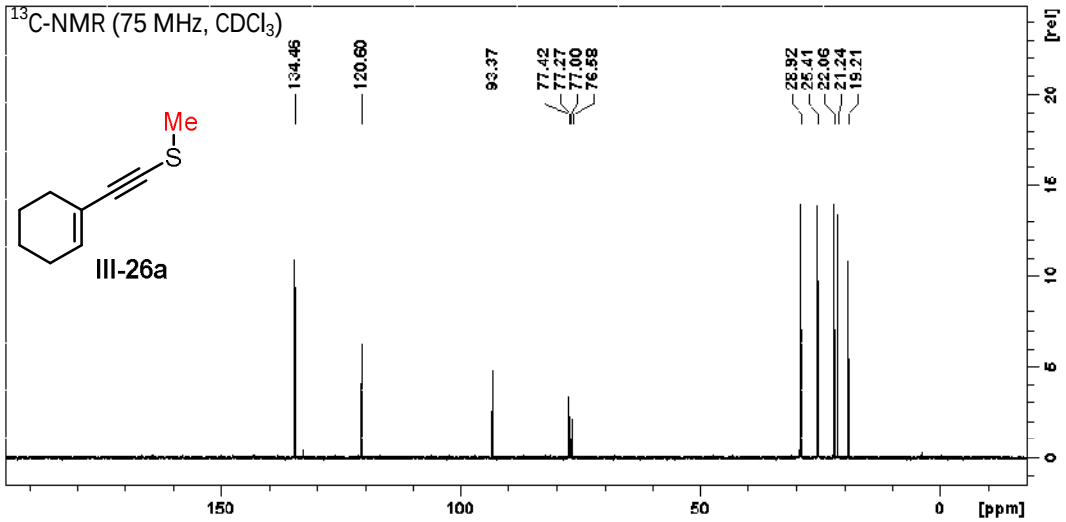

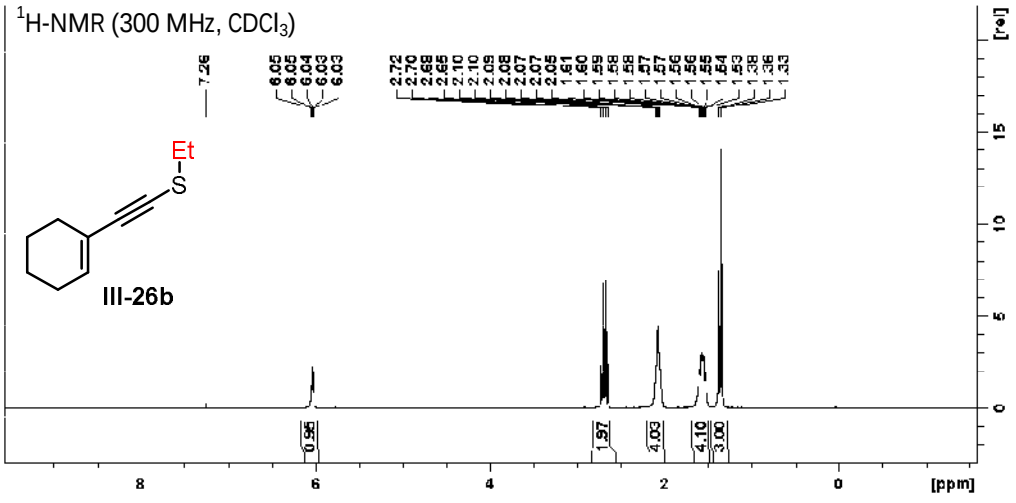
^{1}H-NMR (300 MHz, $CDCl_3$)
Et
S
III-26b
7.26
6.05 6.05 6.04 6.03 6.03
2.72 2.70 2.68 2.65 2.10 2.09 2.08 2.07 2.07 2.05 1.61 1.60 1.59 1.58 1.58 1.57 1.57 1.56 1.56 1.55 1.54 1.53 1.38 1.36 1.33
0.95 1.97 4.03 4.10 3.00
8 6 4 2 0 [ppm]
[rel]

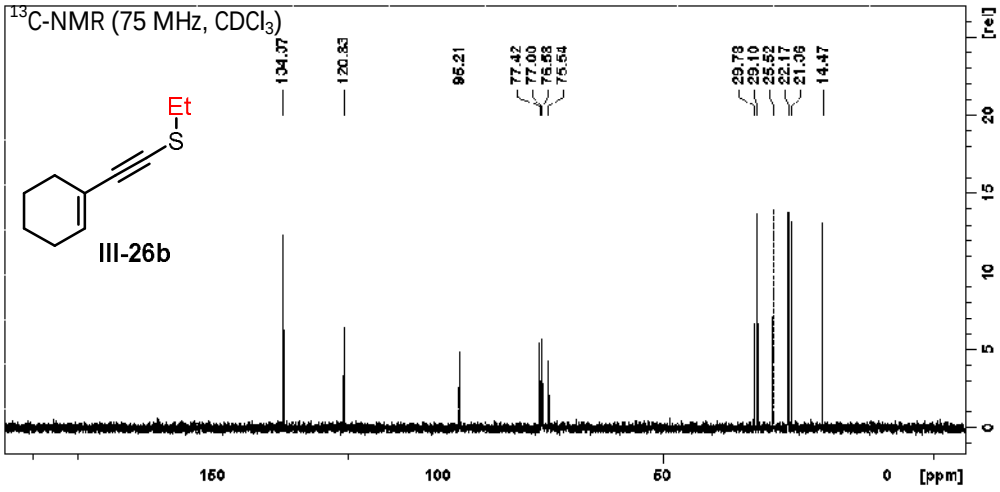
^{13}C-NMR (75 MHz, $CDCl_3$)
Et
S
III-26b
134.37 120.83 95.21 77.42 77.00 76.58 75.54 29.78 29.10 25.52 22.17 21.36 14.47
150 100 50 0 [ppm]
[rel]

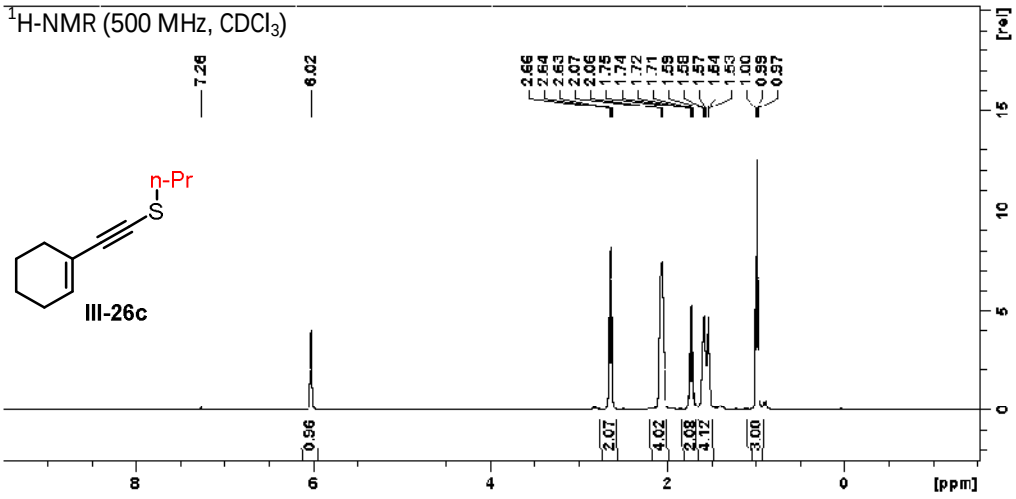
^{1}H-NMR (500 MHz, $CDCl_3$)
n-Pr
S
III-26c
7.26
6.02
2.66
2.64
2.63
2.07
2.06
1.75
1.74
1.72
1.71
1.59
1.58
1.57
1.54
1.53
1.00
0.99
0.97
0.96
2.07
4.02
2.08
4.12
3.00
[rel]
[ppm]

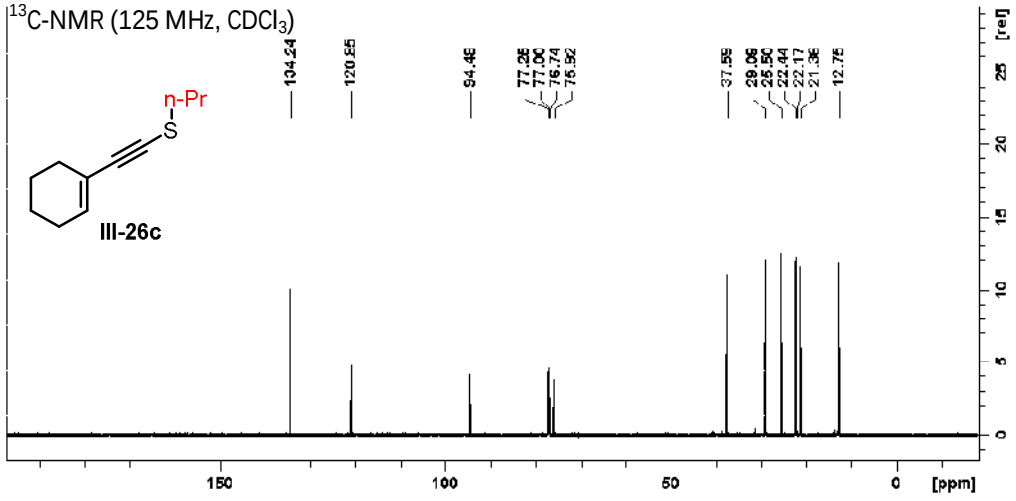
^{13}C-NMR (125 MHz, $CDCl_3$)
n-Pr
S
III-26c
134.24
120.65
94.46
77.26
77.00
76.74
75.92
37.55
29.06
25.50
22.44
22.17
21.36
12.75
[rel]
[ppm]

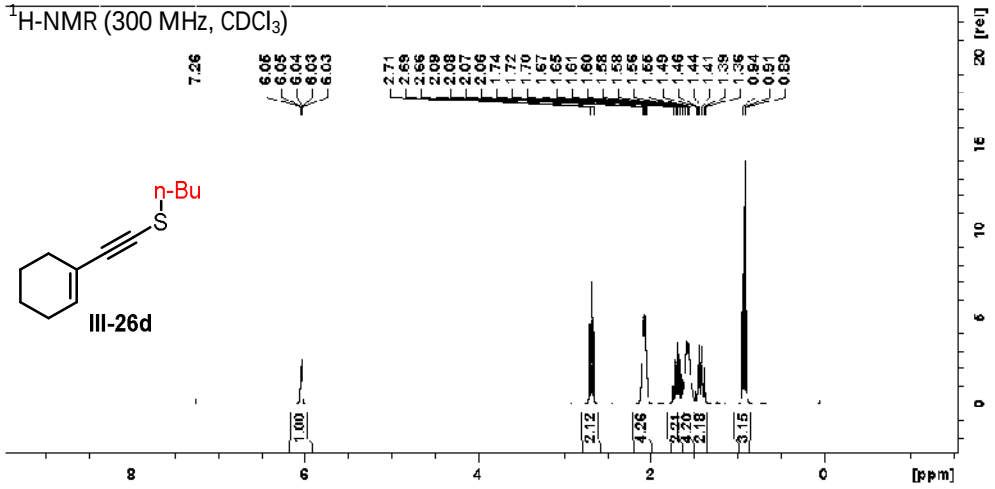
1H-NMR (300 MHz, CDCl3)
n-Bu
S
III-26d
[ppm]
[rel]

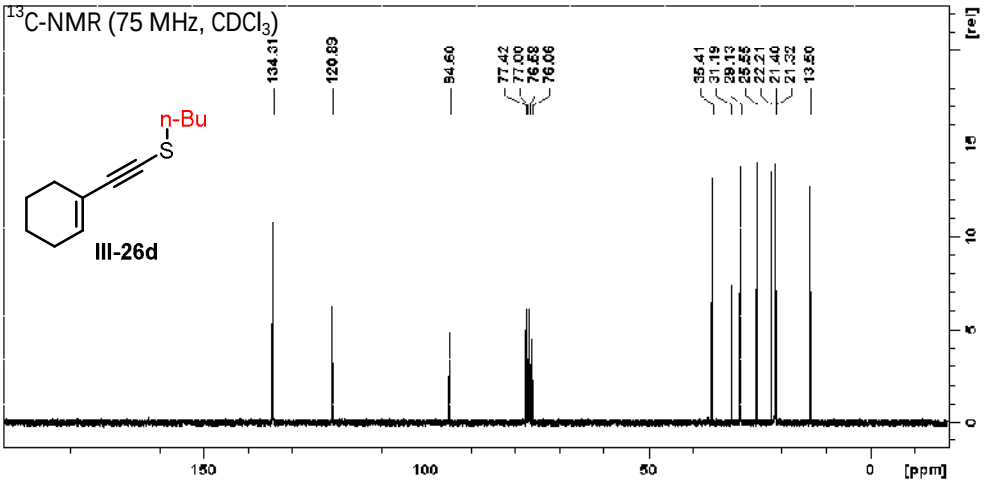
13C-NMR (75 MHz, CDCl3)
n-Bu
S
III-26d
[ppm]
[rel]

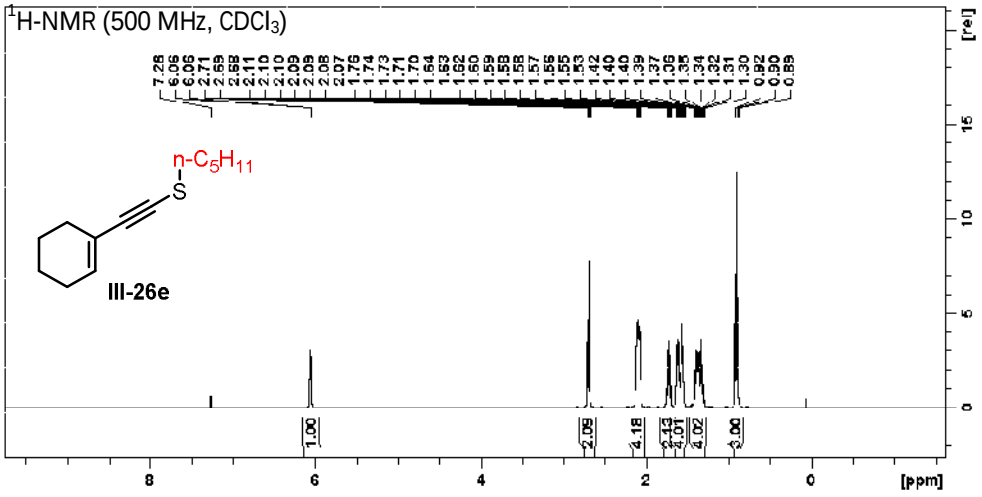
^{1}H-NMR (500 MHz, $CDCl_3$)
n-C_5H_{11}
S
III-26e
[rel]
[ppm]

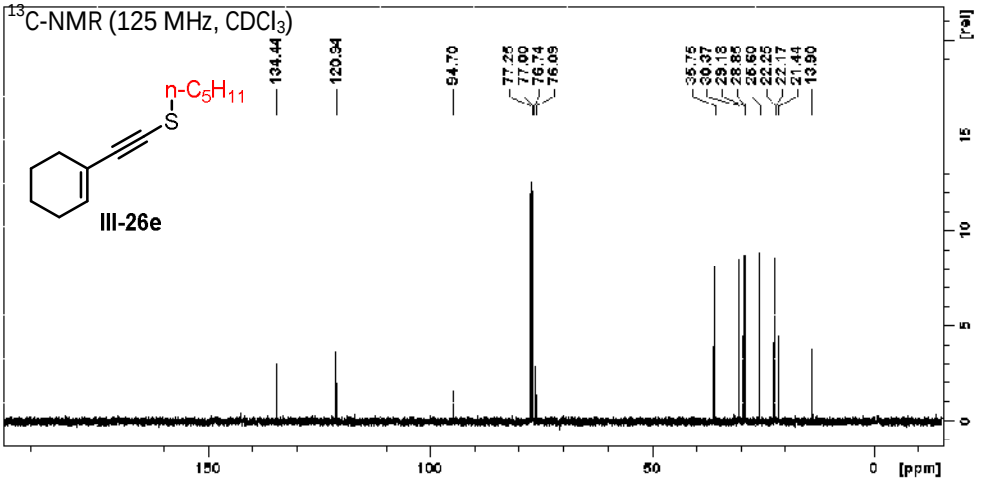
^{13}C-NMR (125 MHz, $CDCl_3$)
n-C_5H_{11}
S
III-26e
134.44
120.94
94.70
77.25
77.00
76.74
76.09
35.75
30.37
29.18
28.85
26.60
22.25
22.17
21.44
13.90
[rel]
[ppm]

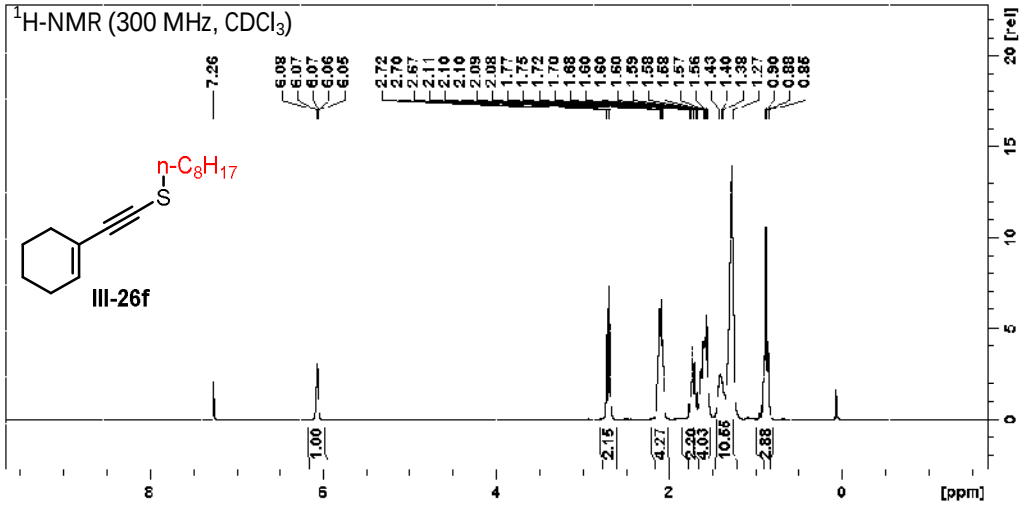
^{1}H-NMR (300 MHz, $CDCl_3$)
n-C_8H_{17}
S
III-26f
7.26
6.08
6.07
6.07
6.06
6.05
2.72
2.70
2.67
2.11
2.10
2.09
2.08
1.77
1.75
1.72
1.70
1.68
1.60
1.60
1.60
1.59
1.58
1.58
1.57
1.56
1.43
1.40
1.38
1.27
0.90
0.88
0.86
1.00
2.15
4.27
2.09
4.03
10.66
2.88
20 [rel]
15
10
5
0
8
6
4
2
0
[ppm]

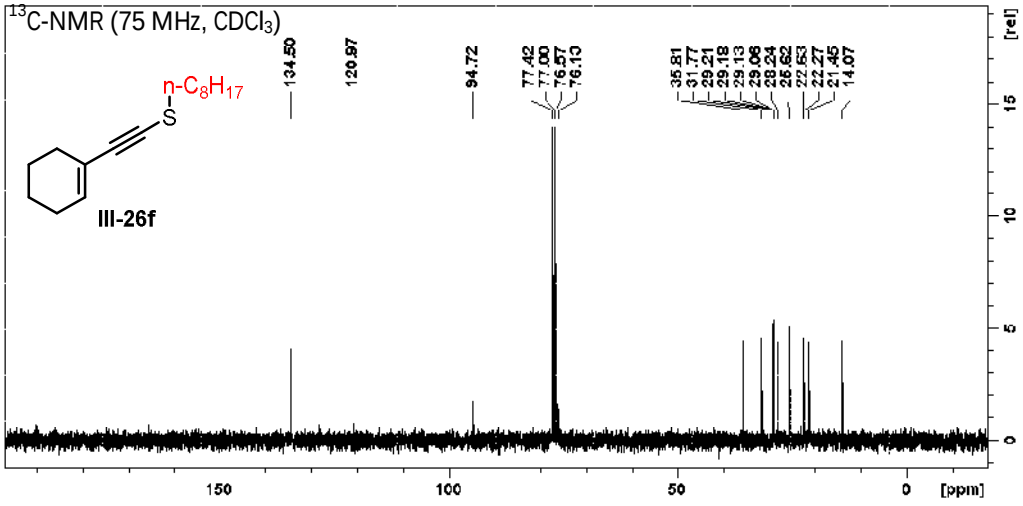
^{13}C-NMR (75 MHz, $CDCl_3$)
n-C_8H_{17}
S
III-26f
134.50
120.97
94.72
77.42
77.00
76.57
76.13
35.81
31.77
29.21
29.18
29.13
29.08
28.24
26.62
22.63
22.27
21.45
14.07
[rel]
15
10
5
0
150
100
50
0
[ppm]

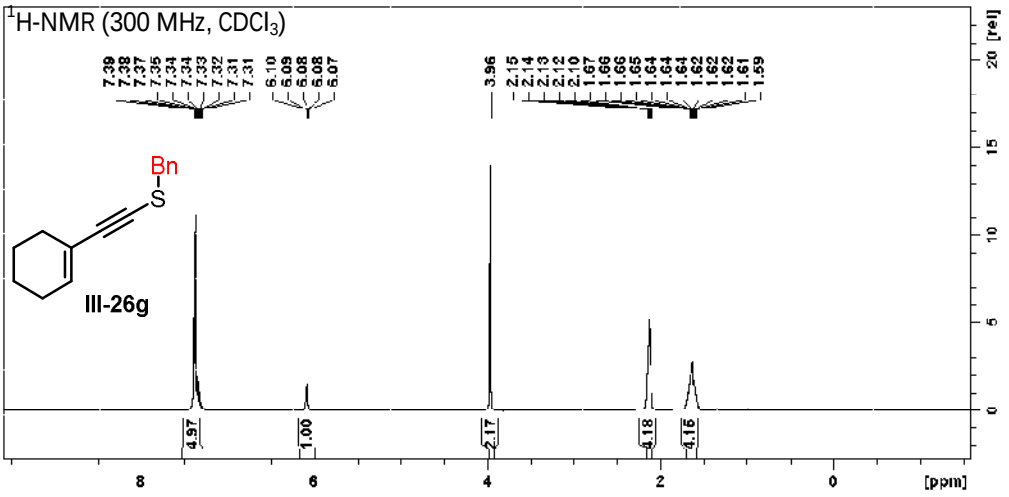
1H-NMR (300 MHz, CDCl3)
7.39
7.38
7.37
7.35
7.34
7.34
7.33
7.32
7.31
7.31
6.10
6.09
6.08
6.08
6.07
3.96
2.15
2.14
2.13
2.12
2.10
1.67
1.66
1.66
1.65
1.64
1.64
1.64
1.62
1.62
1.62
1.61
1.59
Bn
S
III-26g
4.97
1.00
2.17
4.18
4.16
8
6
4
2
0
[ppm]
[rel]

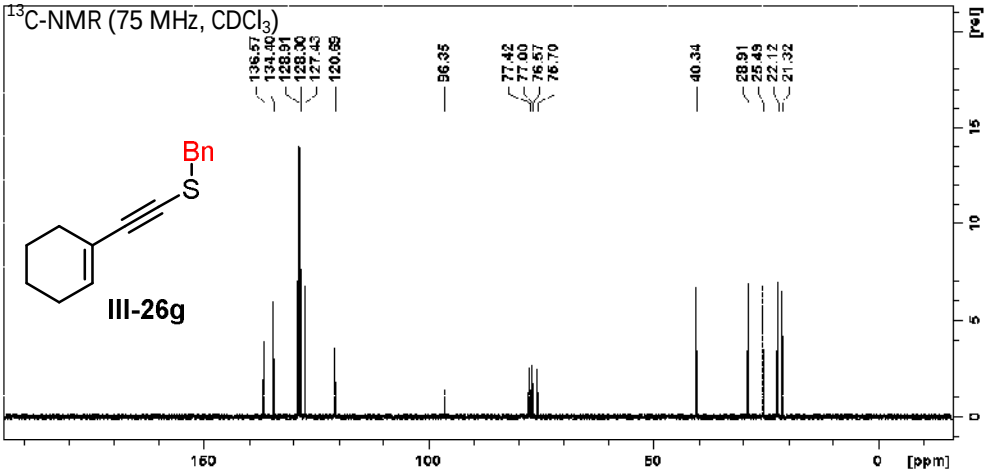
13C-NMR (75 MHz, CDCl3)
136.57
134.40
128.91
128.30
127.43
120.89
96.35
77.42
77.00
76.57
76.70
40.34
28.91
25.49
22.12
21.32
Bn
S
III-26g
150
100
50
0
[ppm]
[rel]

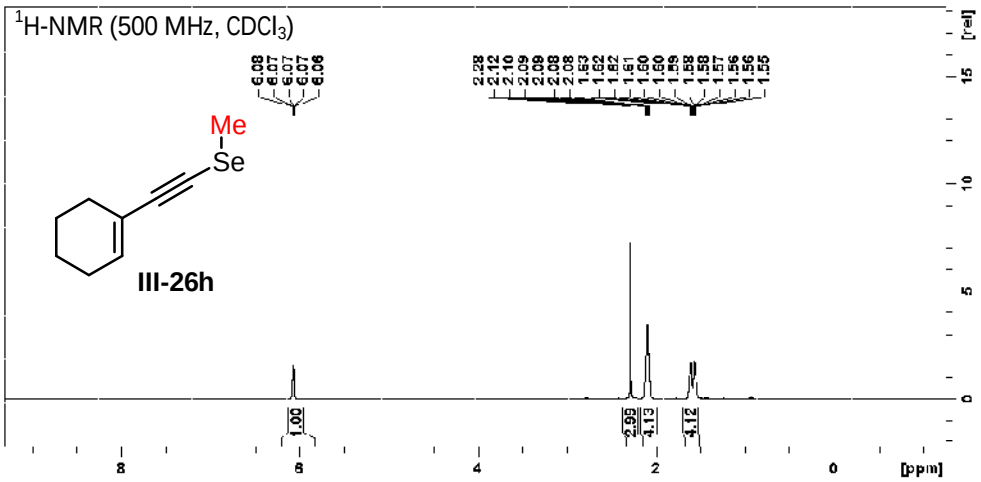
1H-NMR (500 MHz, CDCl3)
Me
Se
III-26h
6.08
6.07
6.07
6.07
6.06
2.28
2.12
2.10
2.09
2.09
2.08
2.08
1.63
1.62
1.61
1.60
1.60
1.59
1.58
1.58
1.57
1.56
1.56
1.55
1.00
2.95
4.13
4.12
8
6
4
2
0
[ppm]
[rel]

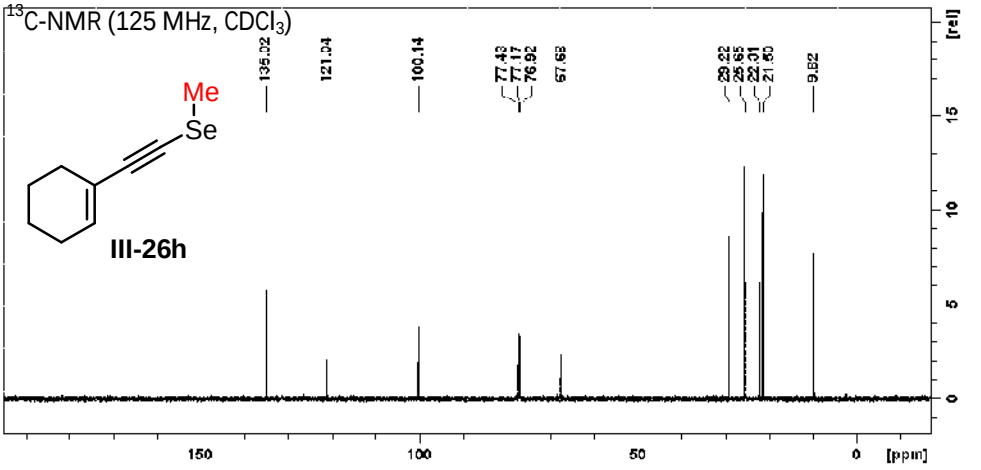
13C-NMR (125 MHz, CDCl3)
Me
Se
III-26h
135.32
121.04
100.14
77.43
77.17
76.92
67.68
29.62
25.65
22.31
21.60
9.62
150
100
50
0
[ppm]
[rel]

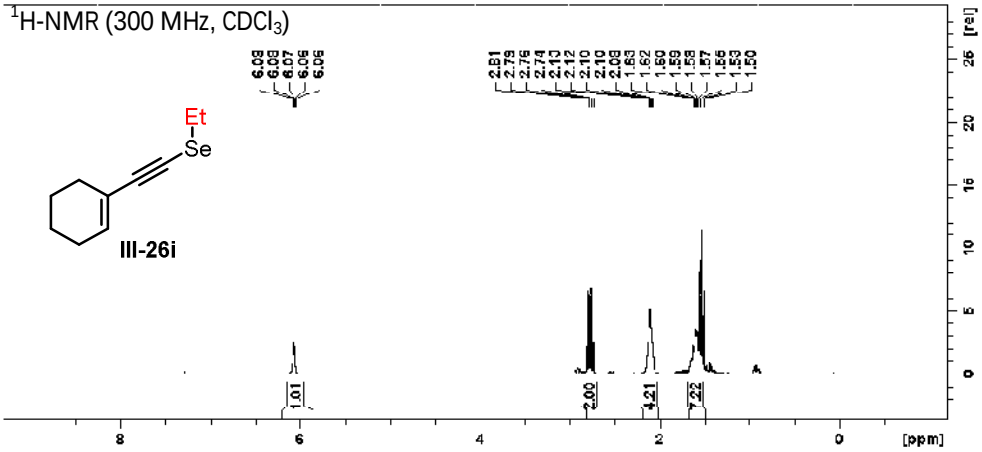
1H-NMR (300 MHz, CDCl3)
Et
Se
III-26i
6.09
6.08
6.07
6.06
6.06
2.81
2.79
2.76
2.74
2.13
2.12
2.10
2.10
2.08
1.63
1.62
1.60
1.59
1.58
1.57
1.55
1.53
1.50
1.01
2.00
1.21
7.22
8
6
4
2
0
[ppm]
[rel]

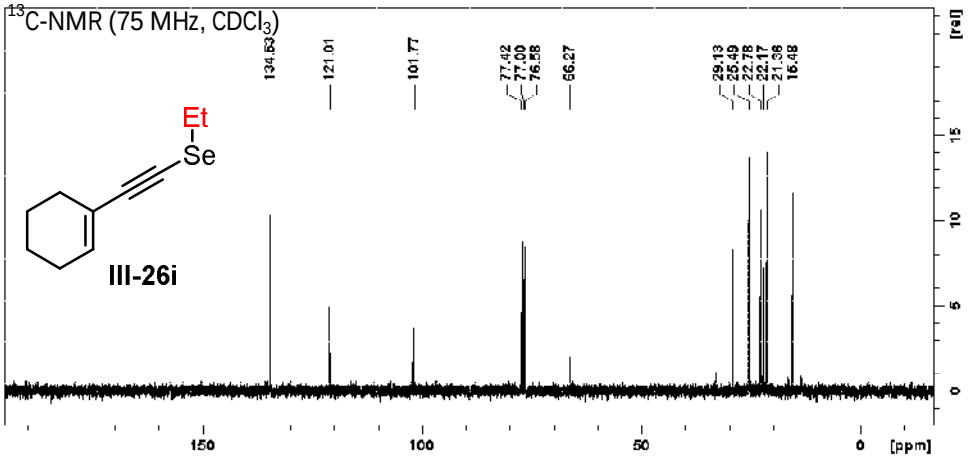
13C-NMR (75 MHz, CDCl3)
Et
Se
III-26i
134.53
121.01
101.77
77.42
77.00
76.58
66.27
29.13
25.49
22.78
22.17
21.38
16.48
150
100
50
0
[ppm]
[rel]

^{1}H-NMR (500 MHz, $CDCl_3$)

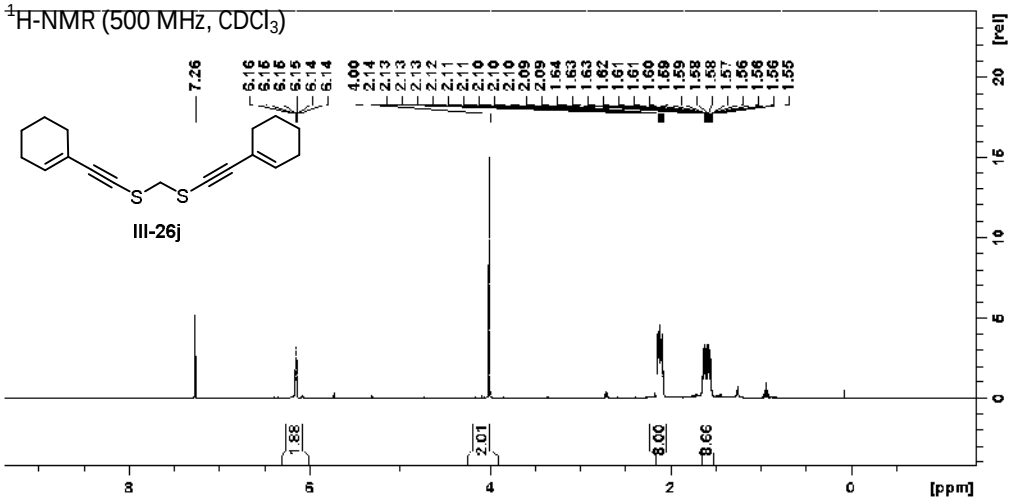

^{13}C-NMR (125 MHz, $CDCl_3$)

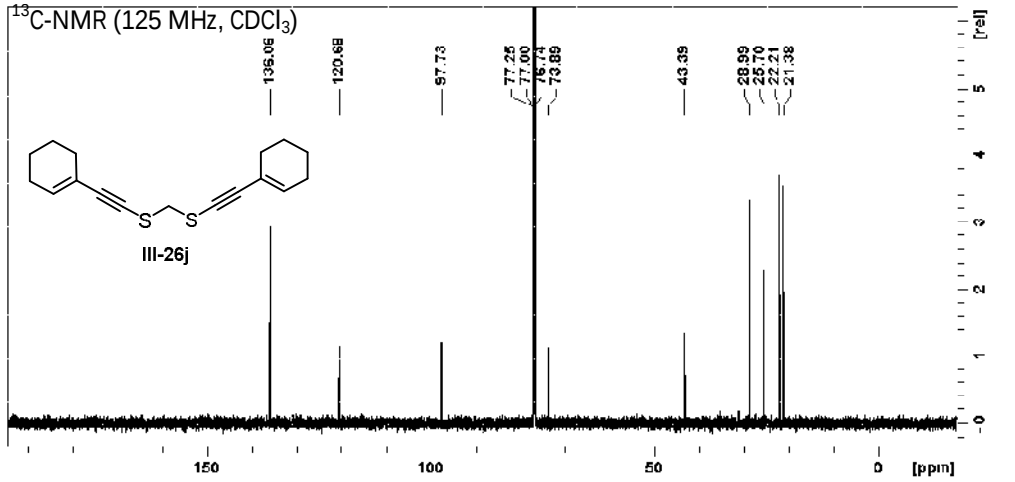

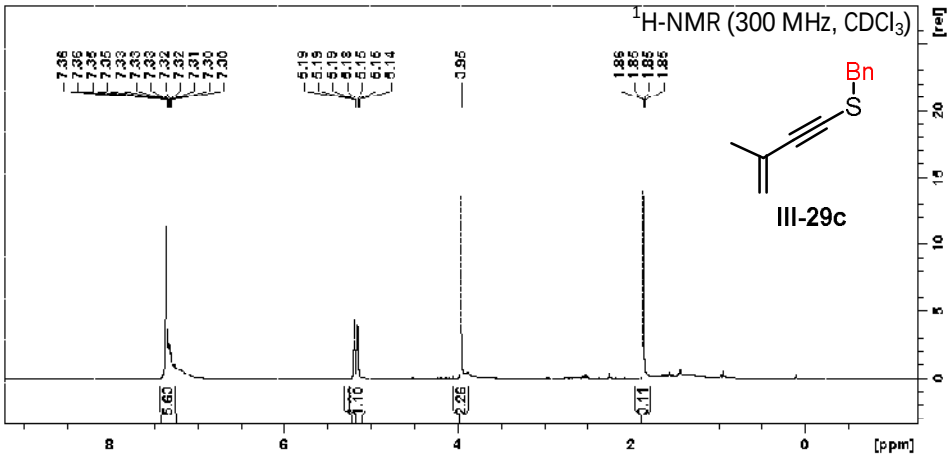
1H-NMR (300 MHz, CDCl3)
Bn
S
III-29c
[ppm]
[rel]

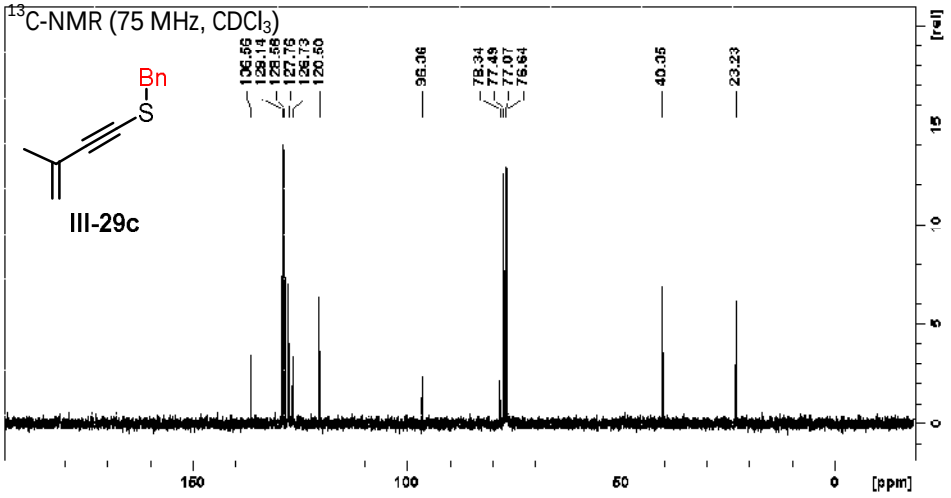
13C-NMR (75 MHz, CDCl3)
Bn
S
III-29c
[ppm]
[rel]

*3.5.22. ^{1}H and ^{13}C NMR spectra for characterization data for tetrahydroindoles (**III-27**)*

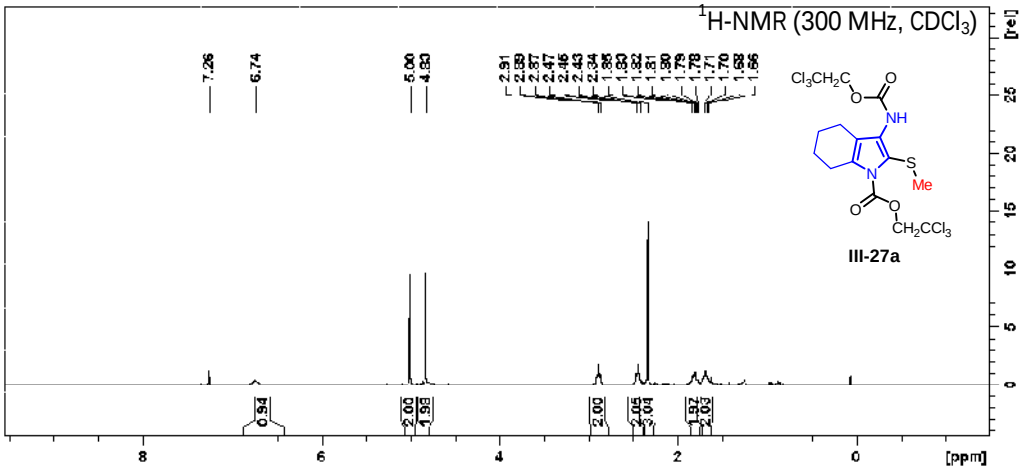

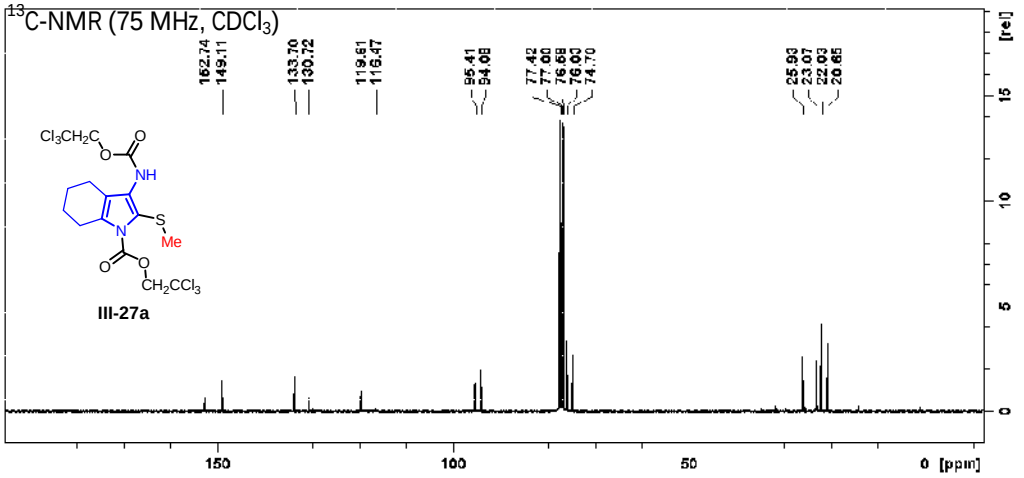

2D-HMQC (F2 = 300 MHz, F1 = 75 MHz, $CDCl_3$) analysis of tetrahydroindole **III-27a**

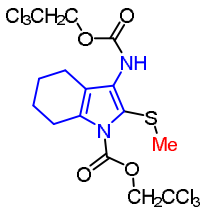

III-27a

Accidental degeneracy of the 22 ppm ^{13}C resonance with the ^{1}H resonances of 2.45 ppm triplet and with the multiplet within the range of 1.90-1.75 ppm.

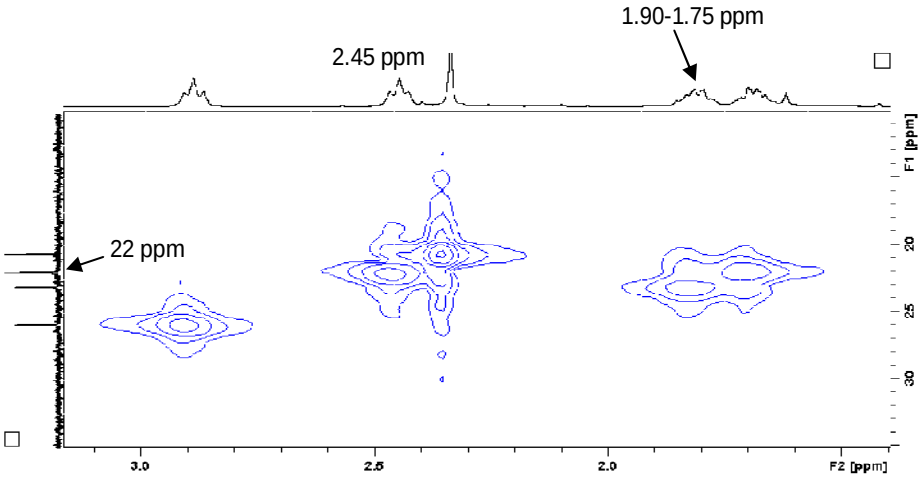

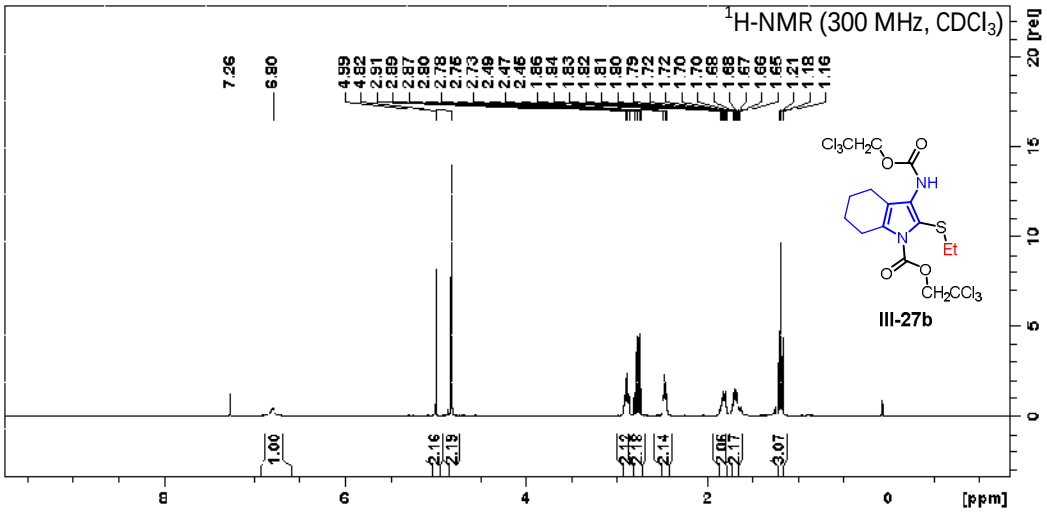
^{1}H-NMR (300 MHz, $CDCl_3$)
7.26
6.80
4.99
4.82
2.91
2.89
2.87
2.80
2.78
2.75
2.73
2.49
2.47
2.45
1.86
1.84
1.83
1.82
1.81
1.80
1.79
1.72
1.72
1.70
1.70
1.68
1.68
1.67
1.66
1.65
1.21
1.18
1.16
1.00
2.16
2.19
2.12
2.18
2.14
2.06
2.17
3.07
8
6
4
2
0
[ppm]
20 [rel]
15
10
5
0
Cl_3CH_2C
O
NH
S
Et
N
CH_2CCl_3
III-27b

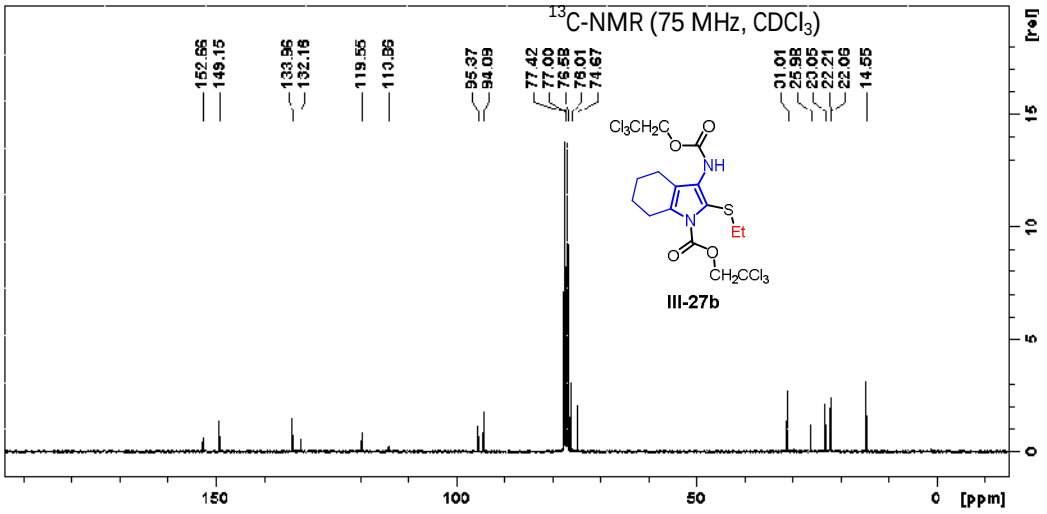
^{13}C-NMR (75 MHz, $CDCl_3$)
152.66
149.15
133.96
132.18
119.55
113.86
95.37
94.09
77.42
77.00
76.58
76.01
74.67
31.01
25.98
23.05
22.21
22.06
14.55
150
100
50
0
[ppm]
[rel]
15
10
5
0
Cl_3CH_2C
O
NH
S
Et
N
CH_2CCl_3
III-27b

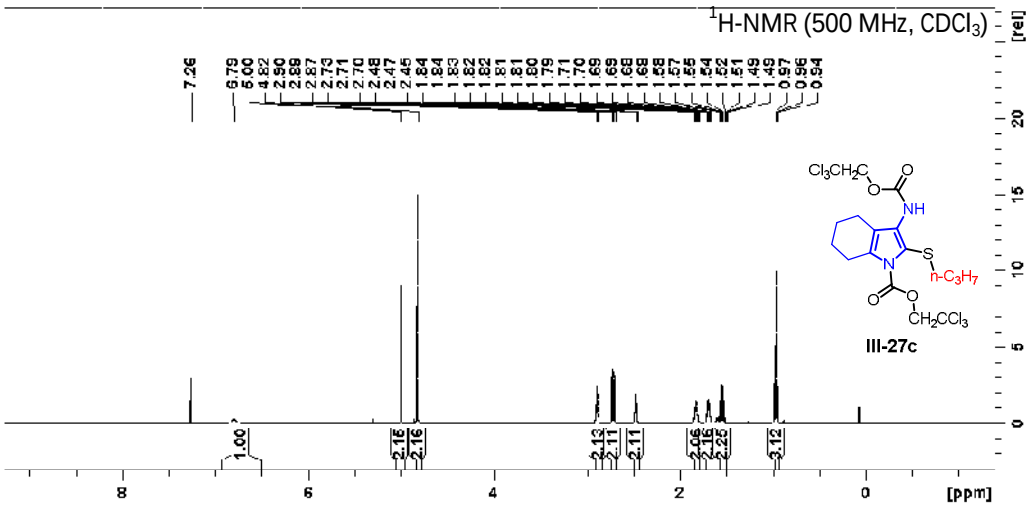
^{1}H-NMR (500 MHz, $CDCl_3$)
III-27c
[ppm]
[rel]

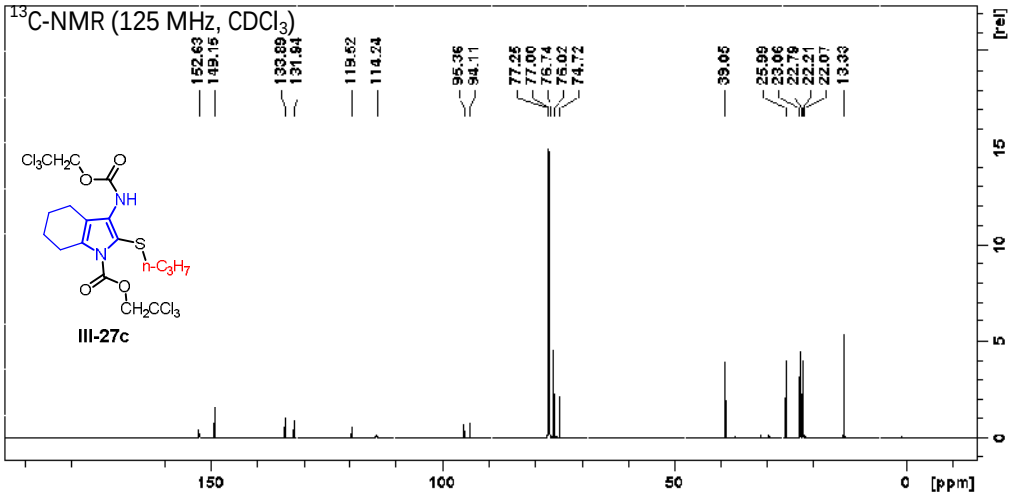
^{13}C-NMR (125 MHz, $CDCl_3$)
III-27c
[ppm]
[rel]

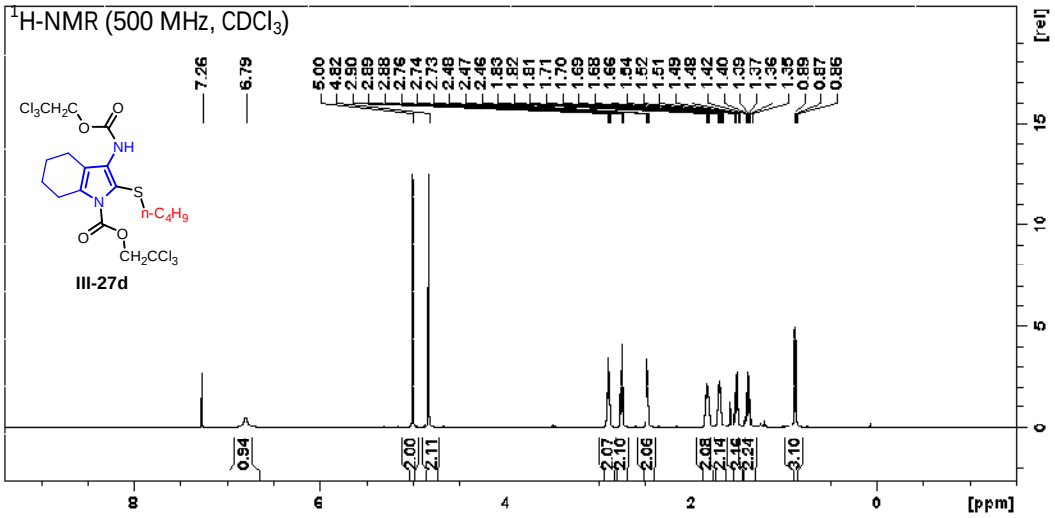
^{1}H-NMR (500 MHz, $CDCl_3$)
III-27d
[ppm]
[rel]

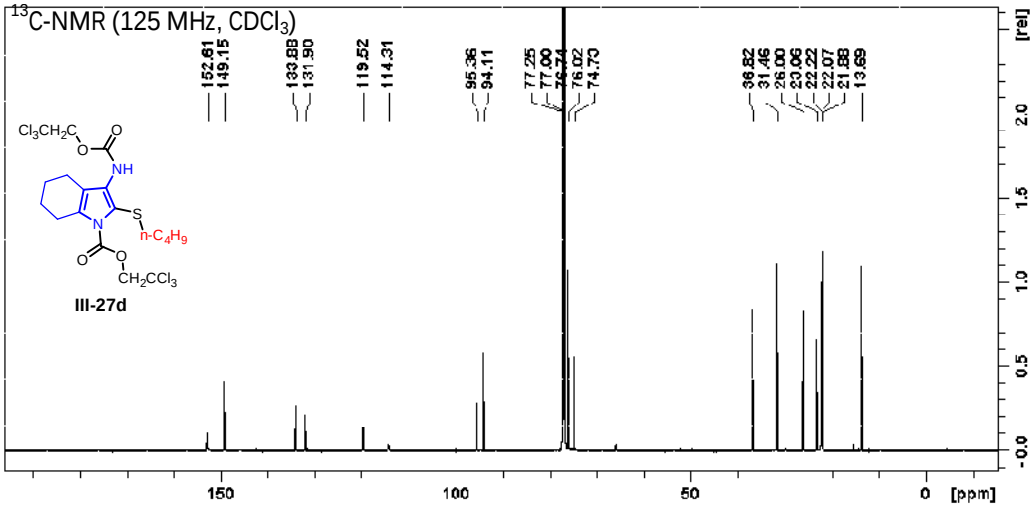
^{13}C-NMR (125 MHz, $CDCl_3$)
III-27d
[ppm]
[rel]

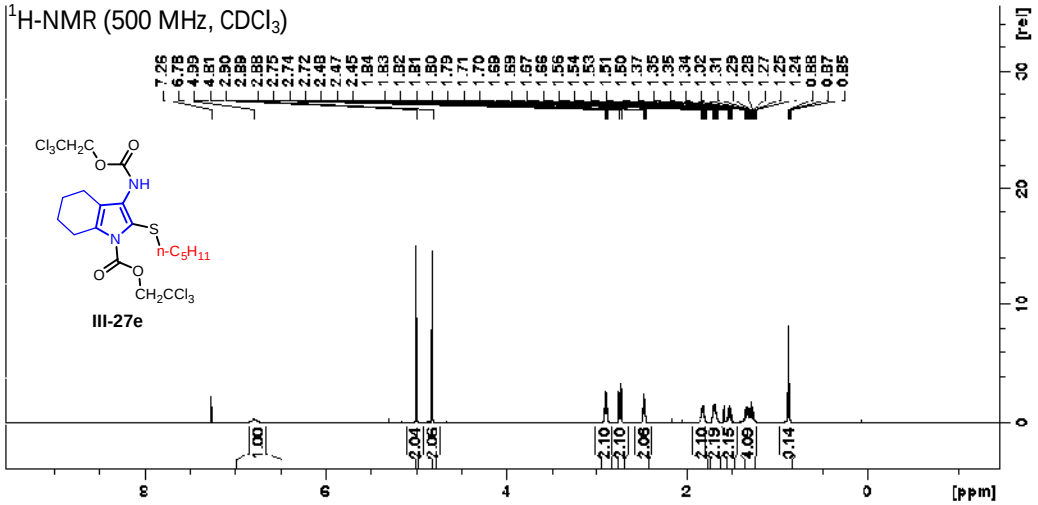
1H-NMR (500 MHz, CDCl3)
III-27e
[ppm]
[rel]

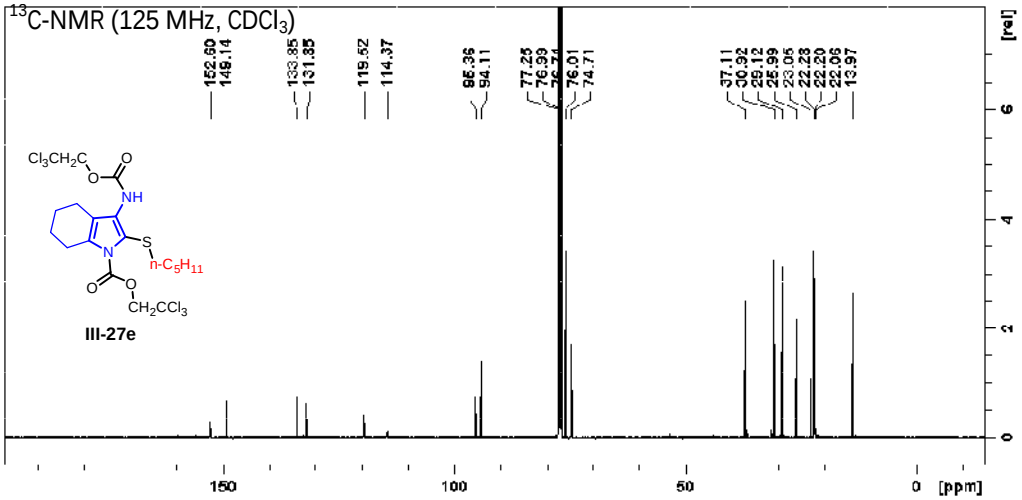
13C-NMR (125 MHz, CDCl3)
III-27e
[ppm]
[rel]

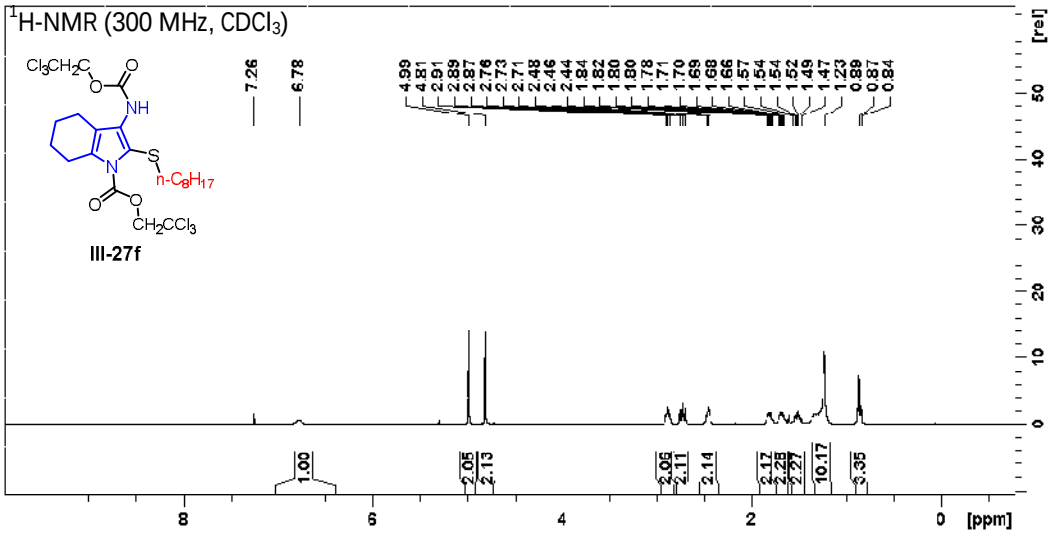
1H-NMR (300 MHz, CDCl3)
III-27f
[ppm]
[rel]

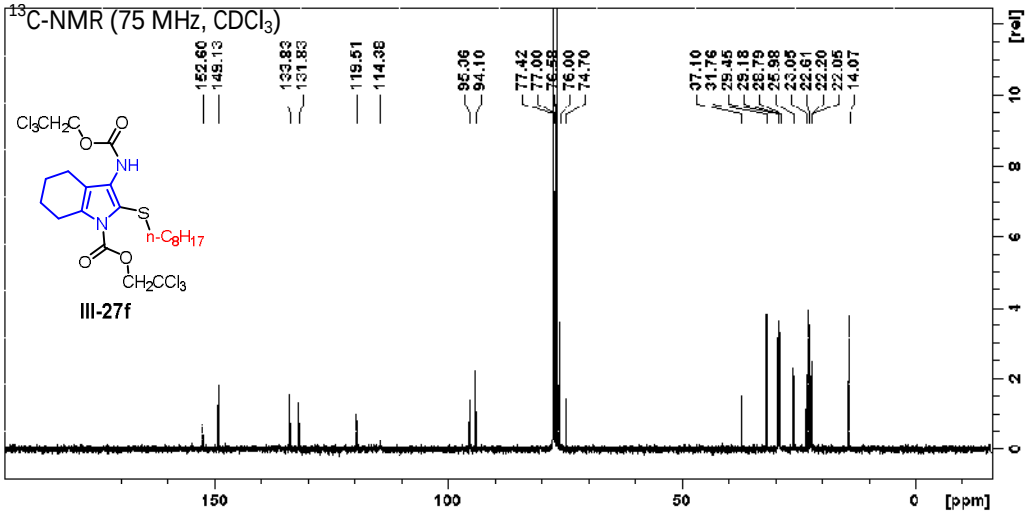
13C-NMR (75 MHz, CDCl3)
III-27f
[ppm]
[rel]

2D-HMQC (F2 = 300 MHz, F1 = 75 MHz, $CDCl_3$) analysis of tetrahydroindole **III-27f**

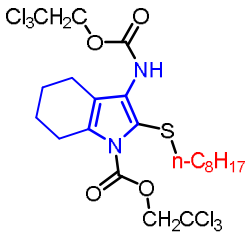

III-27f

- 29.2 ppm ^{13}C resonance has an accidental degeneracy of another ^{13}C resonance.

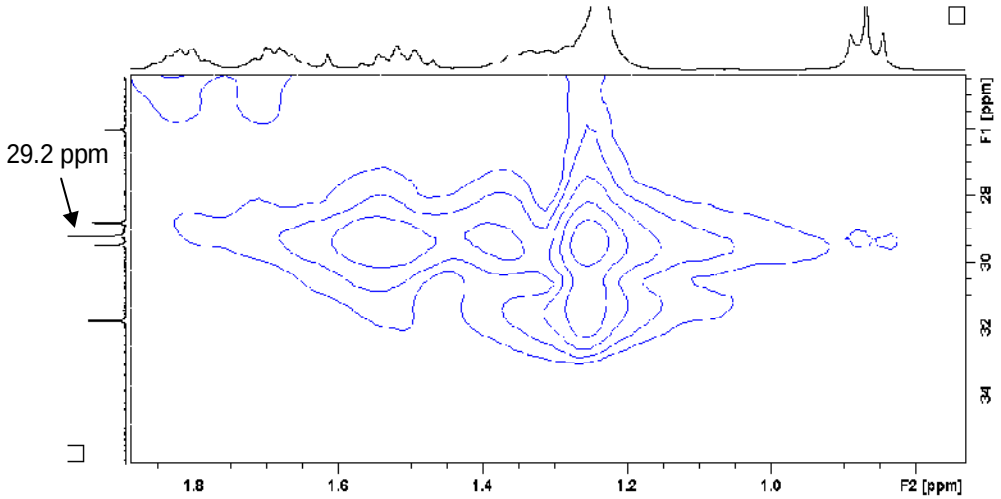

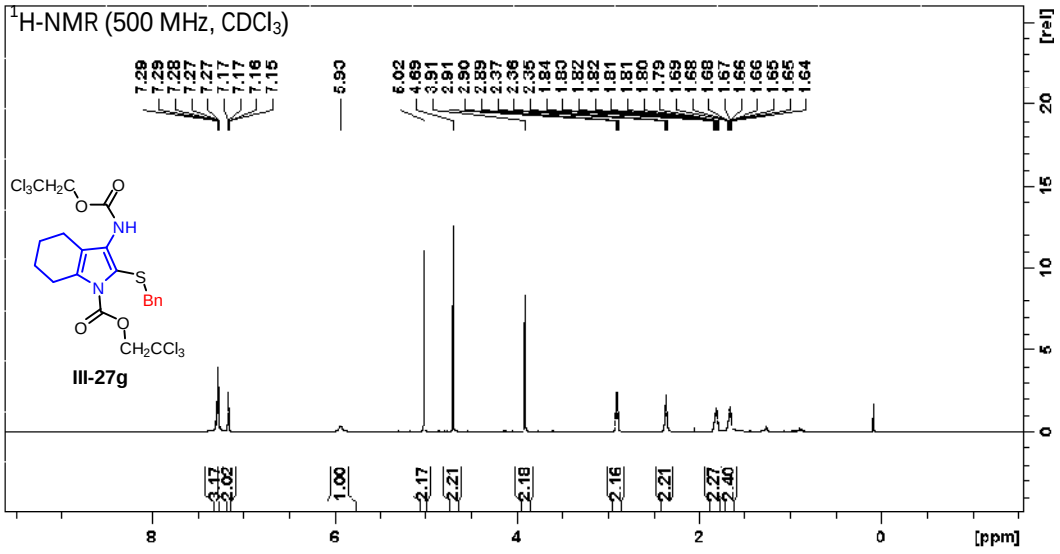
1H-NMR (500 MHz, CDCl3)
III-27g
[ppm]
[rel]

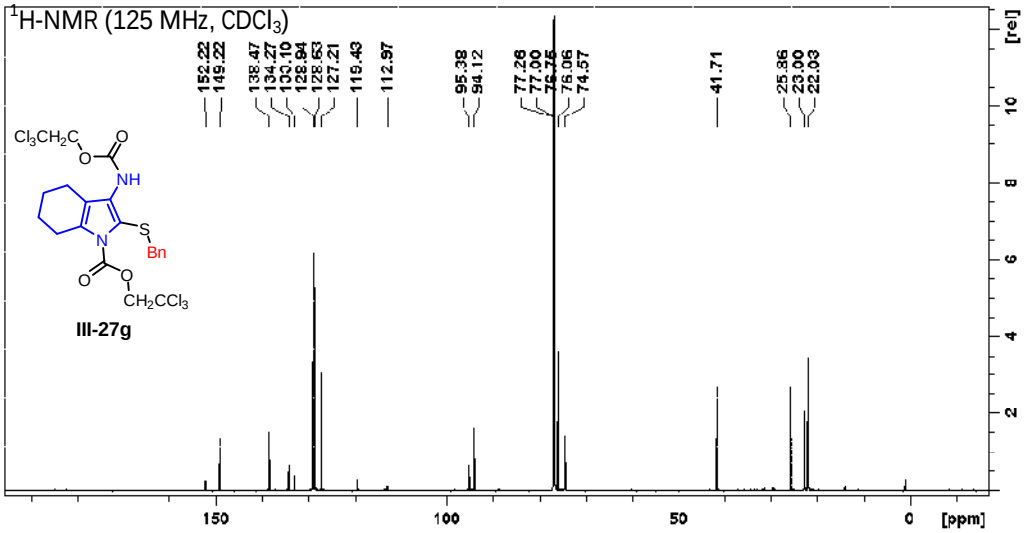
1H-NMR (125 MHz, CDCl3)
III-27g
[ppm]
[rel]

2D-HMQC (F2 = 500 MHz, F1 = 125 MHz, $CDCl_3$) analysis of tetrahydroindole **III-27g**

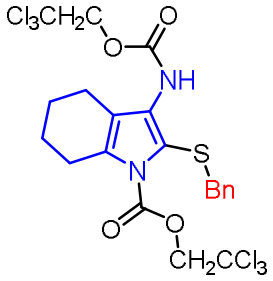

III-27g

- 22.0 ppm ^{13}C resonance has an accidental degeneracy of another ^{13}C resonance.

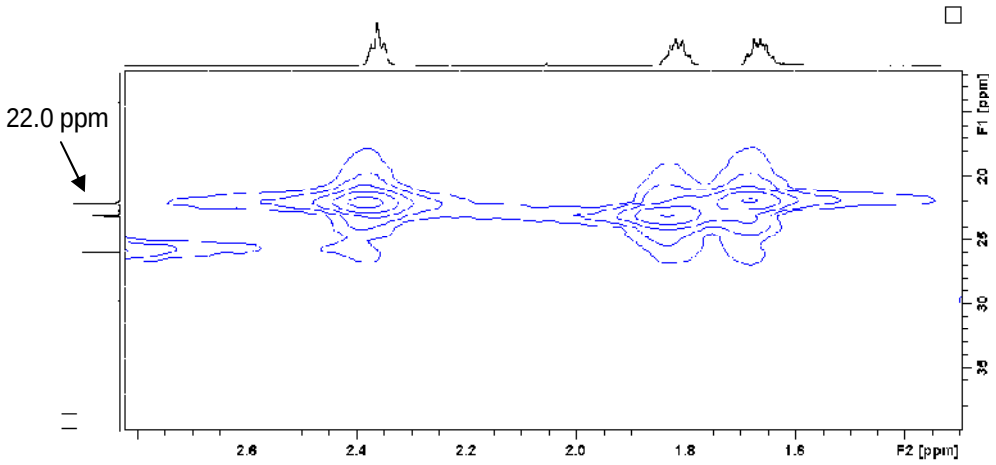

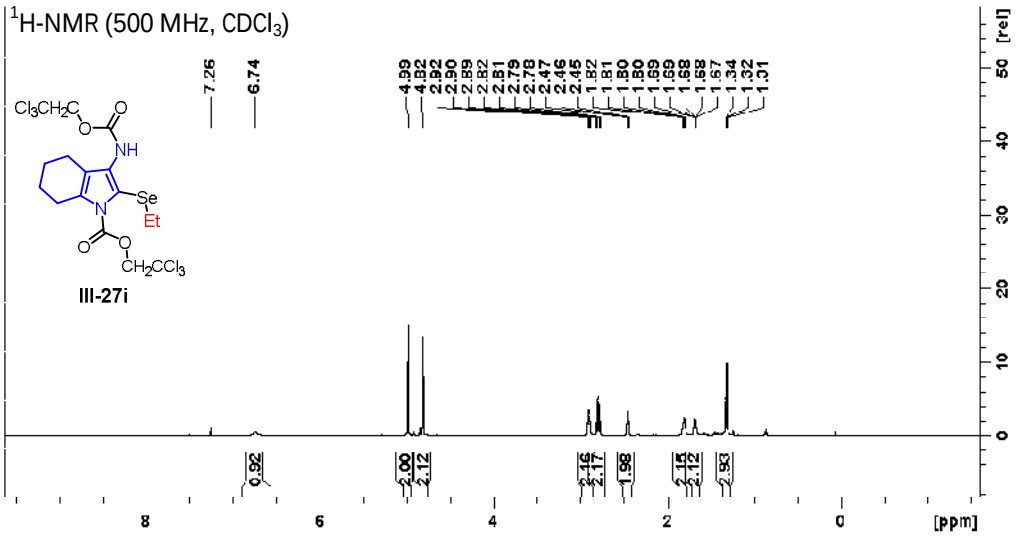
1H-NMR (500 MHz, CDCl3)
III-27i
[ppm]
[rel]

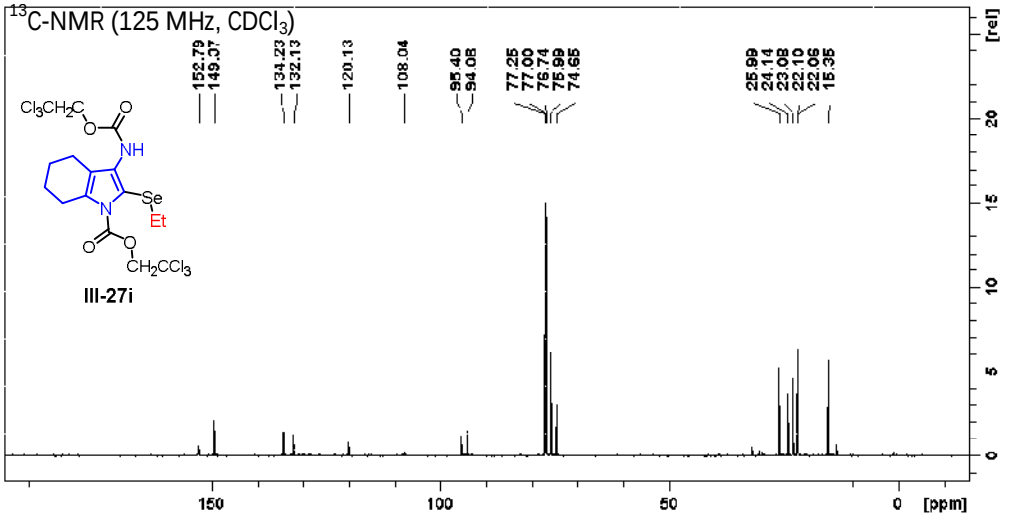
13C-NMR (125 MHz, CDCl3)
III-27i
[ppm]
[rel]

3.5.23. ^{1}H and ^{13}C NMR spectra for Di-tert-butyl 3-(Ethylthio)-4-phenyl-1,2-diazete-1,2-dicarboxylate (III-7y) and oxadiazinone-3-one (III-43)

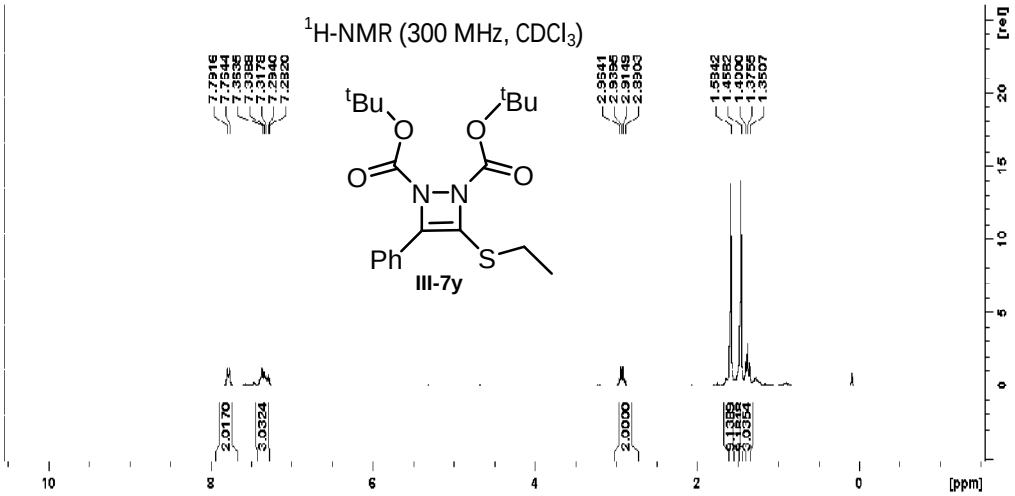

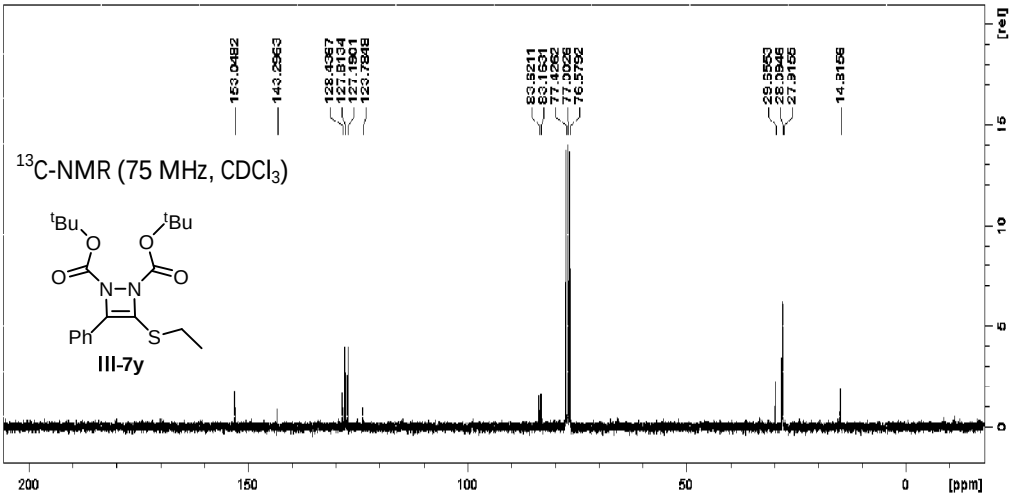

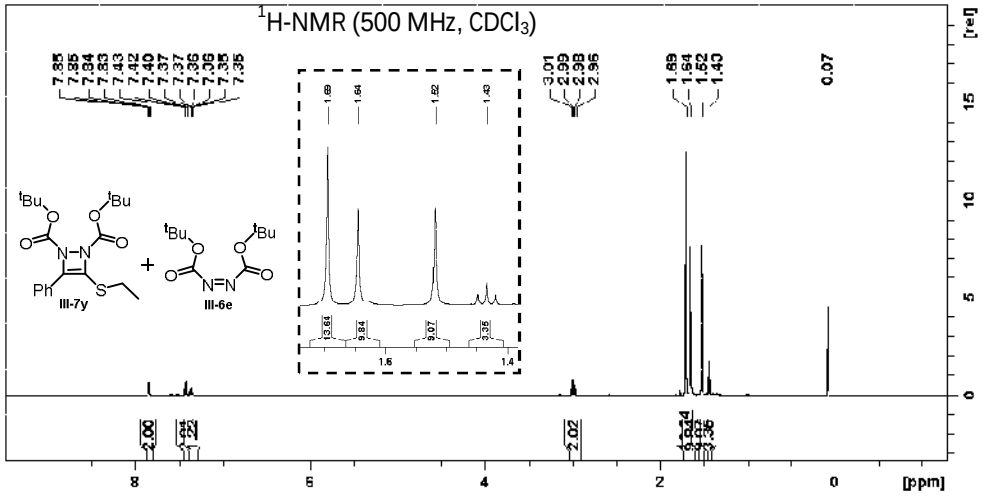
^{1}H-NMR (500 MHz, $CDCl_3$)
III-7y
III-6e
[ppm]
[rel]

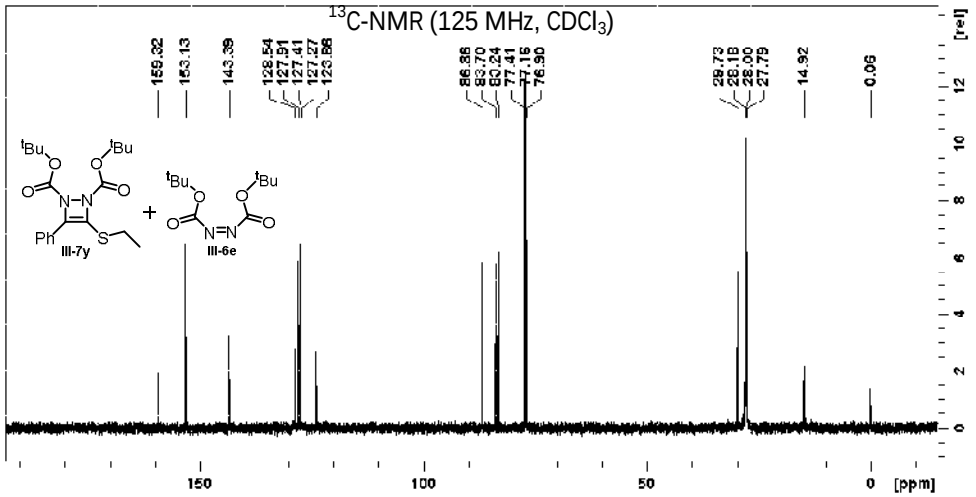
^{13}C-NMR (125 MHz, $CDCl_3$)
III-7y
III-6e
[ppm]
[rel]

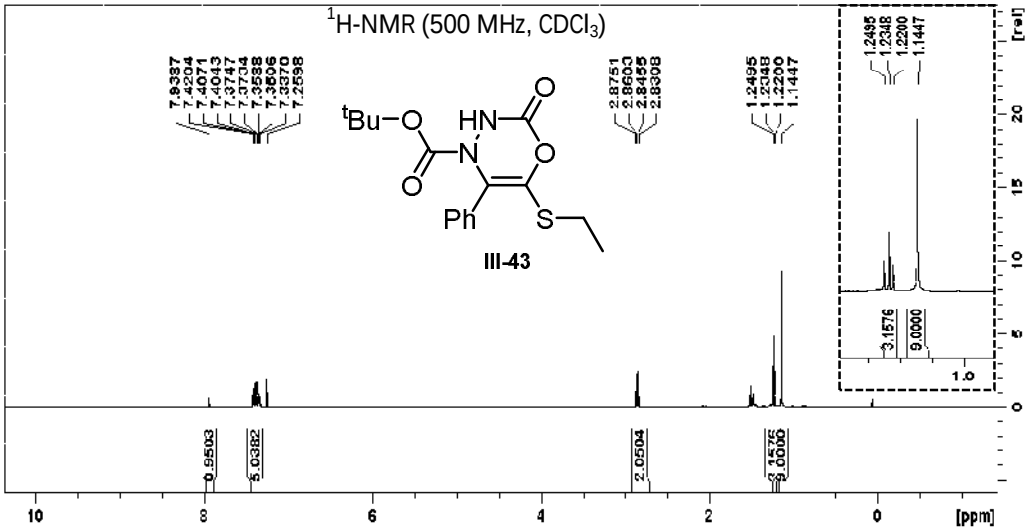
1H-NMR (500 MHz, CDCl3)
III-43
[ppm]

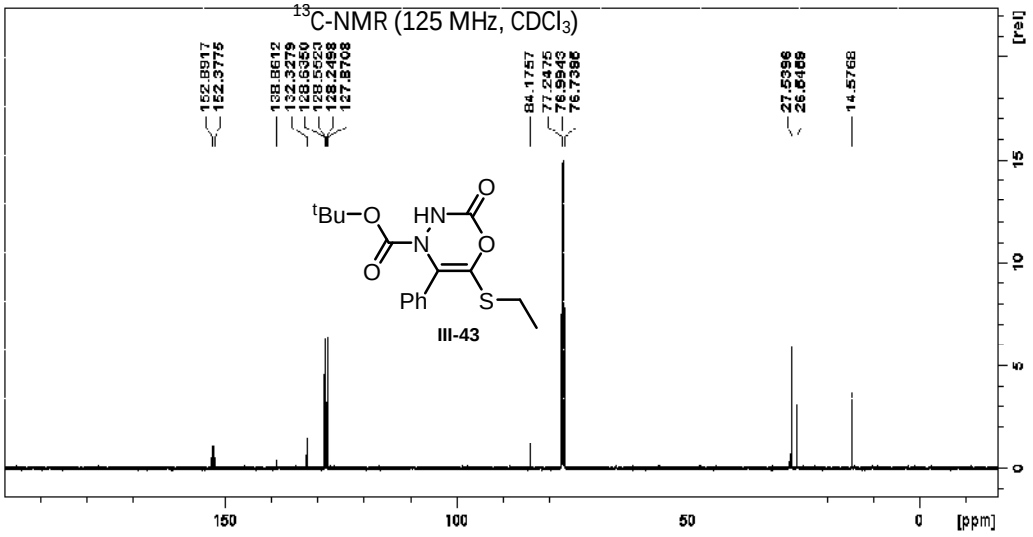
13C-NMR (125 MHz, CDCl3)
III-43
[ppm]

3.6 References

(1) Narangoda, C. J.; Lex, T. R.; Moore, M. A.; McMillen, C. D.; Kitaygorodskiy, A.; Jackson, J. E.; Whitehead, D. C. Accessing the Rare Diazacyclobutene Motif. *Org. Lett.* **2018**, *20* (24), 8009–8013. https://doi.org/10.1021/acs.orglett.8b03590.

(2) Nunn, E. E.; Warrener, R. N. Dimethyl Δ3-1,2-Diazetine-1,2-Dicarboxylate: A New Four-Membered 6π-Ring System. *J. Chem. Soc., Chem. Commun.* **1972**, No. 14, 818–819. https://doi.org/10.1039/C39720000818.

(3) Warrener, R. N.; Nunn, E. E.; Paddon-Row, M. N. The Synthesis and Properties of Dimethyl 1,2-Diazetine-1,2-Dicarboxylate, a Potentially Aromatic Molecule. *Aust. J. Chem.* **1979**, *32* (12), 2659–2674. https://doi.org/10.1071/ch9792659.

(4) Jean, Y.; Devaquet, A. Ab Initio SCF Study of the Disrotatory Closure of 1,4-Diaza-1,3-Dienes to Diazacyclobutene. *J. Am. Chem. Soc.* **1977**, *99* (6), 1949–1952. https://doi.org/10.1021/ja00448a043.

(5) Budzelaar, P. H. M.; Cremer, D.; Wallasch, M.; Wuerthwein, E. U.; Schleyer, P. v. R. Dioxetenes and Diazetines: Nonaromatic 6.Pi.-Systems in Four-Membered Rings. *Journal of the American Chemical Society* **1987**, *109* (21), 6290–6299. https://doi.org/10.1021/ja00255a011.

(6) Mó, O.; Yáñez, M.; Elguero, J. A MO Analysis of the Aromaticity of Some Nitrogen Heterocyclic Compounds. *Journal of Molecular Structure: THEOCHEM* **1989**, *201*, 17–37. https://doi.org/10.1016/0166-1280(89)87059-9.

(7) Jursic, B. S. Study of Ring Opening of 1,2-Diformyl-1,2-Diazacyclobutene by Ab Initio and Density Functional Gaussian-Type-Orbital Approach. *Journal of Molecular Structure: THEOCHEM* **1995**, *357* (3), 243–253. https://doi.org/10.1016/0166-1280(95)04332-6.

(8) Bachrach, S. M.; Liu, M. Ab Initio Study of the Conrotatory Ring Opening of Phospha- and Azacyclobutenes. 2. Diphospha- and Diazacyclobutenes. *The Journal of Organic Chemistry* **1992**, *57* (7), 2040–2047. https://doi.org/10.1021/jo00033a026.

(9) Breton, G. W.; Martin, K. L. Are 1,2-Dihydrodiazetes Aromatic? An Experimental and Computational Investigation. *J. Org. Chem.* **2002**, *67* (19), 6699–6704. https://doi.org/10.1021/jo026082m.

(10) Breton, G. W.; Shugart, J. H.; Hughey, C. A.; Perala, S. M.; Hicks, A. D. Synthesis of Δ1-1,2-Diazetines via a Diels−Alder Cycloaddition Approach. *Org. Lett.* **2001**, *3* (20), 3185–3187. https://doi.org/10.1021/ol0164942.

(11) Narangoda, C. J.; Kakeshpour, T.; Lex, T. R.; Redden, B. K.; Moore, M. A.; Frank, E. M.; McMillen, C. D.; Wiskur, S. L.; Kitaygorodskiy, A.; Jackson, J. E.; Whitehead, D. C. Cycloaddition/Electrocyclic Ring Opening Sequence between Alkynyl Sulfides and Azodicarboxylates To Provide N,N-Dicarbamoyl 2-Iminothioimidates. *J. Org. Chem.* **2019**, *84* (15), 9734–9743. https://doi.org/10.1021/acs.joc.9b01515.

(12) Chaminda Lakmal, H. H.; Xu, J. X.; Xu, X.; Ahmed, B.; Fong, C.; Szalda, D. J.; Ramig, K.; Sygula, A.; Webster, C. E.; Zhang, D.; Cui, X. Synthesis of C-Unsubstituted 1,2-Diazetidines and Their Ring-Opening Reactions via Selective N–N Bond Cleavage. *J. Org. Chem.* **2018**, *83* (16), 9497–9503. https://doi.org/10.1021/acs.joc.8b01223.
(13) Rajkumar, S.; Clarkson, G. J.; Shipman, M. Regio- and Stereocontrolled Synthesis of 3-Substituted 1,2-Diazetidines by Asymmetric Allylic Amination of Vinyl Epoxide. *Org. Lett.* **2017**, *19* (8), 2058–2061. https://doi.org/10.1021/acs.orglett.7b00653.
(14) Brown, M. J.; Clarkson, G. J.; Inglis, G. G.; Shipman, M. Synthesis and Functionalization of 3-Alkylidene-1,2-Diazetidines Using Transition Metal Catalysis. *Org. Lett.* **2011**, *13* (7), 1686–1689. https://doi.org/10.1021/ol200193n.
(15) P. Iacobini, G.; W. Porter, D.; Shipman, M. Chemo- and Enantioselective Rh-Catalysed Hydrogenation of 3-Methylene-1,2-Diazetidines: Application to Vicinal Diamine Synthesis. *Chemical Communications* **2012**, *48* (79), 9852–9854. https://doi.org/10.1039/C2CC35445D.
(16) Viñuelas-Zahínos, E.; Maldonado-Rogado, M. A.; Luna-Giles, F.; Barros-García, F. J. Coordination Behaviour of Schiff Base 2-Acetyl-2-Thiazoline Hydrazone (ATH) towards Cobalt(II), Nickel(II) and Copper(II). *Polyhedron* **2008**, *27* (2), 879–886. https://doi.org/10.1016/j.poly.2007.11.009.
(17) Viñuelas-Zahínos, E.; Luna-Giles, F.; Torres-García, P.; Rodríguez, A. B.; Bernalte-García, A. Effects of a Derivative Thiazoline/Thiazolidine Azine Ligand and Its Cadmium Complexes on Phagocytic Activity by Human Neutrophils. *Inorganica Chimica Acta* **2011**, *366* (1), 373–379. https://doi.org/10.1016/j.ica.2010.11.037.
(18) E. MacKenzie, N.; H. Thomson, R.; W. Greenhalgh, C. New Dyes Based on 3-Aryl-Benzo- and -Naphtho-1,4-Thiazines. *Journal of the Chemical Society, Perkin Transactions 1* **1980**, *0* (0), 2923–2932. https://doi.org/10.1039/P19800002923.
(19) Coustard, J.-M. 1-Arylamino-1-Methylthio-2-Nitroethene in Superacids: NMR Study and Reactivity of the Formed Hydroxynitrilium Lons. *Tetrahedron* **1996**, *52* (28), 9509–9520. https://doi.org/10.1016/0040-4020(96)00485-1.
(20) Cousson, A.; Coustard, J.-M. X-Ray Structure Determination of Products Resulting from Trapping of Hydroxynitrilium Ions. *Tetrahedron* **1998**, *54* (23), 6523–6528. https://doi.org/10.1016/S0040-4020(98)00325-1.
(21) Bamba, F.; Soro, Y.; Siaka, S.; Marrot, J.; Coustard, J. M. A New Way for Synthetizing (E)-Methyl Methylsulfanyl(Phenylamino)Methylene Carbamates via Beckmann Transposition in Triflic Acid. *Bulletin of the Chemical Society of Ethiopia* **2015**, *29* (2), 291–298. https://doi.org/10.4314/bcse.v29i2.11.
(22) Elghandour, A. H. H.; Ibrahim, M. K. A.; El-badry, B.; Waly, H. K. Utility of Hydrazidoyl Halides in Heterocycles: A New Route for the Synthesis of Alkylmercaptoheterocyclic Compounds. *Phosphorus, Sulfur, and Silicon and the Related Elements* **1994**, *88* (1–4), 147–153. https://doi.org/10.1080/10426509408036915.

(23) Deryabina, T. G.; Bel'skaya, N. P.; Kodess, M. I.; Bakulev, V. A. Reaction of 2-Arylhydrazono-2-Cyano-N-Cyclohexylthioacetamides with Halocarbonyl Compounds. *Chem Heterocycl Compd* **2007**, *43* (1), 18–27. https://doi.org/10.1007/s10593-007-0003-3.
(24) Bel'skaya, N. P.; Koksharov, A. V.; Deryabina, T. G.; Bakulev, V. A. Intramolecular Cyclization of 1-[1-Alkylsulfanyl-2-Phenyl- 2-(Phenylhydrazono)Ethylidene]-Pyrrolidinium Salts. *Chem Heterocycl Comp* **2010**, *46* (9), 1156–1157. https://doi.org/10.1007/s10593-010-0647-2.
(25) Brandes, W. D.; Fuehrer, W. D.; Stetter, J. D. Hydroximic Acid Esters, Their Preparation and Their Use as Fungicides. EP0056161A2, July 21, 1982.
(26) Fuganti, C.; Gatti, F. G.; Serra, S. A General Method for the Synthesis of the Most Powerful Naturally Occurring Maillard Flavors. *Tetrahedron* **2007**, *63* (22), 4762–4767. https://doi.org/10.1016/j.tet.2007.03.089.
(27) Beereboom, J. J. 2-Substituted Cyclic Thioimidates as Fungicides. US3471618A, October 7, 1969.
(28) H·拜尔; H·索特; R·本诺伊特; R·米勒; E·阿默曼; G·洛伦兹. Thioimidates, Their Preparation and Their Use. CN1109873A, October 11, 1995.
(29) Muller, M.; Forster, W.-R.; Holst, A.; Kingma, A. J.; Schaumann, E.; Adiwidjaja, G. Synthesis of 4-Silylcyclobut-2-Enethiones and Their Use in Cyclobutadiene Generation. *Chemistry – A European Journal* **1996**, *2* (8), 949–956.
(30) DeKorver, K. A.; Li, H.; Lohse, A. G.; Hayashi, R.; Lu, Z.; Zhang, Y.; Hsung, R. P. Ynamides: A Modern Functional Group for the New Millennium. *Chem. Rev.* **2010**, *110* (9), 5064–5106. https://doi.org/10.1021/cr100003s.
(31) Hall, J. H.; Krishnan, G. The 2 + 2 Cycloaddition of 4-Substituted-1,2,4-Triazoline-3,5-Diones to Diphenylketene. *J. Org. Chem.* **1984**, *49* (13), 2498–2500. https://doi.org/10.1021/jo00187a040.
(32) Staudinger, H. *Die ketene*; F. Enke, 1912.
(33) Hyatt, J. A.; Raynolds, P. W. Ketene Cycloadditions. In *Organic Reactions*; American Cancer Society, 2004; pp 159–646. https://doi.org/10.1002/0471264180.or045.02.
(34) Butler, G. B.; Turner, S. R.; Guilbault, L. J. Cycloaddition of a 1,4 Dipole with Alkyl Ketones. Novel Synthesis of 1,3,4-Tetrahydrooxadiazines. *J. Org. Chem.* **1971**, *36* (19), 2838–2840. https://doi.org/10.1021/jo00818a024.
(35) Hall, J. H.; Jones, M. L. Reactions of Azodiones with Electron-Rich Alkenes. 1,2,4-Triazoline-3,5-Diones and Vinyl Ethers. *J. Org. Chem.* **1983**, *48* (6), 822–826. https://doi.org/10.1021/jo00154a014.
(36) Huisgen, R.; Rapp, W.; Ugi, I.; Walz, H.; Glogger, I. Mittlere Ringe IV Darstellung Und Eigenschaften Der 1,2,3,4-Benzo-cycla-1,3-dienone-(5). *Justus Liebigs Annalen der Chemie* **1954**, *586* (1), 52–69. https://doi.org/10.1002/jlac.19545860104.

(37) Baumann, T.; Bächle, M.; Hartmann, C.; Bräse, S. Thermal Effects in the Organocatalytic Asymmetric α-Amination of Disubstituted Aldehydes with Azodicarboxylates: A High-Temperature Organocatalysis. *European Journal of Organic Chemistry* **2008**, *2008* (13), 2207–2212. https://doi.org/10.1002/ejoc.200701167.
(38) Bøgevig, A.; Juhl, K.; Kumaragurubaran, N.; Zhuang, W.; Jørgensen, K. A. Direct Organo-Catalytic Asymmetric α-Amination of Aldehydes—A Simple Approach to Optically Active α-Amino Aldehydes, α-Amino Alcohols, and α-Amino Acids. *Angewandte Chemie International Edition* **2002**, *41* (10), 1790–1793. https://doi.org/10.1002/1521-3773(20020517)41:10<1790::AID-ANIE1790>3.0.CO;2-Y.
(39) Wiles, D. M.; Gingras, B. A.; Suprunchuk, T. The C=S Stretching Vibration in the Infrared Spectra of Some Thiosemicarbazones. *Canadian Journal of Chemistry* **1967**, *45* (5), 469–473. https://doi.org/10.1139/v67-081.
(40) Rao, C. N. R.; Venkataraghavan, R. The C=S Stretching Frequency and the "-N-C=S Bands" in the Infrared. *Spectrochimica Acta* **1962**, *18* (4), 541–547. https://doi.org/10.1016/S0371-1951(62)80164-7.
(41) Rao, C. N. R.; Venkataraghavan, R.; Kasturi, T. R. CONTRIBUTION TO THE INFRARED SPECTRA OF ORGANOSULPHUR COMPOUNDS. *Canadian Journal of Chemistry* **1964**, *42* (1), 36–42. https://doi.org/10.1139/v64-006.
(42) Blanco, F.; Alkorta, I.; Elguero, J. Barriers about Double Carbon-Nitrogen Bond in Imine Derivatives (Aldimines, Oximes, Hydrazones, Azines). *Croatica Chemica Acta* **2009**, *82* (1), 173–183.
(43) Guerra, A.; Lunazzi, L. Conformational Studies by Dynamic NMR. 54. Trigonal Nitrogen Inversion and Enantiomerization Processes in the Stereolabile Chiral Isomers of N-Naphthylimines. *The Journal of Organic Chemistry* **1995**, *60* (24), 7959–7965. https://doi.org/10.1021/jo00129a042.
(44) Claude H. Yoder; Sandberg, J. A.; Moore, W. S. Electronic and Steric Effects of Substitution at Nitrogen on Hindered Rotation in Formanilides. *Journal of the American Chemical Society* **1974**, *96* (7), 2260–2262.
(45) Maghsoodlou, M. T.; Marandi, G.; Khorassani, M. H.; Saghatforoush, L.; Kabiri, R. Dynamic 1H NMR Study of Rotational Energy Barrier around the Aryl-Nitrogen Single Bond in γ-Spiroiminolactones Derived from Reaction between 2,6-Dimethylphenyl Isocyanide and Dialkyl Acetylenedicarboxylates in the Presence of Phendione. 3.
(46) Bouzzine, S. M.; Bouzakraoui, S.; Bouachrine, M.; Hamidi, M. Density Functional Theory (B3LYP/6-31G*) Study of Oligothiophenes in Their Aromatic and Polaronic States. *Journal of Molecular Structure: THEOCHEM* **2005**, *726* (1), 271–276. https://doi.org/10.1016/j.theochem.2005.04.023.
(47) Shakila, G.; Periandy, S.; Ramalingam, S. Molecular Structure and Vibrational Analysis of 3-Ethylpyridine Using Ab Initio HF and Density Functional Theory (B3LYP) Calculations. *Spectrochimica Acta Part A: Molecular and Biomolecular Spectroscopy* **2011**, *78* (2), 732–739. https://doi.org/10.1016/j.saa.2010.12.005.

(48) Gu, C.-H.; Li, H.; Gandhi, R. B.; Raghavan, K. Grouping Solvents by Statistical Analysis of Solvent Property Parameters: Implication to Polymorph Screening. *International Journal of Pharmaceutics* **2004**, *283* (1), 117–125. https://doi.org/10.1016/j.ijpharm.2004.06.021.
(49) Xie, J.; Xu, C.; Dai, Q.; Wang, X.; Xu, G.; Chen, Y.; Dai, L. Synthesis and Application of a Novel Asymmetric Azo Reagent: 1-(Tert-Butyl)-2-(4-Chlorobenzyl) Azodicarboxylate (TBCAD). *Tetrahedron* **2017**, *73* (35), 5321–5326. https://doi.org/10.1016/j.tet.2017.07.033.
(50) Marenich, A. V.; Cramer, C. J.; Truhlar, D. G. Universal Solvation Model Based on Solute Electron Density and on a Continuum Model of the Solvent Defined by the Bulk Dielectric Constant and Atomic Surface Tensions. *J. Phys. Chem. B* **2009**, *113* (18), 6378–6396. https://doi.org/10.1021/jp810292n.
(51) Biswas, A.; Alves, C. R.; Trevisan, M. T. S.; Berfield, J.; Furtado, R. F.; Liu, Z.; Cheng, H. N.; Biswas, A.; Alves, C. R.; Trevisan, M. T. S.; Berfield, J.; Furtado, R. F.; Liu, Z.; Cheng, H. N. Derivatives of Cardanol through the Ene Reaction with Diethyl Azodicarboxylate. *Journal of the Brazilian Chemical Society* **2016**, *27* (6), 1078–1082. https://doi.org/10.5935/0103-5053.20160003.
(52) Brimble, M. A.; Heathcock, C. H. Allylic Amination by the Lewis Acid-Mediated Ene Reactions of Diethyl Azodicarboxylate with Alkenes. *The Journal of Organic Chemistry* **1993**, *58* (19), 5261–5263. https://doi.org/10.1021/jo00071a042.
(53) Leblanc, Y.; Zamboni, R.; Bernstein, M. A. Amination of Olefinic Compounds with Bis(2,2,2-Trichloroethyl) Azodicarboxylate. *J. Org. Chem.* **1991**, *56* (5), 1971–1972. https://doi.org/10.1021/jo00005a063.
(54) Jacobson, B. M.; Arvanitis, G. M.; Eliasen, C. A.; Mitelman, R. Ene Reactions of Conjugated Dienes. 2. Dependence of Rate on Degree of Hydrogen Removed and s-Cis or s-Trans Diene Character. *J. Org. Chem.* **1985**, *50* (2), 194–201. https://doi.org/10.1021/jo00202a011.
(55) Zhang, H.; Ma, C.; Sun, R.; Liao, X.; Wu, J.; Xie, M. Sustainable Elastomer of Triazolinedione-Modified Eucommia Ulmoides Gum with Enhanced Elasticity and Shape Memory Capability. *Polymer* **2019**, *184*, 121904. https://doi.org/10.1016/j.polymer.2019.121904.
(56) Thaler, W. A.; Franzus, B. The Reaction of Ethyl Azodicarboxylate with Monoolefins. *J. Org. Chem.* **1964**, *29* (8), 2226–2235. https://doi.org/10.1021/jo01031a029.
(57) Jenner, G.; Salem, R. B.; El'yanov, B.; Gonikberg, E. M. Piezochemical Interpretation of (C ⋯ H ⋯ X) Hydrogen Transfer in Ene Reactions. *J. Chem. Soc., Perkin Trans. 2* **1989**, No. 11, 1671–1675. https://doi.org/10.1039/P29890001671.
(58) Jenner, G.; Salem, R. B. Anatomy of Ene and Diels–Alder Reactions between Cyclohexadienes and Azodicarboxylates. *J. Chem. Soc., Perkin Trans. 2* **1990**, No. 11, 1961–1964. https://doi.org/10.1039/P29900001961.
(59) Baldwin, J. E. Rules for Ring Closure. *J. Chem. Soc., Chem. Commun.* **1976**, No. 18, 734–736. https://doi.org/10.1039/C39760000734.

(60) Baldwin, J. E.; Cutting, J.; Dupont, W.; Kruse, L.; Silberman, L.; Thomas, R. C. 5-Endo-Trigonal Reactions: A Disfavoured Ring Closure. *J. Chem. Soc., Chem. Commun.* **1976**, No. 18, 736–738. https://doi.org/10.1039/C39760000736.
(61) Baldwin, J. E.; Thomas, R. C.; Kruse, L. I.; Silberman, L. Rules for Ring Closure: Ring Formation by Conjugate Addition of Oxygen Nucleophiles. *J. Org. Chem.* **1977**, *42* (24), 3846–3852. https://doi.org/10.1021/jo00444a011.
(62) E. Baldwin, J.; I. Kruse, L. Rules for Ring Closure. Stereoelectronic Control in the Endocyclic Alkylation of Ketone Enolates. *Journal of the Chemical Society, Chemical Communications* **1977**, *0* (7), 233–235. https://doi.org/10.1039/C39770000233.
(63) Baldwin, J. E.; Lusch, M. J. Rules for Ring Closure: Application to Intramolecular Aldol Condensations in Polyketonic Substrates. *Tetrahedron* **1982**, *38* (19), 2939–2947. https://doi.org/10.1016/0040-4020(82)85023-0.
(64) V. Alabugin, I.; Gilmore, K. Finding the Right Path: Baldwin "Rules for Ring Closure" and Stereoelectronic Control of Cyclizations. *Chemical Communications* **2013**, *49* (96), 11246–11250. https://doi.org/10.1039/C3CC43872D.
(65) Planas, O.; Wang, F.; Leutzsch, M.; Cornella, J. Fluorination of Arylboronic Esters Enabled by Bismuth Redox Catalysis. *Science* **2020**, *367* (6475), 313–317. https://doi.org/10.1126/science.aaz2258.
(66) Gilmore, K.; Alabugin, I. V. Cyclizations of Alkynes: Revisiting Baldwin's Rules for Ring Closure. *Chem. Rev.* **2011**, *111* (11), 6513–6556. https://doi.org/10.1021/cr200164y.
(67) Alabugin, I. V.; Gilmore, K.; Manoharan, M. Rules for Anionic and Radical Ring Closure of Alkynes. *J. Am. Chem. Soc.* **2011**, *133* (32), 12608–12623. https://doi.org/10.1021/ja203191f.
(68) Xu, X.-T.; Mou, X.-Q.; Xi, Q.-M.; Liu, W.-T.; Liu, W.-F.; Sheng, Z.-J.; Zheng, X.; Zhang, K.; Du, Z.-Y.; Zhao, S.-Q.; Wang, S.-H. Anti-Inflammatory Activity Effect of 2-Substituted-1,4,5,6-Tetrahydrocyclopenta[b]Pyrrole on TPA-Induced Skin Inflammation in Mice. *Bioorganic & Medicinal Chemistry Letters* **2016**, *26* (21), 5334–5339. https://doi.org/10.1016/j.bmcl.2016.09.034.
(69) Doody, R. S.; Gavrilova, S. I.; Sano, M.; Thomas, R. G.; Aisen, P. S.; Bachurin, S. O.; Seely, L.; Hung, D. Effect of Dimebon on Cognition, Activities of Daily Living, Behaviour, and Global Function in Patients with Mild-to-Moderate Alzheimer's Disease: A Randomised, Double-Blind, Placebo-Controlled Study. *The Lancet* **2008**, *372* (9634), 207–215. https://doi.org/10.1016/S0140-6736(08)61074-0.
(70) Wu, J.; Li, Q.; Bezprozvanny, I. Evaluation of Dimebon in Cellular Model of Huntington's Disease. *Mol Neurodegeneration* **2008**, *3* (1), 15. https://doi.org/10.1186/1750-1326-3-15.
(71) Ivachtchenko, A. V.; Frolov, E. B.; Mitkin, O. D.; Tkachenko, S. E.; Okun, I. M.; Khvat, A. V. Synthesis and Biological Activity of 5-Styryl and 5-Phenethyl-Substituted 2,3,4,5-Tetrahydro-1H-Pyrido[4,3-b]Indoles. *Bioorganic & Medicinal Chemistry Letters* **2010**, *20* (1), 78–82. https://doi.org/10.1016/j.bmcl.2009.11.037.

(72) Bergauer, M.; Hübner, H.; Gmeiner, P. Practical Ex-Chiral-Pool Methodology for the Synthesis of Dopaminergic Tetrahydroindoles. *Tetrahedron* **2004**, *60* (5), 1197–1204. https://doi.org/10.1016/j.tet.2003.11.041.
(73) Malone, J. A.; Toussel, C. E.; Fronczek, F. R.; Kartika, R. Brønsted Acid-Catalyzed Formal [2 + 2 + 1] Annulation for the Modular Synthesis of Tetrahydroindoles and Tetrahydrocyclopenta[*b*]Pyrroles. *Org. Lett.* **2019**, *21* (10), 3610–3614. https://doi.org/10.1021/acs.orglett.9b01032.
(74) Mou, X.-Q.; Xu, Z.-L.; Wang, S.-H.; Zhu, D.-Y.; Wang, J.; Bao, W.; Zhou, S.-J.; Yang, C.; Zhang, D. An Au(i)-Catalyzed Rearrangement/Cyclization Cascade toward the Synthesis of 2-Substituted-1,4,5,6-Tetrahydrocyclopenta[b]Pyrrole. *Chemical Communications* **2015**, *51* (60), 12064–12067. https://doi.org/10.1039/C5CC03979G.
(75) Guan, H.; Laird, A. D.; Blake, R. A.; Tang, C.; Liang, C. Design and Synthesis of Aminopropyl Tetrahydroindole-Based Indolin-2-Ones as Selective and Potent Inhibitors of Src and Yes Tyrosine Kinase. *Bioorganic & Medicinal Chemistry Letters* **2004**, *14* (1), 187–190. https://doi.org/10.1016/j.bmcl.2003.09.069.
(76) Patterson, J. M.; Soedigdo, S. Pyrolysis Products of Cycloalkano[a]Pyrroles. *J. Org. Chem.* **1967**, *32* (10), 2969–2972. https://doi.org/10.1021/jo01285a008.
(77) Wu, S.; Fluxe, A.; Janusz, J. M.; Sheffer, J. B.; Browning, G.; Blass, B.; Cobum, K.; Hedges, R.; Murawsky, M.; Fang, B.; Fadayel, G. M.; Hare, M.; Djandjighian, L. Discovery and Synthesis of Tetrahydroindolone Derived Semicarbazones as Selective Kv1.5 Blockers. *Bioorganic & Medicinal Chemistry Letters* **2006**, *16* (22), 5859–5863. https://doi.org/10.1016/j.bmcl.2006.08.057.
(78) Trofimov, B. A.; Mikhaleva, A. I.; Shmidt, E. Yu.; Vasil'tsov, A. M.; Ivanov, A. V.; Protsuk, N. I.; Ryapolov, O. A. A New Technology for the Synthesis of 4,5,6,7-Tetrahydroindole. *Dokl Chem* **2010**, *435* (1), 307–310. https://doi.org/10.1134/S0012500810110091.
(79) Yoshida, M.; Maeyama, Y.; Al-Amin, M.; Shishido, K. Synthesis of Substituted 1,4,5,6-Tetrahydrocyclopenta[b]Pyrroles by Platinum-Catalyzed Cascade Cyclization/Ring Expansion of 2-Alkynyl-1-Azaspiro[2.3]Hexanes. *J. Org. Chem.* **2011**, *76* (14), 5813–5820. https://doi.org/10.1021/jo201000f.
(80) Andreev, I. A.; Belov, D. S.; Kurkin, A. V.; Yurovskaya, M. A. Synthesis of 4,5,6,7-Tetrahydro-1H-Indole Derivatives Through Successive Sonogashira Coupling/Pd-Mediated 5-Endo-Dig Cyclization. *European Journal of Organic Chemistry* **2013**, *2013* (4), 649–652. https://doi.org/10.1002/ejoc.201201417.
(81) Shi, Q.-Q.; Fu, L.-P.; Shi, Y.; Ding, H.-Q.; Luo, J.-H.; Jiang, B.; Tu, S.-J. Three-Component Synthesis of Poly-Substituted Tetrahydroindoles through p-TsOH Promoted Alkoxylation. *Tetrahedron Letters* **2013**, *54* (24), 3176–3179. https://doi.org/10.1016/j.tetlet.2013.04.029.
(82) Brayton, D. F.; Beaumont, P. R.; Fukushima, E. Y.; Sartain, H. T.; Morales-Morales, D.; Jensen, C. M. Synthesis, Characterization, and Dehydrogenation Activity of an Iridium Arsenic Based Pincer Catalyst. *Organometallics* **2014**, *33* (19), 5198–5202. https://doi.org/10.1021/om5005034.

(83) F. Brayton, D.; M. Jensen, C. Solvent Free Selective Dehydrogenation of Indolic and Carbazolic Molecules with an Iridium Pincer Catalyst. *Chemical Communications* **2014**, *50* (45), 5987–5989. https://doi.org/10.1039/C4CC02073A.
(84) Ivanov, A. V.; Shcherbakova, V. S.; Mikhaleva, A. I.; Trofimov, B. A. One-Pot Synthesis of Pyrroles from Ketones, Hydroxylamine, and 1,2-Dibromoethane in the System KOH-DMSO. *Russ J Org Chem* **2014**, *50* (12), 1775–1778. https://doi.org/10.1134/S1070428014120100.
(85) To, Q. H.; Lee, Y. R.; Kim, S. H. One-Step Synthesis of Tetrahydroindoles by Ceric(IV) Ammonium Nitrate-Promoted Oxidative Cycloaddition of Enaminones and Vinyl Ethers. *Tetrahedron* **2014**, *70* (43), 8108–8113. https://doi.org/10.1016/j.tet.2014.08.011.
(86) Mamedov, V. A.; Hafizova, E. A.; Zamaletdinova, A. I.; Rizvanov, I. Kh.; Mirgorodskaya, A. B.; Zakharova, L. Ya.; Latypov, S. K.; Sinyashin, O. G. Sequential Substitution/Ring Cleavage/Addition Reaction of 1-(Cyclohex-1-Enyl)-Piperidine and -Pyrrolidine with Chloropyruvates for the Efficient Synthesis of Substituted 4,5,6,7-Tetrahydro-1H-Indole Derivatives. *Tetrahedron* **2015**, *71* (48), 9143–9153. https://doi.org/10.1016/j.tet.2015.10.004.
(87) Trofimov, B. A.; Mikhaleva, A. I.; Ivanov, A. V.; Shcherbakova, V. S.; Ushakov, I. A. Expedient One-Pot Synthesis of Pyrroles from Ketones, Hydroxylamine, and 1,2-Dichloroethane. *Tetrahedron* **2015**, *71* (1), 124–128. https://doi.org/10.1016/j.tet.2014.11.031.
(88) Zhang, J.-W.; Liu, X.-W.; Gu, Q.; Shi, X.-X.; You, S.-L. Enantioselective Synthesis of 4,5,6,7-Tetrahydroindoles via Olefin Cross-Metathesis/Intramolecular Friedel–Crafts Alkylation Reaction of Pyrroles. *Organic Chemistry Frontiers* **2015**, *2* (5), 476–480. https://doi.org/10.1039/C5QO00034C.
(89) Andreev, I. A.; Ratmanova, N. K.; Novoselov, A. M.; Belov, D. S.; Seregina, I. F.; Kurkin, A. V. Oxidative Dearomatization of 4,5,6,7-Tetrahydro-1H-Indoles Obtained by Metal- and Solvent-Free Thermal 5-Endo-Dig Cyclization: The Route to Erythrina and Lycorine Alkaloids. *Chemistry – A European Journal* **2016**, *22* (21), 7262–7267. https://doi.org/10.1002/chem.201600273.
(90) Peters, B. K.; Liu, J.; Margarita, C.; Rabten, W.; Kerdphon, S.; Orebom, A.; Morsch, T.; Andersson, P. G. Enantio- and Regioselective Ir-Catalyzed Hydrogenation of Di- and Trisubstituted Cycloalkenes. *J. Am. Chem. Soc.* **2016**, *138* (36), 11930–11935. https://doi.org/10.1021/jacs.6b07291.
(91) Xue, S.; Li, Y.; Wang, L.; Liu, J.; Qing, X.; Wang, C. Four-Component Reaction of Substituted β-Nitrostyrenes, Cyclohexanones, Activated Methylene Compounds, and Ammonium Acetate: Efficient Strategy for Construction of Tetrahydroindole Skeletons. *Synlett* **2016**, *27* (07), 1083–1090. https://doi.org/10.1055/s-0035-1560602.
(92) Ficini, J.; Krief, A.; Guingant, A.; Desmaele, D. Influence of Magnesium Bromide on the Regioselectivity of the Cycloaddition of Ynamines with Cyclenones: Difference in Reactivity between Cyclohexenones and Cyclopentenones. *Tetrahedron Letters* **1981**, *22* (8), 725–728. https://doi.org/10.1016/0040-4039(81)80134-7.

(93) Ishitani, H.; Nagayama, S.; Kobayashi, S. A New Reaction of Imines with Alkynyl Sulfides Affording α,β-Unsaturated Thioimidates. *J. Org. Chem.* **1996**, *61* (6), 1902–1903. https://doi.org/10.1021/jo951924l.
(94) Ma, Y.; Qian, C. [2+2] Cycloaddition Reactions of Imines with Alkynyl Selenides Catalyzed by Scandium Triflate. *Tetrahedron Letters* **2000**, *41* (6), 945–947. https://doi.org/10.1016/S0040-4039(99)02178-4.
(95) Qin, Y.; Lv, J.; Luo, S.; Cheng, J.-P. Direct Intramolecular Conjugate Addition of Simple Alkenes to α,β-Unsaturated Carbonyls Catalyzed by Cu(OTf)2. *Org. Lett.* **2014**, *16* (19), 5032–5035. https://doi.org/10.1021/ol502373u.
(96) Matsuo, J.; Sasaki, S.; Hoshikawa, T.; Ishibashi, H. Tin(IV) Chloride Catalyzed Cycloaddition Reactions between 3-Ethoxycyclobutanones and Allylsilanes. *Org. Lett.* **2009**, *11* (17), 3822–3825. https://doi.org/10.1021/ol901329c.
(97) Shen, L.; Zhao, K.; Doitomi, K.; Ganguly, R.; Li, Y.-X.; Shen, Z.-L.; Hirao, H.; Loh, T.-P. Lewis Acid-Catalyzed Selective [2 + 2]-Cycloaddition and Dearomatizing Cascade Reaction of Aryl Alkynes with Acrylates. *Journal of the American Chemical Society* **2017**, *139* (38), 13570–13578. https://doi.org/10.1021/jacs.7b07997.
(98) Santelli-Rouvier, C.; Santelli, M. The Nazarov Cyclisation. *Synthesis* **1983**, *1983* (06), 429–442. https://doi.org/10.1055/s-1983-30367.
(99) Liang, G.; Gradl, S. N.; Trauner, D. Efficient Nazarov Cyclizations of 2-Alkoxy-1,4-Pentadien-3-Ones. *Org. Lett.* **2003**, *5* (26), 4931–4934. https://doi.org/10.1021/ol036019z.
(100) Liang, G.; Trauner, D. Enantioselective Nazarov Reactions through Catalytic Asymmetric Proton Transfer. *J. Am. Chem. Soc.* **2004**, *126* (31), 9544–9545. https://doi.org/10.1021/ja0476664.
(101) Malona, J. A.; Colbourne, J. M.; Frontier, A. J. A General Method for the Catalytic Nazarov Cyclization of Heteroaromatic Compounds. *Org. Lett.* **2006**, *8* (24), 5661–5664. https://doi.org/10.1021/ol062403v.
(102) Marx, V. M.; Burnell, D. J. Synthesis of 5-Hydroxycyclopent-2-Enones from Allenyl Vinyl Ketones via an Interrupted Nazarov Cyclization. *Org. Lett.* **2009**, *11* (6), 1229–1231. https://doi.org/10.1021/ol900029d.
(103) Zhu, L.; Xi, Z.-G.; Lv, J.; Luo, S. In(III)/PhCO2H Binary Acid Catalyzed Tandem [2 + 2] Cycloaddition and Nazarov Reaction between Alkynes and Acetals. *Org. Lett.* **2013**, *15* (17), 4496–4499. https://doi.org/10.1021/ol4020464.
(104) Vaidya, T.; Cheng, R.; Carlsen, P. N.; Frontier, A. J.; Eisenberg, R. Cationic Cyclizations and Rearrangements Promoted by a Heterogeneous Gold Catalyst. *Org. Lett.* **2014**, *16* (3), 800–803. https://doi.org/10.1021/ol403542k.
(105) Melzig, L.; Metzger, A.; Knochel, P. Pd- and Ni-Catalyzed Cross-Coupling Reactions of Functionalized Organozinc Reagents with Unsaturated Thioethers. *Chemistry – A European Journal* **2011**, *17* (10), 2948–2956. https://doi.org/10.1002/chem.201002850.
(106) Zheng, W.; Zheng, F.; Hong, Y.; Hu, L. A One-Pot Synthesis of Alkynyl Sulfides from Terminal Alkynes. *Heteroatom Chemistry* **2012**, *23* (1), 105–110. https://doi.org/10.1002/hc.20744.

(107) Xie, L.-G.; Niyomchon, S.; Mota, A. J.; González, L.; Maulide, N. Metal-Free Intermolecular Formal Cycloadditions Enable an Orthogonal Access to Nitrogen Heterocycles. *Nature Communications* **2016**, *7* (1), 1–9. https://doi.org/10.1038/ncomms10914.
(108) Ying, J.; Pu, L. A Facile Asymmetric Approach to the Multicyclic Core Structure of Mangicol A. *Chemistry – A European Journal* **2014**, *20* (49), 16301–16307. https://doi.org/10.1002/chem.201404142.
(109) Jansone-Popova, S.; May, J. A. Synthesis of Bridged Polycyclic Ring Systems via Carbene Cascades Terminating in C–H Bond Insertion. *Journal of the American Chemical Society* **2012**, *134* (43), 17877–17880. https://doi.org/10.1021/ja308305z.
(110) Arai, S.; Koike, Y.; Hada, H.; Nishida, A. Catalytic Dicyanative [4+2] Cycloaddition Triggered by Cyanopalladation of Conjugated Enynes under Aerobic Conditions. *J. Am. Chem. Soc.* **2010**, *132* (33), 11824–11824. https://doi.org/10.1021/ja1052939.
(111) Dhiman, S.; Ramasastry, S. S. V. One-Pot Relay Gold(I) and Brønsted Acid Catalysis: Cyclopenta[b]Annulation of Indoles via Hydroamination/Nazarov-Type Cyclization Cascade of Enynols. *Org. Lett.* **2015**, *17* (20), 5116–5119. https://doi.org/10.1021/acs.orglett.5b02632.
(112) Ye, C.; Qian, B.; Li, Y.; Su, M.; Li, D.; Bao, H. Iron-Catalyzed Dehydrative Alkylation of Propargyl Alcohol with Alkyl Peroxides To Form Substituted 1,3-Enynes. *Org. Lett.* **2018**, *20* (11), 3202–3205. https://doi.org/10.1021/acs.orglett.8b01043.
(113) Lv, J.; Zhao, B.; Liu, L.; Han, Y.; Yuan, Y.; Shi, Z. Boron Trichloride-Mediated Synthesis of Indoles via the Aminoboration of Alkynes. *Advanced Synthesis & Catalysis* **2018**, *360* (21), 4054–4059. https://doi.org/10.1002/adsc.201800509.
(114) Chen, H.; Zhang, J.; Wang, D. Z. Gold-Catalyzed Rearrangement of Alkynyl Donor–Acceptor Cyclopropanes To Construct Highly Functionalized Alkylidenecyclopentenes. *Org. Lett.* **2015**, *17* (9), 2098–2101. https://doi.org/10.1021/acs.orglett.5b00671.
(115) Sweis, R. F.; Schramm, M. P.; Kozmin, S. A. Silver-Catalyzed [2 + 2] Cycloadditions of Siloxy Alkynes. *Journal of the American Chemical Society* **2004**, *126* (24), 7442–7443. https://doi.org/10.1021/ja048251l.
(116) Ke, S.; Cao, X.; Liang, Y.; Wang, K.; Yang, Z. Synthesis and Biological Properties of Dihydro-Oxadiazine-Based Heterocyclic Derivatives http://www.ingentaconnect.com/content/ben/mrmc/2011/00000011/00000008/art00002 (accessed Mar 20, 2020). https://doi.org/info:doi/10.2174/138955711796268769.
(117) Berkowitz, P. T.; Long, R. A.; Dea, P.; Robins, R. K.; Matthews, T. R. Synthesis and Antimicrobial Activity of Certain 6H-1,2,4-Oxadiazin-3(2H)-Ones. *J. Med. Chem.* **1977**, *20* (1), 134–138. https://doi.org/10.1021/jm00211a028.
(118) Dekeyser, M. A.; Mishra, A.; Moore, R. C. Substituted Oxadiazinone Miticidal Compositions and Use. US4782066A, November 1, 1988.

(119) Khan, K. M.; Rahat, S.; Choudhary, M. I.; Atta-ur-Rahman; Ghani, U.; Perveen, S.; Khatoon, S.; Dar, A.; Malik, A. Synthesis and Biological Screening of 2-Substituted 5,6-Dihydro-5-Oxo- 4H-1,3,4-Oxadiazine-4-Propanenitriles and of Their Intermediates. *Helvetica Chimica Acta* **2002**, *85* (2), 559–570. https://doi.org/10.1002/1522-2675(200202)85:2<559::AID-HLCA559>3.0.CO;2-A.
(120) Sun, L.; Cao, J.; Chen, L.; Lü, D.; Ni, C.; Shen, Z.; Yuan, L.; Zhang, Y. Synthesis and Bioactivity of 4-Substituted-2-[2-(3-(Trifluoromethyl-Phenyl)-Vinyl)]-4H-[1,3,4]-Oxadiazin-5-One. *J. Pestic. Sci.* **2010**, *12*, 221–224.
(121) Nakajima, K.; Zhang, Y.; Nishibayashi, Y. Alkylation Reactions of Azodicarboxylate Esters with 4-Alkyl-1,4-Dihydropyridines under Catalyst-Free Conditions. *Org. Lett.* **2019**, *21* (12), 4642–4645. https://doi.org/10.1021/acs.orglett.9b01537.
(122) Gray, V. J.; Wilden, J. D. The Chemistry of Ynol and Thioynol Ethers. *Org. Biomol. Chem.* **2016**, *14* (41), 9695–9711. https://doi.org/10.1039/C6OB01776B.
(123) Mamone, M.; Morvan, E.; Milcent, T.; Ongeri, S.; Crousse, B. Electrophilic Amination of Fluoroalkyl Groups on Azodicarboxylate Derivatives. *J. Org. Chem.* **2015**, *80* (3), 1964–1971. https://doi.org/10.1021/jo502638y.
(124) APEX3 suite for crystallographic software - single crystal X-ray diffraction https://www.bruker.com/products/x-ray-diffraction-and-elemental-analysis/single-crystal-x-ray-diffraction/sc-xrd-software/apex3.html (accessed May 1, 2020).
(125) Sheldrick, G. M. Crystal Structure Refinement with SHELXL. *Acta Cryst C* **2015**, *71* (1), 3–8. https://doi.org/10.1107/S2053229614024218.

CHAPTER FOUR

POLYETHYLENIMINE (PEI) FUNCTIONALIZED CELLULOSE NANOCRYSTALS FOR USE IN ENVIRONMENTAL REMEDIATION

4.1 Environmental remediation.

The global deterioration of the environment with the rapid industrial development has caused air, soil, and water pollution in high intensity over the past decades.[1] Common air pollutants consist of toxic gases (*e.g.* nitrogen oxides, sulfur oxides, carbon oxides, ozone, *etc.*), volatile organic compounds (VOCs), and suspended airborne particles.[1] Previous studies have shown that the employees working at livestock buildings,[2] waste treatment plants,[3] plants applying spraying processes,[4] and rendering plant of poultry slaughterhouse[5] have a potential health risk from exposure to the hazardous gas emissions beyond the acceptable limits. Consequently, many studies have been conducted in order to measure the quantity of the hazardous volatile gases in such areas and test efficient remediation technologies.[2–12]

On the other hand, as a result of population growth and increasing food demand (*e.g.* milk, eggs, and meat), the crop production industry (*e.g.* grain, fruit, and vegetables) and animal meat industry have grown significantly.[13] Therefore, the use of herbicides, pesticides, and insecticides has increased in order to yield a larger harvest. As a result of increased demand, water and soil are simultaneously contaminated with herbicides, pesticides, and insecticides.[14,15] Apart from organic pollutants, heavy metals (*e.g.* lead, cadmium, arsenic, mercury, *etc.*) and microbial pathogens are also identified among the

soil and water contaminants.[1,16] It has been shown that persistent organic pesticides can migrate through seasonal changes via soil-air exchange.[17] Moreover, when these persistent pollutants get in contact with the soil through rain, irrigation water, or wind, subsequently they enter into the surface water and ground water via surface runoff and infiltration processes.[18] These factors showed that all three natural resources: air, soil, and water can be simultaneously contaminated by the migration processes of pollutants. These issues have gained the attention of researchers to create efficient technologies for environmental remediation.[1] In recent years, nanomaterial-based applications have emerged as effective treatments for air, water, and soil remediation due to their high surface-to-volume ratio and surface properties.[1,19–28]

However, one obvious fact in the environmental remediation research arena is that due to the diverse remediation techniques available, some of techniques are more specific or less broadly applicable.[29–36,36–43] In addition, some of techniques are not generated from bio-compatible, or biodegradable materials.[20,21,27,44,45] Also, it has been noticed that some of the existing techniques for VOC remediation in industries have less efficiency. For instance, wet scrubber outlets have detected VOCs due to their low efficacies.[46] Thus, materials exhibiting high efficiency, biodegradability, broad applicability, and renewability are still in demand.[42,47–49]

4.2 Use of cellulose nanocrystal materials in environmental remediation.

In previous studies, cellulose based materials have proven to be effective for environmental remediation applications due to their biocompatibility, biodegradability, and the ability of further surface modification with reactive functional groups. Indeed, cellulose based materials have shown diverse applications such as: for the removal particulate matter in air filters,[50] rapid removal of polyfluorinated compounds,[51] VOC capture,[52–54] removal of environmentally persistent drugs,[55] removal of heavy metals and dyes,[16,56–59] and pesticide remediation.[23,24,60–62] In addition, among the aforementioned cellulose based studies, amine functionalized cellulose materials are the leading materials which have been used in diverse applications.[16,51,52,52,56–61]

Previous studies in the Whitehead group have shown significant proficiency in the remediation of VOCs using mesoporous organo silica nanoparticles,[63] kaolinite particles,[64] amine functionalized cellulose nanocrystals (CNC)[52] and amine functionalized co-polymeric nanoparticles.[65,66] Recently, the Whitehead group has developed poly(ethylenimine) functionalized cellulose nanocrystals (PEI-*f*-CNC) to capture VOCs.[52]

The objective of this chapter is to describe the recent modification and the follow up work that has been carried out relevant to the poly(ethylenimine) functionalized cellulose nanocrystals (PEI-*f*-CNC). This chapter describes the development of a protocol for the in-house synthesis of cellulose nanocrystals from bulk cotton, and the

optimization of the poly(ethylenimine) functionalization protocol to scale up the PEI-*f*-CNC synthesis. This study served to investigate the possibility of reducing the cost of the PEI-*f*-CNC synthesis while maintaining the environmental remediation properties at the same efficiency.

4.3 In-house synthesis of cellulose nanocrystals (CNC) from bulk cotton.

Cellulose is one of the most abundant materials on earth and is present in a wide range of living species, such as plants, algae, fungi, bacteria, and some sea animals.[67]Cellulose is a fibrous, tough, and water insoluble polysaccharide with β-1,4-linked glucose units (Figure 4.1). Cellulose has characteristic properties such as hydrophilicity, chirality, and due to its hydroxyl groups. Bulk cellulose contains highly organized crystalline regions and disordered amorphous regions in different amounts depending on the source.[67] The ability of the hydroxyl groups in cellulose to form strong hydrogen bonds is the main reason for these crystalline and amorphous regions.

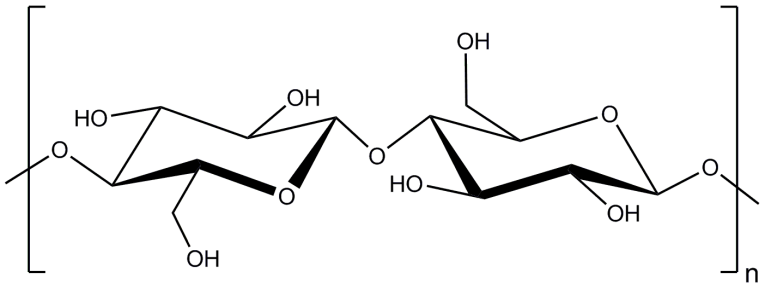

Figure 4.1. The chemical structure of cellulose: linear homopolymer made of glucose units connected with β-1,4-linkages.

Cellulose nanocrystals (CNCs) can be extracted from an appropriate combination of mechanical and chemical treatments. The most typical chemical treatment for the synthesis of cellulose nanocrystals (CNCs) is the acid hydrolysis to extract the most crystalline areas of cellulose. Strong acids such as sulfuric acid or hydrochloric acid can penetrate through the loosely organized amorphous regions of cellulose and hydrolyze those amorphous regions which ultimately leave the crystalline regions.[67,68]

CNC materials consisting of particle sizes below 100 nm have shown good environmental remediation properties in our previous studies.[52] Due to this reason, one of the main objectives of this CNC synthesis was to maintain the particle size of CNC below or around 100 nm in diameter. In order to develop an optimized protocol for the CNC synthesis in our laboratory, we conducted 1 gram scale acid hydrolysis experiments with different types of cotton (Table 4.1). During this study we used aqueous hydrochloric acid (HCl) and aqueous sulfuric acid (H_2SO_4), as the hydrolyzing agents. The particle size was measured using dynamic light scattering (DLS) in order to rapidly optimize the protocol. The cellulose microcrystals (CMC), store bought cotton (Cotton-A) and mechanically processed cotton (Cotton-B, which processed in a magic bullet mini blender with a cross blade for about 10 min) were hydrolyzed with 2.5 M aq. HCl for 0.5 h to 4 h and provided 93 nm, 560 nm and 1800 nm particles, respectively (entry 1-3, Table 4.1). Then, the mechanically processed cotton (Cotton-B) was treated with 50% aq. H_2SO_4 at room temperature and 45°C to provide 175 nm and 52 nm particles respectively (entry 4 and 5).

Table 4.1. Optimization of the cellulose nanocrystal synthesis.

Entry	Source	Acid	Temperature (°C)	Time (h)	Hydrodynamic Diameter from DLS (nm)[a]
1	CMC (20 µm)	2.5M HCl	100	0.5	93
2	Cotton-A	2.5M HCl	100	0.5	560
3	Cotton-B	2.5M HCl	100	4	1800[b]
4	Cotton-B	50% H_2SO_4	RT	4	175
5	**Cotton-B**	**50% H_2SO_4**	**45**	**4**	**52 (375[c])**
6	Cotton-B	25% H_2SO_4	45	4	9970
7	Cotton-B	50% H_2SO_4	60	4	77
8	CMC (20 µm)	64% H_2SO_4	45	1	432
9	Cotton-A	64% H_2SO_4	45	1	91
10	Cotton-B	64% H_2SO_4	45	1	416

RT = room temperature, CMC (20µm) = cellulose microcrystals filtered through 20µm pore size filter, Cotton-A = unprocessed store bought cotton, Cotton B = mechanically processed store bought cotton, a = 90° scattering detection used for small particles, b = forward scattering detection used for larger particles, c = after freeze drying

However, we noticed that upon freeze drying of the slurry of the 52 nm particles, the resulting solid materials had a larger particle size (375 nm) on DLS, which suggests that the removal of the aqueous solution causes the agglomeration of the particles. Lowering the concentration of $H_2SO_4$to a 25% aqueous solution yielded much larger particles (*i.e.,* 9970 nm, entry 6). Attempting to increase the temperature of the acid hydrolysis while maintaining the H_2SO_4 concentration at 50% in water resulted in slightly higher particle size (77 nm, entry 7). The CMC, Cotton-A, and Cotton-B were then treated with a slightly higher concentration of H_2SO_4 (*i.e.,* 64% in water) at 45°C with the hope of shortening the hydrolysis time. However, the resultant cellulose slurries showed polydisperse particle sizes in the range of 90-430 nm (entry 8-10). Since, the 50% aq. H_2SO_4 at 45°C for 4 h afforded the smallest particle size of CNC (entry 5, highlighted in bold), it was selected as the optimized hydrolysis condition for larger scale CNC synthesis.

During the optimization process of CNC synthesis, we noticed that the pH plays a significant role on agglomeration of the CNC particles. If the CNC slurry was freeze dried after the acid hydrolysis, the particles tended to agglomerate and form larger particles (*i.e.,* >1000 nm at pH = 2.7), whereas if the CNC slurry was neutralized by the addition of aqueous sodium hydroxide after the acid hydrolysis, the particle size remained below 100 nm (*i.e.,* 60 nm at pH = 6.9) even after the freeze-drying process. Next, we then turned towards the larger scale CNC synthesis.

The experimental set up and the key steps of the higher scale CNC synthesis are shown in Figure 4.2. A wide mouth brewer's carboy (height = 20", diameter = 4.5") was used in these larger scale reactions (*see* experimental details for more information). The mixing of the reaction was performed using an overhead stirrer equipped with a glass stir rod which was designed to obtain maximum mixing rate. The glass stir rod was designed with a vertical glass rod (16.5 inches length), and several perpendicular glass paddles (4 inches each) (*see* Figure 4.2.A).

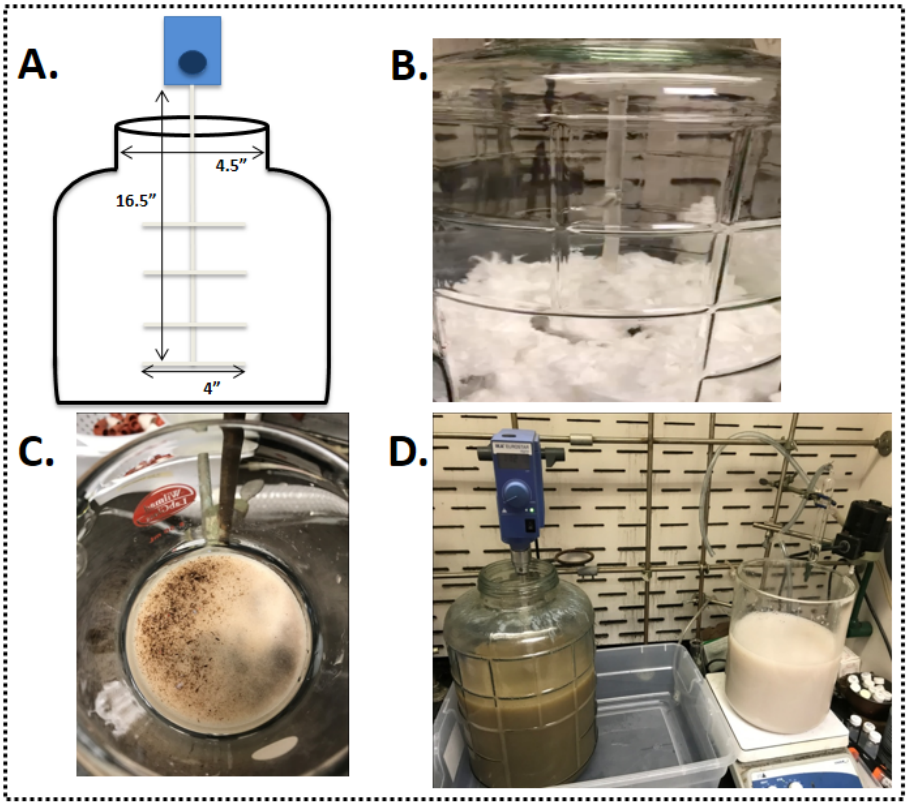

Figure 4.2. The key steps of the larger scale CNC synthesis: A = Apparatus set up, B = mechanically processed cotton, C = removing non-acid hydrolyzed portion of the cotton, D = appearance before (left) and after (right) the work-up

Several modifications such as premixing the 50% aq. H_2SO_4 solution and filtration of the hydrolyzed slurry through a fritted funnel (40-60 µm pore size) were also applied to the optimized protocol to avoid some of the experimental issues such as dehydration, degradation of the cotton with 50% aq. H_2SO_4, and to remove larger cellulose aggregates, respectively. Once the desired particle size was reached (<100 nm), the reaction mixture was subjected to several work-up steps including initial centrifugation (8000 rpm, in 500 mL centrifuge containers, for 20 min) to remove the excess strong acid, re-suspension in water, and filtering through a 40-60 µm fritted funnel to remove non-acid hydrolyzed particles. Then the resulted solution was neutralized with 6 M aq. sodium hydroxide, re-centrifuged and freeze dried to obtain the final dried CNC powder. Figure 4.2.C clearly displays the acid-decomposed cotton and the non-acid hydrolyzed portion of the cotton. Furthermore, a clear difference in the appearance of the CNC slurry after the reaction is complete and after the work-up steps is shown in Figure 4.2.D.

The 100 g and the 500 g scale reactions were performed as shown in Figure 4.2. The final results of these different experimental scales are illustrated in Table 4.2. The experiment of the 100 g scale proceeded to give 60 nm CNC particles in 50% yield and the 500 g scale reaction provided CNCs with an average size of 177 nm in 65% yield (entry 2 and 3, Table 4.2). This shows the applicability of the optimized protocol in the larger scale synthesis of CNCs.

Table 4.2. Results of the different experimental scales of CNC synthesis.

Entry	Experimental scale[a]	Average hydrodynamic diameter	Yield
1	1 g	52 nm	20%
2	100 g	60 nm	50%
3	500 g	177 nm	65%

a = Cotton was mechanically processed before the acid hydrolysis.

It is important to note that the 500 g scale reaction is a 3 week process due to the large reaction volume. Throughout the period, it was thoroughly monitored by DLS measurements. In this reaction, the CNC particle size varied from smaller to larger sizes over time until the smallest particle size was achieved. For instance, Table 4.3 illustrates the CNC particle size at the top layer of the reaction mixture over several days for the 500 g scale reaction. Based on our observations and results, we understood that, first the mechanically processed CNC hydrolyses and provides smaller particles in the top layer of the solution. However, with time, the particle size becomes larger due to the moderately or weakly hydrolized particles which settle in the middle and the bottom layers of the container. Finally, upon further hydrolysis of those moderately larger particles, a more homogenous mixture with an appropriate particle size is reached at the top layer of the container.

Table 4.3. CNC particle size over time for the 500 g scale CNC synthesis.

Days	DLS average hydrodynamic diameter (nm)[a]
1	1220
2	378
3	1540
4	355
5	978
6	635
7	534
8	140

a = DLS measurements were taken for the top layer of the container.

Due to this stepwise hydrolysis event in 500 g scale reaction, the work-up process was also performed in step-wise manner while monitoring the top, middle and the bottom layer of the container by DLS. After the work-up steps described above, DLS measurements showed that the top layer, middle layer, and the bottom layer consisted of CNCs with diameters of 140, 170, and 220 nm, respectively. The CNC particle size of the 500 g scale reaction is somewhat larger (177 nm) than the CNC obtained from the 1 g (52 nm) and the 100 g scale (60 nm) reactions.

However we believe that further modifications of this larger scale CNC synthesis protocol can be made in order to obtain even smaller CNC particles. The pertinent factors that may influence particle size include the reactor dimensions, mixing method/speed, stir rod or the propeller design, and filtering the CNC slurries with a lower pore size filter funnel.

In addition, the slurries resulting from the CNC synthesis (*e.g.* 52 nm size particles from the 1 g scale experiment and 60 nm size particles from the100 g scale experiment) were further characterized by transmission electron microscopy (TEM) (Figure 4.3). The width of the cellulose nanorods captured in TEM images were in good agreement with the DLS data. Furthermore, it suggests that, both the in-house CNC that we synthesized and the commercial CNC (30 nm) have the same needle or rod like crystalline structures and they both are in comparable size range.

As mentioned earlier, another objective of the CNC synthesis in our laboratory was to reduce the cost of the PEI-*f*-CNC synthesis. The cost of the commercial CNC is about $3/gram (Cellulose Lab).[69] According to our improved yield (50%), and based on the cost of the materials for the 100 gram scale in-house CNC synthesis (*i.e.*, concentrated sulfuric acid ($13.00) and a bag of cotton balls (~$2.0)), it will roughly cost about $0.30/gram. For the goal of a 1 kg synthesis of PEI-*f*-CNC, using our in-house protocol in lieu of a commercial source of CNC will save approximately $2,700.

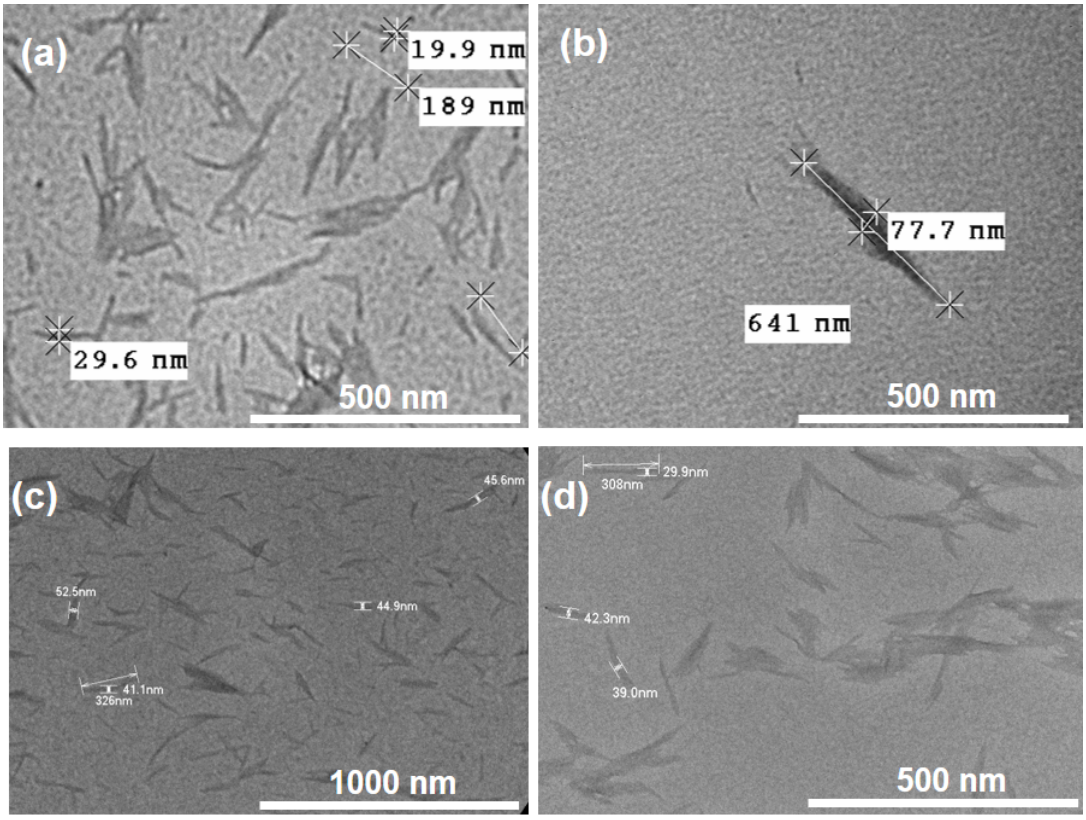

Figure 4.3. TEM images of CNCs at different magnifications which represents the crystalline, needle-like structures. (a) commercial CNC, (b) in-house CNC from 1 g scale synthesis, (c,d) in-house CNC from 100 g scale synthesis.

In conclusion, we developed a reliable and inexpensive laboratory protocol to synthesize cellulose nanocrystals (CNC). This protocol was thoroughly monitored through dynamic light scattering (DLS) measurements and the CNC particles were characterized by DLS, powder X-ray diffraction (PXRD).and transmission electron microscopy (TEM). Moreover, this protocol was further developed to perform an even larger scale synthesis of CNC (*i.e.*, up to 500 g) by designing a large scale reactor while achieving a reasonable size range (100-200 nm) of CNC particles in good yield.

4.4 Optimization of the polyethyelenimine (PEI) functionalization of cellulose nanocrystals.

Our next objective in this study was to optimize the previously developed protocol for the synthesis of the PEI-*f*-CNC. We first used our in-house synthesized CNC to perform the PEI functionalization protocol to see whether the PEI functionalized in-house synthesized CNC can capture VOCs with similar efficiency as compared to our previously synthesized PEI-functionalized commercial CNC material. The typical protocol for this PEI functionalization is illustrated in Scheme 4.1. First, the alcohol functionality at the C6 carbon of the cellulose monomers (**IV-1**) is converted to the corresponding carboxylate group (**IV-2**) by means of a TEMPO mediated oxidation (Scheme 4.1).[70,71]

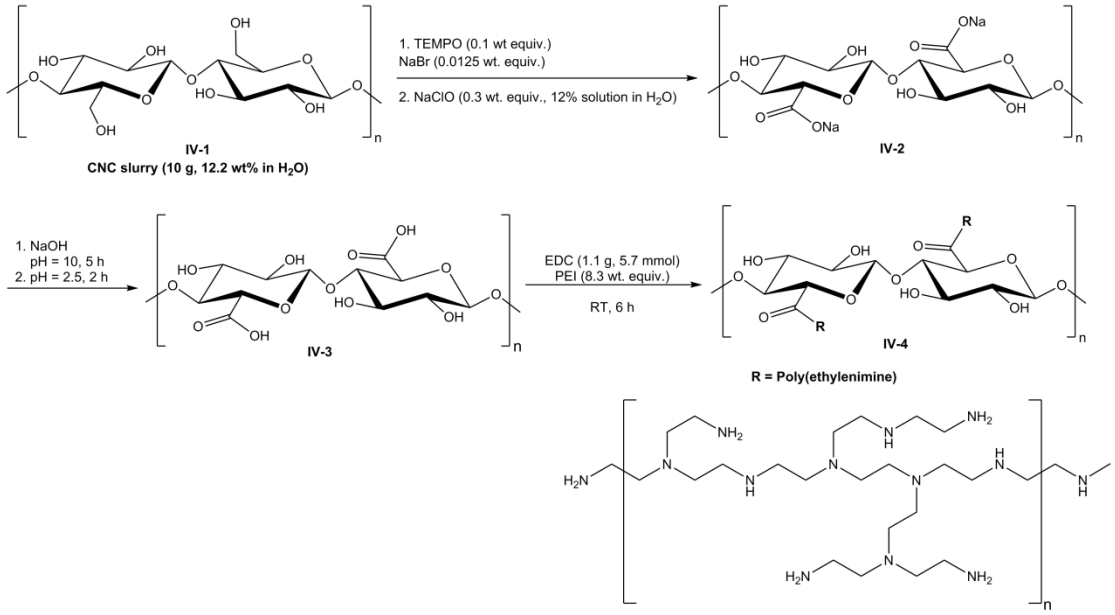

Scheme 4.1. Synthesis of the PEI-*f*-CNC (10 g scale).

Then, the material **IV-2** can be neutralized to the free carboxylic acid form, **IV-3**, followed by functionalization with PEI via amide bond formation using EDC (*i.e.*, 1-ethyl-3-(3-dimethylaminopropyl)carbodiimide) to form the PEI-functionalized CNC material (PEI-*f*-CNC, *eg*: **IV-4**). Finally these functionalized materials were purified via dialysis to remove the unreacted reagents and freeze-dried to obtain the powdered PEI-*f*-CNC material. These materials were then characterized using thermogravimetric analysis (TGA) and attenuated total reflection-Fourier transform infrared spectroscopy (ATR-FTIR). We also evaluated the in-house prepared PEI-*f*-CNC material for their VOC capturing capabilities.

A comparison of the TGA data arising from the PEI-functionalized materials of commercial CNC, in-house synthesized CNC, and related starting materials is shown in Figure 4.4.The commercial CNC showed a rapid thermal weight loss around at 265°C whereas the in-house synthesized CNC showed a gradual thermal weight loss from 150°C. This different thermal property is presumably due to the difference in the amount of uronic acid and suphate ester groups at the surface of CNC during acid hydrolysis.[72–74] In addition, the slight difference in CNC particle size (*i.e.*, 30 nm for commercial CNC vs. 50-60 nm for the in-house CNC) could also influence the thermal degradation profiles which is a manifestation of different amounts of crystallized regions of the corresponding cellulose source. However, the steady decrease of the weight percentage over temperature seen in PEI-*f*-CNC and PEI-*f*-in-house CNC clearly suggest that the materials are successfully functionalized. This amine functionalization was further confirmed by the NH-bending peak observed around 1500-1750 cm^{-1} region in the ATR-FTIR spectra of PEI-*f*-in-house CNC (Figure 4.5).

After the confirmation of successful PEI functionalization from the in-house synthesized CNC, we then turned towards assessing its VOC vapor capture capabilities. Figure 4.6 depicts the hexanal vapor capture studies of the non-functionalized and PEI-functionalized materials of commercial CNC and in-house synthesized CNC.

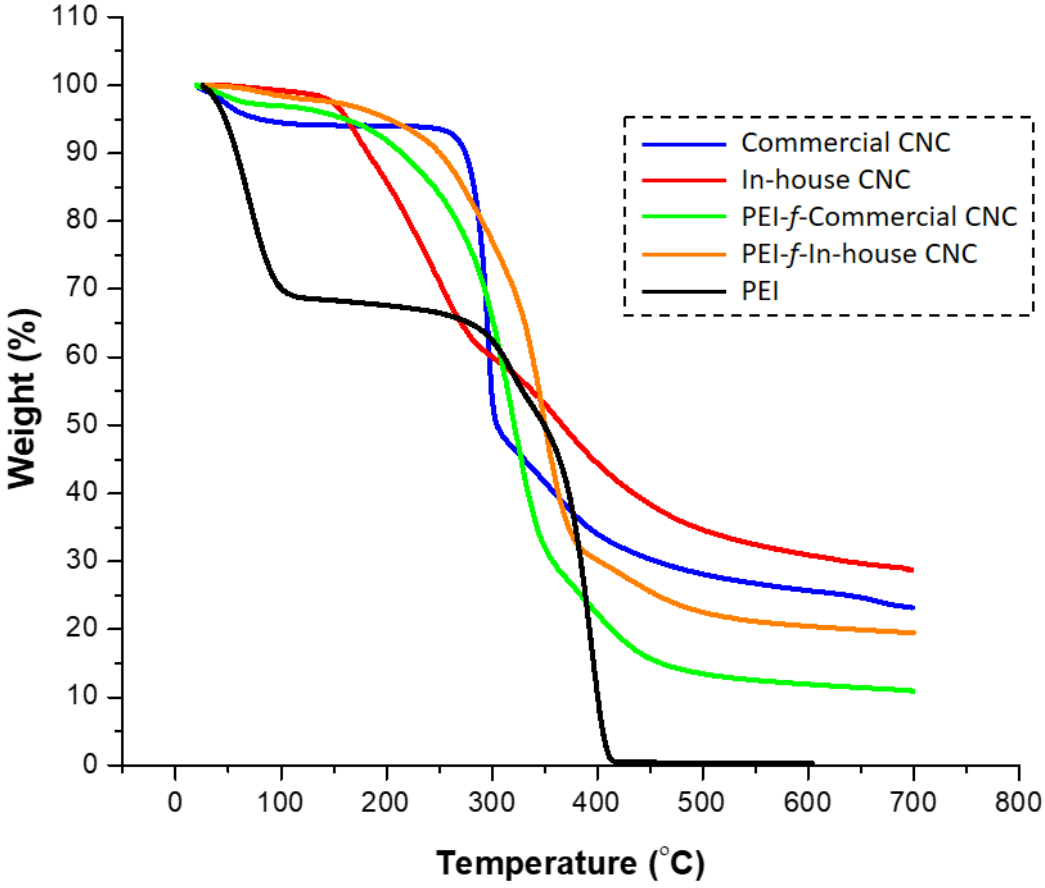

Figure 4.4. TGA curves of the non-functionalized and PEI-functionalized materials of commercial CNC and in-house synthesized CNC.

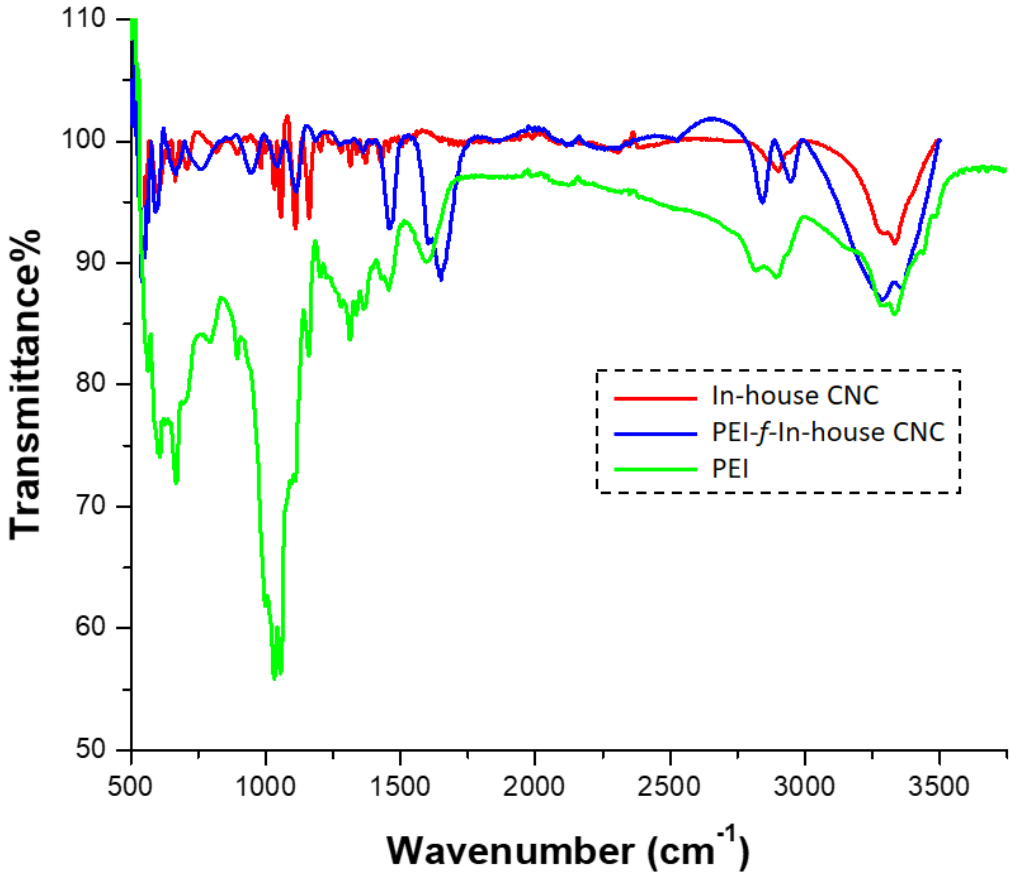

Figure 4.5. ATR-FTIR spectra of the non-functionalized and PEI-functionalized materials of commercial CNC and in-house synthesized CNC.

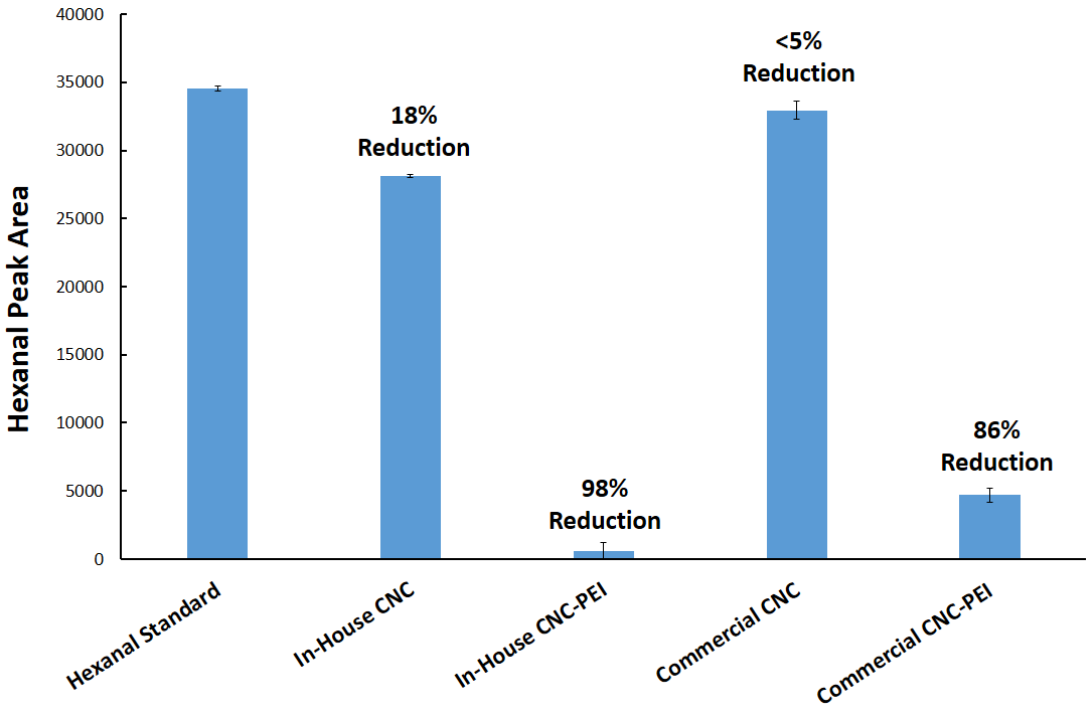

Figure 4.6. Hexanal vapor capture studies of the non-functionalized and PEI-functionalized materials of commercial CNC and in-house synthesized CNC.

These VOC studies were conducted according to our previously published protocol by adding a small amount (*i.e.*, 10 µL) of hexanal into a 1 mL gas chromatography vial, subsequently place the nanomaterial (50 mg) on a tissue paper towel (*i.e.*, Chemwipe) in the headspace of the vial and capping with a rubber septa. The headspace of the vial was then analyzed via GC peak area studies (*see* Experimental section for more details). Thus, the in-house prepared PEI-*f*-CNC reduced volatile hexanal vapors by 98% whereas PEI-*f*-CNC generated from commercial CNCs reduced vapors by 86% (Figure 4.6). These VOC studies shows that the in-house generated PEI-*f*-CNC materials are equally capable of capturing VOCs as compared to our previously developed PEI-*f*-CNC starting from commercially available CNCs.

Furthermore, the pesticide remediation capabilities of the fully in-house prepared PEI-*f*-CNC were also evaluated. These studies were performed with the well-known pesticide malathion using GC peak area analysis. Malathion remediation experiments were set up by adding the modified materials directly into a solution of malathion in DCM followed by filtration and analysis of the amount of malathion present in the solution using GC after a certain period of time (*see* Experimental section for more details). The results of these studies shows that the malathion solutions treated with the fully in-house prepared PEI-*f*-CNC materials can reduce the concentration of pesticide in solution by 74% after 24 h, suggesting that the materials are efficient in pesticide remediation as well (Figure 4.7).

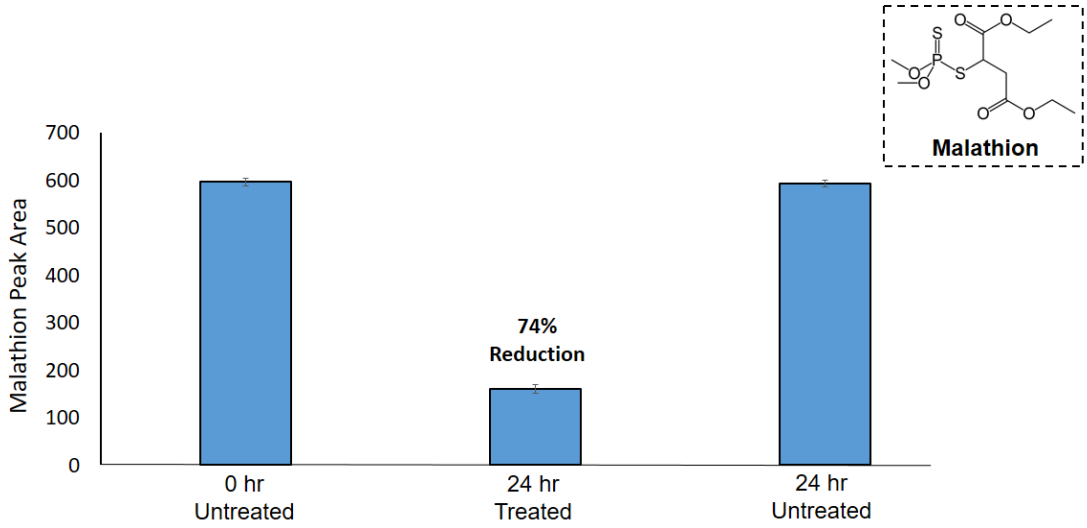

Figure 4.7. Pesticide remediation studies: Malathion degradation from the PEI-functionalized CNC.

After the initial confirmation of the efficient VOC and pesticide remediation of the PEI-*f*-in-house CNC materials, the optimization of the PEI functionalization was carried out in order to reduce the extra cost of the synthesis. As described earlier, it has been showed that the in-house synthesized CNC materials are 10 times less expensive than the commercial CNC sources. In addition, in our early attempts we were also able to show that the solvent demand for the overall PEI-functionalization reaction can be reduced by 50%.

Apart from the aforementioned factors, the other important factors that affect the cost of the synthesis are the materials and reagents involved in the key steps for the PEI functionalization such as TEMPO, NaBr, NaOCl (oxidation step) and EDC coupling reagent, and PEI (amine-functionalization step). In order to understand the optimum TEMPO and PEI amounts for this functionalization reaction while retaining the remediation activity, we then performed the same PEI functionalization reaction (as shown in Scheme 4.1) using commercial CNC with different weight equivalence of the TEMPO catalyst in the first step and PEI in the second step. Two functionalization protocols were conducted without TEMPO and by adding half the amount of TEMPO weight equivalence used in the original protocol. These PEI functionalized samples were denoted with the prefixes such as 0 wt. equiv. and 0.5 wt. equiv. TEMPO, respectively. On the other hand PEI amounts were changed to 2 or 4 weight equivalence compared to the original protocol (8 wt. equiv.) and these samples were denoted with the prefixes such as 2, 4, 8 wt. equiv. PEI, respectively.

In addition, we hypothesized that, CNC could have different types interactions with PEI such as covalent interactions due to the EDC coupling and non-covalent or ionic interactions due to adventitious surface coating since we are adding excess of PEI in these functionalization reactions. In order to understand the critical interaction types of PEI-*f*-CNC for VOC capture; 0.1 g of the functionalized samples prepared with different weight equivalence of TEMPO and PEI were subjected to sonication in 10 mL of water for 30 min. Then both sample types, before sonication (sample type A) and after sonication (sample type B) were characterized using TGA and ATR-FTIR, prior to performing VOC capture studies (*see* Experimental section for more details of the related spectra).

TGA curves of the non-sonicated (A) and sonicated (B) PEI-*f*-CNC materials synthesized with different weight equivalence of TEMPO are shown in Figure 4.8. Interestingly, the sonicated PEI-*f*-CNC samples (both the 0 and 0.5 wt. equiv. TEMPO materials) showed about 5-6% of the weight loss in the char yield after sonication (Figure 4.8). We believe that this could be mainly attributed to the amount of loosely bound PEI to the CNC surface such as non-covalently bound PEI (*i.e.*, *via* hydrogen bonding and Van der Waals interactions). Since TEMPO is important to perform the catalytic oxidation of the hydroxymethylene groups in cellulose; less weight equivalence of TEMPO could potentially result in a fewer number of carboxylic groups on the surface of the CNC, and consequently less covalently bound PEI in the functionalization step.

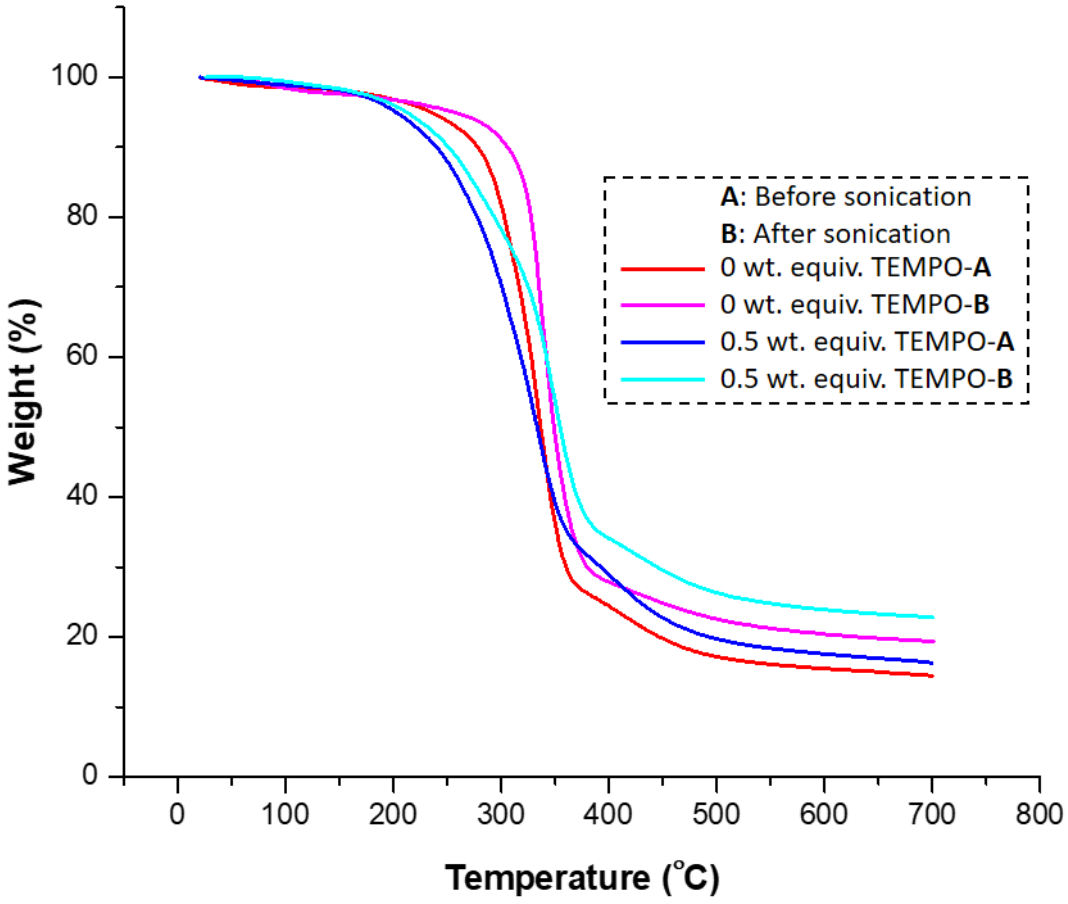

Figure 4.8. Optimization work: TGA curves of the PEI-functionalized CNC materials synthesized with different weight equivalence of TEMPO. (A) - Before sonication, (B) - After sonication

In contrast, the TGA curves of the non-sonicated (A) and sonicated (B) PEI-*f*-CNC materials synthesized with different weight equivalence of PEI shows that the mass loss in char yield is higher in the samples prepared with the 8 weight equivalence of PEI (*i.e.,* about 10%) compared to the samples prepared with 2 weight equivalence of PEI (2% weight loss) (*see* Figure 4.9). These results show that the 2 weight equivalence of PEI is the optimal amount of PEI for the functionalization.

Next, the VOC capture studies of these non-sonicated and sonicated PEI-*f*-CNC materials were performed (Figure 4.10). It is important to note that the changes in VOC activity along with the TGA char yield of the modified materials produced before and after sonication experiment were used as a key tool to decide the optimized protocol for the PEI functionalization of CNC.

Surprisingly, the non-sonicated PEI-*f*-CNC materials showed excellent hexanal vapor reduction (*i.e.*, >90%) regardless of the TEMPO or PEI weight equivalence used in the CNC modification (Figure 4.10). Sonication of the 0 weight equivalence TEMPO material showed a considerable drop in the VOC capture efficiency compared to the corresponding 0.5 weight equivalence TEMPO material. Since the absence of the TEMPO doesn't provide carboxylic functionality to the CNC surface to form covalently bound PEI; we can now assume that some type of a loosely bound PEI or presumably non-covalently bound PEI has been lost during the sonication process which is important for the gas capture activity. Indeed, 5% mass loss in the char yield of PEI-*f*-CNC

materials prepared with 0 weight equivalence of TEMPO reconfirms that there could be non-covalently bound PEI on the CNC surface.

In addition, the slightly higher mass loss in the char yield of PEI-*f*-CNC materials made with 0.5 weight equivalence of TEMPO (*i.e.,* about 1.5% higher) compared to the materials prepared with the 0 weight equivalence of TEMPO; further support the argument that PEI can also have non-covalent or ionic interactions on the oxidized or non-oxidized CNC surface.

Since the characterization of the samples after sonication still showed evidence of the active PEI, we can assume that the covalently bound PEI has not been removed during the sonication. Therefore, the TGA and VOC results both suggest that PEI-*f*-CNC samples prepared with excess PEI such as with 8 weight equivalence of PEI (similar to the previously published protocol), most probably have a combination of covalently bound PEI, non-covalently bound PEI or PEI bound with the ionic interactions with the carboxylic groups.

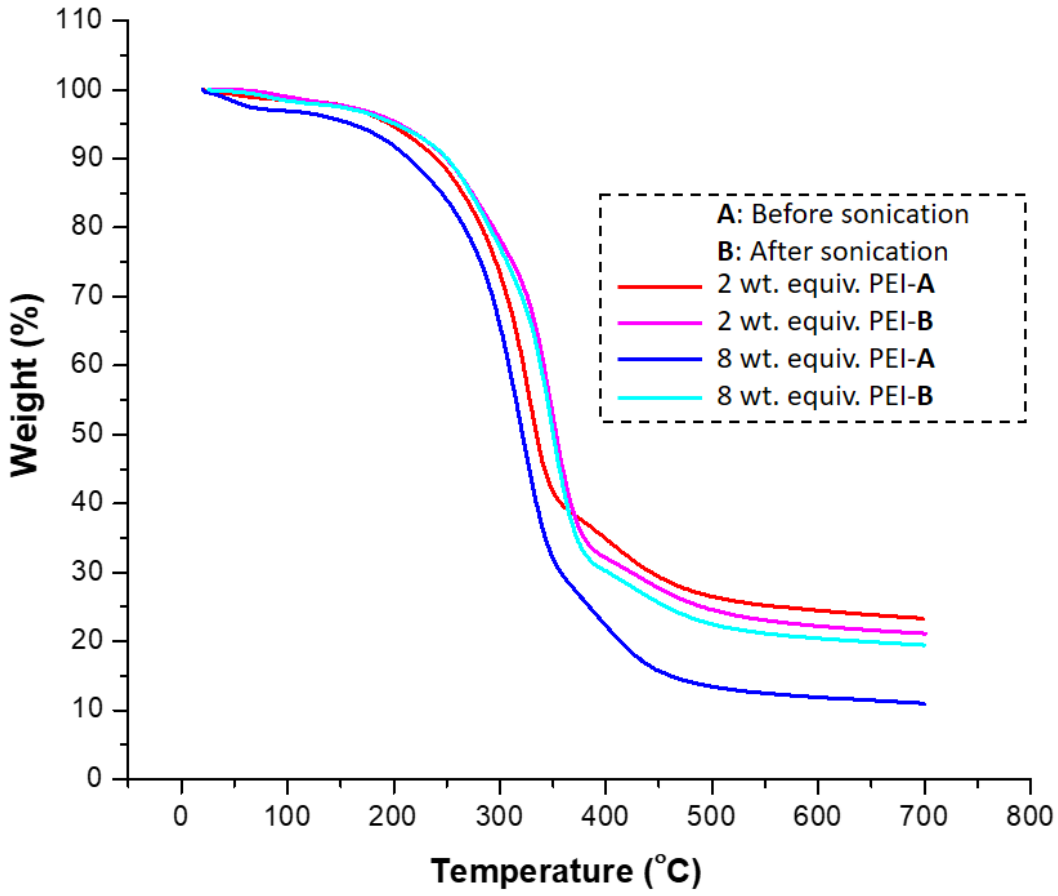

Figure 4.9. Optimization work: TGA curves of the PEI-functionalized CNC materials synthesized with different weight equivalence of PEI. (A) - Before sonication, (B) - After sonication

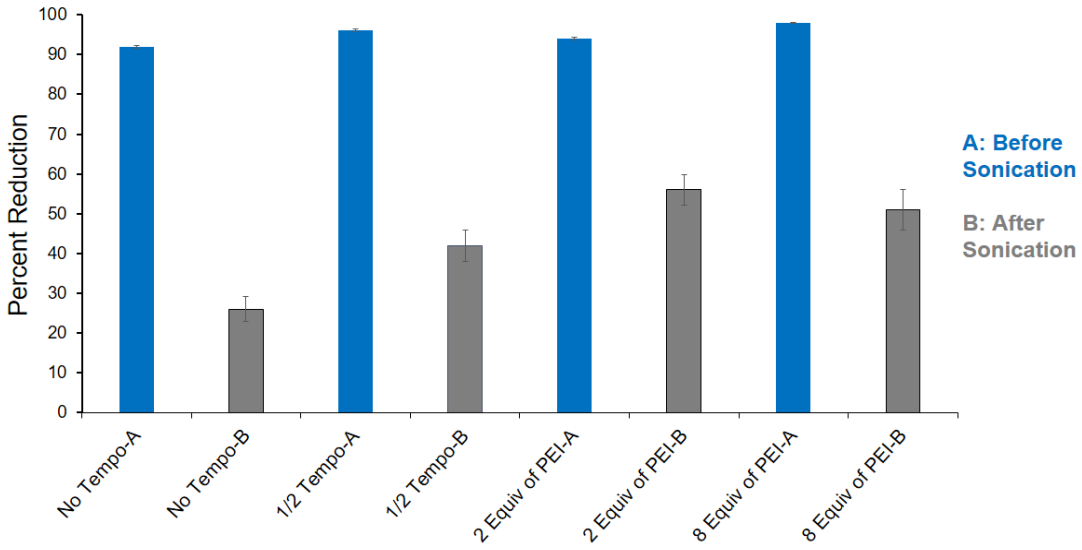

Figure 4.10. Hexanal vapor capture studies of PEI-functionalized CNC materials synthesized with different weight equivalence of TEMPO and PEI. (A: Before Sonication, B: After Sonication).

Furthermore, 2 weight equivalence of PEI and 8 weight equivalence of PEI materials showed similar efficiency in VOC capture before and after the sonication, >90% and about 50% respectively (Figure 4.10). These results suggest that the CNC functionalization with 2 weight equivalence of PEI is an optimum protocol to reduce the cost of the synthesis while retaining the remediation efficiency.

Taken all of these TGA and VOC capture results together, we can envision that the PEI can have different types of interactions with CNC such as covalently bound PEI, non-covalently bound PEI and PEI bound with ionic interactions. These results also suggest that non-covalently bound PEI (*via* hydrogen bonding, Van der Waals interactions) PEI and the PEI bound with ionic interactions also play an equal role in volatile organic capture. Figure 4.11 depicts the plausible modes of CNC and PEI interactions at the interlayer based on the experimental evidences. However, the non-covalent and ionic interactions on the CNC surface are needed to be further proved by more experimental studies such as X-ray photoelectron spectroscopy (XPS) to confirm different types of nitrogens on the CNC surface.

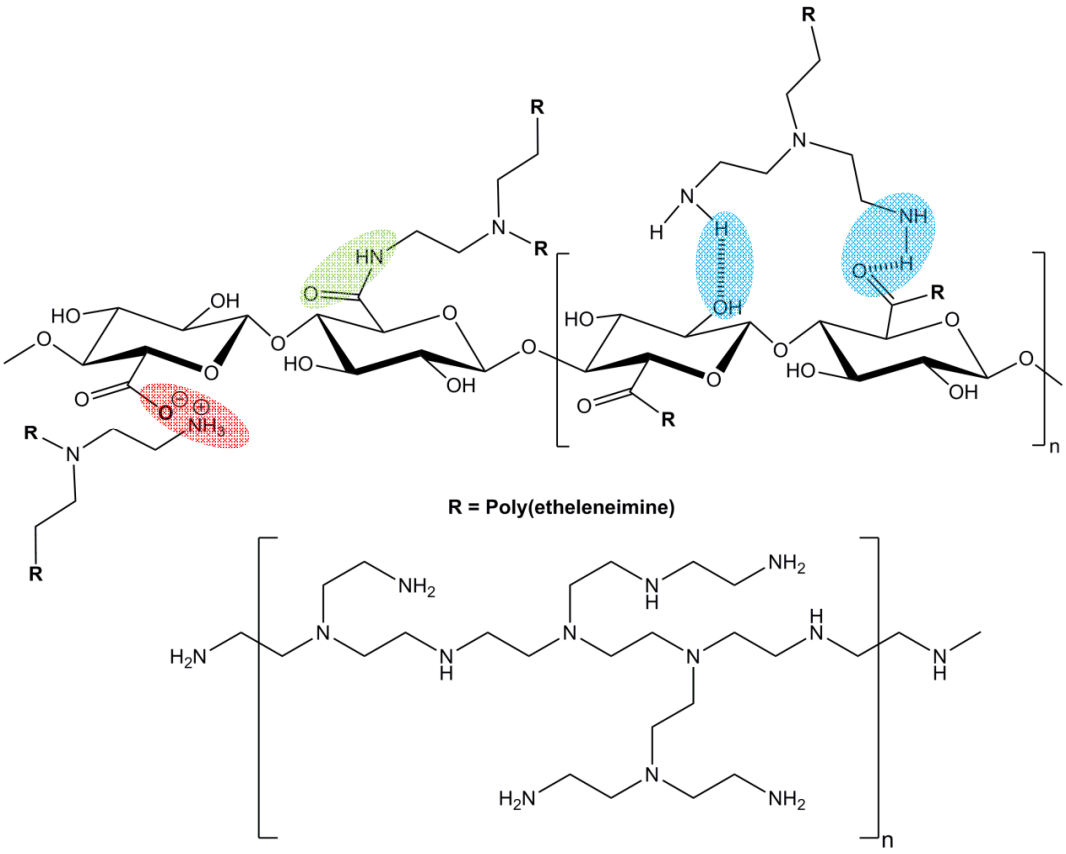

Figure 4.11. Plausible interactions of CNC and PEI at the interlayer. Note: Covalent interactions are shown in green color, hydrogen bonding or the non-covalent interactions are shown in blue color, and ionic interactions are shown in red color.

Furthermore, with the optimized PEI functionalization protocol (with 2 weight equivalence of PEI) in hand, we were successfully able to scale up the functionalization of CNC with PEI up to 100 g scale. Characterization of these modified materials by means of TGA and ATR showed successful modification of CNC. These modified materials were also showed the same hexanal remediation activity similar to the CNC-*f*-PEI produce in 1 g scale (*see* experimental section for more details).

In conclusion, we were able to perform in-house CNC synthesis in 1 g, 10 g, 100 g and 500 g scales in our laboratory. We successfully optimized the PEI functionalization protocol of CNC to reduce the cost of the synthesis while retaining the efficiency of VOC and pesticide remediation. With this optimized protocol, we were able to perform the PEI functionalization protocol of CNC in 1 g, 10 g and 100 g scales. We further confirm these PEI functionalized CNC materials from the scale up synthesis have the same remediation efficiency as the lower scale synthesis. Furthermore, optimization studies indirectly revealed that the PEI can bind to the CNC surface via covalent interactions, non-covalent interactions, and ionic interactions. Moreover, it has been evident that all these interactions play a significant role in the remediation efficiency.

In the future, this optimization study needs to be further tuned in order to obtain a crucial understanding about which synthetic protocols are best applied depending on the type of the desired application. For example if the materials are being applied in an aqueous environment; presumably the covalent PEI interactions would be more

important, whereas if the materials are applied for the capture of a volatile substance; all three types of interactions would be important. Further studies are underway in order to find alternative reagents for TEMPO since this catalyst is a corrosive reagent and somewhat difficult to handle in higher scale reactions. Similar studies also need to be done in order to find more cost effective amide coupling agent instead of EDC. Additionally, further characterization studies of the functionalized materials in X-ray photoelectron spectroscopy (XPS) could be performed in order to identify the different oxidation states of nitrogen to further confirms the different bonding patterns of PEI on the CNC surface.

4.5. Spray experiment to mimic a real-time on site remediation.

In order to further illustrate the capability of hexanal vapor capture in more realistic environment, we set up a spray experiment of the PEI-*f*-CNC materials where the volatile organic material is spread in a larger volume. The objective of this study was to show that these materials can be applied via an aqueous spray to the location where the remediation is needed. Experiments were set up to mimic a real-time, on-site remediation.

Figure 4.12 demonstrates the spray experiment set up. In this experiment, a nitrogen line was used to produce hexanal vapors after hexanal liquid is placed on the watch glass. An aqueous solution of the PEI-*f*-CNC materials was then delivered into the sealed box (dimensions: 7"H x 15.5" W x 22"L; 20 liter HDPE rectangular container) from the side while reading the ppm value corresponding to the hexanal vapors using an Aeroqual VOC probe (*see* Experimental section for more details).

The results from this spray study showed that an aqueous solution of the PEI-*f*-CNC materials (12.5 g/L and 25 g/L slurry) can reduce hexanal vapors ≥90% (Figure 4.13). However, one of the drawbacks in this study was the effect of water in the remediation. The water by itself also showed 34% reduction of the hexanal vapors. In addition, 11% reduction was also observed for the untreated trial due to the experimental errors.

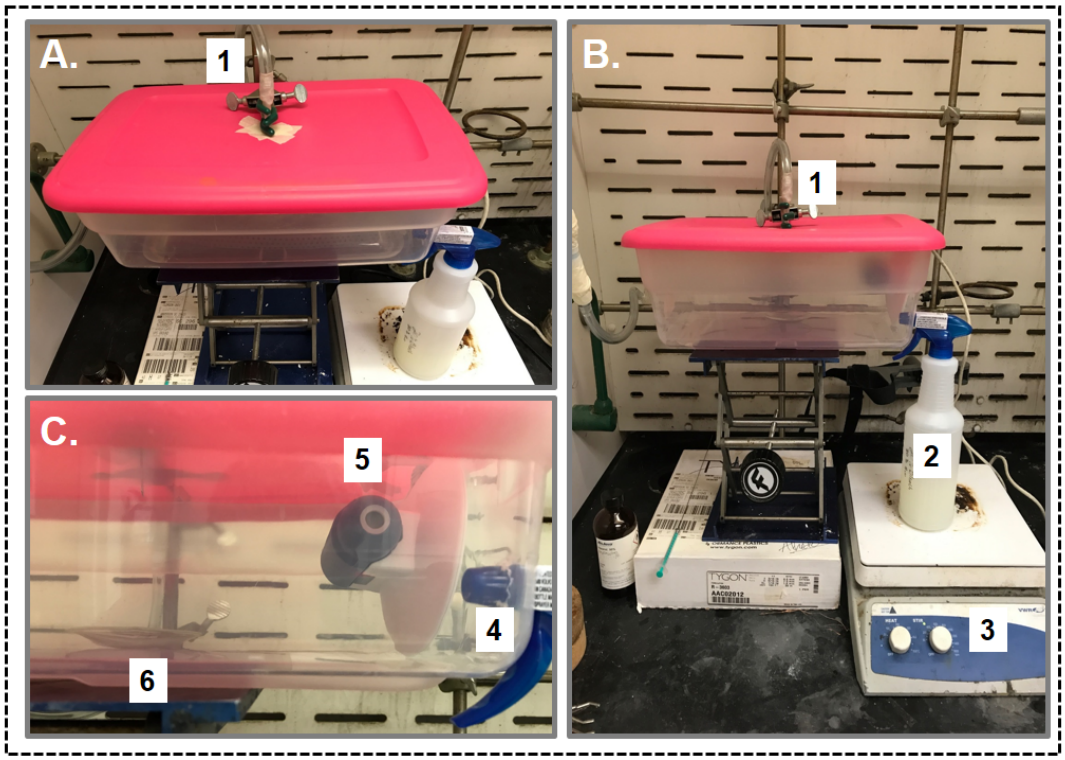

Figure 4.12. Spray experiment set up. **A**: Top view, **B**: Side view, **C**: Aeroqual probe view, **1**: Nitrogen line to produce hexanal vapors, **2**: PEI-*f*-CNC aqueous solution with a stir bar, **3**: Stir plate, **4**: Delivering of the PEI-*f*-CNC solution, **5**: Aeroqual probe, **6**: Hexanal liquid on the watch glass.

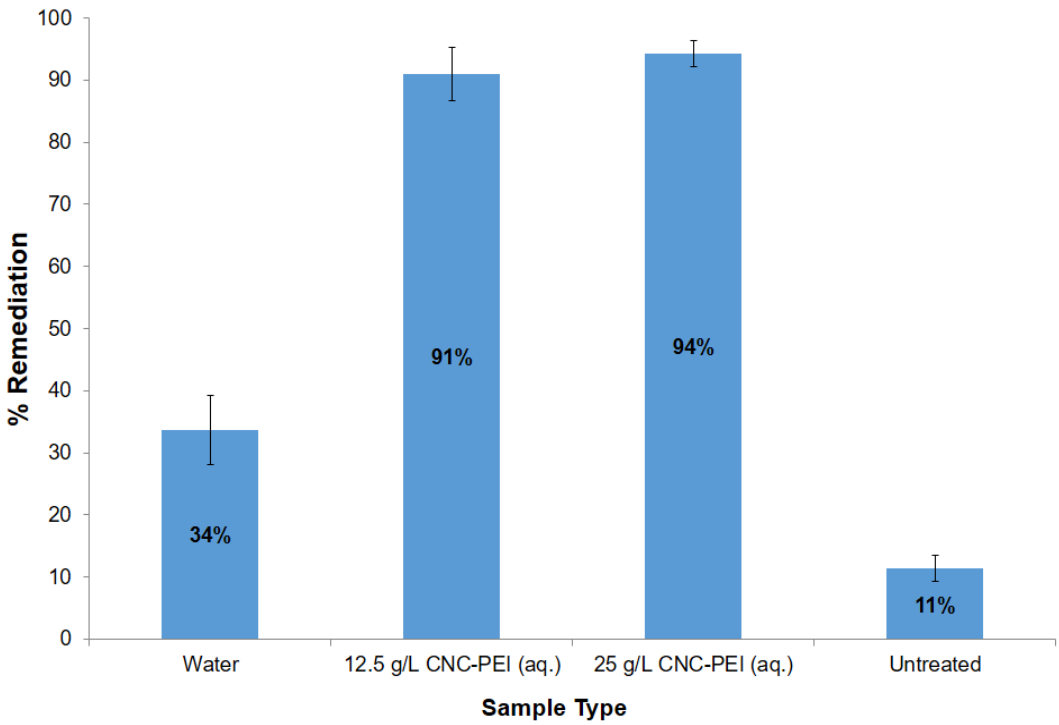

Figure 4.13. Hexanal remediation from the spray experiment.

Hexanal reduction over time from the spray experiment shows that 50% of the reduction occurs within the first minute of treatment and then it slows down gradually over a period of 8-10 minutes (Figure 4.14).

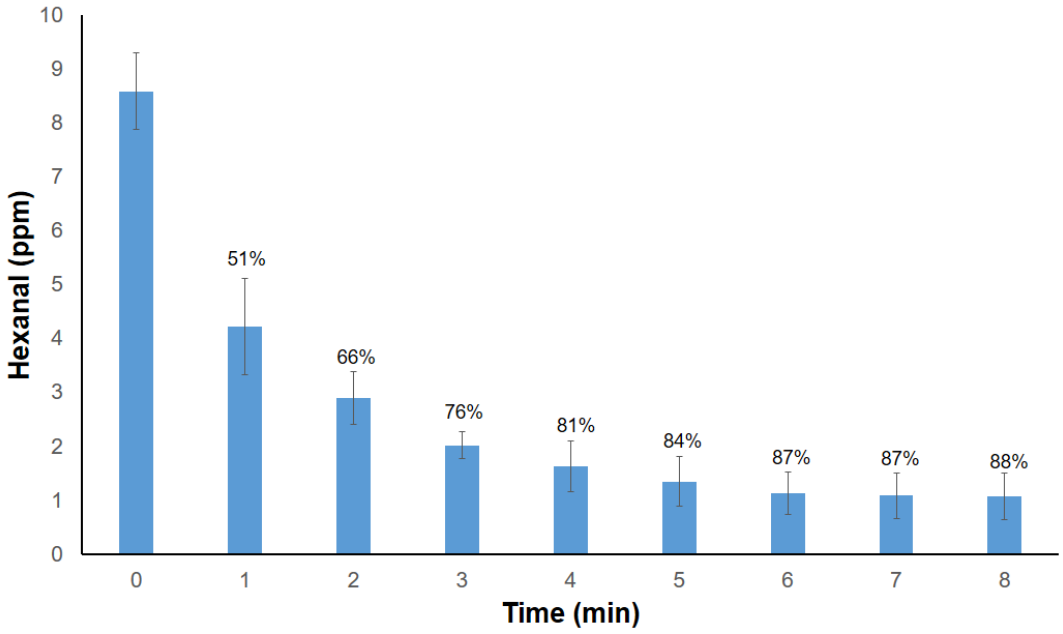

Figure 4.14. Hexanal remediation over time from the spray experiment.

Further studies on this spray experiments to show the effect of the unmodified CNC and other related materials are currently underway.

4.6 Halogenation of the PEI-functionalized cellulose nanocrystals (CNC-*f*-PEI).

Halogenation of polymeric materials is a well-known surface modification technique used to improve adhesion properties and peel strength over the past.[75–78] For instance chlorination of styrene-butadiene rubber has been used to improve the adhesion properties.The inherent non-polar nature arising for these polymers from their structural features, and also with the additives in the formulations can be overcome by such surface modifications.[75,76]

On the other hand, the chlorination of the polymeric materials has been appeared as a successful method to prevent bacterial contamination via polymers. It has been shown that polymeric materials play a significant role in transmission of infectious diseases, especially in the locations where high risk is involved for cross-infections such as hospitals.[79,80] In fact, previous studies have shown that some microbes can survive on polymer surfaces for 3 days.[79,80]As a response for these challenges; *N*-halamine precursors such as hydantoin-based polymer materials, coatings have emerged as a widely used approach to prevent microbial infections.[81–85]Furthermore, previous studiesof the antimicrobial materials such as cotton fibers,[81] polyurethane biofilms,[82] and wound dressings[84] have shown good biocidal properties.

These previous studies encouraged us to further modify the PEI-*f*-CNC materials for the use in antimicrobial applications. As a result of this, the PEI-*f*-CNC materials were treated with trichloroisocyanuric acid (TCCA) and 1,3-dibromo-5,5-

dimethylhydantoin (DBH) and characterized using ATR-FTIR, TGA, SEM and EDX. Figure 4.15 displays the ATR-FTIR of the PEI-*f*-CNC material reacted with TCCA compared to the starting materials. Despite the fact that the characteristic N-Cl stretching of TCCA (*i.e.*, 694, 796 cm^{-1} peaks)[86] is obscured by the fingerprint IR region of the PEI-*f*-CNC material, the shift of the 1597 cm^{-1} (NH bending) peak of the PEI-*f*-CNC to 1726 cm^{-1} is indicative of the successful modification of the material (Figure 4.15).The gradual weight loss in the thermal profile of the PEI-*f*-CNC material reacted with TCCA compared to the original PEI-*f*-CNC further confirms the alteration of the material (Figure 4.16).

The materials modified with DBH also did not show any significant evidence of the N-Br stretching, however they showed two new peaks in the carbonyl IR region (1720 cm^{-1}, 1737 cm^{-1}) which indicates an alteration of the PEI-*f*-CNC material (Figure 4.17). Also, higher thermal stability (*ca.* 229°C at 95% wt. for DBH treated material vs. 129°C at 95% wt. for untreated) with the steady weight loss in the TGA profile of the PEI-*f*-CNC material treated with DBH further confirms the alteration of the material (Figure 4.18).

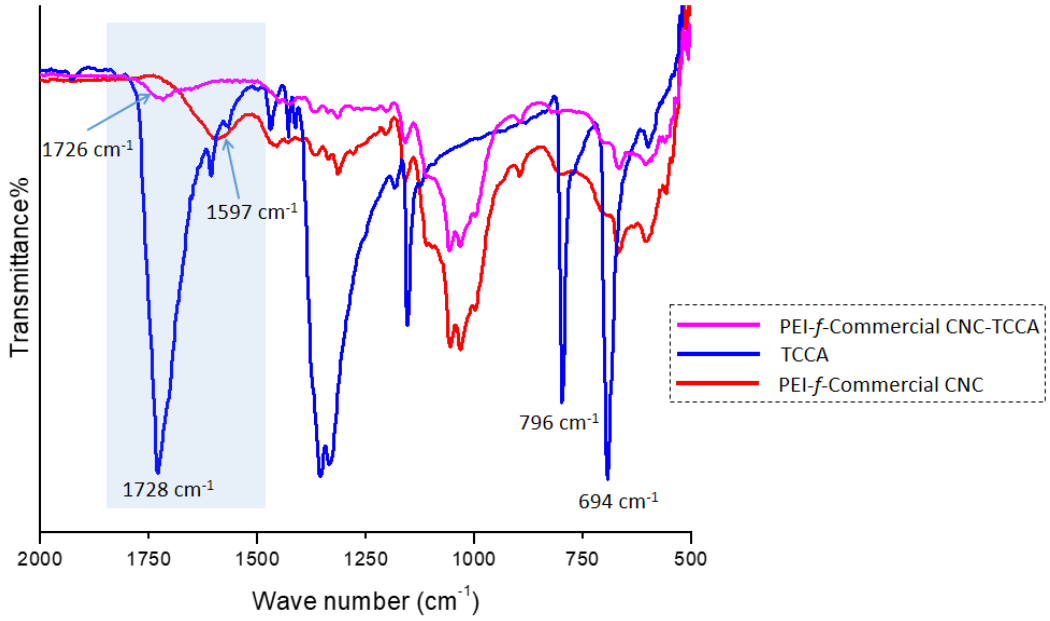

Figure 4.15. ATR-FTIR of the PEI-*f*-CNC material reacted with TCCA compared to the starting materials.

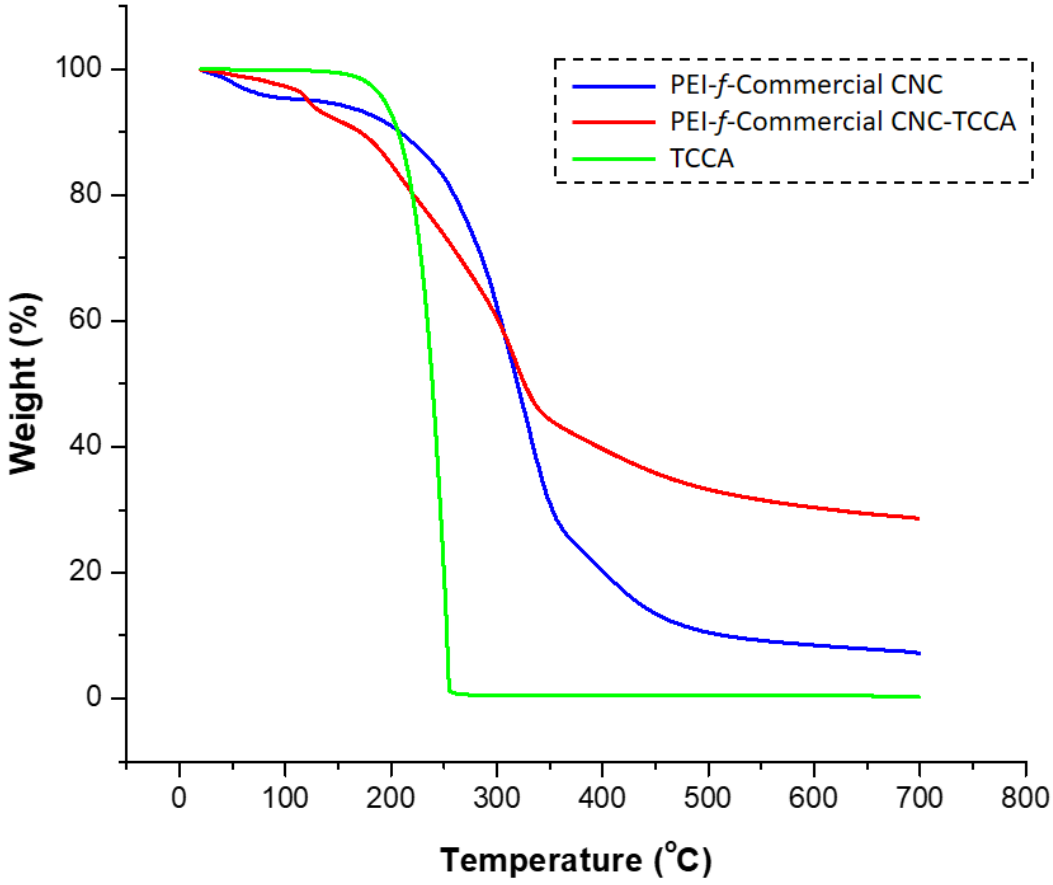

Figure 4.16. TGA curves of the PEI-*f*-CNC material reacted with TCCA compared to the starting materials.

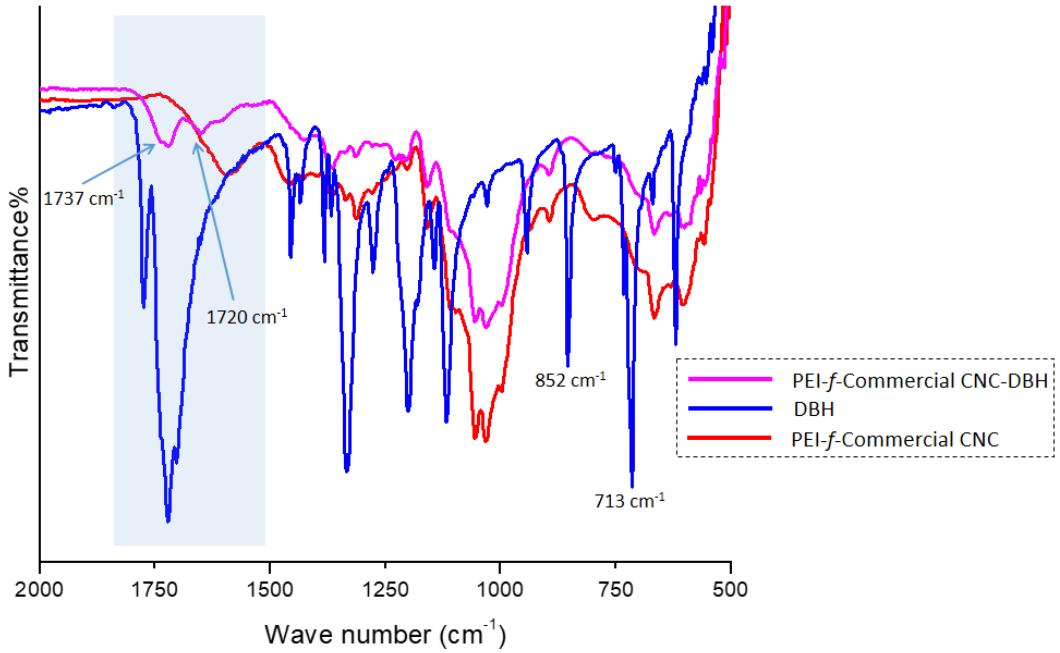

Figure 4.17. ATR-FTIR curves of the PEI-*f*-CNC material reacted with DBH compared to the starting materials.

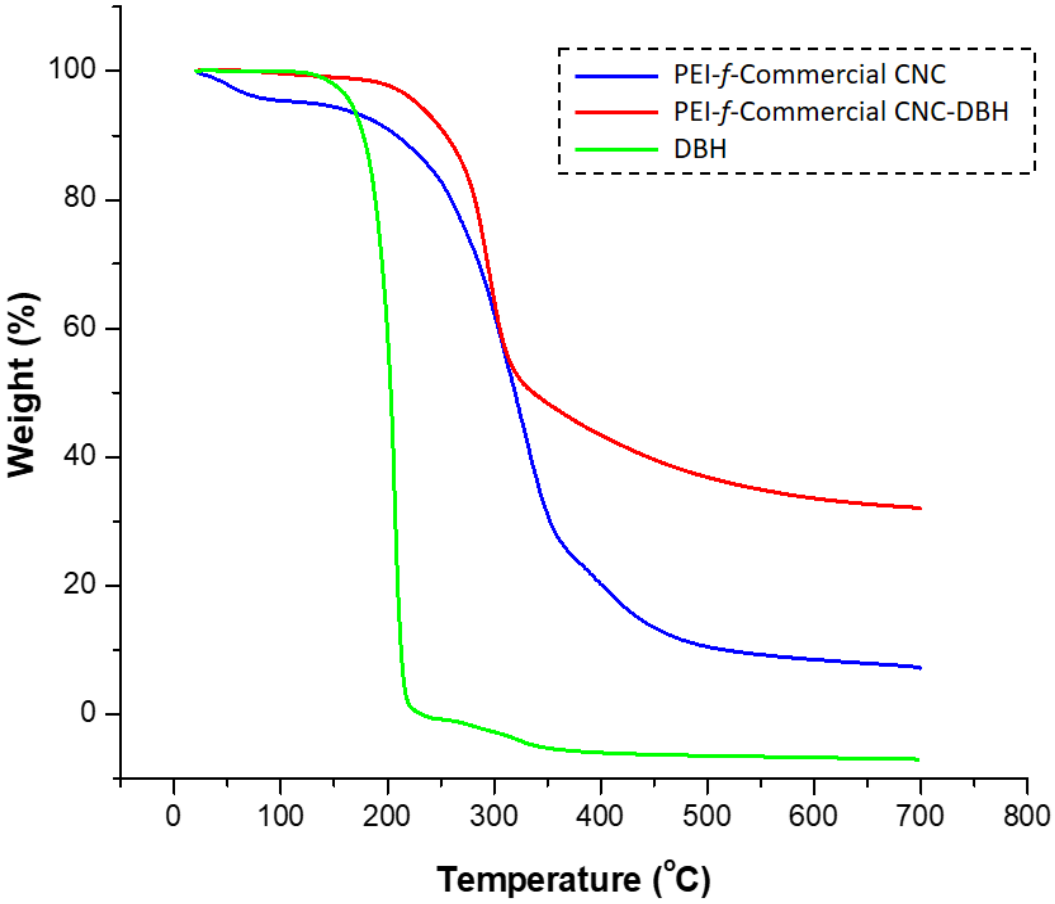

Figure 4.18. TGA curves of the PEI-*f*-CNC material reacted with DBH compared to the starting materials.

However, both TCCA and DBH treated PEI-*f*-CNC materials showed a considerable weight loss (about 20-25%) of the char yield in their thermal profiles. This is presumably due to the loss of non-covalently bound PEI and undesired degradation of the PEI. Figure 4.19 illustrates the surface topography of the untreated PEI-*f*-CNC, TCCA and DBH treated PEI-*f*-CNC materials. This shows the difference in the surface morphology of the TCCA- and DBH-treated materials suggesting the successful modifications of the PEI-*f*-CNC.

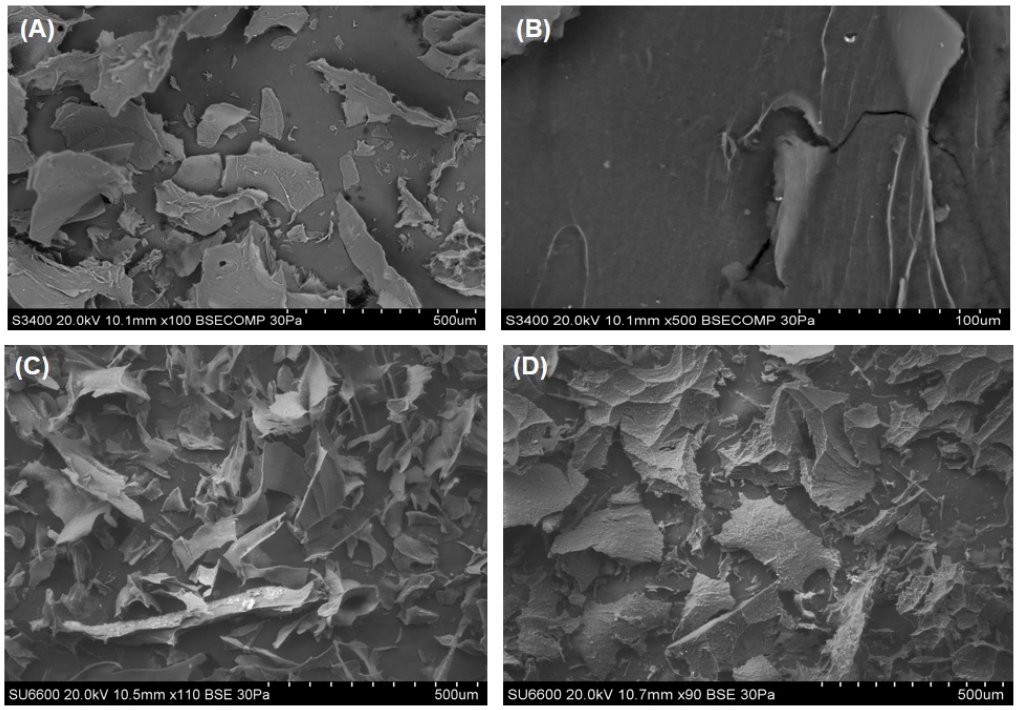

Figure 4.19. SEM images (at different magnifications) of the untreated PEI-*f*-CNC (**A, B**), PEI-*f*-CNC material reacted with TCCA (**C**) and DBH (**D**).

Further characterization of the modified PEI-*f*-CNC materials by means of EDX revealed the presence of chlorine atoms (*i.e.*, about 6 atoms %) in the TCCA treated PEI-*f*-CNC materials, whereas DBH treated materials showed only a very little amount of bromine atoms (*i.e.*, 0.1 atoms %) (Figure 4.20, 4.21).

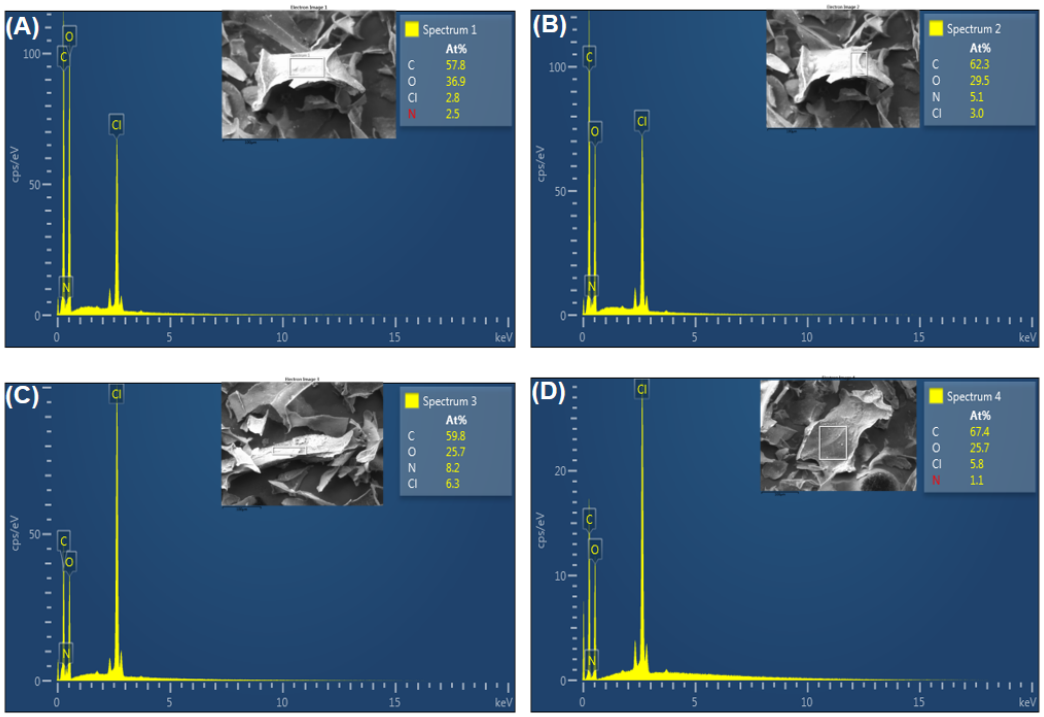

Figure 4.20. Energy dispersive X-ray (EDX) graphs of the PEI-*f*-CNC material reacted with TCCA (at sites **A,B,C,D**).

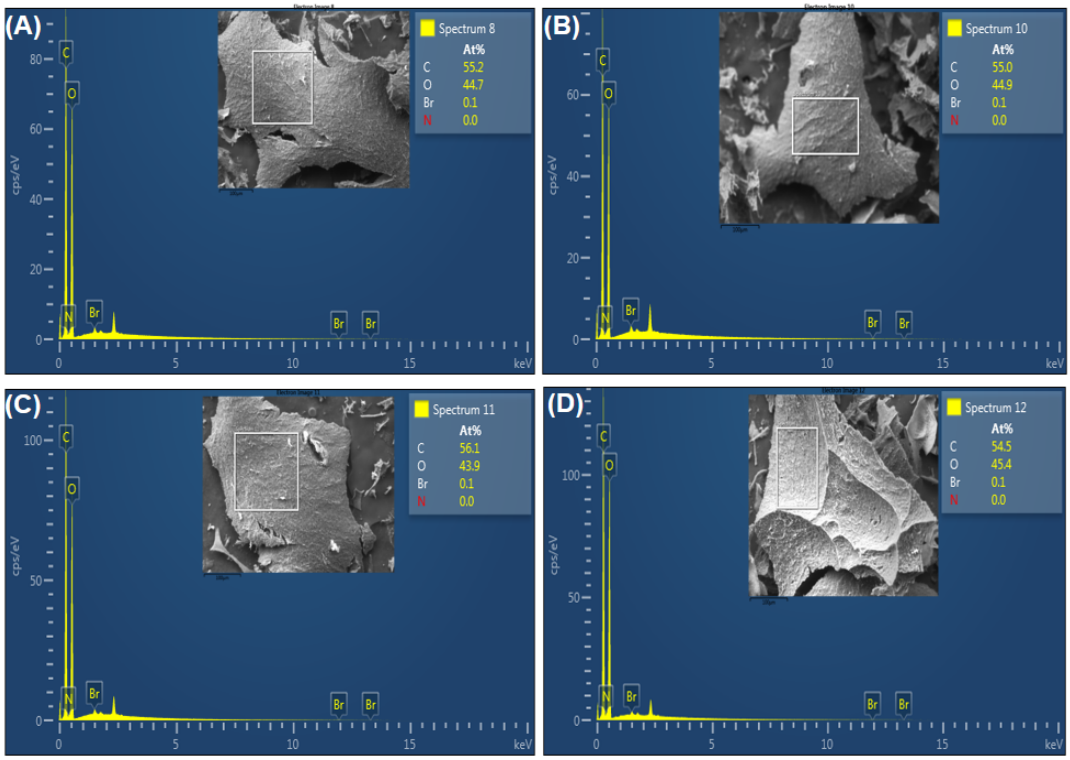

Figure 4.21. Energy dispersive X-ray (EDX) graphs of the PEI-*f*-CNC material reacted with DBH (at sites **A**,**B,C,D**).

In conclusion, we were able to chlorinate the PEI-*f*-CNC materials with TCCA. EDX studies confirmed the presence of chlorine in the modified materials. Further studies to optimize the chlorination, evaluate the degree of active chlorine (*i.e.*, chlorenium (Cl^+) equivalent) using idometric titrations, and investigate the degree of chlorination with different amine functionalized materials such as ethylenediamine (EDA), tris(2-amino-ethyl)amine are underway.[52] In addition, antimicrobial studies for the modified materials are in progress.

4.7. Experimental section

4.7.1 General information and characterization techniques

All commonly available reagents were obtained from commercially available sources and used without purification. The commercial cellulose nanocrystal (CNC) slurry (12.2 wt.% in H_2O) was purchased from Cellulose Lab. Solution of PEI (50% wt. % in H_2O, M_w ~ 1300), 10-15% sodium hypochlorite solution (NaClO), sodium hydroxide, 2,2,6,6-Tetramethylpiperidine 1-oxyl free radical (TEMPO), *N*-(3-Dimethylaminopropyl)-*N'*-ethylcarbodiimide hydrochloride (EDC), and sodium bromide were purchased from Sigma-Aldrich and used without further purification.

Attenuated Total Reflection-Fourier Transform Infrared spectroscopy (ATR-FTIR)

Infrared spectroscopy data were collected using an ATR-FTIR instrument (Shimadzu IRAffinity-1S instrument with MIRacle 10 single reflection ATR accessory) and scanned over the range of 400 to 4000 cm^{-1}.

Thermo gravimetric analysis (TGA)

TGA data were collected using TGA instrument SDT Q600 V20.9 Build 20 over the temperature range of 200 – 800 ˚C, with a ramp rate of 10˚C/min and under a nitrogen flow rate of 100mL/min.

Dynamic light scattering (DLS) measurements

DLS measurements were performed in Brookhaven NanoBrook Omni instrument. Generally, the resultant CNC slurry from the synthesis was filtered through 40-60 µm pore size fritted funnel and centrifuged at 8000 rpm in 25 mL conical vials for 20 min followed by diluted with de-ionized water to obtain a homogeneous transparent solution prior to DLS measurements. Following parameters were used in the DLS measurements; Set duration: 180 seconds, Equilibration time: 180 seconds, Total measurements: 4, Time interval between measurements: 10 seconds, Dust cut off: 50.00, Cell type: Bi-SCP, Angle: 90 degree scattering for smaller particles and forward scattering for larger particles, Refractive index of particles: 1.59, Particle shape: uniform spheres, Baseline normalization: Auto, Size distribution: used CONTIN for broad unimodal distribution. Data correlation was monitored during the DLS measurements for the accuracy and the authenticity of the data. If the correlation graph is breaking in between; multiple measurements, re-preparation of the sample or changed the scattering angle was done accordingly.

Mechanical processing

Mechanical processing of cotton (equate Jumbo Cotton Balls) was performed in a magic bullet blender with a 6 cm × 4 cm cross blade.

Centrifugation

Centrifugation was performed in eppendorf centrifuge 5804 R instrument with 25 mL conical flasks and SORVALL RC 5C PLUS instrument with 500 mL nalgene bottle with a fiberlite screw top cap closure for larger scale experiments.

Dialysis purification

Dialysis was performed using Spectra/Por®2 Dialysis membrane standard RC tubing (MW: 12-14 kD, Flat width: 45 mm, Diameter: 29 mm).

Mixing and agitation

Mixing in 100 g scale CNC synthesis and 500 g scale PEI functionalization of CNC was performed in a wide mouth brewer's glass carboy (height = 20", diameter = 4.5", Volume :~ 25 L). The glass stir rod was designed with a vertical glass rod (16.5 inches length), and several perpendicular glass paddles (4 inches each) (*see* Figure 4.2.A). The glass rod propeller was set at 150-200 rpm during all the synthesis work.

Sonication experiments

Sonication experiments were performed in a 2510 Branson ultrasonic bath.

Transmission electron microscopy (TEM)

Transmission electron microscopy (TEM) images were photographed with a H7600 and HT7830 microscopes (Hitachi High-Tech, Tokyo, Japan) operated at 100 kV and 120.0kV voltage.

Sample preparation for TEM study:

Moderately diluted CNC slurry solution (moderately turbid) was prepared by dissolving approximately 50 mg of freeze dried CNC in 5-10 mL of deionized water. A small drop of this solution was placed on the TEM grid using a plastic dropper and kept it for 1-2 minutes. Then the TEM grid was carefully placed on a Kimwipe paper to remove the excess solution. Then the TEM grid was placed on a small piece of a parafilm and one drop of 3% uranyl acetate was carefully placed on the TEM grid. This was then kept for 30 seconds at room temperature for staining. The excess uranyl acetate solution was then removed by using a Kimwipe paper. This TEM grid was dried in a desiccator with the TEM grid holder for 24 hrs prior to TEM analysis. For rapid analysis this TEM grid was placed on a piece of aluminum foil followed by kept on a hot plate at a mild heat (~40°C) for 0.5-1 hour and then placed in a desiccator with the TEM grid holder prior to TEM analysis.

Scanning electron microscopy (SEM)

Scanning electron microscopy (SEM) images were recorded in S3400 and SU6600 (Hitachi High-Tech, Tokyo, Japan) operated at 20.0kV voltage.

Energy dispersive X-ray analysis (EDX)

Elemental analysis was performed by means of energy dispersive X-ray analysis (EDX) with using SU6600 (Hitachi High-Tech, Tokyo, Japan) scanning electron microscope equipped with an X-Max detector. Data acquisition and manipulation was performed by Oxford Instruments' AZtec software suite. The samples were positioned on a carbon tape attached to a carbon disk and the disk was located inside the SEM chamber. An electron beam with an accelerating voltage of 20.0 kV was used. For each analysis scattered X-ray was collected for 30 seconds.

4.7.2 Synthesis of cellulose nanocrystals (100 g and 500 g scale)

Aqueous solutions of the 50% H_2SO_4 were pre-made and kept chilled prior to the hydrolysis of the cellulose. Then 100 g of mechanically processed cotton (with the use of a magic bullet mini blender with a cross blade for about 10 min) was placed in the large reaction vessel (Figure 4.2). The large glass vessel was then placed in a secondary container and ice was added to the secondary container. The solution of 50% H_2SO_4 was then added drop-wise to the 100 g of processed cotton while stirring via an overhead stirrer with the help of specifically designed glass stir-rod with Teflon propellers (note: glass stir rod allows for stirring of the acidic solution without corrosion). Once the addition of the acidic solution is complete, the ice was replaced with warm water. Warm water was continually replenished in order to maintain the water batch at 45°C in the secondary container.

The hydrolysis progress was continuously monitored via DLS measurements. DLS monitoring was done by first removing a certain volume from the cellulose slurry, filtering through a 40-60 µm pore size fritted funnel and centrifugation (8000 rpm, in 25 mL conical vials for 20 min) to give a precipitate. The resulting precipitate was then used in the DLS experiment. Once the desired particle size was reached (*i.e.*, 50-100 nm), the CNC slurry was centrifuged in 500 mL aliquots for 20 min at 8000 rpm speed to remove excess acid which helps to handle the material in the following steps. Once centrifuged, the solid was re-suspended in water and filtered through a 40-60 µm pore size fritted funnel. After filtration, the solution was neutralized via the addition of 6M aq. NaOH

(approximately about 300-400 mL of 6M aq. NaOH was used to neutralize 4 L of the slurry, *note:* neutralization allows access to the sodium form of the sulfonated ester groups on the CNC and prevents coagulation after freeze drying). The neutralized solution was then centrifuged and the wet precipitate was freeze-dried to obtain the cellulose nanocrystals (CNC).

4.7.3 Powder X-ray diffraction of commercial and in-house CNC.

Powder X-ray diffraction was carried out using a Rigaku Ultima IV diffractometer with CuKα radiation (λ = 1.5406 Å) at 0.02° intervals at a rate of between 0.2-1°/min from a 2θ range of 5°-65°. PXRD-PDXL software was used to analyze the composition and the purity of the product.[87] Origin 8 software was used to plot the powder patterns.

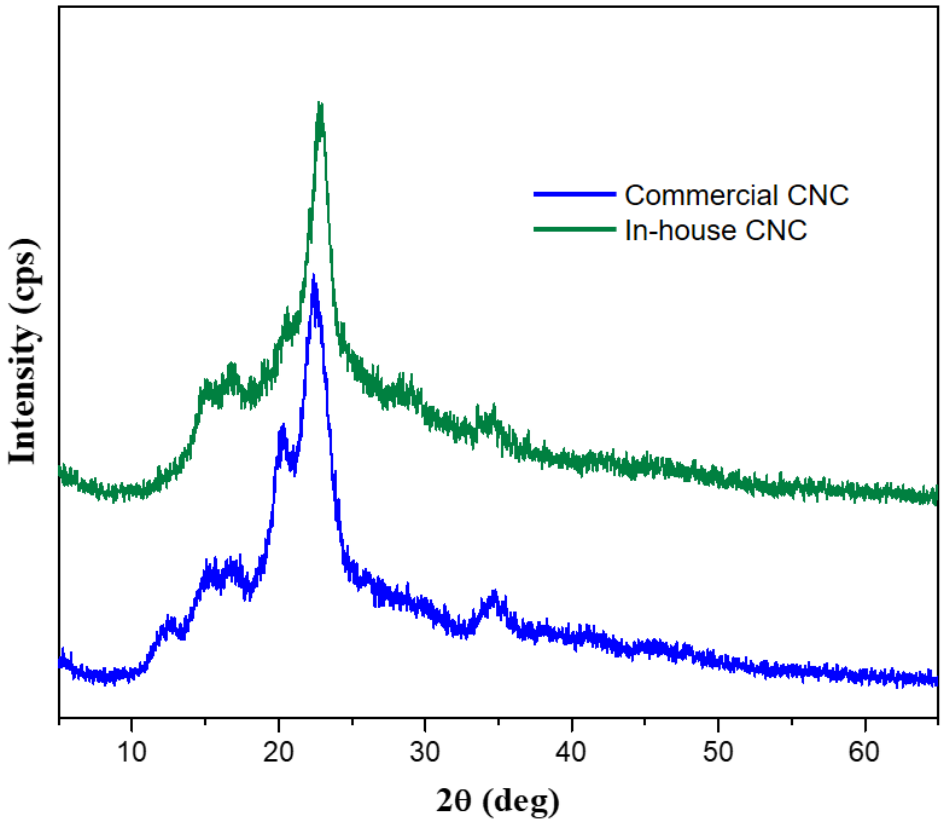

Figure 4.22. PXRD patterns of commercial and in-house CNC.

Commercial and in-house CNC both showed three main diffraction peaks corresponding to cellulose type I which are a sharp high peak at around $2\theta = 22.5°$ and weaker peaks closer to $2\theta = 14.8°$, 16.3°. These diffraction peaks can be assigned to the 200, 110, and $1\bar{1}0$ crystallographic planes of the monoclinic cellulose Iβ lattice, respectively.[72,88]

Due to the more prominent crystalline peaks at 12.4 and 20.3 degrees in the commercial CNC; the crystallinity of the commercial CNC found to be slightly higher (*i.e.*, 45.5%) than the in-house synthesized CNC (*i.e.*, 37.1%).

4.7.4. General procedure for the synthesis of PEI-f-CNC (Optimized)

TEMPO-mediated Oxidation (100 g scale)

First, 1kg of the CNC slurry (10-12% wt in H_2O) was suspended in 5 L of water in a large reaction vessel. To the resultant solution was added 10 g (63 mmol) of TEMPO, 1.25 g (12 mmol) of sodium bromide, and 240 g (387 mmol) of 12% NaClO solution (weight the solution on the scale and added portion-wise) in order to initiate the TEMPO-mediated oxidation. This reaction mixture was stirred at room temperature for 7-10 days. After a couple of hours after the addition of the reagents for the oxidation step, the pH of the solution was checked and maintained at pH 10 by the addition of a 0.5M NaOH solution (approximately 5-10 mL every 24 hrs) throughout the course of the reaction. After 7-10 days, the pH of the resultant suspension was adjusted to 2.5 (by adding approximately 50-75 mL 0.1M HCl) in order to neutralize the sodium carboxylate functional groups formed during the oxidation. The neutralized suspension was left at rest for1-2 days while monitoring and maintaining the pH at 2.5. This resultant mixture was used for the next step without further purification.

PEI-functionalization (100 g scale)

To the above mixture was added 110 g (574 mmol) of EDC (1-Ethyl-3-(3-dimethylaminopropyl)carbodiimide) and 375 mL of PEI solution (50% wt. % in H_2O, M_w ~ 1300), and the resulting mixture was stirred at room temperature for 7-10 days. The resultant slurry was purified using dialysis membrane purification (by using Spectra/Por®2 dialysis membrane standard RC tubing (MW: 12-14 kD, flat width: 45

mm, diameter: 29 mm)). In this dialysis purification, any excess and unreacted reagents were removed while monitoring the pH and replenishing the distilled water frequently. The water was changed every 24 hrs until no significant pH change in the water was observed. (*Note:* The above protocol was successful in the functionalization of CNC with PEI in 1 g, 10 g and 100 g scales).

4.7.5. VOC studies in Gas Chromatography Materials

Hexanal used in VOC studies was purchased fromcommercial sources and used without further purification. Gas Chromatography (GC) studies were performed using a Shimadzu GC-2014 Gas Chromatograph equipped with a Shimadzu AOC-20iAuto Injector and a Flame Ionization Detector (FID). The GC was equipped with a 30 m x 0.25mm x 0.25 μmZebron ZB-WAX Plus capillary GC column. The assays were conducted in Agilent Technologies GasChromatography vials with septum crimp-caps.

Gas Chromatography Analysis

The VOC capture studies were conducted using the same method which is described in our previous studies.[65,66] About 50 mg of the modified or unmodified CNC materials were placed in a tissue paper well, which was positioned inside the 2mL GC vials. The vials were then capped to hold the tissue paper and the materials and the extra tissue paper was trimmed. A 10 μL aliquot of the analyte (*i.e.,* hexanal) was carefully injected into the bottom of the vial without disturbing the material. The vial was then kept at 25°C for 30 min before injection of the gaseous head space of the vial into the GC.

Note: When 1 μL aliquot of the analyte (*i.e.,* hexanal) was used; about 10 mg of the modified or unmodified CNC materials were placed in a tissue paper well.

4.7.6. Malathion remediation study

In order to determine the GC peak area of a malathion standard, a solution of 165 ppm Malathion in DCM was prepared. This solution was immediately added in 1 mL aliquots to 1.5 mL glass screw top GC vials and injected to GC and the peak area was analyzed. This area was taken as the untreated pesticide peak area at t = 0 h. This was done in triplicate before evaluating the remediation activity of the modified materials. Next, 50 mg of the PEI-*f*-CNC materials was placed in the GC vial and 1 mL of the same malathion stock solution was added. Then the GC vial was capped, and sealed with Teflon tape, followed parafilm to avoid unnecessary evaporation. The vial was then maintained at 25℃ for 24 hr on a tilting mixer. Then these vials were also analyzed by GC. Also, an untreated sample was also prepared in a similar fashion without adding any

nanomaterial and maintained for 24 hr as a control. These trials were conducted in triplicate. The percent remediation of all the trials was calculated by comparing the treated samples with the peak area of the untreated sample at t = 0 h, which was taken to be 100%.

4.7.7. ATR-FTIR spectra of the PEI-functionalized CNC materials synthesized with different weight equivalence of TEMPO and PEI

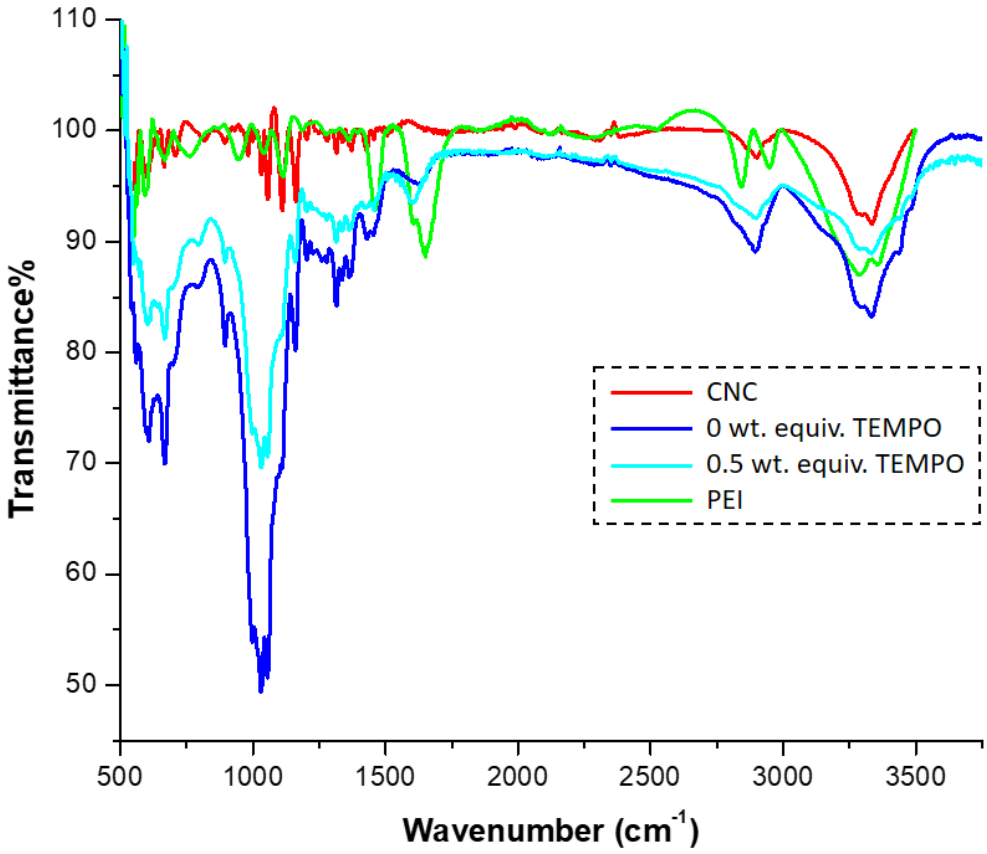

Figure 4.23. Optimization work: ATR-FTIR spectra of the PEI-functionalized CNC materials synthesized with different weight equivalence of TEMPO.

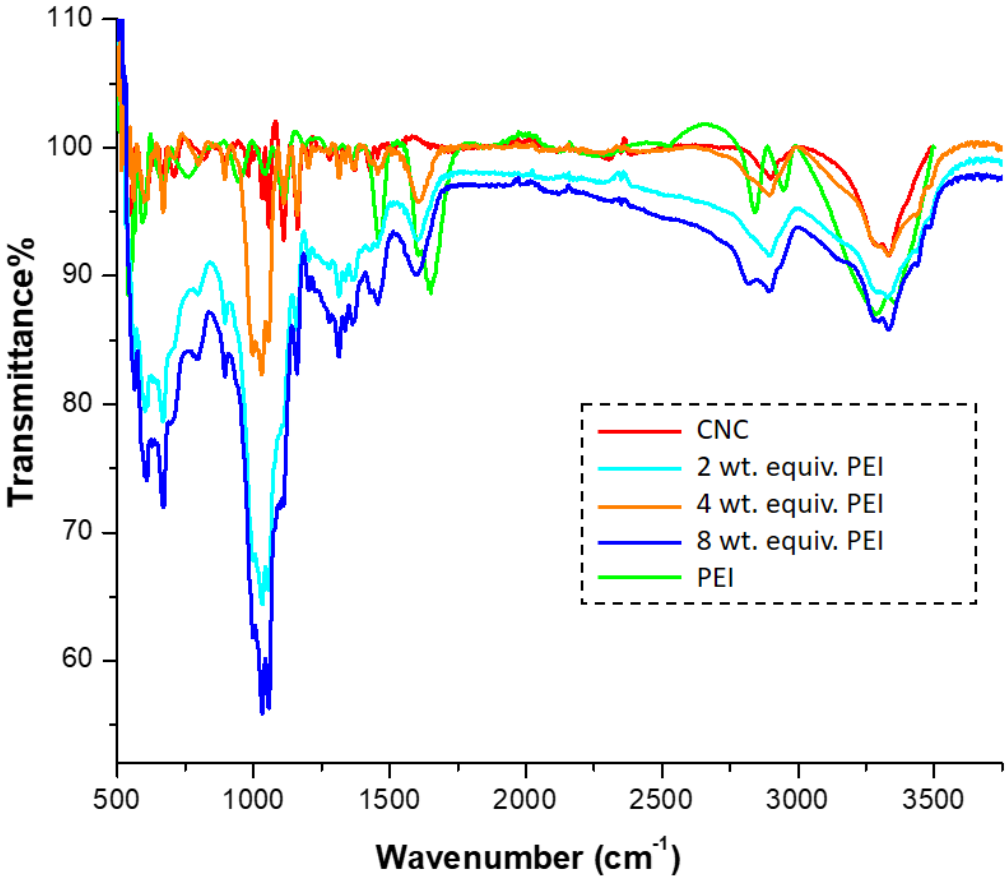

Figure 4.24. Optimization work: ATR-FTIR spectra of the PEI-functionalized CNC materials synthesized with different weight equivalence of PEI.

4.7.8. ATR-FTIR spectra of the Sonicated samples of the PEI-functionalized CNC materials synthesized with different weight equivalence of TEMPO and PEI

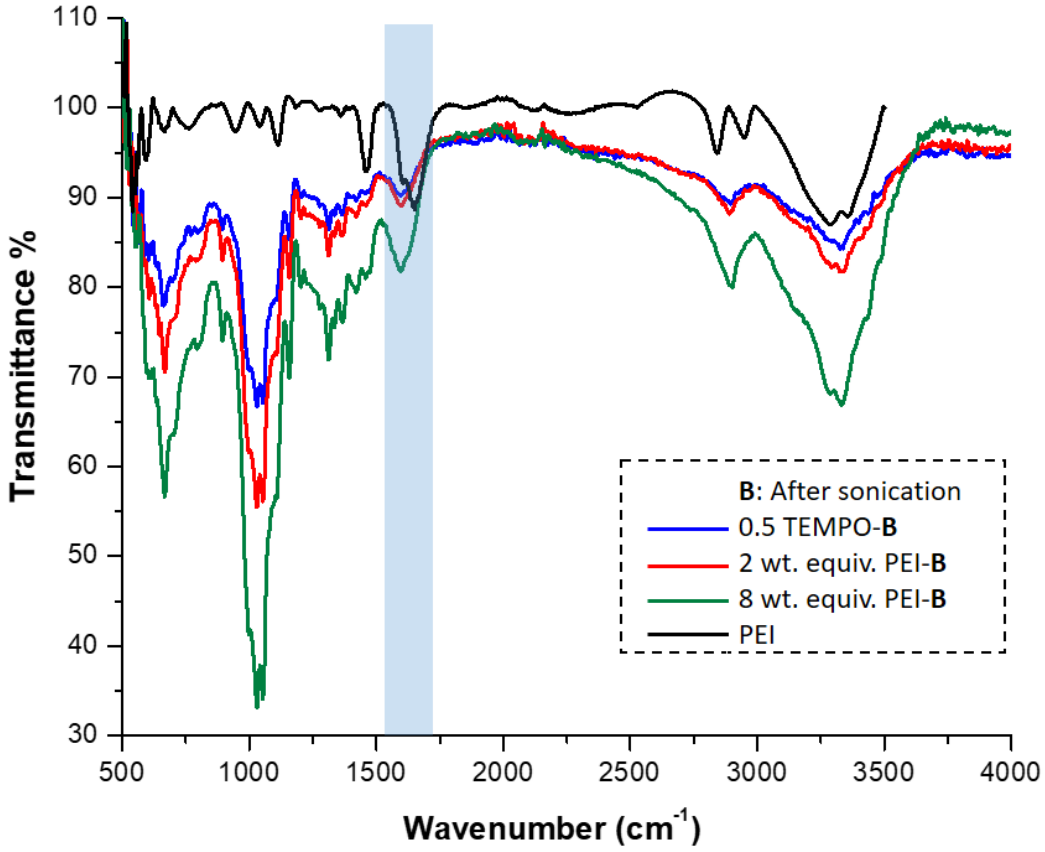

Figure 4.25. ATR-FTIR spectra of the sonicated samples of the PEI-functionalized CNC materials synthesized with different weight equivalence of TEMPO and PEI.

4.7.9. Comparison of the ATR-FTIR spectra of the PEI-functionalized CNC materials synthesized in 1g and 100 g scales

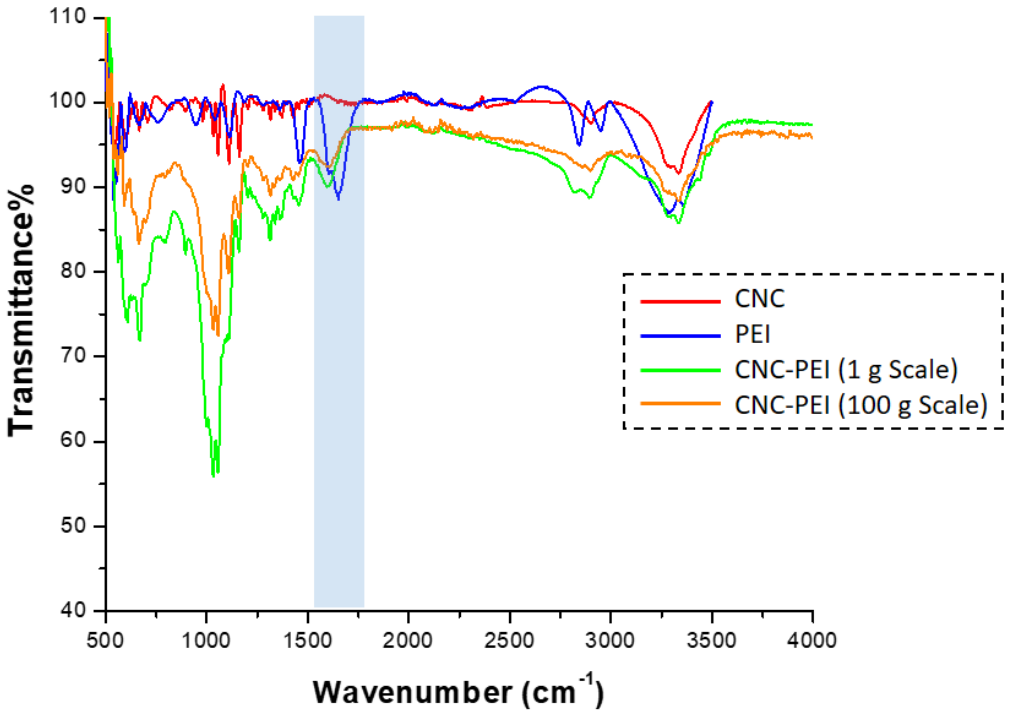

Figure 4.26. ATR-FTIR spectra of the PEI-functionalized CNC materials synthesized in 1g and 100 g scales.

The NH-bending peak observed around 1500-1750 cm^{-1} region in the ATR-FTIR spectra of PEI-*f*-CNC synthesized in 1 g scale and 100 g scale both confirms the successful amine functionalization with PEI. For the extra clarity; this portion has highlighted in blue color square region.

4.7.10. Comparison of the TGA curves of the PEI-functionalized CNC materials synthesized in 1g and 100 g scales

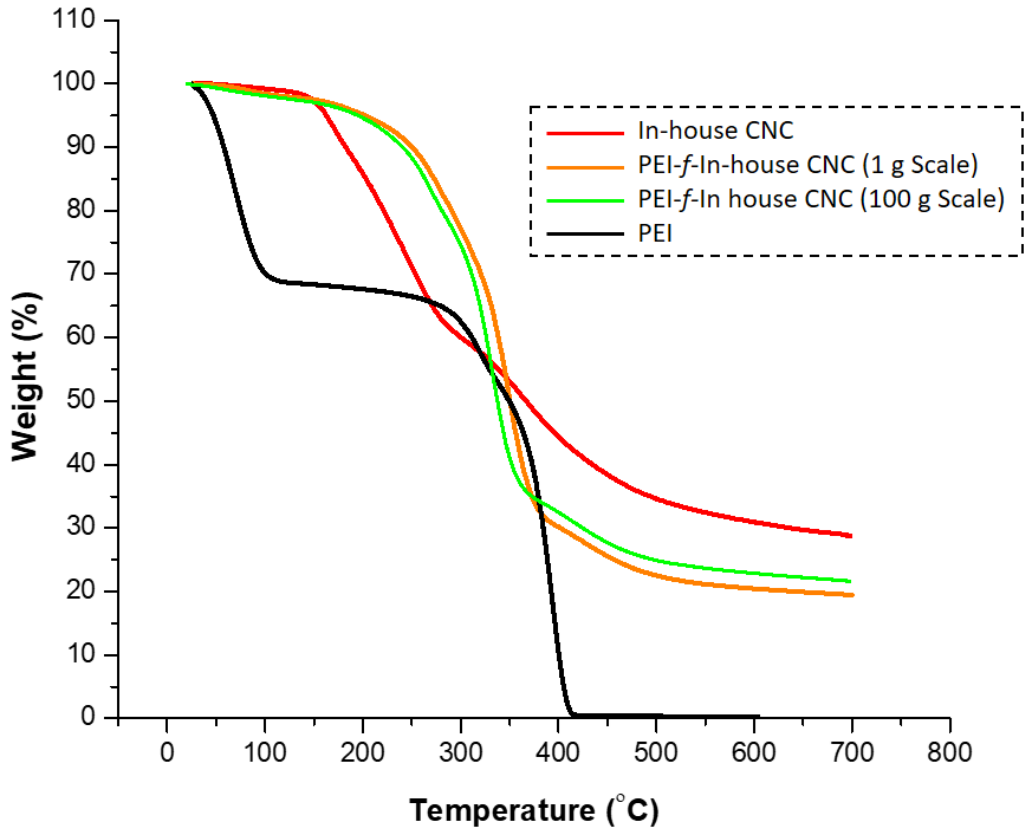

Figure 4.27. TGA curves of the PEI-functionalized CNC materials synthesized in 1g and 100 g scales.

4.7.11. Comparison of the VOC capture studies of the PEI-functionalized CNC materials synthesized in 1g and 100 g scales

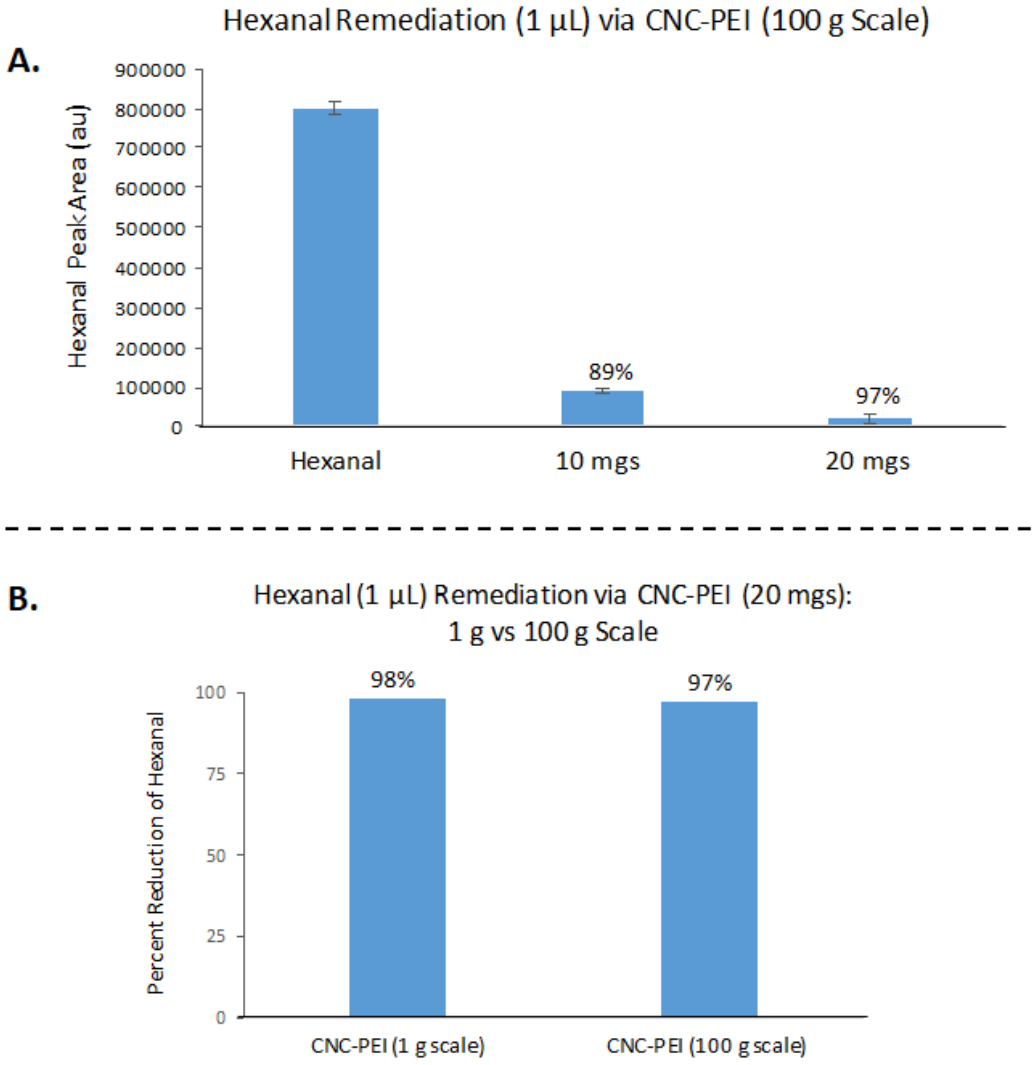

Figure 4.28. VOC capture studies of the PEI-functionalized CNC materials synthesized in 1g and 100 g scales. **A**: 1µL of the analyte with 10 mg and 20 mg of the CNC-*f*-PEI (100 g scale), **B**: 1µL of the analyte with 20 mg of the CNC-*f*-PEI (1 g vs. 100 g scale).

4.7.12. General procedure for the spray experiment of the PEI-f-CNC materials.

The equipment was set up as shown in Figure 4.11. The Aeroqual probe was attached inside the spray chamber (Dimensions: 7"H x 15.5" W x 22"L; 20 Liter HDPE rectangular container). Then the chamber was closed and allowed to equilibrate until the Aeroqual probe read a ppm value in between 0-0.50 ppm for VOCs. This value was taken as the baseline value in each spray experiment attempt. Once the VOC reading fell to within the above range; 0.6-0.8 mL of hexanal was introduced using a syringe from the top of the chamber onto the watch glass that was previously placed in the middle of the chamber. Then the chamber was provided a constant dry nitrogen flow (~200 cycles/min as measured using BELL-ART flow indicator (Cat No: 19935)) from the top of the watch glass. After the VOC ppm value reached 7-9 ppm under nitrogen flow and stabilized, the aqueous solution of the CNC-*f*-PEI was sprayed into the chamber (3 sprays = 2 mL in each spray experiment). Then the VOC ppm reading was recorded until the ppm value stabilized (typically about 8-10 min).All of these spray experiments were performed in triplicate. Due to the low solubility of CNC-*f*-PEI in water, the spray solution was stirred during the entire time of the experiment. Furthermore, similar experiments were conducted using water (*i.e.,* without CNC-PEI). Untreated control samples were measured to acquire the remediation% by water and Aeroqual probe error%, respectively.

4.7.13. General procedure for the halogenation of PEI-f-CNC

A dried 20 mL vial was equipped with a stir bar, and 100 mg (1 weight equiv.) of the PEI-*f*-CNC, 20 mL of water and 100 mg (1 weight equiv.) of the halogenating reagent were added. The resultant suspension was stirred for 24 h and then purified via dialysis purification followed by freeze drying to obtain the dried powder of the halogenated PEI-*f*-CNC materials.

4.8. References.

(1) Ibrahim, R. K.; Hayyan, M.; AlSaadi, M. A.; Hayyan, A.; Ibrahim, S. Environmental Application of Nanotechnology: Air, Soil, and Water. *Environ Sci Pollut Res* **2016**, *23* (14), 13754–13788. https://doi.org/10.1007/s11356-016-6457-z.

(2) Nie, E.; Zheng, G.; Ma, C. Characterization of Odorous Pollution and Health Risk Assessment of Volatile Organic Compound Emissions in Swine Facilities. *Atmospheric Environment* **2020**, *223*, 117233. https://doi.org/10.1016/j.atmosenv.2019.117233.

(3) Zheng, G.; Liu, J.; Shao, Z.; Chen, T. Emission Characteristics and Health Risk Assessment of VOCs from a Food Waste Anaerobic Digestion Plant: A Case Study of Suzhou, China. *Environmental Pollution* **2020**, *257*, 113546. https://doi.org/10.1016/j.envpol.2019.113546.

(4) Hu, R.; Liu, G.; Zhang, H.; Xue, H.; Wang, X.; Lam, P. K. S. Odor Pollution Due to Industrial Emission of Volatile Organic Compounds: A Case Study in Hefei, China. *Journal of Cleaner Production* **2020**, *246*, 119075. https://doi.org/10.1016/j.jclepro.2019.119075.

(5) Omidi, F.; Dehghani, F.; Fallahzadeh, R. A.; Miri, M.; Taghavi, M.; Eynipour, A. Probabilistic Risk Assessment of Occupational Exposure to Volatile Organic Compounds in the Rendering Plant of a Poultry Slaughterhouse. *Ecotoxicology and Environmental Safety* **2019**, *176*, 132–136. https://doi.org/10.1016/j.ecoenv.2019.03.079.

(6) Blount, B. C.; Kobelski, R. J.; McElprang, D. O.; Ashley, D. L.; Morrow, J. C.; Chambers, D. M.; Cardinali, F. L. Quantification of 31 Volatile Organic Compounds in Whole Blood Using Solid-Phase Microextraction and Gas Chromatography–Mass Spectrometry. *Journal of Chromatography B* **2006**, *832* (2), 292–301. https://doi.org/10.1016/j.jchromb.2006.01.019.

(7) Blanes-Vidal, V.; Hansen, M. N.; Adamsen, A. P. S.; Feilberg, A.; Petersen, S. O.; Jensen, B. B. Characterization of Odor Released during Handling of Swine Slurry: Part II. Effect of Production Type, Storage and Physicochemical Characteristics of the Slurry. *Atmospheric Environment* **2009**, *43* (18), 3006–3014. https://doi.org/10.1016/j.atmosenv.2009.01.046.

(8) Domingo, J. L.; Rovira, J.; Vilavert, L.; Nadal, M.; Figueras, M. J.; Schuhmacher, M. Health Risks for the Population Living in the Vicinity of an Integrated Waste Management Facility: Screening Environmental Pollutants. *Science of The Total Environment* **2015**, *518–519*, 363–370. https://doi.org/10.1016/j.scitotenv.2015.03.010.

(9) Jones, A. P. Indoor Air Quality and Health. *Atmospheric Environment* **1999**, *33* (28), 4535–4564. https://doi.org/10.1016/S1352-2310(99)00272-1.

(10) Miri, M.; Rostami Aghdam Shendi, M.; Ghaffari, H. R.; Ebrahimi Aval, H.; Ahmadi, E.; Taban, E.; Gholizadeh, A.; Yazdani Aval, M.; Mohammadi, A.; Azari, A. Investigation of Outdoor BTEX: Concentration, Variations, Sources, Spatial Distribution, and Risk Assessment. *Chemosphere* **2016**, *163*, 601–609. https://doi.org/10.1016/j.chemosphere.2016.07.088.

(11) Ni, J.-Q.; Robarge, W. P.; Xiao, C.; Heber, A. J. Volatile Organic Compounds at Swine Facilities: A Critical Review. *Chemosphere* **2012**, *89* (7), 769–788. https://doi.org/10.1016/j.chemosphere.2012.04.061.
(12) Khan, F. I.; Kr. Ghoshal, A. Removal of Volatile Organic Compounds from Polluted Air. *Journal of Loss Prevention in the Process Industries* **2000**, *13* (6), 527–545. https://doi.org/10.1016/S0950-4230(00)00007-3.
(13) Guffanti, P.; Pifferi, V.; Falciola, L.; Ferrante, V. Analyses of Odours from Concentrated Animal Feeding Operations: A Review. *Atmospheric Environment* **2018**, *175*, 100–108. https://doi.org/10.1016/j.atmosenv.2017.12.007.
(14) Zapata, A.; Malato, S.; Sánchez-Pérez, J. A.; Oller, I.; Maldonado, M. I. Scale-up Strategy for a Combined Solar Photo-Fenton/Biological System for Remediation of Pesticide-Contaminated Water. *Catalysis Today* **2010**, *151* (1), 100–106. https://doi.org/10.1016/j.cattod.2010.01.034.
(15) Malato, S.; Blanco, J.; Maldonado, M. I.; Oller, I.; Gernjak, W.; Pérez-Estrada, L. Coupling Solar Photo-Fenton and Biotreatment at Industrial Scale: Main Results of a Demonstration Plant. *Journal of Hazardous Materials* **2007**, *146* (3), 440–446. https://doi.org/10.1016/j.jhazmat.2007.04.084.
(16) Tang, C.; Brodie, P.; Li, Y.; Grishkewich, N. J.; Brunsting, M.; Tam, K. C. Shape Recoverable and Mechanically Robust Cellulose Aerogel Beads for Efficient Removal of Copper Ions. *Chemical Engineering Journal* **2020**, *392*, 124821. https://doi.org/10.1016/j.cej.2020.124821.
(17) Wang, X.; Sheng, J.; Gong, P.; Xue, Y.; Yao, T.; Jones, K. C. Persistent Organic Pollutants in the Tibetan Surface Soil: Spatial Distribution, Air–Soil Exchange and Implications for Global Cycling. *Environmental Pollution* **2012**, *170*, 145–151. https://doi.org/10.1016/j.envpol.2012.06.012.
(18) Marican, A.; Durán-Lara, E. F. A Review on Pesticide Removal through Different Processes. *Environ Sci Pollut Res* **2018**, *25* (3), 2051–2064. https://doi.org/10.1007/s11356-017-0796-2.
(19) Guerra, F. D.; Attia, M. F.; Whitehead, D. C.; Alexis, F. Nanotechnology for Environmental Remediation: Materials and Applications. *Molecules* **2018**, *23* (7), 1760. https://doi.org/10.3390/molecules23071760.
(20) Huong, P.-T.; Lee, B.-K.; Kim, J.; Lee, C.-H. Nitrophenols Removal from Aqueous Medium Using Fe-Nano Mesoporous Zeolite. *Materials & Design* **2016**, *101*, 210–217. https://doi.org/10.1016/j.matdes.2016.04.020.
(21) Senthilnathan, J.; Philip, L. Removal of Mixed Pesticides from Drinking Water System Using Surfactant-Assisted Nano-TiO2. *Water Air Soil Pollut* **2010**, *210* (1), 143–154. https://doi.org/10.1007/s11270-009-0230-6.
(22) Tyagi, N.; Thangadurai, P.; Suresh, S. Application of Bacterial Cellulose–Silver Nanoprism Composite for Detoxification of Endosulfan and Inactivation of Escherichia Coli Cells. *Int. J. Environ. Sci. Technol.* **2020**, *17* (3), 1713–1726. https://doi.org/10.1007/s13762-019-02510-4.

(23) A, V. B. R.; Jaafar, J.; Abdul Majid, Z.; Aris, A.; Umar, K.; Talib, J.; Madhavi, G. Relative Efficiency Comparison of Carboxymethyl Cellulose (CMC) Stabilized Fe0and Fe0/Ag Nanoparticles for Rapid Degradation of Chlorpyrifos in Aqueous Solutions. *Digest Journal of Nanomaterials and Biostructures* **2015**, *10*, 331–340.
(24) Komal; Gupta, K.; Kumar, V.; Tikoo, K. B.; Kaushik, A.; Singhal, S. Encrustation of Cadmium Sulfide Nanoparticles into the Matrix of Biomass Derived Silanized Cellulose Nanofibers for Adsorptive Detoxification of Pesticide and Textile Waste. *Chemical Engineering Journal* **2020**, *385*, 123700. https://doi.org/10.1016/j.cej.2019.123700.
(25) Lowry, G. V.; Johnson, K. M. Congener-Specific Dechlorination of Dissolved PCBs by Microscale and Nanoscale Zerovalent Iron in a Water/Methanol Solution. *Environ. Sci. Technol.* **2004**, *38* (19), 5208–5216. https://doi.org/10.1021/es049835q.
(26) Baglieri, A.; Nègre, M.; Trotta, F.; Bracco, P.; Gennari, M. Organo-Clays and Nanosponges for Acquifer Bioremediation: Adsorption and Degradation of Triclopyr. *Journal of Environmental Science and Health, Part B* **2013**, *48* (9), 784–792. https://doi.org/10.1080/03601234.2013.780943.
(27) Fiorilli, S.; Rivoira, L.; Calì, G.; Appendini, M.; Bruzzoniti, M. C.; Coïsson, M.; Onida, B. Iron Oxide inside SBA-15 Modified with Amino Groups as Reusable Adsorbent for Highly Efficient Removal of Glyphosate from Water. *Applied Surface Science* **2017**, *411*, 457–465. https://doi.org/10.1016/j.apsusc.2017.03.206.
(28) Rawtani, D.; Khatri, N.; Tyagi, S.; Pandey, G. Nanotechnology-Based Recent Approaches for Sensing and Remediation of Pesticides. *Journal of Environmental Management* **2018**, *206*, 749–762. https://doi.org/10.1016/j.jenvman.2017.11.037.
(29) Tarla, D. N.; Erickson, L. E.; Hettiarachchi, G. M.; Amadi, S. I.; Galkaduwa, M.; Davis, L. C.; Nurzhanova, A.; Pidlisnyuk, V. Phytoremediation and Bioremediation of Pesticide-Contaminated Soil. *Applied Sciences* **2020**, *10* (4), 1217. https://doi.org/10.3390/app10041217.
(30) Khan, S. H.; Pathak, B. ZnO Based Photocatalytic Degradation of Persistent Pesticides: A Comprehensive Review. *Environmental Nanotechnology, Monitoring & Management* **2020**, 100290. https://doi.org/10.1016/j.enmm.2020.100290.
(31) Pérez-Estrada, L. A.; Malato, S.; Gernjak, W.; Agüera, A.; Thurman, E. M.; Ferrer, I.; Fernández-Alba, A. R. Photo-Fenton Degradation of Diclofenac: Identification of Main Intermediates and Degradation Pathway. *Environ. Sci. Technol.* **2005**, *39* (21), 8300–8306. https://doi.org/10.1021/es050794n.
(32) Durán-Lara, E. F.; Ávila-Salas, F.; Galaz, S.; John, A.; Maricán, A.; Gutiérrez, M.; Nachtigall, F. M.; Gonzalez-Nilo, F. D.; Santos, L. S.; Durán-Lara, E. F.; Ávila-Salas, F.; Galaz, S.; John, A.; Maricán, A.; Gutiérrez, M.; Nachtigall, F. M.; Gonzalez-Nilo, F. D.; Santos, L. S. Nano-Detoxification of Organophosphate Agents by PAMAM Derivatives. *Journal of the Brazilian Chemical Society* **2015**, *26* (3), 580–591. https://doi.org/10.5935/0103-5053.20150013.

(33) Nathiya, S.; Janani, R.; Rajesh Kannan, V. Potential of Plant Growth Promoting Rhizobacteria to Overcome the Exposure of Pesticide in Trigonella Foenum - Graecum (Fenugreek Leaves). *Biocatalysis and Agricultural Biotechnology* **2020**, *23*, 101493. https://doi.org/10.1016/j.bcab.2020.101493.
(34) Golash, N.; Gogate, P. R. Degradation of Dichlorvos Containing Wastewaters Using Sonochemical Reactors. *Ultrasonics Sonochemistry* **2012**, *19* (5), 1051–1060. https://doi.org/10.1016/j.ultsonch.2012.02.011.
(35) Durand, G.; Abad, J. L.; Sanchez-Baeza, F.; Messeguer, A.; Barcelo, D. Unequivocal Identification of Compounds Formed in the Photodegradation of Fenitrothion in Water/Methanol and Proposal of Selected Transformation Pathways. *J. Agric. Food Chem.* **1994**, *42* (3), 814–821. https://doi.org/10.1021/jf00039a044.
(36) Beyke, G. L. Thermally Enhanced Hydrolysis for Treatment of Pesticides and Explosives. *Remediation Journal* **2018**, *28* (4), 17–22. https://doi.org/10.1002/rem.21572.
(37) Rodrigo, M. A.; Oturan, N.; Oturan, M. A. Electrochemically Assisted Remediation of Pesticides in Soils and Water: A Review http://pubs.acs.org/doi/full/10.1021/cr500077e (accessed Apr 10, 2020). https://doi.org/10.1021/cr500077e.
(38) Plakas, K. V.; Karabelas, A. J. Removal of Pesticides from Water by NF and RO Membranes — A Review. *Desalination* **2012**, *287*, 255–265. https://doi.org/10.1016/j.desal.2011.08.003.
(39) Cycoń, M.; Mrozik, A.; Piotrowska-Seget, Z. Bioaugmentation as a Strategy for the Remediation of Pesticide-Polluted Soil: A Review. *Chemosphere* **2017**, *172*, 52–71. https://doi.org/10.1016/j.chemosphere.2016.12.129.
(40) Wu, P.; Zhang, Y.; Chen, Z.; Wang, Y.; Zhu, F.; Cao, B.; Wu, Y.; Li, N. The Organophosphorus Pesticides in Soil Was Degradated by Rhodobacter Sphaeroides after Wastewater Treatment. *Biochemical Engineering Journal* **2019**, *141*, 247–251. https://doi.org/10.1016/j.bej.2018.07.019.
(41) Varjani, S.; Kumar, G.; Rene, E. R. Developments in Biochar Application for Pesticide Remediation: Current Knowledge and Future Research Directions. *Journal of Environmental Management* **2019**, *232*, 505–513. https://doi.org/10.1016/j.jenvman.2018.11.043.
(42) Ahmadizad Firozjaei, S. A.; Latifi, A. M.; Khodi, S.; Abolmaali, S.; Choopani, A. A Review on Biodegradation of Toxic Organophosphate Compounds. *Journal of Applied Biotechnology Reports* **2015**, *2* (2), 215–224.
(43) Maya, K.; Upadhyay, S. N.; Singh, R. S.; Dubey, S. K. Degradation Kinetics of Chlorpyrifos and 3,5,6-Trichloro-2-Pyridinol (TCP) by Fungal Communities. *Bioresource Technology* **2012**, *126*, 216–223. https://doi.org/10.1016/j.biortech.2012.09.003.
(44) Ghosh, P.; Kumar, C.; Samanta, A. N.; Ray, S. Comparison of a New Immobilized Fe3+ Catalyst with Homogeneous Fe3+–H2O2 System for Degradation of 2,4-Dinitrophenol. *Journal of Chemical Technology & Biotechnology* **2012**, *87* (7), 914–923. https://doi.org/10.1002/jctb.3699.

(45) Lucas, M. S.; Peres, J. A. Decolorization of the Azo Dye Reactive Black 5 by Fenton and Photo-Fenton Oxidation. *Dyes and Pigments* **2006**, *71* (3), 236–244. https://doi.org/10.1016/j.dyepig.2005.07.007.
(46) Kastner, J. R.; Das, K. C. Wet Scrubber Analysis of Volatile Organic Compound Removal in the Rendering Industry. *Journal of the Air & Waste Management Association* **2002**, *52* (4), 459–469. https://doi.org/10.1080/10473289.2002.10470800.
(47) Herrmann, J.-M.; Guillard, C. Photocatalytic Degradation of Pesticides in Agricultural Used Waters. *Comptes Rendus de l'Académie des Sciences - Series IIC - Chemistry* **2000**, *3* (6), 417–422. https://doi.org/10.1016/S1387-1609(00)01137-3.
(48) Javier Benitez, F.; Acero, J. L.; Gonzalez, T.; Garcia, J. Organic Matter Removal from Wastewaters of the Black Olive Industry by Chemical and Biological Procedures. *Process Biochemistry* **2001**, *37* (3), 257–265. https://doi.org/10.1016/S0032-9592(01)00209-6.
(49) Miltner, R. J.; Baker, D. B.; Speth, T. F.; Fronk, C. A. Treatment of Seasonal Pesticides in Surface Waters. *Journal (American Water Works Association)* **1989**, *81* (1), 43–52.
(50) Zhang, Q.; Li, Q.; Young, T. M.; Harper, D. P.; Wang, S. A Novel Method for Fabricating an Electrospun Poly(Vinyl Alcohol)/Cellulose Nanocrystals Composite Nanofibrous Filter with Low Air Resistance for High-Efficiency Filtration of Particulate Matter. *ACS Sustainable Chem. Eng.* **2019**, *7* (9), 8706–8714. https://doi.org/10.1021/acssuschemeng.9b00605.
(51) Ateia, M.; Attia, M. F.; Maroli, A.; Tharayil, N.; Alexis, F.; Whitehead, D. C.; Karanfil, T. Rapid Removal of Poly- and Perfluorinated Alkyl Substances by Poly(Ethylenimine)-Functionalized Cellulose Microcrystals at Environmentally Relevant Conditions. *Environ. Sci. Technol. Lett.* **2018**, *5* (12), 764–769. https://doi.org/10.1021/acs.estlett.8b00556.
(52) Guerra, F. D.; Campbell, M. L.; Attia, M. F.; Whitehead, Daniel. C.; Alexis, F. Capture of Aldehyde VOCs Using a Series of Amine-Functionalized Cellulose Nanocrystals. *ChemistrySelect* **2018**, *3* (20), 5495–5501. https://doi.org/10.1002/slct.201703149.
(53) Bravo, I.; Figueroa, F.; I. Swasy, M.; F. Attia, M.; Ateia, M.; Encalada, D.; Vizuete, K.; Galeas, S.; H. Guerrero, V.; Debut, A.; C. Whitehead, D.; Alexis, F. Cellulose Particles Capture Aldehyde VOC Pollutants. *RSC Advances* **2020**, *10* (13), 7967–7975. https://doi.org/10.1039/D0RA00414F.
(54) Zhao, Y.; Gao, G.; Liu, D.; Tian, D.; Zhu, Y.; Chang, Y. Vapor Sensing with Color-Tunable Multilayered Coatings of Cellulose Nanocrystals. *Carbohydrate Polymers* **2017**, *174*, 39–47. https://doi.org/10.1016/j.carbpol.2017.06.059.
(55) Fan, L.; Lu, Y.; Yang, L.-Y.; Huang, F.; Ouyang, X. Fabrication of Polyethylenimine-Functionalized Sodium Alginate/Cellulose Nanocrystal/Polyvinyl Alcohol Core–Shell Microspheres ((PVA/SA/CNC)@PEI) for Diclofenac Sodium Adsorption. *Journal of Colloid and Interface Science* **2019**, *554*, 48–58. https://doi.org/10.1016/j.jcis.2019.06.099.

(56) Jin, L.; Li, W.; Xu, Q.; Sun, Q. Amino-Functionalized Nanocrystalline Cellulose as an Adsorbent for Anionic Dyes. *Cellulose* **2015**, *22* (4), 2443–2456. https://doi.org/10.1007/s10570-015-0649-4.
(57) Jin, L.; Sun, Q.; Xu, Q.; Xu, Y. Adsorptive Removal of Anionic Dyes from Aqueous Solutions Using Microgel Based on Nanocellulose and Polyvinylamine. *Bioresource Technology* **2015**, *197*, 348–355. https://doi.org/10.1016/j.biortech.2015.08.093.
(58) Li, J.; Zuo, K.; Wu, W.; Xu, Z.; Yi, Y.; Jing, Y.; Dai, H.; Fang, G. Shape Memory Aerogels from Nanocellulose and Polyethyleneimine as a Novel Adsorbent for Removal of Cu(II) and Pb(II). *Carbohydrate Polymers* **2018**, *196*, 376–384. https://doi.org/10.1016/j.carbpol.2018.05.015.
(59) Xi, C.; Wang, R.; Rao, P.; Zhang, W.; Yan, L.; Li, G.; Chai, F.; Cai, Y.; Luo, T.; Zhou, X. The Fabrication and Arsenic Removal Performance of Cellulose Nanocrystal-Containing Absorbents Based on the "Bridge Joint" Effect of Iron Ions. *Carbohydrate Polymers* **2020**, *237*, 116129. https://doi.org/10.1016/j.carbpol.2020.116129.
(60) Melone, L.; Rossi, B.; Pastori, N.; Panzeri, W.; Mele, A.; Punta, C. TEMPO-Oxidized Cellulose Cross-Linked with Branched Polyethyleneimine: Nanostructured Adsorbent Sponges for Water Remediation. *ChemPlusChem* **2015**, *80* (9), 1408–1415. https://doi.org/10.1002/cplu.201500145.
(61) Zulfiqar, S.; Rafique, U.; Javed Akhtar, M. Removal of Pirimicarb from Agricultural Waste Water Using Cellulose Acetate–Modified Ionic Liquid Membrane. *Environ Sci Pollut Res* **2019**, *26* (16), 15795–15802. https://doi.org/10.1007/s11356-019-04681-6.
(62) Tshikovhi, A.; Mishra, S. B.; Mishra, A. K. Nanocellulose-Based Composites for the Removal of Contaminants from Wastewater. *International Journal of Biological Macromolecules* **2020**, *152*, 616–632. https://doi.org/10.1016/j.ijbiomac.2020.02.221.
(63) F. Attia, M.; I. Swasy, M.; Ateia, M.; Alexis, F.; C. Whitehead, D. Periodic Mesoporous Organosilica Nanomaterials for Rapid Capture of VOCs. *Chemical Communications* **2020**, *56* (4), 607–610. https://doi.org/10.1039/C9CC09024J.
(64) Swasy, M. I.; Campbell, M. L.; Brummel, B. R.; Guerra, F. D.; Attia, M. F.; Smith, G. D.; Alexis, F.; Whitehead, D. C. Poly(Amine) Modified Kaolinite Clay for VOC Capture. *Chemosphere* **2018**, *213*, 19–24. https://doi.org/10.1016/j.chemosphere.2018.08.156.
(65) Guerra, F. D.; Campbell, M. L.; Whitehead, D. C.; Alexis, F. Cover Picture: Tunable Properties of Functional Nanoparticles for Efficient Capture of VOCs (ChemistrySelect 31/2017). *ChemistrySelect* **2017**, *2* (31), 9888–9888. https://doi.org/10.1002/slct.201702287.
(66) Campbell, M. L.; Guerra, F. D.; Dhulekar, J.; Alexis, F.; Whitehead, D. C. Target-Specific Capture of Environmentally Relevant Gaseous Aldehydes and Carboxylic Acids with Functional Nanoparticles. *Chemistry – A European Journal* **2015**, *21* (42), 14834–14842. https://doi.org/10.1002/chem.201502021.

(67) George, J.; Sabapathi, S. Cellulose Nanocrystals: Synthesis, Functional Properties, and Applications. *Nanotechnol Sci Appl* **2015**, *8*, 45–54. https://doi.org/10.2147/NSA.S64386.
(68) Araki, J.; Wada, M.; Kuga, S. Steric Stabilization of a Cellulose Microcrystal Suspension by Poly(Ethylene Glycol) Grafting. *Langmuir* **2001**, *17* (1), 21–27. https://doi.org/10.1021/la001070m.
(69) nanocellulose price; cellulose lab; https://www.celluloselab.com/price/CelluloseLab%20Product%20Price%20List%202020.htm (accessed Sep 6, 2020).
(70) Saito, T.; Kimura, S.; Nishiyama, Y.; Isogai, A. Cellulose Nanofibers Prepared by TEMPO-Mediated Oxidation of Native Cellulose. *Biomacromolecules* **2007**, *8* (8), 2485–2491. https://doi.org/10.1021/bm0703970.
(71) Missoum, K.; Belgacem, M. N.; Bras, J. Nanofibrillated Cellulose Surface Modification: A Review. *Materials* **2013**, *6* (5), 1745–1766. https://doi.org/10.3390/ma6051745.
(72) Huang, S.; Zhou, L.; Li, M.-C.; Wu, Q.; Zhou, D. Cellulose Nanocrystals (CNCs) from Corn Stalk: Activation Energy Analysis. *Materials* **2017**, *10* (1), 80. https://doi.org/10.3390/ma10010080.
(73) Roman, M.; Winter, W. T. Effect of Sulfate Groups from Sulfuric Acid Hydrolysis on the Thermal Degradation Behavior of Bacterial Cellulose. *Biomacromolecules* **2004**, *5* (5), 1671–1677. https://doi.org/10.1021/bm034519+.
(74) Zhou, C.; Shi, Q.; Guo, W.; Terrell, L.; Qureshi, A. T.; Hayes, D. J.; Wu, Q. Electrospun Bio-Nanocomposite Scaffolds for Bone Tissue Engineering by Cellulose Nanocrystals Reinforcing Maleic Anhydride Grafted PLA. *ACS Appl. Mater. Interfaces* **2013**, *5* (9), 3847–3854. https://doi.org/10.1021/am4005072.
(75) Martín-Martínez, J. M.; Fernández-García, J. C.; Huerta, F.; Orgilés-Barceló, A. C. Effect of Different Surface Modifications on the Adhesion of Vulcanized Styrene-Butadiene Rubber. *Rubber Chemistry and Technology* **1991**, *64* (4), 510–521. https://doi.org/10.5254/1.3538569.
(76) Pastor-Blas, M. M.; Ferrándiz-Gómez, T. P.; Martín-Martínez, J. M. Chlorination of Vulcanized Styrene-Butadiene Rubber Using Solutions of Trichloroisocyanuric Acid in Different Solvents. *Journal of Adhesion Science & Technology* **2000**, *14* (4), 561–581. https://doi.org/10.1163/156856100742744.
(77) Romero-Sánchez, M. D.; Pastor-Blas, M. M.; Martín-Martínez, J. M. Adhesion Improvement of SBR Rubber by Treatment with Trichloroisocyanuric Acid Solutions in Different Esters. *International Journal of Adhesion and Adhesives* **2001**, *21* (4), 325–337. https://doi.org/10.1016/S0143-7496(01)00005-7.
(78) García-Martín, C.; Andreu-Gómez, V.; Miguel Martín-Martínez, J. Surface Modification of Vulcanized Styrene–Butadiene Rubber with Trichloroisocyanuric Acid Solutions of Different Active Chlorine Contents. *International Journal of Adhesion and Adhesives* **2010**, *30* (7), 550–558. https://doi.org/10.1016/j.ijadhadh.2010.06.004.

(79) Scott, E.; Bloomfield, S. F. The Survival and Transfer of Microbial Contamination via Cloths, Hands and Utensils. *Journal of Applied Bacteriology* **1990**, *68* (3), 271–278. https://doi.org/10.1111/j.1365-2672.1990.tb02574.x.
(80) Neely, A. N.; Maley, M. P. Survival of Enterococci and Staphylococci on Hospital Fabrics and Plastic. *Journal of Clinical Microbiology* **2000**, *38* (2), 724–726. https://doi.org/10.1128/JCM.38.2.724-726.2000.
(81) Ren, X.; Kou, L.; Kocer, H. B.; Zhu, C.; Worley, S. D.; Broughton, R. M.; Huang, T. S. Antimicrobial Coating of an N-Halamine Biocidal Monomer on Cotton Fibers via Admicellar Polymerization. *Colloids and Surfaces A: Physicochemical and Engineering Aspects* **2008**, *317* (1), 711–716. https://doi.org/10.1016/j.colsurfa.2007.12.007.
(82) Sun, X.; Cao, Z.; Porteous, N.; Sun, Y. An N-Halamine-Based Rechargeable Antimicrobial and Biofilm Controlling Polyurethane. *Acta Biomaterialia* **2012**, *8* (4), 1498–1506. https://doi.org/10.1016/j.actbio.2011.12.027.
(83) Hui, F.; Debiemme-Chouvy, C. Antimicrobial N-Halamine Polymers and Coatings: A Review of Their Synthesis, Characterization, and Applications. *Biomacromolecules* **2013**, *14* (3), 585–601. https://doi.org/10.1021/bm301980q.
(84) Demir, B.; Broughton, R. M.; Qiao, M.; Huang, T.-S.; Worley, S. D. N-Halamine Biocidal Materials with Superior Antimicrobial Efficacies for Wound Dressings. *Molecules* **2017**, *22* (10), 1582. https://doi.org/10.3390/molecules22101582.
(85) Chen, Z.; Sun, Y. N-Halamine-Based Antimicrobial Additives for Polymers: Preparation, Characterization, and Antimicrobial Activity. *Ind. Eng. Chem. Res.* **2006**, *45* (8), 2634–2640. https://doi.org/10.1021/ie060088a.
(86) PETTERSON, R. C.; GRZESKOWIAK, U.; JULES, L. H. N-Halogen Compounds. II.1,2 The N—Cl Stretching Band in Some N-Chloroamides. The Structure of Trichloroisocyanuric Acid. *J. Org. Chem.* **1960**, *25* (9), 1595–1598. https://doi.org/10.1021/jo01079a030.
(87) Sasaki, A.; Himeda, A.; Konaka, H.; Muroyama, N. Ab Initio Crystal Structure Analysis Based on Powder Diffraction Data Using PDXL. **2010**, 5.
(88) Besbes, I.; Alila, S.; Boufi, S. Nanofibrillated Cellulose from TEMPO-Oxidized Eucalyptus Fibres: Effect of the Carboxyl Content. *Carbohydrate Polymers* **2011**, *84* (3), 975–983. https://doi.org/10.1016/j.carbpol.2010.12.052.